Universidade de Lisboa
Faculdade de Medicina



Astrosomes: A Novel Approach for the Regulation of Neuronal Communication

Adam Ioshua d'Armada Moreira

Orientador(es):
Sandra Henriques Vaz, PhD
Brigitte Maria Städler, PhD

Tese especialmente elaborada para obtenção do grau de Doutor em Ciências Biomédicas, com especialidade em Neurociências.

Agosto 2020

Universidade de Lisboa
Faculdade de Medicina



Astrosomes: A Novel Approach for the Regulation of Neuronal Communication

Adam Ioshua d'Armada Moreira

Orientadores:
Sandra Henriques Vaz, PhD
Brigitte Maria Städler, PhD

Tese especialmente elaborada para obtenção do grau de Doutor em Ciências Biomédicas, com especialidade em Neurociências.

Financiado por FCT (PD/BD/114278/2016)

Agosto 2020

A impressão desta tese foi aprovada pelo Conselho Científico da Faculdade de Medicina de Lisboa em reunião de 30 de junho de 2020.

The printing of this dissertation was approved by the Scientific Council of the Faculty of Medicine of the University of Lisbon in the meeting of June 30th, 2020.

All the views expressed in this document are the sole responsibility of the author.

Glia already know how to save neurons,
whereas neuroscientists still have no clue.

– Ben Barres

Abbreviations

3-NT	3-nitrotyrosine
3xTg-AD	triple transgenic AD mouse model
AAK	ammonia assay kit
AD	Alzheimer's disease
Ag-NP	silver nanoparticles
AIBN	azobis(isobutyronitrile)
ALS	amyotrophic lateral sclerosis
AMPAR	α-amino-3-hydroxy-5-methylisoxazole-4-propionate receptors
ANP	atrial natriuretic peptide
ApoE	apolipoprotein E
APP	amyloid precursor protein
AQP4	aquaporin 4
Au-NP	gold nanoparticles
Au-NS	gold nanostars
Aβ	amyloid-β peptide
BDNF	brain-derived neurotrophic factor
BMP	bis(monoacylglycero)phosphate
BSA	bovine serum albumin
C9ORF72	chromosome 9 open reading frame 72
Cat	catalase
CB_1R	cannabinoid receptor 1
CCK-8	cell counting kit 8
CCP	colloidal crystal particles
Chol	cholesterol
CIP	contact inhibition of proliferation
CL	cardiolipin
CLSM	confocal laser scanning microscopy
CNS	central nervous system
CREB	cAMP-regulatory element binding protein

CTA-NHS	N-hydroxysuccinimide 2-(dodecylthiocarbonothioylthio)isobutyrate
CypD	cyclophilin D
D-μF	droplet microfluidics
DA	dopamine hydrochloride
DAPI	4'-6-diamidino-2-phenylindole
DCV	dense-core vesicles
DCX	doublecortin
DG	dentate gyrus
DLS	dynamic light scattering
DMC	dimethyl carbonate
DMEM	Dulbecco's modified Eagle's medium
DMPC	1,2-dimyristoyl-*sn*-glycero-3-phosphocholine
DOPC	1,2-dioleoyl-*sn*-glycero-3-phosphocholine
dPE	dendritic polyethylene
DPPC	1,2-dipalmitoyl-*sn*-glycero-3-phosphocholine
DPPS	1,2-dipalmitoyl-*sn*-glycero-3-phospho-L-serine
EAAT	excitatory amino acid transporters
EDL	electric double layer
EGF	epidermal growth factor
eNMDAR	extrasynaptic NMDAR
ERK	extracellular signal-regulated kinase
F12	Ham's F-12 medium
FBS	fetal bovine serum
FDA	fluorescein diacetate
FE	free enzymes
FGF-2	fibroblast growth factor 2
FITC	fluorescein 5(6)-isothiocyanate
FUS	fused in sarcoma
GABA	γ-aminobutirate
GABAR	GABA receptors
GDH	glutamate dehydrogenase
GDNF	glial cell line-derived neurotrophic factor
GFAP	glial fibrillary acidic protein

GOx	glucose oxidase
GPCR	G protein-coupled receptors
GSH	glutathione
GSSG	oxidized L-glutathione
GTR	glutathione reductase
H_2O_2	hydrogen peroxide
HBSS	Hank's balanced saline solution
HEPES	4-(2-hydroxyethyl)piperazine-1-ethanesulfonic acid
HFF	hydrodynamic flow focusing
hPEG	acrylated hyperbranched PEG
HPMC-AS	hydroxypropylmethylcellulose acetylsuccinate
HRP	horseradish peroxidase
ICC	immunocytochemistry
iGluR	ionotropic glutamate receptors
IL-1β	interleukin 1-β
INF-γ	interferon γ
iNOS	inducible NOS
INT	tetrazolium salt
IP_3	inositol triphosphate
K-ATP	ATP-dependent potassium channels
KAR	kainate receptors
Kir4.1	input rectifier channels for potassium
L	liposomes
L-Glu	L-glutamate
LbL	layer-by-layer deposition
LDH	lactate dehydrogenase
LFP	local field potential
logP	octanol-water partition coefficient
LTP	long-term potentiation
M	microreactors
MAP2	microtubule associated protein 2
Mcu	mitochondrial calcium uniporter
MEA	microelectrode array

mGluR	metabotropic glutamate receptors
MMP	matrix metalloproteinases
Mn-NP	manganese nanoparticles
MNP	magnetic nanoparticles
MPTP	mitochondrial permeability transition pore
NAD	β-nicotinamide adenine dinucleotide
NADP	β-nicotinamide adenine dinucleotide phosphate
NF-κB	nuclear factor κ-B
NFT	neurofibrillary tangles
NGF	nerve growth factor
NH_4^+	ammonia
NMDAR	N-methyl-D-aspartic acid receptors
NO	nitric oxide
NOS	nitric oxide synthase
NP	nanoparticles
NPY	neuropeptide Y
NSC	neural stem cells
NTDPases	nucleotide triphosphate diphosphohydrolases
O_2^-	superoxide anion
O4	oligodendrocyte marker 4
$ONOO^-$	peroxynitrite
PA	phosphatidic acid
PAAm	poly(acrylamide)
PAM	poly(acrylamide)/poly(methyl acrylate)
PBS	phosphate buffered saline
PC	phosphatidylcholine
PCL	polycaprolactone
PDA	poly(dopamine)
PDI	polydispersity index
PDL	poly(D-lysine)
PE	phosphatidylethanolamine
PEG	polyethylene glycol
PEG-*b*-PB	PEG-*b*-polybutadiene block co-polymer

PEG-DA	PEG diacrylate
Pen/Strep	penicillin and streptomycin solution
PFA	paraformaldehyde
PGE2	prostaglandin E2
PI	propidium iodide
PI (ch. V)	phosphatidylinositol
PKA	protein kinase A
PLA	poly(lactic acid)
PLGA	poly(lactic-*co*-glycolic acid)
PLL	poly(L-lysine)
PLL_F	FITC-labeled PLL
PMA	poly(methacrylic acid)
PMAc	poly(methacrylic acid)-*co*-cholesteryl methacrylate
PMA_F	fluorescein *O*-methacrylate-labeled PMA
PMBA	poly(N,N-methylenebisacrylamide)
pNIPAAm	poly(isopropyl acrylamide)
POPC	1-palmitoyl-2-oleoyl-*sn*-glycero-3-phosphocholine
POPS	1-palmitoyl-2-oleoyl-*sn*-glycero-3-phospho-L-serine
PS	polystyrene
PS (ch. V)	phosphatidylserine
PSD-95	postsynaptic density protein of 95 kDa
PSi	mesoporous silicon
Pt-NP	platinum nanoparticles
PUFA	polyunsaturated fatty acid
PVP	poly(vinylpyrrolidone)
QCM-D	quartz crystal microbalance with dissipation monitoring
Rhod	rhodamine
RNS	reactive nitrogen species
ROS	reactive oxygen species
SA	stearylamine
SD	standard deviation
SEC	size exclusion chromatography
SEM	standard error of mean

SICI	short intracortical inhibition
SK	small conductance
SLMV	synaptic-like microvesicles
SM	sphingomyelin
SNARE	soluble N-ethylmaleimide-sensitive factor attachment protein receptor
sNMDAR	synaptic NMDAR
SOD	superoxide dismutase
SPIO	superparamagnetic iron oxide
SVZ	subventricular zone
TARDBP	transactive response DNA-binding protein
TEM	transmission electron microscopy
TLE	temporal lobe epilepsy
TNFα	tumor necrosis factor-α
TRIS	tris(hydroxymethyl)aminomethane
UCMS	unpredictable chronic mild stress
VEGF	vascular endothelial growth factor
VFF	vertical flow focusing
WST-8	2-(2-methoxy-4-nitrophenyl)-3-(4-nitrophenyl)-5-(2,4-disulfophenyl)-2*H*-tetrazolium
x_c^-	cystine-glutamate antiporter
xCT	x_c^- specific light chain protein
ZP	ζ-potential
α-KG	α-ketoglutarate
β-Gal	β-galactosidase

Resumo

O cérebro é uma rede complexa de transmissão de informação que, ao nível celular, depende de um equilíbrio altamente regulado entre excitação e inibição. No sistema nervoso central, o glutamato é o principal neurotransmissor excitatório e a transmissão glutamatérgica está profundamente envolvida numa grande variedade de funções cerebrais, das quais se destacam a aprendizagem e a memória. Este tipo de transmissão excitatória baseia-se na libertação de glutamato na fenda sináptica pelo neurónio pré-sináptico, o que vai ativar os recetores neuronais pós-sinápticos de glutamato, levando a um influxo de iões pelo neurónio pós-sináptico, com despolarização da sua membrana e, caso o limiar de despolarização seja atingido, consequente propagação de potenciais de ação.

A terminação da transmissão glutamatérgica é, na sua maioria, assegurada pela recaptação de glutamato pelos astrócitos vizinhos, onde será metabolizado a glutamina, por ação do enzima sintetase da glutamina. A glutamina é de seguida transportada para o neurónio pré-sináptico onde é novamente convertida a glutamato, por ação do enzima glutaminase, garantindo deste modo a manutenção das reservas intracelulares deste neurotransmissor. Esse ciclo, denominado de ciclo glutamato / glutamina, é também responsável pela destoxificação de amónia, uma vez que a amónia livre é usada para sintetizar glutamina a partir do glutamato. Se algum dos elementos descritos falhar, o cérebro pode facilmente entrar em condições excitotóxicas. A excitotoxicidade é um fenómeno celular que descreve as ações tóxicas de neurotransmissores excitatórios, nomeadamente do glutamato no sistema nervoso central, sendo reconhecido como um mecanismo comum de patogénese em várias doenças neurodegenerativas e outros distúrbios cerebrais, como a doença de Alzheimer, a esclerose lateral amiotrófica, e a epilepsia. Neste cenário excitotóxico, o glutamato ativa em excesso o neurónio pós-sináptico, através da sobreativação dos recetores de glutamato, levando a disfunções dependentes de cálcio. A alteração significativa dos níveis de cálcio desencadeia disfunções mitocondriais e energéticas, stress oxidativo, e superprodução de espécies reativas de oxigénio, que levam a processos de neuroinflamação, culminando eventualmente em morte celular.

Independentemente do papel central da excitotoxicidade em processos patogénicos, nenhum tratamento adequado desta condição foi descrito até ao momento. A maioria das terapias utilizadas no tratamento da excitotoxicidade tende a concentrar-se no bloqueio da libertação de glutamato ou na inativação dos recetores de glutamato. Devido ao papel central da transmissão glutamatérgica no sistema nervoso central, essas terapias tendem a dar origem a efeitos colaterais indesejados e nocivos. Assim, é necessário considerar uma nova abordagem terapêutica para combater a excitotoxicidade. Neste contexto, a biologia sintética aparece como uma estratégia terapêutica promissora. Este campo da bioengenharia está focado na criação de enzimas, organelos, e até células artificiais, usando moléculas biológicas e sintéticas como blocos de construção, com o objetivo de substituir processos biológicos perdidos ou disfuncionais. Alguns avanços notáveis já foram descritos na biologia sintética em contexto biomédico, como a criação de tecido hepático biónico, células artificiais que promovem o crescimento e a regeneração óssea e microrreatores que contêm enzimas biológicos que combatem o stress oxidativo, entre outros.

O presente trabalho de doutoramento teve como objetivo utilizar a biologia sintética como uma ferramenta farmacológica contra a excitotoxicidade. Para isso, desenvolveram-se astrossomas, que se caracterizam por serem células artificiais que mimetizam funções astrocíticas.

Como ponto de partida, duas das funções astrocíticas principais foram consideradas: a remoção de espécies reativas de oxigénio do meio que circunda as células, em particular o peróxido de hidrogénio, e a destoxificação de amónia. Assim, para a primeira geração de astrossomas, foram utilizadas nanopartículas de platina como um mímico artificial de enzima, uma vez que já era sabido que as nanopartículas de platina são capazes de neutralizar simultaneamente espécies reativas de oxigénio e amónia, mesmo que raramente tenham sido aplicadas num contexto biomédico. Além disso, o uso de catalisadores inorgânicos oferece algumas vantagens em relação à utilização de enzimas biológicos. Para além de serem não serem tóxicos para as células, os materiais inorgânicos não são degradados ou inativados quando em contato com células, mantêm sua atividade catalítica por mais tempo quando comparados com os enzimas biológicos e são catalisadores mais eficientes, devido ao seu tamanho reduzido e consequente maior rácio entre área de superfície e volume. Foi utilizada a técnica de deposição camada a camada (*layer-by-layer*), que é uma técnica de

assemblagem baseada na interação de polímeros e materiais com carga oposta, de modo a criar microrreatores de 20 μm de diâmetro contendo nanopartículas de platina. A fim de otimizar a química de superfície para interação celular, diferentes polímeros foram testados, como poli(L-lisina), poli(dopamina), e poli(ácido metacrílico). Foi possível concluir que a poli(dopamina) permitiu uma melhor interação entre o astrossoma e as membranas celulares. Este era já um resultado expectável, dado que a poli(dopamina) tem sido amplamente descrita como uma cola biológica – um material inerte capaz de funcionalizar praticamente qualquer material, proporcionando biocompatibilidade e taxas mais elevadas de interação celular. Foi caracterizada a assemblagem de microrreatores revestidos com poli(dopamina) contendo nanopartículas de platina, garantindo a adsorção bem-sucedida de cada camada e a manutenção da atividade catalítica das nanopartículas de platina. Estes astrossomas foram então testados com a linha celular derivada de neuroblastoma humano SH-SY5Y, onde foi possível concluir que estes microrreatores são biocompatíveis, capazes de interagir com as membranas celulares, e eficientes a resgatar com sucesso a viabilidade celular quando as células foram expostas a peróxido de hidrogénio ou a amónia.

Embora estes sejam resultados promissores, o astrossoma representa uma abordagem bastante simplista e ainda muito distante de um mímico de célula biológica. Existem duas características muito importantes das células biológicas que aumentariam a função e a complexidade dos astrossomas. São essas a existência e a atividade simultânea de vários enzimas, em vez de existir apenas um único catalisador, e a compartimentalização, que permite uma atividade enzimática aprimorada e fornece uma proteção e separação física de vias enzimáticas previamente incompatíveis. Com o objetivo de aprofundar a mimetização de uma célula biológica, desenvolveu-se de seguida um microrreator contendo vários enzimas biológicos e, de forma mais relevante, diferentes vias enzimáticas fisicamente separadas em diferentes compartimentos artificiais. Para isso, duas vias enzimáticas foram consideradas: as reações cíclicas catalisadas pelos enzimas desidrogenase do glutamato e redutase da glutationa, que usam $NADP^+$ e NADPH como cofatores, e a cascata enzimática composta por β-galactosidase, oxidase da glucose, e catalase. Cada via foi então encapsulada em diferentes subunidades lipossómicas que foram incluídas num único microrreator funcional. Com esta abordagem, foi possível criar um microrreator complexo,

contendo cinco enzimas diferentes, trabalhando em duas vias enzimáticas independentes. Com isto, concluiu-se que era possível aumentar a complexidade dos microrreatores sem perder a atividade dos catalisadores.

A aplicação da lógica de compartimentação e múltiplos catalisadores à primeira geração de astrossomas permitiu a criação da segunda geração de astrossomas, desta vez contendo nanopartículas de platina e o enzima desidrogenase do glutamato, encerrados num microrreator revestido com poli(dopamina). Estes astrossomas, quando comparados com a primeira geração, apresentaram maior atividade biológica, sendo capazes de induzir uma maior sobrevivência celular quando neurónios corticais primários de rato foram expostos a peróxido de hidrogénio ou a amónia. Além disso, estes astrossomas foram também capazes de restaurar a comunicação elétrica neuronal, como observado por registros eletrofisiológicos extracelulares realizados em culturas primárias de neurónios expostos a peróxido de hidrogénio ou a amónia na presença ou ausência dos diferentes astrossomas. Estes últimos dados permitiram concluir que estes novos astrossomas não só protegem fisicamente os neurónios, como também são capazes prevenir défices na sua resposta elétrica, o que é uma função essencial para uma ferramenta que combata a excitotoxicidade.

Em conclusão, com este trabalho de doutoramento, foi possível criar uma nova abordagem terapêutica contra a excitotoxicidade. É importante ressaltar que os astrossomas podem ser facilmente adaptáveis a diferentes aplicações, quer por alteração do tipo de nanopartícula quer por alteração dos enzimas utilizados, sendo uma estrutura artificial não tóxica, biocompatível, e biologicamente ativa. As próximas etapas deste projeto envolvem a criação de uma âncora biológica para direcionar os astrossomas especificamente para sinapses excitatórias, a otimização do tamanho destas estruturas, a utilização dos astrossomas em diferentes aplicações, como por exemplo neuroinflamação, e a determinação da sua atividade *in vivo*, num modelo de stress crónico em que a excitotoxicidade está envolvida.

Palavras-chave: excitotoxicidade, astrócitos artificias, nanopartículas de platina, poli(dopamina), catálise encapsulada.

Abstract

The brain is an intricate and complex network of information transmission that, at a cellular level, relies on a highly regulated balance between excitation and inhibition. In the central nervous system, glutamate is the main excitatory neurotransmitter and glutamatergic transmission is deeply involved in a large array of brain functions, such as learning and memory, among many others. This type of excitatory transmission is based on the release of glutamate into the synaptic cleft by the presynaptic neuron, which then activates postsynaptic neuronal glutamate receptors, leading in certain circumstances to an influx of calcium into the postsynaptic neuron, with concomitant membrane depolarization and eventual propagation of action potentials. The synaptically-released glutamate is then taken up into neighboring astrocytes through specific glutamate transporters, where it will be converted into glutamine by the enzyme glutamine synthetase and returned to the presynaptic neuron where it is converted back to glutamate by the enzyme glutaminase, ensuring the maintenance of intracellular glutamate pools. This astrocytic glutamate/glutamine cycle is also responsible for ammonia detoxification, since free ammonia is used to create glutamine from glutamate. If any element of it fails, the brain can easily shift into excitotoxic conditions. Excitotoxicity is a cellular phenomenon that comprises the toxic actions of excitatory neurotransmitters, namely glutamate in the central nervous system, and it is now recognized as a common mechanism for pathogenesis in several neurodegenerative diseases and other brain disorders, such as Alzheimer's disease, amyotrophic lateral sclerosis, and epilepsy. In this excitotoxic scenario, glutamate overactivates the postsynaptic neuron, leading to calcium-dependent dysfunctions. These calcium-dependent dysfunctions include mitochondrial and energetic dysfunctions, oxidative stress and overproduction of reactive oxygen species, and neuroinflammation, culminating eventually in cell death.

Regardless of the central role of excitotoxicity in pathogenesis, no adequate treatment has even been described. Indeed, most therapies against excitotoxicity tend to focus on blocking glutamate release or inactivating glutamate receptors. Because of the central role of glutamatergic transmission in the central nervous system, these

therapies often give rise to undesired and deleterious side effects. Thus, a new therapeutical approach to counteract excitotoxicity needs to be considered. In this context, synthetic biology appears as a promising therapeutical strategy. This field of bioengineering is focused on creating artificial enzymes, organelles, and even cells, using biological and synthetic molecules as building blocks, with the aim to replace for lost or dysfunctional biological processes. Some notable advances have already been described within synthetic biology in a biomedical context, such as the creation of bionic hepatic tissue, artificial cells that promote bone growth and regeneration, and enzyme-based microreactors that tackle oxidative stress, among others.

The aim of this PhD project was to apply synthetic biology as a pharmacological tool against excitotoxicity. For that, we created astrosomes, which are artificial cells that mimic astrocytic functions.

As a starting point, two main astrocytic functions were considered: clearance of reactive oxygen species and ammonia detoxification. Therefore, for the first generation of astrosomes, platinum nanoparticles were used as an artificial enzyme mimic, since it was already known that platinum nanoparticles were able to simultaneously neutralize reactive oxygen species and ammonia, even though they have been rarely applied to a biomedical context. Additionally, the use of inorganic catalysts offers some advantages over biological enzymes. Briefly, inorganic materials cannot be degraded or inactivated when in contact with cells, maintain their catalytic activity longer than biological enzymes, and are more efficient catalysts, due to their reduced size and consequent higher surface area-to-volume ratio. The layer-by-layer deposition technique, which is an assembly technique based on the interaction of polymers and materials with opposite charge, was used to create 20 μm in diameter microreactors containing platinum nanoparticles. In order to optimize the surface chemistry for cell interaction, different polymers were tested, such as poly(L-lysine), poly(dopamine), and poly(methacrylic acid). It was possible to conclude that poly(dopamine) allowed for a higher interaction between the astrosome and cell membranes. This was already to be expected, given that poly(dopamine) has widely been described as a biological glue – an inert material capable of functionalizing virtually any material, providing biocompatibility and higher rates of cell interaction. The assembly of poly(dopamine)-coated microreactors containing platinum nanoparticles was characterized, ensuring the successful adsorption of each layer and the maintenance of the catalytic activity of the

platinum nanoparticles. These astrosomes were then tested with the human neuroblastoma-derived cell line SH-SY5Y, where they were proven to be biocompatible, able to interact with cell membranes, and successfully rescue cell viability when cells were exposed to hydrogen peroxide or ammonia.

While these were promising results, the astrosome remained rather simplistic, and very distant from a biological cell mimic. There were two very important characteristics of biological cells that would increase the function and complexity of the astrosomes. These are the existence and simultaneous activity of several enzymes, as opposed to only one catalyst, and compartmentalization, which allows for enhanced enzymatic activity and provides a physical protection and separation of otherwise incompatible enzymatic pathways. With the aim to better mimic a biological cell, the creation of a microreactor containing biological enzymes and, most importantly, different enzymatic pathways, physically separated in different artificial compartments was investigated. For this, two enzymatic pathways were explored: the cyclical reactions catalyzed by glutamate dehydrogenase and glutathione reductase, using $NADP^+$/NADPH as a co-factor, and the enzymatic cascade comprised of β-galactosidase, glucose oxidase, and catalase. Each pathway was then encapsulated in different liposomal subunits that were included in one microreactor. With this, a complex microreactor, containing five different enzymes, working in two different enzymatic pathways was successfully created, leading to the conclusion that it was possible to increase the complexity of microreactors without losing catalyst activity.

Applying the logic of compartmentalization and multiple catalysts to the first generation astrosome allowed for the creation of the second generation astrosome, containing platinum nanoparticles and the enzyme glutamate dehydrogenase, enclosed in a poly(dopamine)-coated microreactor. These astrosomes, when compared to the first generation, presented enhanced biological activity, leading to a higher cell survival when rat primary cortical neurons were exposed to hydrogen peroxide or ammonia. Furthermore, these astrosomes were also able to restore neuronal electrical communication, as seen by extracellular electrophysiological recordings performed in neurons exposed to hydrogen peroxide or ammonia in the presence or absence of the different astrosomes. These last data led to the conclusion that the astrosomes not only physically protected neurons, but also that they could prevent deficits in neuronal electrical responses, an essential feat when tackling excitotoxicity.

In conclusion, this thesis describes the creation of a novel therapeutical approach against excitotoxicity. Importantly, the astrosomes can be easily tailorable for different applications by changing the catalytically active components, being a non-toxic, biocompatible, and biologically active artificial structure. The next steps for this project involve creating a biological anchor to direct the astrosomes toward excitatory synapses, optimizing the size of these structures, exploring different applications, such as neuroinflammation, and testing their activity *in vivo*, in a model of chronic stress where excitotoxicity is involved.

Keywords: excitotoxicity, artificial astrocytes, platinum nanoparticles, poly(dopamine), encapsulated catalysis.

Acknowledgements

It takes a village to successfully finish a PhD! A lot of people were essential in the process of creating this thesis. First and foremost, I want to deeply thank Sandra Vaz, my supervisor, for embarking in this amazing trip with me, accepting my crazy ideas, teaching me how to be a “grown-up” scientist, and helping me to control my anxiety when things didn’t work out how I wanted them to. I could have never asked for a better supervisor. Following the same line, I am really thankful and happy that Brigitte Städler accepted to be my co-supervisor, even though I knew almost nothing about synthetic biology. My stay in Denmark, in her lab, was one of the most character-defining experiences for me, both personally and scientifically. Thank you Brigitte, for always pushing me to work harder and smarter, and for seeing me not only as a student, but as a collaborator.

I was very lucky during these four years. Not only I was able to find amazing supervisors with whom I could talk to and discuss science as equals, but I was fortunate enough to be part of awesome research teams. The people that worked (and hung out, and partied) with me over these four years are the best colleagues and friends that a person could ask for. So, I feel obliged to thank them individually.

Starting with Denmark people: Essi, Philipp, Fabian, Bo, Laura, Yan, and Martin – I will never forget the comradery, the late-night discussions of science and philosophy, our usual Tuesday beer, and the fact that you made me play football. I do, however, need to highlight two special Scandinavian thanks. First, to Kristine, my first ever student. I was really nervous to be, for the first time, in the role of supervisor, but you made it an amazing experience. And finally, to Sidsel, without whom my life in Denmark would have been a lot less than it was. You will always have a place in my heart.

As for Portugal people, I need to acknowledge my Astropeople! Gomes, Ribeiro, Tati, Oksana, Carolina, Robertta, Sara, Nádia, Filipa, and Miguel (by proxy). You guys made me want to come into work every single day, always looking forward to our coffee breaks, our silliness, and the way we all help each other and push each other to be better.

I would also like to extend my appreciation to all entities that supported my research by awarding me travel grants and awards that allowed me to go to excellent scientific conferences and recognized the quality of my work, deeply contributing to my development as a researcher and science communicator. These are the Portuguese Society for Neuroscience (SPN), for the travel grant and best poster award at the 25th SPN Meeting in Braga, Portugal; the Mind-Brain College of the University of Lisbon, for awarding me a best poster award at the 3rd Meeting of PhD Students from the Mind-Brain Doctoral College of the University of Lisbon; and the Japanese Neuroscience Society, for the travel grant that allowed me to attend and present my work at the 41st Meeting of the Japanese Neuroscience Society in Kobe, Japan.

Finally, it's going to get personal. I could not end this acknowledgement section without thanking my friends and family. I had a lot of ups and downs over the last four years, and I don't know how I could've survived it without their support. So, to all my queers: you bunch of misfits, you rock!

To my mom and my grandma, I don't even know what to say. I am what you made me. I hope I was able to make you proud, both as a person and as a scientist. You two will always be what I aspire to be when I grow up.

Last, but definitely not least at all, I need to thank my wife. Flávia, thank you so much for looking at this very anxious and gender dysphoric tiny scientist and seeing a husband. Your support and your existence in general make everything possible. I love you.

Declaration of authorship

This thesis includes several scientific publications, either already published, accepted, or in preparation. These publications are:

Armada-Moreira A, *et al*. Walking the extra (synaptic) mile: excitotoxicity as the road toward neurodegenerative diseases. Frontiers in Cellular Neuroscience 2020, 14, 90.

Armada-Moreira A, *et al*. Droplet-microfluidics to assemble advanced building blocks in cell mimicry. Nanoscale 2016, 8 (47), 19510–19522.

Armada-Moreira A, *et al*. Artificial astrocytes: not if, but when. In preparation.

Armada-Moreira A, *et al*. Platinum nanoparticle-based microreactors as support for neuroblastoma cells. ACS Applied Materials & Interfaces 2018, 10 (9), 7581–7592.

Armada-Moreira A, *et al*. On the assembly of microreactors with parallel enzymatic pathways. Advanced Biosystems 2018, 2 (5), 1700244.

Armada-Moreira A, *et al*. Multicompartment microreactors prevent excitotoxic dysfunctions in rat primary cortical neurons. Advanced Biosystems 2020, 2000139.

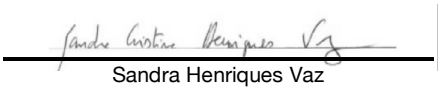
Regarding these publications:

I, Adam Ioshua d'Armada Moreira, hereby declare that all experimental work, data analysis, manuscript writing, and illustrations were created by me, unless otherwise stated in the respective chapter.

I, Sandra Henriques Vaz, as supervisor, agree that this information is correct.



Adam Ioshua d'Armada Moreira



Sandra Henriques Vaz

Table of Contents

vii **abbreviations**

xiii **abstract (portuguese)**

xvii **abstract (english)**

xxi **acknowledgements**

xxiii **declaration of authorship**

1 chapter i. **THE IDEA**

5 chapter ii. **MAIN INTRODUCTION**

7 the biological side

Rationale and publication information

Original review article

"Going the extra (synaptic) mile: excitotoxicity as the road toward neurodegenerative diseases"

36 the engineering side

Rationale

Defining the astrosome size

Choosing a catalyst for the astrosome

42 chapter II references

61 chapter iii. **EMPLOYED METHODOLOGIES**

63 rationale

63 nanoscience and synthetic biology techniques

Fabricating the astrosome

Exploring surface charge

Ensuring layer interaction

Protecting enzymes

Assessing size

66 neuroscience techniques

Determining cell viability

Measuring membrane integrity

Probing neuronal activity

69 chapter III references

71 chapter iv. **SPECIFIC METHODS IN SYNTHETIC BIOLOGY**
73 rationale and publication information
75 original review article
"Droplet-microfluidics to assemble advanced building blocks in cell mimicry"
89 chapter IV references

95 chapter v. **NEUROBIOLOGY AND SYNTHETIC BIOLOGY**
97 rationale and publication information
99 original review article
"Artificial astrocytes: not if, but when"
110 chapter V references

117 chapter vi. **THE FIRST ASTROSOME**
119 rationale and publication information
121 original research article
"Platinum nanoparticle-based microreactors as support for neuroblastoma cells"
137 chapter VI supporting information
142 chapter VI references

147 chapter vii. **INCREASING THE COMPLEXITY OF MICROREACTORS**
149 rationale and publication information
151 original research article
"On the assembly of microreactors with parallel enzymatic pathways"
163 chapter VII supporting information
169 chapter VII references

171 chapter viii. **THE EVOLUTION OF THE ASTROSOME**
173 rationale and publication information
175 original research article
"Multicompartment microreactors prevent excitotoxic dysfunctions in rat primary cortical neurons"
191 chapter VIII supporting information
192 chapter VIII references

195 chapter ix. **MAIN DISCUSSION AND FUTURE WORK**
197 discussion
201 future directions
Anchoring the astrosome to excitatory synapses
Optimizing astrosome size
Change the catalyst, change the application: astrosomes as tools to tackle neuroinflammation
Moving forward: testing the astrosomes in vivo
217 chapter IX references

221 annex i. **FACS SIMILE OF SCIENTIFIC ARTICLES**

Table of Figures

chapter ii. **MAIN INTRODUCTION**

10 II.1. Schematic summary of different aspects of excitotoxicity, including the main cellular defenses against it, the main causes, the players involved in its mechanisms, and general cellular consequences.

17 II.2. Graphical depiction of the main calcium-dependent processes involved in excitotoxicity, leading to oxidative stress and cell death.

23 II.3. Schematic representation of the alterations in excitatory neurotransmission in ALS.

25 II.4. Underlying cellular mechanisms of Alzheimer's Disease.

30 II.5. Aβ-induced astrocytic dysfunctions leading to excitotoxicity and AD pathogenesis.

31 II.6. The connecting railway between Epilepsy and Excitotoxicity: Glutamatergic and GABAergic mechanisms in epilepsy-related excitotoxicity.

chapter iv. **SPECIFIC METHODS IN SYNTHETIC BIOLOGY**

76 IV.1. Cartoon illustrating the use of D-μF for the assembly of nanoparticles, Janus particles, and non-spherical particles as well as their loading with biological cargo and potential application in cell mimicry.

78 IV.2. Nanoparticle assembly.

81 IV.3. Janus-shaped particles.

84 IV.4. Non-spherical particles.

87 IV.5. Cargo loading.

chapter vi. **THE FIRST ASTROSOME**

123 VI.1. Schematic overview of the interaction between neuroblastoma cells and microreactors.

127 VI.2. Pt-NP synthesis.

128 VI.3. Pt-NP as enzyme mimics in solution.

130 VI.4. ζ-potential measurements of the microreactors at the different steps in the LbL assembly including representative images.

131 VI.5. Pt-NP-based microreactors in solution.

133 VI.6. Cell viability/proliferation of neuroblastoma cells incubated with different microreactors.

134 VI.7. Surface coating dependent cell adhesion.

136 VI.8. M^{PDA} offer protection against H_2O_2 and NH_4^+ toxicity.

137 VI.S1. Pt-NP as enzyme mimics for H_2O_2 degradation.
138 VI.S2. Changes in frequency and dissipation of a silica/PDA pre-coated QCM-D crystal upon deposition of polymers.
138 VI.S3. Pt-NP-catalyzed conversion of H_2O_2 by microreactors is not affected by the terminating layer.
139 VI.S4. H_2O_2 degradation by M^{PDA} in cell medium.
140 VI.S5. Effects of the terminating layers of the microreactors in cell proliferation.
140 VI.S6. Cell viability of undifferentiated SH-SY5Y cells incubated with M^{i} or M^{PDA} for 24 h.
140 VI.S7. Cell viability curves of SH-SY5Y cells exposed to different concentrations of H_2O_2 or NH_4^+.

chapter vii. **INCREASING THE COMPLEXITY OF MICROREACTORS**

153 VII.1. Overview schematic of the microreactors containing two different encapsulated enzymatic pathways.
156 VII.2. Cyclical reactions of GDH and GTR.
157 VII.3. Enzymatic cascade of GOx and Cat.
157 VII.4. Enzymatic cascade of β-Gal, GOx, and Cat.
160 VII.5. Enzymatic pathways encapsulated in liposomes.
162 VII.6. Assembly and activity of microreactors with up to five encapsulated enzymes.
163 VII.S1. Cyclical reactions of GDH and GTR throughout time.
163 VII.S2. Cyclical reactions of GDH and GTR in solution when incubated with the enzymatic cascades.
164 VII.S3. Activity of the GOx and Cat cascade in solution when incubated with the GDH and GTR enzymatic cycle.
164 VII.S4. Activity of the β-Gal, GOx, and Cat cascade in solution when incubated with the GDH and GTR enzymatic cycle.
164 VII.S5. Average size and polydispersity index for all fabricated enzyme-loaded liposomes.
165 VII.S6. L_{GDH} activity with different lipid compositions.
166 VII.S7. L_{GDH} activity with different liposome sizes.
166 VII.S8. GDH and GTR cyclical reactions encapsulated in liposomes.
167 VII.S9. BSA calibration curve for the BCA Protein Assay.
168 VII.S10. Highest measured amount of NADPH, in raw values.
168 VII.S11. Amount of NADPH measured after L_{GDH} were incubated for 24 h with L-glutamate, GSSG, and NADP· with or without 0.25% Triton X-100.
168 VII.S12. Bright field microscopy images and population histogram flow cytometry analysis for all the assembled microreactors.

chapter viii. **THE EVOLUTION OF THE ASTROSOME**

176 VIII.1. Schematic representation of rat primary cortical neurons exposed to toxic compounds in the absence and in the presence of first and second generation microreactors.

183 VIII.2. Cell viability and adherence of rat primary cortical neurons exposed to different microreactor concentrations.

186 VIII.3. ζ-potential measurement of the microreactors at the different assembly steps and representative images. Determination of enzymatic and Pt-NP activity in the different microreactors.

190 VIII.4. Biological activity of the different microreactors.

191 VIII.S1. Cell viability of cells at 14 DIV incubated with M^P for 24 h and exposed to different concentrations of H_2O_2 or NH_4^+.

chapter ix. **MAIN DISCUSSION AND FUTURE WORK**

203 IX.1. 3D structure of the dimeric complex neuroligin-1/neurexin-1β, with the identified pocket locations.

204 IX.2. Chemical structure of the top 3 more adequate ligands.

209 IX.3. Representative fluorescence microscopy images of different cell types in the mixed cell culture.

210 IX.4. Representative fluorescence microscopy images of DIV 14 cells exposed for 24 h to particles with 2 or 7 μm in diameter.

214 IX.5. Physical and functional analysis of Mn-NP.

215 IX.6. SOD enzymatic activity of free SOD and SOD-containing liposomes.

Table of Tables

chapter ii. **MAIN INTRODUCTION**

15 II.1. Summary of glutamate receptors' characteristics, including their synaptic location, relationship with calcium, and involvement in excitotoxicity.

chapter v. **NEUROBIOLOGY AND SYNTHETIC BIOLOGY**

97 V.1. A comparison between known astrocytic functions and equivalent artificial mimics.

99 V.2. Characteristics of the different astrocytic vesicles and liposomal mimicking possibilities.

chapter vi. **THE FIRST ASTROSOME**

132 VI.S1. Summary of the steps for the determination of the average activity per microreactor toward H_2O_2.

132 VI.S2. Summary of the steps for the determination of the average activity per microreactor toward NH_4^+.

chapter vii. **INCREASING THE COMPLEXITY OF MICROREACTORS**

151 VII.1. Final concentration of the encapsulated enzymes in liposomes.

151 VII.2. Overview of the enzyme-loaded liposomes encapsulated in the different microreactors.

157 VII.S1. Enzyme encapsulation efficiency.

chapter viii. **THE EVOLUTION OF THE ASTROSOME**

191 VIII.S1. Summary of all the fabricated microreactors.

191 VIII.S2. Two-way ANOVA of H_2O_2 and NH_4^+ consumption.

chapter ix. **MAIN DISCUSSION AND FUTURE WORK**

198 IX.1. Primary antibodies used for ICC, including their origin, type, company, reference, and dilution.

205 IX.2. Size distribution of liposomes with different lipid compositions, either empty or containing SOD.

Chapter I.

The idea.

I am aware that a PhD thesis is supposed to be super scientific. And we'll get to that! I did a lot of scientific things during these past four years that resulted in the thesis you are about to read. But science does not exist in a vacuum and I believe that us scientists should stop pretending we are machines that can only convey pure raw data. We are people and we can tell stories while keeping the scientific part unbiased. So, I think it is important to give context of how a scientific idea appears and comes to life, with all the challenges and detours along the way. So, I will try to turn this bulky piece of written science into something light(er) to read – by providing context and little paragraphs that will hopefully give you an insight on my thinking. Here comes the first one.

In science (and life, mostly), everything starts with an idea. In this particular case, the idea came up to me in 2015. I was finishing my MSc degree and had just been accepted into the NeurULisboa PhD programme. While trying to rush my MSc defense, I asked how the PhD project proposal would work. Did it need to be associated with studying a disease? Were there prepared projects? To this, Prof. Ana Sebastião simply answered: "You have a clean slate and free reign. Come up with something you want to study!".

I went home and got on with the thinking. A lot of possible projects came to mind, but nothing that filled me with the enthusiasm that would get me through four years of frustration and hard work. Then, one day, my "Eureka moment" came to me very cliché-y in the shower. It was very simple: what if I can make artificial astrocytes?

At this point, after two years of studying neurosciences, I had let go of my fascination with neurons, having concluded that they are mere transistors. The cells that started to awe me were astrocytes. They were the true controllers of neurons and, by proxy, of the brain. They were powerful and versatile. I actually have a very nice metaphor about this, that I use with my friends that never heard the word astrocyte before. Imagine that a neuron is that loud friend that, when you go out at night, is annoying, yells, and talks to everyone. While they are fun and the light of the party, that person alone in a club would be a disaster! Now, the astrocyte is the "mom-type" friend, that goes over to the neuron and says things like "maybe you drank enough already, I'm cutting you off", or "how about drinking water now?", or "I'm keeping your wallet from now on!", or even "please, that person does NOT want to talk to you".

So, it would only make sense that when the idea of synthetic biology came to my mind, it would be related to astrocytes. I went back to Prof. Ana, super excited, and the exchange went something like this:

Me: “I know what I want my project to be! I will make artificial astrocytes that will replace the real ones in cases where they lose functions or are dysfunctional.”

Prof. Ana: “...ok. Do you know how to make artificial cells?”

Me: “No.”

Prof. Ana: “Well then, that’s quite risky, isn’t it?”

Me: “If it wasn’t risky, what would be the fun of it?”

Prof. Ana (realizing I’m very stubborn): “Ok, if you can find supervisors that believe that this project is feasible in four years, go for it.”

Long story short, I convinced Sandra Vaz to be my supervisor, since she’s the goddess of astrocytes and molecular neurosciences, and I found Brigitte Städler during my luckiest Google search ever, given that she had been working with artificial cells and organelles for a long time and was looking exactly for a neuronal application for her technology.

With all this in place, I started thinking about the science.

As an editorial note, I would like to use this first chapter to explain how this thesis is organized. Each chapter corresponds to a logical sequence of the project, mostly associated with original articles, and the references are divided by chapter, following the numbering I.1, I.2, (...), II.1, II.2. Each chapter’s references can be found at the end of that chapter, and not at the end of the thesis.

Other than that, some chapters include literature background and my own comments or conclusion of that research. My opinion paragraphs are differentiated from the rest with black lateral lines and italic text, such as this one.

To conclude, all text that has been written in the context of a scientific article is displayed in double column serif font. The remainder is in single column non-serif font.

Chapter II.

Main introduction.

Going the extra (synaptic) mile: excitotoxicity as the road toward neurodegenerative diseases

Armada-Moreira A, Gomes JI, Pina CC, Savchak OK, Gonçalves-Ribeiro J, Rei N, Pinto S, Morais TP, Martins RS, Ribeiro FF, Sebastião AM, Crunelli V, Vaz SH

Frontiers in Cellular Neuroscience **2020**

Rationale

The first application we envisioned for the astrosomes (our artificial astrocytes) was excitotoxicity. This molecular phenomenon comprising the toxic action of excitatory neurotransmitters, namely glutamate, includes various cellular consequences and is involved in several neurodegenerative diseases. All the bibliographic research I did on this issue resulted in the publication in this chapter, a review focusing on the main aspects of excitotoxicity and how this phenomenon manifests in different pathologies. In this article, Filipa F. Ribeiro and Joana Gonçalves-Ribeiro, together with me, wrote the section on excitotoxicity; Nádia Rei and Sara Pinto wrote about amyotrophic lateral sclerosis; Joana I. Gomes and Oksana K. Savchak wrote the Alzheimer's disease section; and Carolina Campos Pina, Robertta Silva Martins, and Tatiana P. Morais wrote about epilepsy. Sandra H. Vaz envisioned the topics, divided the sections amongst authors, coordinated the writing process, and wrote the abstract and conclusion. All was done under the supervision of Vincenzo Crunelli and Ana M. Sebastião, who reviewed the manuscript. All illustrations and titles are my original work.

Publication information

Title. Going the extra (synaptic) mile: excitotoxicity as the road toward neurodegenerative diseases.

Authors. Adam Armada-Moreira, Joana I. Gomes, Carolina Campos Pina, Oksana K. Savchak, Joana Gonçalves-Ribeiro, Nádia Rei, Sara Pinto, Tatiana P. Morais, Robertta Silva Martins, Filipa F. Ribeiro, Ana M. Sebastião, Vincenzo Crunelli, Sandra H. Vaz.

Status of publication. Published.

Journal. Frontiers in Cellular Neuroscience 2020, 14, 90.

DOI. 10.3389/fncell.2020.00090

JCR impact factor, quartile, and field. 4.555; Cellular and Molecular Neuroscience: Q1.

Original review article

Going the extra (synaptic) mile: excitotoxicity as the road toward neurodegenerative diseases

Armada-Moreira A[1,2,3,†], Gomes JI[1,2,†], Pina CC[1,2], Savchak OK[1,2], Gonçalves-Ribeiro J[1,2], Rei N[1,2], Pinto S[1,2], Morais TP[4], Martins RS[5], Ribeiro FF[1,2], Sebastião AM[1,2], Crunelli V[4,6], Vaz SH[1,2*]

[1]Instituto de Farmacologia e Neurociências, Faculdade de Medicina, Universidade de Lisboa, Lisbon, Portugal.
[2]Instituto de Medicina Molecular, Faculdade de Medicina, Universidade de Lisboa, Lisbon, Portugal.
[3]Interdisciplinary Nanoscience Center (iNANO), Aarhus University, Aarhus, Denmark.
[4]Neuroscience Division, School of Bioscience, Cardiff University, Cardiff, UK.
[5]Laboratório de Neurofarmacologia, Instituto Biomédico, Universidade Federal Fluminense, Niterói, Brazil.
[6]Department of Physiology and Biochemistry, Faculty of Medicine and Surgery, University of Malta, Malta.
*Corresponding author. | [†]Co-first authors.

Frontiers in Cellular Neuroscience **2020**, *14*, 90.

Abstract

Excitotoxicity is a phenomenon that describes the toxic actions of excitatory neurotransmitters, primarily glutamate, where the exacerbated or prolonged activation of glutamate receptors starts a cascade of neurotoxicity that ultimately leads to the loss of neuronal function and cell death. In this process, the shift between normal physiological function and excitotoxicity is largely controlled by astrocytes since they are able to control the levels of glutamate on the synaptic cleft. This control is achieved through glutamate clearance from the synaptic cleft and its underlying recycling through the glutamate-glutamine cycle.

The molecular mechanism that triggers excitotoxicity involves alterations in glutamate and calcium metabolism, dysfunction of glutamate transporters, and malfunction of glutamate receptors, particularly NMDAR. On the other hand, excitotoxicity can be regarded as a consequence of other cellular phenomena, such as mitochondrial dysfunction, physical neuronal damage, and oxidative stress. Regardless, it is known that the excessive activation of NMDAR results in the sustained influx of calcium into neurons and leads to a number of deleterious consequences, including mitochondrial dysfunction, reactive oxygen species overproduction, impairment of calcium buffering, release of pro-apoptotic factors, among others, that inevitably contribute to neuronal loss.

A large body of evidence implicates NMDAR-mediated excitotoxicity as a central mechanism in the pathogenesis of many neurodegenerative diseases, including amyotrophic lateral sclerosis, Alzheimer's disease, and epilepsy. In this review, we explore different causes and consequences of excitotoxicity, discuss the involvement of NMDAR-mediated excitotoxicity and its downstream effects on several neurodegenerative disorders, and identify possible strategies to study new aspects of these diseases that may lead to the discovery of new therapeutic approaches. With the understanding that excitotoxicity is a common denominator in neurodegenerative diseases and other disorders, a new perspective on therapy can be considered, where the targets are not specific symptoms, but the underlying cellular phenomena of the disease.

Keywords: excitotoxicity, astrocytes, NMDA receptors, calcium signaling, neurodegenerative diseases, oxidative stress.

Excitotoxicity: what is it, where does it come from, how does it live?

The Good, The Bad, and The Ugly: general definition and summary of consequences

When looking into the glutamatergic system within the central nervous system, one can see three sides of the same biological phenomenon. First, there is The Good: the glutamatergic system is essential for brain functioning. Indeed, with 40% of glutamatergic synapses in the central nervous system,[II.1] glutamate is essential for neuronal communication, as well as for higher level functions, such as learning and memory. Then, there is The Bad: since glutamate plays such an important role in the brain, dysregulation of the glutamatergic system has long been implicated as a key step in the pathophysiology of neuronal death.[II.2] Finally, there is The Ugly: excitotoxicity. This phenomenon, an important aspect of glutamatergic dysregulation, describes the toxic actions of excitatory neurotransmitters, mainly glutamate, that ultimately lead to neuronal death.[II.3] While glutamate does not directly kill neurons, the exacerbated or prolonged activation of glutamate receptors starts a cascade of neurotoxicity,[II.4,5] which includes cationic influx, mitochondrial dysfunction, energetic and oxidative stress, and overproduction of reactive oxygen species (ROS).[II.3,6] Here, we review the main factors involved in excitotoxicity, as summarized in **Figure II.1**, and their role in neurodegenerative diseases and epilepsy.

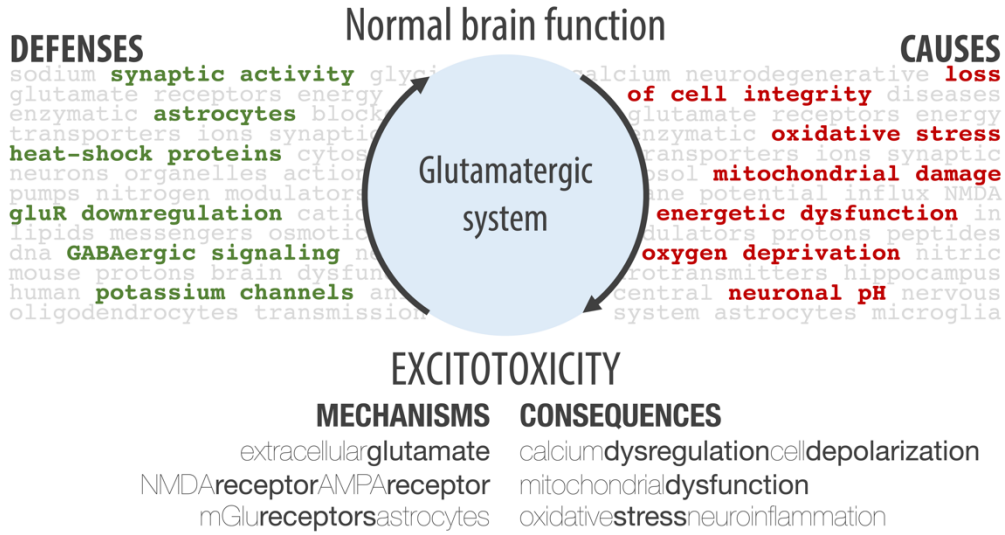


Figure II.1. Schematic summary of different aspects of excitotoxicity, including the main cellular defenses against it, the main causes, the players involved in its mechanisms, and general cellular consequences. The shift from normal brain function to an excitotoxic state is brought about by the main **causes**, and this shift is avoided by the main cellular **defenses**. If the defenses fail, excitotoxicity is amplified by different **mechanisms**, causing cellular **consequences**.

If These Walls Could Talk... About Excitotoxicity: historic review

The term "excitotoxicity" makes its debut in 1969 in a study by Olney where, for the first time, cell death was observed as a consequence of exposure to glutamate or aspartate.[II.7] This type of excitotoxicity can be divided into three steps. It starts with the induction, which begins with the overactivation of ionotropic glutamate receptors (iGluR), such as N-methyl-D-aspartic acid receptors (NMDAR), α-amino-3-hydroxy-5-methylisoxazole-4-propionate receptors (AMPAR), and kainate receptors (KAR). NMDAR activation allows for the influx of calcium, while AMPAR and KAR activation contributes to sodium influx. This ionic influx is followed by water influx, leading to cell swelling and mitochondrial dysfunction. The final step of induction is the activation of metabotropic glutamate receptors (mGluR), activating pathways regulated by diacylglycerol and inositol 1,4,5-triphosphate.[II.8] Amplification and expression are the following stages. These consist in exacerbated metabolic activity, further disruption of ion gradients, elevated electrical neuronal activity, and mitochondrial dysfunction.[II.8]

Other than this classification system for excitotoxicity, this phenomenon can be further categorized as strong or weak excitotoxicity.[II.9] Strong excitotoxicity refers to the classical phenomenon described by Olney, where excitotoxicity is elicited by direct exposure to glutamate or other excitotoxic compound. In strong excitotoxicity, the calcium influx is prolonged, there is depolarization of both cell and mitochondria membranes, excessive consumption of NAD(P)H, and an established bioenergetic failure. Furthermore, cell death is generally brought on by necrosis.[II.3,10] On the other hand, weak excitotoxicity arises from a prolonged alteration of glutamate receptor function, possibly impacting membrane potential and cellular metabolism and increasing cellular sensitivity to the toxic actions of glutamate.[II.9] In this scenario, neurons are transiently able to restore calcium homeostasis, membrane potential, and internal ATP and NAD(P)H pools.[II.11,12] These neurons can then undergo delayed apoptosis, characterized by delayed calcium dysregulation, nuclear compression, and cellular contraction.[II.13–16] This is accompanied by a loss of membrane potential, ATP depletion, and overproduction of ROS.[II.17,18]

A Glutamatergic Mind: glutamate in physiological and excitotoxic conditions

In central nervous system synapses, glutamate clearance is achieved by diffusion and transporter uptake, mainly into neighboring glial cells,[II.19–21] and is practically independent of enzymatic breakdown.[II.22]

It should however be noted that glutamatergic synapses are complex – their morphological characteristics (number of release sites, existence of dendritic spines, etc.) can differ greatly and synapses in different neural circuitries exhibit different time courses of synaptic communication.[II.23] Furthermore, the exact time course of glutamate dynamics can be altered by the microanatomical synaptic properties (synaptic contact size, complexity of synaptic morphology, glial wrapping, etc.) and by the density of glutamate transporters.[II.23]

Even taking all this into account, during a synaptic event, the peak concentration of glutamate in the synapse can be estimated to be

1.1 mM (1.0–1.5 mM), with a decay time constant of 1.2 ms (0.70–2.0 ms),[II.24] while in extrasynaptic locations, the peak concentration can reach 190 μM.[II.25] On the opposite side, the baseline concentration of synaptic glutamate (with no synaptic event occurring) is thought to vary between 25 nM[II.26] and 600 nM,[II.27] depending on the study. This basal concentration is unaltered by synaptic activity, being controlled solely by glutamate transporters.[II.26] Furthermore, this basal concentration does not activate glutamate receptors[II.28–30] nor interferes with neuronal excitability.[II.26]

In excitotoxicity, the time course of glutamate dynamics can be affected in several different manners. The synaptic concentration of glutamate can rise above its usual peak concentration (above 1.1 mM), although this value might plateau due to complete depletion of presynaptic glutamate, or this peak concentration can be maintained for an excessive amount of time, which is translated to an increase in the decay time, or even the baseline concentration of glutamate may be increased, regardless of depolarization-induced release. Regarding this last scenario, it is known that neuronal excitotoxic injury occurs with baseline concentrations of glutamate of 2–5 μM.[II.27]

Glutamate and the depolarization factory: glutamate receptors in excitotoxicity

Glutamatergic neurotransmission is performed through iGluR and mGluR. The iGluR are ligand-gated ion channels permeable to various cations, namely sodium, potassium, and calcium, that produce excitatory glutamate-evoked currents, while mGluR are G protein-coupled receptors that control cellular processes via G protein signaling cascades.[II.31] The main characteristics of these receptors are summarized in **Table II.1** and reviewed in detail in this section.

iGluR can be divided into three functional classes such as NMDAR, AMPAR, and KAR.[II.32] While all iGluR are in the first line of the excitotoxic response, NMDAR have been pinpointed as the main culprit in glutamate-induced neurotoxicity, due to their permeability to calcium ions. NMDAR exhibit a voltage-dependent magnesium-blockade, high permeability to calcium, and require simultaneous binding of glutamate and a co-agonist, such as glycine and D-serine, for activation.[II.33] NMDAR are tetrameric structures composed of GluN1, GluN2A-D and GluN3A-B subunits that form a central ion channel pore. Diversity in NMDAR subunits and assembly results in different receptor subtypes with distinct functional properties, including different channel kinetics, channel opening probability, and conductance. Therefore, these differences in subunit composition can impact both synaptic plasticity and neuronal function. Previous literature reported that GluN2A-containing receptors present faster kinetics, while GluN2B-containing receptors present slower opening, closing, and glutamate

unbinding, indicating that NMDAR containing GluN2A open more reliably and with faster kinetics than NMDAR containing GluN2B subunits.[II.34] These data suggest that NMDAR containing GluN2A are more likely to sense rapid glutamate transients in the synapse and open with a high probability, while NMDAR containing GluN2B seem to be set to sense basal levels of glutamate and open with much lower probability. Moreover, it is known that NMDAR subunit composition also determines single-channel conductance and blockage by magnesium ions,[II.35–37] where both GluN2A- or GluN2B-containing receptors display a high ionic conductance and stronger magnesium block. In mature neurons, GluN2A subunits are predominantly synaptic (sNMDAR), whereas GluN2B-containing receptors are mostly extrasynaptic (eNMDAR).[II.38] In rat hippocampal slices, the amount of eNMDAR has been estimated to be 36% of that of sNMDAR[II.39] and it is known that D-serine mainly binds to sNMDAR, while glycine preferentially binds to eNMDAR.[II.40] Furthermore, previous studies reported a neuroprotective role for sNMDAR and a neurotoxic role for eNMDAR by receptor-mediated influx of calcium.[II.41–43] Moreover, it has been proposed that the activation of NMDAR containing GluN2A subunits stimulates signaling cascades associated with neuroprotection and regulates survival, while stimulation of NMDAR containing GluN2B subunits leads to the activation of excitotoxic pathways, leading to neuronal death.[II.44] sNMDAR (mainly enriched with GluN2A subunits) activation promotes neuroprotection via changes in gene expression that have multiple effects within the cell. Stimulation of sNMDAR is known to result in the enhancement of antioxidant defenses, promoting the transcription of pro-survival factors, including cAMP-regulatory element binding protein (CREB),[II.42] that results in the transcription of brain-derived neurotrophic factor (BDNF), essential for neuronal survival. sNMDAR activity is also implicated in the generation of anti-apoptotic effects, including the inactivation of pro-death transcription factors, such as forkhead box protein O and p53.[II.45] In contrast, stimulation of eNMDAR (mainly enriched with GluN2B subunits) preferentially induces pro-death effects, such as the shut-off of CREB pathway, blocking BDNF expression;[II.41] the inactivation of extracellular signal-regulated kinases 1 and 2, which are necessary for BDNF function on spines;[II.41] activation of forkhead box protein O and calpains, with consequent cleavage of the striatal enriched tyrosine phosphatase, which prevents this phosphatase from inhibiting p38 mitogen-activated protein kinase; and oxidative stress with subsequent neurodegeneration.[II.41,42] Hence, while sNMDAR have a neuroprotective role, eNMDAR preferentially initiate cell death pathways.[II.42] In fact, it is known that low levels of eNMDAR activity have no effects on neuronal survival, while high levels of eNMDAR stimulation enhance cell death pathways and exacerbate neurodegenerative processes, consequently reducing neuronal survival.[II.42] eNMDAR can also be activated by mechanical stimuli and aspartate. Indeed, the GluN2B subunit has been reported to play a role in the mechanosensitive activation of NMDAR.[II.46] On the other hand, although with lower affinity than glutamate, aspartate can bind and activate NMDAR.[II.47] Aspartate levels are severely increased following traumatic brain

injury[II.48,49] and, when present in excessive levels extrasynaptically, are associated with excitotoxicity.[II.50] In summary, while sNMDAR signaling is associated with the suppression of pro-apoptotic transcription factors,[II.45] eNMDAR stimulation increases the activity of pro-apoptotic factors, leading to oxidative stress and cell death.[II.41,42,51] The activation of these pro-apoptotic factors is able to affect gene activity regulation of BDNF and vascular endothelial growth factor,[II.41] essential for the maintenance of synaptic connectivity and architecture.[II.52] Hence, the excessive intracellular calcium levels resulting from the excessive eNMDAR stimulation lead to excitotoxic cell death and contributes to neuronal injury.

Intriguingly, there are conflicting evidences regarding NMDAR involvement in excitotoxicity. Some studies state that NMDAR have a dichotomic effect in excitotoxicity, where activation of sNMDAR counteracts excitotoxicity and activation of eNMDAR is the main contributor to the excitotoxic cascade.[II.53] Other authors propose that NMDAR-induced excitotoxicity requires overactivation of both sNMDAR and eNMDAR.[II.44,54] Finally, other studies even suggest neurotoxicity could be solely dependent on sNMDAR activity, since silencing sNMDAR can act as neuroprotective approach against NMDA-induced excitotoxicity, while inhibiting eNMDAR does not have any protective effect, questioning the role of these receptors in neurotoxicity.[II.40]

AMPAR are tetrameric ionotropic glutamate receptors formed by GluA1-4 subunits. These receptors can be either hetero- or homotetramers and, depending on subunit composition, display different calcium permeability,[II.55] with the GluA2 subunit controling AMPAR calcium permeability. Assemblies of highly calcium-permeable AMPAR have been implicated in excitotoxicity. Moreover, the GluA2 subunit can also be subjected to RNA editing, with conversion of a glutamine codon into an arginine one, and AMPAR are calcium-permeable if they contain the unedited GluA2 subunit or if they lack the GluA2 subunit.[II.56] Given their high calcium permeability, AMPAR lacking GluA2 are thought to contribute to excitotoxic cell death.[II.56]

KAR are composed of GluR5-7 and KA1-2 subunits. KAR properties are similar to AMPAR in that they allow ion flux directly following glutamate exposure, and are mostly impermeable to calcium. Although AMPAR are localized mostly in the postsynaptic membrane, several studies have shown that KAR may be localized in both pre- and post-synaptically.[II.57,58] Post-synaptically, KAR and AMPAR have a similar function in alleviating the magnesium block in NMDAR. This phenomenon leads to an exacerbation of NMDAR activation under glutamate excess.

mGluR are probably the most diverse receptor family of the central nervous system. The mGluR1 and mGluR5 subtypes are located in the peri- and extrasynaptic neuronal regions.[II.59] They are coupled to G_q protein and exert their actions via the inositol trisphosphate/calcium signal pathway, being consequently able to stimulate of calcium release from neuronal stores, thus triggering delayed cell death.[II.55]

Table II.1. Summary of glutamate receptors' characteristics, including their synaptic location, relationship with calcium, and involvement in excitotoxicity.

Receptor type	General description	Receptor subtype	Location	Calcium involvement	Involvement in excitotoxicity
Ionotropic	Ligand-gated ion channels Excitatory glutamate-evoked currents	NMDA	Synaptic and extrasynaptic	Permeable	sNMDA: neuroprotection, cell survival eNMDA: pro-death pathways, excitotoxicity, neuronal dysfunction
		AMPA	Post-synaptic	Permeable if lacking GluA2 subunit	Activation alleviates NMDAR Mg^{2+} block, cell depolarization
		KA	Pre- and post-synaptic	Mostly impermeable	
Metabotropic	GPCR Cellular processes via G protein signaling cascades	mGluR1/5	Peri- and extrasynaptic	Ca^{2+} release from internal stores	Activation of the IP_3/Ca^{2+} signaling pathway Delayed cell death

The Gatekeepers of Homeostasis: astrocytes

In the forebrain, it has been shown that astrocytes are responsible for about 90% of the glutamate clearance from the synaptic cleft. During synaptic transmission, only approximately 20% of synaptically-released glutamate reaches the postsynaptic glutamate receptors, while the remainder can reach the extrasynaptic space.[II.60] Due to the significant role of astrocytes in glutamate re-uptake, impairment of astrocytic glutamate transporters leaves neurons highly susceptible to excitotoxicity.[II.61] During an acute insult, astrocytes are able to prevent excitotoxicity by removing extracellular glutamate with high-affinity sodium-dependent glutamate transporters also known as excitatory amino acid transporters (EAAT). These proteins can clear glutamate from the extracellular space into cells, where it can be metabolized or recycled. Several subtypes of EAAT have already been pharmacologically identified. These transporters were divided into four subtypes in rats (GLAST, GLT-1, EAAC1 and EAAT4) and five in humans (EAAT1-5), and can be found in neurons (EAAT3 or EAAC1 and EAAT4) and in astrocytes (EAAT1 or GLAST and EAAT2 or GLT-1).[II.62–66] Additionally, although it may appear that glutamate transporters activity comes mostly from (if not exclusively) from astrocytes, the role of glutamate transporters in neurons still needs to be further explored. Indeed, neuronal glutamate transporters knockout does not have an influence in terms of preventing excitotoxicity, since mice with this knockout show no differences in survival, weight gain, and seizure activity compared to wild-type. On the other hand, synaptosomes prepared from these

knockout mice showed a reduction of glutamate activity by 40%,[II.67] suggesting that the role of neuronal glutamate transporters is yet to be revealed.

Furthermore, astrocytes are responsible for the maintenance of glutamate homeostasis by sustaining its synthesis, uptake and release via the glutamate-glutamine cycle.[II.19,21,68] Through this cycle, synaptically released glutamate is predominantly taken up into astrocytes, where it is amidated to glutamine by the astrocyte-specific enzyme glutamine synthetase.[II.69] Glutamine is then released to the synapse and uptake by adjacent neurons, where it is converted to glutamate and γ-aminobutyric acid (GABA), which are then repackaged into vesicles and again released in the synapse as neurotransmitters.[II.70,71]

In a different perspective, astrocytes are hypothesized to be the main effectors of glycolysis in order to produce lactate that is then transferred to neurons through the astrocyte-neuron lactate shuttle. This metabolic link between neurons and astrocytes is due to the fact that neurons are highly energy-demanding cells but are unable to perform the citric acid cycle without external supply of lactate, due to the lack of the essential enzyme pyruvate carboxylase.[II.72,73] Since astrocytic glutamate re-uptake is electrogenic, for each glutamate molecule entrance, three sodium ions enter the cell, activating the sodium/potassium ATPase. This, in turn, activates the glycolysis pathway in the astrocytes, stimulating the production of the lactate by either increasing glucose uptake or intracellular glycogen breakdown. Produced lactate is later released into the intracellular space by the monocarboxylate transporter 1 expressed in the astrocytes and received by neurons through the monocarboxylate transporter 2.[II.74] It is later used by the neuron as the carbon source in the Krebs cycle for oxidative phosphorylation. Besides lactate, astrocytes also release citrate, involved in the regulation of neuronal excitability by chelating zinc ions, thus inhibiting NMDAR.[II.72,75] Furthermore, although recent literature suggests that neurons are primarily responsible for the synthesis and release of D-serine,[II.76] several independent studies strongly support that astrocytes are the main source of D-serine, essential for NMDAR function.[II.77–80]

The Butterfly Effect: detailed look into excitotoxicity-induced dysfunctions

One ion to rule them all: the central role of calcium to propagate glutamate toxicity

One of the first consequences of excessive activation of glutamate receptors, namely NMDAR, is a sustained influx of calcium into the neuron.[II.81] Calcium has long been identified as a key player in glutamate neurotoxicity, as summarized in **Figure II.2**. Specifically, early studies proved that scavenging extracellular calcium would decrease excitotoxicity-induced neuronal degeneration, while removal of other cations would not.[II.82,83] This influx synergizes with the release of calcium from intracellular stores, such as the mitochondria and the endoplasmic reticulum, due to membrane damage caused by the disruption of ionic gradients.[II.81]

Together, these phenomena lead to a striking increase in the intracellular calcium concentration, which can activate enzymes that degrade proteins, lipids, and nucleic acids,[II.84] as well as enzymes involved in arachidonic acid pathways,

such as phospholipase A2, cyclooxygenase-2, and lipoxygenases. These latter enzymes, when activated, lead to the production of arachidonic acid and its conversion into prostaglandins, leukotrienes, and thromboxanes with concomitant production of ROS.[II.85–87] Among these molecules, prostaglandin E2 has been shown to have a dual role in excitotoxicity: at low concentration (nanomolar range), prostaglandin E2 presents a neuroprotective effect;[II.88] at higher concentrations (micro- to millimolar), as seen in the calcium-induced arachidonic acid cascade, prostaglandin E2 contributes to neurotoxicity and cell death.[II.89] Additionally, calcium-induced activation of phospholipase A2 inhibits GABA receptors (GABAR), thus preventing neuronal hyperpolarization and further contributing to excitotoxicity.[II.90]

Finally, the calcium dysregulation also activates ATP-dependent ion pumps, in an effort to counteract the cationic influx, such as the sodium/potassium and calcium ATPases, which will drain all available ATP, creating a low-energy neuronal state.[II.91,92]

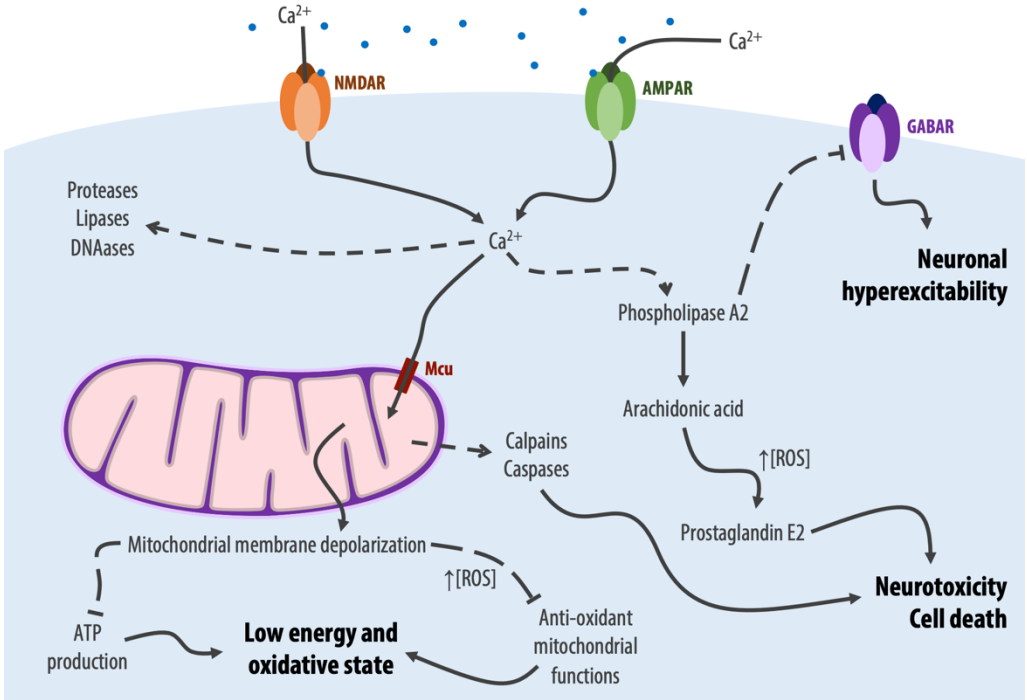


Figure II.2. Graphical depiction of the main calcium-dependent processes involved in excitotoxicity, leading to oxidative stress and cell death. Dotted lines with end arrows represent activation, dotted lines with T ends represent inhibition. Mcu – mitochondrial calcium uniporter.

Eternal dysfunction for the mitochondrial minds: mitochondrial damage

Another large contributor to glutamate neurotoxicity are mitochondria (**Figure II.2**), which are essential in bioenergetic homeostasis and calcium signaling regulation.[II.81] Indeed, following the excitotoxicity-induced calcium influx, mitochondria capture cytosolic calcium via the mitochondrial calcium uniporter, attempting to maintain a low cytosolical calcium concentration.[II.93] While this process temporarily buffers the intracellular calcium concentration, the

excessive cationic uptake eventually leads to the depolarization of the mitochondrial membrane, impairing ATP production and anti-oxidant mitochondrial functions[II.94,95] and leaving neurons in a low-energy and oxidative state with high production of ROS.[II.81] Following this cascade, mitochondrial dysfunction contributes to apoptotic cell death, activating both caspases[II.4] and calpains.[II.96]

The Wizard of ROS: oxidative stress

The excessive activation of glutamate receptors also leads to an imbalance between ROS and their opposing antioxidant forces,[II.97] a phenomenon named oxidative stress. In an excitotoxic scenario, oxidative stress is brought about by a higher intracellular concentration of ROS, which is directly associated with glutamate neurotoxicity.[II.98] ROS are then mediators of enzyme inactivation, lipidic peroxidation and consequent membrane damage, DNA alterations, and apoptosis.[II.99,100]

The excitotoxic production of ROS is related to the activation of the pro-oxidant enzymes xanthine oxidase and NADPH oxidase[II.6] and to mitochondrial dysfunction. Interestingly, NADPH oxidase, and not mitochondria, has been identified as the major source of ROS following glutamate exposure.[II.101]

Additionally, studies have demonstrated that glutamate binding to NMDAR results in the production of nitric oxide (NO) as a consequence of nitric oxide synthase (NOS) activation by calcium influx, which is spatially linked to NMDAR via the postsynaptic density protein of 95 kDa.[II.102–104] It has also been observed that an increase in NO concentration is able to trigger biochemical pathways that contribute to neuronal death and cognitive impairment,[II.105] since NO is able to react with the superoxide anion forming peroxynitrite, known to lead to the formation of 3-nitrotyrosine.[II.106] NO is then responsible for protein degradation by nitration and oxidation, lipid peroxidation, and DNA damage.[II.53] Protein nitration results in the dysfunction of several proteins such as superoxide dismutase (SOD), actin, and tyrosine hydroxylase, and is able to interfere with cell signaling pathways mediated by tyrosine phosphorylation,[II.107] contributing to the intracellular signaling dysregulation.

We Need to Talk About Excitotoxicity: excitotoxicity as consequence of other phenomena

A possible trigger for excitotoxicity is the physical damage of a neuron. In physiological conditions, the extracellular glutamate concentration is around 0.01% of the intracellular concentration, not reaching the threshold for postsynaptic neuronal activation which maintains the glutamate pools in an inactive state.[II.81] However, this percentage can quickly increase if a damaged neuron releases all its glutamate content into the extracellular space, leading to excitotoxicity in neighboring neurons.[II.81]

Oxidative stress is one of the main consequences of glutamate-induced neurotoxicity. However, it is not possible to define an unidirectional cause/effect relationship between the two phenomena, since oxidative stress and excessive intracellular ROS can also induce excitotoxicity by stimulating extracellular glutamate release[II.108] and releasing calcium from mitochondria into the cytosol.[II.109] In another perspective, it has already been shown that astrocytic

glutamine synthetase is especially susceptible to ROS-induced inactivation, which compromises the whole glutamate-glutamine cycle and contributes to an increase in extracellular glutamate concentration and consequent excitotoxicity.[II.110] Additionally, the presence of ROS has been shown to decrease glutamate transporter activity, impairing synaptic clearance of glutamate further contributing to the increase in extracellular glutamate concentration.[II.111]

Oxygen deprivation can also induce excitotoxicity through different mechanisms. In a straight forward manner, hypoxic-ischemic states directly stimulate glutamate release, increasing the extracellular glutamate concentration to neurotoxic levels.[II.6] Additionally, oxygen deprivation leads to energetic stress by impairing mitochondrial oxidative phosphorylation and, consequently, blocking ATP production.[II.112] This blockage leads to the depletion of intracellular ATP, which prevents the reuptake of glutamate, creating an excitotoxic concentration of extracellular glutamate.[II.113]

In a different perspective, while mitochondrial damage is one of the main consequences of excitotoxicity, mitochondria can also be originators of excitotoxicity. Mitochondrial toxins, for instance, can cause energetic impairment, preventing ATP production.[II.114] Over time, cellular ATP pools are then depleted, with a concomitant decline in the activity of the sodium/potassium ATPase, which will depolarize the neuronal membrane.[II.81] By itself, this depolarization can render neurons more prone to firing action potentials.[II.115] It, however, also affects NMDAR by removing their voltage-dependent magnesium-block, lowering their activation threshold so that non-excitotoxic glutamate concentrations become capable of inducing an excitotoxic response.[II.116]

Finally, the physiological brain pH is estimated to be pH 7.2–7.3 in rats,[II.117] and pH 7.33 in humans.[II.118] However, some diseases or disorders can drastically alter the CNS pH, inducing either acidosis or alkalosis. For instance, anaerobic conditions of ischemia promote the alteration of the metabolism of the cells from aerobic oxidation of glucose to anaerobic glycolysis. This alteration in metabolism produces lactate and protons, which is responsible for acidosis.[II.119] Interestingly, a curious phenomenon occurs in acidosis. While severe acidosis ($pH < 6.4$) contributes to excitotoxicity through a loss of ionic gradients[II.120] and activation of acid-sensing ion channels, which intensifies excitotoxicity by providing another entry for calcium,[II.121–123] mild acidosis (pH 6.5–7.0) appears to partly prevent excitotoxicity,[II.124] as well as glutamate-induced neuronal death.[II.125] This phenomenon occurs due to the inhibitory effects of protons on NMDAR activation.[II.126] On the other end of the spectrum, alkalosis ($pH > 8.0$) seems to induce neurotoxicity. When compared to acidosis, alkalosis produces a more severe dysfunction that is more difficult to counteract. Indeed, cortical GABAergic neurons appear to be more susceptible to alkalosis than to acidosis.[II.127] And, considering the inhibitory effect of protons on NMDAR, it is possible to conclude that alkalosis leads to an increase in NMDAR activation. Thus, alkalosis contributes to excitotoxicity by both directly stimulating NMDAR, but also by disrupting inhibitory neurotransmission.

Saving Private Neuron: cellular defenses against excitotoxicity

During excitotoxicity, neurons mobilize a variety of defenses in order to decrease the damaging effects of this process, among which are potassium channels, GABA signaling, acid-sensing ion channels, adenosine, and NO.[II.128]

Potassium channels are responsible for limiting and rectifying neuronal excitability during action potentials. The small-conductance calcium-dependent potassium channels[II.129] are highly calcium-dependent and are quite sensitive to transient increases of cytosolic calcium.[II.130] The small-conductance channels mediate the shift of the excitotoxic calcium mobilization into a protective, hyperpolarizing signal.[II.129,131–133] Other key potassium channels are the ATP-dependent potassium channels, whose conductance is enhanced by ATP depletion,[II.134,135] particularly following excitotoxic insults.[II.136] At presynaptic sites, ATP-dependent potassium channel activation also inhibits glutamate release.[II.137]

NMDAR-mediated calcium influx also increases sodium/potassium ATPase activity, leading to decreased excitability by stabilizing the resting membrane potential.[II.138]

Another defense mechanism against excitotoxicity involves the inhibitory neurotransmitter GABA and GABAergic signaling.[II.139] In addition, taurine released from glial cells during insults,[II.140,141] similarly to GABA, also decreases presynaptic neuronal excitability by increasing chloride influx[II.142] through $GABA_AR$.[II.143,144] Moreover, neuronal networks were shown to offer a fast acting GluN2A-dependent neuroprotective signaling mechanism, which uses the innate capacity of surrounding neuronal networks to quench excitation, through the recruitment of $GABA_BR$.[II.43]

Glutamate receptor number can be also decreased by calcium-mediated activation of calpains. Activation of these proteases can result in the proteolysis of both NMDAR and AMPAR.[II.145–147] Moreover, calcium-dependent activation of calcineurin and calmodulin can inhibit voltage-gated and NMDAR-gated calcium currents, respectively.[II.148–150]

During necrotic insults, energy depletion gives rise to adenosine. Adenosine inhibits presynaptic glutamate release, an action that is accomplished through A_1 adenosine receptors linked by G proteins to both calcium and potassium channels, and decreases postsynaptic calcium currents in response to glutamate.[II.151,152] On the other hand, a downstream consequence of glutamatergic excitotoxicity is the generation of NO, which acts intracellularly to inhibit NMDAR activity by nitrosylation.[II.153]

Another response of neurons to cell stress is the expression of heat-shock proteins, which protect against misfolding, conferring resistance to necrotic injury.[II.154] Neurons can also up-regulate and increase the activity of antioxidant agents following necrotic insults, which includes Mn- and Cu/Zn-SOD,[II.155–157] glutathione peroxidase, and catalase.[II.158]

In addition, recent evidences have shown that synaptic activity is able to protect primary rat hippocampal neurons against mitochondrial oxidative stress and mitochondrial dysfunction derived from acute excitotoxicity, since synaptic activity is able to induce the transcriptional repression of the mitochondrial calcium uniporter, leading to a reduction in excitotoxicity associated with mitochondrial calcium overload.[II.159]

A Brief History of ALS: amyotrophic lateral sclerosis

Amyotrophic Lateral Sclerosis (ALS) is a fatal and progressive neurodegenerative disease, characterized by the degeneration of both upper (motor cortex) and lower (spinal cord) motor neurons that results in motor dysfunction and, ultimately, death. While primary symptoms of ALS are associated with motor dysfunction, other areas of the brain may undergo degeneration, with 40–60% of patients showing evidence of different levels of cognitive impairment.[II.160,161] Although 90% of ALS cases are sporadic with no known cause, in the 10% of familial cases, more than 30 genes have already been implicated,[II.162] with mutations in Cu/Zn-SOD1, transactive response DNA-binding protein, fused in sarcoma, chromosome 9 open reading frame 72, and several others.[II.163]

Despite numerous studies demonstrating the involvement of several altered signaling pathways, the pathogenetic mechanisms behind ALS are still unclear. Indeed, it seems that, in ALS, neurodegeneration is the product of a combination of different concomitant mechanisms. Understanding the cause of motor neuron degeneration is critical for unravelling ALS pathogenesis and there are mainly two hypotheses to explain the origin of the disease.[II.164] The first one is the dying-forward hypothesis, which proposes an anterograde degeneration of motor neurons via glutamate excitotoxicity from the cortex. The second one is the dying-back hypothesis, which suggests that ALS may start distally at the nerve terminal or at the neuromuscular junction, progressing towards the cell body. Despite the numerous hypotheses proposed, alterations in excitatory neurotransmission appear to have a key role in disease progression, mediated by increased susceptibility to excitotoxicity, as schematically depicted in **Figure II.3**.[II.165] Physiological studies have demonstrated cortical hyperexcitability in patients with both sporadic and familial ALS before the onset of symptoms.[II.166] In addition to cortical hyperexcitability, peripheral axons also present changes in their excitability in ALS patients.[II.167] Changes in neuronal activity can also lead to morphological alterations. In the $SOD1^{G93A}$ mouse model, upper motor neurons display reductions in dendritic length and spine density, suggesting a homeostatic response to heightened pre-synaptic activity or even a stressed state of these neurons.[II.168,169] It is however still unclear whether hyperexcitability is one of the causes of motor neuron degeneration or a compensatory mechanism resulting from motor neuron degeneration.

One of the first proposed mechanisms underpinning neurodegeneration in ALS was glutamate-mediated excitotoxicity.[II.170] One suggested way in which glutamate excitotoxicity may occur is through a decrease in the levels of the transporters responsible for the removal of glutamate from the synaptic cleft. In ALS, a likely trigger for neuroinflammation is the motor neuronal and astrocytic release of misfolded proteins, like aberrant SOD1, and other toxic molecules. This release stimulates the activation of microglia, unleashing pro-inflammatory and neurotoxic actions,[II.171–174] which dysregulate the communication between motor neurons and glial cells, compromising neuronal homeostasis. Microglia are considered the immune cells of the brain and may adopt different polarized activated phenotypes, with the M1 and M2 being

the most accepted. The classical M1 phenotype is associated with the release of pro-inflammatory molecules and activation of receptors, and the M2 phenotype is related with the secretion of anti-inflammatory mediators and growth factors. However, recent studies point to the coexistence of different heterogeneous states and mixed phenotypes.[II.126,174] In ALS, microglia function changes along disease progression, displaying the M2 anti-inflammatory phenotype at early stages and switching to the M1 activated subtype as disease progresses. [II.172,175] Activated microglia contribute and enhance motor neuron death, and can even acquire a distinct and impaired phenotype at the end-stage that accelerates disease progression.[II.174,176] In addition to neuroinflammation, glial cells also play a role in glutamate-mediated excitotoxicity. Specifically, astrocyte-mediated downregulation of EAAT2, leading to a decrease in glutamate uptake and subsequent potentiation of excitotoxic effects, has been reported in both ALS patients and SOD1^{G93A} mice,[II.177] as well as in the TDP-43 rat model,[II.178] correlating with regions of motor neuron loss.[II.179] Thus, a decrease in the level of these transporters may lead to the accumulation of glutamate in the extracellular space, resulting in post-synaptic glutamate receptor overstimulation and consequent excitotoxic effects.[II.180,181] Furthermore, not only have astrocytes in ALS been reported to release lower levels of neurotrophic factors, but they have actually been shown to release neurotoxic factors that play a role in furthering neurodegeneration.[II.182–184] Moreover, it has been shown that, in ALS patients carrying *SOD1* gene mutations, there is a decrease in motor neuron levels of calcium binding proteins, which – by decreasing calcium buffering in the cytoplasm – may exacerbate excitotoxicity.[II.185,186] In the SOD1^{G93A} mouse model, overexpression of EAAT2 delays disease onset but not death[II.187] and fails to prevent loss of phrenic nerve motor neurons or rescue respiratory function.[II.188] Several pathways have been implicated in the modulation of EAAT2 levels, such as tumor necrosis factor-α (TNFα) and downstream nuclear factor κ-B signaling.[II.189] Recently, membralin, an endoplasmic reticulum membrane protein, was also shown to have a role in EAAT2-mediated glutamate excitotoxicity in ALS. Membralin levels are reduced in human ALS spinal cord and SOD1^{G93A} mouse models, and its deletion suppresses EAAT2 expression through a TNF-α/TNF receptor 1/nuclear factor κ-B pathway. Overexpression of membralin in astrocytes was shown to increase EAAT2 expression and improve motor neuron survival.[II.190]

However, defects in the clearance of glutamate do not seem to be the only origin of excessive extracellular glutamate. In the SOD1^{G93A} mouse model, activation of Group I mGluR or the GABA/glycine heterotransporter abnormally increases the release of glutamate.[II.191–193] Recently, Bonifacino and colleagues[II.194] demonstrated that mGluR are overexpressed in the spinal cord of SOD1^{G93A} mice at pre-symptomatic stages and that their function is altered early on in the disease, suggesting that it can represent a cause rather than a consequence of disease progression. Group I mGluR may be potential targets for preventing excitotoxicity in ALS, since it has been shown that treatment with an antagonist attenuated cell death, delayed the onset of motor symptoms, and slightly prolonged survival in SOD1^{G93A} mice.[II.195]

Moreover, calcium permeability of AMPAR is largely determined by the presence of the GluA2 subunit and it has been shown that mutant SOD1 astrocytes secrete factors that lower the expression of this subunit in motor neurons, consequently leading to AMPAR-mediated excitotoxicity and cell death.[II.196,197] Moreover, fused in sarcoma-ALS astrocytes trigger changes to motor neuron AMPAR that render them susceptible to excitotoxicity[II.198] and patients with the chromosome 9 open reading frame 72 mutation appear to have increased vulnerability to AMPAR-mediated excitotoxicity.[II.199]

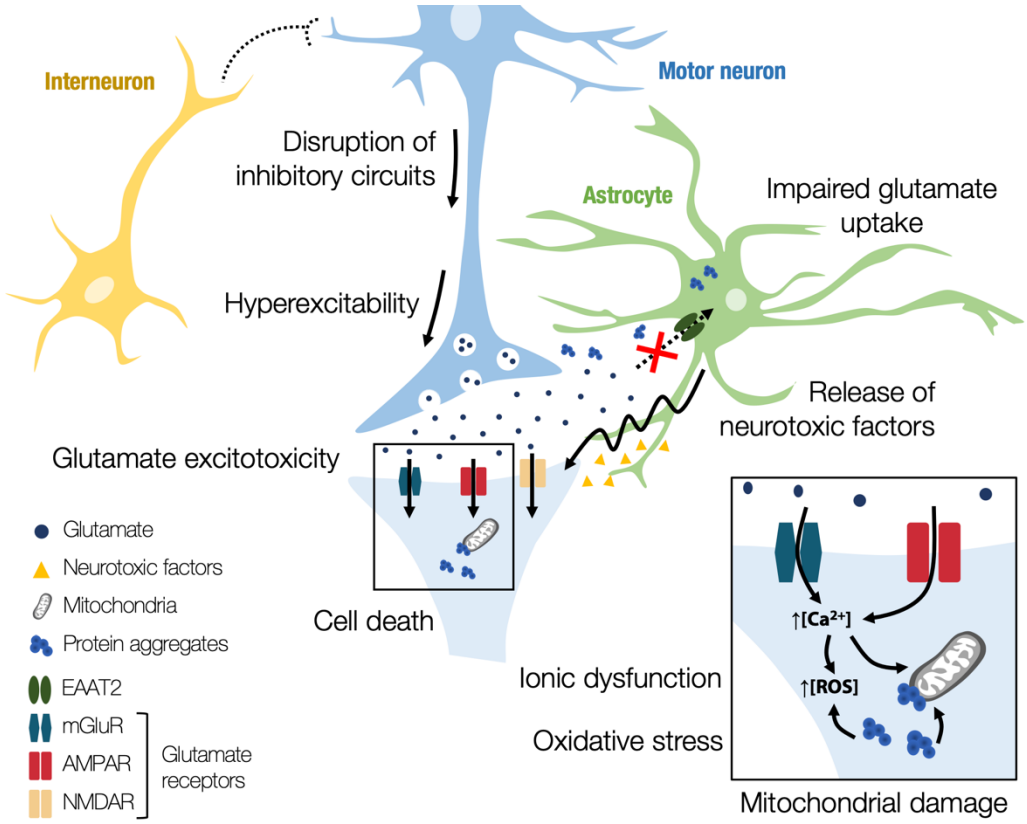


Figure II.3. Schematic representation of the alterations in excitatory neurotransmission in ALS. Different pathophysiological mechanisms have been proposed to explain excitotoxicity in ALS. Interneuron alterations are observed in early disease stages, with a loss of cortical and spinal interneurons, leading to the disruption of inhibitory circuits. Consequently, there is an excitation–inhibition imbalance, increasing subsequent excitability and glutamate release to the synaptic cleft. Glutamate-mediated excitotoxicity may happen through an astrocyte-mediated downregulation of excitatory amino acid transporter 2 (EAAT2), which decreases the glutamate uptake from the synaptic cleft and potentiates the excitotoxic effects. Astrocytes in ALS also release neurotoxic factors that trigger changes to motor neuron glutamate receptors and render them susceptible to excitotoxicity, furthering neurodegeneration. Moreover, the excessive firing and the dysregulated calcium influx through atypical glutamate receptors results in an ionic dysfunction in motor neurons. Excessive entry of calcium into motor neurons results in mitochondrial overload and in the generation of reactive oxygen species, which ultimately causes oxidative stress. The presence of protein aggregates in mitochondria can also lead to alterations in normal cell metabolism, increasing the susceptibility to glutamatergic overstimulation as well as the activation of apoptotic pathways.

Besides glutamate-mediated excitotoxicity, excitotoxicity may arise from an altered regulation by interneurons. Interneurons are one of the main regulators of neuronal signaling and the majority in the cortex is inhibitory, using GABA or glycine as a neurotransmitter. In healthy individuals, a subthreshold stimulus of the motor cortex generally leads to the activation of inhibitory GABAergic interneurons, thus reducing subsequent excitability, in a process called short intracortical inhibition.[II.200] In ALS patients, however, cortical inhibition is impaired, with reduced or complete absence of short intracortical inhibition. Importantly, reduction of short intracortical inhibition was shown to be an adverse prognostic factor in ALS.[II.201] Several post-mortem reports indicate a loss of cortical and spinal interneurons, in addition to motor neuron losses.[II.202] These observations are seen in different mouse models that also exhibit interneuron alterations in early disease stages. The wobbler mouse model displays hippocampal hyperexcitability, together with a reduced number of interneurons.[II.203] Also, in the SOD1^{G93A} mouse model, decreases in calretinin interneurons and subsequent increases in parvalbumin interneurons in motor and somatosensory cortex may be compensatory changes to improve excitation–inhibition balance.[II.204,205] In the spinal cord of the SOD1^{G93A} mice, interneurons degenerate prior to the loss of motor neurons.[II.206] Further studies on a mutant SOD1 zebrafish model revealed that interneurons are the first to exhibit neuronal stress and, once more, that the reduction of inhibitory currents or interneurons preceded any defects in motor neurons.[II.207]

Another known mechanism involved in ALS neurodegeneration is oxidative stress. The major enzyme involved in the prevention of oxidative damage is the Cu/Zn-SOD1 enzyme. Congruently, mutations in the *SOD1* gene – resulting in either a decrease/loss or a dominant gain of function – have been found to contribute to cytotoxicity. In line with this, a study demonstrated that the cerebrospinal fluid, serum, and urine samples of ALS patients had increased levels of free radicals and concomitant oxidative stress.[II.181] Another source of oxidative damage is mitochondrial dysfunction. The existence of alterations in normal cell metabolism due to misfolded mutant SOD1 deposits in mitochondria has been reported in both ALS patients and mouse models. Furthermore, dysfunctions in energy, alterations in the triggering of apoptotic signals, disruptions in mitochondrial transport along axons, and atypical production of ATP and ROS have been also associated with ALS.[II.208–211] Moreover, the presence of mutant SOD1 in mitochondria can lead to an increase of the motor neurons sensitization to glutamatergic (over)-stimulation and therefore to excitotoxicity. In addition, the inflammation and associated microglial activation, both hallmarks of ALS, may contribute to increasing the motor neurons susceptibility to excitotoxicity.

The Old Man and the Alzheimer's disease

Alzheimer's Disease (AD) is an age-dependent neurodegenerative disease, considered the most common form of dementia worldwide.[II.212] AD is firstly manifested by the loss of episodic memory and later loss of executive functions like language, attention, and reasoning.[II.213] AD is commonly characterized by the presence of senile plaques, large extracellular aggregates of fibrillary amyloid-β peptide (Aβ),

originated by the abnormal cleavage of amyloid precursor protein where the sequential cleavage of amyloid precursor protein by β- and γ-secretase produces the neurotoxic Aβ peptide.[II.214,215] The presence of intracellular neurofibrillary tangles of hyperphosphorylated tau protein is also a characteristic of AD.[II.216,217] Many pieces of evidence suggests that $A\beta_{1-42}$ oligomers are the most toxic Aβ species, exerting their pathological actions by disrupting glutamatergic transmission, mainly by acting on NMDAR and mGluR.[II.218] Aβ can also increase glutamate release from both neurons[II.219] and astrocytes,[II.220] resulting in abnormally high extracellular glutamate levels capable of activating eNMDAR and, thus, leading to the activation of pro-death pathways and consequent excitotoxicity. Hence, the harmful effects of Aβ in AD may be mediated by the excessive activation of eNMDAR containing predominantly GluN2B subunits.[II.221] In addition, it has been demonstrated that the presence of Aβ is able to induce a sustained calcium influx via NMDAR,[II.222] which is able to trigger a cascade of events leading to mitochondrial and synaptic dysfunction, excitotoxicity, production of ROS, and neuronal death,[II.223] as depicted in **Figure II.4**.

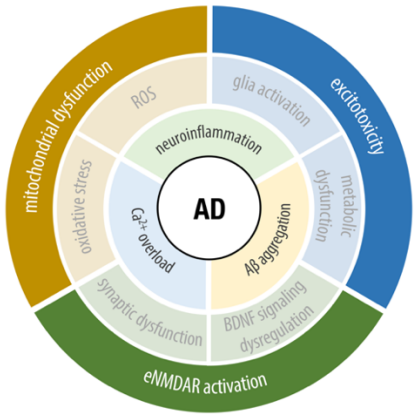


Figure II.4. Underlying cellular mechanisms of Alzheimer's Disease. The upstream key hallmarks of AD ranges from ionic dysfunction to the impairment of several cellular processes, including calcium-signaling dysregulation, abnormal Aβ production and aggregation and neuroinflammation. The crosstalk between the mentioned factors, leads to the pathological phenotype, involving mitochondrial dysfunction, excitotoxicity and eNMDAR activation. As the symptomatic circle closes, the dysfunction of one leads to further activation of the others, altogether contributing to neurodegeneration and cognitive deficits, characteristics of the disease.

An imbalance between sNMDAR and eNMDAR activity was observed in brain samples from AD patients, which can contribute to the Aβ-triggered neurotoxicity observed in this disease. In parallel, it is also known that stimulation of eNMDAR plays a critical role in AD. Recent studies performed in rat acute hippocampal slices under Aβ exposure and in Aβ-injected mice support the idea that enhancement of sNMDAR activity, together with the inhibition of eNMDAR, has protective effects against Aβ-induced neurotoxicity.[II.224] eNMDAR stimulation is also associated with the inactivation of extracellular signal-regulated kinase/mitogen-activated protein kinase signaling,[II.225] which is crucial for memory consolidation and synaptic plasticity, suggesting that eNMDAR activation leads to the impairment of the molecular mechanisms underlying memory and learning processes.[II.226] In the presence of Aβ, the exacerbated calcium influx via eNMDAR is also associated with excessive activation of calpains, which are calcium-dependent proteases involved in multiple cellular functions, including proliferation, differentiation, and modulation of synaptic function.[II.227] The overactivation of calpains in AD is associated with functional changes in several proteins involved in neuronal

transmission, such as BDNF. In fact, previous reports have shown that Aβ impairs BDNF function in a calpain-dependent manner,[II.228] whereas inhibition of eNMDAR is able to prevent Aβ-triggered impairment of BDNF action in long-term synaptic potentiation.[II.229]

Under physiological conditions, mitochondrial calcium signaling stimulates oxidative phosphorylation and ATP synthesis. In AD, as a consequence of the exacerbated calcium levels derived from eNMDAR activation, mitochondria form a non-specific pore in their internal membrane, termed mitochondrial permeability transition pore.[II.230] With the pore opening, protons are able to cross this membrane, leading to the loss of mitochondrial membrane potential and dysregulation of pH gradient. Consequently, this affects ATP synthesis by oxidative phosphorylation, resulting in ionic and metabolic impairment, inevitably leading to cell death. Moreover, this decrease in mitochondrial bioenergetic capacity and consequent impairment of oxidative phosphorylation is associated with free radical production and subsequent oxidative damage. There are evidences of cyclophilin D (CypD), an integral part of the mitochondrial permeability transition pore,[II.230] playing a critical role in Aβ-induced mitochondrial and synaptic injury.[II.231,232] Neuronal CypD is linked to Aβ-mediated ROS production, whereas CypD-deficient neurons appear to be resistant to Aβ-mediated inactivation of protein kinase A/CREB signaling, thus revealing that the absence of CypD is able to prevent Aβ-induced mitochondrial and synaptic dysfunction.[II.233] Additionally, mitochondrial dysfunction in AD includes respiration deficits, increased generation and accumulation of free radicals, and impaired energy metabolism.[II.234–237] Changes in mitochondrial dynamics, including decreased transport, increased fission, and, eventually, loss of mitochondrial function, are also observed in AD.[II.234–237]

Dysfunctional mitochondria are considered the main generator of ROS and consequent oxidative stress in AD, where oxidative stress is able to alter protein kinase A/CREB signaling, a signaling pathway necessary for neuronal survival.[II.238] Indeed, several reports indicate that alterations in brain glucose metabolism in AD patients contribute to synaptic dysfunction and neuronal loss.[II.239,240] ROS, as well as reactive nitrogen species, are associated with the formation of protein carbonyls and 3-nitrotyrosine, which correlates with the level of protein oxidation within a cell. The determination of protein carbonyls levels and tyrosine nitration are considered viable measures of oxidative damage, where tyrosine nitration is one specific form of protein oxidation that is associated with AD,[II.241] which culminates in loss of protein function, cellular dysfunction and, ultimately, cell death.[II.107,242]

In AD, glial cell activation and consequent pro-inflammatory response is associated with an increased expression of NOS, an enzyme responsible for NO production. Indeed, inducible NOS, one of the NOS isoforms, has been found in activated astrocytes and microglia, suggesting a critical role of this enzyme in pathological conditions.[II.243] In addition, inducible NOS has been described as the main culprit behind the NO increase to neurotoxic levels, whereas its inhibition was found to be an useful target for neuronal protection against Aβ-mediated toxicity.[II.243] Furthermore, a recent report found

that, in adult rats injected with $A\beta_{25-35}$, a neurotoxic Aβ fragment, there is an increase in inducible NOS expression and consequent upsurge of NO levels, which was prevented by the administration of a highly selective cannabinoid receptor 1 agonist, ACEA.[II.244] Additionally, animals injected with ACEA and $A\beta_{25-35}$ presented an improvement in learning and memory when compared with animals injected with $A\beta_{25-35}$ alone,[II.244] suggesting the involvement of the cannabinoid receptor 1 in neuroprotective mechanisms in AD.

Growing evidence has identified reactive astrocytes as a key player in glutamate-mediated excitotoxicity, since astrogliosis results in the loss of astrocytic physiological function and consequent impairment of neuronal synaptic transmission. This phenomenon is common in AD, where Aβ induces functional, morphological, and metabolic astrocytic dysfunction.[II.245,246] Specifically, a downregulation of astrocytic glutamate transporters has been shown in both animal models and AD human brain samples, impairing glutamate uptake and causing excitatory overload in the synaptic cleft. Moreover, in astrocytic cell culture, Aβ reduces the expression of GLT-1 through a mechanism that involves the calcineurin/nuclear factor of activated T cells pathway[II.247] and oxidative stress.[II.248] This reduction of GLT-1 expression in astrocytes results in increased glutamate levels at the synapse, which, by acting on eNMDAR, contribute to the progression of AD pathology in the human brain.[II.249] Additionally, a study performed in *postmortem* human samples suggests that the preservation of GLT-1 expression in reactive astrocytes could act as a neuroprotective mechanism against AD neuropathological changes.[II.250]

Astrocytic glutamate uptake is not only essential for synaptic glutamate clearance, but also for the activation of the astrocytic glycolysis cycle. The impaired glutamate uptake will then lead to glycolysis deficiency. In this scenario, neurons not only suffer the consequences of the excessive extracellular glutamate but also of metabolic insufficiency as the astrocytes fail to fulfill the necessary energetic needs. In the hippocampus, glycogen-derived lactate is responsible for memory formation and long-term synaptic potentiation.[II.251] Inhibition of lactate production and neuronal delivery weakens synaptic plasticity and memory formation, by impairment of the Krebs cycle and cell signaling dysregulation.[II.252–254] Indeed, when Long-Evans rats with induced astrocytic metabolic impairment were treated with downstream glycolytic metabolites, such as pyruvate or β-hydroxybutyrate, memory improvement and consolidation were observed.[II.255] This may suggest that astrocytic metabolic impairment is responsible for memory loss and cognitive impairment, even in the premature stages of AD.[II.256]

Metabolic dysfunction is a very early sign of disease onset. Some studies suggest that glucose hypometabolism is a hallmark of AD that can be detected long before any significant Aβ plaques and neurofibrillary tangles.[II.257,258] As the first aggregates occur with concomitant astrocytic dysfunction, signaling for glycolysis starts to drop and leads to the onset of energetic failure, causing metabolic starvation and consequent excitotoxicity. So far, it has been difficult to determine the causal relationship between astrocytic

glutamate uptake dysregulation and metabolic disturbance. Nevertheless, the contribution of the metabolic processes in the pathological excitotoxicity is undeniable.

The role of neuroinflammation in the chemically induced AD animal models has been proven significant for the neurodegenerative profile and assumed to be a crucial factor in disease progression.[II.259–261] In the early stages of AD, activated microglia express both neurodegenerative (M1) and neuroprotective (M2) phenotypes.[II.262] The M2 phenotype exhibits a great capacity for Aβ and tau protein aggregates clearance through phagocytosis. During disease progression, however, the M2 phenotype appears to undergo polarization into an M1 phenotype, resulting in the overproduction of neurotoxic factors. Indeed, in all stages of AD, significant aggregation of M1 microglia has been observed surrounding neurofibrillary tangles.[II.263,264] M1 microglia not only release neurotoxic factors but have also been shown to downregulate or even block neuroprotective mechanisms involved in phagocytosis of Aβ.[II.265] This inhibition is mainly due to the impairment of Aβ receptor complex, complement receptor 3, and insulin-degrading enzyme expression.[II.266] Among neurotoxic factors released by microglia, microglial glutamate release can stimulate excitotoxicity,[II.267] while release of pro-inflammatory cytokines such as interferon γ and TNFα impair the uptake and internal degradation of extracellular glutamate.[II.265,268] In AD, reactive astrocytes are also able to release pro-inflammatory cytokines, such as, TNFα and interleukin 1-β, which, while not directly cytotoxic, have the ability to impair astrocytic glutamate uptake and to enhance NMDAR-induced calcium release, contributing to AD progression. Moreover, it is known that inhibitors of these inflammatory mediators attenuate both synaptic and cognitive deficits in Aβ-treated mice, suggesting that these inflammatory responses mediated by astrocytes have negative effects upon synaptic plasticity mechanisms.[II.269]

Though not often discussed, the cystine-glutamate (x_c^-) antiporter system is essential for cystine homeostasis and considered only a secondary mechanism in the glutamate release and uptake. However, its contribution to pathological states such as glutamate excitotoxicity should not be ignored. The x_c^- antiporter system is highly expressed in microglia and astrocytes. It is a sodium-independent anionic amino acid transporter with high specificity for negative species of cystine and glutamate.[II.270] It is also electroneutral, instead of electrogenic as most common EAAT systems.[II.271] This antiporter is a heterodimer,[II.272] composed of heavy 4F2 chain and a specific light chain, named xCT, linked by a disulfide bridge.[II.273] It uptakes cystine in exchange of releasing glutamate in the molar ratio 1:1.[II.274] Although less discussed, the x_c^- system significantly increases extracellular and, more specifically, synaptic levels of glutamate, releasing up to 60% of all extracellular glutamate in the striatum.[II.275] This antiporter is able to release up to 0.6 μM s^{-1} of glutamate into the extracellular space,[II.276] which is then uptaken by GLT-1.[II.275,277] Depending on the influx and overall capacity to uptake glutamate, this release can either activate or desensitize the NMDAR.[II.276] The cystine-glutamate antiporter was reported to exhibit neuroprotective effects in neurodegenerative diseases, as it is linked to

the production of glutathione and rise of antioxidant cellular capacity.[II.277] This protective effect is observed in AD models, where the x_c^- system uptakes cystine, showing great potential at lowering Aβ-induced toxicity, oxidative stress, and later apoptosis. However, when activated either by oxidative stress, TNF-α, or amyloid precursor protein, this antiporter can release cytotoxic amounts of glutamate.[II.278,279] Not only is this antiporter involved in the release of glutamate, contributing to excitotoxicity, but it has also been shown to block microglial neuroprotective functions in AD. Indeed, activated microglia in both AD patients and in AD mouse models show an increased expression of this antiporter and, specifically, the xCT protein.[II.277] In mice, transgenic depletion of the *Slca11* gene ($xCT^{-/-}$ mice) impaired microglial polarization into the neurotoxic phenotype and reduced up to 70% pathological glutamate release in cultured microglial cells.[II.280] Upon blockade of either NMDAR or the x_c^- system, microglia act in a neuroprotective way when exposed to Aβ and attenuate neuronal death. However, when neurons were cultured with microglia depleted of lipid-associated apolipoprotein E expression, the neuroprotective phenotype was lost,[II.281] implying that the neuroprotective phenotype of microglia in AD is related to apolipoprotein E. In neuron-microglia co-cultures, the activation of the x_c^- system by the Aβ deposits not only exacerbates excitotoxicity, but also lowers the neuronal threshold for glutamate toxicity, allowing non-toxic concentrations of glutamate to exert excitotoxic actions.[II.281] Although very sparse in current literature, the neuroprotective role of the x_c^- system *in vivo* showed similar effects, where the activation of microglial cells by Aβ can cause both phenotypes, the neurotoxic being mostly related to glutamate release and increased neuronal susceptibility to excitotoxicity, and the neuroprotective related to expression of apolipoprotein E and glutathione.[II.281–283]

As stated before, another AD hallmark is hypoglycemia. Removal of glucose in mixed astrocyte-neuron cell cultures leads to aglycemic neuronal injury and death.[II.284] However, the neuronal death observed in glucose deprivation conditions is not connected to energy failure but most likely tied to glutamate accumulation in the synaptic cleft.[II.285] Astrocytes express significant levels of the cystine-glutamate antiporter and are also the main metabolic factories and energy suppliers for neurons. As these processes are tightly linked, the dysfunction of one is likely to mediate the function of the other system, for benefit or for damage. Upon glucose deprivation in cultured astrocytes, xCT protein expression rose in a time dependent matter.[II.284]

In the triple transgenic AD mouse model (3xTg-AD), astrocytic glutamine synthetase expression was found to be decreased in the hippocampus, suggesting a critical role of astrocytes in AD-related disruption of glutamate homeostasis, which may affect the efficiency of glutamatergic transmission, contributing to the cognitive deficits of the disease.[II.286] In addition, it is known that glutamine synthetase activity is sensitive to oxidation and may be impaired by oxidative stress in AD.[II.236,287,288] In the 3xTg-AD mouse model, Aβ near to astrocytes leads to the extrasynaptic release of glutamate and consequent eNMDAR activation,[II.220] which contributes to synaptic dysfunction and neuronal death. Furthermore, there are also evidences that eNMDAR activity is able to trigger the

generation of toxic Aβ,[II.220] which suggests a key role of eNMDAR and astrocytic glutamate release in mediating Aβ neurotoxicity.

As mentioned before, astrocytes are responsible for the supply of D-serine to neurons.[II.78] Indeed, recent evidences reveal that serine racemase, the enzyme responsible for D-serine synthesis is strongly expressed in reactive astrocytes in both human AD samples and AD rat models.[II.289] Moreover, changes in intracellular signaling cascades, consistent with excitotoxicity and decreased neuronal survival were found.[II.289] Hence, these findings support a model where D-serine released from reactive astrocytes could bind to extrasynaptic GluN2B-containing NMDAR, triggering the activation of excitotoxic signaling pathways and consequent neuronal damage and death. It has however been shown that, in AD-like conditions, the selective blockade of eNMDAR together with the administration of a D-serine-like NMDAR co-agonist significantly improved spatial and related forms of learning and memory.[II.224] Moreover, there are evidences that blocking eNMDAR provide neuroprotection against Aβ-triggered deficits, together with the enhancement of sNMDAR activity.[II.224] In conclusion, while it is known that D-serine is mainly a co-agonist of sNMDAR, the role of D-serine as a mediator of neuronal excitotoxicity cannot be excluded.

In line with what was described above, many studies support the active involvement of glial cells, in particular astrocytes, in early stages of AD pathogenesis, where Aβ is able to dysregulate astrocytic calcium signaling both *in vitro* and *in vivo*,[II.290,291] which can result in the excessive release of glutamate and other gliotransmitters, enhancing extrasynaptic glutamatergic signaling and consequent excitotoxicity in AD, as summarized in **Figure II.5**.

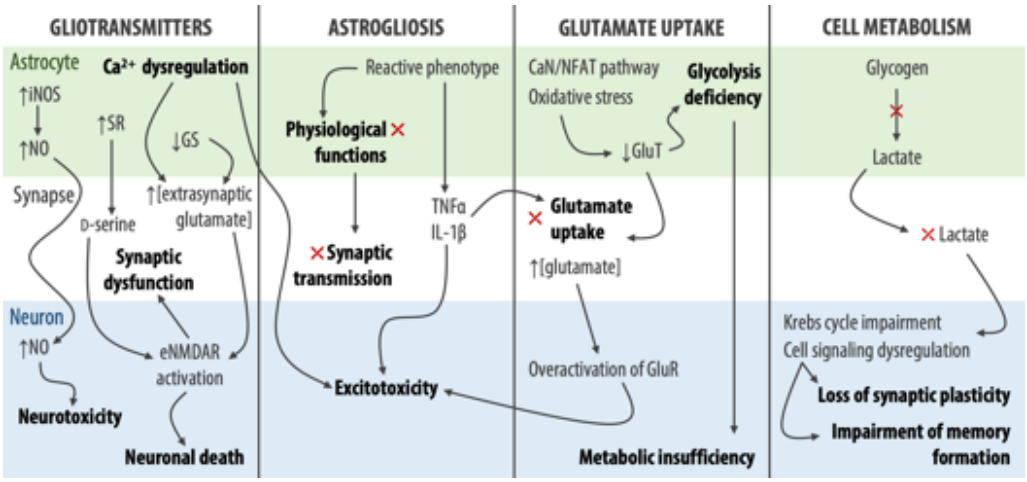


Figure II.5. Aβ-induced astrocytic dysfunctions leading to excitotoxicity and AD pathogenesis. iNOS – inducible nitric oxide synthase; NO – nitric oxide; SR – serine racemase; GS – glutamine synthetase; CaN/NFAT – calcineurin/nuclear factor of activated T cells; GluT – glutamate transporters; GluR – glutamate receptors.

The Phantom of the Brain: epilepsy

Epilepsy is one of the most common neurological disorders, estimated to affect more than 70 million people worldwide.[II.292] Epilepsy can be regarded as a family of disorders which comprise several diseases and conditions, and can be defined by (i) the unprovoked occurrence of at least two seizures more than 24 hours apart, (ii) one unprovoked seizure and further seizure probability of at least 60%, or (iii) diagnosis of an epilepsy syndrome. There are multiple types of seizures, which are characterized in accordance to their onset, physical manifestation, and level of consciousness, differing in the corresponding pathophysiological mechanisms.[II.293] Nevertheless, all epileptic seizures involve persistent changes in synaptic events such as neurotransmitter release, and receptor and transporter activity, and are underpinned by an abnormal excessive or synchronous neuronal firing activity, typically resulting from an imbalance between excitatory and inhibitory processes mediated by the neurotransmitters glutamate and GABA, respectively. Excessive neuronal firing is accompanied by increased extracellular levels of glutamate, leading to excitotoxicity,[II.294] one of the primary sources of neuronal damage in epilepsy. The processes by which excitotoxicity results in neuronal damage and/or death have previously been described and, in this section, we will focus on the underlying pathophysiological mechanisms of different types of epilepsy and how they correlate with excitotoxicity. The main findings discussed here are summarized in **Figure II.6**.

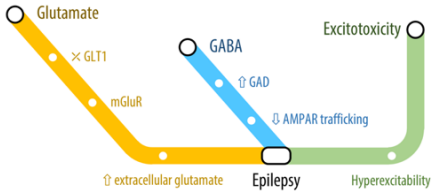


Figure II.6. The connecting railway between Epilepsy and Excitotoxicity: Glutamatergic and GABAergic mechanisms in epilepsy-related excitotoxicity. Schematic representation of alterations in excitatory and inhibitory neurotransmission and their relationship with epilepsy-excitotoxicity dynamic. Both alterations in glutamate- and GABA-mediated neurotransmission have been reported to play a role in epileptogenesis. Increased glutamate levels are a key-feature of temporal lobe epilepsy, resulting from an impairment in GLT-1, which are compensated by increased GAD. The excessive and hypersynchronous neuronal firing promotes network hyperexcitability, culminating in glutamate-mediated excitotoxicity.

Temporal Side Story: temporal lobe epilepsy

Temporal lobe epilepsy (TLE) is the most common form of epilepsy, affecting up to 40 million people worldwide.[II.295,296] TLE is characterized by the occurrence of focal seizures that may impair individuals and is often associated with treatment resistance, where approximately 30% of patients taking antiepileptic drugs present drug resistance that prevents them from living seizure free.[II.65,295,296]

The increase in local excitation and cytotoxicity in the epileptogenic focus of TLE is linked to an increase in extracellular glutamate levels.[II.65,297,298] Changes in glutamate levels have been reported in the hippocampus of epileptic patients before, during, and after seizures, which may occur due to increased glutamate release or its impaired reuptake.[II.295,297,299]

As mentioned before, glutamate uptake is a major determinant of extracellular glutamate levels and evidences show that the alteration of glutamate concentrations in epilepsy may result

from aberrant EAAT expression or function.[II.63,297] Indeed, an increase in EAAT3 expression in the hippocampus of both patients and animal models with TLE has been observed.[II.63] This enhanced expression may lead to the increased glutamate release during seizures by increasing intracellular glutamate, which will be stored in vesicles and synaptically released by the classical calcium-dependent pathway.[II.63,300] Another mechanism by which increased glutamate release may occur is EAAT3 reversal due to alteration of cellular excitability promoted during epileptogenesis.[II.113] However, the increase in EAAT3 expression may be a compensatory mechanism, leading to the improvement of GABAergic inhibitory transmission, as shown in the granular cells of the dentate gyrus of TLE animal models, which had increased glutamate decarboxylase expression and GABA release.[II.63,301]

Additionally, reactive astrocytes with morphological and functional alterations may be important in epileptogenesis since they contribute to the increase of neuronal excitability. In TLE, this astrocyte-induced excitotoxicity occurs by dysregulation of glutamate astrocytic transporters (EAAT1 or GLAST and EAAT2 or GLT-1), which are responsible for maintaining extracellular glutamate homeostasis.[II.295,296] In fact, different studies have shown that there is a reduction in EAAT1 and EAAT2 expression in the sclerotic hippocampus of TLE patients at RNA or protein levels.[II.297,302] Furthermore, modifications in GLT-1 function and expression contribute to TLE hyperexcitability and seizure generation.[II.295,296] Different studies have already shown that knockout animal models for GLT-1 exhibit severe spontaneous seizures that can lead to early postnatal death,[II.295,296,303] and that GLT-1 overexpression may generate pilocarpine-induced epileptogenesis resistant mice.[II.304,305] In fact, in the intrahippocampal kainic acid mouse model of TLE, a down-regulation of hippocampal astrocytic GLT-1 has been reported, coinciding with the increased excitability.[II.296] In addition, there seems to be a temporal regulation of GLT-1 expression during epileptic seizures, with an increase in GLT-1 levels 1–4 days after seizure and a reduction 4–7 days after seizure.[II.295,296] This difference in GLT-1 expression after epileptic seizures can arise from changes in the membrane anchor and trafficking system, since, upon glutamate release, GLT-1 can be trafficked to synaptic and non-synaptic regions to ensure glutamate clearance.[II.306] Different drugs are able to ameliorate epilepsy intensity by targeting GLT-1. Among these drugs, antibiotics such as β-lactam and ceftriaxone show antiepileptic effects and are able increase GLT-1 levels,[II.307,308] and, in a pilocarpine-induced TLE model, a GLT-1 activator was able to promote an increase in GLT-1 expression and reduction of spontaneous seizures frequency by 50%.[II.305,309] However, GLT-1 internalization and degradation are still observed, suggesting that these are the causes of GLT-1 deficiency and the limiting factors for the use of these drugs in the treatment of TLE.[II.310] Thus, some studies have shown that besides increasing GLT-1 expression, it would be necessary to use inhibitors of proteins responsible for its degradation. Studies have been performed with a Hsp90B inhibitor (17AAG), which is one of the proteins that recruit GLT-1 for degradation.[II.311] Not only was this drug able to increase GLT-1 expression, it also maintained

GLT-1 protein levels more effectively than ceftriaxone and exhibited a remarkable seizure suppression effect in the TLE model.[II.305]

Besides glutamate homeostasis, astrocytes can also modulate water flow and potassium homeostasis in the extracellular space.[II.312] Potassium concentration is regulated by astrocytes through its uptake by the sodium/potassium ATPase, sodium/potassium/chloride cotransporters, and input rectifier channels for potassium (Kir 4.1).[II.313–316] Increased potassium concentration in the extracellular space can generate sustained neuronal depolarization and neuronal hyperexcitability,[II.312,315,317] and evidence in the literature suggests an association between the uncontrolled increase of extracellular potassium levels and epilepsy, both in humans and in animal models.[II.318]

In recent years, studies have shown an association between the glial water channel aquaporin-4 (AQP4) and Kir 4.1, forming an astrocytic protein complex responsible for removing potassium from the extracellular space, being an important mechanism in establishing an hyperpolarized neuronal membrane potential which may play an important role in epilepsy.[II.312,319,320] Indeed, reduced expression of Kir 4.1 has been described in the hippocampus of patients with TLE,[II.320] where actrocytes showed deficits in potassium and glutamate uptake similar to those found in Kir 4.1 knockout animal models.[II.315,321,322] Furthermore, AQP4 knockout animals are also more susceptible to seizures and epilepsy[II.312,323] and, in kainate-induced epileptic animal models, a reduction in AQP4 expression was also reported.[II.312,324] Similarly, patients with TLE who have hippocampal sclerosis show a decrease or loss of AQP4 expression, suggesting the involvement of these channels in early epileptogenesis.[II.325–327] Taken together, these findings show that, in addition to the glutamate transporters, the control of potassium homeostasis and water flow is involved in neuronal excitability and TLE, even though further studies are needed to better elucidate their underlying mechanisms for controlling neuronal excitability.

Not only is ion homeostasis, such as sodium and potassium, altered in various forms of epilepsy, but cell metabolism has also been shown to be deeply affected in the epileptic brain. For instance, it is well known that there is a high energy demand during seizures, accompanied by high glucose consumption by neural networks. However, cerebral glucose hypometabolism is a feature of interictal phases in different forms of epilepsy, in regions that encompass but are generally larger than the region of seizure onset.[II.328,329] The exact mechanisms underpinning such alterations are not clear, but mitochondrial dysfunction, linked with deficient glycolysis, remains an plausible hypothesis. Indeed, glutamate is known to promote astrocytic glycolysis,[II.330,331] a process in which glucose is converted into lactate. In epilepsy, where extracellular glutamate levels are increased, this process is most likely heightened when in comparison with control conditions. Thus, this results in a rapid depletion of glucose and quick increase in lactate levels, indicating that, following seizure activity, in which there is a high consumption of glucose, neurons likely rely mostly on astrocyte-derived lactate. The lactate surplus is released into the extracellular space, creating a gradient between astrocytes and neurons.[II.332] Accompanying these alterations, the expression

of astroglial monocarboxylate transporters, which lead to an efflux of monocarboxylates in astrocytes, has been reported to be increased in animal models of TLE,[II.333] further suggesting that this astroglial-neuronal metabolic coupling pathway is affected in epilepsy. This pathway is vital for several brain functions, including for long-term memory formation,[II.334] which might indicate a compromise of several neural functions, as a consequence of disrupted energy homeostasis. Due to the accumulating evidence of metabolic disruption in epilepsy, treatment strategies targetting cell metabolism have been gaining more attention, including the revival of the ketogenic diet.[II.335] Pyruvate has been proposed as a possible treatment for epilepsy on account of being an anaplerotic mitochondrial fuel and because of its protective features, including acting as a potent ROS scavenger and normalizing cytosolic redox state. This molecule also facilitates brain-to-blood glutamate flux, preventing neuronal excitability.[II.336] Finally, since blood glutamate can be converted into 2-ketoglutarate in the presence of pyruvate, mediated by glutamate-pyruvate transaminase,[II.337] treatment with pyruvate can be a protective measure against excitotoxicity.[II.338]

In addition to alterations in cell metabolism in epilepsy, which include the hypermetabolism and hypometabolism during ictal and interictal phases, respectively, intracellular ATP levels are also affected. Indeed, depletion of intracellular ATP has been reported in seizures,[II.339] and considering that the major source of ATP is the mitochondria, the possibility of mitochondrial dysfunction in epilepsy has gained considerable attention. While it is known that mitochondrial dysfunction is involved in seizure-related neuronal death,[II.340] it has also been associated with increased ROS and NO production during seizures,[II.341,342] which is related with the activation of glutamate receptors and depolarization of the mitochondrial membrane. As the major sources of ATP are glycolysis and mitochondrial respiration, alterations in the rate of these processes in epilepsy will also impact ATP production which, reciprocally, influences mitochondrial activity. Mitochondrial dysfunction has been profoundly linked with neuronal damage and death,[II.343] and this organelle is particularly relevant for calcium homeostasis. Mitochondria serve as a key regulator of cytosolic calcium, via the mitochondrial calcium uniporter and, in its turn, the influx of calcium into the mitochondria can activate the respiratory chain as well as promote the production of ATP. During seizure activity, in which neurons are exposed to high concentrations of glutamate, the subsequent activation of NMDAR induces calcium oscillations and a subsequent depolarization of the mitochondrial membrane,[II.344] which can be a trigger for neuronal death.[II.345] In rats where epileptic status was induced by L-allylglycine and bicuculline, the influx of calcium into neurons led to mitochondrial calcium overload, resulting in cell death.[II.346,347] This issue has been overcome in the pilocarpine model of epilepsy by the inhibition of the mitochondrial calcium uniporter system, which decreased neuronal death, suggesting this system plays a role in seizure activity.[II.348] In addition, increasing ATP production by providing a substrate such as pyruvate has also been demonstrated to prevent neuronal death.[II.344] It should be noted that not only mitochondrial alterations can be observed but also in the endoplasmic reticulum, another

intracellular pool of calcium. Indeed, debilitation of endoplasmic reticulum calcium with thapsigargin results in decreased neuronal excitation triggered by bicuculline in cultures[II.349] as well as in slices, where (RS)-3,5-dihydroxyphenylglycine and pilocarpine-induced ictal discharges were shown to be dependent on the endoplamic reticulum calcium pool.[II.350] Although very few studies have focused on the contribution of endoplamic reticulum calcium stores toward seizure activity, it has been demonstrated that depleting intracellular endoplamic reticulum calcium stores can counteract neuronal excitability.[II.349]

Another major consequence of intracellular calcium accumulation and mitochondrial dysregulation is the exacerbated production of ROS, which is an essential mechanism in excitotoxicity-induced neuronal injury.[II.351] Indeed, oxidative stress has been implicated in both immediate and later excitotoxic neuronal damage, and increased ROS production has been reported in the ictal and interictal phases of epilepsy.[II.352] Furthermore, this increase is also known to inhibit mitochondrial complex 1 activity and decrease mitochondrial membrane potential.[II.353,354]

Additionally, calcium influx also leads to NOS activation and consequent NO overproduction, which is known to be increased in the cerebral cortex of rodents and epilepsy patients[II.355,356] and has been suggested to contribute to seizure-induced neuronal death. It has also been demonstrated that NO-mediated activation of the type 1 ryanodine receptor is crucial for seizure-induced neuronal death, and that antagonists of the this receptor have a neuroprotective effect, emerging as suitable candidates for ameliorating conditions following seizures.[II.357] Supporting this fact, it has been described that non-selectively blocking NOS can potentiate rubidium chloride anti-convulsive effects.[II.358] Thus, given the onset of metabolic and mitochondrial alterations as a consequence of excitotoxicity in seizure activity and their relevance for neuronal damage, there has been a growing interest in the use of antioxidants and other neuroprotective drugs that prevent neuronal damage following seizures.[II.359–362]

Final Curtain Call: conclusions

Excitotoxicity relies on multiple pathways that are involved in several regulatory cell mechanisms. Studies reviewed here suggest that, although the glutamatergic system is essential for brain functioning, its dysregulation is implicated as a key step in the pathophysiology of neuronal impairment, which is closely associated with excitotoxicity. This dysregulation may occur at receptor, transporter, or metabolic levels, leading to different types of cellular responses that ultimately culminate in oxidative stress and neuronal death. Several neurodegenerative diseases display excitotoxic events or characteristics, and possibly this chronic mild excitotoxicity contributes, among other factors, to the neuronal death observed in these pathophysiological conditions. Thus, it is urgent to discover new therapeutic targets that counteract the excitotoxicity mediated by glutamatergic system, with a positive impact on neurological diseases such as ALS, AD, and TLE.

the engineering side

Rationale

After researching excitotoxicity, the first steps toward the creation of the astrosomes were deciding what should be their size and which catalysts would be used in the assembly process. Given that excitotoxicity gives rise to various cellular consequences, we chose to focus on the main one: excessive extracellular glutamate levels. The research on glutamate-degrading enzymes led us to conclude that the best theoretical approach would be to tackle not only glutamate, but also the overproduction of ROS and ammonia toxicity, since these are tightly connected to astrocytic dysfunction.

Defining the astrosome size

The shape and size of neurons are highly variable parameters, both between different species and between different brain areas. Indeed, it is known that the diameter of human neuronal somas can range from 5 to 100 μm.[II.363] Importantly, a study conducted in rat pyramidal neurons defined the mean soma diameter as 17 μm at P7, with a significant enlargement to 20 μm at P14.[II.364] After this time point, no more significant differences in neuron soma diameter were observed.

> *The astrosomes have been envisioned as artificial cells. Thus, as a starting point, we concluded that the diameter of the astrosomes should be roughly equal to that of a neuronal soma. So, we chose to create astrosomes with 20 μm in diameter.*

Choosing a catalyst for the astrosome

There are several different enzymes capable of glutamate degradation that could be incorporated into the astrosome. However, when choosing an enzyme for this end, several aspects have to be considered, such as how realistically we can equip the astrosomes with the necessary substrates and co-factors, what effects the end products might have, and how the enzyme can impact endogenous cellular metabolism. With this in mind, the following enzymes were considered as a catalyst: glutamine synthetase, transaminase, glutamate dehydrogenase, and glutamate decarboxylase.

As a first candidate, the astrocyte-specific glutamine synthetase (EC6.3.1.2)[II.365] appears as a strong contender, being a key enzyme in the glutamate/glutamine cycle where it is responsible for the conversion of most synaptically-released glutamate.[II.366] This enzyme plays an important part in nitrogen metabolism by catalyzing the condensation of glutamate and ammonia to form glutamine, via the reaction schematized below:

$$\text{L-glutamate} + \text{ATP} + NH_4^+ \rightarrow \text{Glutamine} + \text{ADP} + P_i$$

It should be noted that, although the ammonium ion binds more strongly to the enzyme than water due to electrostatic forces between the cation and the negatively charged binding site,[II.367] water can compete with the ammonium ion for the binding site, which prevents the conversion of L-glutamate into glutamine.[II.365,368]

Similarly, transaminases (or aminotransferases) are enzymes that catalyze a reaction between an amino acid and an α-keto acid in which the amino group ($-NH_2$) in the first is exchanged by the keto group (=O) in the latter.[II.369] The reaction can be generally schematized as follows:

$$R_1\text{-amino acid} + R_2\text{-α-keto acid} \leftrightarrow R_1\text{-α-keto acid} + R_2\text{-amino acid}$$

It is important to point out that all reactions catalyzed by transaminases are reversible. For glutamate specifically, two main reactions can occur:[II.369]

$$\text{alanine} + \text{α-ketoglutarate} \leftrightarrow \text{pyruvate} + \text{glutamate}$$

$$\text{aspartate} + \text{α-ketoglutarate} \leftrightarrow \text{oxaloacetate} + \text{glutamate}$$

These two enzymes are excluded since their co-factors cannot be introduced in the astrosome. Specifically, glutamine synthetase uses ATP as a co-factor. It would be impossible to obtain a constant exogenous supply of this molecule to ensure astrosome activity – it would likely impact cellular ATP levels. The same arguments can be used for transaminases – given that these enzymes require different amino acids for their reaction, their activity in the astrosome could create an imbalance in endogenous amino acid pathways. Furthermore, transaminases catalyze reversible reactions, which could result in an even higher production of L-glutamate. We are then left with glutamate dehydrogenase and glutamate decarboxylase.

Glutamate dehydrogenases (EC1.4.1.2 / EC1.4.1.3 / EC1.4.1.4) are a family of mitochondrial enzymes that catalyze the reversible conversion of glutamate to α-ketoglutarate. The glutamate dehydrogenase subtypes differ on the necessary co-factors:[II.370]

EC1.4.1.2: L-glutamate + H_2O + NAD^+ ↔ α-ketoglutarate + NH_4^+ + NADH + H^+

EC1.4.1.3: L-glutamate + H_2O + $NAD(P)^+$ ↔ α-ketoglutarate + NH_4^+ + NAD(P)H + H^+

EC1.4.1.4: L-glutamate + H_2O + $NADP^+$ ↔ α-ketoglutarate + NH_4^+ + NADPH + H^+

Importantly, contrarily to transaminases, these reactions occur mainly in the direction of α-ketoglutarate formation, since glutamate dehydrogenase shows very low affinity for ammonia, which implies that the reverse reaction would only occur in the presence of toxic levels of ammonia.[II.366]

Glutamate decarboxylase (EC4.1.1.15), on the other hand, is an enzyme that catalyzes the decarboxylation of L-glutamate, originating GABA and CO_2.[II.371] The reaction catalyzed by this enzyme can be schematized as follows:

L-glutamate + H^+ → GABA + CO_2

This enzyme is essential in the synthesis of GABA in the brain and its low expression has been found in excitotoxicity-related diseases, such as schizophrenia.[II.372]

Looking into the end products of these two enzymes (glutamate dehydrogenase and glutamate decarboxylase), α-ketoglutarate is a glutamate-derived ketone that can be transported across the neuronal cell membrane by both high and low affinity carriers specifically in nerve terminals,[II.373] where this transport mechanism has been shown to be involved in *de novo* synthesis of neuronal L-glutamate.[II.373] Indeed, studies have shown that extracellular α-ketoglutarate, in the presence of an amino acid such as alanine, can be utilized for L-glutamate synthesis in the glutamatergic cerebellar granule cell neurons.[II.374] Alanine, in turn, can be synthesized from pyruvate in astrocytes and released to the extracellular space in large amounts.[II.375] Furthermore, the amino group in alanine can be incorporated into L-glutamate in neurons,[II.375] which corroborates the existence of this cycle. In human CSF, the concentration of α-ketoglutarate has been reported to be c. 20 μM.[II.376] Although this concentration is much lower than that of glutamine (c. 500 μM), another possible source for neuronal glutamate synthesis, it appears to be enough to form new neuronal L-glutamate.[II.373] The conversion from α-ketoglutarate to L-glutamate within the neuron is mainly catalyzed by the enzyme aspartate aminotransferase (both cytosolic and mitochondrial subtypes). Moreover, aspartate aminotransferase levels appear to be outstandingly high in

glutamatergic neurons,[II.377] supporting the role of α-ketoglutarate as a precursor for neuronal L-glutamate.[II.373]

Differently, GABA is the main inhibitory neurotransmitter in the CNS, playing an important role in reducing and modulating neuronal excitability.[II.378] Imbalances in GABA levels and GABAergic neurons have been encountered in excitotoxicity-associated disorders, such as autism spectrum disorders,[II.379] in Huntington's disease with loss of striatal GABAergic neurons,[II.380] and in epileptic seizure activity with changes in GABA metabolism involved in the origin and spreading of this activity[II.381–383] and death of GABAergic neurons in the epileptic neocortex.[II.384,385] Moreover, excitotoxicity promotes a decrease in GABAergic communication in the hippocampus.[II.386] In the brain, GABA is synthetized from glutamate but the contrary reaction can also occur, in which GABA is used as a substrate for glutamate production, through the actions of the enzyme GABA transaminase, as shown below:

α-ketoglutarate + GABA ↔ succinate semialdehyde + L-glutamate

It should however be noted that the reactions catalyzed by the enzymes aspartate aminotransferase and glutaminase are responsible for most of the glutamate production in the brain.[II.387] Even so, evidence suggests the existence of this glutamate/GABA cycle,[II.371] based on the finding that glutamatergic neurons seem to express GABA transporters and GABA transaminase,[II.388] and can uptake GABA released from GABAergic neurons to synthetize glutamate.[II.371]

In physiological L-glutamate synaptic clearance, the astrocytes ensure two important steps for glutamate metabolism: first, they are able to convert glutamate into glutamine, ending its excitatory effect on neighboring neurons; secondly, they are able to supply this newly-formed glutamine back to the pre-synaptic neuron, where it will be converted back to L-glutamate, to safeguard the maintenance of the intracellular L-glutamate pool. So, when choosing an enzyme for the astrosome, we have to guarantee that their actions do not destroy the L-glutamate pool.

Regarding the replenishment of presynaptic glutamate, both α-ketoglutarate and GABA (the end products of glutamate dehydrogenase and glutamate decarboxylase, respectively) can be transported into glutamatergic neurons and have been described as possible sources for de novo neuronal synthesis of glutamate. Importantly, GABA is a central neurotransmitter in the brain, which means that using glutamate

decarboxylase could impact inhibitory transmission, with unforeseen consequences. Thus, glutamate decarboxylase will no longer be considered.

The last detail to consider is the co-products generated by the enzymatic activity. Glutamate dehydrogenase produces ammonia (NH_4^+), which, in excess, has negative effects on the brain. Indeed, NH_4^+ is molecularly comparable to K^+, showing a similar ionic radius and diffusion coefficient, being able to compete with this ion on K^+ transporters and channels, such as the Na^+/K^+ and H^+/K^+ ATPases.[II.389] Also, NH_4^+ has been shown to be transported by the NH_4^+/Cl^- and the $Na^+/K^+/Cl^-$ co-transporters,[II.390,391] as well as by aquaporin-8.[II.392] Due to the facilitated transport of NH_4^+, this ion can have unfavorable effects on the cell pH and membrane potential.[II.390] Particularly, high concentrations of intracellular neuronal NH_4^+ can raise the membrane potential of both neurons and astrocytes, where 2 mM of NH_4Cl was shown to have an effect of +10 mV in neuronal membrane potential.[II.390] It should be noted that the physiological concentration of NH_4^+ in the brain is estimated to be 0.1–0.2 mM.[II.371] Nevertheless, free NH_4^+ is used in the brain to convert α-keto acids into amino acids, which means that the astrosome-generated NH_4^+ can be detoxified. Additionally, in the context of the astrosome, it is possible to place within the particle a secondary enzyme or enzyme mimic, such as platinum nanoparticles. When compared to biological enzymes, these inorganic nanoparticles offer the advantage of enhanced stability and surpass the issue of loss of enzymatic activity. Platinum nanoparticles, as described later on in Chapter VI of this thesis, are known to convert H_2O_2 into water and oxygen[II.393] and NH_4^+ into nitric oxide (NO),[II.394] without needing any co-factors. NO is a free radical and an important signaling molecule in mammals, associated with several physiological and pathological processes.[II.395] Some of its functions have been associated with vasodilation and protection from ischemic damage in several tissues. Particularly in the brain, NO has been shown to be involved in processes of learning and memory, cortical arousal, nociception, and immune response.[II.396] Indeed, NO is considered a physiological messenger in the brain[II.397] and all brain cells are capable of synthetizing this molecule.[II.398,399] Moreover, due to its molecular properties, NO is capable of freely crossing cell membranes and has a half-life of 5 seconds, which is in agreement with its role as a cellular messenger.[II.396] Within neurotransmitters and cellular messengers, NO seems to be an atypical case. This molecule is not taken up into synaptic vesicles,

its release depends solely on the rate of synthesis and is independent of membrane depolarization, and it does not bind to any membrane receptor, crossing the membrane through diffusion and acting directly on intracellular components.[II.396]

NO appears to have two opposing effects in the brain. In low or physiological concentrations, NO has been associated with hippocampal long-term potentiation (LTP) induction, via the NO-cGMP pathway.[II.396] Moreover, NO seems to induce neuronal activity, both through direct neuronal actions[II.400] as well as by dilating blood vessels and thus increasing blood supply to the brain.[II.401] On the other hand, higher concentrations of NO can become neurotoxic[II.402,403] and contribute to cognitive impairment[II.404] and neurodegeneration,[II.405,406] mostly due to accumulation of peroxynitrite, a toxic NO metabolite.[II.396,401] In a pathological situation, however, the outcome of NO actions in the brain is not so clear. One pathologic event that exemplifies this apparently contradictory duality of NO brain effects is cerebral ischemia. The brain is especially vulnerable to blood supply shortage,[II.398] since its metabolism is highly dependent on a continuous supply of glucose and oxygen. So, in an ischemic scenario, compensatory phenomena take over, aiming to maintain cerebral blood circulation.[II.398] NO has been shown to be involved in the control of these physiological responses to brain hypoxia-ischemia,[II.398] with the concentration of NO increasing with higher degrees of ischemic insult.[II.407,408] Furthermore, it has suggested that the control of cerebral blood flow caused by excessive release of NO during and after ischemic episodes can have a beneficial and neuroprotective role.[II.398] However, another consequence of brain ischemia is the exacerbated neuronal glutamate release, which leads to excitotoxicity.[II.409] This will then cause the hyperactivation of NMDA receptors in postsynaptic neurons, leading to an increase in intracellular calcium levels and consequent overactivation of the neuronal subtype of nitric oxide synthase[II.410] which, in turn, can lead to mitochondrial dysfunction and cell death.[II.411] These deleterious effects of NO are thought to occur via energy depletion, lipid and protein peroxidation, protein nitrosylation, and DNA damage[II.406], predominantly due to endogenous production of peroxynitrite.[II.412] This duality means that the effects of nitric oxide in the brain can be either neuroprotective or neurotoxic. So, it is possible that, in an excitotoxic environment, low concentrations of nitric oxide, such as the ones generated by platinum nanoparticles, may contribute to neuroprotection.

In conclusion, glutamate dehydrogenase was chosen as the enzyme to incorporate in the astrosomes, together with platinum nanoparticles. In this manner, we can provide the astrosome with catalysts for glutamate degradation, ROS scavenging, and NH_4^+ detoxification. However, since platinum nanoparticles are theoretically able to counteract excitotoxicity per se, the first astrosome will only contain these nanoparticles. With this first proof of concept concluded, glutamate dehydrogenase will also be included.

chapter II references

II.1 Fairman WA, Amara SG. Functional Diversity of Excitatory Amino Acid Transporters: Ion Channel and Transport Modes. *Am J Physiol* **1999**, *277* (4), F481–486.

II.2 Bano D, Young KW, Guerin CJ, Lefeuvre R, Rothwell NJ, Naldini L, Rizzuto R, Carafoli E, Nicotera P. Cleavage of the Plasma Membrane Na+/Ca2+ Exchanger in Excitotoxicity. *Cell* **2005**, *120* (2), 275–285.

II.3 Connolly NMC, Prehn JHM. The Metabolic Response to Excitotoxicity - Lessons from Single-Cell Imaging. *J Bioenerg Biomembr* **2015**, *47* (1–2), 75–88.

II.4 Lipton SA. NMDA Receptor Activity Regulates Transcription of Antioxidant Pathways. *Nat Neurosci* **2008**, *11* (4), 381–382.

II.5 Vincent P, Mulle C. Kainate Receptors in Epilepsy and Excitotoxicity. *Neuroscience* **2009**, *158* (1), 309–323.

II.6 Prentice H, Modi JP, Wu J-Y. Mechanisms of Neuronal Protection against Excitotoxicity, Endoplasmic Reticulum Stress, and Mitochondrial Dysfunction in Stroke and Neurodegenerative Diseases. *Oxid Med Cell Longev* **2015**, *2015*, 964518.

II.7 Olney JW. Brain Lesions, Obesity, and Other Disturbances in Mice Treated with Monosodium Glutamate. *Science* **1969**, *164* (3880), 719–721.

II.8 Zivin JA, Choi DW. Stroke Therapy. *Sci Am* **1991**, *265* (1), 56–65.

II.9 Albin RL, Greenamyre JT. Alternative Excitotoxic Hypotheses. *Neurology* **1992**, *42* (4), 733–738.

II.10 Castilho RF, Hansson O, Ward MW, Budd SL, Nicholls DG. Mitochondrial Control of Acute Glutamate Excitotoxicity in Cultured Cerebellar Granule Cells. *J Neurosci* **1998**, *18* (24), 10277–10286.

II.11 Ward MW, Rego AC, Frenguelli BG, Nicholls DG. Mitochondrial Membrane Potential and Glutamate Excitotoxicity in Cultured Cerebellar Granule Cells. *J Neurosci* **2000**, *20* (19), 7208–7219.

II.12 Weisová P, Concannon CG, Devocelle M, Prehn JHM, Ward MW. Regulation of Glucose Transporter 3 Surface Expression by the AMP-Activated Protein Kinase Mediates Tolerance to Glutamate Excitation in Neurons. *J Neurosci* **2009**, *29* (9), 2997–3008.

II.13 Ankarcrona M, Dypbukt JM, Bonfoco E, Zhivotovsky B, Orrenius S, Lipton SA, Nicotera P. Glutamate-Induced Neuronal Death: A Succession of Necrosis or Apoptosis Depending on Mitochondrial Function. *Neuron* **1995**, *15* (4), 961–973.

II.14 Bonfoco E, Krainc D, Ankarcrona M, Nicotera P, Lipton SA. Apoptosis and Necrosis: Two Distinct Events Induced, Respectively, by Mild and Intense Insults with N-Methyl-D-Aspartate or Nitric Oxide/Superoxide in Cortical Cell Cultures. *Proc Natl Acad Sci USA* **1995**, *92* (16), 7162–7166.

II.15 D'Orsi B, Bonner H, Tuffy LP, Düssmann H, Woods I, Courtney MJ, Ward MW, Prehn JHM. Calpains Are Downstream Effectors of Bax-Dependent Excitotoxic Apoptosis. *J Neurosci* **2012**, *32* (5), 1847–1858.

II.16 Ward MW, Huber HJ, Weisová P, Düssmann H, Nicholls DG, Prehn JHM. Mitochondrial and Plasma Membrane Potential of Cultured Cerebellar Neurons during Glutamate-Induced Necrosis, Apoptosis, and Tolerance. *J Neurosci* **2007**, *27* (31), 8238–8249.

II.17 Luetjens CM, Bui NT, Sengpiel B, Münstermann G, Poppe M, Krohn AJ, Bauerbach E, Krieglstein J, Prehn JHM. Delayed Mitochondrial Dysfunction in Excitotoxic Neuron Death: Cytochrome c Release and a Secondary Increase in Superoxide Production. *J Neurosci* **2000**, *20* (15), 5715–5723.

II.18 Vesce S, Kirk L, Nicholls DG. Relationships between Superoxide Levels and Delayed Calcium Deregulation in Cultured Cerebellar Granule Cells Exposed Continuously to Glutamate. *J Neurochem* **2004**, *90* (3), 683–693.

II.19 Benjamin AM, Quastel JH. Locations of Amino Acids in Brain Slices from the Rat. Tetrodotoxin-Sensitive Release of Amino Acids. *Biochem J* **1972**, *128* (3), 631–646.

II.20 Hertz L, Dringen R, Schousboe A, Robinson SR. Astrocytes: Glutamate Producers for Neurons. *J Neurosci Res* **1999**, *57* (4), 417–428.

II.21 van den Berg CJ, Garfinkel D. A Simulation Study of Brain Compartments. Metabolism of Glutamate and Related Substances in Mouse Brain. *Biochem J* **1971**, *123* (2), 211–218.

II.22 Watkins JC, Evans RH. Excitatory Amino Acid Transmitters. *Annu Rev Pharmacol Toxicol* **1981**, *21*, 165–204.

II.23 Jonas P. The Time Course of Signaling at Central Glutamatergic Synapses. *Physiology* **2000**, *15* (2), 83–89.

II.24 Clements JD, Lester RA, Tong G, Jahr CE, Westbrook GL. The Time Course of Glutamate in the Synaptic Cleft. *Science* **1992**, *258* (5087), 1498–1501.

II.25 Dzubay JA, Jahr CE. The Concentration of Synaptically Released Glutamate Outside of the Climbing Fiber-Purkinje Cell Synaptic Cleft. *J Neurosci* **1999**, *19* (13), 5265–5274.

II.26 Herman MA, Jahr CE. Extracellular Glutamate Concentration in Hippocampal Slice. *J Neurosci* **2007**, *27* (36), 9736–9741.

II.27 Mark LP, Prost RW, Ulmer JL, Smith MM, Daniels DL, Strottmann JM, Brown WD, Hacein-Bey L. Pictorial Review of Glutamate Excitotoxicity: Fundamental Concepts for Neuroimaging. *Am J Neuroradiol* **2001**, *22* (10), 1813–1824.

II.28 Conn PJ, Pin JP. Pharmacology and Functions of Metabotropic Glutamate Receptors. *Annu Rev Pharmacol Toxicol* **1997**, *37*, 205–237.

II.29 Patneau DK, Mayer ML. Structure-Activity Relationships for Amino Acid Transmitter Candidates Acting at N-Methyl-D-Aspartate and Quisqualate Receptors. *J Neurosci* **1990**, *10* (7), 2385–2399.

II.30 Trussell LO, Fischbach GD. Glutamate Receptor Desensitization and Its Role in Synaptic Transmission. *Neuron* **1989**, *3* (2), 209–218.

II.31 Reiner A, Levitz J. Glutamatergic Signaling in the Central Nervous System: Ionotropic and Metabotropic Receptors in Concert. *Neuron* **2018**, *98* (6), 1080–1098.

II.32 Hansen KB, Yi F, Perszyk RE, Menniti FS, Traynelis SF. NMDA Receptors in the Central Nervous System. In *NMDA Receptors*; Methods in Molecular Biology; Burnashev N, Szepetowski P, Eds.; Humana Press: New York, USA, **2017**; Vol. 1677, pp 1–80.

II.33 Guo H, Camargo LM, Yeboah F, Digan ME, Niu H, Pan Y, Reiling S, Soler-Llavina G, Weihofen WA, Wang H-R, *et al*. A NMDA-Receptor Calcium Influx Assay Sensitive to Stimulation by Glutamate and Glycine/D-Serine. *Sci Rep* **2017**, *7* (1), 11608.

II.34 Erreger K, Dravid SM, Banke TG, Wyllie DJA, Traynelis SF. Subunit-Specific Gating Controls Rat NR1/NR2A and NR1/NR2B NMDA Channel Kinetics and Synaptic Signalling Profiles. *J Physiol* **2005**, *563* (Pt 2), 345–358.

II.35 Kuner T, Schoepfer R. Multiple Structural Elements Determine Subunit Specificity of Mg2+ Block in NMDA Receptor Channels. *J Neurosci* **1996**, *16* (11), 3549–3558.

II.36 Cull-Candy S, Brickley S, Farrant M. NMDA Receptor Subunits: Diversity, Development and Disease. *Curr Opin Neurobiol* **2001**, *11* (3), 327–335.

II.37 Brimecombe JC, Boeckman FA, Aizenman E. Functional Consequences of NR2 Subunit Composition in Single Recombinant N-Methyl-D-Aspartate Receptors. *Proc Natl Acad Sci USA* **1997**, *94* (20), 11019–11024.

II.38 Rönicke R, Mikhaylova M, Rönicke S, Meinhardt J, Schröder UH, Fändrich M, Reiser G, Kreutz MR, Reymann KG. Early Neuronal Dysfunction by Amyloid β Oligomers Depends on Activation of NR2B-Containing NMDA Receptors. *Neurobiol Aging* **2011**, *32* (12), 2219–2228.

II.39 Harris AZ, Pettit DL. Extrasynaptic and Synaptic NMDA Receptors Form Stable and Uniform Pools in Rat Hippocampal Slices. *J Physiol* **2007**, *584* (Pt 2), 509–519.

II.40 Papouin T, Ladépêche L, Ruel J, Sacchi S, Labasque M, Hanini M, Groc L, Pollegioni L, Mothet JP, Oliet SHR. Synaptic and Extrasynaptic NMDA Receptors Are Gated by Different Endogenous Coagonists. *Cell* **2012**, *150* (3), 633–646.

II.41 Hardingham GE, Fukunaga Y, Bading H. Extrasynaptic NMDARs Oppose Synaptic NMDARs by Triggering CREB Shut-off and Cell Death Pathways. *Nat Neurosci* **2002**, *5* (5), 405–414.

II.42 Hardingham GE, Bading H. Synaptic versus Extrasynaptic NMDA Receptor Signalling: Implications for Neurodegenerative Disorders. *Nat Rev Neurosci* **2010**, *11* (10), 682–696.

II.43 Samson AJ, Robertson G, Zagnoni M, Connolly CN. Neuronal Networks Provide Rapid Neuroprotection against Spreading Toxicity. *Sci Rep* **2016**, *6*, 33746.

II.44 Zhou X, Ding Q, Chen Z, Yun H, Wang H. Involvement of the GluN2A and GluN2B Subunits in Synaptic and Extrasynaptic N-Methyl-D-Aspartate Receptor Function and Neuronal Excitotoxicity. *J Biol Chem* **2013**, *288* (33), 24151–24159.

II.45 Dick O, Bading H. Synaptic Activity and Nuclear Calcium Signaling Protect Hippocampal Neurons from Death Signal-Associated Nuclear Translocation of FoxO3a Induced by Extrasynaptic N-Methyl-D-Aspartate Receptors. *J Biol Chem* **2010**, *285* (25), 19354–19361.

II.46 Maneshi MM, Maki B, Gnanasambandam R, Belin S, Popescu GK, Sachs F, Hua SZ. Mechanical Stress Activates NMDA Receptors in the Absence of Agonists. *Sci Rep* **2017**, *7*, 39610.

II.47 Chen PE, Geballe MT, Stansfeld PJ, Johnston AR, Yuan H, Jacob AL, Snyder JP, Traynelis SF, Wyllie DJA. Structural Features of the Glutamate Binding Site in Recombinant NR1/NR2A N-Methyl-D-Aspartate Receptors Determined by Site-Directed Mutagenesis and Molecular Modeling. *Mol Pharmacol* **2005**, *67* (5), 1470–1484.

II.48 Amorini AM, Lazzarino G, Di Pietro V, Signoretti S, Lazzarino G, Belli A, Tavazzi B. Severity of Experimental Traumatic Brain Injury Modulates Changes in Concentrations of Cerebral Free Amino Acids. *J Cell Mol Med* **2017**, *21* (3), 530–542.

II.49 Palmer AM, Marion DW, Botscheller ML, Bowen DM, DeKosky ST. Increased Transmitter Amino Acid Concentration in Human Ventricular CSF after Brain Trauma. *Neuroreport* **1994**, *6* (1), 153–156.

II.50 Choi DW, Viseskul V, Amirthanayagam M, Monyer H. Aspartate Neurotoxicity on Cultured Cortical Neurons. *J Neurosci Res* **1989**, *23* (1), 116–121.

II.51 Parsons MP, Raymond LA. Extrasynaptic NMDA Receptor Involvement in Central Nervous System Disorders. *Neuron* **2014**, *82* (2), 279–293.

II.52 Bading H. Nuclear Calcium Signalling in the Regulation of Brain Function. *Nat Rev Neurosci* **2013**, *14* (9), 593–608.

II.53 Jia M, Njapo SAN, Rastogi V, Hedna VS. Taming Glutamate Excitotoxicity: Strategic Pathway Modulation for Neuroprotection. *CNS Drugs* **2015**, *29* (2), 153–162.

II.54 Zhou X, Chen Z, Yun W, Ren J, Li C, Program N, Lansing E. Revisiting the Function of Extrasynaptic NMDA Receptor in Excitotoxicity. *Neuroscientist* **2015**, *21* (4), 337–344.

II.55 Pál B. Involvement of Extrasynaptic Glutamate in Physiological and Pathophysiological Changes of Neuronal Excitability. *Cell Mol Life Sci* **2018**, *75* (16), 2917–2949.

II.56 Wright A, Vissel B. The Essential Role of AMPA Receptor GluR2 Subunit RNA Editing in the Normal and Diseased Brain. *Front Mol Neurosci* **2012**, *5*, 34.

II.57 Chittajallu R, Vignes M, Dev KK, Barnes JM, Collingridge GL, Henley JM. Regulation of Glutamate Release by Presynaptic Kainate Receptors in the Hippocampus. *Nature* **1996**, *379* (6560), 78–81.

II.58 Castillo PE, Malenka RC, Nicoll RA. Kainate Receptors Mediate a Slow Postsynaptic Current in Hippocampal CA3 Neurons. *Nature* **1997**, *388* (6638), 182–186.

II.59 Ferraguti F, Crepaldi L, Nicoletti F. Metabotropic Glutamate 1 Receptor: Current Concepts and Perspectives. *Pharmacol Rev* **2008**, *60* (4), 536–581.

II.60 Kojima S, Nakamura T, Nidaira T, Nakamura K, Ooashi N, Ito E, Watase K, Tanaka K, Wada K, Kudo Y, Miyakawa H. Optical Detection of Synaptically Induced Glutamate Transport in Hippocampal Slices. *J Neurosci* **1999**, *19* (7), 2580–2588.

II.61 Rothstein JD, Dykes-Hoberg M, Pardo CA, Bristol LA, Jin L, Kuncl RW, Kanai Y, Hediger MA, Wang Y, Schielke JP, Welty DF. Knockout of Glutamate Transporters Reveals a Major Role for Astroglial Transport in Excitotoxicity and Clearance of Glutamate. *Neuron* **1996**, *16* (3), 675–686.

II.62 Danbolt NC. Glutamate Uptake. *Prog Neurobiol* **2001**, *65* (1), 1–105.

II.63 Crino PB, Jin H, Shumate MD, Robinson MB, Coulter DA, Brooks-Kayal AR. Increased Expression of the Neuronal Glutamate Transporter (EAAT3/EAAC1) in Hippocampal and Neocortical Epilepsy. *Epilepsia* **2002**, *43* (3), 211–218.

II.64 Beart PM, O'Shea RD. Transporters for L-Glutamate: An Update on Their Molecular Pharmacology and Pathological Involvement. *Br J Pharmacol* **2007**, *150* (1), 5–17.

II.65 Sarac S, Afzal S, Broholm H, Madsen FF, Ploug T, Laursen H. Excitatory Amino Acid Transporters EAAT-1 and EAAT-2 in Temporal Lobe and Hippocampus in Intractable Temporal Lobe Epilepsy. *APMIS* **2009**, *117* (4), 291–301.

II.66 Gonçalves-Ribeiro J, Pina CC, Sebastião AM, Vaz SH. Glutamate Transporters in Hippocampal LTD/LTP: Not Just Prevention of Excitotoxicity. *Front Cell Neurosci* **2019**, *13*, 357.

II.67 Petr GT, Sun Y, Frederick NM, Zhou Y, Dhamne SC, Hameed MQ, Miranda C, Bedoya EA, Fischer KD, Armsen W, Wang J, Danbolt NC, Rotenberg A, Aoki CJ, Rosenberg PA. Conditional Deletion of the Glutamate Transporter GLT-1 Reveals That Astrocytic GLT-1 Protects against Fatal Epilepsy While Neuronal GLT-1 Contributes Significantly to Glutamate Uptake into Synaptosomes. *J Neurosci* **2015**, *35* (13), 5187–5201.

II.68 Ottersen OP, Zhang N, Walberg F. Metabolic Compartmentation of Glutamate and Glutamine: Morphological Evidence Obtained by Quantitative Immunocytochemistry in Rat Cerebellum. *Neuroscience* **1992**, *46* (3), 519–534.

II.69 Norenberg MD, Martinez-Hernandez A. Fine Structural Localization of Glutamine Synthetase in Astrocytes of Rat Brain. *Brain Res* **1979**, *161* (2), 303–310.

II.70 Allen NJ. Astrocyte Regulation of Synaptic Behavior. *Annu Rev Cell Dev Biol* **2014**, *30* (1), 439–463.

II.71 Rodríguez-Arellano JJ, Parpura V, Zorec R, Verkhratsky A. Astrocytes in Physiological Aging and Alzheimer's Disease. *Neuroscience* **2016**, *323*, 170–182.

II.72 Schousboe A, Westergaard N, Waagepetersen HS, Larsson OM, Bakken IJ, Sonnewald U. Trafficking between Glia and Neurons of TCA Cycle Intermediates and Related Metabolites. *Glia* **1997**, *21* (1), 99–105.

II.73 Magistretti PJ, Allaman I. A Cellular Perspective on Brain Energy Metabolism and Functional Imaging. *Neuron* **2015**, *86* (4), 883–901.

II.74 Stobart JL, Anderson CM. Multifunctional Role of Astrocytes as Gatekeepers of Neuronal Energy Supply. *Front Cell Neurosci* **2013**, *7*, 38.

II.75 Westergaard N, Banke TUE, Wahl P, Sonnewaldt U, Schousboe A. Citrate Modulates the Regulation by Zn2+ of N-Methyl-D-Aspartate Receptor-Mediated Channel Current and Neurotransmitter Release. *Proc Natl Acad Sci USA* **1995**, *92* (8), 3367–3370.

II.76 Wolosker H, Balu DT, Coyle JT. The Rise and Fall of the D-Serine-Mediated Gliotransmission Hypothesis. *Trends Neurosci* **2016**, *39* (11), 712–721.

II.77 Martineau M, Shi T, Puyal J, Knolhoff AM, Dulong J, Gasnier B, Klingauf J, Sweedler JV, Jahn R, Mothet J-P. Storage and Uptake of D-Serine into Astrocytic Synaptic-like Vesicles Specify Gliotransmission. *J Neurosci* **2013**, *33* (8), 3413–3423.

II.78 Henneberger C, Papouin T, Oliet SHR, Rusakov DA. Long-Term Potentiation Depends on Release of D-Serine from Astrocytes. *Nature* **2010**, *463* (7278), 232–236.

II.79 Bergersen LH, Morland C, Ormel L, Rinholm JE, Larsson M, Wold JFH, Røe AT, Stranna A, Santello M, Bouvier D, Ottersen OP, Volterra A, Gundersen V. Immunogold Detection of L-Glutamate and D-Serine in Small Synaptic-like Microvesicles in Adult Hippocampal Astrocytes. *Cereb Cortex* **2012**, *22* (7), 1690–1697.

II.80 Sultan S, Li L, Moss J, Petrelli F, Cassé F, Gebara E, Lopatar J, Pfrieger FW, Bezzi P, Bischofberger J, Toni N. Synaptic Integration of Adult-Born Hippocampal Neurons Is Locally Controlled by Astrocytes. *Neuron* **2015**, *88* (5), 957–972.

II.81 Mehta A, Prabhakar M, Kumar P, Deshmukh R, Sharma PL. Excitotoxicity: Bridge to Various Triggers in Neurodegenerative Disorders. *Eur J Pharmacol* **2013**, *698* (1–3), 6–18.

II.82 Berdichevsky E, Riveros N, Sánchez-Armáss S, Orrego F. Kainate, N-Methylaspartate and Other Excitatory Amino Acids Increase Calcium Influx into Rat Brain Cortex Cells in Vitro. *Neurosci Lett* **1983**, *36* (1), 75–80.

II.83 Choi DW, Koh JY, Peters S. Pharmacology of Glutamate Neurotoxicity in Cortical Cell Culture: Attenuation by NMDA Antagonists. *J Neurosci* **1988**, *8* (1), 185–196.

II.84 Berliocchi L, Bano D, Nicotera P. Ca2+ Signals and Death Programmes in Neurons. *Philos Trans R Soc Lond B Biol Sci* **2005**, *360* (1464), 2255–2258.

II.85 Freeman BA, Crapo JD. Biology of Disease: Free Radicals and Tissue Injury. *Lab Investig* **1982**, *47* (5), 412–426.

II.86 Murphy EJ, Behrmann D, Bates CM, Horrocks LA. Lipid Alterations Following Impact Spinal Cord Injury in the Rat. *Mol Chem Neuropathol* **1994**, *23* (1), 13–26.

II.87 Pazdernik TL, Layton M, Nelson SR, Samson FE. The Osmotic/Calcium Stress Theory of Brain Damage: Are Free Radicals Involved? *Neurochem Res* **1992**, *17* (1), 11–21.

II.88 Akaike A, Kaneko S, Tamura Y, Nakata N, Shiomi H, Ushikubi F, Narumiya S. Prostaglandin E2 Protects Cultured Cortical Neurons against N-Methyl-D-Aspartate Receptor-Mediated Glutamate Cytotoxicity. *Brain Res* **1994**, *663* (2), 237–243.

II.89 Hewett SJ, Uliasz TF, Vidwans AS, Hewett JA. Cyclooxygenase-2 Contributes to N-Methyl-D-Aspartate-Mediated Neuronal Cell Death in Primary Cortical Cell Culture. *J Pharmacol Exp Ther* **2000**, *293* (2), 417–425.

II.90 Hamano H, Nabekura J, Nishikawa M, Ogawa T. Docosahexaenoic Acid Reduces GABA Response in Substantia Nigra Neuron of Rat. *J Neurophysiol* **1996**, *75* (3), 1264–1270.

II.91 Connolly NMC, Düssmann H, Anilkumar U, Huber HJ, Prehn JHM. Single-Cell Imaging of Bioenergetic Responses to Neuronal Excitotoxicity and Oxygen and Glucose Deprivation. *J Neurosci* **2014**, *34* (31), 10192–10205.

II.92 Surin AM, Gorbacheva LR, Savinkova IG, Sharipov RR, Khodorov BI, Pinelis VG. Study on ATP Concentration Changes in Cytosol of Individual Cultured Neurons during Glutamate-Induced Deregulation of Calcium Homeostasis. *Biochemistry* **2014**, *79* (2), 146–157.

II.93 Qiu J, Tan Y-W, Hagenston AM, Martel M-A, Kneisel N, Skehel PA, Wyllie DJA, Bading H, Hardingham GE. Mitochondrial Calcium Uniporter Mcu Controls Excitotoxicity and Is Transcriptionally Repressed by Neuroprotective Nuclear Calcium Signals. *Nat Commun* **2013**, *4* (1), 2034.

II.94 Kushnareva YE, Wiley SE, Ward MW, Andreyev AY, Murphy AN. Excitotoxic Injury to Mitochondria Isolated from Cultured Neurons. *J Biol Chem* **2005**, *280* (32), 28894–28902.

II.95 Nicholls DG, Budd SL. Mitochondria and Neuronal Survival. *Physiol Rev* **2000**, *80* (1), 315–360.

II.96 Caldeira MV, Salazar IL, Curcio M, Canzoniero LMT, Duarte CB. Role of the Ubiquitin-Proteasome System in Brain Ischemia: Friend or Foe? *Prog Neurobiol* **2014**, *112*, 50–69.

II.97 Bondy SC, LeBel CP. The Relationship between Excitotoxicity and Oxidative Stress in the Central Nervous System. *Free Radic Biol Med* **1993**, *14* (6), 633–642.

II.98 Nicholls DG. Mitochondrial Dysfunction and Glutamate Excitotoxicity Studied in Primary Neuronal Cultures. *Curr Mol Med* **2004**, *4* (2), 149–177.

II.99 Floyd RA. Antioxidants, Oxidative Stress, and Degenerative Neurological Disorders. *Proc Soc Exp Biol Med* **1999**, *222* (3), 236–245.

II.100 Lucca G, Comim CM, Valvassori SS, Réus GZ, Vuolo F, Petronilho F, Dal-Pizzol F, Gavioli EC, Quevedo J. Effects of Chronic Mild Stress on the Oxidative Parameters in the Rat Brain. *Neurochem Int* **2009**, *54* (5–6), 358–362.

II.101 Brennan AM, Suh SW, Won SJ, Narasimhan P, Kauppinen TM, Lee H, Edling Y, Chan PH, Swanson RA. NADPH Oxidase Is the Primary Source of Superoxide Induced by NMDA Receptor Activation. *Nat Neurosci* **2009**, *12* (7), 857–863.

II.102 Aarts M, Liu Y, Liu L, Besshoh S, Arundine M, Gurd JW, Wang Y-T, Salter MW, Tymianski M. Treatment of Ischemic Brain Damage by Perturbing NMDA Receptor-PSD-95 Protein Interactions. *Science* **2002**, *298* (5594), 846–850.

II.103 Jones N. Stroke: Disruption of the nNOS–PSD-95 Complex Is Neuroprotective in Models of Cerebral Ischemia. *Nat Rev Neurol* **2011**, *7* (2), 61.

II.104 Zhou L, Li F, Xu H-B, Luo C-X, Wu H-Y, Zhu M-M, Lu W, Ji X, Zhou Q-G, Zhu D-Y. Treatment of Cerebral Ischemia by Disrupting Ischemia-Induced Interaction of nNOS with PSD-95. *Nat Med* **2010**, *16* (12), 1439–1443.

II.105 Díaz A, De Jesús L, Mendieta L, Calvillo M, Espinosa B, Zenteno E, Guevara J, Limón ID. The Amyloid-B25-35 Injection into the CA1 Region of the Neonatal Rat Hippocampus Impairs the Long-Term Memory Because of an Increase of Nitric Oxide. *Neurosci Lett* **2010**, *468* (2), 151–155.

II.106 Butterfield DA, Kanski J. Brain Protein Oxidation in Age-Related Neurodegenerative Disorders That Are Associated with Aggregated Proteins. *Mech Ageing Dev* **2001**, *122* (9), 945–962.

II.107 Butterfield DA, Stadtman ER. Protein Oxidation Processes in Aging Brain. *Adv Cell Aging Gerontol* **1997**, *2*, 161–191.

II.108 Pellegrini-Giampietro DE, Cherici G, Alesiani M, Carla V, Moroni F. Excitatory Amino Acid Release and Free Radical Formation May Cooperate in the Genesis of Ischemia-Induced Neuronal Damage. *J Neurosci* **1990**, *10* (3), 1035–1041.

II.109 Richter C, Kass GE. Oxidative Stress in Mitochondria: Its Relationship to Cellular Ca2+ Homeostasis, Cell Death, Proliferation, and Differentiation. *Chem Biol Interact* **1991**, *77* (1), 1–23.

II.110 Schor NF. Inactivation of Mammalian Brain Glutamine Synthetase by Oxygen Radicals. *Brain Res* **1988**, *456* (1), 17–21.

II.111 Anderson CM, Swanson RA. Astrocyte Glutamate Transport: Review of Properties, Regulation, and Physiological Functions. *Glia* **2000**, *32* (1), 1–14.

II.112 Doyle KP, Simon RP, Stenzel-Poore MP. Mechanisms of Ischemic Brain Damage. *Neuropharmacology* **2008**, *55* (3), 310–318.

II.113 Rossi DJ, Oshima T, Attwell D. Glutamate Release in Severe Brain Ischaemia Is Mainly by Reversed Uptake. *Nature* **2000**, *403* (6767), 316–321.

II.114 Dong X, Wang Y, Qin Z. Molecular Mechanisms of Excitotoxicity and Their Relevance to Pathogenesis of Neurodegenerative Diseases. *Acta Pharmacol Sin* **2009**, *30* (4), 379–387.

II.115 Dutta R, Trapp BD. Mechanisms of Neuronal Dysfunction and Degeneration in Multiple Sclerosis. *Prog Neurobiol* **2011**, *93* (1), 1–12.

II.116 Stavrovskaya IG, Kristal BS. The Powerhouse Takes Control of the Cell: Is the Mitochondrial Permeability Transition a Viable Therapeutic Target against Neuronal Dysfunction and Death? *Free Radic Biol Med* **2005**, *38* (6), 687–697.

II.117 Siemkowicz E, Hansen AJ. Brain Extracellular Ion Composition and EEG Activity Following 10 Minutes Ischemia in Normo- and Hyperglycemic Rats. *Stroke* **1981**, *12* (2), 236–240.

II.118 Mutch WA, Hansen AJ. Extracellular pH Changes during Spreading Depression and Cerebral Ischemia: Mechanisms of Brain pH Regulation. *J Cereb Blood Flow Metab* **1984**, *4* (1), 17–27.

II.119 Li M-H, Leng T-D, Feng X-C, Yang T, Simon RP, Xiong Z-G. Modulation of Acid-Sensing Ion Channel 1a by Intracellular pH and Its Role in Ischemic Stroke. *J Biol Chem* **2016**, *291* (35), 18370–18383.

II.120 Kraig RP, Petito CK, Plum F, Pulsinelli WA. Hydrogen Ions Kill Brain at Concentrations Reached in Ischemia. *J Cereb Blood Flow Metab* **1987**, *7* (4), 379–386.

II.121 Cheng Y-R, Jiang B-Y, Chen C-C. Acid-Sensing Ion Channels: Dual Function Proteins for Chemo-Sensing and Mechano-Sensing. *J Biomed Sci* **2018**, *25* (1), 46.

II.122 Qiang M, Dong X, Zha Z, Zuo X-K, Song X-L, Zhao L, Yuan C, Huang C, Tao P, Hu Q, *et al*. Selection of an ASIC1a-Blocking Combinatorial Antibody That Protects Cells from Ischemic Death. *Proc Natl Acad Sci USA* **2018**, *115* (32), E7469–E7477.

II.123 Waldmann R, Champigny G, Bassilana F, Heurteaux C, Lazdunski M. A Proton-Gated Cation Channel Involved in Acid-Sensing. *Nature* **1997**, *386* (6621), 173–177.

II.124 Simon RP, Niro M, Gwinn R. Brain Acidosis Induced by Hypercarbic Ventilation Attenuates Focal Ischemic Injury. *J Pharmacol Exp Ther* **1993**, *267* (3), 1428–1431.

II.125 Tombaugh GC, Sapolsky RM. Mild Acidosis Protects Hippocampal Neurons from Injury Induced by Oxygen and Glucose Deprivation. *Brain Res* **1990**, *506* (2), 343–345.

II.126 Tang CM, Dichter M, Morad M. Modulation of the N-Methyl-D-Aspartate Channel by Extracellular H+. *Proc Natl Acad Sci USA* **1990**, *87* (16), 6445–6449.

II.127 Zhang S, Sun P, Sun Z, Zhang J, Zhou J, Gu Y. Cortical GABAergic Neurons Are More Severely Impaired by Alkalosis than Acidosis. *BMC Neurol* **2013**, *13*, 192.

II.128 Sapolsky RM. Cellular Defenses against Excitotoxic Insults. *J Neurochem* **2001**, *76* (6), 1601–1611.

II.129 Sah P. Ca(2+)-Activated K+ Currents in Neurones: Types, Physiological Roles and Modulation. *Trends Neurosci* **1996**, *19* (4), 150–154.

II.130 Blatz AL, Magleby KL. Calcium-Activated Potassium Channels. *Trends Neurosci* **1987**, *10* (11), 463–467.

II.131 Honrath B, Krabbendam IE, Culmsee C, Dolga AM. Small Conductance Ca2+-Activated K+ Channels in the Plasma Membrane, Mitochondria and the ER: Pharmacology and Implications in Neuronal Diseases. *Neurochem Int* **2017**, *109*, 13–23.

II.132 Lancaster B, Adams PR. Calcium-Dependent Current Generating the Afterhyperpolarization of Hippocampal Neurons. *J Neurophysiol* **1986**, *55* (6), 1268–1282.

II.133 Madison DV, Nicoll RA. Control of the Repetitive Discharge of Rat CA1 Pyramidal Neurones in Vitro. *J Physiol* **1984**, *354*, 319–331.

II.134 Politi DM, Rogawski MA. Glyburide-Sensitive K+ Channels in Cultured Rat Hippocampal Neurons: Activation by Cromakalim and Energy-Depleting Conditions. *Mol Pharmacol* **1991**, *40* (2), 308–315.

II.135 Riepe M, Hori N, Ludolph AC, Carpenter DO, Spencer PS, Allen CN. Inhibition of Energy Metabolism by 3-Nitropropionic Acid Activates ATP-Sensitive Potassium Channels. *Brain Res* **1992**, *586* (1), 61–66.

II.136 Trapp S, Ballanyi K. KATP Channel Mediation of Anoxia-Induced Outward Current in Rat Dorsal Vagal Neurons in Vitro. *J Physiol* **1995**, *487* (1), 37–50.

II.137 Bancila V, Nikonenko I, Dunant Y, Bloc A. Zinc Inhibits Glutamate Release via Activation of Pre-Synaptic KATP Channels and Reduces Ischaemic Damage in Rat Hippocampus. *J Neurochem* **2004**, *90* (5), 1243–1250.

II.138 Marcaida G, Kosenko E, Miñana MD, Grisolía S, Felipo V. Glutamate Induces a Calcineurin-Mediated Dephosphorylation of Na+,K(+)-ATPase That Results in Its Activation in Cerebellar Neurons in Culture. *J Neurochem* **1996**, *66* (1), 99–104.

II.139 Bradford HF. Glutamate, GABA and Epilepsy. *Prog Neurobiol* **1995**, *47* (6), 477–511.

II.140 Magnusson KR, Koerner JF, Larson AA, Smullin DH, Skilling SR, Beitz AJ. NMDA-, Kainate- and Quisqualate-Stimulated Release of Taurine from Electrophysiologically Monitored Rat Hippocampal Slices. *Brain Res* **1991**, *549* (1), 1–8.

II.141 Torp R, Andiné P, Hagberg H, Karagülle T, Blackstad TW, Ottersen OP. Cellular and Subcellular Redistribution of Glutamate-, Glutamine- and Taurine-like Immunoreactivities during Forebrain Ischemia: A Semiquantitative Electron Microscopic Study in Rat Hippocampus. *Neuroscience* **1991**, *41* (2), 433–447.

II.142 Huxtable RJ. Physiological Actions of Taurine. *Physiol Rev* **1992**, *72* (1), 101–163.

II.143 O'Byrne MB, Tipton KF. Taurine-Induced Attenuation of MPP+ Neurotoxicity In Vitro. *J Neurochem* **2000**, *74* (5), 2087–2093.

II.144 Winkler P, Luhmann HJ, Kilb W. Taurine Potentiates the Anticonvulsive Effect of the GABAA Agonist Muscimol and Pentobarbital in the Immature Mouse Hippocampus. *Epilepsia* **2019**, *60* (3), 464–474.

II.145 Bi X, Chen J, Baudry M. Calpain-Mediated Proteolysis of GluR1 Subunits in Organotypic Hippocampal Cultures Following Kainic Acid Treatment. *Brain Res* **1998**, *781* (1–2), 355–357.

II.146 Bi X, Rong Y, Chen J, Dang S, Wang Z, Baudry M. Calpain-Mediated Regulation of NMDA Receptor Structure and Function. *Brain Res* **1998**, *790* (1–2), 245–253.

II.147 Bi X, Chang V, Molnar E, McIlhinney RAJ, Baudry M. The C-Terminal Domain of Glutamate Receptor Subunit 1 Is a Target for Calpain-Mediated Proteolysis. *Neuroscience* **1996**, *73* (4), 903–906.

II.148 Ehlers MD, Zhang S, Bernhardt JP, Huganir RL. Inactivation of NMDA Receptors by Direct Interaction of Calmodulin with the NR1 Subunit. *Cell* **1996**, *84* (5), 745–755.

II.149 Lieberman DN, Mody I. Regulation of NMDA Channel Function by Endogenous Ca(2+)-Dependent Phosphatase. *Nature* **1994**, *369* (6477), 235–239.

II.150 Vyklický L. Calcium-Mediated Modulation of N-Methyl-D-Aspartate (NMDA) Responses in Cultured Rat Hippocampal Neurones. *J Physiol* **1993**, *470*, 575–600.

II.151 Cunha RA. Neuroprotection by Adenosine in the Brain: From A1 Receptor Activation to A2A Receptor Blockade. *Purinergic Signal* **2005**, *1* (2), 111–134.

II.152 Phillis JW, Wu PH. The Role of Adenosine and Its Nucleotides in Central Synaptic Transmission. *Prog Neurobiol* **1981**, *16* (3), 187–239.

II.153 Lipton SA, Choi YB, Pan ZH, Lei SZ, Chen HS, Sucher NJ, Loscalzo J, Singel DJ, Stamler JS. A Redox-Based Mechanism for the Neuroprotective and Neurodestructive Effects of Nitric Oxide and Related Nitroso-Compounds. *Nature* **1993**, *364* (6438), 626–632.

II.154 Yenari MA, Giffard RG, Sapolsky RM, Steinberg GK. The Neuroprotective Potential of Heat Shock Protein 70 (HSP70). *Mol Med Today* **1999**, *5* (12), 525–531.

II.155 Fukuhara T, Nishio S, Ono Y, Kawauchi M, Asari S, Ohmoto T. Induction of Cu,Zn-Superoxide Dismutase after Cortical Contusion Injury during Hypothermia. *Brain Res* **1994**, *657* (1–2), 333–336.

II.156 Matsuyama T, Shimizu S, Nakamura H, Michishita H, Tagaya M, Sugita M. Effects of Recombinant Superoxide Dismutase on Manganese Superoxide Dismutase Gene Expression in Gerbil Hippocampus after Ischemia. *Stroke* **1994**, *25* (7), 1417–1424.

II.157 Ohtsuki T, Matsumoto M, Suzuki K, Taniguchi N, Kamada T. Effect of Transient Forebrain Ischemia on Superoxide Dismutases in Gerbil Hippocampus. *Brain Res* **1993**, *620* (2), 305–309.

II.158 Goss JR, Taffe KM, Kochanek PM, DeKosky ST. The Antioxidant Enzymes Glutathione Peroxidase and Catalase Increase Following Traumatic Brain Injury in the Rat. *Exp Neurol* **1997**, *146* (1), 291–294.

II.159 Depp C, Bas-Orth C, Schroeder L, Hellwig A, Bading H. Synaptic Activity Protects Neurons Against Calcium-Mediated Oxidation and Contraction of Mitochondria during Excitotoxicity. *Antioxid Redox Signal* **2018**, *29* (12), 1109–1124.

II.160 Witgert M, Salamone AR, Strutt AM, Jawaid A, Massman PJ, Bradshaw M, Mosnik D, Appel SH, Schulz PE. Frontal-Lobe Mediated Behavioral Dysfunction in Amyotrophic Lateral Sclerosis. *Eur J Neurol* **2010**, *17* (1), 103–110.

II.161 Ferrari R, Kapogiannis D, Huey ED, Momeni P. FTD and ALS: A Tale of Two Diseases. *Curr Alzheimer Res* **2011**, *8* (3), 273–294.

II.162 Chen S, Sayana P, Zhang X, Le W. Genetics of Amyotrophic Lateral Sclerosis: An Update. *Mol Neurodegener* **2013**, *8*, 28.

II.163 Ajroud-Driss S, Siddique T. Sporadic and Hereditary Amyotrophic Lateral Sclerosis (ALS). *Biochim Biophys Acta* **2015**, *1852* (4), 679–684.

II.164 Kiernan MC, Vucic S, Cheah BC, Turner MR, Eisen A, Hardiman O, Burrell JR, Zoing MC. Amyotrophic Lateral Sclerosis. *Lancet* **2011**, *377* (9769), 942–955.

II.165 Bae JS, Simon NG, Menon P, Vucic S, Kiernan MC. The Puzzling Case of Hyperexcitability in Amyotrophic Lateral Sclerosis. *J Clin Neurol* **2013**, *9* (2), 65–74.

II.166 Vucic S, Kiernan MC. Utility of Transcranial Magnetic Stimulation in Delineating Amyotrophic Lateral Sclerosis Pathophysiology. *Handb Clin Neurol* **2013**, *116*, 561–575.

II.167 Vucic S, Kiernan MC. Axonal Excitability Properties in Amyotrophic Lateral Sclerosis. *Clin Neurophysiol* **2006**, *117* (7), 1458–1466.

II.168 Fogarty MJ, Mu EWH, Noakes PG, Lavidis NA, Bellingham MC. Marked Changes in Dendritic Structure and Spine Density Precede Significant Neuronal Death in Vulnerable Cortical Pyramidal Neuron Populations in the SOD1(G93A) Mouse Model of Amyotrophic Lateral Sclerosis. *Acta Neuropathol Commun* **2016**, *4* (1), 77.

II.169 Saba L, Viscomi MT, Caioli S, Pignataro A, Bisicchia E, Pieri M, Molinari M, Ammassari-Teule M, Zona C. Altered Functionality, Morphology, and Vesicular Glutamate Transporter Expression of Cortical Motor Neurons from a Presymptomatic Mouse Model of Amyotrophic Lateral Sclerosis. *Cereb Cortex* **2016**, *26* (4), 1512–1528.

II.170 Bendotti C, Carrì MT. Lessons from Models of SOD1-Linked Familial ALS. *Trends Mol Med* **2004**, *10* (8), 393–400.

II.171 Appel SH, Zhao W, Beers DR, Henkel JS. The Microglial-Motoneuron Dialogue in ALS. *Acta Myol* **2011**, *30* (1), 4–8.

II.172 Zhao W, Beers DR, Appel SH. Immune-Mediated Mechanisms in the Pathoprogression of Amyotrophic Lateral Sclerosis. *J Neuroimmune Pharmacol* **2013**, *8* (4), 888–899.

II.173 Brites D, Vaz AR. Microglia Centered Pathogenesis in ALS: Insights in Cell Interconnectivity. *Front Cell Neurosci* **2014**, *8*, 117.

II.174 Pinto S, Cunha C, Barbosa M, Vaz AR, Brites D. Exosomes from NSC-34 Cells Transfected with HSOD1-G93A Are Enriched in miR-124 and Drive Alterations in Microglia Phenotype. *Front Neurosci* **2017**, *11*, 273.

II.175 Gravel M, Béland L-C, Soucy G, Abdelhamid E, Rahimian R, Gravel C, Kriz J. IL-10 Controls Early Microglial Phenotypes and Disease Onset in ALS Caused by Misfolded Superoxide Dismutase 1. *J Neurosci* **2016**, *36* (3), 1031–1048.

II.176 Nikodemova M, Small AL, Smith SMC, Mitchell GS, Watters JJ. Spinal but Not Cortical Microglia Acquire an Atypical Phenotype with High VEGF, Galectin-3 and Osteopontin, and Blunted Inflammatory Responses in ALS Rats. *Neurobiol Dis* **2014**, *69*, 43–53.

II.177 Howland JG, Taepavarapruk P, Phillips AG. Glutamate Receptor-Dependent Modulation of Dopamine Efflux in the Nucleus Accumbens by Basolateral, but Not Central, Nucleus of the Amygdala in Rats. *J Neurosci* **2002**, *22* (3), 1137–1145.

II.178 Tong J, Huang C, Bi F, Wu Q, Huang B, Liu X, Li F, Zhou H, Xia X-G. Expression of ALS-Linked TDP-43 Mutant in Astrocytes Causes Non-Cell-Autonomous Motor Neuron Death in Rats. *EMBO J* **2013**, *32* (13), 1917–1926.

II.179 Sasaki S, Komori T, Iwata M. Excitatory Amino Acid Transporter 1 and 2 Immunoreactivity in the Spinal Cord in Amyotrophic Lateral Sclerosis. *Acta Neuropathol* **2000**, *100* (2), 138–144.

II.180 Lin CL, Bristol LA, Jin L, Dykes-Hoberg M, Crawford T, Clawson L, Rothstein JD. Aberrant RNA Processing in a Neurodegenerative Disease: The Cause for Absent EAAT2, a Glutamate Transporter, in Amyotrophic Lateral Sclerosis. *Neuron* **1998**, *20* (3), 589–602.

II.181 Zarei S, Carr K, Reiley L, Diaz K, Guerra O, Altamirano P, Pagani W, Lodin D, Orozco G, Chinea A. A Comprehensive Review of Amyotrophic Lateral Sclerosis. *Surg Neurol Int* **2015**, *6* (1), 171.

II.182 Komine O, Yamanaka K. Neuroinflammation in Motor Neuron Disease. *Nagoya J Med Sci* **2015**, *77* (4), 537–549.

II.183 Cunha C, Santos C, Gomes C, Fernandes A, Correia AM, Sebastião AM, Vaz AR, Brites D. Downregulated Glia Interplay and Increased miRNA-155 as Promising Markers to Track ALS at an Early Stage. *Mol Neurobiol* **2018**, *55* (5), 4207–4224.

II.184 Gomes C, Cunha C, Nascimento F, Ribeiro JA, Vaz AR, Brites D. Cortical Neurotoxic Astrocytes with Early ALS Pathology and miR-146a Deficit Replicate Gliosis Markers of Symptomatic SOD1G93A Mouse Model. *Mol Neurobiol* **2019**, *56* (3), 2137–2158.

II.185 Bernard-Marissal N, Moumen A, Sunyach C, Pellegrino C, Dudley K, Henderson CE, Raoul C, Pettmann B. Reduced Calreticulin Levels Link Endoplasmic Reticulum Stress and Fas-Triggered Cell Death in Motoneurons Vulnerable to ALS. *J Neurosci* **2012**, *32* (14), 4901–4912.

II.186 Mattson MP. Excitation BolsTORs Motor Neurons in ALS Mice. *Neuron* **2013**, *80* (1), 1–3.

II.187 Guo H, Lai L, Butchbach MER, Stockinger MP, Shan X, Bishop GA, Lin CG. Increased Expression of the Glial Glutamate Transporter EAAT2 Modulates Excitotoxicity and Delays the Onset but Not the Outcome of ALS in Mice. *Hum Mol Genet* **2003**, *12* (19), 2519–2532.

II.188 Li K, Hala TJ, Seetharam S, Poulsen DJ, Wright MC, Lepore AC. GLT1 Overexpression in SOD1(G93A) Mouse Cervical Spinal Cord Does Not Preserve Diaphragm Function or Extend Disease. *Neurobiol Dis* **2015**, *78*, 12–23.

II.189 Boycott HE, Wilkinson JA, Boyle JP, Pearson HA, Peers C. Differential Involvement of TNFα in Hypoxic Suppression of Astrocyte Glutamate Transporters. *Glia* **2008**, *56* (9), 998–1004.

II.190 Jiang LL, Zhu B, Zhao Y, Li X, Liu T, Pina-Crespo J, Zhou L, Xu W, Rodriguez MJ, Yu H, *et al*. Membralin Deficiency Dysregulates Astrocytic Glutamate Homeostasis Leading to ALS-like Impairment. *J Clin Invest* **2019**, *129* (8), 3103–3120.

II.191 Giribaldi F, Milanese M, Bonifacino T, Anna Rossi PI, Di Prisco S, Pittaluga A, Tacchetti C, Puliti A, Usai C, Bonanno G. Group I Metabotropic Glutamate Autoreceptors Induce Abnormal Glutamate Exocytosis in a Mouse Model of Amyotrophic Lateral Sclerosis. *Neuropharmacology* **2013**, *66*, 253–263.

II.192 Raiteri L, Paolucci E, Prisco S, Raiteri M, Bonanno G. Activation of a Glycine Transporter on Spinal Cord Neurons Causes Enhanced Glutamate Release in a Mouse Model of Amyotrophic Lateral Sclerosis. *Br J Pharmacol* **2003**, *138* (6), 1021–1025.

II.193 Milanese M, Bonifacino T, Fedele E, Rebosio C, Cattaneo L, Benfenati F, Usai C, Bonanno G. Exocytosis Regulates Trafficking of GABA and Glycine Heterotransporters in Spinal Cord Glutamatergic Synapses: A Mechanism for the Excessive Heterotransporter-Induced Release of Glutamate in Experimental Amyotrophic Lateral Sclerosis. *Neurobiol Dis* **2015**, *74*, 314–324.

II.194 Bonifacino T, Rebosio C, Provenzano F, Torazza C, Balbi M, Milanese M, Raiteri L, Usai C, Fedele E, Bonanno G. Enhanced Function and Overexpression of Metabotropic Glutamate Receptors 1 and 5 in the Spinal Cord of the SOD1G93A Mouse Model of Amyotrophic Lateral Sclerosis during Disease Progression. *Int J Mol Sci* **2019**, *20* (18), E4552.

II.195 Rossi D, Brambilla L, Valori CF, Roncoroni C, Crugnola A, Yokota T, Bredesen DE, Volterra A. Focal Degeneration of Astrocytes in Amyotrophic Lateral Sclerosis. *Cell Death Differ* **2008**, *15* (11), 1691–1700.

II.196 Van Damme P, Braeken D, Callewaert G, Robberecht W, Van Den Bosch L. GluR2 Deficiency Accelerates Motor Neuron Degeneration in a Mouse Model of Amyotrophic Lateral Sclerosis. *J Neuropathol Exp Neurol* **2005**, *64* (7), 605–612.

II.197 Van Damme P, Bogaert E, Dewil M, Hersmus N, Kiraly D, Scheveneels W, Bockx I, Braeken D, Verpoorten N, Verhoeven K, *et al*. Astrocytes Regulate GluR2 Expression in Motor Neurons and Their Vulnerability to Excitotoxicity. *Proc Natl Acad Sci USA* **2007**, *104* (37), 14825–14830.

II.198 Kia A, McAvoy K, Krishnamurthy K, Trotti D, Pasinelli P. Astrocytes Expressing ALS-Linked Mutant FUS Induce Motor Neuron Death through Release of Tumor Necrosis Factor-Alpha. *Glia* **2018**, *66* (5), 1016–1033.

II.199 Selvaraj BT, Livesey MR, Zhao C, Gregory JM, James OT, Cleary EM, Chouhan AK, Gane AB, Perkins EM, Dando O, *et al*. C9ORF72 Repeat Expansion Causes Vulnerability of Motor Neurons to Ca2+-Permeable AMPA Receptor-Mediated Excitotoxicity. *Nat Commun* **2018**, *9* (1), 347.

II.200 Wagle-Shukla A, Ni Z, Gunraj CA, Bahl N, Chen R. Effects of Short Interval Intracortical Inhibition and Intracortical Facilitation on Short Interval Intracortical Facilitation in Human Primary Motor Cortex. *J Physiol* **2009**, *587* (23), 5665–5678.

II.201 Shibuya K, Park SB, Geevasinga N, Menon P, Howells J, Simon NG, Huynh W, Noto Y-I, Götz J, Kril JJ, *et al*. Motor Cortical Function Determines Prognosis in Sporadic ALS. *Neurology* **2016**, *87* (5), 513–520.

II.202 Stephens B, Guiloff RJ, Navarrete R, Newman P, Nikhar N, Lewis P. Widespread Loss of Neuronal Populations in the Spinal Ventral Horn in Sporadic Motor Neuron Disease. A Morphometric Study. *J Neurol Sci* **2006**, *244* (1–2), 41–58.

II.203 Thielsen KD, Moser JM, Schmitt-John T, Jensen MS, Jensen K, Holm MM. The Wobbler Mouse Model of Amyotrophic Lateral Sclerosis (ALS) Displays Hippocampal Hyperexcitability, and Reduced Number of Interneurons, but No Presynaptic Vesicle Release Impairments. *PloS One* **2013**, *8* (12), e82767.

II.204 Chung YH, Joo KM, Nam RH, Cho MH, Kim DJ, Lee WB, Cha CI. Decreased Expression of Calretinin in the Cerebral Cortex and Hippocampus of SOD1G93A Transgenic Mice. *Brain Res* **2005**, *1035* (1), 105–109.

II.205 Minciacchi D, Kassa RM, Del Tongo C, Mariotti R, Bentivoglio M. Voronoi-Based Spatial Analysis Reveals Selective Interneuron Changes in the Cortex of FALS Mice. *Exp Neurol* **2009**, *215* (1), 77–86.

II.206 Martin LJ, Liu Z, Chen K, Price AC, Pan Y, Swaby JA, Golden WC. Motor Neuron Degeneration in Amyotrophic Lateral Sclerosis Mutant Superoxide Dismutase-1 Transgenic Mice: Mechanisms of Mitochondriopathy and Cell Death. *J Comp Neurol* **2007**, *500* (1), 20–46.

II.207 McGown A, McDearmid JR, Panagiotaki N, Tong H, Al Mashhadi S, Redhead N, Lyon AN, Beattie CE, Shaw PJ, Ramesh TM. Early Interneuron Dysfunction in ALS: Insights from a Mutant SOD1 Zebrafish Model. *Ann Neurol* **2013**, *73* (2), 246–258.

II.208 Damiano M, Starkov AA, Petri S, Kipiani K, Kiaei M, Mattiazzi M, Flint Beal M, Manfredi G. Neural Mitochondrial Ca2+ Capacity Impairment Precedes the Onset of Motor Symptoms in G93A Cu/Zn-Superoxide Dismutase Mutant Mice. *J Neurochem* **2006**, *96* (5), 1349–1361.

II.209 Mattiazzi M, D'Aurelio M, Gajewski CD, Martushova K, Kiaei M, Beal MF, Manfredi G. Mutated Human SOD1 Causes Dysfunction of Oxidative Phosphorylation in Mitochondria of Transgenic Mice. *J Biol Chem* **2002**, *277* (33), 29626–29633.

II.210 Menzies FM, Ince PG, Shaw PJ. Mitochondrial Involvement in Amyotrophic Lateral Sclerosis. *Neurochem Int* **2002**, *40* (6), 543–551.

II.211 Pasinelli P, Houseweart MK, Brown RH, Cleveland DW. Caspase-1 and -3 Are Sequentially Activated in Motor Neuron Death in Cu,Zn Superoxide Dismutase-Mediated Familial Amyotrophic Lateral Sclerosis. *Proc Natl Acad Sci USA* **2000**, *97* (25), 13901–13906.

II.212 Alzheimer's Association. 2009 Alzheimer's Disease Facts and Figures. *Alzheimers Dement* **2009**, *5* (3), 234–270.

II.213 LaFerla FM, Green KN, Oddo S. Intracellular Amyloid-Beta in Alzheimer's Disease. *Nat Rev Neurosci* **2007**, *8* (7), 499–509.

II.214 Ertekin-Taner N. Genetics of Alzheimer's Disease: A Centennial Review. *Neurol Clin* **2007**, *25* (3), 611–667.

II.215 Scheuner D, Eckman C, Jensen M, Song X, Citron M, Suzuki N, Bird TD, Hardy J, Hutton M, Kukull W, *et al*. Secreted Amyloid β-Protein Similar to That in the Senile Plaques of Alzheimer's Disease Is Increased in Vivo by the Presenilin 1 and 2 and APP Mutations Linked to Familial Alzheimer's Disease. *Nat Med* **1996**, *2* (8), 864–870.

II.216 Grundke-Iqbal I, Iqbal K, Tung YC, Quinlan M, Wisniewski HM, Binder LI. Abnormal Phosphorylation of the Microtubule-Associated Protein Tau (Tau) in Alzheimer Cytoskeletal Pathology. *Proc Natl Acad Sci USA* **1986**, *83* (13), 4913–4917.

II.217 Ferrer I. Defining Alzheimer as a Common Age-Related Neurodegenerative Process Not Inevitably Leading to Dementia. *Prog Neurobiol* **2012**, *97* (1), 38–51.

II.218 Walsh DM, Klyubin I, Fadeeva JV, Cullen WK, Anwyl R, Wolfe MS, Rowan MJ, Selkoe DJ. Naturally Secreted Oligomers of Amyloid β Protein Potently Inhibit Hippocampal Long-Term Potentiation in Vivo. *Nature* **2002**, *416* (6880), 535–539.

II.219 Brito-Moreira J, Paula-Lima AC, Bomfim TR, Oliveira FB, Sepúlveda FJ, De Mello FG, Aguayo LG, Panizzutti R, Ferreira ST. Aβ Oligomers Induce Glutamate Release from Hippocampal Neurons. *Curr Alzheimer Res* **2011**, *8* (5), 552–562.

II.220 Talantova M, Sanz-Blasco S, Zhang X, Xia P, Waseem M, Okamoto S. Aβ Induces Astrocytic Glutamate Release, Extrasynaptic NMDA Receptor Activation, and Synaptic Loss. *Proc Natl Acad Sci USA* **2013**, *110* (27), E2518–E2527.

II.221 Li S, Jin M, Koeglsperger T, Shepardson N, Shankar G, Selkoe D. Soluble Aβ Oligomers Inhibit Long-Term Potentiation through a Mechanism Involving Excessive Activation of Extrasynaptic NR2B-Containing NMDA Receptors. *J Neurosci* **2011**, *31* (18), 6627–6638.

II.222 Texidó L, Martín-Satué M, Alberdi E, Solsona C, Matute C. Amyloid β Peptide Oligomers Directly Activate NMDA Receptors. *Cell Calcium* **2011**, *49* (3), 184–190.

II.223 Ferreira IL, Bajouco LM, Mota SI, Auberson YP, Oliveira CR, Rego AC. Amyloid Beta Peptide 1-42 Disturbs Intracellular Calcium Homeostasis through Activation of GluN2B-Containing N-Methyl-D-Aspartate Receptors in Cortical Cultures. *Cell Calcium* **2012**, *51* (2), 95–106.

II.224 Huang Y, Shen W, Su J, Cheng B, Li D, Liu G, Zhou WX, Zhang YX. Modulating the Balance of Synaptic and Extrasynaptic NMDA Receptors Shows Positive Effects against Amyloid-β-Induced Neurotoxicity. *J Alzheimers Dis* **2017**, *57* (3), 885–897.

II.225 Mulholland PJ, Luong NT, Woodward JJ, Chandler LJ. Brain-Derived Neurotrophic Factor Activation of Extracellular Signal-Regulated Kinase Is Autonomous from the Dominant Extrasynaptic NMDA Receptor Extracellular Signal-Regulated Kinase Shutoff Pathway. *Neuroscience* **2008**, *151* (2), 419–427.

II.226 Schafe GE, Atkins CM, Swank MW, Bauer EP, Sweatt JD, Ledoux JE. Activation of ERK/MAP Kinase in the Amygdala Is Required for Memory Consolidation of Pavlovian Fear Conditioning. *J Neurosci* **2000**, *20* (21), 8177–8187.

II.227 Wu HY, Lynch DR. Calpain and Synaptic Function. *Mol Neurobiol* **2006**, *33* (3), 215–236.

II.228 Jerónimo-Santos A, Vaz SH, Parreira S, Rapaz-Lérias S, Caetano AP, Buée-Scherrer V, Castrén E, Valente CA, Blum D, Sebastião AM, *et al*. Dysregulation of TrkB Receptors and BDNF Function by Amyloid-β Peptide Is Mediated by Calpain. *Cereb Cortex* **2015**, *25* (9), 3107–3121.

II.229 Tanqueiro SR, Ramalho RM, Rodrigues TM, Lopes LV, Sebastião AM, Diógenes MJ. Inhibition of NMDA Receptors Prevents the Loss of BDNF Function Induced by Amyloid β. *Front Pharmacol* **2018**, *9*, 237.

II.230 Leung AWC, Varanyuwatana P, Halestrap AP. The Mitochondrial Phosphate Carrier Interacts with Cyclophilin D and May Play a Key Role in the Permeability Transition. *J Biol Chem* **2008**, *283* (39), 26312–26323.

II.231 Du H, Guo L, Fang F, Chen D, Sosunov AA, McKhann GM, Yan Y, Wang C, Zhang H, Molkentin JD, *et al*. Cyclophilin D Deficiency Attenuates Mitochondrial and Neuronal Perturbation and Ameliorates Learning and Memory in Alzheimer's Disease. *Nat Med* **2008**, *14* (10), 1097–1105.

II.232 Du H, Guo L, Zhang W, Rydzewska M, Yan S. Cyclophilin D Deficiency Improves Mitochondrial Function and Learning/Memory in Aging Alzheimer Disease Mouse Model. *Neurobiol Aging* **2011**, *32* (3), 398–406.

II.233 Du H, Guo L, Wu X, Sosunov AA, McKhann GM, Chen JX, Yan SS. Cyclophilin D Deficiency Rescues Aβ-Impaired PKA/CREB Signaling and Alleviates Synaptic Degeneration. *Biochim Biophys Acta* **2014**, *1842* (12), 2517–2527.

II.234 Yao J, Irwin RW, Zhao L, Nilsen J, Hamilton RT, Brinton RD. Mitochondrial Bioenergetic Deficit Precedes Alzheimer's Pathology in Female Mouse Model of Alzheimer's Disease. *PNAS* **2009**, *106* (34), 14670–14675.

II.235 Manczak M, Anekonda TS, Henson E, Park BS, Quinn J, Reddy PH. Mitochondria Are a Direct Site of Aβ Accumulation in Alzheimer's Disease Neurons: Implications for Free Radical Generation and Oxidative Damage in Disease Progression. *Hum Mol Genet* **2006**, *15* (9), 1437–1449.

II.236 Hensley K, Carney JM, Mattson MP, Aksenova M, Harris M, Wu JF, Floyd RA, Butterfield DA. A Model for β-Amyloid Aggregation and Neurotoxicity Based on Free Radical Generation by the Peptide: Relevance to Alzheimer Disease. *Proc Natl Acad Sci USA* **1994**, *91* (8), 3270–3274.

II.237 Calkins MJ, Manczak M, Mao P, Shirendeb U, Reddy PH. Impaired Mitochondrial Biogenesis, Defective Axonal Transport of Mitochondria, Abnormal Mitochondrial Dynamics and Synaptic Degeneration in a Mouse Model of Alzheimer's Disease. *Hum Mol Genet* **2011**, *20* (23), 4515–4529.

II.238 Wang X, Wang W, Li L, Perry G, Lee H, Zhu X. Oxidative Stress and Mitochondrial Dysfunction in Alzheimer's Disease. *Biochim Biophys Acta* **2014**, *1842* (8), 1240–1247.

II.239 Ishii K, Sasaki M, Kitagaki H, Yamaji S, Sakamoto S, Matsuda K, Mori E. Reduction of Cerebellar Glucose Metabolism in Advanced Alzheimer's Disease. *J Nucl Med* **1997**, *38* (6), 925–928.

II.240 Kennedy AM, Frackowiak RSJ, Newman SK, Bloomfield PM, Seaward J, Roques P, Lewington G, Cunningham VJ, Rossor MN. Deficits in Cerebral Glucose Metabolism Demonstrated by Positron Emission Tomography in Individuals at Risk of Familial Alzheimer's Disease. *Neurosci Lett* **1995**, *186* (1), 17–20.

II.241 Castegna A, Thongboonkerd V, Klein JB, Lynn B, Markesberyl WR, Butterfield DA. Proteomic Identification of Nitrated Proteins in Alzheimer's Disease Brain. *J Neurochem* **2003**, *85* (6), 1394–1401.

II.242 Butterfield DA, Reed T, Perluigi M, De Marco C, Coccia R, Cini C, Sultana R. Elevated Protein-Bound Levels of the Lipid Peroxidation Product, 4-Hydroxy-2-Nonenal, in Brain from Persons with Mild Cognitive Impairment. *Neurosci Lett* **2006**, *397* (3), 170–173.

II.243 Diaz A, Mendieta L, Zenteno E, Guevara J, Limon ID. The Role of NOS in the Impairment of Spatial Memory and Damaged Neurons in Rats Injected with Amyloid Beta 25-35 into the Temporal Cortex. *Pharmacol Biochem Behav* **2011**, *98* (1), 67–75.

II.244 Patricio-Martínez A, Sánchez-Zavaleta R, Angulo-Cruz I, Gutierrez-Praxedis L, Ramírez E, Martínez-García I, Limón ID. The Acute Activation of the CB1 Receptor in the Hippocampus Decreases Neurotoxicity and Prevents Spatial Memory Impairment in Rats Lesioned with β-Amyloid 25–35. *Neuroscience* **2019**, *416*, 239–254.

II.245 Angelova PR, Abramov AY. Interaction of Neurons and Astrocytes Underlies the Mechanism of Aβ-Induced Neurotoxicity. *Biochem Soc Trans* **2014**, *42*, 1286–1290.

II.246 Brawek B, Garaschuk O. Network-Wide Dysregulation of Calcium Homeostasis in Alzheimer's Disease. *Cell Tissue Res* **2014**, *357*, 427–438.

II.247 Abdul HM, Sama MA, Furman JL, Mathis DM, Beckett TL, Weidner AM, Patel ES, Baig I, Murphy MP, LeVine H, *et al*. Cognitive Decline in Alzheimer's Disease Is Associated with Selective Changes in Calcineurin/NFAT Signaling. *J Neurosci* **2009**, *29* (41), 12957–12969.

II.248 Scimemi A, Meabon JS, Woltjer RL, Sullivan JM, Diamond JS, Cook DG. Amyloid-β1-42 Slows Clearance of Synaptically Released Glutamate by Mislocalizing Astrocytic GLT-1. *J Neurosci* **2013**, *33* (12), 5312–5318.

II.249 Simpson JE, Ince PG, Lace G, Forster G, Shaw PJ, Matthews F, Savva G, Brayne C, Wharton SB. Astrocyte Phenotype in Relation to Alzheimer-Type Pathology in the Ageing Brain. *Neurobiol Aging* **2010**, *31* (4), 578–590.

II.250 Kobayashi E, Nakano M, Kubota K, Himuro N, Mizoguchi S, Chikenji T, Otani M, Mizue Y, Nagaishi K, Fujimiya M. Activated Forms of Astrocytes with Higher GLT-1 Expression Are Associated with Cognitive Normal Subjects with Alzheimer Pathology in Human Brain. *Sci Rep* **2018**, *8* (1), 1712.

II.251 Newman LA, Korol DL, Gold PE. Lactate Produced by Glycogenolysis in Astrocytes Regulates Memory Processing. *PloS One* **2011**, *6* (12), e28427.

II.252 Barros LF. Metabolic Signaling by Lactate in the Brain. *Trends Neurosci* **2013**, *36* (7), 396–404.

II.253 Dienel GA. The Metabolic Trinity, Glucose-Glycogen-Lactate, Links Astrocytes and Neurons in Brain Energetics, Signaling, Memory, and Gene Expression. *Neurosci Lett* **2017**, *637*, 18–25.

II.254 Schurr A. Cerebral Glycolysis: A Century of Persistent Misunderstanding and Misconception. *Front Neurosci* **2014**, *8*, 360.

II.255 Descalzi G, Gao V, Steinman MQ, Suzuki A, Alberini CM. Lactate from Astrocytes Fuels Learning-Induced mRNA Translation in Excitatory and Inhibitory Neurons. *Commun Biol* **2019**, *2* (1), 247.

II.256 Merlini M, Meyer EP, Nitsch AURM. Vascular β-Amyloid and Early Astrocyte Alterations Impair Cerebrovascular Function and Cerebral Metabolism in Transgenic arcAβ Mice. *Acta Neuropathol* **2011**, *122* (3), 293–311.

II.257 Chen Z, Zhong C. Decoding Alzheimer's Disease from Perturbed Cerebral Glucose Metabolism: Implications for Diagnostic and Therapeutic Strategies. *Prog Neurobiol* **2013**, *108*, 21–43.

II.258 Mosconi L, Pupi A, De Leon MJ. Brain Glucose Hypometabolism and Oxidative Stress in Preclinical Alzheimer's Disease. *Ann NY Acad Sci* **2008**, *1147*, 180–195.

II.259 Liu B, Hong J-S. Role of Microglia in Inflammation-Mediated Neurodegenerative Diseases: Mechanisms and Strategies for Therapeutic Intervention. *J Pharmacol Exp Ther* **2003**, *304* (1), 1–7.

II.260 Reynolds A, Laurie C, Mosley RL, Gendelman HE. Oxidative Stress and the Pathogenesis of Neurodegenerative Disorders. *Int Rev Neurobiol* **2007**, *82*, 297–325.

II.261 Taylor JM, Main BS, Crack PJ. Neuroinflammation and Oxidative Stress: Co-Conspirators in the Pathology of Parkinson's Disease. *Neurochem Int* **2013**, *62* (5), 803–819.

II.262 Edwards JP, Zhang X, Frauwirth KA, Mosser DM. Biochemical and Functional Characterization of Three Activated Macrophage Populations. *J Leukoc Biol* **2006**, *80* (6), 1298–1307.

II.263 Sheffield LG, Marquis JG, Berman NEJ. Regional Distribution of Cortical Microglia Parallels That of Neurofibrillary Tangles in Alzheimer's Disease. *Neurosci Lett* **2000**, *285* (3), 165–168.

II.264 Yao K, Zu H-B. Microglial Polarization: Novel Therapeutic Mechanism against Alzheimer's Disease. *Inflammopharmacol* **2019**, *28*, 95–110.

II.265 Yamamoto M, Kiyota T, Walsh SM, Liu J, Kipnis J, Ikezu T. Cytokine-Mediated Inhibition of Fibrillar Amyloid-β Peptide Degradation by Human Mononuclear Phagocytes. *J Immunol* **2008**, *181* (6), 3877–3886.

II.266 Koenigsknecht-Talboo J, Landreth GE. Microglial Phagocytosis Induced by Fibrillar β-Amyloid and IgGs Are Differentially Regulated by Proinflammatory Cytokines. *J Neurosci* **2005**, *25* (36), 8240–8249.

II.267 Barger SW, Goodwin ME, Porter MM, Beggs ML. Glutamate Release from Activated Microglia Requires the Oxidative Burst and Lipid Peroxidation. *J Neurochem* **2007**, *101* (5), 1205–1213.

II.268 Hu S, Sheng WS, Ehrlich LC, Peterson PK, Chao CC. Cytokine Effects on Glutamate Uptake by Human Astrocytes. *Neuroimmunomodulation* **2000**, *7* (3), 153–159.

II.269 Ralay Ranaivo H, Craft JM, Hu W, Guo L, Wing LK, Van Eldik LJ, Watterson DM. Glia as a Therapeutic Target: Selective Suppression of Human Amyloid-β-Induced Upregulation of Brain Proinflammatory Cytokine Production Attenuates Neurodegeneration. *J Neurosci* **2006**, *26* (2), 662–670.

II.270 Sato H, Tamba M, Okuno S, Sato K, Keino-Masu K, Masu M, Bannai S. Distribution of Cystine/Glutamate Exchange Transporter, System x(c)-, in the Mouse Brain. *J Neurosci* **2002**, *22* (18), 8028–8033.

II.271 Lo M, Wang Y-Z, Gout PW. The x(c)- Cystine/Glutamate Antiporter: A Potential Target for Therapy of Cancer and Other Diseases. *J Cell Physiol* **2008**, *215* (3), 593–602.

II.272 Lutgen V, Resch J, Qualmann K, Raddatz NJ, Panhans C, Olander EM, Kong L, Choi S, Mantsch JR, Baker DA. Behavioral Assessment of Acute Inhibition of System Xc- in Rats. *Psychopharmacology* **2014**, *231* (24), 4637–4647.

II.273 Lewerenz J, Maher P, Methner A. Regulation of xCT Expression and System x(c)- Function in Neuronal Cells. *Amino Acids* **2012**, *42* (1), 171–179.

II.274 Sato H, Tamba M, Ishii T, Bannai S. Cloning and Expression of a Plasma Membrane Cystine/Glutamate Exchange Transporter Composed of Two Distinct Proteins. *J Biol Chem* **1999**, *274* (17), 11455–11458.

II.275 Baker DA, Xi ZX, Shen H, Swanson CJ, Kalivas PW. The Origin and Neuronal Function of in Vivo Nonsynaptic Glutamate. *J Neurosci* **2002**, *22* (20), 9134–9141.

II.276 Warr O, Takahashi M, Attwell D. Modulation of Extracellular Glutamate Concentration in Rat Brain Slices by Cystine-Glutamate Exchange. *J Physiol* **1999**, *514* (Pt 3), 783–793.

II.277 Bridges R, Lutgen V, Lobner D, Baker DA. Thinking Outside the Cleft to Understand Synaptic Activity: Contribution of the Cystine-Glutamate Antiporter (System Xc-) to Normal and Pathological Glutamatergic Signaling. *Pharmacol Rev* **2012**, *64* (3), 780–802.

II.278 Barger SW, Basile AS. Activation of Microglia by Secreted Amyloid Precursor Protein Evokes Release of Glutamate by Cystine Exchange and Attenuates Synaptic Function. *J Neurochem* **2001**, *76* (3), 846–854.

II.279 Sato H, Kuriyama-Matsumura K, Hashimoto T, Sasaki H, Wang H, Ishii T, Mann GE, Bannai S. Effect of Oxygen on Induction of the Cystine Transporter by Bacterial Lipopolysaccharide in Mouse Peritoneal Macrophages. *J Biol Chem* **2001**, *276* (13), 10407–10412.

II.280 Mesci P, Zaïdi S, Lobsiger CS, Millecamps S, Escartin C, Seilhean D, Sato H, Mallat M, Boillée S. System XC- Is a Mediator of Microglial Function and Its Deletion Slows Symptoms in Amyotrophic Lateral Sclerosis Mice. *Brain J Neurol* **2015**, *138* (2014), 53–68.

II.281 Qin S, Colin C, Hinners I, Gervais A, Cheret C, Mallat M. System Xc- and Apolipoprotein E Expressed by Microglia Have Opposite Effects on the Neurotoxicity of Amyloid-Beta Peptide 1-40. *J Neurosci* **2006**, *26* (12), 3345–3356.

II.282 Shih AY, Erb H, Sun X, Toda S, Kalivas PW, Murphy TH. Cystine/Glutamate Exchange Modulates Glutathione Supply for Neuroprotection from Oxidative Stress and Cell Proliferation. *J Neurosci* **2006**, *26* (41), 10514–10523.

II.283 Bannai S, Tateishi N. Role of Membrane Transport in Metabolism and Function of Glutathione in Mammals. *J Membr Biol* **1986**, *89* (1), 1–8.

II.284 Thorn TL, He Y, Jackman NA, Lobner D, Hewett JA, Hewett SJ. A Cytotoxic, Co-Operative Interaction between Energy Deprivation and Glutamate Release from System Xc-Mediates Aglycemic Neuronal Cell Death. *ASN Neuro* **2015**, *7* (6), 1759091415614301.

II.285 Jackman NA, Melchior SE, Hewett JA, Hewett SJ. Non-Cell Autonomous Influence of the Astrocyte System Xc- on Hypoglycaemic Neuronal Cell Death. *ASN Neuro* **2012**, *4* (1), e00074.

II.286 Olabarria M, Noristani HN, Verkhratsky A, Rodríguez JJ. Age-Dependent Decrease in Glutamine Synthetase Expression in the Hippocampal Astroglia of the Triple Transgenic Alzheimer's Disease Mouse Model: Mechanism for Deficient Glutamatergic Transmission? *Mol Neurodegener* **2011**, *6* (1), 55.

II.287 Smith CD, Carney JM, Starke-Reed PE, Oliver CN, Stadtman ER, Floyd RA, Markesbery WR. Excess Brain Protein Oxidation and Enzyme Dysfunction in Normal Aging and in Alzheimer Disease. *Proc Natl Acad Sci USA* **1991**, *88* (23), 10540–10543.

II.288 Hensley K, Hall N, Subramaniam R, Cole P, Harris M, Aksenov M, Aksenova M, Gabbita SP, Wu JF, Carney JM, *et al*. Brain Regional Correspondence Between Alzheimer's Disease Histopathology and Biomarkers of Protein Oxidation. *J Neurochem* **1995**, *65* (5), 2146–2156.

II.289 Balu DT, Pantazopoulos H, Huang CCY, Muszynski K, Harvey TL, Uno Y, Rorabaugh JM, Galloway CR, Botz-Zapp C, Berretta S, *et al*. Neurotoxic Astrocytes Express the D-Serine Synthesizing Enzyme, Serine Racemase, in Alzheimer's Disease. *Neurobiol Dis* **2019**, *130*, 104511.

II.290 Haughey NJ, Mattson MP. Alzheimer's Amyloid Beta-Peptide Enhances ATP/Gap Junction-Mediated Calcium-Wave Propagation in Astrocytes. *Neuromolecular Med* **2003**, *3* (3), 173–180.

II.291 Kuchibhotla KV, Lattarulo CR, Hyman BT, Bacskai BJ. Synchronous Hyperactivity and Intercellular Calcium Waves in Astrocytes in Alzheimer Mice. *Science* **2009**, *323* (5918), 1211–1215.

II.292 Singh A, Trevick S. The Epidemiology of Global Epilepsy. *Neurol Clin* **2016**, *34* (4), 837–847.

II.293 Fisher RS, Cross JH, French JA, Higurashi N, Hirsch E, Jansen FE, Lagae L, Moshé SL, Peltola J, Roulet Perez E, *et al*. Operational Classification of Seizure Types by the International League Against Epilepsy: Position Paper of the ILAE Commission for Classification and Terminology. *Epilepsia* **2017**, *58* (4), 522–530.

II.294 Soukupová M, Binaschi A, Falcicchia C, Zucchini S, Roncon P, Palma E, Magri E, Grandi E, Simonato M. Impairment of GABA Release in the Hippocampus at the Time of the First Spontaneous Seizure in the Pilocarpine Model of Temporal Lobe Epilepsy. *Exp Neurol* **2014**, *257*, 39–49.

II.295 Hubbard JA, Szu JI, Yonan JM, Binder DK. Regulation of Astrocyte Glutamate Transporter-1 (GLT1) and Aquaporin-4 (AQP4) Expression in a Model of Epilepsy. *Exp Neurol* **2016**, *283* (Pt A), 85–96.

II.296 Peterson AR, Binder DK. Regulation of Synaptosomal GLT-1 and GLAST during Epileptogenesis. *Neuroscience* **2019**, *411*, 185–201.

II.297 Proper EA, Hoogland G, Kappen SM, Jansen GH, Rensen MG, Schrama LH, van Veelen CW, van Rijen PC, van Nieuwenhuizen O, Gispen WH, *et al*. Distribution of Glutamate Transporters in the Hippocampus of Patients with Pharmaco-Resistant Temporal Lobe Epilepsy. *Brain* **2002**, *125* (Pt 1), 32–43.

II.298 Albrecht J, Zielinska M. Mechanisms of Excessive Extracellular Glutamate Accumulation in Temporal Lobe Epilepsy. *Neurochem Res* **2017**, *42* (6), 1724–1734.

II.299 Hoogland G, van Oort RJ, Proper EA, Jansen GH, van Rijen PC, van Veelen CW, van Nieuwenhuizen O, Troost D, de Graan PN. Alternative Splicing of Glutamate Transporter EAAT2 RNA in Neocortex and Hippocampus of Temporal Lobe Epilepsy Patients. *Epilepsy Res* **2004**, *59* (2–3), 75–82.

II.300 During MJ, Spencer DD. Extracellular Hippocampal Glutamate and Spontaneous Seizure in the Conscious Human Brain. *Lancet* **1993**, *341* (8861), 1607–1610.

II.301 Sloviter RS, Dichter MA, Rachinsky TL, Dean E, Goodman JH, Sollas AL, Martin DL. Basal Expression and Induction of Glutamate Decarboxylase and GABA in Excitatory Granule Cells of the Rat and Monkey Hippocampal Dentate Gyrus. *J Comp Neurol* **1996**, *373* (4), 593–618.

II.302 Rakhade SN, Loeb JA. Focal Reduction of Neuronal Glutamate Transporters in Human Neocortical Epilepsy. *Epilepsia* **2008**, *49* (2), 226–236.

II.303 Tanaka K, Watase K, Manabe T, Yamada K, Watanabe M, Takahashi K, Iwama H, Nishikawa T, Ichihara N, Kikuchi T, *et al*. Epilepsy and Exacerbation of Brain Injury in Mice Lacking the Glutamate Transporter GLT-1. *Science* **1997**, *276* (5319), 1699–1702.

II.304 Kong Q, Takahashi K, Schulte D, Stouffer N, Lin Y, Lin CL. Increased Glial Glutamate Transporter EAAT2 Expression Reduces Epileptogenic Processes Following Pilocarpine-Induced Status Epilepticus. *Neurobiol Dis* **2012**, *47* (2), 145–154.

II.305 Sha L, Wang X, Li J, Shi X, Wu L, Shen Y, Xu Q. Pharmacologic Inhibition of Hsp90 to Prevent GLT-1 Degradation as an Effective Therapy for Epilepsy. *J Exp Med* **2017**, *214* (2), 547–563.

II.306 Murphy-Royal C, Dupuis JP, Varela JA, Panatier A, Pinson B, Baufreton J, Groc L, Oliet SH. Surface Diffusion of Astrocytic Glutamate Transporters Shapes Synaptic Transmission. *Nat Neurosci* **2015**, *18* (2), 219–226.

II.307 Rothstein JD, Patel S, Regan MR, Haenggeli C, Huang YH, Bergles DE, Jin L, Dykes Hoberg M, Vidensky S, Chung DS, *et al*. Beta-Lactam Antibiotics Offer Neuroprotection by Increasing Glutamate Transporter Expression. *Nature* **2005**, *433* (7021), 73–77.

II.308 Zeng LH, Bero AW, Zhang B, Holtzman DM, Wong M. Modulation of Astrocyte Glutamate Transporters Decreases Seizures in a Mouse Model of Tuberous Sclerosis Complex. *Neurobiol Dis* **2010**, *37* (3), 764–771.

II.309 Kong Q, Chang LC, Takahashi K, Liu Q, Schulte DA, Lai L, Ibabao B, Lin Y, Stouffer N, Das Mukhopadhyay C, *et al*. Small-Molecule Activator of Glutamate Transporter EAAT2 Translation Provides Neuroprotection. *J Clin Invest* **2014**, *124* (3), 1255–1267.

II.310 Susarla BT, Robinson MB. Internalization and Degradation of the Glutamate Transporter GLT-1 in Response to Phorbol Ester. *Neurochem Int* **2008**, *52* (4–5), 709–722.

II.311 Whitesell L, Lindquist SL. HSP90 and the Chaperoning of Cancer. *Nat Rev Cancer* **2005**, *5* (10), 761–772.

II.312 Devinsky O, Vezzani A, Najjar S, De Lanerolle NC, Rogawski MA. Glia and Epilepsy: Excitability and Inflammation. *Trends Neurosci* **2013**, *36* (3), 174–184.

II.313 D'Ambrosio R, Gordon DS, Winn HR. Differential Role of KIR Channel and Na(+)/K(+)-Pump in the Regulation of Extracellular K(+) in Rat Hippocampus. *J Neurophysiol* **2002**, *87* (1), 87–102.

II.314 Kofuji P, Newman EA. Potassium Buffering in the Central Nervous System. *Neuroscience* **2004**, *129* (4), 1045–1056.

II.315 Nikolic L, Nobili P, Shen W, Audinat E. Role of Astrocyte Purinergic Signaling in Epilepsy. *Glia* **2019**. [Epub ahead of print].

II.316 Ransom CB, Ransom BR, Sontheimer H. Activity-Dependent Extracellular K+ Accumulation in Rat Optic Nerve: The Role of Glial and Axonal Na+ Pumps. *J Physiol* **2000**, *522* (Pt 3), 427–442.

II.317 Walz W. Role of Astrocytes in the Clearance of Excess Extracellular Potassium. *Neurochem Int* **2000**, *36* (4–5), 291–300.

II.318 Steinhäuser C, Grunnet M, Carmignoto G. Crucial Role of Astrocytes in Temporal Lobe Epilepsy. *Neuroscience* **2016**, *323*, 157–169.

II.319 Aronica E, van Vliet EA, Mayboroda OA, Troost D, da Silva FH, Gorter JA. Upregulation of Metabotropic Glutamate Receptor Subtype MGluR3 and MGluR5 in Reactive Astrocytes in a Rat Model of Mesial Temporal Lobe Epilepsy. *Eur J Neurosci* **2000**, *12* (7), 2333–2344.

II.320 Das A, Wallace GC, Holmes C, McDowell ML, Smith JA, Marshall JD, Bonilha L, Edwards JC, Glazier SS, Ray SK, Banik NL. Hippocampal Tissue of Patients with Refractory Temporal Lobe Epilepsy Is Associated with Astrocyte Activation, Inflammation, and Altered Expression of Channels and Receptors. *Neuroscience* **2012**, *220*, 237–246.

II.321 Chever O, Djukic B, McCarthy KD, Amzica F. Implication of Kir4.1 Channel in Excess Potassium Clearance: An in Vivo Study on Anesthetized Glial-Conditional Kir4.1 Knock-out Mice. *J Neurosci* **2010**, *30* (47), 15769–15777.

II.322 Djukic B, Casper KB, Philpot BD, Chin L-S, McCarthy KD. Conditional Knock-out of Kir4.1 Leads to Glial Membrane Depolarization, Inhibition of Potassium and Glutamate Uptake, and Enhanced Short-Term Synaptic Potentiation. *J Neurosci* **2007**, *27* (42), 11354–11365.

II.323 Dudek FE, Rogawski MA. Regulation of Brain Water: Is There a Role for Aquaporins in Epilepsy? *Epilepsy Curr* **2005**, *5* (3), 104–106.

II.324 Lee DJ, Hsu MS, Seldin MM, Arellano JL, Binder DK. Decreased Expression of the Glial Water Channel Aquaporin-4 in the Intrahippocampal Kainic Acid Model of Epileptogenesis. *Exp Neurol* **2012**, *235* (1), 246–255.

II.325 Amiry-Moghaddam M, Otsuka T, Hurn PD, Traystman RJ, Haug F-M, Froehner SC, Adams ME, Neely JD, Agre P, Ottersen OP, Bhardwaj A. An Alpha-Syntrophin-Dependent Pool of AQP4 in Astroglial End-Feet Confers Bidirectional Water Flow between Blood and Brain. *Proc Natl Acad Sci USA* **2003**, *100* (4), 2106–2111.

II.326 Eid T, Lee T-SW, Thomas MJ, Amiry-Moghaddam M, Bjørnsen LP, Spencer DD, Agre P, Ottersen OP, de Lanerolle NC. Loss of Perivascular Aquaporin 4 May Underlie Deficient Water and K+ Homeostasis in the Human Epileptogenic Hippocampus. *Proc Natl Acad Sci USA* **2005**, *102* (4), 1193–1198.

II.327 Seifert G, Carmignoto G, Steinhäuser C. Astrocyte Dysfunction in Epilepsy. *Brain Res Rev* **2010**, *63* (1–2), 212–221.

II.328 Goffin K, Dedeurwaerdere S, Van Laere K, Van Paesschen W. Neuronuclear Assessment of Patients with Epilepsy. *Semin Nucl Med* **2008**, *38* (4), 227–239.

II.329 Pittau F, Grouiller F, Spinelli L, Seeck M, Michel CM, Vulliemoz S. The Role of Functional Neuroimaging in Pre-Surgical Epilepsy Evaluation. *Front Neurol* **2014**, *5*, 31.

II.330 Bittner CX, Valdebenito R, Ruminot I, Loaiza A, Larenas V, Sotelo-Hitschfeld T, Moldenhauer H, Martín AS, Gutiérrez R, Zambrano M, Barros LF. Fast and Reversible Stimulation of Astrocytic Glycolysis by K+ and a Delayed and Persistent Effect of Glutamate. *J Neurosci* **2011**, *31* (12), 4709–4713.

II.331 Yan X, Shi ZF, Xu LX, Li JX, Wu M, Wang XX, Jia M, Dong LP, Yang SH, Yuan,F. Glutamate Impairs Mitochondria Aerobic Respiration Capacity and Enhances Glycolysis in Cultured Rat Astrocytes. *Biomed Environ Sci* **2017**, *30* (1), 44–51.

II.332 Mächler P, Wyss MT, Elsayed M, Stobart J, Gutierrez R, von Faber-Castell A, Kaelin V, Zuend M, San Martín A, Romero-Gómez I, Baeza-Lehnert F, Lengacher S, Schneider BL, Aebischer P, Magistretti PJ, Barros LF, Weber B. In Vivo Evidence for a Lactate Gradient from Astrocytes to Neurons. *Cell Metab* **2016**, *23* (1), 94–102.

II.333 Liu B, Niu L, Shen M-Z, Gao L, Wang C, Li J, Song L-J, Tao Y, Meng Q, Yang Q-L, Gao G-D, Zhang H. Decreased Astroglial Monocarboxylate Transporter 4 Expression in Temporal Lobe Epilepsy. *Mol Neurobiol* **2014**, *50* (2), 327–338.

II.334 Suzuki A, Stern SA, Bozdagi O, Huntley GW, Walker RH, Magistretti PJ, Alberini CM. Astrocyte-Neuron Lactate Transport Is Required for Long-Term Memory Formation. *Cell* **2011**, *144* (5), 810–823.

II.335 Walczyk T, Wick JY. The Ketogenic Diet: Making a Comeback. *Consult Pharm* **2017**, *32* (7), 388–396.

II.336 Popova I, Malkov A, Ivanov AI, Samokhina E, Buldakova S, Gubkina O, Osypov A, Muhammadiev RS, Zilberter T, Molchanov M, Paskevich S, Zilberter M, Zilberter Y. Metabolic Correction by Pyruvate Halts Acquired Epilepsy in Multiple Rodent Models. *Neurobiol Dis* **2017**, *106*, 244–254.

II.337 Gottlieb M, Wang Y, Teichberg VI. Blood-Mediated Scavenging of Cerebrospinal Fluid Glutamate. *J Neurochem* **2003**, *87* (1), 119–126.

II.338 Carvalho AS, Torres LB, Persike DS, Fernandes MJ, Amado D, Naffah-Mazzacoratti M da G, Cavalheiro EA, da Silva AV. Neuroprotective Effect of Pyruvate and Oxaloacetate during Pilocarpine Induced Status Epilepticus in Rats. *Neurochem Int* **2011**, *58* (3), 385–390.

II.339 Wasterlain CG, Thompson KW, Suchomelova L, Niquet J. Brain Energy Metabolism during Experimental Neonatal Seizures. *Neurochem Res* **2010**, *35* (12), 2193–2198.

II.340 Kovac S, Abramov AY, Walker MC. Energy Depletion in Seizures: Anaplerosis as a Strategy for Future Therapies. *Neuropharmacology* **2013**, *69*, 96–104.

II.341 Frantseva MV, Velazquez JL, Hwang PA, Carlen PL. Free Radical Production Correlates with Cell Death in an in Vitro Model of Epilepsy. *Eur J Neurosci* **2000**, *12* (4), 1431–1439.

II.342 Jarrett SG, Liang L-P, Hellier JL, Staley KJ, Patel M. Mitochondrial DNA Damage and Impaired Base Excision Repair during Epileptogenesis. *Neurobiol Dis* **2008**, *30* (1), 130–138.

II.343 Rose J, Brian C, Woods J, Pappa A, Panayiotidis MI, Powers R, Franco R. Mitochondrial Dysfunction in Glial Cells: Implications for Neuronal Homeostasis and Survival. *Toxicology* **2017**, *391*, 109–115.

II.344 Kovac S, Domijan A-M, Walker MC, Abramov AY. Prolonged Seizure Activity Impairs Mitochondrial Bioenergetics and Induces Cell Death. *J Cell Sci* **2012**, *125* (Pt 7), 1796–1806.

II.345 Vergun O, Keelan J, Khodorov BI, Duchen MR. Glutamate-Induced Mitochondrial Depolarisation and Perturbation of Calcium Homeostasis in Cultured Rat Hippocampal Neurones. *J Physiol* **1999**, *519* (Pt 2), 451–466.

II.346 Griffiths T, Evans MC, Meldrum BS. Intracellular Calcium Accumulation in Rat Hippocampus during Seizures Induced by Bicuculline or L-Allylglycine. *Neuroscience* **1983**, *10* (2), 385–395.

II.347 De Stefani D, Raffaello A, Teardo E, Szabò I, Rizzuto R. A Forty-Kilodalton Protein of the Inner Membrane Is the Mitochondrial Calcium Uniporter. *Nature* **2011**, *476* (7360), 336–340.

II.348 Wang C, Xie N, Wang Y, Li Y, Ge X, Wang M. Role of the Mitochondrial Calcium Uniporter in Rat Hippocampal Neuronal Death After Pilocarpine-Induced Status Epilepticus. *Neurochem Res* **2015**, *40* (8), 1739–1746.

II.349 Sokal DM, Mason R, Parker TL. Multi-Neuronal Recordings Reveal a Differential Effect of Thapsigargin on Bicuculline- or Gabazine-Induced Epileptiform Excitability in Rat Hippocampal Neuronal Networks. *Neuropharmacology* **2000**, *39* (12), 2408–2417.

II.350 Rutecki PA, Sayin U, Yang Y, Hadar E. Determinants of Ictal Epileptiform Patterns in the Hippocampal Slice. *Epilepsia* **2002**, *43* (Suppl 5), 179–183.

II.351 Patel M, Day BJ, Crapo JD, Fridovich I, McNamara JO. Requirement for Superoxide in Excitotoxic Cell Death. *Neuron* **1996**, *16* (2), 345–355.

II.352 Liang LP, Ho YS, Patel M. Mitochondrial Superoxide Production in Kainate-Induced Hippocampal Damage. *Neuroscience* **2000**, *101* (3), 563–570.

II.353 Ryan K, Backos DS, Reigan P, Patel M. Post-Translational Oxidative Modification and Inactivation of Mitochondrial Complex I in Epileptogenesis. *J Neurosci* **2012**, *32* (33), 11250–11258.

II.354 Rowley S, Liang L-P, Fulton R, Shimizu T, Day B, Patel M. Mitochondrial Respiration Deficits Driven by Reactive Oxygen Species in Experimental Temporal Lobe Epilepsy. *Neurobiol Dis* **2015**, *75*, 151–158.

II.355 Mülsch A, Busse R, Mordvintcev PI, Vanin AF, Nielsen EO, Scheel-Krüger J, Olesen SP. Nitric Oxide Promotes Seizure Activity in Kainate-Treated Rats. *Neuroreport* **1994**, *5* (17), 2325–2328.

II.356 González-Hernández T, García-Marín V, Pérez-Delgado MM, González-González ML, Rancel-Torres N, González-Feria L. Nitric Oxide Synthase Expression in the Cerebral Cortex of Patients with Epilepsy. *Epilepsia* **2000**, *41* (10), 1259–1268.

II.357 Mikami Y, Kanemaru K, Okubo Y, Nakaune T, Suzuki J, Shibata K, Sugiyama H, Koyama R, Murayama T, Ito A, Yamazawa T, Ikegaya Y, Sakurai T, Saito N, Kakizawa S, Iino M. Nitric Oxide-Induced Activation of the Type 1 Ryanodine Receptor Is Critical for Epileptic Seizure-Induced Neuronal Cell Death. *EBioMedicine* **2016**, *11*, 253–261.

II.358 Rahimi N, Hassanipour M, Yarmohammadi F, Faghir-Ghanesefat H, Pourshadi N, Bahramnejad E, Dehpour AR. Nitric Oxide and Glutamate Are Contributors of Anti-Seizure Activity of Rubidium Chloride: A Comparison with Lithium. *Neurosci Lett* **2019**, *708*, 134349.

II.359 Petkova Z, Tchekalarova J, Pechlivanova D, Moyanova S, Kortenska L, Mitreva R, Popov D, Markova P, Lozanov V, Atanasova D, Lazarov N, Stoynev A. Treatment with Melatonin after Status Epilepticus Attenuates Seizure Activity and Neuronal Damage but Does Not Prevent the Disturbance in Diurnal Rhythms and Behavioral Alterations in Spontaneously Hypertensive Rats in Kainate Model of Temporal Lobe Epilepsy. *Epilepsy Behav* **2014**, *31*, 198–208.

II.360 Mishra V, Shuai B, Kodali M, Shetty GA, Hattiangady B, Rao X, Shetty AK. Resveratrol Treatment after Status Epilepticus Restrains Neurodegeneration and Abnormal Neurogenesis with Suppression of Oxidative Stress and Inflammation. *Sci Rep* **2015**, *5*, 17807.

II.361 Williams S, Hamil N, Abramov AY, Walker MC, Kovac S. Status Epilepticus Results in Persistent Overproduction of Reactive Oxygen Species, Inhibition of Which Is Neuroprotective. *Neuroscience* **2015**, *303*, 160–165.

II.362 Pauletti A, Terrone G, Shekh-Ahmad T, Salamone A, Ravizza T, Rizzi M, Pastore A, Pascente R, Liang L-P, Villa BR, Balosso S, Abramov AY, van Vliet EA, Del Giudice E, Aronica E, Patel M, Walker MC, Vezzani A. Targeting Oxidative Stress Improves Disease Outcomes in a Rat Model of Acquired Epilepsy. *Brain J Neurol* **2019**, *142* (7), e39.

II.363 Pannese E. III. Shape and Size of Neurons. In *Neurocytology: Fine Structure of Neurons, Nerve Processes, and Neuroglial Cells*; Pannese E, Ed.; Springer International Publishing: Cham, Switzerland, **2015**; pp 13–23.

II.364 Romand S, Wang Y, Toledo-Rodriguez M, Markram H. Morphological Development of Thick-Tufted Layer V Pyramidal Cells in the Rat Somatosensory Cortex. *Front Neuroanat* **2011**, *5*, 5.

II.365 Eisenberg D, Gill HS, Pfluegl GMU, Rotstein SH. Structure–Function Relationships of Glutamine Synthetases. *Biochim Biophys Acta* **2000**, *1477* (1), 122–145.

II.366 Bak LK, Schousboe A, Waagepetersen HS. The Glutamate/GABA-Glutamine Cycle: Aspects of Transport, Neurotransmitter Homeostasis and Ammonia Transfer. *J Neurochem* **2006**, *98* (3), 641–653.

II.367 Liaw SH, Kuo I, Eisenberg D. Discovery of the Ammonium Substrate Site on Glutamine Synthetase, A Third Cation Binding Site. *Protein Sci* **1995**, *4* (11), 2358–2365.

II.368 Liaw SH, Eisenberg D. Structural Model for the Reaction Mechanism of Glutamine Synthetase, Based on Five Crystal Structures of Enzyme-Substrate Complexes. *Biochemistry* **1994**, *33* (3), 675–681.

II.369 Nelson D, Cox M, Eds. *Lehninger Principles of Biochemistry*; WH Freeman: New York, USA, **2008**.

II.370 Botman D, Tigchelaar W, Noorden CJFV. Determination of Glutamate Dehydrogenase Activity and Its Kinetics in Mouse Tissues Using Metabolic Mapping (Quantitative Enzyme Histochemistry). *J Histochem Cytochem* **2014**, *62* (11), 802–812.

II.371 Farooqui AA, Ong W-Y, Horrocks LA. *Neurochemical Aspects of Excitotoxicity*; Springer-Verlag: New York, USA, **2008**.

II.372 Woo T-UW, Walsh JP, Benes FM. Density of Glutamic Acid Decarboxylase 67 Messenger RNA–Containing Neurons That Express the N-Methyl-D-Aspartate Receptor Subunit NR2A in the Anterior Cingulate Cortex in Schizophrenia and Bipolar Disorder. *Arch Gen Psychiatry* **2004**, *61* (7), 649–657.

II.373 Shank RP, Campbell GL. Glutamine and Alpha-Ketoglutarate Uptake and Metabolism by Nerve Terminal Enriched Material from Mouse Cerebellum. *Neurochem Res* **1982**, *7* (5), 601–616.

II.374 Peng LA, Schousboe A, Hertz L. Utilization of Alpha-Ketoglutarate as a Precursor for Transmitter Glutamate in Cultured Cerebellar Granule Cells. *Neurochem Res* **1991**, *16* (1), 29–34.

II.375 Yudkoff M, Nissim I, Hertz L. Precursors of Glutamic Acid Nitrogen in Primary Neuronal Cultures: Studies With 15N. *Neurochem Res* **1990**, *15* (12), 1191–1196.

II.376 Juggi J, Iyng Karan N, Prathap K. Hyperammonemia in Reye's Syndrome. In *Reye's Syndrome II*; Crocker J, Ed.; Grune and Stratton: New York, USA, **1979**; pp 411–432.

II.377 Donoghue JP, Wenthold RJ, Altschuler RA. Localization of Glutaminase-like and Aspartate Aminotransferase-like Immunoreactivity in Neurons of Cerebral Neocortex. *J Neurosci* **1985**, *5* (10), 2597–2608.

II.378 Petroff OAC. GABA and Glutamate in the Human Brain. *Neuroscientist* **2002**, *8* (6), 562–573.

II.379 El-Ansary A, Al-Ayadhi L. GABAergic/Glutamatergic Imbalance Relative to Excessive Neuroinflammation in Autism Spectrum Disorders. *J Neuroinflammation* **2014**, *11*, 189.

II.380 Cepeda C, Ariano MA, Calvert CR, Flores-Hernández J, Chandler SH, Leavitt BR, Hayden MR, Levine MS. NMDA Receptor Function in Mouse Models of Huntington Disease. *J Neurosci Res* **2001**, *66* (4), 525–539.

II.381 Meldrum BS. Epilepsy and Gamma-Aminobutyric Acid-Mediated Inhibition. *Int Rev Neurobiol* **1975**, *17*, 1–36.

II.382 Hamberger A, van Gelder NM. Metabolic Manipulation of Neural Tissue to Counter the Hypersynchronous Excitation of Migraine and Epilepsy. *Neurochem Res* **1993**, *18* (4), 503–509.

II.383 Sherwin AL. Neuroactive Amino Acids in Focally Epileptic Human Brain: A Review. *Neurochem Res* **1999**, *24* (11), 1387–1395.

II.384 Haglund MM, Berger MS, Kunkel DD, Franck JE, Ghatan S, Ojemann GA. Changes in Gamma-Aminobutyric Acid and Somatostatin in Epileptic Cortex Associated with Low-Grade Gliomas. *J Neurosurg* **1992**, *77* (2), 209–216.

II.385 Marco P, Sola RG, Pulido P, Alijarde MT, Sánchez A, Ramón y Cajal S, DeFelipe J. Inhibitory Neurons in the Human Epileptogenic Temporal Neocortex. An Immunocytochemical Study. *Brain* **1996**, *119 (Pt 4)*, 1327–1347.

II.386 Rodríguez-Moreno A, Lerma J. Kainate Receptor Modulation of GABA Release Involves a Metabotropic Function. *Neuron* **1998**, *20* (6), 1211–1218.

II.387 McGeer P, Eccles J, McGeer E. Putative Excitatory Neurons: Glutamate and Aspartate. In *Molecular Neurobiology of the Mammalian Brain*; Plenum Press: New York, USA, **1987**.

II.388 Roettger VR, Amara SG. GABA and Glutamate Transporters: Therapeutic and Etiologic Implications for Epilepsy. *Adv Neurol* **1999**, *79*, 551–560.

II.389 Moser H. Electrophysiological Evidence for Ammonium as a Substitute for Potassium in Activating the Sodium Pump in a Crayfish Sensory Neuron. *Can J Physiol Pharmacol* **1987**, *65* (2), 141–145.

II.390 Bosoi CR, Rose CF. Identifying the Direct Effects of Ammonia on the Brain. *Metab Brain Dis* **2009**, *24* (1), 95–102.

II.391 Aickin CC, Deisz RA, Lux HD. Ammonium Action on Post-Synaptic Inhibition in Crayfish Neurones: Implications for the Mechanism of Chloride Extrusion. *J Physiol* **1982**, *329*, 319–339.

II.392 Saparov SM, Liu K, Agre P, Pohl P. Fast and Selective Ammonia Transport by Aquaporin-8. *J Biol Chem* **2007**, *282* (8), 5296–5301.

II.393 Liu Y, Wu H, Li M, Yin J-J, Nie Z. pH Dependent Catalytic Activities of Platinum Nanoparticles with Respect to the Decomposition of Hydrogen Peroxide and Scavenging of Superoxide and Singlet Oxygen. *Nanoscale* **2014**, *6* (20), 11904–11910.

II.394 Rafti M, Brunsen A, Fuertes MC, Azzaroni O, Soler-Illia GJAA. Heterogeneous Catalytic Activity of Platinum Nanoparticles Hosted in Mesoporous Silica Thin Films Modified with Polyelectrolyte Brushes. *ACS Appl Mater Interfaces* **2013**, *5* (18), 8833–8840.

II.395 Hou YC, Janczuk A, Wang PG. Current Trends in the Development of Nitric Oxide Donors. *Curr Pharm Des* **1999**, *5* (6), 417–441.

II.396 Paul V, Ekambaram P. Involvement of Nitric Oxide in Learning & Memory Processes. *Indian J Med Res* **2011**, *133* (5), 471–478.

II.397 Rickard NS, Gibbs ME. Hemispheric Dissociation of the Involvement of NOS Isoforms in Memory for Discriminated Avoidance in the Chick. *Learn Mem* **2003**, *10* (5), 314–318.

II.398 Bolaños JP, Almeida A. Roles of Nitric Oxide in Brain Hypoxia-Ischemia. *Biochim Biophys Acta* **1999**, *1411* (2–3), 415–436.

II.399 Murphy S, Simmons ML, Agullo L, Garcia A, Feinstein DL, Galea E, Reis DJ, Minc-Golomb D, Schwartz JP. Synthesis of Nitric Oxide in CNS Glial Cells. *Trends Neurosci* **1993**, *16* (8), 323–328.

II.400 Yildiz Akar F, Ulak G, Tanyeri P, Erden F, Utkan T, Gacar N. 7-Nitroindazole, a Neuronal Nitric Oxide Synthase Inhibitor, Impairs Passive-Avoidance and Elevated plus-Maze Memory Performance in Rats. *Pharmacol Biochem Behav* **2007**, *87* (4), 434–443.

II.401 Garthwaite J, Boulton CL. Nitric Oxide Signaling in the Central Nervous System. *Annu Rev Physiol* **1995**, *57*, 683–706.

II.402 Dawson VL, Dawson TM, London ED, Bredt DS, Snyder SH. Nitric Oxide Mediates Glutamate Neurotoxicity in Primary Cortical Cultures. *Proc Natl Acad Sci USA* **1991**, *88* (14), 6368–6371.

II.403 Dawson VL, Dawson TM, Bartley DA, Uhl GR, Snyder SH. Mechanisms of Nitric Oxide-Mediated Neurotoxicity in Primary Brain Cultures. *J Neurosci* **1993**, *13* (6), 2651–2661.

II.404 dos Reis EA, de Oliveira LS, Lamers ML, Netto CA, Wyse AT. Arginine Administration Inhibits Hippocampal Na(+),K(+)-ATPase Activity and Impairs Retention of an Inhibitory Avoidance Task in Rats. *Brain Res* **2002**, *951* (2), 151–157.

II.405 Schulz JB, Matthews RT, Beal MF. Role of Nitric Oxide in Neurodegenerative Diseases. *Curr Opin Neurol* **1995**, *8* (6), 480–486.

II.406 Bolaños JP, Almeida A, Stewart V, Peuchen S, Land JM, Clark JB, Heales SJ. Nitric Oxide-Mediated Mitochondrial Damage in the Brain: Mechanisms and Implications for Neurodegenerative Diseases. *J Neurochem* **1997**, *68* (6), 2227–2240.

II.407 Sato S, Tominaga T, Ohnishi T, Ohnishi ST. EPR Spin-Trapping Study of Nitric Oxide Formation during Bilateral Carotid Occlusion in the Rat. *Biochim Biophys Acta* **1993**, *1181* (2), 195–197.

II.408 Tominaga T, Sato S, Ohnishi T, Ohnishi ST. Potentiation of Nitric Oxide Formation Following Bilateral Carotid Occlusion and Focal Cerebral Ischemia in the Rat: In Vivo Detection of the Nitric Oxide Radical by Electron Paramagnetic Resonance Spin Trapping. *Brain Res* **1993**, *614* (1–2), 342–346.

II.409 Beppu K, Sasaki T, Tanaka KF, Yamanaka A, Fukazawa Y, Shigemoto R, Matsui K. Optogenetic Countering of Glial Acidosis Suppresses Glial Glutamate Release and Ischemic Brain Damage. *Neuron* **2014**, *81* (2), 314–320.

II.410 Dawson VL, Dawson TM. Nitric Oxide Neurotoxicity. *J Chem Neuroanat* **1996**, *10* (3–4), 179–190.

II.411 Almeida A, Heales SJ, Bolaños JP, Medina JM. Glutamate Neurotoxicity Is Associated with Nitric Oxide-Mediated Mitochondrial Dysfunction and Glutathione Depletion. *Brain Res* **1998**, *790* (1–2), 209–216.

II.412 Radi R, Beckman JS, Bush KM, Freeman BA. Peroxynitrite Oxidation of Sulfhydryls. The Cytotoxic Potential of Superoxide and Nitric Oxide. *J Biol Chem* **1991**, *266* (7), 4244–4250.

Chapter III.

Employed methodologies.

rationale

The main idea behind my PhD project is to combine some aspects of neurosciences and synthetic biology. Given that these are two different and separate fields, each has very specific methodologies that might seem foreign to field-outsiders. So, for clarity and to ensure that more people are able to understand the work here described, this chapter will highlight details of different used techniques.

nanoscience and synthetic biology techniques

Fabricating the astrosome

Among the many film fabrication techniques, layer-by-layer (LbL) deposition is one of the most widely used to coat and functionalize materials.[III.1] In its classical form, LbL relies on the diffusion-driven sequential deposition of oppositely charged polymers or other materials separated by washing steps, where the assembly is exposed to a solution of a given polymer, creating a new layer.[III.1,2] In very broad terms, the LbL process can be summarized as a cycle of positive coating – wash – negative coating – wash.[III.3]

The interaction between the different layers of the assembly depends on different factors. In the first place, given that this technique relies on ionic charge, electrostatic attraction between polymers plays a major role in ensuring the interaction and stability of two consecutive layers, while electrostatic repulsion within the same polymer limits the rate of adsorption of a given layer, allowing for the formation of very thin polymer layers.[III.2] Nonetheless, this type of interaction does not fully explain LbL. Other types of interaction have to be considered, such as hydrophobic attraction between nonpolar regions,[III.2] and charge transfer interactions between non-ionic materials that have electron-accepting or electron-donating groups.[III.4] Interestingly, while electrostatic interactions are always considered as the driving force for LbL assembly, a thermodynamic analysis of the assembly process points to close-range hydrophobic attraction as the most important factor for layer interaction.[III.2]

With the popularization and wider use of LbL, different protocols have arisen, competing with the canonical diffusion by immersion, yielding films with different physical and chemical properties, as recently thoroughly reviewed.[III.1] Regardless of the used protocol, LbL is a simple and cheap technique,[III.2] with nearly endless flexibility, since

virtually any material can be used to form a layer, including polycations, polyanions, metals, nanoparticles, lipids, proteins, nucleic acids, etc.,[III.1] and tight control over layer thickness, which can be controlled down to 1 nm.[III.5] Due to the overwhelming advantages of LbL over other film fabrication techniques, LbL has been used to create both 2D and 3D assemblies[III.5] in very diverse fields, with applications in proteomics,[III.6] material science,[III.7] biomedicine,[III.1,5] among others.

To characterize the and ensure the successful layer deposition in the microreactors, several methods can be used, such as visual color change, fluorescent microscopy, transmission electron microscopy (TEM), ζ-potential (ZP) determination, and quartz crystal microbalance with dissipation monitoring (QCM-D). While visual and microscopy techniques are widely used among different research areas, ZP and QCM-D are more specific to synthetic biology. Those two methods are explained below.

Exploring surface charge

ζ-potential (ZP) measurement is a light scattering technique that allows for the determination of the surface charge of a colloidal particle or assembly.[III.8] While the actual physical surface charge of a particle cannot be directly determined, specific electrostatic interactions occur between the solid particle and dispersant liquid,[III.9] which can be used as an estimation of the surface charge. Specifically, when a charged particle is in an aqueous solution, the ions in the dispersant will interact with the particle surface, generating an ionic electric double layer (EDL).[III.10] The EDL consists of two main regions, distinguishable by their ionic composition and interaction strength. The inner layer, also called the Stern layer, is enriched with ions of opposite charge in relation to the particle. The ions in the Stern layer are firmly attached to the particle and move with it in the presence of an electric field.[III.9] The outer layer is called the diffuse layer and is composed of ions more loosely attached to the assembly. Within the diffuse layer, a theoretical boundary is defined – the slipping plane. The slipping plane represents the limit between ions that move with the particle and ions in the surrounding dispersant, that will not move.[III.9] The difference in potential between the stationary outer ions and the electrophoretically active particle and EDL at the slipping plane is called the ZP[III.8] and can be used as a proxy to monitor particle charge.

Ensuring layer interaction

Another method for evaluating the successful interaction between different materials is quartz crystal microbalance with dissipation monitoring (QCM-D). This method relies on acoustic sensing, using a thin quartz crystal between two electrodes,[III.11] and allows for the measurement of small changes in mass brought upon by the adsorption of different materials onto the crystal.[III.12] When an alternating current is supplied to those electrodes, the crystal will oscillate in its defined acoustic resonance frequency.[III.13] If the current is then turned off, the oscillation will decay in an exponential manner, which allows for the determination of the energy dissipation factor.[III.13] With this setup, by allowing different materials to adsorb onto the crystal, two parameters can be extracted: the change in acoustic resonance frequency (Δf) and the change in the energy dissipation factor (ΔD). The first parameter is associated with changes in crystal thickness or mass, where a higher frequency can be translated into a higher thickness or more successfully adsorbed layers, and the second is related to the viscoelastic properties of the crystal.[III.14] A higher dissipation factor is associated with higher sample softness, resulting from structural changes brought upon by different adsorbed materials on the crystal surface.[III.14]

Protecting enzymes

Within the field of drug delivery, liposomes are one of the most versatile and widely used structures due to their biocompatibility, ability to entrap both hydrophilic and hydrophobic molecules, and possibility to fine-tune their size and surface chemistry.[III.15] Liposomes are lipid vesicles, composed of at least one lipid bilayer that surrounds an aqueous solution core.[III.16] The lipid bilayer is created by the self-assembly of phospholipids, either natural or synthetic, upon exposure to an aqueous solution.[III.17] Depending on the number of concentric lipid bilayers, liposomes can be classified as unilamellar or multilamellar vesicles, which are more adequate to entrap hydrophilic or hydrophobic molecules, respectively,[III.18] since hydrophilic content can be loaded into the liposomal core and hydrophobic content can be contained inside the lipid bilayer.[III.17] Other than the flexibility in substrate choice, liposomes can be tailored by adjusting the lipid composition of the bilayer, which allows for the fabrication of differently permeable liposomes with well-defined rigidity and different surface charge.[III.19]

Interestingly, some types of liposomes are able to change their permeability in response to external stimuli, such as temperature or pH changes.[III.17]

Liposomes are important structures in the field of encapsulated catalysis since they allow for the successful incorporation of enzymes in microreactors. When using the LbL technique, for instance, adsorbing an enzyme directly onto an interacting polymer can lead to protein misfolding or blockage of the catalytic or binding sites.[III.20] Entrapping the enzyme in a liposome bypasses these issues, since the solubility of the enzyme in the aqueous solution core preserves its structure and activity.[III.21] Furthermore, entrapping enzymes in liposomes can even enhance the enzymatic activity, by creating a confined microenvironment where substrates and products can reach the enzymes faster and where the enzymes are protected against proteolysis, inhibitors, or denaturating agents.[III.22,23]

Assessing size

In order to fully characterize the liposomes and measure their diameter, liposome size can be determined using dynamic light scattering (DLS). This technique analyzes the size distribution of nanoparticles in suspension.[III.24] Briefly, a laser is shot through the sample and nanoparticle size is then mathematically determined, based on the premise that nanoparticles dispersed in an aqueous solution will scatter incident light proportionally to their radii.[III.25]

neuroscience techniques

Determining cell viability

Cell counting kit-8 (CCK) is a very simple and versatile cell viability assay. Similarly to other cell viability assays, CCK is able to quantify cell viability in an index between 0 and 1 (or 0 and 100%),[III.26] by reacting with cellular metabolism and generating a colored product in a proportional manner to the amount of healthy cells.[III.27] Specifically, the CCK solution contains a tetrazolium salt, 2-(2-methoxy-4-nitrophenyl)-3-(4-nitrophenyl)-5-(2,4-disulfophenyl)-2*H*-tetrazolium (WST-8), that is able to react with endogenous NAD(P)H, leading to its reduction to WST-8 formazan.[III.28] NAD(P)H and consequent WST-8 formazan production can be used as proxies for cell viability since

these compounds echo the activity level of NAD(P)H-dependent oxidoreductase enzymes, which play a central role in cellular metabolism[III.29] and reflect the bioenergetic and redox status of the cell.[III.30] After incubating the cells with WST-8 for 2 h, the colored end product present in cell culture medium can be measured by its absorbance at 450 nm.

Measuring membrane integrity

The lactate dehydrogenase (LDH) release assay can be used as tool to measure cell membrane integrity. LDH is a cytosolic enzyme that exists in most eukaryotic cells and is released into the cell medium upon membrane damage.[III.31] The activity of this enzyme in cell culture supernatant will then be proportional to the number of cells with damaged membrane, i.e., in the process of cell death. This activity can be measured when the cell medium is incubated with lactate, NAD^+, tetrazolium salt (INT), and the enzyme diaphorase via the absorbance at 490 nm, which corresponds to the product formazan,[III.31] generated according to the following reactions:

$$\text{Lactate} + NAD^+ \xrightarrow{\text{LDH}} \text{Pyruvate} + NADH$$

$$\text{INT} + NADH \xrightarrow{diaphorase} \text{Formazan} + NAD^+$$

Thus, measuring formazan production in cell medium of cells incubated with a lysis agent and cell medium of healthy control cells, it is possible to obtain a positive and negative control, respectively. This allows for the quantification of the general membrane integrity of cells exposed to any other stimuli, by comparing to these controls.

Probing neuronal activity

To explore the capacity of the astrosomes to control neuronal communication, it is indispensable to be able to measure said activity. Neurons are electrically excitable cells that communicate electrochemically via synapses.[III.32] In general, neurons receive chemical inputs through their dendrites and soma, triggering an electrical signal, called an action potential, that travels across those structures until the end of the axon, where it prompts the release of neurotransmitters onto the synaptic space.[III.33] The transformation from chemical signal into an electrical one occurs due to neurotransmitters binding to their postsynaptic receptors, leading to cation influx into the postsynaptic neuron and consequent depolarization of its membrane.[III.34] Importantly, the action potential is an all-or-nothing signal. It is known that the resting membrane potential of a

neuron is around –70 mV and the threshold for action potential propagation is around –55 mV.[III.35] Thus, if, over a very short period of time, the cation influx is strong enough for the membrane potential to reach the threshold value, that neuron will fire a stereotyped signal, that does not change its wave parameters regardless of magnitude of membrane depolarization, being only able to increase in frequency.[III.36]

Given the physical nature of neuronal signaling, electrophysiology has arisen as a field to measure changes in voltage and electric current resulting from neuronal activity in cell culture, brain slices, or even *in vivo*.[III.37,38] One modality of electrophysiological recordings consists of measuring extracellular local field potentials (LFP), which are transient extracellular signals resulting from the integrated and synchronous activity of neurons surrounding an electrode.[III.39] By measuring electrically how a neuronal network behaves or responds to external electrical stimulation, it is possible to compare the impact of different stimuli or conditions in terms of neuronal communication, health, and network connectivity.

To achieve a high-definition LFP measurement, a very promising and attractive device is the microelectrode array (MEA). MEA systems are interfaces between neural networks and electronic circuitry, containing multiple microelectrodes that are able to not only read neuronal signals, but also to deliver external electrical stimuli to the local neural network.[III.40] For *in vitro* applications, MEA systems can contain 10–100 microelectrodes, with diameters around 5–50 µm,[III.41] and can be used to probe electrical activity of cultured neurons or brain slices.[III.40]

With this technology, it is possible to obtain a high-resolution measurement of local voltage values, which allows for the identification of LFP.[III.39,42] Analyzing this data with computational tools and algorithms then leads to the extraction of important parameters of the neuronal response, such as the amplitude (how large is the voltage change compared to baseline) and slope (how fast is the response) of the LFP.[III.43,44] These parameters can change in different conditions or pathologies and provide insight on the health, function, and connectivity of a given neuronal network.[III.45,46]

chapter III references

III.1 Richardson JJ, Björnmalm M, Caruso F. Technology-Driven Layer-by-Layer Assembly of Nanofilms. *Science* **2015**, *348* (6233), aaa2491.

III.2 Kotov NA. Layer-by-Layer Self-Assembly: The Contribution of Hydrophobic Interactions. *Nanostructured Mater* **1999**, *12* (5), 789–796.

III.3 Decher G. Fuzzy Nanoassemblies: Toward Layered Polymeric Multicomposites. *Science* **1997**, *277* (5330), 1232–1237.

III.4 Shimazaki Y, Mitsuishi M, Ito S, Yamamoto M. Preparation of the Layer-by-Layer Deposited Ultrathin Film Based on the Charge-Transfer Interaction. *Langmuir* **1997**, *13* (6), 1385–1387.

III.5 Ai H, Jones SA, Lvov YM. Biomedical Applications of Electrostatic Layer-by-Layer Nano-Assembly of Polymers, Enzymes, and Nanoparticles. *Cell Biochem Biophys* **2003**, *39* (1), 23.

III.6 Wijeratne S, Liu W, Dong J, Ning W, Ratnayake ND, Walker KD, Bruening ML. Layer-by-Layer Deposition with Polymers Containing Nitrilotriacetate, A Convenient Route to Fabricate Metal- and Protein-Binding Films. *ACS Appl Mater Interfaces* **2016**, *8* (16), 10164–10173.

III.7 Tang Z, Kotov NA, Magonov S, Ozturk B. Nanostructured Artificial Nacre. *Nat Mater* **2003**, *2* (6), 413–418.

III.8 Bhattacharjee S. DLS and Zeta Potential - What They Are and What They Are Not? *J Control Release* **2016**, *235*, 337–351.

III.9 Salgin S, Salgin U, Bahadir S. Zeta Potentials and Isoelectric Points of Biomolecules: The Effects of Ion Types and Ionic Strengths. *Int J Electrochem Sci* **2012**, *7*, 12404–12414.

III.10 Montes Ruiz-Cabello FJ, Trefalt G, Maroni P, Borkovec M. Electric Double-Layer Potentials and Surface Regulation Properties Measured by Colloidal-Probe Atomic Force Microscopy. *Phys Rev E Stat Nonlin Soft Matter Phy* **2014**, *90* (1), 012301.

III.11 Johannsmann D. Studies of Viscoelasticity with the QCM. In *Piezoelectric Sensors*; Steinem C, Janshoff A, Eds.; Springer Series on Chemical Sensors and Biosensors; Springer-Verlag: Berlin, Germany, **2007**; pp 49–109.

III.12 Chen Q, Xu S, Liu Q, Masliyah J, Xu Z. QCM-D Study of Nanoparticle Interactions. *Adv Colloid Interface Sci* **2016**, *233*, 94–114.

III.13 Dixon MC. Quartz Crystal Microbalance with Dissipation Monitoring: Enabling Real-Time Characterization of Biological Materials and Their Interactions. *J Biomol Tech* **2008**, *19* (3), 151–158.

III.14 Johannsmann D. Viscoelastic, Mechanical, and Dielectric Measurements on Complex Samples with the Quartz Crystal Microbalance. *Phys Chem Chem Phys* **2008**, *10* (31), 4516–4534.

III.15 Abu Lila AS, Ishida T. Liposomal Delivery Systems: Design Optimization and Current Applications. *Biol Pharm Bull* **2017**, *40* (1), 1–10.

III.16 Lamichhane N, Udayakumar TS, D'Souza WD, Simone CB, Raghavan SR, Polf J, Mahmood J. Liposomes: Clinical Applications and Potential for Image-Guided Drug Delivery. *Molecules* **2018**, *23* (2), 288.

III.17 Lee Y, Thompson DH. Stimuli-Responsive Liposomes for Drug Delivery. *Wiley Interdiscip Rev Nanomed Nanobiotechnol* **2017**, *9* (5), e1450.

III.18 Bozzuto G, Molinari A. Liposomes as Nanomedical Devices. *Int J Nanomedicine* **2015**, *10*, 975–999.

III.19 Akbarzadeh A, Rezaei-Sadabady R, Davaran S, Joo SW, Zarghami N, Hanifehpour Y, Samiei M, Kouhi M, Nejati-Koshki K. Liposome: Classification, Preparation, and Applications. *Nanoscale Res Lett* **2013**, *8* (1), 102.

III.20 Caruso F, Schüler C. Enzyme Multilayers on Colloid Particles: Assembly, Stability, and Enzymatic Activity. *Langmuir* **2000**, *16* (24), 9595–9603.

III.21 Sakr OS, Borchard G. Encapsulation of Enzymes in Layer-by-Layer (LbL) Structures: Latest Advances and Applications. *Biomacromolecules* **2013**, *14* (7), 2117–2135.

III.22 Zhu H, McShane MJ. Macromolecule Encapsulation in Diazoresin-Based Hollow Polyelectrolyte Microcapsules. *Langmuir* **2005**, *21* (1), 424–430.

III.23 Tiourina OP, Antipov AA, Sukhorukov GB, Larionova NI, Lvov Y, Möhwald H. Entrapment of α-Chymotrypsin into Hollow Polyelectrolyte Microcapsules. *Macromol Biosci* **2001**, *1* (5), 209–214.

III.24 Berne BJ, Pecora R. *Dynamic Light Scattering: With Applications to Chemistry, Biology, and Physics*; Dover Publications: New York, USA, **2000**.

III.25 Rademeyer P, Carugo D, Lee JY, Stride E. Microfluidic System for High Throughput Characterisation of Echogenic Particles. *Lab Chip* **2015**, *15* (2), 417–428.

III.26 Pegg DE. Viability Assays for Preserved Cells, Tissues, and Organs. *Cryobiology* **1989**, *26* (3), 212–231.

III.27 Ishiyama M, Miyazono Y, Sasamoto K, Ohkura Y, Ueno K. A Highly Water-Soluble Disulfonated Tetrazolium Salt as a Chromogenic Indicator for NADH as Well as Cell Viability. *Talanta* **1997**, *44* (7), 1299–1305.

III.28 Tominaga H, Ishiyama M, Ohseto F, Sasamoto K, Hamamoto T, Suzuki K, Watanabe M. A Water-Soluble Tetrazolium Salt Useful for Colorimetric Cell Viability Assay. *Anal Commun* **1999**, *36* (2), 47–50.

III.29 Stockert JC, Horobin RW, Colombo LL, Blázquez-Castro A. Tetrazolium Salts and Formazan Products in Cell Biology: Viability Assessment, Fluorescence Imaging, and Labeling Perspectives. *Acta Histochem* **2018**, *120* (3), 159–167.

III.30 Veskoukis AS, Margaritelis NV, Kyparos A, Paschalis V, Nikolaidis MG. Spectrophotometric Assays for Measuring Redox Biomarkers in Blood and Tissues: The NADPH Network. *Redox Rep* **2018**, *23* (1), 47–56.

III.31 Korzeniewski C, Callewaert DM. An Enzyme-Release Assay for Natural Cytotoxicity. *J Immunol Methods* **1983**, *64* (3), 313–320.

III.32 Palay SL. Synapses In The Central Nervous System. *J Biophys Biochem Cytol* **1956**, *2* (4), 193–202.

III.33 Rutecki P. Neuronal Excitability: Voltage-Dependent Currents and Synaptic Transmission. *J Clin Neurophysiol* **1992**, *9* (2), 195–211.

III.34 Purves D, Augustine GJ, Fitzpatrick D, Hall WC, LaMantia A-S, White LE. How Ionic Movements Produce Electrical Signals. In *Neuroscience*; Sinauer Associates: Sunderland, USA, **2001**; pp 29–32.

III.35 Barnett MW, Larkman PM. The Action Potential. *Pract Neurol* **2007**, *7* (3), 192–197.

III.36 Kalat JW. *Biological Psychology*, 12th edition; Cengage Learning: Boston, USA, **2016**.

III.37 Llinas RR. The Intrinsic Electrophysiological Properties of Mammalian Neurons: Insights into Central Nervous System Function. *Science* **1988**, *242* (4886), 1654–1664.

III.38 Assad JA, Berdondini L, Cancedda L, De Angelis F, Diaspro A, Dipalo M, Fellin T, Maccione A, Panzeri S, Sileo L. Brain Function: Novel Technologies Driving Novel Understanding. In *Bioinspired Approaches for Human-Centric Technologies*; Cingolani R, Ed.; Springer International Publishing: Cham, Switzerland, **2014**; pp 299–334.

III.39 Buzsáki G, Anastassiou CA, Koch C. The Origin of Extracellular Fields and Currents — EEG, ECoG, LFP and Spikes. *Nat Rev Neurosci* **2012**, *13* (6), 407–420.

III.40 Obien MEJ, Deligkaris K, Bullmann T, Bakkum DJ, Frey U. Revealing Neuronal Function through Microelectrode Array Recordings. *Front Neurosci* **2014**, *8*, 423.

III.41 Kim R, Joo S, Jung H, Hong N, Nam Y. Recent Trends in Microelectrode Array Technology for in Vitro Neural Interface Platform. *Biomed Eng Lett* **2014**, *4* (2), 129–141.

III.42 Anastassiou C, Buzsáki G, Koch C. Biophysics of Extracellular Spikes. In *Principles of Neural Coding*; Quiroga R, Panzeri S, Eds.; CRC Press: Boca Raton, USA, **2013**; pp 15–36.

III.43 Gray CM, Maldonado PE, Wilson M, McNaughton B. Tetrodes Markedly Improve the Reliability and Yield of Multiple Single-Unit Isolation from Multi-Unit Recordings in Cat Striate Cortex. *J Neurosci Methods* **1995**, *63* (1), 43–54.

III.44 Einevoll GT, Kayser C, Logothetis NK, Panzeri S. Modelling and Analysis of Local Field Potentials for Studying the Function of Cortical Circuits. *Nat Rev Neurosci* **2013**, *14* (11), 770–785.

III.45 Black BJ, Atmaramani R, Kumaraju R, Plagens S, Romero-Ortega M, Dussor G, Price TJ, Campbell ZT, Pancrazio JJ. Adult Mouse Sensory Neurons on Microelectrode Arrays Exhibit Increased Spontaneous and Stimulus-Evoked Activity in the Presence of Interleukin-6. *J Neurophysiol* **2018**, *120* (3), 1374–1385.

III.46 Zhang S, Song Y, Wang M, Xiao G, Gao F, Li Z, Tao G, Zhuang P, Yue F, Chan P, *et al*. Real-Time Simultaneous Recording of Electrophysiological Activities and Dopamine Overflow in the Deep Brain Nuclei of a Non-Human Primate with Parkinson's Disease Using Nano-Based Microelectrode Arrays. *Microsyst Nanoeng* **2018**, *4* (1), 1–9.

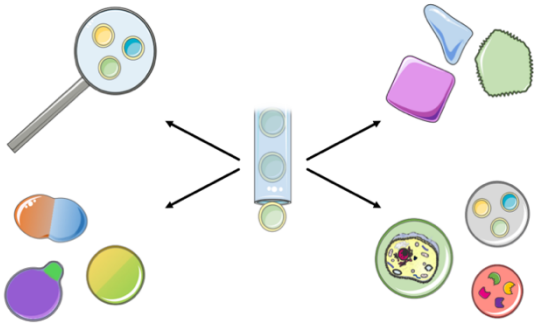
Chapter IV.

Specific methods in synthetic biology.

Droplet-microfluidics towards the assembly of advanced building blocks in cell mimicry

Armada-Moreira A, Taipaleenmäki E, Itel F, Zhang Y, Städler B

Nanoscale **2016**



While searching for the layer-by-layer (LbL) technique described above, I ventured into the world of synthetic biology techniques. Within that world, I considered using droplet microfluidics (D-μF) for my astrosomes – an idea that was dropped due to the advantages that LbL offered. Specifically, we encountered serious issues with the reproducibility of particles generated using D-μF. The size and shape of these particles varied beyond our control, and adding different polymers as capping layers further impacted particle shape. On the other hand, with LbL we were able to generate reproducible particles, all with the same shape, size, and polymer interactions. Regardless, while researching D-μF techniques and innovations, I was part of this publication: a mini-review focused on the advances in droplet microfluidics in the context of artificial cells and organelles.

In this publication, each author wrote a topic. Nanoparticles were explored by Essi Taipaleenmäki, Janus particles by Yan Zhang, biological cargo by Fabian Itel, and non-spherical particles by me, all under the supervision of Brigitte Städler. I was also responsible for the final figures and illustrations. Importantly, the illustrations in the rationale and introduction are my original creations.

publication information

Title. Droplet-microfluidics to assemble advanced building blocks in cell mimicry.

Authors. Adam Armada-Moreira, Essi Taipaleenmäki, Fabian Itel, Yan Zhang, Brigitte Städler.

Status of publication. Published.

Journal. Nanoscale 2016, 8 (47), 19510–19522.

DOI. 10.1039/c6nr07807a

JCR impact factor, quartile, and field. 7.367; Physics, Applied: Q1; Chemistry, Multidisciplinary: Q1; Nanoscience & Nanotechnology: Q1; Materials Science, Multidisciplinary: Q1.

Droplet-microfluidics to assemble advanced building blocks in cell mimicry

Armada-Moreira A[1,2,3], Taipaleenmäki E[1], Itel F[1], Zhang Y[1], Städler B[1]*

[1]Interdisciplinary Nanoscience Center (iNANO), Aarhus University, Aarhus, Denmark.
[2]Instituto de Farmacologia e Neurociências, Faculdade de Medicina, Universidade de Lisboa, Lisbon, Portugal.
[3]Instituto de Medicina Molecular, Faculdade de Medicina, Universidade de Lisboa, Lisbon, Portugal.
*Corresponding author.

Nanoscale **2016**, *8* (47), 19510–19522.

Abstract

Therapeutic cell mimicry is an approach in nanomedicine aiming at substituting for missing or lost cellular functions employing nature-inspired concepts. Pioneered decades ago, only now is this technology empowered with the arsenal of nanotechnological tools and ready to provide radically new solutions such as assembly of synthetic organelles and artificial cells. One of these tools is droplet microfluidics (D-μF), which provides the flexibility to generate cargo-loaded particles with tunable size and shape in a fast and reliable manner, an essential requirement in cell mimicry. This Minireview aims at outlining the developments in D-μF from the past four years focusing on the assembly of nanoparticles, Janus-shaped and other non-spherical particles as well as their loading with biological payload.

Introduction

Since its introduction in 2001,[IV.1] droplet microfluidics (D-μF) has developed into widely applied methods in diverse fields due to its versatility, reliability, low sample consumption, high throughput, etc. With the advent of companies selling microfluidic chips and accessories, D-μF has also become even more spread since access to micro- (or nano-) fabrication facilities became unnecessary.

In the context of nanomedicine and biology,[IV.2] D-μF has been applied for sensing,[IV.3] drug discovery,[IV.4] and assembly of micro/nanoparticles and reaction vessels. Therapeutic cell mimicry is an emerging field of research which aims at providing nature-inspired approaches to address biomedical challenges by substituting for missing or lost cellular function. The assembly of such mimics, including artificial organelles,[IV.5] artificial cells,[IV.6] and biological nanobots,[IV.7] requires access to flexible yet reliable fabrication methods, which can accommodate for the complexity of the natural role models in terms of size, shape, and function, among others. D-μF is such an approach that can fulfil these prerequisites, as recently reviewed for artificial cells by the deMello group.[IV.8] Traditional assembly methods such as the self-assembly of lipids and block copolymers into liposomes[IV.9,10] and polymersomes,[IV.5] respectively, or layer-by-layer based techniques[IV.11] have been successful in fabricating building blocks for cell mimicry. However, D-μF is uniquely amendable for diverse requirements in terms of sizes (from nanometer particles to large micrometer sized beads), shape, or type of loaded cargo.

The aim of this Minireview is to highlight the latest developments in D-µF which have the potential to provide innovative tools and methods to be applied in cell mimicry (**Figure IV.1**). Specifically, we will focus on the assembly of nanoparticles, Janus- and other non-spherical particles as well as the use of biological cargo. We will discuss their relevance and envisioned biomedical applications by providing selected examples from the past four years.

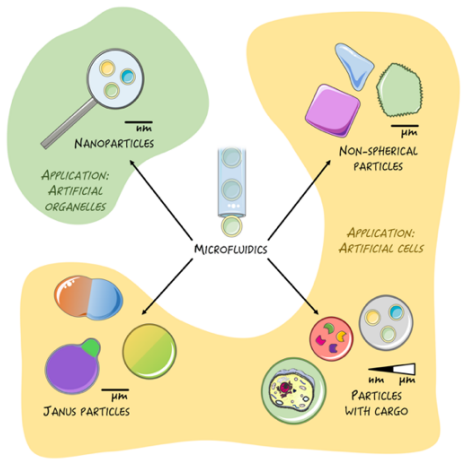


Figure IV.1. Cartoon illustrating the use of D-µF for the assembly of nanoparticles, Janus particles, and non-spherical particles as well as their loading with biological cargo and potential application in cell mimicry.

Nanoparticles

Artificial organelles are envisioned to be nano-sized entities with intracellular biocatalytic activity. Among the crucial prerequisites for their assembly is access to sub-300 nm-sized, colloidally stable, monodisperse nanoparticles. D-µF has been applied in the assembly of various kinds of polymeric,[IV.12,13] lipid-based,[IV.14,15] inorganic,[IV.16,17] and composite nanoparticles.[IV.18,19] While traditional macroscale methods often lack the precise control over the nucleation and growth processes that are required to produce nanoparticles with well-defined properties, D-µF allows for rapid and uniform heat and mass transfer via accurate control of fluids and their interfaces, leading to a more controlled and homogeneous reactive environment.[IV.20] A detailed discussion about what makes D-µF an appealing method for nanoparticle fabrication is available in an excellent review.[IV.20]

In recent years, the most favored fabrication technique for both polymer-[IV.12,13,21–27] and lipid-based[IV.14,15,28–32] nanoparticles has been the hydrodynamic flow focusing (HFF) approach. In HFF, polymers or lipids are dissolved in an organic solvent which is then hydrodynamically focused by two co-axial aqueous streams into a thin sheet (**Figure IV.2A**). This sheet of organic solvent diffuses into water until a critical concentration is reached, where the nanoparticles start to precipitate.

A variety of biodegradable polymers including poly(lactic-*co*-glycolic acid) (PLGA),[IV.13,24,25,27,33,34] alginate,[IV.21] chitosan,[IV.22,23,35] poly(lactic acid) (PLA),[IV.36,37] and polycaprolactone (PCL)[IV.36,38] have been used to fabricate nanoparticles in microfluidic devices for medical applications. Low flow ratio and fast mixing in HFF allowed for the one-step synthesis of drug-loaded polymeric nanoparticles with higher drug loading, smaller particle diameter, smaller size distribution and a slower and more sustained release rate of the drug compared to bulk synthesized nanoparticles. For instance, Majedi *et al.* reported a solvent-free synthesis of paclitaxel-loaded chitosan nanoparticles via HFF with loading efficiencies above 95%, with a 1.7-fold higher cellular uptake compared to the particles prepared by a bulk method

and the ability to hold their cargo in physiological pH until they reach the more acidic pH of a tumor environment.[IV.23] In a similar study, Hasani-Sadrabadi *et al*. utilized HFF to assemble paclitaxel-loaded hydrophobic-hydrophilic core-shell structures of dendritic polyethylene (dPE) and triblock copolymers.[IV.12] It was shown that, within the time period of two weeks, the nanoparticles formed at flow ratios of 0.03, 0.075, and 0.2 released 86%, 76%, and 98% of their cargo, respectively, while nanoparticles prepared by the bulk synthesis released almost 100% of the cargo (**Figure IV.2B**).

In addition to polymer-based nanoparticles, liposomes have also been widely applied in pharmaceutical and cosmetic industries.[IV.39] Microfluidic techniques for the preparation of liposomes have recently been critically reviewed by Carugo.[IV.39] To address demand for preparation techniques with a high throughput, Hood and DeVoe designed a microfluidic vertical flow focusing (VFF) device with an exceptionally high channel aspect ratio (100:1).[IV.15] This setting enabled the production of unilamellar, nearly monodisperse 80–200 nm liposomes with a production rate of 1.6 mg min^{-1} which was nearly two orders of magnitude higher than that of a traditional HFF device (**Figure IV.2C**). By applying a proper channel design, it is also possible to have several HFF regions in one chip.[IV.14,29] For instance, Conde *et al*. used a 10-inlet channel configuration to produce four parallel HFF regions.[IV.14] The set-up was used to fabricate liposomes loaded with magnetic nanoparticles. These magnetoliposomes had diameters between 90–220 nm and showed responsiveness to external magnetic field gradients. Such particles hold promise in targeted delivery of anticancer drugs[IV.40] and as contrast agents for magnetic resonance imaging.[IV.41]

Examples of lipid-polymer hybrid nanoparticles produced in D-μF have also emerged in the last four years.[IV.42–45] This new class of potential drug carriers enables the loading of a hydrophobic cargo in a polymer core, which also gives rigidity to the assembly, while an outer lipid shell prolongs the circulation half-life. Zhang *et al*. demonstrated the synthesis of PLGA nanoparticles coated with mono- and bilayered lipid shells by using a two-stage microfluidic chip (**Figure IV.2Di**).[IV.44] In the first stage of the chip, PLGA-nanoparticles or intermediate liposomes were produced by applying a typical HFF-geometry. These intermediate products were then guided via two separated channels to the second stage of the chip where a new inlet channel was introduced in the middle. All three channels combined formed a spiral synthesis channel. The second inlet channel was used to add either lipids to a PLGA-nanoparticle solution or PLGA to a liposome solution to form the final mono- and bi-layered nanoparticles, respectively. These nanoparticles, especially the less flexible monolayered ones, showed good cellular uptake and allowed for dual drug delivery via the encapsulation of doxorubicin in the PLGA-core and combretastatin A4 in the lipid shell for tumor growth inhibition *in vivo* (**Figure IV.2Dii**). A similar kind of multi-stage microfluidic setting was also employed to synthetize nanovesicles consisting of a water core loaded with hydrophilic drugs, a rigid PLGA-core and an outermost lipid layer to act as a safe and biocompatible nanocarrier for *in vivo* cancer treatment.[IV.45]

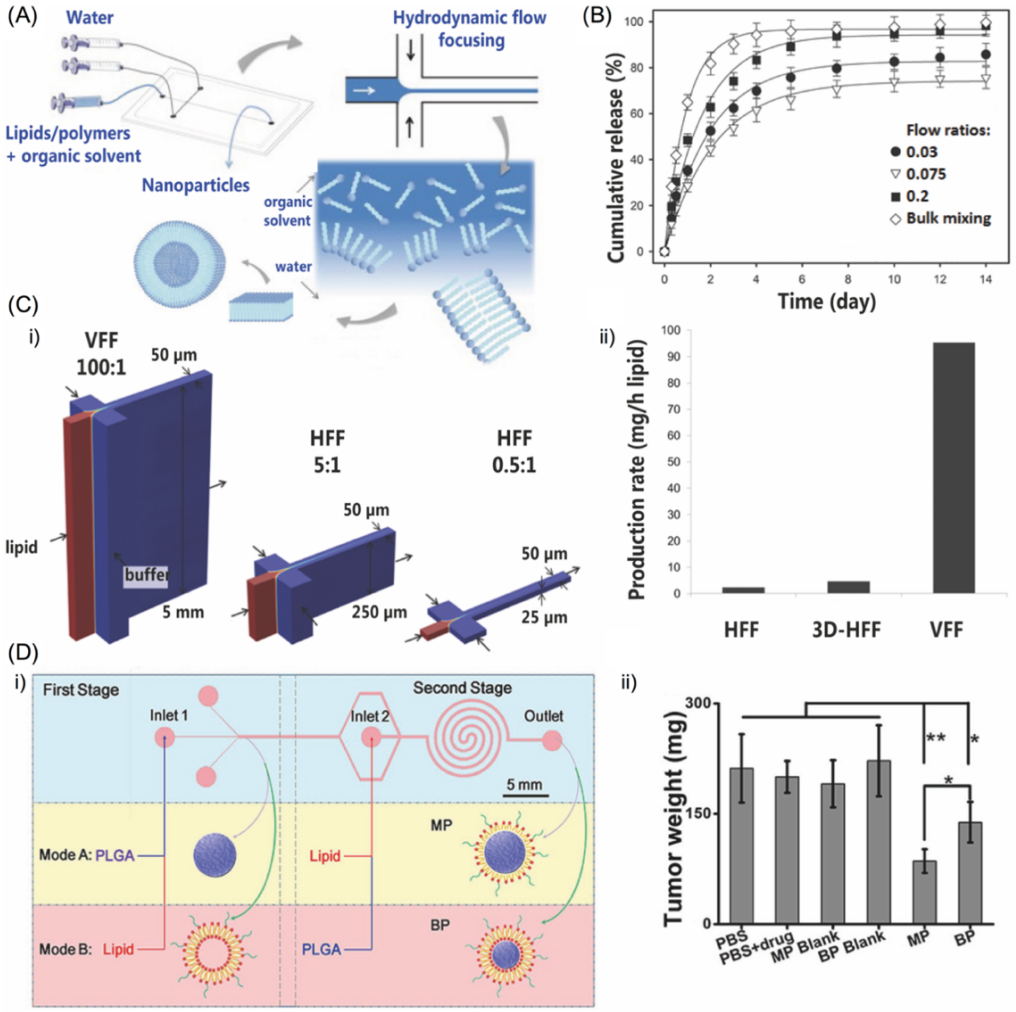


Figure IV.2. Nanoparticle assembly: (**A**) A schematic representation of a HFF set-up where an organic stream is focused into a narrow sheet by two aqueous streams. When the organic sheet mixes with aqueous solvent, nanoparticle precursors, originally dissolved in the organic phase, self-assemble into nanoparticles. Adapted from (IV.29) with permission from Elsevier. (**B**) A cumulative in vitro release of paclitaxel from dPE-based nanoparticles formed at different flow ratios by using HFF illustrating the sustained drug release of microfluidically fabricated nanoparticles. Adapted with permission from (IV.12). (**C**) (**i**) A schematic representation of a microfluidic VFF device with an exceptionally high channel aspect ratio of 100:1 compared with common HFF devices with channel aspect ratios of 5:1 and 0.5:1. Adapted with permission from (IV.15). (**ii**) Comparison of liposome production rates across various microfluidic methods illustrating that VFF enables the generation of liposomes at significantly higher rate than a planar HFF device. Reprinted with permission from (IV.15). (**D**) (**i**) A schematic representation of a two-stage microfluidic chip for the production of PLGA nanoparticles coated with mono- and bi-layered lipid shells. Stage one: PLGA nanoparticles or liposomes are formed via HFF; stage two: lipids or PLGA are introduced to produce mono- and bi-layered core-shell nanoparticles, respectively. Reprinted with permission from (IV.45). Copyright 2015 American Chemical Society. (**ii**) The effect of doxorubicin and combretastatin A4 loaded polymer-lipid nanoparticles with mono- (MP) and bi-layered (BP) lipid shells on tumor growth in vivo is shown. Reprinted with permission from (IV.44). Copyright 2015 American Chemical Society.

For the fabrication of inorganic nanomaterials, such as metallic nanocrystals and quantum dots, microfluidic systems are typically modified to produce a train of discrete droplets which contain the reaction solution.[IV.16,17,46–49] By doing so, the reaction volume is minimized and the reagent concentrations can be easily tuned by varying the droplet size.[IV.46] D-μF has also been presented as a new platform for scaling up the production of inorganic nanocrystals.[IV.50] These nanoparticles are useful not only in biomedicine but also in applications related to photonics, electronics, catalysis, energy conversion, environment protection and information storage, to mention a few.[IV.50] It was demonstrated recently that D-μF enabled not only a high-throughput synthesis, but also allowed for an *in situ* optical detection of the synthesis process when integrated with an online absorbance and fluorescence detection.[IV.48] By using this method, the authors were able to quantitatively measure the growth kinetics of lead-sulfide quantum dots with millisecond time resolution, which revealed a two-stage mechanism for the nanoparticle formation.

Apart from the direct production of nanoparticles, D-μF has also been used to manufacture innovative composite systems via encapsulation of nanoparticles. Recently, Araújo *et al*. developed a PLGA- and mesoporous silicon (PSi)-based composite system for oral delivery of two peptide drugs for the treatment of type 2 diabetes mellitus.[IV.51] The system was composed of an antidiabetic peptide, glucagon-like peptide-1 (GLP-1), loaded on PLGA or PSi nanoparticles which were further functionalized with mucoadhesive chitosan and cell penetrating peptides to enhance the delivery across intestinal endothelial cells protected by a mucus layer. These functionalized nanoparticles were further encapsulated within an enteric polymer hydroxypropylmethylcellulose acetylsuccinate (HPMC-AS) to protect the peptides from degradation. This was done in a microfluidic setting with flow-focusing geometry where functionalized nanoparticles along with the dipeptidyl peptidase 4 (DPP4) enzyme inhibitor were dissolved in ethyl acetate. Then, an aqueous solution of F127 was used to force the organic stream through a narrow orifice where high shear and capillary instability broke bubbles off the tip resulting in the formation of monodisperse particles. The drug delivery system was tested *in vivo* in a non-obese type 2 diabetes mellitus rat model and an increase in the hypoglycemic effects was observed.[IV.52]

Janus particles

Cell polarity, i.e., the asymmetric non-random arrangement of cellular components and structures, is a central feature of cells that allows them to perform specialized tasks such as neurotransmitter release in specialized sites and uptake in neurons,[IV.53] or asymmetric front–back polarity in migrating cells as they move towards attractive cues,[IV.54] among others. Although the biological relevance of cell polarity is tremendous,[IV.55] our group was recently the first one to consider this aspect in cell mimicry employing Janus-shaped particles.[IV.56] Janus particles possess asymmetrical spatial regions with physical and/or chemical differences, as recently discussed in two reviews,[IV.57,58] which is the fundamental prerequisite for polarity. Compared to other assembly methods of Janus particles (e.g., pickering emulsions,[IV.59] self-assembly,[IV.60]

surface modification,[IV.61] particle lithography,[IV.62] photo-polymerization,[IV.63] biphasic electro-jetting/spraying,[IV.64] etc.), D-μF-based assembly benefits from the highly adjustable nature of microfluidic devices, providing a flexible platform to construct Janus particles from monomers,[IV.65] polymers,[IV.66] hydrogels,[IV.67] or nanoparticles,[IV.68] equipped with multiple functions or multiple components.[IV.69,70] It is straightforward to assemble Janus particles by D-μF using either two miscible[IV.71–75] or immiscible regions,[IV.76] followed by parallel crosslinking or polymerization of the building blocks. Furthermore, Janus particles can be assembled by phase separation of mixed droplets employing different driving forces including temperature,[IV.77] co-polymerization,[IV.78] solvent diffusion,[IV.79] or gravity.[IV.79,80]

When assembling Janus droplets using two miscible phases, the main challenges are the risk of their mixing and breaking the Janus configuration due to the interface convection effect. The major preventive strategies are controlling the size of droplet by adjusting the viscosities of the two dispersed phases, matching the flow rates of both continuous phase and disperse phase, and increasing the solidifying rate of the Janus droplets.[IV.67,71,75] Alternatively, when the Janus particles are assembled based on two immiscible phases, undesired mixing can be inherently avoided. An interesting example in this context was reported by Khan *et al*. They constructed amphiphilic poly(acrylamide) (PAAm)/poly(methyl acrylate) (PAM) Janus particles from hydrophilic acrylamide and hydrophobic methyl acrylate monomers through UV-initiated polymerization (**Figure IV.3A**).[IV.65] In those Janus particles, hydrophobic ketoprofen and hydrophilic sodium fluorescein model cargo were encapsulated separately in two areas. In this system, the flow rates of the two dispersed phases and the presence of surfactants in the dispersed phase were the key factors for yielding asymmetric droplet/particle structures. In the absence of surfactants and together with high flow rates of the hydrophobic monomer phase, “acorn-like” Janus particle were obtained. On the other hand, when there was a low amount of surfactant (0.75%) in the hydrophilic dispersed phase, Janus particles were obtained. In addition, they managed to form “helmet-like” and “UFO-like” Janus particles by changing the acrylamide monomer composition. Phase separation of a single droplet is a common strategy for Janus particle formation. The following section highlights a selection of new strategies which are particularly interesting in the context of this Minireview. Lone *et al.* applied a light- and thermo-responsive random copolymer of poly(isopropyl acrylamide) (pNIPAAm) modified with fluorescent dye and photochromic spironaphthoxazine (named poly(NIPAAm-co-SPO-co-fluorophore)) to assemble Janus particles with a poly(NIPAAm-co-SPO-co-fluorophore) copolymer part and a hollow poly(N,N-methylenebisacrylamide) (PMBA) part.[IV.78] First, light-responsive polymer poly(NIPAAm-co-SPO-co-fluorophore) and MBA-monomer mixed droplets were formed, followed by UV-exposure which led to phase separation of the copolymer poly(NIPAAm-co-SPO-co-fluorophore) to one side of the droplet while the MBA monomers in the droplets polymerized at the water/oil interface to form a hollow structure with a PMBA shell (**Figure IV.3B**).

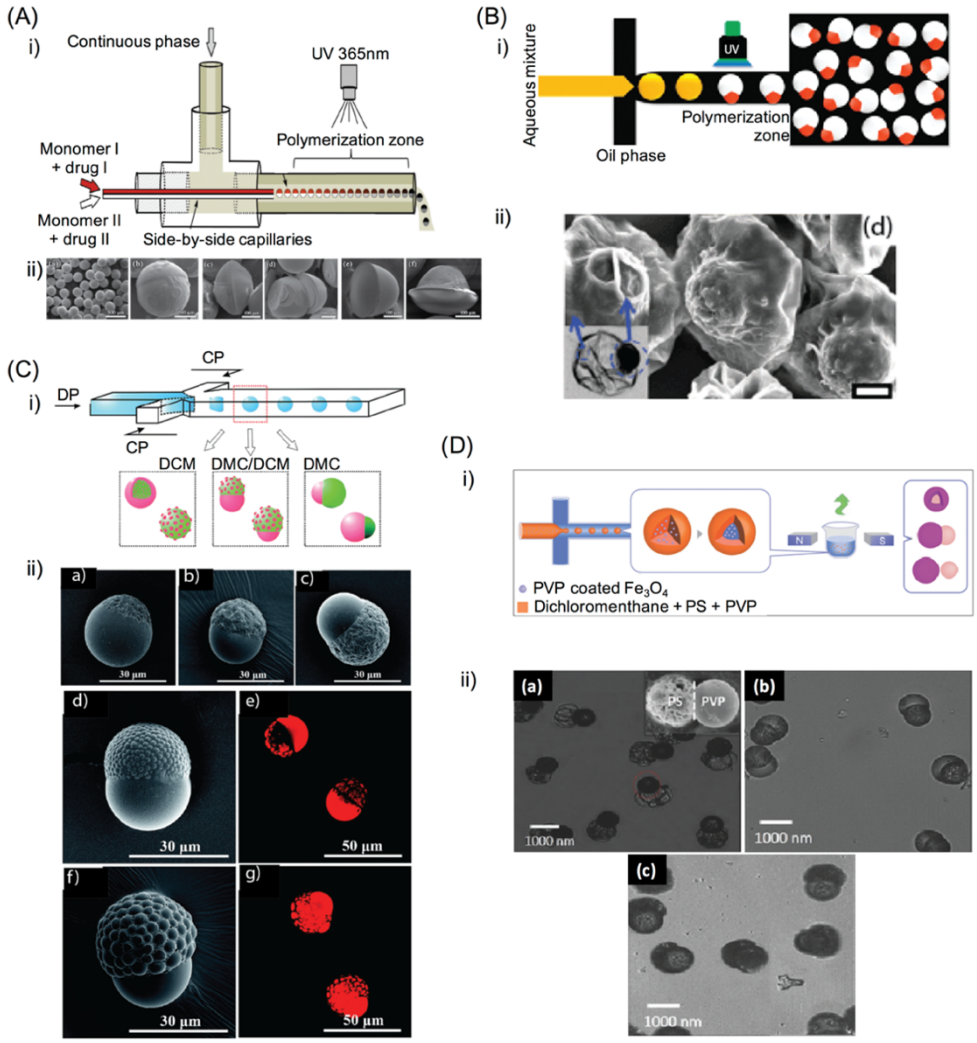


Figure IV.3. Janus-shaped particles: (**A**) (**i**) Schematic of cargo loaded Janus poly(acrylamide)/poly(methyl acrylate) particles fabricated from side-by-side capillary-based microfluidic setup; (**ii**) SEM image of Janus PAAm/PMA particles in different morphologies. Reprinted with permission from (IV.65). (**B**) (**i**) Schematic of the poly(NIPAAm-co-SPO-co-fluorophore)/PMBA Janus particle forming process. (**ii**) Scanning electron micrograph of dried Janus particles with two distinct regions (inset: optical image of the Janus particle). Reprinted with permission from (IV.78). (**C**) (**i**) Schematic illustration of Janus PLGA/PCL particles formation through solvent diffusing reduced phase separation. (**ii**) SEM and CLSM images of Janus PLGA/PCL particles made from different solvent, PLGA, and PCL ratios. Reprinted with permission from (IV.81). (**D**) (**i**) Schematic illustration of the Janus PS/Fe_3O_4@PVP particle formation. (**ii**) TEM images of PS/Fe_3O_4@PVP, PS/Fe_3O_4@PAA and PS/Fe_3O_4@PEG Janus particles. Reprinted with permission from (IV.82).

In another example, Cao and co-workers fabricated PLGA and PCL (patchy) Janus particles by phase separation.[IV.81] The authors controlled the particle architectures by adjusting the polymer ratios and the solvent compositions (**Figure IV.3C**). When dimethyl carbonate (DMC) was used as sole solvent, due to the complete phase separation of PLGA and PCL during

the particle solidification, Janus particles with clear demarcation between two regions were obtained. However, when a dichloromethane and DMC mixture was used, patchy Janus particles with a smooth PLGA hemisphere and a rough PCL hemisphere were formed. In another report, Janus particles with a polystyrene (PS) part and a poly(vinylpyrrolidone) (PVP) containing Fe_3O_4 part (named PS/Fe_3O_4@PVP Janus particle) were assembled by solvent diffusion-induced phase separation (**Figure IV.3D**).[IV.82] The mixture droplets, containing PS, PVP, and PVP-coated Fe_3O_4 nanoparticles (NPs) in dichloromethane, were first formed. Following on, water diffused into the droplets and formed reversed PVP and NPs tiny droplets, followed by coalescence of those tiny droplets. During this process, Fe_3O_4@PVP were located on one side of the droplet under magnetic field, while the hydrophilic PVP with located NPs totally phase separated from hydrophobic PS regions with the assist of solvent evaporation, and thus PS/Fe_3O_4@PVP Janus particles were obtained. Replacing PVP with PAA or polyethylene glycol (PEG) allowed for the assembly of other amphiphilic Janus particles. These Janus particles were used to assemble hydrophilic or hydrophobic monolayers for cell adhesion studies.

Non-spherical particles

In nature, particles exist in several different shapes and sizes. In fact, this shape diversity is crucial for the optimization of different functions. When considering artificial particles, however, most are spherical, due to fabrication techniques generally involving emulsion and suspension polymerization,[IV.83] where surface tension between the polymer and surrounding solutions comes into play, leading to contact area minimization and, thus, the creation of spherical particles.[IV.84] Despite this fact, particle morphology plays a very important role in particle function, and is a main factor in several applications such as intracellular particle delivery,[IV.85] particle stability in emulsions,[IV.86] Brownian motion,[IV.87] three-dimensional tissue formation,[IV.88] as well as drug delivery, bioimaging, and biomimetics.[IV.89] For a recent comprehensive review on non-spherical particles, their fabrication techniques, and their applications, the reader is referred to a review by Mathaes and colleagues.[IV.90] Indeed, non-spherical particles offer larger surface areas, display anisotropic behavior in response to external stimuli[IV.91] and can, for example, be packed more densely than spherical particles.[IV.92] Numerous techniques can be used to produce non-spherical particles. Batch methods include dispersion and precipitation polymerization, copolymer self-assembly, and phase-separated polymer precipitation as recently reviewed by Wang and co-workers.[IV.34] These methods, however, lack control over the precise shape and size of the produced particles. Microfluidic systems solve this problem by allowing a stronger control over particle characteristics. With microfluidics, non-spherical particles can be generated from spherical ones via simple processing steps such as arrested coalescence, asymmetric polymer solidification, polymerization in microfluidic flow, and evaporation-driven clustering as discussed in two recent reviews.[IV.84,93]

There have been, in the last few years, several innovations in the context of differently shaped particles fabricated with microfluidics, including the production of bullet-shaped

magnetic microparticles useful for drug delivery and cell-based therapies,[IV.94] biconcave microlenses for microoptics,[IV.95] differently shaped particles ranging from spheres to rods using a magnetic-field-assisted method of fabrication,[IV.83] and hollow microcapsules capable of maintaining complex rod-like shapes.[IV.96] A detailed discussion on this subject can be found in specific reviews.[IV.69,93] Specifically for biotechnological applications, numerous advances have been accomplished over the last couple of years and a selection will be highlighted here. Cheng and collaborators developed a microfluidic technique to create anisotropic colloidal crystal particles (CCPs), using silica nanoparticles and hexadecane, and achieving different colors by using different concentrations of PEG diacrylate (PEG-DA) (**Figure IV.4A**). With this technique, it was possible to generate anisotropic non-close-packed CCPs by photo-polymerizing droplet templates in a capillary. Applying a thermal process to these non-close-packed CCPs, the group created anisotropic close-packed CCPs. The authors showed that this technique could be used to generate CCPs with several sizes, colors, and shapes (rods, cuboids, and disks) with dimensions in the range of 200 µm to 1 mm. These crystals were employed as a marker for DNA multiplex detection as an example for a high-throughput assay.[IV.97] Notably, this is one of the rare examples where the authors went beyond the assembly and characterization of non-spherical particles, but illustrated their relevance in an nanomedicine-related application. In a different effort, Hu and collaborators created mushroom-shaped alginate/pNIPAAm microgels with tunable size and shape, originated from 300 µm spherical droplets (**Figure IV.4B**). For the fabrication of these particles, Hu and collaborators used a glass capillary microfluidic device, with which they created single water-in-oil emulsions. These alginate/pNIPAAm emulsions were then collected in a solution containing barium acetate and different concentrations of glycerol. By adjusting the glycerol concentration and the initial droplet size, the authors were able to fully control the final particle size and morphology. These non-spherical, mushroom-like particles could be valuable for applications in stimulus-responsive drug delivery, cell attachment, and constructing complex and porous 3D tissues and scaffolds.[IV.77] Apart from particle shape, it is also important to address surface morphology and texture. Indeed, texturized and wrinkled particles are widely found in nature, for example in plant biology[IV.98] and in the mammalian immune system.[IV.99] Therefore, artificial wrinkled particles have been produced, and their different surface morphology and texture might make them quite unique in controlled drug delivery,[IV.100] fabrication of absorbent materials,[IV.101] inkjet recording,[IV.102] and self-assembly.[IV.103] Within this field, Li and collaborators were able to generate wrinkled PEG-DA particles, with a diameter of around 50 µm with controllable morphology, size, and wrinkle pattern (**Figure IV.4C**). The authors resorted to stop-flow lithography combined with a rapid wrinkling post-process that consisted of UV exposure and different concentrations of washing agents. The originated particles were able to promote cell attachment in cell cultures without any extra chemical treatment, showing great promise in the field of cell attachment and scaffold fabrication.[IV.104]

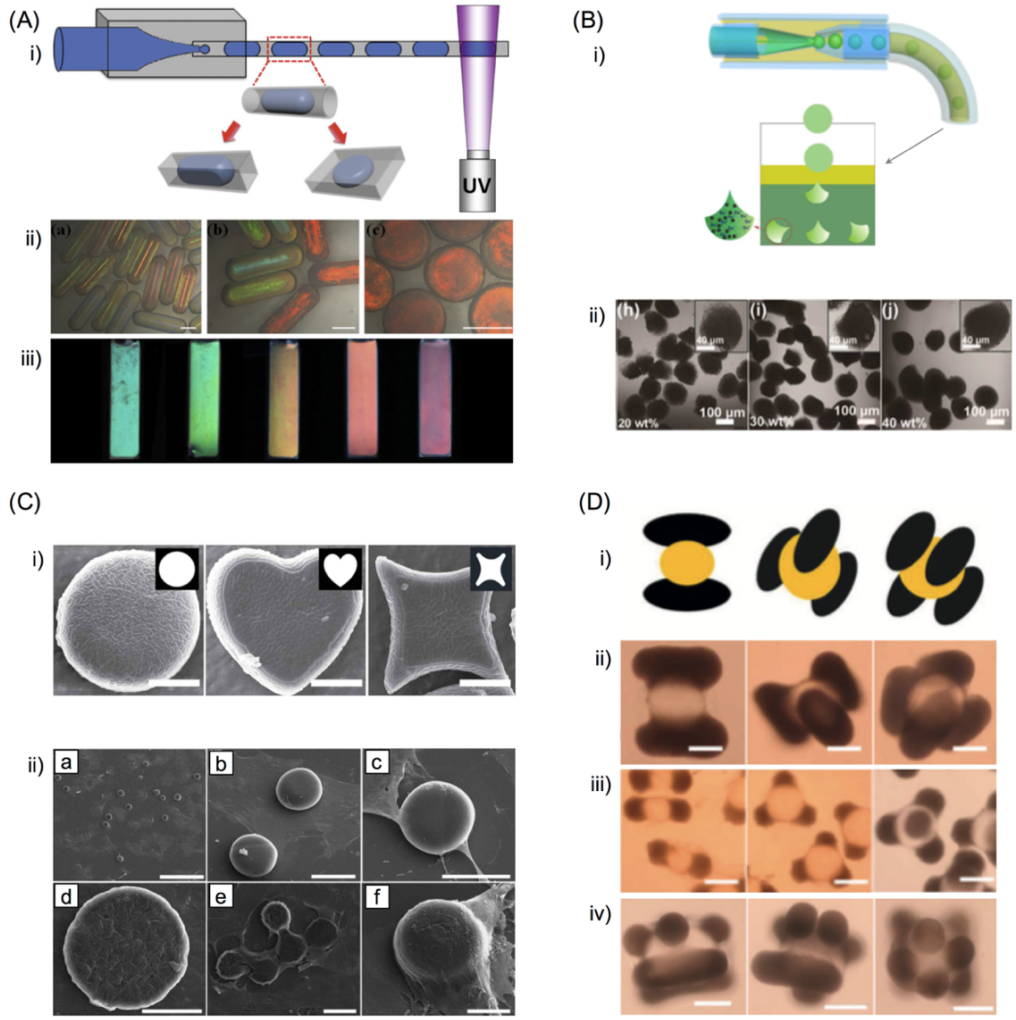


Figure IV.4. Non-spherical particles: (**A**) (**i**) Schematic representation of the microfluidic production of anisotropic particles with different geometries. (**ii**) Optical microscopy images of CCPs with different geometries: a) rods, b) cuboids, c) disks. Scale bars: 200 µm. (**iii**) Digital photographs of different types of colloidal crystal PEG-DA solutions. Reprinted with permission from (IV.97). (**B**) (**i**) Schematic representation of the microfluidic device used for the creation of mushroom-like shaped particles. (**ii**) Optical microscopy images of the resulting particles. Reprinted with permission from (IV.77). (**C**) (**i**) Wrinkled particles with different shapes. Scale bars: 20 µm. (**ii**) Smooth (top) vs. wrinkled particles (bottom) in cell cultures: the cells ignore the smooth particles but attach to the wrinkled ones. Scale bars: (a) 300 µm, (b, c, e) 40 µm, (d, f) 20 µm. Reprinted with permission from (IV.104). (**D**) (**i**) Model for multiple rod-like cores. (**ii**) Optical microscopy images of multiple rod-like cores. (**iii**) and (**iv**) Optical microscopy images of other multicore particle shapes. Scale bars: 200 µm. Reprinted with permission from (IV.108).

Microfluidics also allows for the creation of multicompartmental particles, where it is possible to individually control the function of each compartment, meaning that these particles are capable of controllably releasing several different payloads, in response to diverse external cues,[IV.105,106] aiming towards controlled and sustained drug delivery.[IV.107] Guo and collaborators

were able to produce different shapes of anisotropic PAAm/PEG core/shell droplets and hydrogels with diameters of 250 µm using polymerization-induced phase separation and droplet coalescence.[IV.108] More importantly, this group was able to create multicore emulsion droplets using single-core droplets as building blocks producing several complex two- and three-dimensional structures that can display different release rates depending on their hierarchical organization (**Figure IV.4D**). As a proof of concept, the authors compared the release rate of bovine serum albumin (BSA) in single and quadruple core PAAm/PEG hydrogels and concluded that the kinetics of release changes significantly within those particles. While both particles are able to release most of the entrapped BSA, the quadruple core particles show a much faster release rate when compared to single core particles (70% of release in one hour vs. four hours).[IV.108]

Biological cargo

The use of nano/microparticles in the context of nanobiomedicine requires their loading with bioactive cargo, i.e., biomolecules that are encapsulated as proteins or enzymes, but also as entire living cells. In this way, their encapsulation offers the possibility to create new materials in the fields of drug delivery, cell mimicry, tissue engineering, and diagnosis. In addition to the prior outlined advantages, D-µF allows for 100% cargo loading at efficient rates (10^3–10^9 particles per second).[IV.8,109] Small cargo, e.g. enzymes, proteins, and DNA, can be easily loaded homogenously within the particles. For larger cargo, on the other hand, such as living cells, it has to be considered that the particles can contain zero to multiple cells per particle. An approach to avoid empty particles has recently been reported by either improving the cell-to-particle ratio before forming the particles or by sorting the particles after their formation.[IV.110] Sorting of particles is also important in cell-free protein expression and flow-PCR techniques, where proteins are expressed and DNA is amplified, respectively, within water-oil droplets. After analysis and particle sorting, the cargo could then be recovered and the particles were discarded.[IV.111,112] However, in the context of cell mimicry, the particles have to be structurally stable, i.e., they need to be manipulated in order to be handled over extended period of time or to modify their surfaces. As such, stable particles have been generated as soft particles from biocompatible/biodegradable polymers (PEG,[IV.113,114] PLGA,[IV.115] PCL,[IV.116] PLA[IV.117]), as hydrogel particles from alginate,[IV.118,119] agarose,[IV.120] chitosan,[IV.121] polyacrylamide,[IV.122] DNA,[IV.123,124] etc., as fibrous particles from natural collagen fibrils[IV.125] or peptides,[IV.126] and as hollow structures like liposomes,[IV.127,128] polymersomes,[IV.105,129] or capsules.[IV.130,131] Stable particles are useful for delivering (DNA, siRNA) and producing drugs, as microreactors/nanoreactors or to encapsulate cells for tissue engineering.[IV.132] On the other hand, the field of microfluidics is still relatively new and other techniques to encapsulate protein moieties have been used, e.g., droplet emulsification. Therefore, the number of publications regarding enzyme/protein/DNA-loaded particles prepared by D-µF remains scarce.

The loading of sensitive biomolecules, such as enzymes or proteins, into polymer matrices can result in the loss of the protein 3D structure

and, therefore, the biomolecules can lose their activity due to the small mesh sizes of certain polymers. In addition, denatured proteins can aggregate within the particles, which can lead to strong immunological responses when administered to the body.[IV.133] Thus, hydrogels are more suited to encapsulate proteins due to their large water content and increased mesh sizes. On the other hand, the larger mesh size might involve the need for a covalent immobilization of the proteins to avoid uncontrolled cargo leakage. As an alternative, the particle surface can be rendered less permeable by depositing interacting polymer layers in order to keep the enzymes entrapped as illustrated, for instance, by Fischlechner and co-workers (**Figure IV.5A**).[IV.130] They recently generated gel-shell beads, where an agarose hydrogel core served as the interior compartment while a polyelectrolyte shell functioned as the membrane. In order to functionalize one single droplet with the specific plasmid and expressed enzyme of one specific *E. coli* cell, one of the aqueous channels contained the *E. coli* cells while the second aqueous channel contained the supplements for *E. coli* cell lysis and the third channel contained the non-fluorescent substrate for the enzyme. Within the still liquid core of the droplets, the enzyme converted the substrate to the fluorescent product. After gelation by cooling below 30 °C and consequent gel-shell bead formation, the beads were sorted by FACS. By doing so, a directed evolution of the enzyme was established and the positive mutants could be analyzed at a rate of ~10^7 particles per hour. The plasmid was selectively isolated from the positive beads. These gel-shell beads offer a promising tool for the encapsulation of enzymes or multiple enzymes and proteins to fulfil cascade reactions for the generation of artificial cells. Besides protein encapsulation, proteins can also be immobilized on the surface of particles for applications in affinity tests, disease diagnosis, etc. In a one-step synthesis, Chen *et al*. prepared antibody-presenting alginate microparticles to be used in binding affinity assays.[IV.30] *E. coli* bacteria bound onto the anti-*E. coli* IgG-functionalized alginate microparticles at a comparable specificity than that of an ELISA. Although the non-specific binding has to be further improved, the large surface to volume ratio of microparticles offers a promising approach for a simpler operation procedure and lower costs than ELISA.

In the field of tissue engineering, cell-laden microgels are an approach to engineer a physiologically relevant microenvironment for cells.[IV.134,135] In general, the single-emulsion technique in D-µF has the disadvantage that the cell viability is drastically reduced, as recently reported even down to 20%.[IV.134] The reason for this is the long time the cells are exposed to the different chemical components for the droplet formation, while they endure reduced nutrient- and oxygen-availability due to the oil phase, cell membrane-active surfactants, toxic photo-initiators, UV-light exposure, etc. A possibility to overcome this problem was recently shown, where the gelation of the particles happens without the addition of a polymerization initiator.[IV.135] In this case, three different aqueous microchannels were used, and all of them were mixed just before the droplet formation. The cell-containing solution was mixed with a solution of dithiolated PEG macro-cross-linker, which reacted with the third solution containing acrylated hyperbranched PEG (hPEG) via a

nucleophilic Michael addition. Thus, the cross-linking happens almost immediately after mixing. Yeast and mammalian (lymphoblasts and fibroblasts) cell viability within these particles was increased up to 90%. Another approach was recently reported by the Weitz group.[IV.134] A double emulsion microfluidic technique reduced the time of the cell-loaded particles being in contact with the oil phase, which led to an improved cell viability (**Figure IV.5B**). Specifically, monodispersed PEG-DA or gelatin-methacrylate droplets were polymerized in presence of a photoinitiator for only 2 s after droplet formation. Upon polymerization, the thin oil-shell around the particles spontaneously dewetted and the oil separated immediately from the particles. In this way, the authors were able to reduce the preparation time of the particles and minimize oil-related toxicity effects that are harmful to living cells. This double-emulsion technique showed 100% cell viability for three different cell types (myelogenous leukemia cells (K562), Madin-Darby canine kidney epithelial (MDCK) cells, and NIH/3T3 fibroblast cells). In addition, the cells were cultured in 3D tissues and it was shown that cells were viable and growing within the microgels, even forming cell-cell connections between the microparticles after four days (NIH/3T3 fibroblasts).

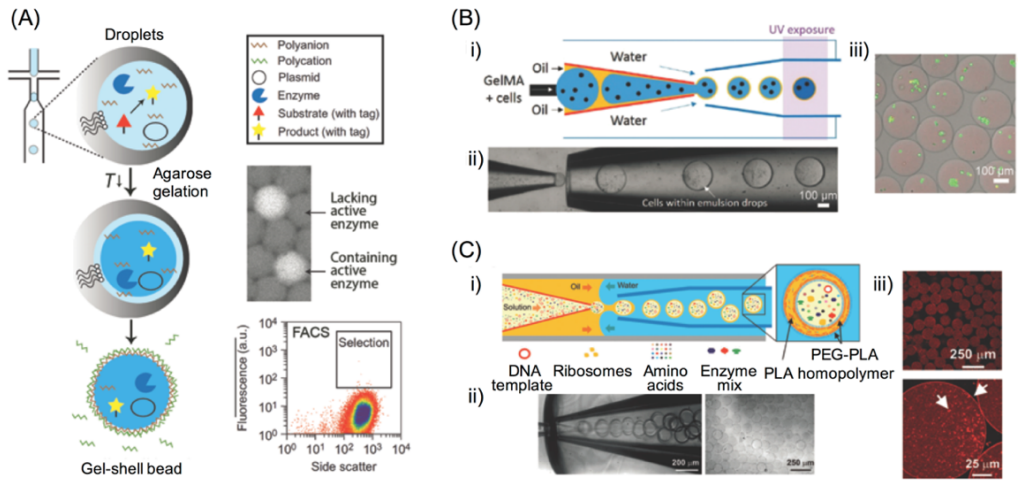


Figure IV.5. Cargo loading: (**A**) Assembly and directed evolution in gel-shell-beads. Assembly is performed by the droplet microfluidic technique. Single *E. coli* cells harboring the expressed enzyme and its encoding plasmid are mixed with the fluorescent substrate and a lysis agent to form the droplets. The aqueous solution also contains agarose and alginate that gelates on cooling to form solid beads. After FACS sorting the positive beads, the coding plasmid is recovered and selected variants are sequenced or further characterized (adapted by permission from Macmillan Publishers Ltd.: Nature Chemistry (IV.130), copyright 2014). (**B**) Production of cell-laden microparticles. (**i**) Schematic illustration showing the encapsulation of living cells using the thin shell double emulsion drops formed with a photo-crosslinkable polymer. (**ii**) Optical image showing cell encapsulation within the drops. (**iii**) Fluorescence microscopy image showing calcein-AM stained (living) and ethidium homodimer-stained (dead) cells embedded within microgels. Adapted from (IV.134) with permission of The Royal Society of Chemistry. (**C**) PEG-*b*-PLA polymersomes made by D-µF and encapsulation of cell-free protein expression machinery. (**i**) Schematic illustration of the double emulsion technique. (**ii**) Optical micrographs of the droplets and the generated polymersomes. (**iii**) Fluorescence microscopy image of expressed MreB-RFP proteins within the giant polymersomes. Arrows indicate the formation of polymerized MreB-RFP patches dispersed in the inner phase and the adhesion of the protein on the membrane. Reproduced with permission of John Wiley & Sons from (IV.136).

D-μF also allowed for generating giant polymersomes loaded with the complete protein expression machinery (**Figure IV.5C**).[IV.136] To mimic the bacterial cytoskeleton, actin-like proteins (MreB) were selectively expressed within PEG-PLA block copolymer vesicles. The advantage of the D-μF technique is that the giant polymersomes can be generated in homogenous sizes without any loss of material (block copolymer and cell-free machinery). Within a few hours, a fluorescent version of MreB was expressed inside the giant polymersomes and a network of actin filaments was achieved. Another work showed the feasibility of having an induced polymersome membrane rupture on demand.[IV.137] Catalase-loaded giant polymersomes, with diameters between 50–100 μm, were prepared by double-emulsion D-μF, with the membrane consisting of a PEG-*b*-polybutadiene (PEG-PB) block copolymer. The polymersomes were then incubated within a glucose and glucose oxidase (GOx) solution, which produces hydrogen peroxide (H_2O_2). H_2O_2 enters the polymersomes and is enzymatically converted to oxygen and water. However, due to the solvent evaporation, large clusters of polymer stuck on the polymersome membrane and, in addition, catalase partially associated with the membrane. Thus, the polymersome membrane ruptured upon H_2O_2 generation. Nevertheless, the exact mechanism of membrane rupture is not clear and might be not applicable for other enzymes/proteins. These two examples of polymersome preparation by D-μF showed the feasibility towards artificial cells by improving the homogeneity and loading of giant polymersomes with biomolecules.

Conclusions and future perspective

This Minireview emphasizes selected aspects that illustrate the impact D-μF could have in different areas of cell mimicry and nanomedicine.

Examples from recent years demonstrated the applicability of D-μF for the production of several different types of nanoparticles. Advantages compared to the traditional bulk synthesis methods include better control over the synthesis process leading to increased uniformity of the produced nanoparticles. Multiple inlet channel set-ups allow fabrication of complex core-shell structures and combination of different materials into hybrid nanoparticles. Moreover, D-μF provides a possibility for in situ monitoring of the nanomaterial production process. It also offers great opportunities to assemble Janus particles. Diverse types of non-spherical particles have been assembled by D-μF including wrinkled particles, multi-core particles, and other particles with controlled shape and size. In the context of loading biological cargo, the generation of artificial cells became technically feasible by D-μF and examples have been shown, such as enzyme encapsulation into hydrogel particles, cell-laden hydrogel particles for tissue engineering and giant polymersomes/liposomes. The advantages of D-μF lie mainly in the extremely high efficiency of cargo loading and the generation of uniform particles at high rates.

Despite all the outlined advantages, the use of D-μF-assembled particles remains largely unexplored, given that most examples found in literature refer only to proofs of concept and simple applications. Future directions will involve the combination of the above outlined aspects including the cargo loading of the

non-spherical particles or their down-scaling to the nano-range. The D-μF based nanoparticle fabrication needs to overcome the small production rates, while achieving Janus particle assembly avoiding organic solvents or long phase separation processes is imperative when loading with biological cargo is envisioned. Cell encapsulation became feasible using D-μF, but improving cargo retention and cell survival (e.g., shortening the time cell loaded particles stay in contact with the oil-phase), and thus prolonging the life-time of the artificial cells, are key challenges to be addressed.

chapter IV references

IV.1 Thorsen T, Roberts RW, Arnold FH, Quake SR. Dynamic Pattern Formation in a Vesicle-Generating Microfluidic Device. *Phys Rev Lett* **2001**, *86* (18), 4163–4166.

IV.2 Mashaghi S, Abbaspourrad A, Weitz DA, van Oijen AM. Droplet Microfluidics: A Tool for Biology, Chemistry and Nanotechnology. *Trends Anal Chem* **2016**, *82*, 118–125.

IV.3 Guo MT, Rotem A, Heyman JA, Weitz DA. Droplet Microfluidics for High-Throughput Biological Assays. *Lab Chip* **2012**, *12* (12), 2146–2155.

IV.4 Shembekar N, Chaipan C, Utharala R, Merten CA. Droplet-Based Microfluidics in Drug Discovery, Transcriptomics and High-Throughput Molecular Genetics. *Lab Chip* **2016**, *16* (8), 1314–1331.

IV.5 Peters RJRW, Louzao I, van Hest JCM. From Polymeric Nanoreactors to Artificial Organelles. *Chem Sci* **2012**, *3* (2), 335–342.

IV.6 Schoonen L, van Hest JCM. Compartmentalization Approaches in Soft Matter Science: From Nanoreactor Development to Organelle Mimics. *Adv Mater* **2016**, *28* (6), 1109–1128.

IV.7 Sánchez S, Soler L, Katuri J. Chemically Powered Micro- and Nanomotors. *Angew Chem Int Ed* **2015**, *54* (5), 1414–1444.

IV.8 Martino C, deMello AJ. Droplet-Based Microfluidics for Artificial Cell Generation: A Brief Review. *Interface Focus* **2016**, *6* (4), 20160011.

IV.9 Bozzuto G, Molinari A. Liposomes as Nanomedical Devices. *Int J Nanomedicine* **2015**, *10*, 975–999.

IV.10 Hosta-Rigau L, Schattling P, Teo BM, Lynge ME, Städler B. Recent Progress of Liposomes in Nanomedicine. *J Mater Chem B* **2014**, *2* (39), 6686–6691.

IV.11 Cui J, Richardson JJ, Björnmalm M, Faria M, Caruso F. Nanoengineered Templated Polymer Particles: Navigating the Biological Realm. *Acc Chem Res* **2016**, *49* (6), 1139–1148.

IV.12 Hasani-Sadrabadi MM, Karimkhani V, Majedi FS, Dersarl JJV, Dashtimoghadam E, Afshar-Taromi F, Mirzadeh H, Bertsch A, Jacob KI, Renaud P, *et al*. Microfluidic-Assisted Self-Assembly of Complex Dendritic Polyethylene Drug Delivery Nanocapsules. *Adv Mater* **2014**, *26* (19), 3118–3123.

IV.13 Lim J-M, Bertrand N, Valencia PM, Rhee M, Langer R, Jon S, Farokhzad OC, Karnik R. Parallel Microfluidic Synthesis of Size-Tunable Polymeric Nanoparticles Using 3D Flow Focusing towards in Vivo Study. *Nanomedicine* **2014**, *10* (2), 401–409.

IV.14 Conde AJ, Batalla M, Cerda B, Mykhaylyk O, Plank C, Podhajcer O, Cabaleiro JM, Madrid RE, Policastro L. Continuous Flow Generation of Magnetoliposomes in a Low-Cost Portable Microfluidic Platform. *Lab Chip* **2014**, *14* (23), 4506–4512.

IV.15 Hood RR, DeVoe DL. High-Throughput Continuous Flow Production of Nanoscale Liposomes by Microfluidic Vertical Flow Focusing. *Small* **2015**, *11* (43), 5790–5799.

IV.16 Kim YH, Zhang L, Yu T, Jin M, Qin D, Xia Y. Droplet-Based Microreactors for Continuous Production of Palladium Nanocrystals with Controlled Sizes and Shapes. *Small* **2013**, *9* (20), 3462–3467.

IV.17 Zhang L, Wang Y, Tong L, Xia Y. Synthesis of Colloidal Metal Nanocrystals in Droplet Reactors: The Pros and Cons of Interfacial Adsorption. *Nano Lett* **2014**, *14* (7), 4189–4194.

IV.18 Lu M, Yang S, Ho Y-P, Grigsby CL, Leong KW, Huang TJ. Shape-Controlled Synthesis of Hybrid Nanomaterials via Three-Dimensional Hydrodynamic Focusing. *ACS Nano* **2014**, *8* (10), 10026–10034.

IV.19 Lu M, Ho Y-P, Grigsby CL, Nawaz AA, Leong KW, Huang TJ. Three-Dimensional Hydrodynamic Focusing Method for Polyplex Synthesis. *ACS Nano* **2014**, *8* (1), 332–339.

IV.20 Capretto L, Carugo D, Mazzitelli S, Nastruzzi C, Zhang X. Microfluidic and Lab-on-a-Chip Preparation Routes for Organic Nanoparticles and Vesicular Systems for Nanomedicine Applications. *Adv Drug Deliv Rev* **2013**, *65* (11), 1496–1532.

IV.21 Bazban-Shotorbani S, Dashtimoghadam E, Karkhaneh A, Hasani-Sadrabadi MM, Jacob KI. Microfluidic Directed Synthesis of Alginate Nanogels with Tunable Pore Size for Efficient Protein Delivery. *Langmuir* **2016**, *32* (19), 4996–5003.

IV.22 Dashtimoghadam E, Mirzadeh H, Taromi FA, Nyström B. Microfluidic Self-Assembly of Polymeric Nanoparticles with Tunable Compactness for Controlled Drug Delivery. *Polymer* **2013**, *54* (18), 4972–4979.

IV.23 Majedi FS, Hasani-Sadrabadi MM, VanDersarl JJ, Mokarram N, Hojjati-Emami S, Dashtimoghadam E, Bonakdar S, Shokrgozar MA, Bertsch A, Renaud P. On-Chip Fabrication of Paclitaxel-Loaded Chitosan Nanoparticles for Cancer Therapeutics. *Adv Funct Mater* **2014**, *24* (4), 432–441.

IV.24 Martín-Banderas L, Sáez-Fernández E, Holgado MÁ, Durán-Lobato MM, Prados JC, Melguizo C, Arias JL. Biocompatible Gemcitabine-Based Nanomedicine Engineered by Flow Focusing® for Efficient Antitumor Activity. *Int J Pharm* **2013**, *443* (1–2), 103–109.

IV.25 Sun J, Xianyu Y, Li M, Liu W, Zhang L, Liu D, Liu C, Hu G, Jiang X. A Microfluidic Origami Chip for Synthesis of Functionalized Polymeric Nanoparticles. *Nanoscale* **2013**, *5* (12), 5262–5265.

IV.26 Tresset G, Marculescu C, Salonen A, Ni M, Iliescu C. Fine Control Over the Size of Surfactant–Polyelectrolyte Nanoparticles by Hydrodynamic Flow Focusing. *Anal Chem* **2013**, *85* (12), 5850–5856.

IV.27 Valencia PM, Pridgen EM, Rhee M, Langer R, Farokhzad OC, Karnik R. Microfluidic Platform for Combinatorial Synthesis and Optimization of Targeted Nanoparticles for Cancer Therapy. *ACS Nano* **2013**, *7* (12), 10671–10680.

IV.28 Andar AU, Hood RR, Vreeland WN, DeVoe DL, Swaan PW. Microfluidic Preparation of Liposomes to Determine Particle Size Influence on Cellular Uptake Mechanisms. *Pharm Res* **2014**, *31* (2), 401–413.

IV.29 Balbino TA, Aoki NT, Gasperini AAM, Oliveira CLP, Azzoni AR, Cavalcanti LP, de la Torre LG. Continuous Flow Production of Cationic Liposomes at High Lipid Concentration in Microfluidic Devices for Gene Delivery Applications. *Chem Eng J* **2013**, *226*, 423–433.

IV.30 Hood RR, Shao C, Omiatek DM, Vreeland WN, DeVoe DL. Microfluidic Synthesis of PEG- and Folate-Conjugated Liposomes for One-Step Formation of Targeted Stealth Nanocarriers. *Pharm Res* **2013**, *30* (6), 1597–1607.

IV.31 Hood RR, DeVoe DL, Atencia J, Vreeland WN, Omiatek DM. A Facile Route to the Synthesis of Monodisperse Nanoscale Liposomes Using 3D Microfluidic Hydrodynamic Focusing in a Concentric Capillary Array. *Lab Chip* **2014**, *14* (14), 2403–2409.

IV.32 Mijajlovic M, Wright D, Zivkovic V, Bi JX, Biggs MJ. Microfluidic Hydrodynamic Focusing Based Synthesis of POPC Liposomes for Model Biological Systems. *Colloids Surf B Biointerfaces* **2013**, *104*, 276–281.

IV.33 Wang J, Chen W, Sun J, Liu C, Yin Q, Zhang L, Xianyu Y, Shi X, Hu G, Jiang X. A Microfluidic Tubing Method and Its Application for Controlled Synthesis of Polymeric Nanoparticles. *Lab Chip* **2014**, *14* (10), 1673–1677.

IV.34 Wang W, Zhang M-J, Chu L-Y. Functional Polymeric Microparticles Engineered from Controllable Microfluidic Emulsions. *Acc Chem Res* **2014**, *47* (2), 373–384.

IV.35 Majedi FS, Hasani-Sadrabadi MM, Hojjati Emami S, Shokrgozar MA, VanDersarl JJ, Dashtimoghadam E, Bertsch A, Renaud P. Microfluidic Assisted Self-Assembly of Chitosan Based Nanoparticles as Drug Delivery Agents. *Lab Chip* **2013**, *13* (2), 204–207.

IV.36 Othman R, Vladisavljević GT, Nagy ZK. Preparation of Biodegradable Polymeric Nanoparticles for Pharmaceutical Applications Using Glass Capillary Microfluidics. *Chem Eng Sci* **2015**, *137*, 119–130.

IV.37 Othman R, Vladisavljević GT, Thomas NL, Nagy ZK. Fabrication of Composite Poly(D,L-Lactide)/Montmorillonite Nanoparticles for Controlled Delivery of Acetaminophen by Solvent-Displacement Method Using Glass Capillary Microfluidics. *Colloids Surf B Biointerfaces* **2016**, *141*, 187–195.

IV.38 Bains A, Wulff JE, Moffitt MG. Microfluidic Synthesis of Dye-Loaded Polycaprolactone-Block-Poly(Ethylene Oxide) Nanoparticles: Insights into Flow-Directed Loading and in Vitro Release for Drug Delivery. *J Colloid Interface Sci* **2016**, *475*, 136–148.

IV.39 Carugo D, Bottaro E, Owen J, Stride E, Nastruzzi C. Liposome Production by Microfluidics: Potential and Limiting Factors. *Sci Rep* **2016**, *6* (1), 25876.

IV.40 Dandamudi S, Campbell RB. The Drug Loading, Cytotoxicty and Tumor Vascular Targeting Characteristics of Magnetite in Magnetic Drug Targeting. *Biomaterials* **2007**, *28* (31), 4673–4683.

IV.41 Mikhaylov G, Mikac U, Magaeva AA, Itin VI, Naiden EP, Psakhye I, Babes L, Reinheckel T, Peters C, Zeiser R, *et al*. Ferri-Liposomes as an MRI-Visible Drug-Delivery System for Targeting Tumours and Their Microenvironment. *Nat Nanotechnol* **2011**, *6* (9), 594–602.

IV.42 Feng Q, Zhang L, Liu C, Li X, Hu G, Sun J, Jiang X. Microfluidic Based High Throughput Synthesis of Lipid-Polymer Hybrid Nanoparticles with Tunable Diameters. *Biomicrofluidics* **2015**, *9* (5), 052604.

IV.43 Sun J, Zhang L, Wang J, Feng Q, Liu D, Yin Q, Xu D, Wei Y, Ding B, Shi X, *et al*. Tunable Rigidity of (Polymeric Core)-(Lipid Shell) Nanoparticles for Regulated Cellular Uptake. *Adv Mater* **2015**, *27* (8), 1402–1407.

IV.44 Zhang L, Feng Q, Wang J, Zhang S, Ding B, Wei Y, Dong M, Ryu J-Y, Yoon T-Y, Shi X, *et al*. Microfluidic Synthesis of Hybrid Nanoparticles with Controlled Lipid Layers: Understanding Flexibility-Regulated Cell–Nanoparticle Interaction. *ACS Nano* **2015**, *9* (10), 9912–9921.

IV.45 Zhang L, Feng Q, Wang J, Sun J, Shi X, Jiang X. Microfluidic Synthesis of Rigid Nanovesicles for Hydrophilic Reagents Delivery. *Angew Chem Int Ed* **2015**, *54* (13), 3952–3956.

IV.46 Dai J, Yang X, Hamon M, Kong L. Particle Size Controlled Synthesis of CdS Nanoparticles on a Microfluidic Chip. *Chem Eng J* **2015**, *280*, 385–390.

IV.47 Gu H, Rong F, Tang B, Zhao Y, Fu D, Gu Z. Photonic Crystal Beads from Gravity-Driven Microfluidics. *Langmuir* **2013**, *29* (25), 7576–7582.

IV.48 Lignos I, Stavrakis S, Kilaj A, deMello AJ. Millisecond-Timescale Monitoring of PbS Nanoparticle Nucleation and Growth Using Droplet-Based Microfluidics. *Small* **2015**, *11* (32), 4009–4017.

IV.49 Shu Y, Jiang P, Pang D-W, Zhang Z-L. Droplet-Based Microreactor for Synthesis of Water-Soluble Ag2S Quantum Dots. *Nanotechnology* **2015**, *26* (27), 275701.

IV.50 Niu G, Ruditskiy A, Vara M, Xia Y. Toward Continuous and Scalable Production of Colloidal Nanocrystals by Switching from Batch to Droplet Reactors. *Chem Soc Rev* **2015**, *44* (16), 5806–5820.

IV.51 Araújo F, Shrestha N, Shahbazi M-A, Liu D, Herranz-Blanco B, Mäkilä EM, Salonen JJ, Hirvonen JT, Granja PL, Sarmento B, *et al*. Microfluidic Assembly of a Multifunctional Tailorable Composite System Designed for Site Specific Combined Oral Delivery of Peptide Drugs. *ACS Nano* **2015**, *9* (8), 8291–8302.

IV.52 Araújo F, Shrestha N, Gomes MJ, Herranz-Blanco B, Liu D, Hirvonen JJ, Granja PL, Santos HA, Sarmento B. In Vivo Dual-Delivery of Glucagon like Peptide-1 (GLP-1) and Dipeptidyl Peptidase-4 (DPP4) Inhibitor through Composites Prepared by Microfluidics for Diabetes Therapy. *Nanoscale* **2016**, *8* (20), 10706–10713.

IV.53 Yamada S, Nelson WJ. Synapses: Sites of Cell Recognition, Adhesion, and Functional Specification. *Annu Rev Biochem* **2007**, *76* (1), 267–294.

IV.54 Iglesias PA, Devreotes PN. Navigating through Models of Chemotaxis. *Curr Opin Cell Biol* **2008**, *20* (1), 35–40.

IV.55 Bryant DM, Mostov KE. From Cells to Organs: Building Polarized Tissue. *Nat Rev Mol Cell Biol* **2008**, *9* (11), 887–901.

IV.56 Schattling P, Dreier C, Städler B. Janus Subcompartmentalized Microreactors. *Soft Matter* **2015**, *11* (26), 5327–5335.

IV.57 Kaewsaneha C, Tangboriboonrat P, Polpanich D, Eissa M, Elaissari A. Janus Colloidal Particles: Preparation, Properties, and Biomedical Applications. *ACS Appl Mater Interfaces* **2013**, *5* (6), 1857–1869.

IV.58 Walther A, Müller AHE. Janus Particles: Synthesis, Self-Assembly, Physical Properties, and Applications. *Chem Rev* **2013**, *113* (7), 5194–5261.

IV.59 Ruhland TM, McKenzie HS, Skelhon TS, Bon SAF, Walther A, Müller AHE. Nanoscale Hybrid Silica/Polymer Janus Particles with a Double-Responsive Hemicorona. *Polymer* **2015**, *79*, 299–308.

IV.60 Maggi C, Simmchen J, Saglimbeni F, Katuri J, Dipalo M, De Angelis F, Sanchez S, Di Leonardo R. Self-Assembly of Micromachining Systems Powered by Janus Micromotors. *Small* **2016**, *12* (4), 446–451.

IV.61 Bradley LC, Stebe KJ, Lee D. Clickable Janus Particles. *J Am Chem Soc* **2016**, *138* (36), 11437–11440.

IV.62 Seidel P, Ravoo BJ. Preparation of Microscale Polymer Janus Particles by Sandwich Microcontact Printing. *Macromol Chem Phys* **2016**, *217* (13), 1467–1472.

IV.63 Kim JW, Cho J, Cho J, Park BJ, Kim Y-J, Choi K-H, Kim JW. Synthesis of Monodisperse Bi-Compartmentalized Amphiphilic Janus Microparticles for Tailored Assembly at the Oil-Water Interface. *Angew Chem Int Ed* **2016**, *55* (14), 4509–4513.

IV.64 Nakagawa Y, Kageyama H, Oaki Y, Imai H. Direction Control of Oriented Self-Assembly for 1D, 2D, and 3D Microarrays of Anisotropic Rectangular Nanoblocks. *J Am Chem Soc* **2014**, *136* (10), 3716–3719.

IV.65 Khan IU, Serra CA, Anton N, Li X, Akasov R, Messaddeq N, Kraus I, Vandamme TF. Microfluidic Conceived Drug Loaded Janus Particles in Side-by-Side Capillaries Device. *Int J Pharm* **2014**, *473* (1–2), 239–249.

IV.66 Sun X-T, Yang C-G, Xu Z-R. Controlled Production of Size-Tunable Janus Droplets for Submicron Particle Synthesis Using an Electrospray Microfluidic Chip. *RSC Adv* **2016**, *6* (15), 12042–12047.

IV.67 Marquis M, Renard D, Cathala B. Microfluidic Generation and Selective Degradation of Biopolymer-Based Janus Microbeads. *Biomacromolecules* **2012**, *13* (4), 1197–1203.

IV.68 Hu Y, Wang J, Li C, Wang Q, Wang H, Zhu J, Yang Y. Janus Photonic Crystal Microspheres: Centrifugation-Assisted Generation and Reversible Optical Property. *Langmuir* **2013**, *29* (50), 15529–15534.

IV.69 Kim JH, Jeon TY, Choi TM, Shim TS, Kim S-H, Yang S-M. Droplet Microfluidics for Producing Functional Microparticles. *Langmuir* **2014**, *30* (6), 1473–1488.

IV.70 Lone S, Cheong IW. Fabrication of Polymeric Janus Particles by Droplet Microfluidics. *RSC Adv* **2014**, *4* (26), 13322–13333.

IV.71 Lan J, Chen J, Li N, Ji X, Yu M, He Z. Microfluidic Generation of Magnetic-Fluorescent Janus Microparticles for Biomolecular Detection. *Talanta* **2016**, *151*, 126–131.

IV.72 Liu M, Sun X-T, Yang C-G, Xu Z-R. On-Chip Preparation of Calcium Alginate Particles Based on Droplet Templates Formed by Using a Centrifugal Microfluidic Technique. *J Colloid Interface Sci* **2016**, *466*, 20–27.

IV.73 Maeda K, Onoe H, Takinoue M, Takeuchi S. Controlled Synthesis of 3D Multi-Compartmental Particles with Centrifuge-Based Microdroplet Formation from a Multi-Barrelled Capillary. *Adv Mater* **2012**, *24* (10), 1340–1346.

IV.74 Yin S-N, Wang C-F, Yu Z-Y, Wang J, Liu S-S, Chen S. Versatile Bifunctional Magnetic-Fluorescent Responsive Janus Supraballs Towards the Flexible Bead Display. *Adv Mater* **2011**, *23* (26), 2915–2919.

IV.75 Zhao LB, Pan L, Zhang K, Guo SS, Liu W, Wang Y, Chen Y, Zhao XZ, Chan HLW. Generation of Janus Alginate Hydrogel Particles with Magnetic Anisotropy for Cell Encapsulation. *Lab Chip* **2009**, *9* (20), 2981–2986.

IV.76 Yang Y-T, Wei J, Li X, Wu L-J, Chang Z-Q, Serra CA. A Side-by-Side Capillaries-Based Microfluidic System for Synthesizing Size- and Morphology-Controlled Magnetic Anisotropy Janus Beads. *Adv Powder Technol* **2015**, *26* (1), 156–162.

IV.77 Hu Y, Wang S, Abbaspourrad A, Ardekani AM. Fabrication of Shape Controllable Janus Alginate/pNIPAAm Microgels via Microfluidics Technique and off-Chip Ionic Cross-Linking. *Langmuir* **2015**, *31* (6), 1885–1891.

IV.78 Lone S, Kim SH, Nam SW, Park S, Joo J, Cheong IW. Microfluidic Synthesis of Janus Particles by UV-Directed Phase Separation. *Chem Commun* **2011**, *47* (9), 2634–2636.

IV.79 Jeong J, Um E, Park J-K, Kim MW. One-Step Preparation of Magnetic Janus Particles Using Controlled Phase Separation of Polymer Blends and Nanoparticles. *RSC Adv* **2013**, *3* (29), 11801–11806.

IV.80 Chen Y, Nurumbetov G, Chen R, Ballard N, Bon SAF. Multicompartmental Janus Microbeads from Branched Polymers by Single-Emulsion Droplet Microfluidics. *Langmuir* **2013**, *29* (41), 12657–12662.

IV.81 Cao X, Li W, Ma T, Dong H. One-Step Fabrication of Polymeric Hybrid Particles with Core–Shell, Patchy, Patchy Janus and Janus Architectures via a Microfluidic-Assisted Phase Separation Process. *RSC Adv* **2015**, *5* (97), 79969–79975.

IV.82 Wang X, Feng X, Ma G, Yao L, Ge M. Amphiphilic Janus Particles Generated via a Combination of Diffusion-Induced Phase Separation and Magnetically Driven Dewetting and Their Synergistic Self-Assembly. *Adv Mater* **2016**, *28* (16), 3131–3137.

IV.83 Zhu T, Cheng R, Sheppard GR, Locklin J, Mao L. Magnetic-Field-Assisted Fabrication and Manipulation of Nonspherical Polymer Particles in Ferrofluid-Based Droplet Microfluidics. *Langmuir* **2015**, *31* (31), 8531–8534.

IV.84 Shum HC, Abate AR, Lee D, Studart AR, Wang B, Chen C-H, Thiele J, Shah RK, Krummel A, Weitz DA. Droplet Microfluidics for Fabrication of Non-Spherical Particles. *Macromol Rapid Commun* **2010**, *31* (2), 108–118.

IV.85 Muro S, Garnacho C, Champion JA, Leferovich J, Gajewski C, Schuchman EH, Mitragotri S, Muzykantov VR. Control of Endothelial Targeting and Intracellular Delivery of Therapeutic Enzymes by Modulating the Size and Shape of ICAM-1-Targeted Carriers. *Mol Ther* **2008**, *16* (8), 1450–1458.

IV.86 Madivala B, Vandebril S, Fransaer J, Vermant J. Exploiting Particle Shape in Solid Stabilized Emulsions. *Soft Matter* **2009**, *5* (8), 1717–1727.

IV.87 Han Y, Alsayed AM, Nobili M, Zhang J, Lubensky TC, Yodh AG. Brownian Motion of an Ellipsoid. *Science* **2006**, *314* (5799), 626–630.

IV.88 Du Y, Lo E, Ali S, Khademhosseini A. Directed Assembly of Cell-Laden Microgels for Fabrication of 3D Tissue Constructs. *Proc Natl Acad Sci USA* **2008**, *105* (28), 9522–9527.

IV.89 Whitehead KA, Colligon J, Verran J. Retention of Microbial Cells in Substratum Surface Features of Micrometer and Sub-Micrometer Dimensions. *Colloids Surf B Biointerfaces* **2005**, *41* (2–3), 129–138.

IV.90 Mathaes R, Winter G, Besheer A, Engert J. Non-Spherical Micro- and Nanoparticles: Fabrication, Characterization and Drug Delivery Applications. *Expert Opin Drug Deliv* **2015**, *12* (3), 481–492.

IV.91 Champion JA, Katare YK, Mitragotri S. Making Polymeric Micro- and Nanoparticles of Complex Shapes. *Proc Natl Acad Sci USA* **2007**, *104* (29), 11901–11904.

IV.92 Donev A, Cisse I, Sachs D, Variano EA, Stillinger FH, Connelly R, Torquato S, Chaikin PM. Improving the Density of Jammed Disordered Packings Using Ellipsoids. *Science* **2004**, *303* (5660), 990–993.

IV.93 Seiffert S. Microgel Capsules Tailored by Droplet-Based Microfluidics. *ChemPhysChem* **2013**, *14* (2), 295–304.

IV.94 Moon B-U, Hakimi N, Hwang DK, Tsai SSH. Microfluidic Conformal Coating of Non-Spherical Magnetic Particles. *Biomicrofluidics* **2014**, *8* (5), 052103.

IV.95 Nisisako T, Ando T, Hatsuzawa T. Capillary-Assisted Fabrication of Biconcave Polymeric Microlenses from Microfluidic Ternary Emulsion Droplets. *Small* **2014**, *10* (24), 5116–5125.

IV.96 Chen L, An HZ, Doyle PS. Synthesis of Nonspherical Microcapsules through Controlled Polyelectrolyte Coating of Hydrogel Templates. *Langmuir* **2015**, *31* (33), 9228–9235.

IV.97 Cheng Y, Zhu C, Xie Z, Gu H, Tian T, Zhao Y, Gu Z. Anisotropic Colloidal Crystal Particles from Microfluidics. *J Colloid Interface Sci* **2014**, *421*, 64–70.

IV.98 Edlund AF, Swanson R, Preuss D. Pollen and Stigma Structure and Function: The Role of Diversity in Pollination. *Plant Cell* **2004**, *16* (suppl 1), S84–S97.

IV.99 Hallett MB, Dewitt S. Ironing out the Wrinkles of Neutrophil Phagocytosis. *Trends Cell Biol* **2007**, *17* (5), 209–214.

IV.100 Chan HK, Chew NYK. Novel Alternative Methods for the Delivery of Drugs for the Treatment of Asthma. *Adv Drug Deliv Rev* **2003**, *55* (7), 793–805.

IV.101 Stanley F, Lamphere J, Wilson L. Wrinkled Absorbent Particles of High Effective Surface Area Having Fast Absorption Rate. US Patent No. 5744564.

IV.102 Landry-Coltrain C, Leon J. Ink Recording Element Utilizing Wrinkled Particles. US Patent No. 6753051 B1.

IV.103 Yin J, Bar-Kochba E, Chen X. Mechanical Self-Assembly Fabrication of Gears. *Soft Matter* **2009**, *5* (18), 3469–3474.

IV.104 Li M, Joung D, Hughes B, Waldman SD, Kozinski JA, Hwang DK. Wrinkling Non-Spherical Particles and Its Application in Cell Attachment Promotion. *Sci Rep* **2016**, *6*, 30463.

IV.105 Kim S-H, Shum HC, Kim JW, Cho J-C, Weitz DA. Multiple Polymersomes for Programmed Release of Multiple Components. *J Am Chem Soc* **2011**, *133* (38), 15165–15171.

IV.106 Luo R, Cao Y, Shi P, Chen C-H. Near-Infrared Light Responsive Multi-Compartmental Hydrogel Particles Synthesized through Droplets Assembly Induced by Superhydrophobic Surface. *Small* **2014**, *10* (23), 4886–4894.

IV.107 Mitragotri S, Lahann J. Physical Approaches to Biomaterial Design. *Nat Mater* **2009**, *8* (1), 15–23.

IV.108 Guo S, Yao T, Ji X, Zeng C, Wang C, Zhang L. Versatile Preparation of Nonspherical Multiple Hydrogel Core PAM/PEG Emulsions and Hierarchical Hydrogel Microarchitectures. *Angew Chem Int Ed* **2014**, *53* (29), 7504–7509.

IV.109 Teh S-Y, Lin R, Hung L-H, Lee AP. Droplet Microfluidics. *Lab Chip* **2008**, *8* (2), 198–220.

IV.110 Mazutis L, Gilbert J, Ung WL, Weitz DA, Griffiths AD, Heyman JA. Single-Cell Analysis and Sorting Using Droplet-Based Microfluidics. *Nat Protoc* **2013**, *8* (5), 870–891.

IV.111 Fallah-Araghi A, Baret J-C, Ryckelynck M, Griffiths AD. A Completely in Vitro Ultrahigh-Throughput Droplet-Based Microfluidic Screening System for Protein Engineering and Directed Evolution. *Lab Chip* **2012**, *12* (5), 882–891.

IV.112 Leman M, Abouakil F, Griffiths AD, Tabeling P. Droplet-Based Microfluidics at the Femtolitre Scale. *Lab Chip* **2015**, *15* (3), 753–765.

IV.113 Wang KW, Lee KG, Park TJ, Lee Y-C, Yang J-W, Kim DH, Lee SJ, Park JY. Organoclay-Assisted Interfacial Polymerization for Microfluidic Production of Monodisperse PEG-Microdroplets and in Situ Encapsulation of E. Coli. *Biotechnol Bioeng* **2012**, *109* (1), 289–294.

IV.114 Ziemecka I, van Steijn V, Koper GJM, Rosso M, Brizard AM, van Esch JH, Kreutzer MT. Monodisperse Hydrogel Microspheres by Forced Droplet Formation in Aqueous Two-Phase Systems. *Lab Chip* **2011**, *11* (4), 620–624.

IV.115 Kim CM, Park SJ, Kim GM. Applications of PLGA Microcarriers Prepared Using Geometrically Passive Breakup on Microfluidic Chip. *Int J Precis Eng Manuf* **2015**, *16* (12), 2545–2551.

IV.116 Yang C-H, Huang K-S, Lin Y-S, Lu K, Tzeng C-C, Wang E-C, Lin C-H, Hsu W-Y, Chang J-Y. Microfluidic Assisted Synthesis of Multi-Functional Polycaprolactone Microcapsules: Incorporation of CdTe Quantum Dots, Fe2O4 Superparamagnetic Nanoparticles and Tamoxifen Anticancer Drugs. *Lab Chip* **2009**, *9* (7), 961–965.

IV.117 Watanabe T, Ono T, Kimura Y. Continuous Fabrication of Monodisperse Polylactide Microspheres by Droplet-to-Particle Technology Using Microfluidic Emulsification and Emulsion–Solvent Diffusion. *Soft Matter* **2011**, *7* (21), 9894–9897.

IV.118 Huang K-S, Lai T-H, Lin Y-C. Manipulating the Generation of Ca-Alginate Microspheres Using Microfluidic Channels as a Carrier of Gold Nanoparticles. *Lab Chip* **2006**, *6* (7), 954–957.

IV.119 Martinez CJ, Kim JW, Ye C, Ortiz I, Rowat AC, Marquez M, Weitz D. A Microfluidic Approach to Encapsulate Living Cells in Uniform Alginate Hydrogel Microparticles. *Macromol Biosci* **2012**, *12* (7), 946–951.

IV.120 Eun Y-J, Utada AS, Copeland MF, Takeuchi S, Weibel DB. Encapsulating Bacteria in Agarose Microparticles Using Microfluidics for High-Throughput Cell Analysis and Isolation. *ACS Chem Biol* **2011**, *6* (3), 260–266.

IV.121 Yang C-H, Huang K-S, Chang J-Y. Manufacturing Monodisperse Chitosan Microparticles Containing Ampicillin Using a Microchannel Chip. *Biomed Microdevices* **2007**, *9* (2), 253–259.

IV.122 Shibata H, Heo YJ, Okitsu T, Matsunaga Y, Kawanishi T, Takeuchi S. Injectable Hydrogel Microbeads for Fluorescence-Based in Vivo Continuous Glucose Monitoring. *Proc Natl Acad Sci USA* **2010**, *107* (42), 17894–17898.

IV.123 Kahn JS, Ruiz RCH, Sureka S, Peng S, Derrien TL, An D, Luo D. DNA Microgels as a Platform for Cell-Free Protein Expression and Display. *Biomacromolecules* **2016**, *17* (6), 2019–2026.

IV.124 Ruiz RCH, Kiatwuthinon P, Kahn JS, Roh YH, Luo D. Cell-Free Protein Expression from DNA-Based Hydrogel (P-Gel) Droplets for Scale-Up Production. *Ind Biotechnol* **2012**, *8* (6), 372–377.

IV.125 Huang S-B, Chang Y-H, Lee H-C, Tsai S-W, Wu M-H. A Pneumatically-Driven Microfluidic System for Size-Tunable Generation of Uniform Cell-Encapsulating Collagen Microbeads with the Ultrastructure Similar to Native Collagen. *Biomed Microdevices* **2014**, *16* (3), 345–354.

IV.126 Tsuda Y, Morimoto Y, Takeuchi S. Monodisperse Cell-Encapsulating Peptide Microgel Beads for 3D Cell Culture. *Langmuir* **2010**, *26* (4), 2645–2649.

IV.127 Deshpande S, Caspi Y, Meijering AEC, Dekker C. Octanol-Assisted Liposome Assembly on Chip. *Nat Commun* **2016**, *7* (1), 10447.

IV.128 Tan Y-C, Hettiarachchi K, Siu M, Pan Y-R, Lee AP. Controlled Microfluidic Encapsulation of Cells, Proteins, and Microbeads in Lipid Vesicles. *J Am Chem Soc* **2006**, *128* (17), 5656–5658.

IV.129 Martino C, Lee TY, Kim S-H, deMello AJ. Microfluidic Generation of PEG-b-PLA Polymersomes Containing Alginate-Based Core Hydrogel. *Biomicrofluidics* **2015**, *9* (2), 024101.

IV.130 Fischlechner M, Schaerli Y, Mohamed MF, Patil S, Abell C, Hollfelder F. Evolution of Enzyme Catalysts Caged in Biomimetic Gel-Shell Beads. *Nat Chem* **2014**, *6* (9), 791–796.

IV.131 Liu L, Wu F, Ju X-J, Xie R, Wang W, Niu CH, Chu L-Y. Preparation of Monodisperse Calcium Alginate Microcapsules via Internal Gelation in Microfluidic-Generated Double Emulsions. *J Colloid Interface Sci* **2013**, *404*, 85–90.

IV.132 Chung BG, Lee K-H, Khademhosseini A, Lee S-H. Microfluidic Fabrication of Microengineered Hydrogels and Their Application in Tissue Engineering. *Lab Chip* **2012**, *12* (1), 45–59.

IV.133 van Beers MMC, Jiskoot W, Schellekens H. On the Role of Aggregates in the Immunogenicity of Recombinant Human Interferon Beta in Patients with Multiple Sclerosis. *J Interferon Cytokine Res* **2010**, *30* (10), 767–775.

IV.134 Choi C-H, Wang H, Lee H, Kim JH, Zhang L, Mao A, Mooney DJ, Weitz DA. One-Step Generation of Cell-Laden Microgels Using Double Emulsion Drops with a Sacrificial Ultra-Thin Oil Shell. *Lab Chip* **2016**, *16* (9), 1549–1555.

IV.135 Rossow T, Heyman JA, Ehrlicher AJ, Langhoff A, Weitz DA, Haag R, Seiffert S. Controlled Synthesis of Cell-Laden Microgels by Radical-Free Gelation in Droplet Microfluidics. *J Am Chem Soc* **2012**, *134* (10), 4983–4989.

IV.136 Martino C, Kim S-H, Horsfall L, Abbaspourrad A, Rosser SJ, Cooper J, Weitz DA. Protein Expression, Aggregation, and Triggered Release from Polymersomes as Artificial Cell-like Structures. *Angew Chem Int Ed* **2012**, *51* (26), 6416–6420.

IV.137 Jang W-S, Park SC, Reed EH, Dooley KP, Wheeler SF, Lee D, Hammer DA. Enzymatically Triggered Rupture of Polymersomes. *Soft Matter* **2016**, *12* (4), 1014–1020.

Chapter V.

Neurobiology and synthetic biology.

Artificial astrocytes: not if, but when

Armada-Moreira A, Morais TP, Sebastião AM, Crunelli V, Städler B, Vaz SH

In preparation

rationale

An important step in creating the astrosomes was to research what are the functions of astrocytes and what equivalents can be found in synthetic biology, and locate the knowledge gap between those two. After reviewing literature, I found that neuro- and synthetic biology seem to exist in two different parallel universes. All the recent efforts in artificial cells and organelles, while impressive and with a huge potential for biomedical application, are created in a sort of vacuum, with no regard for nor parallel with biological cells. For me, this is a missed opportunity. The communication between these two fields has to exist, neurobiology has to look into synthetic methodologies in order to advance, and artificial cell design should look into biological cell function, so as to create artificial cells that can eventually be equivalent to natal cells. With no bridge between these two distant, yet close, scientific fields, I decided to write this review in a first effort to combine knowledge to create something new and better.

For that, Tatiana Morais and me wrote this publication together, under the supervision of Vincenzo Crunelli and Sandra Vaz, respectively. Tatiana wrote the topic on astrocytic biology and functions and I wrote the remainder of the publication.

publication information

Title. Artificial astrocytes: not if, but when.

Authors. Adam Armada-Moreira, Tatiana P. Morais, Ana M. Sebastião, Vincenzo Crunelli, Brigitte Städler, Sandra H. Vaz.

Status of publication. Manuscript in preparation.

Journal. N/A.

DOI. N/A.

JCR impact factor, quartile, and field. N/A.

Artificial astrocytes: not if, but when

Armada-Moreira A[1,2,3], Morais TP[4], Sebastião AM[1,2], Crunelli V[4,5], Städler B[3], Vaz SH[1,2*]

[1]Instituto de Farmacologia e Neurociências, Faculdade de Medicina, Universidade de Lisboa, Lisbon, Portugal.
[2]Instituto de Medicina Molecular, Faculdade de Medicina, Universidade de Lisboa, Lisbon, Portugal.
[3]Interdisciplinary Nanoscience Center (iNANO), Aarhus University, Aarhus, Denmark.
[4]Neuroscience Division, School of Bioscience, Cardiff University, Cardiff, UK.
[5]Department of Physiology and Biochemistry, Faculty of Medicine and Surgery, University of Malta, Malta.
*Corresponding author.

In preparation.

Abstract

Artificial cells, organelles, and enzymes have recently emerged as new therapeutic tools. Although several successes have been achieved with these new biotechnologies, there is still a disconnect between the current knowledge of (neuro)biology and the design of artificial mimics. Indeed, the design and fabrication of biologically active artificial structures is generally not guided by the functions of their biological counterparts. Thus, most artificial cells remain very simple and normally directed into a single active component, whereas biological cells are able to perform multiple functions simultaneously. Within the central nervous system, astrocytes play major roles in the regulation of neuronal activity and maintenance of brain homeostasis. Indeed, loss of astrocytic function is tied to several neurological diseases. Thus, being able to mimic and replace lost astrocytic functions would be crucial to develop new therapeutic tools with a very wide application in neuropathology. With this in mind, the emerging questions are: (1) How close are we to fully mimic an astrocyte? And (2) how can a deeper understanding of neurobiology be used to inform and enhance the design of next generation cell mimics?

In this review, we focus on compiling what is currently known about astrocytic functions in the healthy brain and in disease, dividing it in two approaches: (1) what functions astrocytes perform (a more holistic view of end results) and (2) what molecules are important in astrocytic functions (a more literal approach for the functions these cells perform). Following this, we look into the most recent literature regarding cell mimicry and synthetic biology and identify which astrocytic functions can be achieved artificially and what technology is already available. Finally, we discuss how neurobiology and a profound understanding of astrocytic functions and mechanisms can accelerate the development of efficient and truly complex artificial astrocyte mimics. We argue that bioengineering, synthetic biology, and neurobiology need better communication to take biotechnology to a whole new level.

Keywords: artificial astrocytes, synthetic biology, neurobiology, cell mimics, biological engineering

Astrocytes in all their glory

The role of astrocytes in proper brain function

Astrocytes are star shaped cells, often noted for their unique morphology but whose essential functions for a proper brain function are often overlooked. So, let us stare at the stars and talk about their functions.

Upon their discovery, astrocytes were considered no more than brain connective tissue, providing a "cushion" for neurons to work. This view was changed when some astrocytic functions were discovered and astrocytes started being considered "helper cells", providing nutrients and support to neurons.[V.1] Nowadays, however, it is largely accepted that astrocytes play an active role in the regulation of neuronal communication, via a diverse and long array of functions.

Scar formation upon brain damage,[V.2] tissue repair,[V.3] gliotransmitters release for modulation of synaptic activity,[V.4] synapse formation and remodeling,[V.5] as well as maintenance of the homeostasis of ions,[V.6] water,[V.7] GABA[V.8] and glutamate,[V.9] defense against oxidative stress,[V.10] and energy storage[V.11] are among the roles played by astrocytes, as reviewed by Perea *et al*.[V.4] To perform the described tasks, astrocytes secrete several astrocytic transmitters, named gliotransmitters, such as glutamate,[V.12,13] D-serine,[V.14] ATP,[V.15] adenosine,[V.16] GABA,[V.17] tumor necrosis factor α (TNFα),[V.18] prostaglandins,[V.11] atrial natriuretic peptide (ANP),[V.19] and brain-derived neurotrophic factor (BDNF),[V.20] which can influence synaptic function and, in this way, modulate neuronal activity.[V.4,21] For instance, CA1 hippocampal long-term potentiation (LTP) can be triggered when postsynaptic neuronal activity and astrocytic calcium-dependent glutamate release occur simultaneously.[V.22] This form of LTP is independent of postsynaptic N-methyl-D-aspartic acid receptor (NMDAR)-mediated signaling but requires metabotropic glutamate receptor (mGluR) activation.[V.22] Differently, the calcium-dependent release of D-serine from CA1 hippocampal astrocytes controls NMDAR-dependent plasticity in excitatory synapses[V.14] and extracellular adenosine, derived from astrocytic ATP, regulates synaptic transmission and modulates LTP.[V.23]

Currently, brain function is understood as a network with concerted activity of neuronal and non-neuronal cells. A concept named tripartite synapse was introduced in the 90s[V.24] and highlights the importance of glial cells, particularly astrocytes, in synaptic physiology. In the tripartite synapse, neurons and astrocytes communicate bidirectionally, meaning that information not only flows between the pre- and postsynaptic neurons but also to astrocytes, which can respond to synaptic activity and regulate synaptic transmission through the release of gliotransmitters.[V.4] Thus, while enwrapping nerve terminals, astrocytes are perfectly located to integrate and process synaptic information and, through gliotransmitter release, control synaptic transmission and plasticity.[V.4]

Contrary to neurons that show electrical excitability, firing and propagation of action potentials are not ways of communication used by astrocytes. Expression of sodium and potassium channels can be observed in astrocytes, as well as evoked inward currents,[V.25] but astrocytic excitability is mainly regulated by elevations in cytosolic calcium concentration.[V.26,27]

Astrocytic calcium elevations occur mostly due to calcium release from intracellular stores evoked by intrinsic spontaneous oscillations or due to the release of transmitters, such as glutamate, during neuronal activity that activate specific receptors in astrocytes. On the other hand, calcium elevations can be propagated to neighboring astrocytes and/or can provoke release of gliotransmitters that have the power to activate neighboring neurons.[V.4,25,28] Astrocytes are connected by gap junctions, originating a functional network that allows for the diffusion of ions or even small molecules, like glutamate, glutathione, glucose, and ATP. This coupling plays an important role both in the healthy and diseased brain, where, within the astrocytic network, small molecules can be rapidly diffused, preventing harmful accumulations.[V.29]

It is commonly accepted that astrocytic mechanisms for transmitter release can be divided in two main pathways: (1) astrocytes secrete gliotransmitters and molecules by calcium-regulated exocytosis and (2) non-exocytic release from cytosolic pools. The latter may occur by diffusion through connexin/pannexin hemichannels,[V.30] calcium-dependent anion channel bestrophin 1,[V.31] pore-forming purinergic P2X7 receptors,[V.32] volume regulated anion channels,[V.33] two-pore potassium channels,[V.34] and reversal of specific transporters, such as cysteine-glutamate exchanger, and glutamate and GABA transporters.[V.21] Calcium-dependent exocytosis, on the other hand, appears as the main release mechanism in astrocytes, in which gliotransmitters are released through vesicles[V.35] or lysosomes,[V.36] where the cargo contained and carried by these vesicles is quite diverse, including neurotransmitters, neuromodulators, transporters, water channels, and receptors. Nowadays it is unquestionable that astrocytic vesicular release is an essential mechanism for the astrocyte-to-neuron communication in the brain.[V.37] In astrocytes, the fusion/secretory process is mediated by the soluble N-ethylmaleimide-sensitive factor attachment protein receptor (SNARE) machinery, which is constituted by vesicular and target membrane-associated proteins forming the called SNARE complex.[V.38]

At the synapse, transmitter homeostasis is also controlled by astrocytic processes. The processes regulate synaptic homeostasis through the expression of neurotransmitter transporters, like the ones for GABA, glycine, and glutamate, that are responsible clearing those neurotransmitters from the synaptic cleft. Following the uptake, astrocytes convert the transmitters, using their enzymatic machinery, into transmitter precursors that can be re-located to neurons where new transmitters can be formed.[V.39,40] Therefore, the astrocytic enzymatic machinery is essential for synaptic communication.

Glutamate uptake is one of the most vital functions performed by astrocytes, through the glutamate transporters GLAST and GLT-1, preventing excitotoxicity and controlling excitability.[V.41] Since neurons cannot perform *de novo* synthesis of glutamate,[V.42–45] this task is left for astrocytes, that convert the synaptic released glutamate into glutamine, through the actions of the enzyme glutamine synthetase[V.46] and return this molecule to the presynaptic neuron, where it will be converted back into glutamate, thus maintaining the intracellular neurotransmitter pool.[V.47] The glutamate-glutamine cycle is also crucial for ammonia detoxification, since

glutamine synthetase uses free ammonia to generate glutamine from glutamate.[V.48] Indeed, this cycle is the main ammonia detoxifying mechanism in the brain.[V.39]

Astrocytes are also essential housekeepers responsible for the maintenance of ionic homeostasis, controlling pH levels and regulating oxidative stress and redox balance. Reactive oxygen species (ROS) are harmful for the central nervous system (CNS) due to the CNS high levels of oxidative metabolic activity and fatty acids. It is important to note that ROS are capable of inhibiting glutamate transporters, which leads to glutamate excitotoxicity, through an elevation of extracellular glutamate concentration and excessive stimulation of glutamate receptors, leading to neuronal death.[V.10] Thankfully, astrocytes express antioxidant systems such as the glutathione system,[V.49] which helps to prevent the possible detrimental effects of oxidative stress.

After this overview on the physiology of astrocytes one should be aware of the inestimable role of these brain stars for the proper brain function. So, if the stars fail, how can we mimic astrocytic functions? And can we enhance the functions already performed by astrocytes? How close we are to artificially develop astrocytic functions? These are some of the hot topics in neuroscience nowadays and, as Ben Barres wrote, "glia already knows how to save neurons, whereas neuroscientists still have no clue".[V.50]

Cell-based therapies: astrocytes as saviors?

Astrocytes as cell-based therapies and their limitations

Cell-based therapy can be defined as a therapeutical approach that uses cells, either endogenous or exogenous, as therapy for a disease.[V.51] This approach offers advantages over pharmacological treatments due to its higher versatility and longer administration window, following the onset of acute pathologies.[V.52] Within this field, two main tactics have been applied, one being the stimulation of stem and progenitor cell mobility, proliferation, and differentiation,[V.52,53] and other being the implantation of exogenous cells.[V.54]

While promising, cell-based therapies present numerous setbacks. Specifically, when using stem and progenitor cells, the level of proliferation and differentiation is sub-optimal. Indeed, one major issue is ensuring that the stimulated stem and progenitor cells generate enough new neurons, with specific neuronal types, and that these newly generated neurons actually integrate the pre-existing neuronal circuits.[V.55] An even more relevant problem with stem cell-based therapies is the potential development of tumors, as it has already been demonstrated in both rodents and humans.[V.56,57]

Given the importance of astrocytes for proper brain function and their control over multiple neuronal functions, these cells have been explored in the context of cell-based therapy[V.58,59] as an alternative source for neuron production.[V.60] The use of cortical astrocytes as cell-based therapy provides several advantages over the use of stem and progenitor cells. Given that stem and progenitor cells reside in neurogenic niches, their use is dependent on their translocation into the affected area.[V.61] This issue does not exist with astrocytes, since these cells are already endogenously located in the affected site.[V.55] Furthermore, in pathological situations, such as stroke, the local astrocytic

population is increased, thus surpassing the proliferation problem that stem and progenitor cells face.[V.62] Finally, astrocytes can be reprogrammed into specific neuronal types and oligodendrocytes using simple molecular strategies, which allows for a higher control over the cell types being generated.[V.63–65] For a detailed report on how to generate different neuronal types from cortical astrocytes, the reader is referred to a review by Couchane and Costa.[V.55]

Despite all the advantages listed, the use of astrocytes in cell-based therapies remains rather unexplored, due to the fear of astrocytic reactivation into a neurotoxic phenotype.[V.66] Nonetheless, a recent study showed that bioengineered midbrain astrocytes, expressing the transcription factors Nurr1 and Foxa2, known to direct glial cells into a neuroprotective phenotype, could be successfully co-grafted with dopaminergic neurons in the context of Parkinson's disease. The use of these astrocytes largely enhanced the yield of the neuronal engraftment and led to a robust improvement of the behavioral patterns in a rat model of Parkinson's disease.[V.58] Moreover, the transplanted immature astrocytes did not mature into reactive neurotoxic astrocyte phenotypes, contributing instead to neurite growth and to a reduction of glial scar generation,[V.58] which showcases the great potential of astrocytes as cell-based therapies.[V.67]

Cell transplantation is a developing field with an impressive potential within cell-based therapies. However, there are major setbacks that need to be overcome for an efficient and clinical use of this technology. Due to the existing toxic environment in several neuronal pathologies and to the physical stress of grafting foreign cells,[V.68,69] the survival of transplanted cells is highly compromised, with grafted cells activating the host's immune system and leading to the onset of inflammation.[V.70] This immune response not only affects the transplanted cells survival, but also their differentiation, maturation, and function.[V.71] In general, this hostile brain environment is responsible for the low yields and side effects of cell-based therapies.[V.58]

Given all the advances in cell-based therapies and their unfortunate setbacks, a viable next step within these types of therapies would be to either bioengineer astrocytes to overcome these problems or to create fully controllable artificial astrocytes.

When the biological fails, the artificial comes to the rescue

Synthetic biology and cell mimicry as a therapeutic approach

The path for both bioengineering astrocytes or creating artificial structures relies on synthetic biology. Synthetic biology is a growing field that combines biology and engineering to create artificial biologically active entities or to re-design existing biological elements,[V.72] in order to achieve controllable functions and structures.[V.73] Within this field, therapeutic cell mimicry aims to replace for missing or lost cellular functions, using two different approaches: the top-down approach, which consists in encapsulating biological cells into hydrogel or polymeric capsules, using the same principles as cell-based therapies while providing a permeable but immunoprotective shell that counteracts many issues of these therapies;[V.74] and the bottom-up approach, which comprises the design

and assembly of artificial structures that mimic functions and/or the organization of biological cells, using polymers, inorganic materials, and enzymes, among others, as building blocks.[V.75]

Even though this is a new and growing field, some notable examples have already been successfully used in a biomedical context. Cell encapsulation has been used to implant microencapsulated islets in animal models of diabetes, where the encapsulated cells were viable and provided long-term control over glucose levels.[V.76]

Recent successes in the bottom-up approach include the fabrication of artificial enzymes, such as ceria nanoparticles encapsulated in apoferritin cages that have been used as super oxide dismutase (SOD) mimics with HepG2 cells, where these nanoparticles showed 50% more ROS scavenging activity than the SOD enzyme.[V.77] Another notable example comprises the use of vanadium oxide nanowires as glutathione peroxidase mimics. These nanowires were internalized by HEK293T cells and successfully reduced oxidative stress.[V.78]

In a different approach, nanoreactors containing glucose oxidase-loaded liposomes were fabricated, acting as artificial organelles, with demonstrated cellular uptake and intracellular activity in endothelial cells and macrophages.[V.79] The concept of artificial organelles was then further explored with nanoreactors composed of gold nanoclusters and two different enzymes (trypsin and horseradish peroxidase) encapsulated in different liposomal subunits. These nanoreactors were successfully internalized by macrophages and were capable of performing two parallel enzymatic reactions.[V.80] The same group then advanced this concept by changing the encapsulated enzymes to glucose oxidase and horseradish peroxidase, creating nanoreactors capable of performing a two-step enzymatic cascade, also with demonstrated intracellular activity.[V.81]

On the other hand, microreactors carrying the enzyme phenylalanine ammonia lyase were considered as artificial cells, with successful activity in the presence of human intestinal epithelial HT-29 cells toward alleviating the effects of phenylketonuria.[V.82] Additionally, microreactors containing the enzyme catalase were successfully co-cultured with hepatocytes, forming a bionic tissue and protecting these cells against the toxic actions of hydrogen peroxide.[V.83] This latter concept was recently further developed, using microreactors composed of catalase-containing liposomes entrapped in alginate hydrogel particles. These microreactors were able to detoxify hydrogen peroxide when co-cultured with HepG2 cells, both in planar cell cultures and in the form of microreactor-cell aggregates.[V.84] For more examples of biologically active enzyme, organelle, and cell mimics, the reader is referred to a review by Itel *et al*.[V.85]

Nano- and microcyborgs: cell mimics in the brain

Cell mimicry in neuronal applications

Regardless of the promising cell mimicry examples, the application of this technology in a neuronal context is mostly focused on inorganic nanoparticles, while more complex cell mimics remain to be fully explored.

Top-down synthetic biology approaches include the encapsulation of nerve growth factor (NGF)-releasing astrocytes in collagen microspheres. The encapsulated astrocytes were

viable for several days in culture, presenting a star shaped morphology with complex arborization, and were able to release NGF into the cell medium. Furthermore, when these astrocyte-containing microspheres were co-cultured with dorsal root ganglion neurons, they were able to significantly enhance axonal growth.[V.70] In a different example, neural stem cells (NSC) genetically modified to express the NT-3 and TrkC genes were seeded in a poly(lactic-*co*-glycolic acid) (PLGA) scaffold, forming an artificial neural construct. This scaffold allowed for NSC neural differentiation, with proved synaptogenesis and inter-neuron communication. When applied *in vivo*, in the damaged spinal cord of rats, this construct was able to enhance neuronal fiber regeneration and re-myelination, contributing to tissue repair.[V.86]

The top-down approach, however, presents some limitations: (1) it is always dependent on the cell functions of the encapsulated cells, (2) the transfection of exogenous cells can lead to immunologic issues, and (3) it is not fully controllable due to the inherent variability of natural cells.

Looking into bottom-up synthetic biology, some successes have been accomplished with inorganic nanoparticles (NP), which are known to interact extensively with cells, and, compared to more traditional therapeutic approaches, offer higher efficiency due to their high surface to volume ratio and the versatility of their surface chemistry allows for a more controlled cellular interaction.[V.87–89] Indeed, it has been shown that NP surface charge is a critical factor in the interaction between NP and neurons, while other characteristics such as morphology, size, and composition only play minor roles. In a recent study, it was concluded that negatively charged NP show a better interaction with neuronal membranes and induce measurable cell depolarization. Importantly, these NP interacted only with excitable neuronal membranes and not with astrocytic membranes. Additionally, when cells were treated with tetrodotoxin, a sodium channel blocker that inhibits electrical neuronal activity,[V.90] the NP did not interact with neuronal membranes, showing that this interaction is electrically driven.[V.91]

In a different study, silver nanoparticles (Ag-NP) were shown to promote neurite growth in the human neuroblastoma-derived cell line SH-SY5Y by acting as topographical anchors,[V.92] which, combined with the already known antibacterial features of these NP,[V.93] proves that Ag-NP can be used as a dual action therapeutic tool.

Gold nanoparticles (Au-NP) have been widely used in neuronal applications. Examples include the promotion of neurite growth,[V.94–96] neuronal protection and recovery after injury,[V.97] induction of neuron depolarization,[V.98,99] inhibition of neuronal activity,[V.100] and control over intracellular calcium transients.[V.101–103] For a detailed analysis of the wide range of applications of Au-NP in a neuronal context, the reader is referred to a review by Paviolo and Stoddart.[V.104] Specifically as neuronal depolarizing agents, Au-NP are able to convert pulses of light into heat, thus affecting membrane potential and leading to the firing of action potentials.[V.87] In an opposing example, gold nanostars (Au-NS) that generate heat by absorbing near-infrared light have been used in primary rat hippocampal cultures to specifically inhibit neuronal activity in zones illuminated

with near-infrared light, with proven cell interaction and biocompatibility.[V.105]

In a similar fashion, magnetic nanoparticles (MNP) have been used to promote neuronal excitation and control intracellular calcium levels. When exposed to a magnetic field, these MNP generate heat that activates heat-sensitive capsaicin receptors, leading to calcium influx and consequent membrane depolarization, in a controlled and reversible manner.[V.106]

In more complex advances, PLGA nanoparticles containing the enzyme catalase were able to prevent the deleterious actions of H_2O_2 in primary human neuronal cultures.[V.107] In a different effort, microreactors equipped with platinum nanoparticles (Pt-NP) were used as ROS and ammonia scavengers, in a study where these microreactors were able to rescue cell viability when SH-SY5Y cells were exposed to H_2O_2 or ammonia.[V.108] Additionally, PLGA microparticles loaded with glial cell line-derived neurotrophic factor (GDNF) were administered to parkinsonian monkeys, achieving a prolonged maintenance of GDNF levels in the brain, ameliorating motor performance, and contributing to the increase of dopaminergic neuron density.[V.109] Another example comprises the use of polyethylene glycol-*co*-polycaprolactone (PEG-*co*-PLC) polymersomes loaded with a NGF mimic that can activate TrkB receptors in SHSY-G7 cells, enhancing neuronal survival.[V.110] Similarly, NGF-loaded superparamagnetic iron oxide-gold nanoparticles (SPIO-Au-NP) were able to promote neuronal growth when incubated with PC-12 cells.[V.111]

Thiolated chitosan nanoparticles containing buspirone hydrochloride, a serotonin 5-HT_{1A} receptor agonist, have also been successfully delivered intranasally to rats, enhancing the delivery of this drug to the brain and allowing for the modulation of neuronal activity.[V.112] Also with the goal of modulating neuronal communication, GABA-containing PEGylated poly(N,N-dimethylacrylamide) nanoparticles were able to enhance inhibitory neurotransmission and consequently decrease seizure intensity in epileptic rats.[V.113]

More than its parts: cell mimics inspired by astrocytes

Engineered astrocyte mimics as a therapeutic approach

While the achievements in cell mimicry in a neuronal context cannot be denied, the design of cell mimics still tastes of promise unfulfilled. This because (1) they remain very simple, normally focusing on only one active component, when the versatility of cell mimicry allows for so much more, (2) most artificial structures lack the tight control that is characteristic of biological phenomena and mechanisms, and (3) the development of these artificial entities is mostly detached from neurobiology knowledge and lacks inspiration from biological cell function. If we aim to truly create artificial cells, there needs to be a parallel between what exists in biology and what we are creating. Thus, looking into astrocytic functions and control mechanisms could deeply favor the design of better cell mimics. In this perspective, the pertinent question is: how close are we to creating an artificial astrocyte?

In **Table V.1**, a parallel is drawn between known and explored astrocytic functions and artificial entities that mimic those functions. Several astrocytic functions, such as regulation of neuronal communication or enhancement of

neuronal survival, are already achieved by artificial entities, with proven biological activity. However, each function is explored in different studies, and there is a lack of more holistic approaches, where several functions are considered simultaneously. While there is a large overlap between biological and artificial, the creation of complex and multifaceted astrocyte mimics is left to be explored.

Table V.1. A comparison between known astrocytic functions and equivalent artificial mimics.

Function	In astrocytes	In mimics
Neurite growth	N-Cadherin and integrins[V.114]	Ag-NP[V.92] Au-NP[V.104]
Modulation of intracellular calcium signaling	Voltage-activated calcium channels	Au-NP[V.101] MNP[V.106]
Neuron depolarization / Excitatory neurotransmission	Glutamate[V.12,13] ATP[V.11]	Au-NP[V.98,99] Au-NP[V.87] MNP[V.106] Negatively charged inorganic NP[V.91]
Neuron hyperpolarization / Inhibitory neurotransmission	GABA Glycine[V.17]	GABA-loaded PEGylated poly(N,N-dimethylacrylamide) NP[V.113]
Suppression of neuronal activity	Neurotransmitter transporters[V.11]	Au-NP[V.100] Au-NS[V.105]
Enhancement of neuronal excitability	Release of gliotransmitters[V.11]	Au-NP[V.115]
ROS clearance	Glutathione and ascorbate[V.10]	Pt-NP-based microreactors[V.108] Catalase-containing NP[V.107]
Ammonia detoxification	Glutamate/glutamine cycle[V.116]	Pt-NP-based microreactors[V.108]
Modulation of neuronal communication	Neuropeptide Y[V.117] D-serine[V.11] Taurine[V.118] L-aspartate[V.6] Kynurenic acid[V.119]	Buspirone-loaded thiolated chitosan NP[V.112]
Regulation of neuronal survival, growth, and regeneration	Neurotrophins (NGF, NT-3, BDNF)[V.20]	GDNF-loaded PLGA microparticles[V.109] NGF mimic-loaded PEG-*co*-PLC polymersomes[V.110] NGF-loaded SPIO-Au-NP[V.111]
Regulation of synaptogenesis and synaptic connectivity	Thrombospondin-1[V.5]	PLGA scaffold with NT-3 and TrkC-expressing NSC[V.86]

Astrocytic vesicles and liposomes: looking into a mirror?

Astrocytic vesicles and their mimics

Astrocytes are known to secrete different types of vesicles, each containing different cargo and performing different functions, in a targeted and regulated manner. So, when looking into the possibilities of mimicking astrocytes, a relevant approach would be to mimic specific astrocytic vesicles.

The vesicles secreted by astrocytes can be divided in different categories, based on their size, cargo, membrane composition, and exocytosis mechanism. These vesicles include synaptic-like microvesicles (SLMV),[V.120–122] dense-core vesicles (DCV),[V.123] lysosomes,[V.36,124,125] exosomes,[V.6] and ectosomes.[V.6]

A seemingly simple way of mimicking astrocytic vesicles consists of using liposomes. Liposomes are lipidic nanoparticles formed by the self-assembly of phospholipids in an aqueous medium, containing one or more lipidic bilayers and a hollow hydrophilic core.[V.126] Liposomes are highly versatile structures, where it is possible to fine tune lipid composition, size, type of cargo, and surface chemistry,[V.127] and have already been broadly used in biomedical contexts.[V.128–130]

Considering all the different vesicle characteristics, the question we pose is: could liposomes mimic astrocytic vesicles?

Regarding size, it is known that SLMV and exosomes are around 30–100 nm in diameter,[V.120,122,126,131,132] while DCV and lysosomes vary between 100–600 nm[V.123,133] and 300–500 nm,[V.134] respectively, and ectosomes, being larger vesicles, present diameters from 100 nm to more than 1 μm.[V.135,136]

The production of liposomes between 20–200 nm has been extensively explored,[V.126] being possible to generate liposomes with sizes equivalent to SLMV and exosomes. Although not as explored, it is also possible to generate liposomes up to some micrometers in diameter,[V.137] where the liposome size would be comparable to that of DCV, lysosomes, and ectosomes.

An important aspect in vesicle mimics is their lipid composition, since this will define the release rate of cargo and interaction with cell membranes. All astrocytic vesicles have a lipid composition similar to that of astrocytes,[V.6] although some are enriched in specific lipids. The astrocytic membrane has a high phospholipid content (around 70–80%), where the majority of phospholipids is phosphatidylcholine (PC, c. 46%), followed by phosphatidylethanolamine (PE, c. 18%), sphingomyelin (SM, c. 8%), phosphatidylserine (PS, c. 6%), phosphatidylinositol (PI, c. 5%), and cardiolipin (CL, c. 3%).[V.138] Of the remainder, around 15% corresponds to cholesterol, and 5% to other sphingolipids.[V.138] Regarding the vesicles, SLMV and DCV have a similar lipid composition to the astrocytic membrane, while lysosomal membranes are enriched with bis(monoacylglycero)phosphate (BMP),[V.6] exosomes are enriched in cholesterol, phosphatidic acid (PA), and SM,[V.139,140] and ectosomes show a higher content of PS in their membrane.[V.136]

Interestingly, all these lipids are common in the manufacturing of liposomes. For a detailed analysis of the most common phospholipids, including PC, PE, PS, PI, SM, CL, and PA, the reader is referred to a review by Li and colleagues.[V.141] Cholesterol is easily inserted into liposomal membranes and cholesterol-containing liposomes have also been widely used in the field of cell mimicry.[V.142,143] Furthermore, it is also possible to create liposomes with different combinations and ratios of different lipids,[V.141] which implies that it would be possible to accurately mimic astrocytic vesicle membranes.

Finally, regarding cargo, each astrocytic vesicle carries different molecules: SLMV carry glutamate[V.144] and D-serine;[V.122,131] DCV can contain ANP,[V.145] neuropeptide Y (NPY),[V.146] and ATP;[V.147,148] lysosomes are responsible for the release of ATP[V.124] and proteolytic enzymes;[V.6] exosomes are known to carry mRNA, miRNA, and cytokines[V.149] and have been reported to contain mtDNA;[V.150] and ectosomes carry regulatory factors, such as fibroblast

growth factor 2 (FGF2) and vascular endothelial growth factor (VEGF),[V.135] interleukin 1-β (IL-1β),[V.6] nucleoside triphosphate diphosphohydrolases (NTDPases),[V.151] matrix metalloproteinases (MMP),[V.152] as well as miRNA.[V.149]

The molecules carried by astrocytic vesicles can be divided into amino acids and small peptides, nucleic acids, and more complex proteins (growth factors and enzymes). It has already been reported the use of liposomes for encapsulated catalysis, where several enzymes were successfully encapsulated in one liposome, maintaining their catalytic activity.[V.153] Furthermore, it is also known the liposomes show interaction with nucleic acids, protecting DNA and RNA against nucleases and providing intracellular delivery.[V.154] Finally, some on-going clinical trials are now using liposomes as a delivery system for peptidic drugs,[V.154] showing that these structures can also successfully encapsulate small peptides and amino acids.

With this comparative analysis, it is possible to conclude that liposomes show great potential as astrocytic vesicle mimics, since they can display all the relevant characteristics of astrocytic vesicles, as seen in **Table V.2**. However, this is a mostly unexplored field that could give rise to new, versatile, and powerful therapeutic tools.

Table V.2. Characteristics of the different astrocytic vesicles and liposomal mimicking possibilities, where ○ represents "currently unexplored", ◐ represents "partially explored", and ● represents "explored".

Type of vesicle	Size	Membrane composition	Content
SLMV	30–100 nm ●	PC, PE, SM, PS, PI, CL, cholesterol ●	Glutamate, D-serine ◐
DCV	100–600 nm ●	PC, PE, SM, PS, PI, CL, cholesterol ●	ANP, NPY, ATP ●
Lysosomes	300–500 nm ●	PC, PE, SM, PS, PI, CL, cholesterol Enriched with BMP ◐	ATP, proteolytic enzymes ●
Exosomes	40–100 nm ●	PC, PE, SM, PS, PI, CL, cholesterol Enriched with cholesterol, PA, SM ●	PAR-4, Hsp70, miRNA, mtDNA ○
Ectosomes	100–1000 nm ●	PC, PE, SM, PS, PI, CL, cholesterol Enriched with PS ●	FGF2, VEGF, IL-1β, MMP, NTDPases, miRNA ◐

So, what now?

Concluding remarks and future perspectives

Astrocytes play important roles within the CNS, providing unique and irreplaceable support for neurons, both in physiological and pathological conditions. In several neurological diseases, however, there is a need to enhance this neuronal support, either due to astrocytic malfunction or neuronal damage.

Cell-based therapy tried to fulfill this loss, having major setbacks. These setbacks are mainly based on the fact that stem and progenitor cells tend to generate tumors upon implantation and, while astrocytes are good candidates for this type of therapy, the disease-driven toxic neuronal environment poses a complex challenge for new cells to integrate the existing circuitries and function properly.

Synthetic biology, specifically cell mimicry, is then a beacon of hope for replacement therapies, even though it is still a fairly new and developing field. Currently, one of the biggest issues with artificial cell mimics is that most studies describing new artificial structures only focus on proof of concept, with no

biological application. Additionally, cell mimics with proven biological activity, as the ones described in this review, often lack in complexity and are still not comparable to the functions and regulation of their biological counterparts.

Drawing inspiration from neurobiology will rapidly advance the field of cell mimicry and the complexity and efficiency of artificial mimics. In a neuronal context, astrocytes are good candidate cells to inspire the design of therapeutic cell mimics, due to their importance in the maintenance of proper brain function and the vast array of reactions they are able to perform. And, indeed, the scientific community could be close to creating an artificial astrocyte. In fact, it is already possible to mimic several astrocytic functions, as it was outlined in this review.

The complexity of astrocyte mimics is however stalled and, for it to reach the next step, there needs to be an open communication between fields of knowledge, so that the design of cell mimics is informed not by general shallow knowledge of a disease, but by a deep understanding of the cellular and molecular machinery of the brain. This open line of communication and a true interdisciplinary approach will bring tremendous advantages for both cell mimicry and neurosciences, offering new and completely unexplored therapeutic options for several neurological diseases.

chapter V references

V.1 Kettenmann H, Verkhratsky A. Neuroglia: The 150 Years After. *Trends Neurosci* **2008**, *31* (12), 653–659.

V.2 Fitch MT, Doller C, Combs CK, Landreth GE, Silver J. Cellular and Molecular Mechanisms of Glial Scarring and Progressive Cavitation: In Vivo and in Vitro Analysis of Inflammation-Induced Secondary Injury after CNS Trauma. *J Neurosci* **1999**, *19* (19), 8182–8198.

V.3 Sofroniew MV. Reactive Astrocytes in Neural Repair and Protection. *Neuroscientist* **2005**, *11* (5), 400–407.

V.4 Perea G, Navarrete M, Araque A. Tripartite Synapses: Astrocytes Process and Control Synaptic Information. *Trends Neurosci* **2009**, *32* (8), 421–431.

V.5 Jayakumar AR, Tong XY, Curtis KM, Ruiz-Cordero R, Shamaladevi N, Abuzamel M, Johnstone J, Gaidosh G, Rama Rao KV, Norenberg MD. Decreased Astrocytic Thrombospondin-1 Secretion After Chronic Ammonia Treatment Reduces the Level of Synaptic Proteins: In Vitro and In Vivo Studies. *J Neurochem* **2014**, *131* (3), 333–347.

V.6 Verkhratsky A, Matteoli M, Parpura V, Mothet J-P, Zorec R. Astrocytes as Secretory Cells of the Central Nervous System: Idiosyncrasies of Vesicular Secretion. *EMBO J* **2016**, *35* (3), 239–257.

V.7 Nagelhus EA, Horio Y, Inanobe A, Fujita A, Haug FM, Nielsen S, Kurachi Y, Ottersen OP. Immunogold Evidence Suggests That Coupling of K+ Siphoning and Water Transport in Rat Retinal Müller Cells Is Mediated by a Coenrichment of Kir4.1 and AQP4 in Specific Membrane Domains. *Glia* **1999**, *26* (1), 47–54.

V.8 Borden LA. GABA Transporter Heterogeneity: Pharmacology and Cellular Localization. *Neurochem Int* **1996**, *29* (4), 335–356.

V.9 Bergles DE, Jahr CE. Synaptic Activation of Glutamate Transporters in Hippocampal Astrocytes. *Neuron* **1997**, *19* (6), 1297–1308.

V.10 Rao SD, Yin HZ, Weiss JH. Disruption of Glial Glutamate Transport by Reactive Oxygen Species Produced in Motor Neurons. *J Neurosci* **2003**, *23* (7), 2627–2633.

V.11 Sofroniew MV, Vinters HV. Astrocytes: Biology and Pathology. *Acta Neuropathol* **2010**, *119* (1), 7–35.

V.12 Lovinger DM, Weight FF. Glutamate Induces a Depolarization of Adult Rat Dorsal Root Ganglion Neurons That Is Mediated Predominantly by NMDA Receptors. *Neurosci Lett* **1988**, *94* (3), 314–320.

V.13 Angulo MC, Kozlov AS, Charpak S, Audinat E. Glutamate Released from Glial Cells Synchronizes Neuronal Activity in the Hippocampus. *J Neurosci* **2004**, *24* (31), 6920–6927.

V.14 Henneberger C, Papouin T, Oliet SHR, Rusakov DA. Long-Term Potentiation Depends on Release of D-Serine from Astrocytes. *Nature* **2010**, *463* (7278), 232–236.

V.15 Chen J, Tan Z, Zeng L, Zhang X, He Y, Gao W, Wu X, Li Y, Bu B, Wang W, *et al*. Heterosynaptic Long-Term Depression Mediated by ATP Released from Astrocytes. *Glia* **2013**, *61* (2), 178–191.

V.16 Martín ED, Fernández M, Perea G, Pascual O, Haydon PG, Araque A, Ceña V. Adenosine Released by Astrocytes Contributes to Hypoxia-Induced Modulation of Synaptic Transmission. *Glia* **2007**, *55* (1), 36–45.

V.17 Bowery NG, Smart TG. GABA and Glycine as Neurotransmitters: A Brief History. *Br J Pharmacol* **2006**, *147* (Suppl 1), S109-119.

V.18 Beattie EC, Stellwagen D, Morishita W, Bresnahan JC, Ha BK, Von Zastrow M, Beattie MS, Malenka RC. Control of Synaptic Strength by Glial TNFalpha. *Science* **2002**, *295* (5563), 2282–2285.

V.19 Krzan M, Stenovec M, Kreft M, Pangrsic T, Grilc S, Haydon PG, Zorec R. Calcium-Dependent Exocytosis of Atrial Natriuretic Peptide from Astrocytes. *J Neurosci* **2003**, *23* (5), 1580–1583.

V.20 Krüttgen A, Möller JC, Heymach JV, Shooter EM. Neurotrophins Induce Release of Neurotrophins by the Regulated Secretory Pathway. *Proc Natl Acad Sci USA* **1998**, *95* (16), 9614–9619.

V.21 Hamilton NB, Attwell D. Do Astrocytes Really Exocytose Neurotransmitters? *Nat Rev Neurosci* **2010**, *11* (4), 227–238.

V.22 Perea G, Araque A. Astrocytes Potentiate Transmitter Release at Single Hippocampal Synapses. *Science* **2007**, *317* (5841), 1083–1086.

V.23 Pascual O, Casper KB, Kubera C, Zhang J, Revilla-Sanchez R, Sul J-Y, Takano H, Moss SJ, McCarthy K, Haydon PG. Astrocytic Purinergic Signaling Coordinates Synaptic Networks. *Science* **2005**, *310* (5745), 113–116.

V.24 Araque A, Parpura V, Sanzgiri RP, Haydon PG. Tripartite Synapses: Glia, the Unacknowledged Partner. *Trends Neurosci* **1999**, *22* (5), 208–215.

V.25 Nedergaard M, Ransom B, Goldman SA. New Roles for Astrocytes: Redefining the Functional Architecture of the Brain. *Trends Neurosci* **2003**, *26* (10), 523–530.

V.26 Charles AC, Merrill JE, Dirksen ER, Sanderson MJ. Intercellular Signaling in Glial Cells: Calcium Waves and Oscillations in Response to Mechanical Stimulation and Glutamate. *Neuron* **1991**, *6* (6), 983–992.

V.27 Cornell-Bell AH, Finkbeiner SM, Cooper MS, Smith SJ. Glutamate Induces Calcium Waves in Cultured Astrocytes: Long-Range Glial Signaling. *Science* **1990**, *247* (4941), 470–473.

V.28 Volterra A, Meldolesi J. Astrocytes, from Brain Glue to Communication Elements: The Revolution Continues. *Nat Rev Neurosci* **2005**, *6* (8), 626–640.

V.29 Le HT, Sin WC, Lozinsky S, Bechberger J, Vega JL, Guo XQ, Sáez JC, Naus CC. Gap Junction Intercellular Communication Mediated by Connexin43 in Astrocytes Is Essential for Their Resistance to Oxidative Stress. *J Biol Chem* **2014**, *289* (3), 1345–1354.

V.30 Montero TD, Orellana JA. Hemichannels: New Pathways for Gliotransmitter Release. *Neuroscience* **2015**, *286*, 45–59.

V.31 Park H, Han K-S, Oh S-J, Jo S, Woo J, Yoon B-E, Lee CJ. High Glutamate Permeability and Distal Localization of Best1 Channel in CA1 Hippocampal Astrocyte. *Mol Brain* **2013**, *6* (1), 54.

V.32 Duan S, Anderson CM, Keung EC, Chen Y, Chen Y, Swanson RA. P2X7 Receptor-Mediated Release of Excitatory Amino Acids from Astrocytes. *J Neurosci* **2003**, *23* (4), 1320–1328.

V.33 Kimelberg HK, Macvicar BA, Sontheimer H. Anion Channels in Astrocytes: Biophysics, Pharmacology, and Function. *Glia* **2006**, *54* (7), 747–757.

V.34 Zhou M, Xu G, Xie M, Zhang X, Schools GP, Ma L, Kimelberg HK, Chen H. TWIK-1 and TREK-1 Are Potassium Channels Contributing Significantly to Astrocyte Passive Conductance in Rat Hippocampal Slices. *J Neurosci* **2009**, *29* (26), 8551–8564.

V.35 Martineau M, Galli T, Baux G, Mothet J-P. Confocal Imaging and Tracking of the Exocytotic Routes for D-Serine-Mediated Gliotransmission. *Glia* **2008**, *56* (12), 1271–1284.

V.36 Li D, Ropert N, Koulakoff A, Giaume C, Oheim M. Lysosomes Are the Major Vesicular Compartment Undergoing Ca2+-Regulated Exocytosis from Cortical Astrocytes. *J Neurosci* **2008**, *28* (30), 7648–7658.

V.37 Verkhratsky A, Rodríguez JJ, Parpura V. Neurotransmitters and Integration in Neuronal-Astroglial Networks. *Neurochem Res* **2012**, *37* (11), 2326–2338.

V.38 Parpura V, Fang Y, Basarsky T, Jahn R, Haydon P. Expression of Synaptobrevin II, Cellubrevin and Syntaxin but Not SNAP-25 in Cultured Astrocytes. *FEBS Lett* **1996**, *377*, 489–492.

V.39 Sattler R, Rothstein JD. Regulation and Dysregulation of Glutamate Transporters. In *Neurotransmitter Transporters*; Handbook of Experimental Pharmacology; Sitte HH, Freissmuth M, Eds.; Springer-Verlag: Berlin, Germany, **2006**; Vol. 175, pp 277–303.

V.40 Seifert G, Schilling K, Steinhäuser C. Astrocyte Dysfunction in Neurological Disorders: A Molecular Perspective. *Nat Rev Neurosci* **2006**, *7* (3), 194–206.

V.41 Gonçalves-Ribeiro J, Pina CC, Sebastião AM, Vaz SH. Glutamate Transporters in Hippocampal LTD/LTP: Not Just Prevention of Excitotoxicity. *Front Cell Neurosci* **2019**, *13*, 357.

V.42 Yu AC, Drejer J, Hertz L, Schousboe A. Pyruvate Carboxylase Activity in Primary Cultures of Astrocytes and Neurons. *J Neurochem* **1983**, *41* (5), 1484–1487.

V.43 Shank RP, Bennett GS, Freytag SO, Campbell GL. Pyruvate Carboxylase: An Astrocyte-Specific Enzyme Implicated in the Replenishment of Amino Acid Neurotransmitter Pools. *Brain Res* **1985**, *329* (1–2), 364–367.

V.44 Schousboe A, Westergaard N, Waagepetersen HS, Larsson OM, Bakken IJ, Sonnewald U. Trafficking between Glia and Neurons of TCA Cycle Intermediates and Related Metabolites. *Glia* **1997**, *21* (1), 99–105.

V.45 Hertz L, Dringen R, Schousboe A, Robinson SR. Astrocytes: Glutamate Producers for Neurons. *J Neurosci Res* **1999**, *57* (4), 417–428.

V.46 Norenberg MD, Martinez-Hernandez A. Fine Structural Localization of Glutamine Synthetase in Astrocytes of Rat Brain. *Brain Res* **1979**, *161* (2), 303–310.

V.47 Kvamme E, Torgner IA, Roberg B. Kinetics and Localization of Brain Phosphate Activated Glutaminase. *J Neurosci Res* **2001**, *66* (5), 951–958.

V.48 Bak LK, Schousboe A, Waagepetersen HS. The Glutamate/GABA-Glutamine Cycle: Aspects of Transport, Neurotransmitter Homeostasis and Ammonia Transfer. *J Neurochem* **2006**, *98* (3), 641–653.

V.49 Kimelberg HK. Functions of Mature Mammalian Astrocytes: A Current View. *Neuroscientist* **2010**, *16* (1), 79–106.

V.50 Barres BA. The Mystery and Magic of Glia: A Perspective on Their Roles in Health and Disease. *Neuron* **2008**, *60* (3), 430–440.

V.51 Buzhor E, Leshansky L, Blumenthal J, Barash H, Warshawsky D, Mazor Y, Shtrichman R. Cell-Based Therapy Approaches: The Hope for Incurable Diseases. *Regen Med* **2014**, *9* (5), 649–672.

V.52 Lindvall O, Kokaia Z. Stem Cell Research in Stroke: How Far from the Clinic? *Stroke* **2011**, *42* (8), 2369–2375.

V.53 Leker RR, Lasri V, Chernoguz D. Growth Factors Improve Neurogenesis and Outcome after Focal Cerebral Ischemia. *J Neural Transm* **2009**, *116* (11), 1397–1402.

V.54 Benchoua A, Onteniente B. Intracerebral Transplantation for Neurological Disorders. Lessons from Developmental, Experimental, and Clinical Studies. *Front Cell Neurosci* **2012**, *6*, 2.

V.55 Chouchane M, Costa MR. Cell Therapy for Stroke: Use of Local Astrocytes. *Front Cell Neurosci* **2012**, *6*, 49.

V.56 Erdö F, Bührle C, Blunk J, Hoehn M, Xia Y, Fleischmann B, Föcking M, Küstermann E, Kolossov E, Hescheler J, *et al*. Host-Dependent Tumorigenesis of Embryonic Stem Cell Transplantation in Experimental Stroke. *J Cereb Blood Flow Metab* **2003**, *23* (7), 780–785.

V.57 Amariglio N, Hirshberg A, Scheithauer BW, Cohen Y, Loewenthal R, Trakhtenbrot L, Paz N, Koren-Michowitz M, Waldman D, Leider-Trejo L, *et al*. Donor-Derived Brain Tumor Following Neural Stem Cell Transplantation in an Ataxia Telangiectasia Patient. *PLoS Med* **2009**, *6* (2), e1000029.

V.58 Song J-J, Oh S-M, Kwon O-C, Wulansari N, Lee H-S, Chang M-Y, Lee E, Sun W, Lee S-E, Chang S, *et al*. Cografting Astrocytes Improves Cell Therapeutic Outcomes in a Parkinson's Disease Model. *J Clin Invest* **2018**, *128* (1), 463–482.

V.59 Hamby ME, Sofroniew MV. Reactive Astrocytes as Therapeutic Targets for CNS Disorders. *Neurotherapeutics* **2010**, *7* (4), 494–506.

V.60 Robel S, Berninger B, Götz M. The Stem Cell Potential of Glia: Lessons from Reactive Gliosis. *Nat Rev Neurosci* **2011**, *12* (2), 88–104.

V.61 Taupin P. Adult Neural Stem Cells, Neurogenic Niches, and Cellular Therapy. *Stem Cell Rev* **2006**, *2* (3), 213–219.

V.62 Buffo A, Rite I, Tripathi P, Lepier A, Colak D, Horn A-P, Mori T, Götz M. Origin and Progeny of Reactive Gliosis: A Source of Multipotent Cells in the Injured Brain. *Proc Natl Acad Sci USA* **2008**, *105* (9), 3581–3586.

V.63 Berninger B, Costa MR, Koch U, Schroeder T, Sutor B, Grothe B, Götz M. Functional Properties of Neurons Derived from In Vitro Reprogrammed Postnatal Astroglia. *J Neurosci* **2007**, *27* (32), 8654–8664.

V.64 Heinrich C, Blum R, Gascón S, Masserdotti G, Tripathi P, Sánchez R, Tiedt S, Schroeder T, Götz M, Berninger B. Directing Astroglia from the Cerebral Cortex into Subtype Specific Functional Neurons. *PLoS Biol* **2010**, *8* (5), e1000373.

V.65 Blum R, Heinrich C, Sánchez R, Lepier A, Gundelfinger ED, Berninger B, Götz M. Neuronal Network Formation from Reprogrammed Early Postnatal Rat Cortical Glial Cells. *Cereb Cortex* **2011**, *21* (2), 413–424.

V.66 Liddelow SA, Guttenplan KA, Clarke LE, Bennett FC, Bohlen CJ, Schirmer L, Bennett ML, Münch AE, Chung W-S, Peterson TC, *et al*. Neurotoxic Reactive Astrocytes Are Induced by Activated Microglia. *Nature* **2017**, *541* (7638), 481–487.

V.67 Chen C, Chan A, Wen H, Chung S-H, Deng W, Jiang P. Stem and Progenitor Cell-Derived Astroglia Therapies for Neurological Diseases. *Trends Mol Med* **2015**, *21* (11), 715–729.

V.68 Widner H, Brundin P. Immunological Aspects of Grafting in the Mammalian Central Nervous System. A Review and Speculative Synthesis. *Brain Res* **1988**, *472* (3), 287–324.

V.69 Barker RA, Widner H. Immune Problems in Central Nervous System Cell Therapy. *NeuroRx* **2004**, *1* (4), 472–481.

V.70 Berndt M, Li Y, Seyedhassantehrani N, Yao L. Fabrication and Characterization of Microspheres Encapsulating Astrocytes for Neural Regeneration. *ACS Biomater Sci Eng* **2017**, *3* (7), 1313–1321.

V.71 Ideguchi M, Shinoyama M, Gomi M, Hayashi H, Hashimoto N, Takahashi J. Immune or Inflammatory Response by the Host Brain Suppresses Neuronal Differentiation of Transplanted ES Cell-Derived Neural Precursor Cells. *J Neurosci Res* **2008**, *86* (9), 1936–1943.

V.72 Nakano T, Eckford AW, Haraguchi T. *Molecular Communication*; Cambridge University Press: Cambridge, England, **2013**.

V.73 Agustín-Pavón C, Isalan M. Synthetic Biology and Therapeutic Strategies for the Degenerating Brain: Synthetic Biology Approaches Can Transform Classical Cell and Gene Therapies, to Provide New Cures for Neurodegenerative Diseases. *BioEssays* **2014**, *36* (10), 979–990.

V.74 Orive G, Santos E, Poncelet D, Hernández RM, Pedraz JL, Wahlberg LU, De Vos P, Emerich D. Cell Encapsulation: Technical and Clinical Advances. *Trends Pharmacol Sci* **2015**, *36* (8), 537–546.

V.75 Schoonen L, van Hest JCM. Compartmentalization Approaches in Soft Matter Science: From Nanoreactor Development to Organelle Mimics. *Adv Mater* **2016**, *28* (6), 1109–1128.

V.76 Ricci M, Blasi P, Giovagnoli S, Rossi C, Macchiarulo G, Luca G, Basta G, Calafiore R. Ketoprofen Controlled Release from Composite Microcapsules for Cell Encapsulation: Effect on Post-Transplant Acute Inflammation. *J Control Release* **2005**, *107* (3), 395–407.

V.77 Liu X, Wei W, Yuan Q, Zhang X, Li N, Du Y, Ma G, Yan C, Ma D. Apoferritin-CeO2 Nano-Truffle That Has Excellent Artificial Redox Enzyme Activity. *Chem Commun* **2012**, *48* (26), 3155–3157.

V.78 Vernekar AA, Sinha D, Srivastava S, Paramasivam PU, D'Silva P, Mugesh G. An Antioxidant Nanozyme That Uncovers the Cytoprotective Potential of Vanadia Nanowires. *Nat Commun* **2014**, *5* (1), 1–13.

V.79 Thingholm B, Schattling P, Zhang Y, Städler B. Subcompartmentalized Nanoreactors as Artificial Organelle with Intracellular Activity. *Small* **2016**, *12* (13), 1806–1814.

V.80 Godoy-Gallardo M, Labay C, Jansman MMT, Ek PK, Hosta-Rigau L. Intracellular Microreactors as Artificial Organelles to Conduct Multiple Enzymatic Reactions Simultaneously. *Adv Healthc Mater* **2017**, *6* (4), 1601190.

V.81 Godoy-Gallardo M, Labay C, Trikalitis VD, Kempen PJ, Larsen JB, Andresen TL, Hosta-Rigau L. Multicompartment Artificial Organelles Conducting Enzymatic Cascade Reactions inside Cells. *ACS Appl Mater Interfaces* **2017**, *9* (19), 15907–15921.

V.82 Hosta-Rigau L, York-Duran MJ, Kang TS, Städler B. Extracellular Microreactor for the Depletion of Phenylalanine Toward Phenylketonuria Treatment. *Adv Funct Mater* **2015**, *25* (25), 3860–3869.

V.83 Zhang Y, Baekgaard-Laursen M, Städler B. Small Subcompartmentalized Microreactors as Support for Hepatocytes. *Adv Healthc Mater* **2017**, *6* (15), 1601141.

V.84 Zhang Y, Schattling PS, Itel F, Städler B. Planar and Cell Aggregate-Like Assemblies Consisting of Microreactors and HepG2 Cells. *ACS Omega* **2017**, *2* (10), 7085–7095.

V.85 Itel F, Schattling PS, Zhang Y, Städler B. Enzymes as Key Features in Therapeutic Cell Mimicry. *Adv Drug Deliv Rev* **2017**, *118*, 94–108.

V.86 Du B-L, Xiong Y, Zeng C-G, He L-M, Zhang W, Quan D-P, Wu J-L, Li Y, Zeng Y-S. Transplantation of Artificial Neural Construct Partly Improved Spinal Tissue Repair and Functional Recovery in Rats with Spinal Cord Transection. *Brain Res* **2011**, *1400*, 87–98.

V.87 Carvalho-de-Souza JL, Treger JS, Dang B, Kent SBH, Pepperberg DR, Bezanilla F. Photosensitivity of Neurons Enabled by Cell-Targeted Gold Nanoparticles. *Neuron* **2015**, *86* (1), 207–217.

V.88 Kotov NA, Winter JO, Clements IP, Jan E, Timko BP, Campidelli S, Pathak S, Mazzatenta A, Lieber CM, Prato M, *et al*. Nanomaterials for Neural Interfaces. *Adv Mater* **2009**, *21* (40), 3970–4004.

V.89 Nel AE, Mädler L, Velegol D, Xia T, Hoek EMV, Somasundaran P, Klaessig F, Castranova V, Thompson M. Understanding Biophysicochemical Interactions at the Nano–Bio Interface. *Nat Mater* **2009**, *8* (7), 543–557.

V.90 Bane V, Lehane M, Dikshit M, O'Riordan A, Furey A. Tetrodotoxin: Chemistry, Toxicity, Source, Distribution and Detection. *Toxins* **2014**, *6* (2), 693–755.

V.91 Dante S, Petrelli A, Petrini EM, Marotta R, Maccione A, Alabastri A, Quarta A, De Donato F, Ravasenga T, Sathya A, *et al*. Selective Targeting of Neurons with Inorganic Nanoparticles: Revealing the Crucial Role of Nanoparticle Surface Charge. *ACS Nano* **2017**, *11* (7), 6630–6640.

V.92 Alon N, Miroshnikov Y, Perkas N, Nissan I, Gedanken A, Shefi O. Silver Nanoparticles Promote Neuronal Growth. *Procedia Eng* **2013**, *59*, 25–29.

V.93 Pelgrift RY, Friedman AJ. Nanotechnology as a Therapeutic Tool to Combat Microbial Resistance. *Adv Drug Deliv Rev* **2013**, *65* (13–14), 1803–1815.

V.94 Paviolo C, Haycock JW, Yong J, Yu A, Stoddart PR, McArthur SL. Laser Exposure of Gold Nanorods Can Increase Neuronal Cell Outgrowth. *Biotechnol Bioeng* **2013**, *110* (8), 2277–2291.

V.95 Bhang SH, Han J, Jang H-K, Noh M-K, La W-G, Yi M, Kim W-S, Kwon YK, Yu T, Kim B-S. pH-Triggered Release of Manganese from MnAu Nanoparticles That Enables Cellular Neuronal Differentiation without Cellular Toxicity. *Biomaterials* **2015**, *55*, 33–43.

V.96 Baranes K, Shevach M, Shefi O, Dvir T. Gold Nanoparticle-Decorated Scaffolds Promote Neuronal Differentiation and Maturation. *Nano Lett* **2016**, *16* (5), 2916–2920.

V.97 Papastefanaki F, Jakovcevski I, Poulia N, Djogo N, Schulz F, Martinovic T, Ciric D, Loers G, Vossmeyer T, Weller H, *et al*. Intraspinal Delivery of Polyethylene Glycol-Coated Gold Nanoparticles Promotes Functional Recovery After Spinal Cord Injury. *Mol Ther* **2015**, *23* (6), 993–1002.

V.98 Yong J, Needham K, Brown WGA, Nayagam BA, McArthur SL, Yu A, Stoddart PR. Gold-Nanorod-Assisted near-Infrared Stimulation of Primary Auditory Neurons. *Adv Healthc Mater* **2014**, *3* (11), 1862–1868.

V.99 Eom K, Kim J, Choi JM, Kang T, Chang JW, Byun KM, Jun SB, Kim SJ. Enhanced Infrared Neural Stimulation Using Localized Surface Plasmon Resonance of Gold Nanorods. *Small* **2014**, *10* (19), 3853–3857.

V.100 Yoo S, Hong S, Choi Y, Park J-H, Nam Y. Photothermal Inhibition of Neural Activity with Near-Infrared-Sensitive Nanotransducers. *ACS Nano* **2014**, *8* (8), 8040–8049.

V.101 Paviolo C, Haycock JW, Cadusch PJ, McArthur SL, Stoddart PR. Laser Exposure of Gold Nanorods Can Induce Intracellular Calcium Transients. *J Biophotonics* **2014**, *7* (10), 761–765.

V.102 Lin Y-L, Jen J-C, Hsu S, Chiu I-M. Sciatic Nerve Repair by Microgrooved Nerve Conduits Made of Chitosan-Gold Nanocomposites. *Surg Neurol* **2008**, *70* (Suppl 1), S9-18.

V.103 Eom K, Hwang S, Yun S, Byun KM, Jun SB, Kim SJ. Photothermal Activation of Astrocyte Cells Using Localized Surface Plasmon Resonance of Gold Nanorods. *J Biophotonics* **2017**, *10* (4), 486–493.

V.104 Paviolo C, Stoddart PR. Gold Nanoparticles for Modulating Neuronal Behavior. *Nanomater* **2017**, *7* (4), 92.

V.105 Lee JW, Jung H, Cho HH, Lee JH, Nam Y. Gold Nanostar-Mediated Neural Activity Control Using Plasmonic Photothermal Effects. *Biomaterials* **2018**, *153*, 59–69.

V.106 Chen R, Romero G, Christiansen MG, Mohr A, Anikeeva P. Wireless Magnetothermal Deep Brain Stimulation. *Science* **2015**, *347* (6229), 1477–1480.

V.107 Singhal A, Morris VB, Labhasetwar V, Ghorpade A. Nanoparticle-Mediated Catalase Delivery Protects Human Neurons from Oxidative Stress. *Cell Death Dis* **2013**, *4* (11), e903.

V.108 Armada-Moreira A, Taipaleenmäki E, Baekgaard-Laursen M, Schattling PS, Sebastião AM, Vaz SH, Städler B. Platinum Nanoparticle-Based Microreactors as Support for Neuroblastoma Cells. *ACS Appl Mater Interfaces* **2018**, *10* (9), 7581–7592.

V.109 Garbayo E, Ansorena E, Lana H, Carmona-Abellan MDM, Marcilla I, Lanciego JL, Luquin MR, Blanco-Prieto MJ. Brain Delivery of Microencapsulated GDNF Induces Functional and Structural Recovery in Parkinsonian Monkeys. *Biomaterials* **2016**, *110*, 11–23.

V.110 Soumen R, Johnston AH, Moin ST, Dudas J, Newman TA, Hausott B, Schrott-Fischer A, Glueckert R. Activation of TrkB Receptors by NGFβ Mimetic Peptide Conjugated Polymersome Nanoparticles. *Nanomedicine* **2012**, *8* (3), 271–274.

V.111 Yuan M, Wang Y, Qin Y-X. Promoting Neuroregeneration by Applying Dynamic Magnetic Fields to a Novel Nanomedicine: Superparamagnetic Iron Oxide (SPIO)-Gold Nanoparticles Bounded with Nerve Growth Factor (NGF). *Nanomedicine* **2018**, *14* (4), 1337–1347.

V.112 Bari NK, Fazil M, Hassan MQ, Haider MR, Gaba B, Narang JK, Baboota S, Ali J. Brain Delivery of Buspirone Hydrochloride Chitosan Nanoparticles for the Treatment of General Anxiety Disorder. *Int J Biol Macromol* **2015**, *81*, 49–59.

V.113 Kırımlıoğlu GY, Menceloğlu Y, Erol K, Yazan Y. In Vitro/in Vivo Evaluation of Gamma-Aminobutyric Acid-Loaded N,N-Dimethylacrylamide-Based PEGylated Polymeric Nanoparticles for Brain Delivery to Treat Epilepsy. *J Microencapsul* **2016**, *33* (7), 625–635.

V.114 Tomaselli KJ, Neugebauer KM, Bixby JL, Lilien J, Reichardt LF. N-Cadherin and Integrins: Two Receptor Systems That Mediate Neuronal Process Outgrowth on Astrocyte Surfaces. *Neuron* **1988**, *1* (1), 33–43.

V.115 Jung S, Bang M, Kim BS, Lee S, Kotov NA, Kim B, Jeon D. Intracellular Gold Nanoparticles Increase Neuronal Excitability and Aggravate Seizure Activity in the Mouse Brain. *PloS One* **2014**, *9* (3), e91360.

V.116 Martinez-Hernandez A, Bell KP, Norenberg MD. Glutamine Synthetase: Glial Localization in Brain. *Science* **1977**, *195* (4284), 1356–1358.

V.117 Prada I, Marchaland J, Podini P, Magrassi L, D'Alessandro R, Bezzi P, Meldolesi J. REST/NRSF Governs the Expression of Dense-Core Vesicle Gliosecretion in Astrocytes. *J Cell Biol* **2011**, *193* (3), 537–549.

V.118 Kimelberg HK, Goderie SK, Higman S, Pang S, Waniewski RA. Swelling-Induced Release of Glutamate, Aspartate, and Taurine from Astrocyte Cultures. *J Neurosci* **1990**, *10* (5), 1583–1591.

V.119 Wu H-Q, Pereira EFR, Bruno JP, Pellicciari R, Albuquerque EX, Schwarcz R. The Astrocyte-Derived A7 Nicotinic Receptor Antagonist Kynurenic Acid Controls Extracellular Glutamate Levels in the Prefrontal Cortex. *J Mol Neurosci* **2010**, *40* (1–2), 204–210.

V.120 Bezzi P, Gundersen V, Galbete JL, Seifert G, Steinhäuser C, Pilati E, Volterra A. Astrocytes Contain a Vesicular Compartment That Is Competent for Regulated Exocytosis of Glutamate. *Nat Neurosci* **2004**, *7* (6), 613–620.

V.121 Crippa D, Schenk U, Francolini M, Rosa P, Verderio C, Zonta M, Pozzan T, Matteoli M, Carmignoto G. Synaptobrevin2-Expressing Vesicles in Rat Astrocytes: Insights into Molecular Characterization, Dynamics and Exocytosis. *J Physiol* **2006**, *570* (Pt 3), 567–582.

V.122 Martineau M, Shi T, Puyal J, Knolhoff AM, Dulong J, Gasnier B, Klingauf J, Sweedler JV, Jahn R, Mothet J-P. Storage and Uptake of D-Serine into Astrocytic Synaptic-like Vesicles Specify Gliotransmission. *J Neurosci* **2013**, *33* (8), 3413–3423.

V.123 Calegari F, Coco S, Taverna E, Bassetti M, Verderio C, Corradi N, Matteoli M, Rosa P. A Regulated Secretory Pathway in Cultured Hippocampal Astrocytes. *J Biol Chem* **1999**, *274* (32), 22539–22547.

V.124 Zhang Z, Chen G, Zhou W, Song A, Xu T, Luo Q, Wang W, Gu X, Duan S. Regulated ATP Release from Astrocytes through Lysosome Exocytosis. *Nat Cell Biol* **2007**, *9* (8), 945–953.

V.125 Verderio C, Cagnoli C, Bergami M, Francolini M, Schenk U, Colombo A, Riganti L, Frassoni C, Zuccaro E, Danglot L, *et al*. TI-VAMP/VAMP7 Is the SNARE of Secretory Lysosomes Contributing to ATP Secretion from Astrocytes. *Biol Cell* **2012**, *104* (4), 213–228.

V.126 Maeki M, Kimura N, Sato Y, Harashima H, Tokeshi M. Advances in Microfluidics for Lipid Nanoparticles and Extracellular Vesicles and Applications in Drug Delivery Systems. *Adv Drug Deliv Rev* **2018**, *128*, 84–100.

V.127 McClements DJ. Encapsulation, Protection, and Delivery of Bioactive Proteins and Peptides Using Nanoparticle and Microparticle Systems: A Review. *Adv Colloid Interface Sci* **2018**, *253*, 1–22.

V.128 Safra T, Muggia F, Jeffers S, Tsao-Wei DD, Groshen S, Lyass O, Henderson R, Berry G, Gabizon A. Pegylated Liposomal Doxorubicin (Doxil): Reduced Clinical Cardiotoxicity in Patients Reaching or Exceeding Cumulative Doses of 500 mg/m2. *Ann Oncol* **2000**, *11* (8), 1029–1033.

V.129 Weissig V, Pettinger TK, Murdock N. Nanopharmaceuticals (Part 1): Products on the Market. *Int J Nanomedicine* **2014**, *9*, 4357–4373.

V.130 Xu L, Huang C-C, Huang W, Tang W-H, Rait A, Yin YZ, Cruz I, Xiang L-M, Pirollo KF, Chang EH. Systemic Tumor-Targeted Gene Delivery by Anti-Transferrin Receptor ScFv-Immunoliposomes. *Mol Cancer Ther* **2002**, *1* (5), 337–346.

V.131 Bergersen LH, Morland C, Ormel L, Rinholm JE, Larsson M, Wold JFH, Røe AT, Stranna A, Santello M, Bouvier D, *et al*. Immunogold Detection of L-Glutamate and D-Serine in Small Synaptic-like Microvesicles in Adult Hippocampal Astrocytes. *Cereb Cortex* **2012**, *22* (7), 1690–1697.

V.132 Mathivanan S, Ji H, Simpson RJ. Exosomes: Extracellular Organelles Important in Intercellular Communication. *J Proteomics* **2010**, *73* (10), 1907–1920.

V.133 Hur YS, Kim KD, Paek SH, Yoo SH. Evidence for the Existence of Secretory Granule (Dense-Core Vesicle)-Based Inositol 1,4,5-Trisphosphate-Dependent Ca2+ Signaling System in Astrocytes. *PloS One* **2010**, *5* (8), e11973.

V.134 Liu T, Sun L, Xiong Y, Shang S, Guo N, Teng S, Wang Y, Liu B, Wang C, Wang L, *et al*. Calcium Triggers Exocytosis from Two Types of Organelles in a Single Astrocyte. *J Neurosci* **2011**, *31* (29), 10593–10601.

V.135 Proia P, Schiera G, Mineo M, Ingrassia AMR, Santoro G, Savettieri G, Di Liegro I. Astrocytes Shed Extracellular Vesicles That Contain Fibroblast Growth Factor-2 and Vascular Endothelial Growth Factor. *Int J Mol Med* **2008**, *21* (1), 63–67.

V.136 Bianco F, Perrotta C, Novellino L, Francolini M, Riganti L, Menna E, Saglietti L, Schuchman EH, Furlan R, Clementi E, *et al*. Acid Sphingomyelinase Activity Triggers Microparticle Release from Glial Cells. *EMBO J* **2009**, *28* (8), 1043–1054.

V.137 Lamichhane N, Udayakumar TS, D'Souza WD, Simone CB, Raghavan SR, Polf J, Mahmood J. Liposomes: Clinical Applications and Potential for Image-Guided Drug Delivery. *Molecules* **2018**, *23* (2), 288.

V.138 Kanfer JN. Astrocytic Lipids And Their Metabolism. In *Astrocytes: Biochemistry, Physiology, and Pharmacology of Astrocytes*; Fedoroff S, Vernadakis A, Eds.; Academic Press: London, England, **1986**; Vol. 2, pp 251–278.

V.139 Kobayashi T, Stang E, Fang KS, de Moerloose P, Parton RG, Gruenberg J. A Lipid Associated with the Antiphospholipid Syndrome Regulates Endosome Structure and Function. *Nature* **1998**, *392* (6672), 193–197.

V.140 Chevallier J, Chamoun Z, Jiang G, Prestwich G, Sakai N, Matile S, Parton RG, Gruenberg J. Lysobisphosphatidic Acid Controls Endosomal Cholesterol Levels. *J Biol Chem* **2008**, *283* (41), 27871–27880.

V.141 Li J, Wang X, Zhang T, Wang C, Huang Z, Luo X, Deng Y. A Review on Phospholipids and Their Main Applications in Drug Delivery Systems. *Asian J Pharm Sci* **2015**, *10* (2), 81–98.

V.142 Raffy S, Teissié J. Control of Lipid Membrane Stability by Cholesterol Content. *Biophys J* **1999**, *76* (4), 2072–2080.

V.143 Briuglia M-L, Rotella C, McFarlane A, Lamprou DA. Influence of Cholesterol on Liposome Stability and on in Vitro Drug Release. *Drug Deliv Transl Res* **2015**, *5* (3), 231–242.

V.144 Montana V, Malarkey EB, Verderio C, Matteoli M, Parpura V. Vesicular Transmitter Release from Astrocytes. *Glia* **2006**, *54* (7), 700–715.

V.145 Kreft M, Stenovec M, Rupnik M, Grilc S, Krzan M, Potokar M, Pangrsic T, Haydon PG, Zorec R. Properties of Ca(2+)-Dependent Exocytosis in Cultured Astrocytes. *Glia* **2004**, *46* (4), 437–445.

V.146 Ramamoorthy P, Whim MD. Trafficking and Fusion of Neuropeptide Y-Containing Dense-Core Granules in Astrocytes. *J Neurosci* **2008**, *28* (51), 13815–13827.

V.147 Coco S, Calegari F, Pravettoni E, Pozzi D, Taverna E, Rosa P, Matteoli M, Verderio C. Storage and Release of ATP from Astrocytes in Culture. *J Biol Chem* **2003**, *278* (2), 1354–1362.

V.148 Pangrsic T, Potokar M, Stenovec M, Kreft M, Fabbretti E, Nistri A, Pryazhnikov E, Khiroug L, Giniatullin R, Zorec R. Exocytotic Release of ATP from Cultured Astrocytes. *J Biol Chem* **2007**, *282* (39), 28749–28758.

V.149 Mause SF, Weber C. Microparticles: Protagonists of a Novel Communication Network for Intercellular Information Exchange. *Circ Res* **2010**, *107* (9), 1047–1057.

V.150 Guescini M, Genedani S, Stocchi V, Agnati LF. Astrocytes and Glioblastoma Cells Release Exosomes Carrying mtDNA. *J Neural Transm* **2010**, *117* (1), 1–4.

V.151 Ceruti S, Colombo L, Magni G, Viganò F, Boccazzi M, Deli MA, Sperlágh B, Abbracchio MP, Kittel A. Oxygen-Glucose Deprivation Increases the Enzymatic Activity and the Microvesicle-Mediated Release of Ectonucleotidases in the Cells Composing the Blood-Brain Barrier. *Neurochem Int* **2011**, *59* (2), 259–271.

V.152 Sbai O, Ould-Yahoui A, Ferhat L, Gueye Y, Bernard A, Charrat E, Mehanna A, Risso J-J, Chauvin J-P, Fenouillet E, *et al*. Differential Vesicular Distribution and Trafficking of MMP-2, MMP-9, and Their Inhibitors in Astrocytes. *Glia* **2010**, *58* (3), 344–366.

V.153 Armada-Moreira A, Thingholm B, Andreassen K, Sebastião AM, Vaz SH, Städler B. On the Assembly of Microreactors with Parallel Enzymatic Pathways. *Adv Biosyst* **2018**, *2* (5), 1700244.

V.154 Tyagi P, Santos JL. Macromolecule Nanotherapeutics: Approaches and Challenges. *Drug Discov Today* **2018**, *23* (5), 1053–1061.

Chapter VI.

The first astrosome.

Platinum nanoparticle-based microreactors

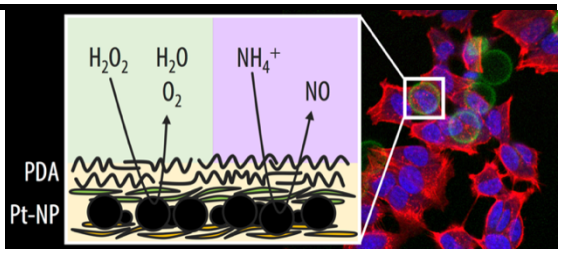
as support for neuroblastoma cells

Armada-Moreira A, Taipaleenmäki E, Baekgaard-Laursen M, Schattling PS,

Sebastião AM, Vaz SH, Städler B

ACS Applied Materials & Interfaces **2018**

rationale



The work developed in this chapter was the first concrete proof that all my theoretical research made sense and could be done in the "real world". Most of the work was carried out by me at Aarhus University during the first half of 2017. With the guidance of Brigitte Städler, I designed, assembled, and characterized the first generation of astrosomes, which use platinum nanoparticles as the active component and rely on poly(dopamine) to improve their biocompatibility. Since this work was performed in Denmark and I came back to Portugal before reviewers asked for more experiments, Essi Taipaleenmäki was responsible for the ζ-potential measurements, LDH release assay, and microreactor activity assay in cell medium. Marie Baekgaard-Laursen was responsible for the QCM-D experiments. Philipp Schattling synthesized platinum nanoparticles and characterized them using TEM. All illustrations are my original design.

publication information

Title. Platinum nanoparticle-based microreactors as support for neuroblastoma cells.

Authors. Adam Armada-Moreira, Essi Taipaleenmäki, Marie Baekgaard-Laursen, Philipp S. Schattling, Ana M. Sebastião, Sandra H. Vaz, Brigitte Städler.

Status of publication. Published.

Journal. ACS Applied Materials & Interfaces 2018, 10 (9), 7581–7592.

DOI. 10.1021/acsami.7b10724

JCR impact factor, quartile, and field. 8.456; Nanoscience & Nanotechnology: Q1; Materials Science, multidisciplinary: Q1.

original research article

Platinum nanoparticle-based microreactors as support for neuroblastoma cells

Armada-Moreira A[1,2,3], Taipaleenmäki E[1], Baekgaard-Laursen M[1], Schattling PS[1], Sebastião AM[2,3], Vaz SH[2,3], Städler B[1]*

[1]Interdisciplinary Nanoscience Center (iNANO), Aarhus University, Aarhus, Denmark.
[2]Instituto de Farmacologia e Neurociências, Faculdade de Medicina, Universidade de Lisboa, Lisbon, Portugal.
[3]Instituto de Medicina Molecular, Faculdade de Medicina, Universidade de Lisboa, Lisbon, Portugal.
*Corresponding author.

ACS Applied Materials & Interfaces **2018**, *10* (9), 7581–7592.

Abstract

Excitotoxicity is a common phenomenon in several neurological diseases, associated with an impaired clearance of synaptically released glutamate, which leads to an overactivation of postsynaptic glutamate receptors. This will, in turn, start an intracellular cascade of neurotoxic events, which include exacerbated production of reactive oxygen species and ammonia toxicity. We report the assembly of microreactors equipped with platinum nanoparticles as artificial enzymes and polymer terminating layers including poly(dopamine). The biological response to these microreactors is assessed in human neuroblastoma cell culture. The microreactors' function to deplete hydrogen peroxide (H_2O_2) and ammonia is confirmed. While the proliferation of the cells depends on the number of microreactors present, no inherent toxicity is found. Furthermore, the microreactors are able to ameliorate the effects of excitotoxicity in cell culture by scavenging H_2O_2 and ammonia, thus having the potential to provide a therapeutic approach for several neurological diseases in which excitotoxicity is observed.

Keywords: polydopamine, neuroblastoma cells, excitotoxicity, oxidative stress, ammonia toxicity, platinum nanoparticles.

Introduction

Excitotoxicity can be described as neuronal injury and death triggered by toxic actions of excitatory neurotransmitters, mainly glutamate in the central nervous system (CNS).[VI.1] Excitotoxicity is present in several neurodegenerative diseases,[VI.2] as well as in cerebral ischemia and traumatic brain injury.[VI.3,4] In the mammalian CNS, this phenomenon involves a rise in intracellular calcium levels, as well as mitochondria dysfunction, free radical accumulation, and production of reactive oxygen species (ROS), among other toxic intracellular events.[VI.5,6] Furthermore, if associated with an impairment of the glutamate/glutamine cycle, which is the main mechanism of ammonia (NH_4^+) detoxification in the brain,[VI.7] excitotoxicity can lead to NH_4^+ toxicity,[VI.8] exacerbating the overactivation of NMDA glutamate receptors.[VI.9]

Although excitotoxicity is a very complex and not yet fully understood phenomenon (the

reader is referred to a review on excitotoxicity by Mehta *et al*.),[VI.2] it is widely accepted that excitotoxicity-induced production of ROS is an important contributor to the onset of pathology.[VI.10,11] It is known that high intracellular ROS levels induce oxidative stress by causing irreversible oxidative damage to lipids, membranes, proteins, and nucleic acids.[VI.12] Importantly, some intracellularly produced ROS, for example hydrogen peroxide (H_2O_2), are capable of crossing cell membranes and affecting neighboring cells.[VI.13]

Several treatments to counteract excitotoxicity focus on limiting glutamate release or blocking glutamate receptors, as reviewed by Jia *et al*.[VI.14] However, this type of permanent blockage interferes with physiological glutamate functions, generating considerable side effects.[VI.3] Therefore, there is a need for the development of alternative therapeutic strategies.

Therapeutic cell mimicry aims at replacing missing or lost cellular functions. A core focus of this field comprises the bottom-up fabrication of micro- and nanostructures with tunable size, shape, chemistry, and biological activity,[VI.15] including the assembly of artificial cells, organelles, and enzymes.[VI.16]

The field of artificial enzymes, which includes organic or inorganic materials with enzyme-like activity, has attracted considerable interest in the past few years.[VI.17] Nanozymes are a particular subset of artificial enzymes that are based on nanomaterials and nanoparticles that possess catalytic activity, including metal oxides, noble metals, and carbon,[VI.18] with potential applications in biomedicine[VI.19] or prodrug therapy.[VI.20] Inorganic nanoparticles show great promise as enzyme mimics since they circumvent problems that natural enzymes face (such as low stability, progressive loss of activity, and high purification costs),[VI.21] although they predominantly exhibit peroxidase, oxidase, catalase, and/or superoxide dismutase (SOD) activity.[VI.18] Noble metals-based nanozymes have inherent beneficial properties, including low susceptibility to corrosion, higher resistance toward oxidation, inertness, and absence of complex formation with other elements, giving them higher stability and lower levels of toxicity.[VI.18] Platinum nanoparticles (Pt-NP) are interesting artificial enzyme candidates.[VI.22] For instance, citrate-capped Pt-NP have been shown to be more efficient peroxidases than horseradish peroxidase (HRP) at the same concentration.[VI.23] Moreover, while soluble platinum ($PtCl_4$) is cytotoxic and leads to oxidative stress, Pt-NP do not dissolve in culture medium and do not lead to a rise in the intracellular ROS levels and consequent cytotoxicity or apoptosis.[VI.23,24] Thus, Pt-NP have been widely used in biomedical applications.[VI.25,26] For a detailed discussion on the applications of noble metal-based nanozymes and Pt-NP, the reader is referred to the review by Cheng and Liu.[VI.27]

From a different perspective, the field of artificial cells considers two different approaches. The top-down approach includes the encapsulation of whole cells or components of cells, as reviewed by Orive *et al*.[VI.28] On the other hand, the bottom-up approach aims to construct microreactors often with biocatalytic activity, using polymers, lipids, and enzymes as building blocks.[VI.29,30] Although impressive progress in the assembly of artificial cells has been accomplished, yielding multi-compartmentalized

systems[VI.31,32] hosting up to three enzymes simultaneously,[VI.33] only few reports have succeeded in confirming their biocatalytic activity in the presence of their natural counterparts. Unlike artificial organelles,[VI.34] artificial cells are expected to show extracellular biocatalytic function and no cell internalization is required.

Poly(dopamine) (PDA), first introduced by Lee *et al.*,[VI.35] is assembled via the self-oxidative polymerization of dopamine at slightly basic pH, has been proven useful for several biomedical applications as recently extensively outlined in reviews providing an excellent historical overview over the developments of PDA.[VI.36,37] The early findings illustrating the biocompatibility of PDA in cell culture[VI.38] and *in vivo*[VI.39] contributed to the wide use of this material, which is known to possess strong adhesive properties, being able to adhere to virtually any type of substrate.[VI.40] In addition to rendering surfaces adhesive to proteins and cells, PDA has been used as a building block for the assembly of colloidal carriers, such as polymer capsules introduced by the Caruso group,[VI.41] and microreactors.[VI.33,42]

The aim of this report was to create a microreactor that can act as an artificial astrocyte toward counteracting ROS production and NH_4^+ toxicity triggered by excitotoxicity (**Figure VI.1**). Specifically, we (i) assessed the conversion of H_2O_2 and NH_4^+ by Pt-NP in solution, (ii) assembled Pt-NP-based microreactors with different surface charges and assessed their catalytic activity towards H_2O_2 and NH_4^+, (iii) determined the effects of different microreactor to cell ratios in terms of cell viability and proliferation, (iv) compared the microreactors' cell adhesive properties, and (v) demonstrated the protective effects of the microreactors towards H_2O_2 and NH_4^+ cell toxicity.

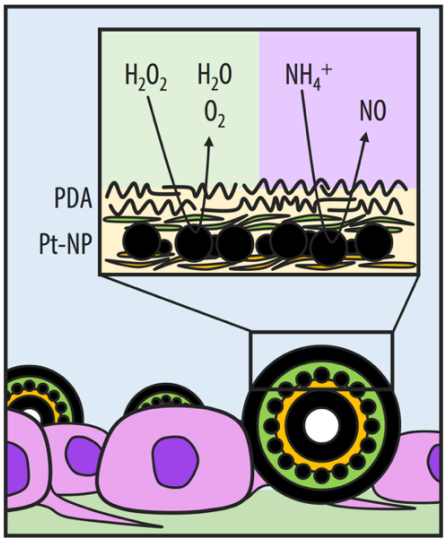


Figure VI.1. Schematic overview of the interaction between neuroblastoma cells and microreactors. The inset shows the protective activity of the Pt-NP, which can convert hydrogen peroxide (H_2O_2) into water and oxygen as well as ammonia (NH_4^+) into nitric oxide (NO). The microreactors consist of a polystyrene carrier particle (white) coated with poly(L-lysine) (PLL, yellow and green), Pt-NP (black circles), and poly(dopamine) (PDA, black layers), PLL, or poly(methacrylic acid) as terminating layers.

Materials and methods

Materials. 4-(2-hydroxyethyl)piperazine-1-ethanesulfonic acid (HEPES), hexachloroplatinic acid, sodium borohydride, trisodium citrate, poly(L-lysine) (PLL, MW 40 000−70 000 Da), poly(methacrylic acid) (PMA, MW 18 600 Da), fluorescein 5(6)-isothiocyanate (FITC), tris(hydroxymethyl)aminomethane (TRIS), fluorescein *O*-methacrylate, N-hydroxysuccinimide 2-(dodecylthiocarbonothioylthio)isobutyrate (CTA-NHS), dopamine hydrochloride (DA), phosphate buffered saline (PBS), Hoechst 33342, fluorescein diacetate (FDA), propidium iodide (PI), horseradish peroxidase (HRP,

250−330 U mg^{-1}), cell counting kit (CCK-8), hydrogen peroxide (H_2O_2, 30% (w/w)), ammonium acetate (NH_4^+), SH-SY5Y cells, ammonia assay kit (AAK, MAK310), paraformaldehyde (PFA), bovine serum albumin (BSA), Triton X-100, and *o*-dianisidine were purchased from Sigma-Aldrich (St. Louis, MO, USA). Amplex UltraRed and Pierce LDH Cytotoxicity Assay Kit were obtained from ThermoFisher Scientific (Waltham, MA, USA). Dulbecco's modified Eagle's medium (DMEM, high glucose), Ham's F12 Nutrient Mix (Ham's F12), fetal bovine serum (FBS), and 100 U mL^{-1} penicillin and 100 µg mL^{-1} streptomycin (Pen/Strep) were purchased from Life Technologies (Camarillo, CA, USA). Diethyl ether and dimethylformamide (DMF) were purchased from VWR (Radnor, PA, USA). Methacrylic acid and azobis(isobutyronitrile) (AIBN) were purchased for Merck (Kenilworth, NJ, USA). Polystyrene (PS) particles (19.30 µm in diameter) were purchased from Microparticles GmbH (Berlin, Germany). Uncoated, IbiTreat- and PLL-coated µ-Slides $VI^{0.4}$ were purchased from ibidi GmbH (Martinsried, Germany). Ultrapure water (18.2 MΩ cm^{-1} resistance) was provided by an ELGA Purelab Ultra system (ELGA LabWater, Lane End, UK). FITC-labeled PLL (PLL_F) was synthesized according to the procedure previously published.[VI.43]

Two types of buffer solutions were used throughout all experiments: HEPES buffer consisting of 10 mM HEPES, pH 7.3, and TRIS buffer consisting of 10 mM TRIS, pH 8.5. All buffer solutions were prepared using ultrapure water.

Pt-NP fabrication. 1 mL of an aqueous solution of hexachloroplatinic acid (16 mM) and 1 mL of an aqueous solution of trisodium citrate (40 mM) were added to 32 mL of ultrapure water and stirred for 30 min at room temperature. After the addition of 200 µL of an aqueous solution of sodium borohydride (50 mM), the solution turned brownish. The reaction was allowed to proceed for 1 h at room temperature.

Synthesis of fluorescein O-methacrylate labeled PMA (PMA_F). 1 g (11.6 mmol) of methacrylic acid, 116 mg (0.3 mmol) of fluorescein *O*-methacrylate, 30.8 mg (0.07 mmol) of CTA-NHS, and 1.10 mg (6.7 µmol) of AIBN were dissolved in 3 mL of DMF. The solution was purged with Argon for 2 min. Oxygen was removed by three consecutive freeze thaw cycles. Between each cycle the tubes were backfilled with Argon. The solution was placed in an oil bath preheated at 75 °C and stirred overnight. After the solution was cooled down to room temperature, the polymer was purified by precipitation with diethyl ether. The purification was repeated three times, by dissolving the polymer again in DMF. The polymer was dried under reduced pressure.

Microreactor assembly. PS particles (ø 19.30 µm, 0.1 g mL^{-1}) were washed 2× in TRIS buffer (1 800 rpm, 45 s). The particles were suspended in a DA solution (2.5 mg mL^{-1} in TRIS buffer, 3 h) to generate inactive PDA-coated particles (M^i). To assemble active microreactors, the particles were then incubated with either a PLL or a PLL_F solution (1 mg mL^{-1} in HEPES buffer, 10 min), followed by incubation with a Pt-NP solution (20 min) to obtain Pt-NP-coated particles (M^{Pt}). The assemblies were always washed 3× in HEPES buffer between the different coating steps. To generate microreactors with a positively charged terminating layer

(M^+), M^{Pt} were incubated with a solution of either PLL or PLL_F (1 mg mL^{-1} in HEPES buffer, 10 min). To obtain microreactors with a PDA terminating layer (M^{PDA}) and with a negatively charged terminating layer (M^-), M^+ were exposed to a DA solution (2.5 mg mL^{-1} in TRIS buffer, 3 h) and to a solution of either PMA or PMA_F (4 mg mL^{-1} in HEPES buffer, 15 min), respectively.

ζ-potential measurements. The ζ-potential of the different layers in the microreactors assembly were analyzed using a Zetasizer Nano ZS (Malvern Instruments, Malvern, UK), employing a material refractive index of 1.590 and a dispersant (water at 25 °C) refractive index of 1.330.

H_2O_2 detection assay. H_2O_2 detection was achieved using the Amplex UltraRed assay for H_2O_2 detection. 50 µL of the samples were incubated with 0.2 U mL^{-1} HRP and 50 µM Amplex UltraRed in ultrapure water, in a total volume of 100 µL. The mix was incubated at room temperature protected from light for 30 min. The fluorescence of the solutions (λ_{ex} = 545 nm, λ_{em} = 590 nm) was measured by a multiplate reader.

NH_4^+ detection assay. NH_4^+ was detected using the commercially available AAK. 10 µL of the samples were incubated with 90 µL of the AAK detection mix and left to incubate for 15 min at room temperature, protected from light. The fluorescence of the solutions (λ_{ex} = 360 nm, λ_{em} = 450 nm) was measured by a multiplate reader.

Confocal laser scanning microscopy (CLSM). Microreactors were deposited in uncoated Ibidi µ-Slides $VI^{0.4}$ and imaged with a confocal laser scanning microscope (CLSM, LSM700, Carl Zeiss, Germany), with a 40× objective. Images were recorded with the software ZEN (Carl Zeiss).

Transmission electron microscopy (TEM). Microreactors with and without Pt-NP were imaged by TEM (Tecnai G^2 Spirit TWIN/BioTWIN, FEI Company, Hillsboro, OR, USA). The grids for TEM were prepared by depositing 5 µL of sample on a glow discharge-treated (20 s, PELCO easiGlow, Ted Pella Inc., Redding, CA, USA) grid followed by washing after 1 min with 2 × 5 µL ultrapure water and staining with 2 × 5 µL 2% (v/v) uranyl acetate.

Cell culture. The human neuroblastoma cell line (SH-SY5Y) was obtained from European Collection of Cell Cultures. The cells were cultured at a density of 3 000 cells cm^{-2} in 75 cm^2 culture flasks in DMEM/Ham's F12 medium (1:1) supplemented with 10% (v/v) FBS and 1% (v/v) Pen/Strep, at 37 °C in a humidified atmosphere of 95% air−5% CO_2.

Immunocytochemistry (ICC). For the cell attachment assay, 50 000 cells cm^{-2} were adhered for 48 h onto IbiTreat-coated µ-Slides $VI^{0.4}$. Microreactors were then added, at a 1:1 or 1:10 microreactor to cell ratio. After 24 h of incubation, cells were washed 3× with PBS, fixed for 30 min in 4% (w/v) PFA in PBS, and permeabilized and blocked for nonspecific binding sites for 20 min with 0.1% (v/v) Triton X-100 and 1% (w/v) BSA in PBS. Cells were subsequently incubated for 30 min at room temperature with Hoechst 33342 (12 µg mL^{-1}) and 1% (w/v) BSA in PBS protected from light. The samples were stored at 4 °C in PBS in the µ-Slides. For the Live/Dead assay, 50 000 cells cm^{-2} were adhered for 48 h onto PLL-coated µ-Slides $VI^{0.4}$. Microreactors were then added, at a 1:1

microreactor to cell ratio. After 24 h of incubation, cells were washed 3× with PBS and incubated for 5 min at room temperature, protected from light, with FDA (8 μg mL^{-1}) and PI (20 μg mL^{-1}) in PBS. The samples were stored at 4 °C in PBS in the μ-Slides. Fluorescence images were captured using an Olympus XM10 monochrome digital camera (Olympus Corp., Tokyo, Japan) mounted on an Olympus IX81 inverted wide field fluorescence microscope (Olympus Corp.), with either a 10× or a 40× objective. Images were recorded using the software CellSens (Olympus Corp.).

Lactate dehydrogenase (LDH) cytotoxicity assay. 100 000 cells cm^{-2} were plated in 96-well plates and allowed to adhere for 24 h. At this point, microreactors were added to the cell medium, at a ratio of one microreactor per one cell, and left to incubate for 24 h. Then, the activity of released LDH was measured for the different conditions by using Pierce LDH Cytotoxicity Assay Kit. Cells grown in the absence of microreactors were used as a negative control, in order to establish the baseline spontaneous LDH activity, and cells exposed to lysis buffer for 45 min were used as a positive control, to determine the maximum LDH activity. 50 μL of each sample was mixed with 50 μL of the LDH cytotoxicity assay reaction mix and incubated for 30 min at room temperature, after which 10 μL of stop solution was added to each well. Absorbance of samples was measured at 490 and 680 nm. The absorbance at 680 nm corresponds to background absorbance and was subtracted from that at 490 nm in order to determine LDH release.

Cell viability assay. 100 000 cells cm^{-2} were plated in 96-well plates and allowed to adhere for 24 h. Then, to study the effects of the microreactors in cell proliferation, microreactors were added to the cell medium at different microreactor to cell ratios (1:20, 1:10, 1:2, and 1:1) and incubated for 24 h. Alternatively, for the determination of the biological activity of the microreactors, microreactors (1:10 ratio) and different concentrations of H_2O_2 or NH_4^+ were incubated with the cells during 24 h instead. Then, the cell medium was renewed and 10% (v/v) of CCK-8 was added to each well. After 2 h of incubation at 37 °C in a humidified atmosphere of 95% air−5% CO_2, 100 μL of the cell medium was transferred into a new 96-well plate and the solution absorbance (λ = 460 nm), which is proportional to the number of cells, was measured using a multiplate reader.

Statistical analysis. All assays in solution were performed with duplicates, with at least three independent repeats. For cell viability assays, every condition was measured in triplicates within every independent repeat. For ICC, five random fields were imaged per condition in each independent repeat. Data are expressed as mean ± standard deviation (SD). Statistical significance was determined using one-way analysis of variance followed by Sidak's multiple comparison test, with $p < 0.05$ considered to represent statistical significance. All data were analyzed in GraphPad Prism (GraphPad Software, Inc., La Jolla, CA, USA).

Results

Pt-NP activity in solution

Pt-NP can act as ROS scavengers due to their SOD- and catalase-like activity and ability to quench superoxide anion (O_2^-), H_2O_2, and free radicals.[VI.22] This property of Pt-NP has been extensively studied, proving that Pt-NP decompose H_2O_2, converting it into hydroxyl radicals in acidic pH, and into water and oxygen in neutral and basic pH.[VI.22] Likewise, it was shown that Pt-NP scavenge O_2^- at neutral pH but not at acidic pH, and that the Pt-NP scavenging activity for $^1O_2$ increases with pH. In addition, smaller Pt-NP show higher catalytic activity due to the increased surface-to-volume ratio.[VI.23] Multiple studies showed that Pt-NP, acting as ROS and free radical scavengers, reduced oxidative damage both *in vitro*[VI.44,45] and *in vivo* for several applications, including bone diseases and pulmonary inflammation.[VI.46,47] In the context of neuronal applications, Pt-NP were able to restore ROS homeostasis in an *in vitro* model of an oxidative stress-related disorder, proving that these particles can act as active ROS scavengers in the brain.[VI.23] Furthermore, Pt-NP have been used as scavengers of O_2^- and H_2O_2 in an mouse model of ischemic stroke,[VI.48] where an i.v. injection of Pt-NP improved neurological function and motor performance and decreased neuronal damage.[VI.48,49]

We aimed to employ Pt-NP as the active entities in microreactors. Therefore, citrate-capped Pt-NP were synthesized by a procedure published earlier,[VI.25] yielding ~2 nm in diameter Pt-NP with narrow dispersity, as confirmed using TEM (**Figure VI.2**).

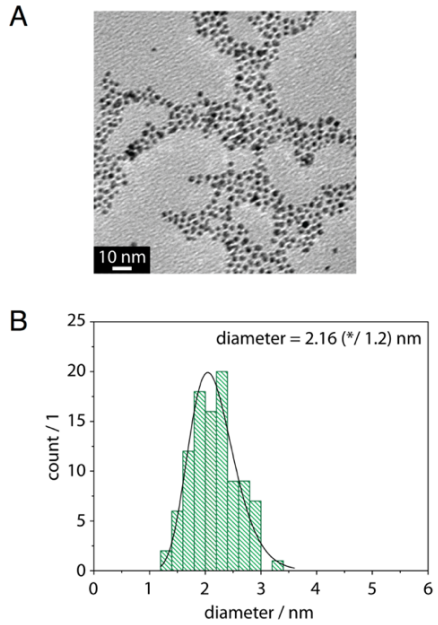


Figure VI.2. Pt-NP synthesis. Representative TEM image (**A**) and the size distribution (**B**) of the Pt-NP is shown. Scale bar = 10 nm.

With the goal to characterize the activity of these Pt-NP in solution, 0.25 mM, 0.50 mM, or 1.0 mM H_2O_2 were incubated with Pt-NP and its consumption was measured after 2, 4, and 24 h. As expected, the Pt-NP were capable of drastically reducing the concentration of H_2O_2 in solution, that is, after 2 h of incubation less than 5% of the original H_2O_2 concentration was left for all tested conditions, with no further significant reduction observed for the later time points (**Figure VI.3A**). It should be noted that the amount of H_2O_2 left in every condition refers to a baseline amount, equal for every condition (Chapter VI Supporting Information, **Figure VI.S1**).

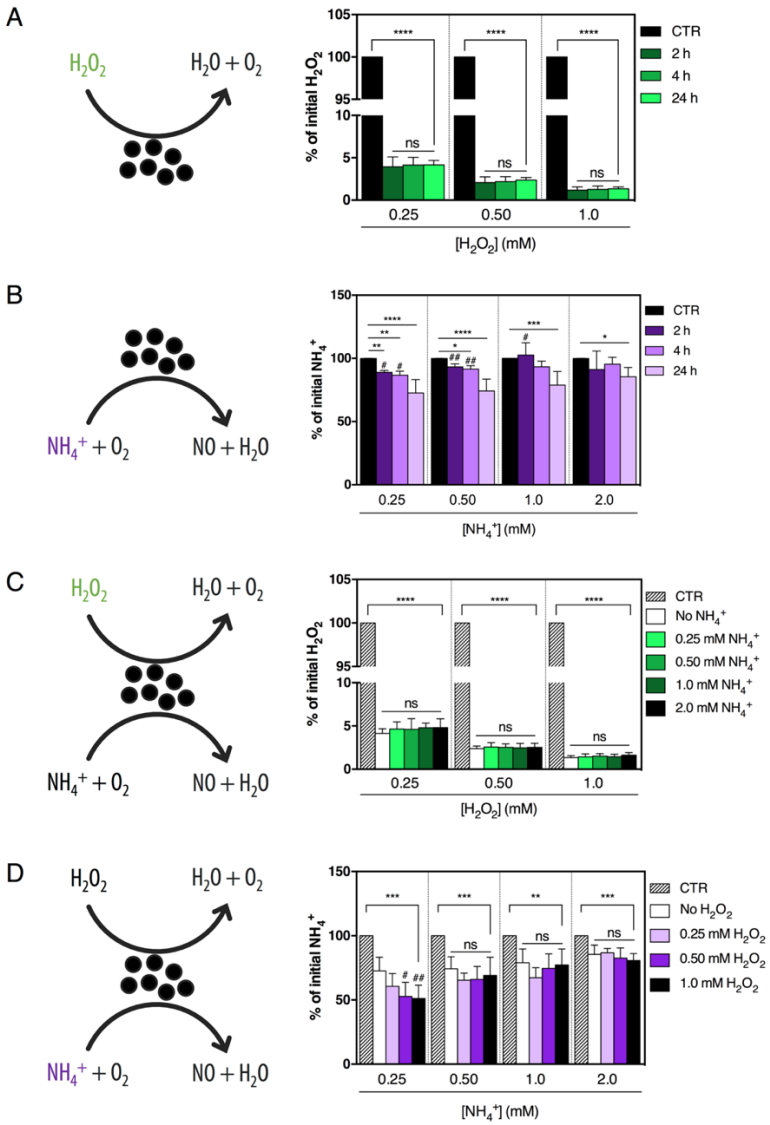


Figure VI.3. Pt-NP as enzyme mimics in solution. (**A**) H_2O_2 degradation. The remaining amount of H_2O_2 was measured at different time points (2, 4, and 24 h) when incubated with Pt-NP using different initial concentrations of H_2O_2 (0.25 mM, 0.50 mM, and 1.0 mM). N=3. ****$p < 0.0001$ compared to control, $^{ns}p > 0.05$ between time points. (**B**) NH_4^+ conversion. The remaining concentration of NH_4^+ in solution was measured after 2, 4, and 24 h when incubated with Pt-NP using different initial NH_4^+ concentrations (0.25 mM, 0.50 mM, 1.0 mM, and 2.0 mM). N=4. *$p < 0.05$, **$p < 0.01$, ***$p < 0.001$, ****$p < 0.0001$ compared to respective control. $^{\#}p < 0.05$, $^{\#\#}p < 0.01$ for comparison with the 24 h time point. (**C**) H_2O_2 degradation in the presence of NH_4^+. Pt-NP were incubated with different combinations of initial concentrations of H_2O_2 (0.25 mM, 0.50 mM, and 1.0 mM) and NH_4^+ (0.25 mM, 0.50 mM, 1.0 mM, and 2.0 mM) for 24 h. N=3. ****$p < 0.0001$ for all conditions compared to control, $^{ns}p > 0.05$ between conditions. (**D**) Degradation of NH_4^+ in the presence of H_2O_2. Pt-NP were incubated with different combinations of initial concentrations of NH_4^+ (0.25 mM, 0.50 mM, 1.0 mM, and 2.0 mM) and H_2O_2 (0.25 mM, 0.50 mM, and 1.0 mM) for 24 h. N=4–9. **$p < 0.01$, ***$p < 0.001$ compared to control. $^{ns}p > 0.05$, $^{\#}p < 0.05$, $^{\#\#}p < 0.01$ for comparison of conditions with the H_2O_2-free condition. All values were normalized to the control condition (no Pt-NP) and are represented as mean ± SD. All controls were set to 100%. All graphs are accompanied by a schematic representation of the measured reaction.

From a different perspective, in bulk, platinum can catalyze the conversion of NH_4^+ into nitric oxide (NO) with high efficiency.[VI.50,51] Interestingly, Pt-NP enclosed in mesoporous silica films were shown to maintain platinum catalytic activity in NH_4^+ degradation in a near ultrahigh-vacuum regime.[VI.51] However, to the best of our knowledge, biomedical applications of this specific Pt-NP activity remain so far unexplored.

With the goal to assess the ability of the Pt-NP to convert NH_4^+ in solution, Pt-NP were exposed to different concentrations of NH_4^+ and the remaining amount of NH_4^+ in solution was monitored after 2, 4, and 24 h. After 2 and 4 h of incubation, it was possible to detect a significant decrease in NH_4^+ for 0.25 mM and 0.50 mM NH_4^+ starting concentrations. Importantly, after 24 h of incubation, it was possible to observe that the Pt-NP converted a significant amount of NH_4^+ for all tested conditions (**Figure VI.3B**).

In order to investigate if the Pt-NP activity was affected by the presence of both H_2O_2 and NH_4^+, Pt-NP were incubated with different concentrations of both compounds simultaneously for 24 h. The results showed that adding increasing amounts of NH_4^+ had no effect on the ability of Pt-NP to convert H_2O_2 (**Figure VI.3C**). On the other hand, adding increasing amounts of H_2O_2 to a Pt-NP solution containing 0.25 mM NH_4^+ significantly improved the Pt-NP-catalyzed conversion of NH_4^+ by ~20% in the presence of 1.0 mM H_2O_2 in comparison to the H_2O_2-free condition. This effect could only be detected for the lowest concentration of NH_4^+ tested, with no H_2O_2-dependent significant changes in NH_4^+ conversion by the Pt-NP observed for higher NH_4^+ starting concentrations (**Figure VI.3D**). This observation might be explainable, considering that H_2O_2 can be used as a source of hydroxyl radicals and these oxidizing molecules can lead to the oxidation of NH_4^+.[VI.52] Indeed, mixtures of NH_4^+ and H_2O_2 have been used in wet chemical cleaning processes, in the form of ammonium hydroxide-hydrogen peroxide mixtures.[VI.53] It was shown that, in these mixtures, the concentration of both NH_4^+ and H_2O_2 decreased over time, probably due to the decomposition of H_2O_2 and the hydroxyl-induced conversion of NH_4^+.[VI.53] In our work, since the Pt-NP decompose H_2O_2 and NH_4^+ simultaneously, it is possible to hypothesize that the products of H_2O_2 degradation might, by themselves, exacerbate the oxidation of NH_4^+, thus contributing to an enhanced decrease in NH_4^+ in solution.

Microreactor assembly

Microreactors were assembled by the layer-by-layer (LbL) technique using 19.30 μm PS particles coated with PDA (M^i) and PLL prior to the deposition of the catalytically active Pt-NP (M^{Pt}) and different terminating polymer layers. The deposition of the initial PDA layer makes the assembly of the microreactors independent of the template particles, that is, instead of PS, other materials such as silica, melamine resin, or poly(methyl methacrylate) could be used without the need to re-evaluate the assembly protocol. First, the LbL film deposition was confirmed on planar surfaces using quartz crystal microbalance with dissipation monitoring (Chapter VI Supporting Information, **Figure VI.S2**). Following on, the multilayers were assembled onto PS particles and the ζ-potential was monitored after each adsorption step. The assembly of M^i was confirmed by the color

change of the initially white PS particles into dark gray particles (**Figure VI.4A**). The subsequent deposition of PLL was illustrated by the ζ-potential change from ~ −34 mV to ~26 mV and visualized using CLSM employing PLL_F (**Figure VI.4B**). The successful Pt-NP adsorption onto the PDA/PLL precoated carrier particles yielding M^{Pt} was confirmed by the ζ-potential change from ~26 mV to ~2 mV and TEM images (**Figure VI.4C**). In the latter case, the particle surfaces were smooth and rough in the absence and presence of the Pt-NP, respectively. Different terminating layers were employed with the aim to optimize the interaction of the microreactors with the neuroblastoma cells. To this end, positively and negatively charged microreactors were assembled.

Additionally, PDA was chosen as a terminating layer due to its known beneficial effects on cell adhesion as, for instance, shown by Yang *et al.*[VI.54] and Xu *et al.*[VI.55] Positively charged microreactors (M^+) were obtained by coating M^{Pt} with PLL. The obtained positive ζ-potential (~19 mV) and the visualization by CLSM using PLL_F confirmed the deposition of this PLL layer (**Figure VI.4D**). PDA-coated (M^{PDA}) and negatively charged (M^-) microreactors were yielded by an additional deposition of PDA and PMA, respectively, on M^+. The deposition of the PDA terminating layer was illustrated by the negative ζ-potential (~ −18 mV) and the color change of the microreactors from dark gray to black (**Figure VI.4E**). The negative ζ-potential (~ −60 mV) and the green fluorescence in the CLSM images originating from the deposited PMA_F confirmed the assembly of M^- (**Figure VI.4F**). Microreactors without a terminating layer (M^{Pt}) were used as control, to ensure that the terminating layers did not block the catalytic activity of Pt-NP.

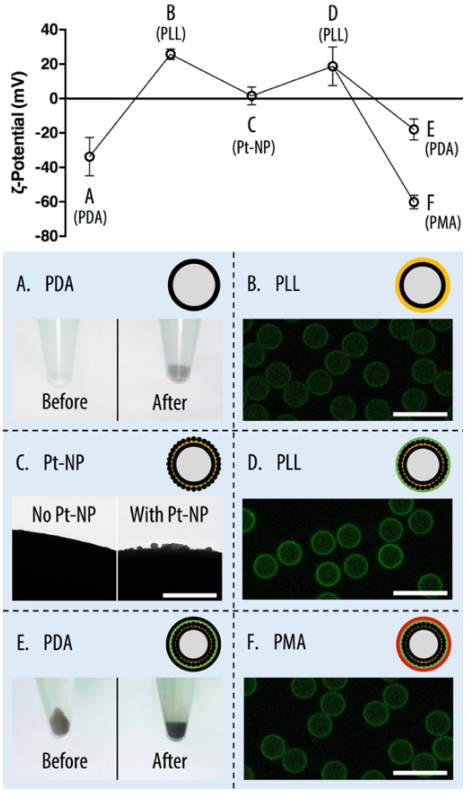


Figure VI.4. ζ-potential measurements of the microreactors at the different steps in the LbL assembly (N=2) including representative images. The PDA deposition is confirmed by color change (**A**: M^i: color change from white to dark gray, **E**: M^{PDA}: color change from dark gray to black). The deposition of the PLL_F and PMA_F layers are imaged using CLSM (**B**, **D**: M^+, **F**: M^-). Pt-NP deposition is confirmed by TEM (**C**: M^{Pt}). CLSM scale bar = 40 µm. TEM scale bar = 1 µm.

Following on, the catalytic activity of the microreactors was assessed. 10^4 or 10^5 microreactors were incubated with 1.0 mM H_2O_2 for 24 h before the remaining H_2O_2 was detected. In the first case (10^4 microreactors) ~ 30% of H_2O_2 was consumed, while almost all H_2O_2 was used up in the latter case (10^5 microreactors) (**Figure VI.5A**). The average conversion of a single microreactor was estimated to be (2.59 ± 0.249) ×

10^{-4} nmol H_2O_2 h^{-1}. The terminating layer did not significantly affect the Pt-NP activity (Chapter VI Supporting Information, **Figure VI.S3**), indicating that neither the deposition of the terminating layer(s) displaced Pt-NP from the carrier particle surface, nor did their presence hinder the access of H_2O_2 to the Pt-NP surface. As expected, M^i did not show catalytic activity toward H_2O_2. In addition, it was confirmed that the catalytic activity toward H_2O_2 of M^{PDA} was maintained in cell medium (Chapter VI Supporting Information, **Figure VI.S4**). Furthermore, although PDA degradation due to H_2O_2 was shown before,[VI.56] the H_2O_2 concentrations used here were ~2000× lower and the pH was neutral and not basic.

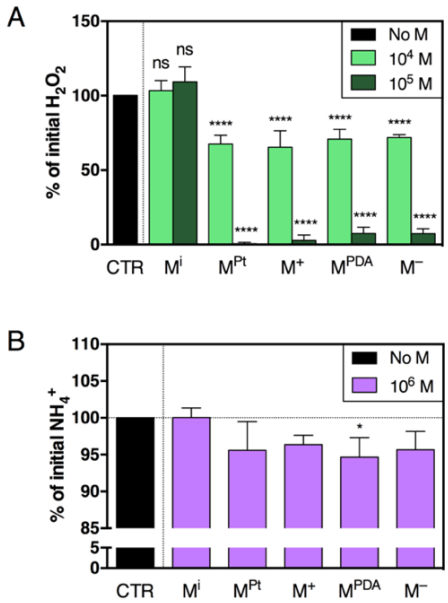


Figure VI.5. Pt-NP-based microreactors in solution. (**A**) Pt-NP-based microreactors as H_2O_2 scavengers. The amount of remaining H_2O_2 in solution after incubation of 1.0 mM H_2O_2 with 10^4 or 10^5 microreactors (M) for 24 h is shown. N=3. $^{ns}p > 0.05$, ****$p < 0.0001$ compared to control (no microreactors). (**B**) Pt-NP-based microreactors for NH_4^+ degradation. The remaining amount of NH_4^+ was measured after 10^6 microreactors (M) were incubated with 1.0 mM NH_4^+ for 24 h. N=3−4. *$p < 0.05$ compared to control (no microreactors). Controls were set to 100%. All values were normalized to the respective control and are represented as mean ± SD.

Similarly, 10^6 microreactors were exposed to 1.0 mM NH_4^+ for 24 h and the amount of remaining NH_4^+ in solution was measured (**Figure VI.5B**). It was observed that all microreactors were catalytically active, consuming similar amounts of NH_4^+. It was estimated that, in average, a single microreactor converted $(1.84 \pm 0.291) \times 10^{-6}$ nmol NH_4^+ h^{-1}. M^i did not show catalytic activity toward NH_4^+.

Taken together, functional Pt-NP-based microreactors, with controllable surface chemistry and capability to convert H_2O_2 and NH_4^+, were assembled.

Microreactors and neuroblastoma cells: proliferation

With the aim to assess the effects of the microreactors on the cell viability and proliferation of neuroblastoma cells, 100 000 cells cm^{-2} were seeded in 96 well-plates and incubated for 24 h at 37 °C in a humidified atmosphere of 95% air−5% CO_2. Subsequently, different numbers of microreactors were added to the cell medium and incubated for 24 h before the cell viability was measured. The cell viability was normalized to cells grown in the absence of microreactors. In general, increasing the number of microreactors led to a decrease in the number of cells, compared to the control condition.

Incubating the cells with microreactors, regardless of the terminating layer, at a ratio of one microreactor per one or two cells led to a decrease of ~50% or more in the number of cells present in culture, compared to the control condition (no microreactors). In these conditions,

the differences between the terminating layers of the microreactors might be caused by how these different coatings interact with the cells. Since the neuronal cell membrane has a negative charge, both M^+ (**Figure VI.6B**) and M^{PDA} (**Figure VI.6C**) will adhere more to the cells compared to M^{Pt} (**Figure VI.6A**), causing a bigger impact in the reduction of number of cells. For the same reason, M^- might not interact as much with the cells, possibly impeding their proliferation due to its surface charge (**Figure VI.6D**). Interestingly, at lower ratios, no significant differences in the number of cells were found between different microreactors co-cultured at the same ratio (Chapter VI Supporting Information, **Figure VI.S5**). The decreasing cell numbers with increasing number of microreactors could be explained by either the microreactors inducing more cell death, or their presence having a negative effect in cell proliferation. In order to clarify the reason for the decreased cell count, a Live/Dead staining assay was employed. 50 000 cells cm^{-2} were grown for 48 h and then exposed to 10^5 microreactors for 24 h. Then, the cells were stained with FDA and PI to visualize the live and dead cells, respectively. The number of dead cells (magenta cells) was negligible in every condition (**Figure VI.6E**). Additionally, a LDH cytotoxicity assay was performed, to ensure the cell membrane integrity when the cells were exposed to the microreactors. LDH release occurs when cell membranes are compromised and the cells begin processes of cell death.[VI.57] This assay was performed on cell cultures prepared in the same manner as for the cell viability assay described above. After the 24 h incubation, the activity of released LDH was measured for all conditions, using cells not exposed to microreactors as a negative control (to establish baseline spontaneous LDH release) and using cells exposed to lysis buffer as a positive control (to determine the maximum LDH release). It was observed that the levels of LDH release in cells exposed to microreactors were undistinguishable from the baseline spontaneous LDH release (**Figure VI.6F**). On the other hand, cells exposed to the lysis buffer, that is, cells with compromised membranes, showed significantly higher levels of LDH release. Thus, it can be concluded that the microreactors did not interfere with the membrane integrity. Therefore, taking all these assays into account, it can be hypothesized that the microreactors are not cytotoxic, but interfere with cell proliferation, likely due to contact inhibition of proliferation (CIP). CIP refers to the process by which cells stop or slow their proliferation due to high confluence and mechanical constraints, and is one of the factors that lead to monolayer cell growth. For a review on the subject, the reader is referred to the publication of McClatchey and Yap.[VI.58] Indeed, it has been shown that, when the free space available per cell was reduced, the affected cells slowed their proliferation and eventually reached a quiescent state.[VI.59] In our experimental setup, increasing the number of microreactors in culture led to less available space for the cells and, thus, might have caused a higher mechanical stress with concomitant arrest of proliferation. In light of these results, a ratio of one microreactor per ten cells was chosen for most of the following experiments, to ensure high catalytic activity while minimizing the negative effects on the cell proliferation.

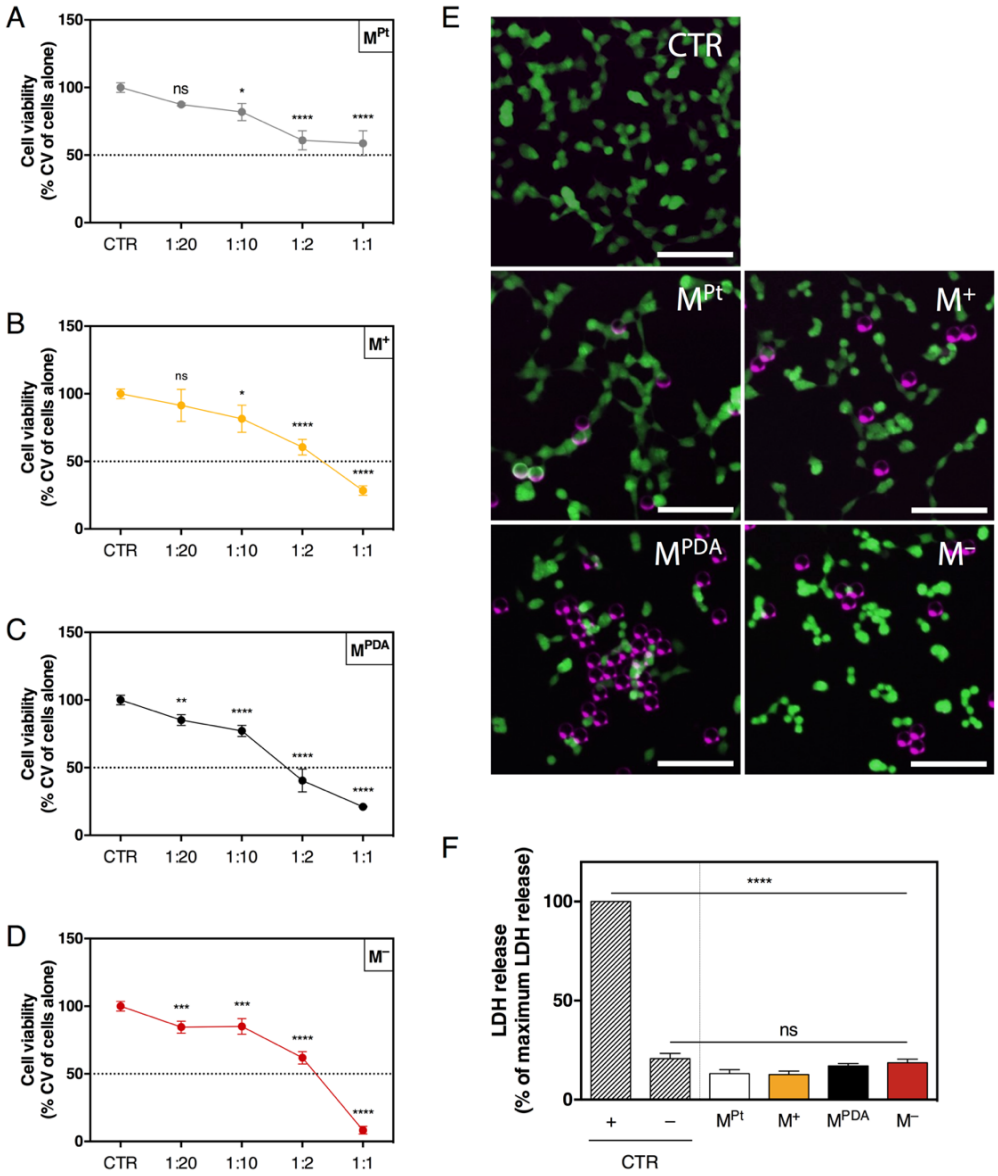


Figure VI.6. Cell viability/proliferation of neuroblastoma cells incubated with (**A**) Pt-NP-coated microreactors (M^{Pt}; N=3; *p < 0.05, **p < 0.01, ****p < 0.0001 compared to control), (**B**) positively charged microreactors (M^{+}; N=3; ^{ns}p > 0.05, *p < 0.01, ****p < 0.0001 compared to control), (**C**) PDA-coated microreactors (M^{PDA}; N=4−5; **p < 0.01, ****p < 0.0001 compared to control), and (**D**) negatively charged microreactors (M^{-}; N=3; ****p < 0.0001 compared to control). All values were normalized to the control (no microreactors) and are represented as mean ± SD. Controls were set to 100% of cell viability. (**E**) Representative fluorescent images of the Live/Dead assay, showing live cells (green) and microreactors (magenta). No dead cells (magenta cells) were found in any condition. Scale bars = 100 µm. (**F**) LDH cytotoxicity assay. The levels of LDH release were measured in cells treated with lysis buffer (positive control), cells grown in the absence of microreactors (negative control), and cells exposed to the differently coated microreactors, at a 1:1 ratio, for 24 h. The maximum LDH release, shown in the negative control, was set to 100% and other values were normalized to it. N=3. ^{ns}p > 0.05 for comparison with negative control, ****p < 0.0001 for comparison with positive control. Data are represented as mean ± SD.

Microreactors and neuroblastoma cells: attachment

In a next step, the cell attachment to the microreactors was analyzed in more detail. To this end, the microreactors were incubated with the neuroblastoma cells in a theoretical microreactor to cell ratio of 1:1 and 1:10 and allowed to adhere for 24 h, followed by medium change, cell fixing and staining for microscopy analysis. In this experimental set up, only microreactors which were attached to the cells were detected – the free or loosely bound microreactors were washed away. The experimental microreactor to cell ratios were then calculated. When incubated at a theoretical ratio of 1:1, that is, when the number of microreactors and cells should be the same, all microreactors were present at a much lower ratio (**Figure VI.7A**, left bars). For instance, there were 10× more cells than M^{Pt} present in the culture. While M^{Pt}, M^{+}, and M^{-} attached in the same amounts, significantly more M^{PDA} could be found, indicating that PDA had a beneficial effect on the cell adhesion to the microreactors. Similarly, at the theoretical ratio 1:10, that is, the number of microreactors should be 10× lower than the number of cells, the experimental microreactor to cell ratio was significantly lower for all the tested microreactors (**Figure VI.7A**, right bars). Representative microscopy images reflect these observations (**Figure VI.7B**), where the number of microreactors (green) in comparison to the number of cells (blue nuclei) varies with the microreactor surface coating. For M^{Pt}, representative bright field images are shown.

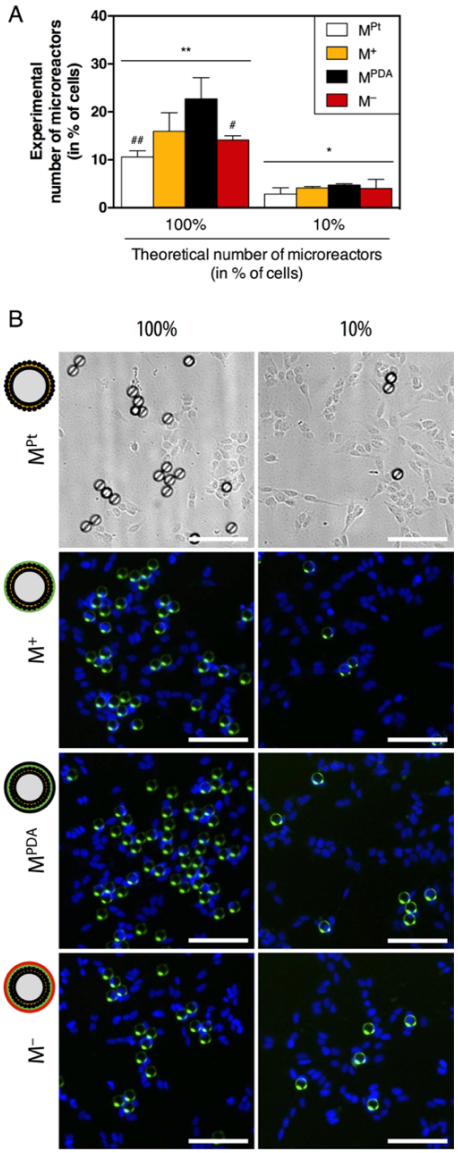


Figure VI.7. Surface coating dependent cell adhesion. (**A**) Number of microreactors, expressed as % of cells, present after medium change and ICC. The number of microreactors and cells per field was counted. The total number of cells was set to 100% and the number of microreactors was normalized to it. N=3–4. *$p < 0.05$, **$p < 0.01$ compared to the theoretical ratio. $^{\#}p < 0.05$, $^{\#\#}p < 0.01$ compared to M^{PDA}. (**B**) Representative fluorescence images of microreactors (green: PLL_F) incubated with neuroblastoma cells (blue nuclei). For M^{Pt}, representative bright field images are shown. Scale bars = 100 µm.

Taking these results into account, M^{PDA} were chosen for further studies, due to their higher cell adhesive properties. PDA was previously shown to be noncytotoxic[VI.60,61] and beneficial for neuronal cells.[VI.62,63] Specifically, PDA-coated substrates exhibited increased neuronal adhesion, causing no alterations in neuronal communication and excitability, and possessing no neurotoxic effects.[VI.63] Furthermore, while detailed studies on PDA degradation in biological environments are rare, it was shown that PDA neither led to the formation of monomeric dopamine[VI.39] nor did it present dopaminergic activity.[VI.64]

Microreactors and neuroblastoma cells: activity

Prior efforts have been attempted to enzymatically alleviate the toxic effects of H_2O_2 in neuronal cell cultures. For instance, it has been shown, in rat striatal neuronal culture, that pharmacological-induced production of H_2O_2 could be blocked by co-administration of the inducing drug and catalase.[VI.65] Additionally, catalase-containing nanoparticles have also been recently used to prevent the toxic effects of H_2O_2, in a study where primary human neuronal cultures were exposed to exogenous H_2O_2.[VI.66]

In contrast to these prior reports, we employed a simple microreactor to support neuroblastoma cells. To evaluate the protective effects of M^{PDA} toward cell toxicity, neuroblastoma cells were incubated with M^{PDA} (one microreactor per ten cells ratio) and different concentrations of H_2O_2 or NH_4^+. Control experiments were performed using inactive microreactors (M^i) at the same ratio. It should be noted that, in the absence of toxic compounds, there were no significant differences in cell viability of cells incubated with M^i and with M^{PDA} at a 1:10 ratio (Chapter VI Supporting Information, **Figure VI.S6**). 100 000 cells cm^{-2} were plated and allowed to stabilize for 24 h and, then, microreactors (M^i or M^{PDA}) and different concentrations of H_2O_2 or NH_4^+ were simultaneously added to the cell medium and incubated for another 24 h (**Figure VI.8A**). The range of concentrations for both toxic compounds was determined by performing the same assay in neuroblastoma cells not exposed to microreactors (Chapter VI Supporting Information, **Figure VI.S7**). In the described experimental setup, not all microreactors are attached to the cells, as discussed in the attachment section above, being present both loose in solution and adhered to cells (**Figure VI.8B**). Thus, their catalytic activity will affect the cell medium in general, and not only in the immediate surrounding of cells. Cell viability data showed that M^{PDA} have a significant protective effect against the cytotoxic effects of H_2O_2, compared to cells exposed to M^i (**Figure VI.8Ci**). Although these findings are not surprising, since Pt-NP were expected to have a protective effect toward H_2O_2 due to their catalase-like activity, converting H_2O_2 into H_2O and O_2, nontoxic products,[VI.22] this is the first time that Pt-NP were integrated into microreactors to be used as artificial cells.

Additionally, M^{PDA} also showed a beneficial effect toward NH_4^+ toxicity as illustrated by the cell viability data (**Figure VI.8Cii**). Interestingly, while no cell toxicity in the presence of low NH_4^+ concentrations and M^i was detected, M^{PDA} increased the cell viability at these NH_4^+ concentrations. This observation could be explained by the fact that NH_4^+ is converted into NO by M^{PDA}.[VI.51] Although NH_4^+ and NO can

be neurotoxic at high concentrations,[VI.8,67,68] it is possible to hypothesize that the cells were only exposed to low concentrations of NO due to the NH_4^+ conversion by M^{PDA}. More specifically, according to our *in vitro* data (**Figure VI.5B**), only ~7% of the initial low concentration NH_4^+ (max. 5 mM) would be converted into NO. NO, in lower concentrations, is known to promote neuronal activity,[VI.69,70] illustrating that M^{PDA} could not only prevent the cytotoxic actions of H_2O_2, but these artificial entities seemed to also convert the toxic compound NH_4^+, yielding a positive cell response.

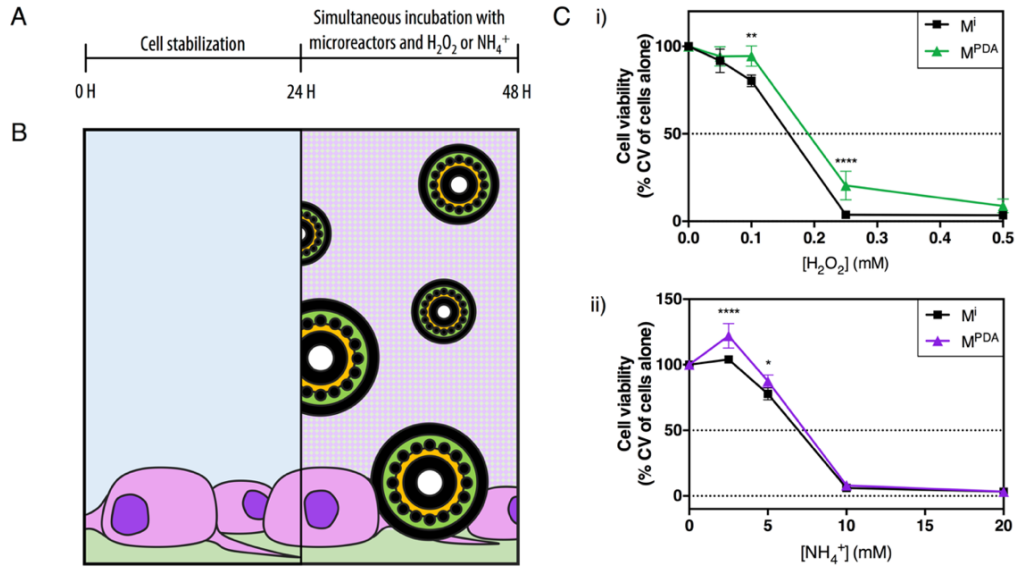


Figure VI.8. M^{PDA} offer protection against H_2O_2 and NH_4^+ toxicity. (**A**) Schematic representation of the experimental setup. (**B**) Illustration of microreactor-cell interaction. In the first frame, cells grow and stabilize for 24 h. In the second frame, microreactors (M^{PDA} or M^i) and toxic compounds (either H_2O_2 or NH_4^+) are incubated with the cells for more 24 h. (**C**) Cell viability assays performed in the presence of different concentrations of H_2O_2 or NH_4^+, with active (M^{PDA}) or inactive (M^i) microreactors. (**i**) Neuroblastoma cells were exposed to different concentrations of H_2O_2 and M^{PDA} or M^i (1:10 ratio) for 24 h. N=3. **p < 0.01, ****p < 0.0001 compared to M^i. (**ii**) Neuroblastoma cells were incubated for 24 h with M^{PDA} or M^i (1:10 ratio) and different concentrations of NH_4^+. N=3−5. *p < 0.05, ****p < 0.0001 compared to M^i. For each condition, cell viability in the absence of toxic compounds was set to 100%. All values were normalized to the respective cell viability in the absence of toxic compounds and are represented and mean ± SD.

Conclusion

Taken together, we demonstrated the assembly of a microreactor using Pt-NP as ROS and NH_4^+ scavengers and showed their protective and stimulating effects on neuroblastoma cells. Furthermore, this work represents the first attempt to create a simple artificial astrocyte to counteract excitotoxicity and it is, to our knowledge, the first study that focuses on PDA/Pt-NP- based cell mimics as a therapeutic approach in a neuronal setting. Admittedly, the supportive effect of the microreactors needs to be improved, for instance by adding multiple layers of Pt-NP. Moreover, more in-depth biological evaluations, including the effect of the microreactors on endogenous H_2O_2 or assessing the intracellular responses to the presence of the microreactors, are required. Nonetheless, these findings are considerably advancing the field of cell mimicry, opening up vast possibilities to address the tremendous need for novel therapeutic concepts to counteract neurological medical challenges. Considering the diverse assembly possibilities of microreactors (e.g., compartmentalization, targeting, multiple biocatalytic cargo, etc.), tailor-made artificial cells might be feasible depending on the targeted neurological condition.

chapter VI supporting information

Raw fluorescence intensity data for Pt-NP-catalyzed H_2O_2 degradation.

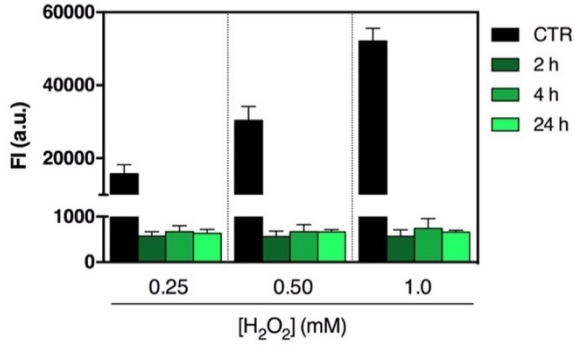


Figure VI.S1. Pt-NP as enzyme mimics for H_2O_2 degradation. Pt-NP were incubated with different concentrations of H_2O_2 (0.25 mM, 0.50 mM, and 1.0 mM) and the remaining amount of H_2O_2 in solution was measured after 2, 4, and 24 h. Only a baseline fluorescent signal was measured after the incubation time in all cases. N=3. Data are represented as mean ± SD.

Film assembly on planar surface.

Methods

Quartz crystal microbalance with dissipation monitoring (QCM-D) measurements (Q-Sense E4, Sweden) were used to analyze the adsorption behavior of Pt-NP-containing polymer films. Silica-coated crystals (QSX300, Q-Sense) were cleaned in a 2% (w/w) SDS solution overnight, rinsed with ultrapure water and dried with nitrogen, exposed to UV/ozone for 30 min, and pre-coated with PDA (2.5 mg mL^{-1} in TRIS buffer, 30 min). Then the crystals were dried and mounted into the chambers of the QCM-D instrument. The frequency changes (Δf) and dissipation changes (ΔD) were monitored at 20 ± 0.02 °C. After a stable baseline was obtained in HEPES buffer, a PLL solution

(1 mg mL^{-1} in HEPES buffer) was introduced into the chambers and let to adsorb. When the surface was saturated, the chambers were rinsed with HEPES buffer. The pre-coated PLL crystals were exposed to a Pt-NP solution until the surface was saturated and the chambers were rinsed with HEPES buffer. A layer of PLL (1 mg mL^{-1} in HEPES buffer) was adsorbed onto these pre-coated crystals prior to the exposure to either PMA (4 mg mL^{-1} in HEPES buffer) or PDA (2.5 mg mL^{-1} in TRIS buffer, 1 h, flow rate 56 µL min^{-1}). Normalized frequencies using the third harmonics are presented.

Results

The detected changes in frequency change (Δf, **Figure VI.S2A**) and dissipation change (ΔD, **Figure VI.S2B**) of the PDA pre-coated QCM-D crystals confirmed that the film assembly via the LbL technique was successful.

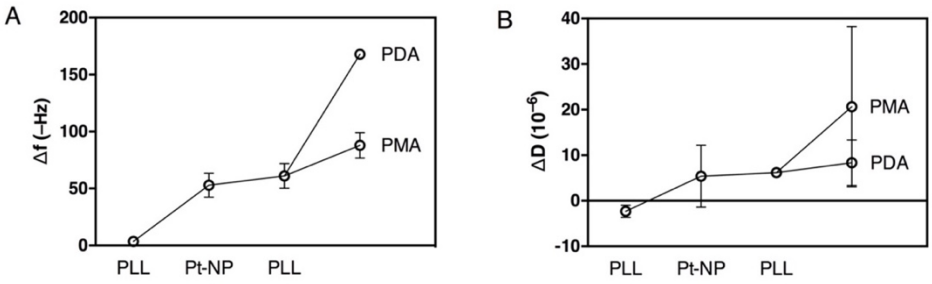


Figure VI.S2. Changes in frequency (Δf, **A**) and dissipation (ΔD, **B**) of a silica/PDA pre-coated QCM-D crystal upon deposition of PLL, Pt-NP, and PLL. Finally, either PMA or PDA were used as terminating layers.

Effects of different terminating layers on microreactor H_2O_2 scavenging properties.

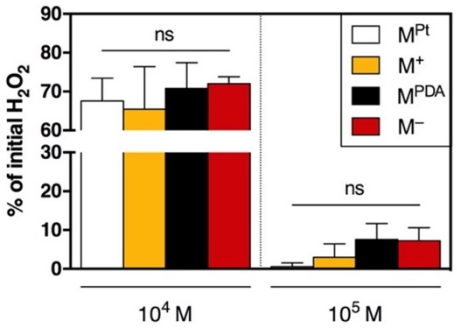


Figure VI.S3. Pt-NP-catalyzed conversion of H_2O_2 by microreactors (M) is not affected by the terminating layer, for both 10^4 or 10^5 microreactors incubated with 1.0 mM H_2O_2 for 24 h. $^{ns}p > 0.05$ for comparison between the different microreactors. The initial concentration of H_2O_2 was set to 100% and all values were normalized to it. Data are represented as mean ± SD.

Detection of H_2O_2 consumption by microreactors in cell medium.

Methods

Cell medium was exposed to 1.0 mM H_2O_2 and 10^4 or 10^5 microreactors (M^i or M^{PDA}) for 24 h at 37 °C. At this point, samples were centrifuged (1 min, 9 000 rpm), in order to separate the microreactors from the solution, and the supernatant was incubated with 0.16 mM *o*-dianisidine and 2 U mL^{-1} HRP for 30 min at room temperature. The absorbance of the solutions was read at 500 nm. To ascertain the linearity of this H_2O_2 detection assay, different concentrations of H_2O_2 (0.25 mM, 0.50 mM, and 1.0 mM) were added to cell medium in the absence of microreactors and the same protocol was performed.

Results

With this detection method, it was possible to linearly detect the concentration of H_2O_2 in cell medium for all concentrations tested (**Figure VI.S4A**). Furthermore, when the microreactors were incubated with H_2O_2 in cell medium, it was possible to confirm the catalytic activity of M^{PDA}, whose actions lead to a considerable decrease of the initial H_2O_2 concentration (**Figure VI.S4B**). On the other hand, no consumption of H_2O_2 was detected when H_2O_2-containing cell medium was mixed with M^i. These data corroborate that M^{PDA} maintain their catalytic activity in cell medium, thus being able to ameliorate cell viability in the presence of H_2O_2.

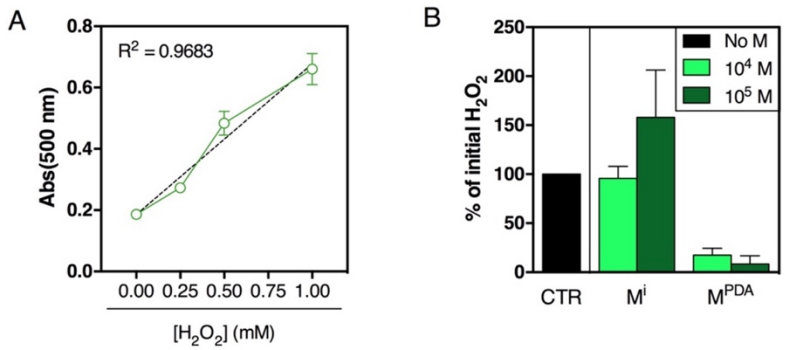


Figure VI.S4. H_2O_2 degradation by M^{PDA} in cell medium. (**A**) Cell medium was exposed to different concentrations of H_2O_2 (0.25 mM, 0.50 mM, and 1.0 mM) and its concentration was measured, to ensure a linear response within this range of concentrations. A linear regression applied to the values obtained led to R^2 = 0.9683. N=3. Data are represented as mean ± SD. (**B**) 10^4 or 10^5 microreactors (either M^i or M^{PDA}) were incubated with 1.0 mM H_2O_2 for 24 h in cell medium. At that point, the remaining concentration of H_2O_2 in solution was measured. The value obtained for H_2O_2 in cell medium without microreactors was set to 100% and other values normalized to it. N=2. Data are represented as mean ± SD.

Cell viability: comparison between different microreactor terminating layers and different microreactor to cell ratios.

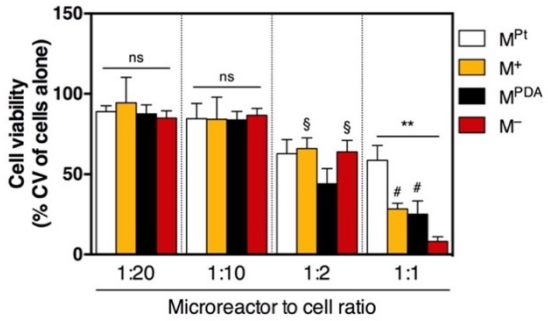


Figure VI.S5. Effects of the terminating layers of the microreactors in cell proliferation. At lower microreactor to cell ratios, the decrease in the number of cells is independent of the terminating layer of the microreactors. $^{ns}p > 0.05$ for comparison between different microreactors. $^{**}p < 0.01$ for comparison with M^{Pt}. $^{\S}p < 0.05$ for comparison with M^{PDA}. $^{\#}p < 0.05$ for comparison with M^{-}. Cell viability for cells not exposed to microreactors was set to 100% and all other values were normalized to it. Data are represented as mean ± SD.

Cell viability in the presence of active and inactive microreactors at a one microreactor to ten cells ratio.

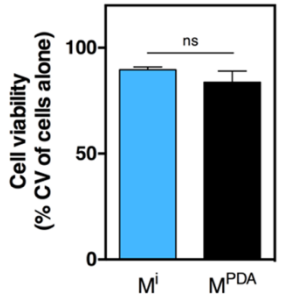


Figure VI.S6. Cell viability of undifferentiated SH-SY5Y cells incubated with M^{i} or M^{PDA} at a ratio of one microreactor per ten cells for 24 h, normalized to the cell viability of cells not exposed to microreactors (100%). No significant differences can be observed between the two tested microreactors. $^{ns}p > 0.05$. Data represented as mean ± SD.

Dose-response curves for neuroblastoma cells in the presence of H_2O_2 or NH_4^+.

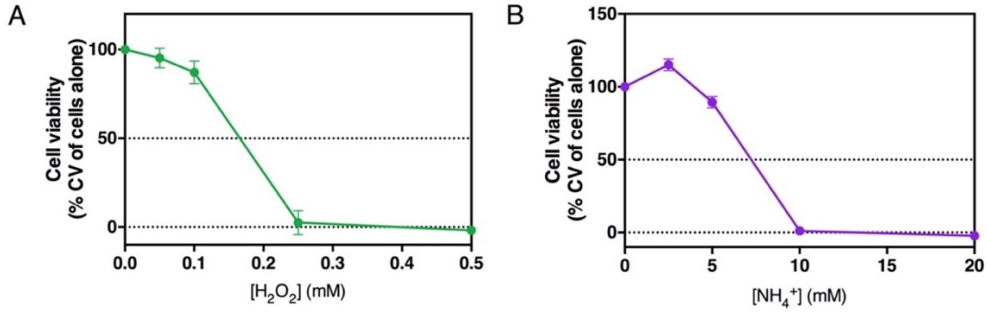


Figure VI.S7. Cell viability curves of undifferentiated SH-SY5Y cells exposed to different concentrations of H_2O_2 or NH_4^+. Cells were exposed to different concentrations of H_2O_2 (**A**) and NH_4^+ (**B**) for 24 h prior to the cell viability measurements. **A**: N=3, **B**: N=4. The cell viability of cells not exposed to any toxic compound was set to 100% and all other values were normalized to it. Data are represented as mean ± SD.

Calculation of average activity per microreactor in solution.

Both H_2O_2 and NH_4^+ were detected using fluorescence intensity methods that provide a linear response for the range of concentrations used. Also, for both assays, a positive control was measured, using a solution with the initial concentration of H_2O_2 or NH_4^+ and no microreactors (no enzymatic consumption of the substrates).

For the H_2O_2 detection assay, the 100% of the positive control corresponds to 1.0 mM H_2O_2 (the initial concentration added to each condition), in a reaction volume of 200 µL. The percentage of H_2O_2 measured after 24 h for each condition corresponds to the amount of H_2O_2 not consumed. The results obtained using 10^4 microreactors were used for the determination of the activity per microreactor. For the 10^5 microreactors, the measured values were almost negligible, which could mean that all H_2O_2 had been already consumed over the course of the 24 h incubation. Taking the 10^4 M^{Pt} condition as an example:

$$[H_2O_2]_{initial} = 1.0 \text{ mM } (100\%) \qquad n(H_2O_2)_{initial} = 200 \text{ nmol}$$

$$[H_2O_2]_{final} = 675.7 \text{ µM } (67.57\%) \qquad n(H_2O_2)_{final} = 135.14 \text{ nmol}$$

$$v_{reaction} = 200 \text{ µL}$$

$$n(H_2O_2)_{consumed} = n(H_2O_2)_{initial} - n(H_2O_2)_{final} = 200 - 135.14 = 64.86 \text{ nmol}$$

Considering there were 10^4 microreactors in solution:

$$n(H_2O_2)_{consumed} \text{ microreactor}^{-1} = 64.86 / 10\,000 = 6.49 \times 10^{-3} \text{ nmol}$$

This value represents the amount of H_2O_2 one microreactor consumed over 24 h. To obtain the activity of one microreactor per hour:

$$n(H_2O_2)_{consumed} \text{ h}^{-1} \text{ microreactor}^{-1} = (6.49 \times 10^{-3}) / 24 = 2.70 \times 10^{-4} \text{ nmol h}^{-1}$$

Since there were no significant differences in activity between the differently coated microreactors, it is possible to repeat this process for all tested microreactors and average their activity, as shown in **Table VI.S1**.

Table VI.S1. Summary of the steps for the determination of the average activity per microreactor towards H_2O_2.

Microreactor	% H_2O_2	nmol$(H_2O_2)_{final}$	nmol$(H_2O_2)_{consumed}$	nmol$(H_2O_2)_{consumed}$ microreactor^{-1}	nmol$(H_2O_2)_{consumed}$ h^{-1} microreactor^{-1}
M^{Pt}	67.57	135.14	64.86	6.49×10^{-3}	2.70×10^{-4}
M^{+}	65.44	130.88	69.12	6.91×10^{-3}	2.88×10^{-4}
M^{PDA}	70.81	141.62	58.38	5.84×10^{-3}	2.43×10^{-4}
M^{-}	71.98	143.96	56.04	5.60×10^{-3}	2.34×10^{-4}

Which leads to a final average activity per microreactor of:

$$A_{average} = (2.59 \pm 0.249) \times 10^{-4} \text{ nmol}(H_2O_2)\ h^{-1}$$

The same approach was applied to the NH_4^+ detection assay to determine the average activity per microreactor. In this case, 10^6 microreactors were incubated with 1.0 mM NH_4^+ during 24 h, in a reaction volume of 1 mL. The 100% of the positive control corresponds to 1.0 mM (and, thus, 1 000 nmol) NH_4^+.

Table VI.S2. Summary of the steps for the determination of the average activity per microreactor towards NH_4^+.

Microreactor	% NH_4^+	nmol$(NH_4^+)_{final}$	nmol$(NH_4^+)_{consumed}$	nmol$(NH_4^+)_{consumed}$ microreactor^{-1}	nmol$(NH_4^+)_{consumed}$ h^{-1} microreactor^{-1}
M^{Pt}	95.61	956.1	43.9	4.39×10^{-5}	1.83×10^{-6}
M^{+}	96.37	963.7	36.3	3.63×10^{-5}	1.51×10^{-6}
M^{PDA}	94.67	946.7	53.3	5.33×10^{-5}	2.22×10^{-6}
M^{-}	95.68	956.8	43.2	4.32×10^{-5}	1.80×10^{-6}

Since no significant differences between differently coated microreactors were found, averaging all determined activity values leads to a final average activity per microreactor of:

$$A_{average} = (1.84 \pm 0.291) \times 10^{-6} \text{ nmol}(NH_4^+)\ h^{-1}$$

chapter VI references

VI.1 Dong X, Wang Y, Qin Z. Molecular Mechanisms of Excitotoxicity and Their Relevance to Pathogenesis of Neurodegenerative Diseases. *Acta Pharmacol Sin* **2009**, *30* (4), 379–387.

VI.2 Mehta A, Prabhakar M, Kumar P, Deshmukh R, Sharma PL. Excitotoxicity: Bridge to Various Triggers in Neurodegenerative Disorders. *Eur J Pharmacol* **2013**, *698* (1–3), 6–18.

VI.3 Sattler R, Tymianski M. Molecular Mechanisms of Glutamate Receptor-Mediated Excitotoxic Neuronal Cell Death. *Mol Neurobiol* **2001**, *24* (1–3), 107–129.

VI.4 Yi J-H, Hazell AS. Excitotoxic Mechanisms and the Role of Astrocytic Glutamate Transporters in Traumatic Brain Injury. *Neurochem Int* **2006**, *48* (5), 394–403.

VI.5 Connolly NMC, Prehn JHM. The Metabolic Response to Excitotoxicity - Lessons from Single-Cell Imaging. *J Bioenerg Biomembr* **2015**, *47* (1–2), 75–88.

VI.6 Kritis AA, Stamoula EG, Paniskaki KA, Vavilis TD. Researching Glutamate-Induced Cytotoxicity in Different Cell Lines: A Comparative/Collective Analysis/Study. *Front Cell Neurosci* **2015**, *9*, 91.

VI.7 Bak LK, Schousboe A, Waagepetersen HS. The Glutamate/GABA-Glutamine Cycle: Aspects of Transport, Neurotransmitter Homeostasis and Ammonia Transfer. *J Neurochem* **2006**, *98* (3), 641–653.

VI.8 Suárez I, Bodega G, Fernández B. Glutamine Synthetase in Brain: Effect of Ammonia. *Neurochem Int* **2002**, *41* (2–3), 123–142.

VI.9 Marcaida G, Felipo V, Hermenegildo C, Miñana MD, Grisolía S. Acute Ammonia Toxicity Is Mediated by the NMDA Type of Glutamate Receptors. *FEBS Lett* **1992**, *296* (1), 67–68.

VI.10 Coyle JT, Puttfarcken P. Oxidative Stress, Glutamate, and Neurodegenerative Disorders. *Science* **1993**, *262* (5134), 689–695.

VI.11 Kontos HA. Oxygen Radicals in Cerebral Ischemia: The 2001 Willis Lecture. *Stroke* **2001**, *32* (11), 2712–2716.

VI.12 Poli G, Leonarduzzi G, Biasi F, Chiarpotto E. Oxidative Stress and Cell Signalling. *Curr Med Chem* **2004**, *11* (9), 1163–1182.

VI.13 Halliwell B. Antioxidants in Human Health and Disease. *Annu Rev Nutr* **1996**, *16* (1), 33–50.

VI.14 Jia M, Njapo SAN, Rastogi V, Hedna VS. Taming Glutamate Excitotoxicity: Strategic Pathway Modulation for Neuroprotection. *CNS Drugs* **2015**, *29* (2), 153–162.

VI.15 Armada-Moreira A, Taipaleenmäki E, Itel F, Zhang Y, Städler B. Droplet-Microfluidics towards the Assembly of Advanced Building Blocks in Cell Mimicry. *Nanoscale* **2016**, *8* (47), 19510–19522.

VI.16 Itel F, Schattling PS, Zhang Y, Städler B. Enzymes as Key Features in Therapeutic Cell Mimicry. *Adv Drug Deliv Rev* **2017**, *118*, 94–108.

VI.17 Mancin F, Prins LJ, Pengo P, Pasquato L, Tecilla P, Scrimin P. Hydrolytic Metallo-Nanozymes: From Micelles and Vesicles to Gold Nanoparticles. *Molecules* **2016**, *21* (8), E1014.

VI.18 Wei H, Wang E. Nanomaterials with Enzyme-like Characteristics (Nanozymes): Next-Generation Artificial Enzymes. *Chem Soc Rev* **2013**, *42* (14), 6060–6093.

VI.19 Rai M, Ingle AP, Birla S, Yadav A, Santos CAD. Strategic Role of Selected Noble Metal Nanoparticles in Medicine. *Crit Rev Microbiol* **2016**, *42* (5), 696–719.

VI.20 Du B, Li D, Wang J, Wang E. Designing Metal-Contained Enzyme Mimics for Prodrug Activation. *Adv Drug Deliv Rev* **2017**, *118*, 78–93.

VI.21 Lin Y, Ren J, Qu X. Catalytically Active Nanomaterials: A Promising Candidate for Artificial Enzymes. *Acc Chem Res* **2014**, *47* (4), 1097–1105.

VI.22 Liu Y, Wu H, Li M, Yin J-J, Nie Z. pH Dependent Catalytic Activities of Platinum Nanoparticles with Respect to the Decomposition of Hydrogen Peroxide and Scavenging of Superoxide and Singlet Oxygen. *Nanoscale* **2014**, *6* (20), 11904–11910.

VI.23 Moglianetti M, De Luca E, Pedone D, Marotta R, Catelani T, Sartori B, Amenitsch H, Retta SF, Pompa PP. Platinum Nanozymes Recover Cellular ROS Homeostasis in an Oxidative Stress-Mediated Disease Model. *Nanoscale* **2016**, *8* (6), 3739–3752.

VI.24 Horie M, Kato H, Endoh S, Fujita K, Nishio K, Komaba LK, Fukui H, Nakamura A, Miyauchi A, Nakazato T, *et al*. Evaluation of Cellular Influences of Platinum Nanoparticles by Stable Medium Dispersion. *Metallomics* **2011**, *3* (11), 1244–1252.

VI.25 Wu G-W, He S-B, Peng H-P, Deng H-H, Liu A-L, Lin X-H, Xia X-H, Chen W. Citrate-Capped Platinum Nanoparticle as a Smart Probe for Ultrasensitive Mercury Sensing. *Anal Chem* **2014**, *86* (21), 10955–10960.

VI.26 Yan L, Bo X, Zhu D, Guo L. Well-Dispersed Pt Nanoparticles on Polydopamine-Coated Ordered Mesoporous Carbons and Their Electrocatalytic Application. *Talanta* **2014**, *120*, 304–311.

VI.27 Cheng Q, Liu Y. Multifunctional Platinum-Based Nanoparticles for Biomedical Applications. *Wiley Interdiscip Rev Nanomed Nanobiotechnol* **2017**, *9* (2), E1410.

VI.28 Orive G, Santos E, Poncelet D, Hernández RM, Pedraz JL, Wahlberg LU, De Vos P, Emerich D. Cell Encapsulation: Technical and Clinical Advances. *Trends Pharmacol Sci* **2015**, *36* (8), 537–546.

VI.29 Gao C, Wu Z, Lin Z, Lin X, He Q. Polymeric Capsule-Cushioned Leukocyte Cell Membrane Vesicles as a Biomimetic Delivery Platform. *Nanoscale* **2016**, *8* (6), 3548–3554.

VI.30 Zhang Y, Baekgaard-Laursen M, Städler B. Small Subcompartmentalized Microreactors as Support for Hepatocytes. *Adv Healthc Mater* **2017**, *6* (15), 1601141.

VI.31 Marguet M, Bonduelle C, Lecommandoux S. Multicompartmentalized Polymeric Systems: Towards Biomimetic Cellular Structure and Function. *Chem Soc Rev* **2012**, *42* (2), 512–529.

VI.32 Trantidou T, Friddin M, Elani Y, Brooks NJ, Law RV, Seddon JM, Ces O. Engineering Compartmentalized Biomimetic Micro- and Nanocontainers. *ACS Nano* **2017**, *11* (7), 6549–6565.

VI.33 Hosta-Rigau L, York-Duran MJ, Zhang Y, Goldie KN, Städler B. Confined Multiple Enzymatic (Cascade) Reactions within Poly(Dopamine)-Based Capsosomes. *ACS Appl Mater Interfaces* **2014**, *6* (15), 12771–12779.

VI.34 Schoonen L, van Hest JCM. Compartmentalization Approaches in Soft Matter Science: From Nanoreactor Development to Organelle Mimics. *Adv Mater* **2016**, *28* (6), 1109–1128.

VI.35 Lee H, Dellatore SM, Miller WM, Messersmith PB. Mussel-Inspired Surface Chemistry for Multifunctional Coatings. *Science* **2007**, *318* (5849), 426–430.

VI.36 Liu Y, Ai K, Lu L. Polydopamine and Its Derivative Materials: Synthesis and Promising Applications in Energy, Environmental, and Biomedical Fields. *Chem Rev* **2014**, *114* (9), 5057–5115.

VI.37 Lynge ME, Schattling P, Städler B. Recent Developments in Poly(Dopamine)-Based Coatings for Biomedical Applications. *Nanomed* **2015**, *10* (17), 2725–2742.

VI.38 Ku SH, Ryu J, Hong SK, Lee H, Park CB. General Functionalization Route for Cell Adhesion on Non-Wetting Surfaces. *Biomaterials* **2010**, *31* (9), 2535–2541.

VI.39 Hong S, Kim KY, Wook HJ, Park SY, Lee KD, Lee DY, Lee H. Attenuation of the in Vivo Toxicity of Biomaterials by Polydopamine Surface Modification. *Nanomed* **2011**, *6* (5), 793–801.

VI.40 Sedó J, Saiz-Poseu J, Busqué F, Ruiz-Molina D. Catechol-Based Biomimetic Functional Materials. *Adv Mater* **2013**, *25* (5), 653–701.

VI.41 Postma A, Yan Y, Wang Y, Zelikin AN, Tjipto E, Caruso F. Self-Polymerization of Dopamine as a Versatile and Robust Technique to Prepare Polymer Capsules. *Chem Mater* **2009**, *21* (14), 3042–3044.

VI.42 Zhang L, Shi J, Jiang Z, Jiang Y, Qiao S, Li J, Wang R, Meng R, Zhu Y, Zheng Y. Bioinspired Preparation of Polydopamine Microcapsule for Multienzyme System Construction. *Green Chem* **2011**, *13* (2), 300–306.

VI.43 Schattling P, Dreier C, Städler B. Janus Subcompartmentalized Microreactors. *Soft Matter* **2015**, *11* (26), 5327–5335.

VI.44 Hamasaki T, Kashiwagi T, Imada T, Nakamichi N, Aramaki S, Toh K, Morisawa S, Shimakoshi H, Hisaeda Y, Shirahata S. Kinetic Analysis of Superoxide Anion Radical-Scavenging and Hydroxyl Radical-Scavenging Activities of Platinum Nanoparticles. *Langmuir* **2008**, *24* (14), 7354–7364.

VI.45 Watanabe A, Kajita M, Kim J, Kanayama A, Takahashi K, Mashino T, Miyamoto Y. In Vitro Free Radical Scavenging Activity of Platinum Nanoparticles. *Nanotechnology* **2009**, *20* (45), 455105.

VI.46 Nomura M, Yoshimura Y, Kikuiri T, Hasegawa T, Taniguchi Y, Deyama Y, Koshiro K, Sano H, Suzuki K, Inoue N. Platinum Nanoparticles Suppress Osteoclastogenesis through Scavenging of Reactive Oxygen Species Produced in RAW264.7 Cells. *J Pharmacol Sci* **2011**, *117* (4), 243–252.

VI.47 Onizawa S, Aoshiba K, Kajita M, Miyamoto Y, Nagai A. Platinum Nanoparticle Antioxidants Inhibit Pulmonary Inflammation in Mice Exposed to Cigarette Smoke. *Pulm Pharmacol Ther* **2009**, *22* (4), 340–349.

VI.48 Takamiya M, Miyamoto Y, Yamashita T, Deguchi K, Ohta Y, Abe K. Strong Neuroprotection with a Novel Platinum Nanoparticle against Ischemic Stroke- and Tissue Plasminogen Activator-Related Brain Damages in Mice. *Neuroscience* **2012**, *221*, 47–55.

VI.49 Takamiya M, Miyamoto Y, Yamashita T, Deguchi K, Ohta Y, Ikeda Y, Matsuura T, Abe K. Neurological and Pathological Improvements of Cerebral Infarction in Mice with Platinum Nanoparticles. *J Neurosci Res* **2011**, *89* (7), 1125–1133.

VI.50 Nowak EJ. Catalytic Oxidation of Ammonia on Platinum. *Chem Eng Sci* **1966**, *21* (1), 19–27.

VI.51 Rafti M, Brunsen A, Fuertes MC, Azzaroni O, Soler-Illia GJAA. Heterogeneous Catalytic Activity of Platinum Nanoparticles Hosted in Mesoporous Silica Thin Films Modified with Polyelectrolyte Brushes. *ACS Appl Mater Interfaces* **2013**, *5* (18), 8833–8840.

VI.52 Huang L, Li L, Dong W, Liu Y, Hou H. Removal of Ammonia by OH Radical in Aqueous Phase. *Environ Sci Technol* **2008**, *42* (21), 8070–8075.

VI.53 Siddiqui S, Keswani M, Brooks B, Fuerst A, Raghavan S. A Study of Hydrogen Peroxide Decomposition in Ammonia-Peroxide Mixtures (APM). *Microelectron Eng* **2013**, *102*, 68–73.

VI.54 Yang Z, Tu Q, Zhu Y, Luo R, Li X, Xie Y, Maitz MF, Wang J, Huang N. Mussel-Inspired Coating of Polydopamine Directs Endothelial and Smooth Muscle Cell Fate for Re-Endothelialization of Vascular Devices. *Adv Healthc Mater* **2012**, *1* (5), 548–559.

VI.55 Xu M, Zhang Y, Zhai D, Chang J, Wu C. Mussel-Inspired Bioactive Ceramics with Improved Bioactivity, Cell Proliferation, Differentiation and Bone-Related Gene Expression of MC3T3 Cells. *Biomater Sci* **2013**, *1* (9), 933–941.

VI.56 Lin J-H, Yu C-J, Yang Y-C, Tseng W-L. Formation of Fluorescent Polydopamine Dots from Hydroxyl Radical-Induced Degradation of Polydopamine Nanoparticles. *Phys Chem Chem Phys* **2015**, *17* (23), 15124–15130.

VI.57 Decker T, Lohmann-Matthes ML. A Quick and Simple Method for the Quantitation of Lactate Dehydrogenase Release in Measurements of Cellular Cytotoxicity and Tumor Necrosis Factor (TNF) Activity. *J Immunol Methods* **1988**, *115* (1), 61–69.

VI.58 McClatchey AI, Yap AS. Contact Inhibition (of Proliferation) Redux. *Curr Opin Cell Biol* **2012**, *24* (5), 685–694.

VI.59 Puliafito A, Hufnagel L, Neveu P, Streichan S, Sigal A, Fygenson DK, Shraiman BI. Collective and Single Cell Behavior in Epithelial Contact Inhibition. *Proc Natl Acad Sci USA* **2012**, *109* (3), 739–744.

VI.60 Liu X, Cao J, Li H, Li J, Jin Q, Ren K, Ji J. Mussel-Inspired Polydopamine: A Biocompatible and Ultrastable Coating for Nanoparticles in Vivo. *ACS Nano* **2013**, *7* (10), 9384–9395.

VI.61 van der Westen R, Hosta-Rigau L, Sutherland DS, Goldie KN, Albericio F, Postma A, Städler B. Myoblast Cell Interaction with Polydopamine Coated Liposomes. *Biointerphases* **2012**, *7* (1–4), 8.

VI.62 Bhang SH, Kwon S-H, Lee S, Kim GC, Han AM, Kwon YHK, Kim B-S. Enhanced Neuronal Differentiation of Pheochromocytoma 12 Cells on Polydopamine-Modified Surface. *Biochem Biophys Res Commun* **2013**, *430* (4), 1294–1300.

VI.63 Kang K, Choi IS, Nam Y. A Biofunctionalization Scheme for Neural Interfaces Using Polydopamine Polymer. *Biomaterials* **2011**, *32* (27), 6374–6380.

VI.64 Park J, Brust TF, Lee HJ, Lee SC, Watts VJ, Yeo Y. Polydopamine-Based Simple and Versatile Surface Modification of Polymeric Nano Drug Carriers. *ACS Nano* **2014**, *8* (4), 3347–3356.

VI.65 Okuda S, Nishiyama N, Saito H, Katsuki H. Hydrogen Peroxide-Mediated Neuronal Cell Death Induced by an Endogenous Neurotoxin, 3-Hydroxykynurenine. *Proc Natl Acad Sci USA* **1996**, *93* (22), 12553–12558.

VI.66 Singhal A, Morris VB, Labhasetwar V, Ghorpade A. Nanoparticle-Mediated Catalase Delivery Protects Human Neurons from Oxidative Stress. *Cell Death Dis* **2013**, *4* (11), e903.

VI.67 Dawson VL, Dawson TM. Nitric Oxide Neurotoxicity. *J Chem Neuroanat* **1996**, *10* (3–4), 179–190.

VI.68 Dawson VL, Dawson TM, Bartley DA, Uhl GR, Snyder SH. Mechanisms of Nitric Oxide-Mediated Neurotoxicity in Primary Brain Cultures. *J Neurosci* **1993**, *13* (6), 2651–2661.

VI.69 Paul V, Ekambaram P. Involvement of Nitric Oxide in Learning & Memory Processes. *Indian J Med Res* **2011**, *133* (5), 471–478.

VI.70 Yildiz Akar F, Ulak G, Tanyeri P, Erden F, Utkan T, Gacar N. 7-Nitroindazole, a Neuronal Nitric Oxide Synthase Inhibitor, Impairs Passive-Avoidance and Elevated Plus-Maze Memory Performance in Rats. *Pharmacol Biochem Behav* **2007**, *87* (4), 434–443.

Chapter VII.

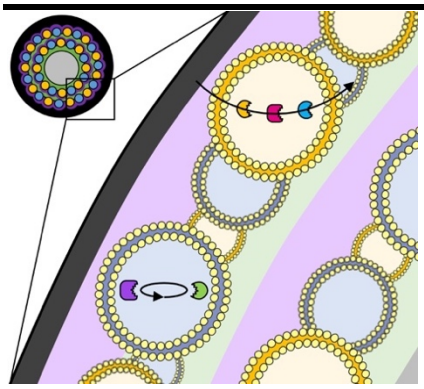
Increasing the complexity of microreactors

On the assembly of microreactors with parallel enzymatic pathways

Armada-Moreira A, Thingholm B, Andreassen K, Sebastião AM, Vaz SH, Städler B

Advanced Biosystems **2018**

rationale



During my stay in Aarhus, I had my debut as a supervisor. Kristine Andreassen was a BSc student in Nanotechnology that chose Städler's lab to do her final project. Since I somehow became the "group's expert" in enzymology and all things biological, Brigitte called on me to design and supervise Kristine's project. With our first proof of concept confirmed, we started thinking about increasing the complexity of our astrosomes by incorporating enzymes. Following that line of thought, we designed a project that originated the work presented in this chapter, where we explore multiple enzyme encapsulation into a functional microreactor. Although not directly relevant for the astrosomes, this work helped us understand how to optimize the use of enzymes in a cell mimicry context. This knowledge could then be transposed for our main aim. No spoilers, but we apply this knowledge to astrosomes in the next chapter.

I was responsible for most of the experimental work performed, as well as all data analysis, manuscript writing, experimental design, and original illustrations. Bo Thingholm was responsible for protein quantification assays and, together with me, calculation of encapsulation efficiencies. Kristine Andreassen performed the experimental work with me.

publication information

Title. On the assembly of microreactors with parallel enzymatic pathways.

Authors. Adam Armada-Moreira, Bo Thingholm, Kristine Andreassen, Ana M. Sebastião, Sandra H. Vaz, Brigitte Städler.

Status of publication. Published.

Journal. Advanced Biosystems 2018, 2 (5), 1700244.

DOI. 10.1002/adbi.201700244

JCR impact factor, quartile, and field. N/A.

original research article

On the assembly of microreactors with parallel enzymatic pathways

Armada-Moreira A[1,2,3], Thingholm B[1], Andreassen K[1], Sebastião AM[2,3], Vaz SH[2,3], Städler B[1]*

[1]Interdisciplinary Nanoscience Center (iNANO), Aarhus University, Aarhus, Denmark.
[2]Instituto de Farmacologia e Neurociências, Faculdade de Medicina, Universidade de Lisboa, Lisbon, Portugal.
[3]Instituto de Medicina Molecular, Faculdade de Medicina, Universidade de Lisboa, Lisbon, Portugal.
*Corresponding author.

Advanced Biosystems **2018**, *2* (5), 1700244.

Abstract

Cell mimicry aims to create artificial structures capable of mimicking certain functions of living cells. However, cell mimics are tremendously simpler than their natural role models. Thus, increasing their complexity is of great importance for the advancement of cell mimicry concepts and for further understanding of biological intracellular processes. Here, the successful co-encapsulation of two enzymatic pathways with up to five enzymes into compartmentalized microreactors is reported. The microreactors are assembled by combining polymer layers and enzyme-loaded liposomal subunits, which physically separate the two encapsulated enzymatic pathways. Specifically, this report confirms the activity of an encapsulated enzymatic cycle that conjugates the actions of glutamate dehydrogenase and glutathione reductase, using $NADP^+$/NADPH as a common co-factor, as well as an encapsulated enzymatic cascade combining β-galactosidase, glucose oxidase, and catalase. This work represents a relevant advancement in encapsulated catalysis toward the assembly of therapeutic cell mimics.

Keywords: encapsulated catalysis, microreactors, enzymatic cascades, enzymatic cycles.

Introduction

Living cells are complex structures and yet, at the same time, represent the simplest form of life. In terms of function, it is possible to look at cells as advanced catalytic reactors.[VII.1] A notable feature of living cells that enables the performance of said catalytic activity is compartmentalization, that is, the presence of several different organelles enclosed by a lipid bilayer.[VII.2,3] This hierarchical structure allows for the performance of multiple and simultaneous complex biochemical processes with high specificity and selectivity[VII.3] in confined microenvironments, often with different physical and biochemical characteristics, without interference of unwanted external stimuli.[VII.4] In fact, there is a large consensus that compartmentalization and catalyst separation are important mechanisms in the spatial and temporal control of intracellular processes and flux regulation of metabolic pathways.[VII.2] For a detailed review on the control of specific cellular functions by compartmentalization, the reader is referred to a report by Zecchin *et al*.[VII.5]

Researchers have been fascinated with the complexity and efficiency of living cells and,

consequently, dedicated a considerable effort toward creating artificial cells and organelles that mimic specific features. With that aim, bottom-up synthetic biology focuses on creating artificial structures with functions and architectures similar to those of living cells[VII.6–8] by combining both biological and synthetic building blocks (such as polymers, enzymes, enzyme mimics, lipids, among others)[VII.9–11] to construct functional artificial structures, namely artificial cells and organelles,[VII.12] capable of interacting with cells.[VII.13]

Taking all this into account, a simple model of an artificial cell can be achieved by creating compartmentalized assemblies where the encapsulated cargo is protected from unwanted degradation or interference and where exchange of molecules between the interior and exterior of the reactor is possible. The latter aspect gives the cargo the opportunity to react to external cues.[VII.14] Moreover, being able to mimic biological compartmentalization is essential in the field of cell mimicry, since it creates an isolated micro/nano-environment for the entrapped catalyst, avoiding biocompatibility problems and enhancing the selectivity and efficiency of the catalyst.[VII.13,15] Furthermore, compartmentalization in cell mimics allows for the entrapment of different cargo in each compartment, making it possible to combine different therapeutic compounds in a single carrier.[VII.16] For an overview on recent advances in compartmentalization approaches in cell mimicry, as well as their applications, the reader is referred to reviews by York-Duran *et al*.[VII.3] and Buddingh' and van Hest.[VII.1]

A recent highlight from polymersomes-in-polymersome assemblies was reported by Peters and colleagues, where three incompatible enzymes were compartmentalized in different compartments to form an enzymatic cascade, and communication between the different compartments was achieved by substrate and product diffusion.[VII.17] Alternatively, Elani and colleagues designed a complex artificial structure based on liposomes-in-liposomes comprised of a network of tightly bound aqueous liposomal compartments, used to encapsulate a three-step enzymatic cascade, where transmembrane protein pores were used to navigate substrates and products toward adjacent compartments.[VII.18]

Capsosomes (structures combining polymer capsules and liposomes), on the other hand, were employed to trigger release of encapsulated cargo using the actions of an entrapped enzyme on its substrate,[VII.19] to catalyze a two-enzyme coupled reaction in parallel with a single-enzyme conversion by incorporating three types of liposomal subunits, each encapsulating a different type of enzyme,[VII.20] and to perform localized encapsulated catalysis in Janus capsosomes.[VII.21] Also, capsosomes are the only compartmentalized system that has been proven functional in biologically relevant settings, as both nanoreactors with organelle-like function[VII.22–24] and microreactors with cell-like function.[VII.10,11] Furthermore, capsosome-like microreactors composed of catalase-containing liposomes entrapped in alginate hydrogel particles were used to detoxify hydrogen peroxide when co-cultured with HepG2 cells, both in planar cell cultures and in the form of microreactor-cell aggregates.[VII.25] Another recent variation of capsosomes with demonstrated biological activity entailed the replacement of enzyme-loaded

liposomes by platinum nanoparticles acting as catalysts. These microreactors were able to detoxify both hydrogen peroxide and ammonia when co-cultured with human neuroblastoma cells.[VII.26] Although still scarce in the literature, these successful examples describing the biological activity of microreactors demonstrate the potential of these systems as therapeutic strategies in a biological and biomedical context.

It should be noted that, although tremendous advances were made in assembling functional compartmentalized microreactors, metabolic clustering, that is, the encapsulation of enzymatic pathways within the same compartment and not only the same microreactor, is largely unexplored. Together with compartmentalization, metabolic clustering is relevant for the field of cell mimicry. Indeed, biological compartments often contain several enzymes that work together, forming enzymatic pathways.[VII.27] Furthermore, computational simulations of enzyme kinetics have already shown that enzymatic clustering, that is, the physical proximity of the elements of enzymatic pathways, increases the efficiency of the pathway flux by 6-fold for a simple two-step enzymatic pathway, compared to the distribution of these elements in a bigger structure, such as the cytosol.[VII.28] Within the field of cell mimicry, some notable examples highlight the advantages of metabolic clustering. For instance, Liu and colleagues describe the assembly and activity *in vivo* of non-compartmentalized polymer capsules containing two enzymes working in tandem. In their work, the authors compared the activity of two polymer capsules containing one enzyme each with that of a capsule containing both, concluding that metabolic clustering lead to a significant enhancement of the enzymatic pathway activity.[VII.27]

Taking into account that the highest number of co-encapsulated enzymes in a single microreactor is three and that metabolic clustering is often overlooked, the aim of this work was to create a compartmentalized microreactor containing up to five liposome-entrapped enzymes forming two enzymatic pathways – an enzymatic cycle containing the enzymes glutamate dehydrogenase and glutathione reductase, using $NADP^+$/NADPH as a self-renewable co-factor, and an enzymatic cascade combining the enzymes β-galactosidase, glucose oxidase, and catalase, using lactose as substrate and generating water and oxygen (**Figure VII.1**). Specifically, we assessed the performance of the two different enzymatic pathways using either free enzymes in solution (i) or enzymes entrapped in liposomes (ii) and confirmed the biocatalytic activity of microreactors containing these enzyme-loaded liposomes (iii). The microreactors were successfully assembled, maintaining the activity of both encapsulated enzymatic pathways.

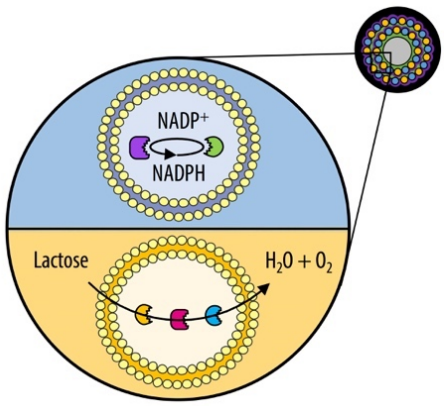


Figure VII.1. Overview schematic of the microreactors containing two different encapsulated enzymatic pathways.

Experimental section

Materials. 4-(2-hydroxyethyl)piperazine-1-ethanesulfonic acid (HEPES), tris(hydroxymethyl)aminomethane (TRIS), sodium chloride (NaCl), L-glutamic acid dehydrogenase from bovine liver (GDH, EC1.4.1.3, 48 U mg^{-1}), glutathione reductase from baker's yeast (GTR, EC1.8.1.7, 170 U mg^{-1}), β-galactosidase from *Aspergillus oryzae* (β-Gal, EC3.2.1.23, 12 U mg^{-1}), glucose oxidase from *Aspergillus niger* (GOx, EC1.1.3.4, 173 U mg^{-1}), catalase from bovine liver (Cat, EC1.11.1.6, 5 000 U mg^{-1}), L-glutamic acid monosodium salt hydrate (L-glutamate), L-glutathione oxidized disodium salt (GSSG), β-nicotinamide adenine dinucleotide phosphate sodium salt hydrate ($NADP^+$), D-glucose, D-lactose, poly(L-lysine) (PLL, MW 30 000−70 000 Da), dopamine hydrochloride (DA), horseradish peroxidase (HRP, 250–330 U mg^{-1}), hydrogen peroxide (H_2O_2, 30% (w/w)), and Triton X-100 were purchased from Sigma-Aldrich (MO, USA). Amplex UltraRed and Pierce BCA Protein Assay Kit were obtained from ThermoFisher Scientific (MA, USA). 1,2-dioleoyl-*sn*-glycero-3-phosphocholine (DOPC) was purchased from Avanti Polar Lipids (Alabama, USA). SiO_2 particles (2.12 ± 0.06 μm in diameter) were purchased from Microparticles GmbH (Berlin, Germany). Ultrapure water (18.2 MΩ cm^{-1} resistance) was provided by an ELGA Purelab Ultra system (ELGA LabWater, Lane End, UK).

Poly(methacrylic acid)-*co*-(cholesteryl methacrylate) (PMAc) was synthesized according to a previously published protocol.[VII.29]

Two types of buffer solutions were used: HEPES2 buffer consisting of 20 mM HEPES and 130 mM NaCl, pH 7.4, and TRIS buffer consisting of 10 mM TRIS, pH 8.5. All buffer solutions were prepared using ultrapure water.

Liposome preparation. Unilamellar liposomes were prepared by evaporation of 100 μL of a DOPC solution (25 mg mL^{-1} in chloroform) under vacuum for 1 h, followed by rehydration of the lipids with 200 μL of an enzyme-containing solution (see **Table VII.1** for specific enzymes and concentrations used) in HEPES2 buffer. The liposomes were then further hydrated with 800 μL of HEPES2 buffer. The solutions were extruded through 200 nm filters (13×) to obtain monodispersed liposomes. Non-encapsulated enzymes were removed by size exclusion chromatography, which diluted each sample by a factor of 2. Liposome formation was confirmed through dynamic light scattering (DLS, Zetasizer Nano S90, Malvern Instruments, UK) using a material refractive index of 1.590 and a dispersant (water at 25 °C) refractive index of 1.330.

Microreactor assembly. Silica particles (2.12 μm in diameter, 50 mg mL^{-1}) were washed 3× in HEPES2 buffer (1 800 rpm, 45 s). The particles were then incubated with a PLL solution (1.0 mg mL^{-1} in HEPES2 buffer, 10 min). The assemblies were washed 3× in HEPES2 buffer between coating steps, unless otherwise stated. The positively charged particles were incubated with enzyme-loaded liposomes (1:1 mix of L_{GDH} and L_{GOx} for M1, $L_{GDH:GTR}$ and $L_{GOx:Cat}$ for M2, L_{GDH} and $L_{β\text{-}Gal:GOx}$ for M3, and $L_{GDH:GTR}$ and $L_{β\text{-}Gal:GOx:Cat}$ for M4) for 40 min. In order to anchor and fix the liposomes, the microreactors were incubated with PMAc (2.0 mg mL^{-1} in HEPES2 buffer, 10 min). These three coating steps were

repeated to increase the amount of adsorbed enzyme-loaded liposomes. Finally, the microreactors were washed 2× in HEPES2 buffer and 1× in TRIS buffer and incubated with a DA solution (2.5 mg mL^{-1} in TRIS buffer, overnight) to generate a PDA layer. The final concentration of microreactors was determined by flow cytometry (C6 Flow Cytometer, Accuri Cytometers, Inc., MI, USA).

NADPH detection assay. Samples were incubated with 30 mM L-glutamate, 2.0 mM GSSG, and 2.0 mM $NADP^+$ in HEPES2 buffer at 37 °C. The production of NADPH was followed by measuring the absorbance of the solutions (λ = 340 nm) at different time points. For the determination of NADPH produced by the different microreactors, samples were centrifuged (1 800 rpm, 45 s) prior to absorbance measurements.

H_2O_2 detection assay. Samples were incubated with 10 μM D-glucose (for the two-step enzymatic cascade) or 10 μM D-lactose (for the three-step enzymatic cascade) during 3 h (for the free enzyme assay) or 24 h (for the liposome and microreactor assays) at 37 °C. After these incubations, H_2O_2 was detected using the Amplex UltraRed assay for H_2O_2 detection. 50 μL of the samples were incubated with 0.2 U mL^{-1} HRP and 50 μM Amplex UltraRed in ultrapure water (reaction mix), in a total volume of 100 μL. The mix was incubated at room temperature protected from light for 30 min. The fluorescence of the solutions (λ_{ex} = 545 nm, λ_{em} = 590 nm) was measured by a multiplate reader. For the microreactor assay, samples were centrifuged (1 800 rpm, 45 s) prior to incubation with the reaction mix.

Statistical analysis. All assays were performed with duplicates, with at least three independent repeats (N>=3). All data are presented as percentage of enzymatically-generated NADPH, for the GDH and GTR cycle, or H_2O_2, for the two-step and the three-step enzymatic cascades. For each independent repeat, the amount of the monitored molecules generated by the incomplete pathways (GDH alone, GOx alone, or β-Gal and GOx) was set to 100% and the amount of the monitored molecules generated by the respective complete pathways was normalized to it. Considering the data from all the repeats, values outside of the range mean ± 2× standard deviation (SD) were considered outliers. Data are represented as mean ± SD. Statistical significance was determined using two-tailed paired t-tests comparing incomplete and complete pathway values, with $p < 0.05$ considered to represent statistical significance. All data were analyzed in GraphPad Prism (GraphPad Software, Inc., CS, USA).

Results and discussion

Enzymatic pathways using free enzymes in solution

As a first step, we aimed to illustrate that the activity of the envisioned enzymatic pathways could be monitored. To this end, we employed enzymes in solution considering two different enzymatic pathways. The first investigated pathway consisted of cyclical reactions catalyzed by glutamate dehydrogenase (GDH) and glutathione reductase (GTR). GDH reversibly converts L-glutamate into α-ketoglutarate and ammonia (NH_4^+), while simultaneously converting nicotinamide adenine dinucleotide phosphate ($NADP^+$) into its reduced form, NADPH.[VII.30]

GTR, on the other hand, catalyzes the reduction of glutathione disulphide (GSSG) into glutathione (GSH), concomitantly converting NADPH into $NADP^+$ (**Figure VII.2A**).[VII.31] Thus, it was expected that the activity of GDH alone would lead to a high production of NADPH, while the presence of both enzymes would only lead to the generation of a basal amount of NADPH, which would be constant over time. The successful performance of this enzymatic pathway was confirmed. The amount of NADPH in solution was followed by changes in the absorbance (λ = 340 nm), using two different conditions. On the one hand, when only GDH (10 U mL^{-1}) was incubated for 1 h with L-glutamate, GSSG, and $NADP^+$, the enzymatic pathway was incomplete and NADPH was enzymatically generated, serving as the control condition. On the other hand, when GDH and GTR (1:1 enzymatic activity ratio, 10 U mL^{-1}) were employed with the same substrates for 1 h, the enzymatic pathway was complete and the NADPH generated by GDH was consumed by GTR. Indeed, the normalized amount of NADPH produced by GDH was significantly higher than the monitored amount of NADPH when both enzymes were present (**Figure VII.2B**). Furthermore, in the latter case, an equilibrium was reached, where the amount of NADPH in solution was constant over time (Chapter VII Supporting Information, **Figure VII.S1**). Additionally, although there was a significant difference between the two conditions in all measured time points, the levels of NADPH produced by GDH alone decreased with increasing incubation time (Chapter VII Supporting Information, **Figure VII.S1**). This finding might be due to the non-enzymatic oxidation of NADPH into $NADP^+$, given the instability of the former molecule,[VII.32] or due to the reversal of the GDH-catalyzed reaction. However, the reaction catalyzed by GDH is known to mainly occur in the direction of α-ketoglutarate formation, since GDH shows very low affinity for NH_4^+ (Km ≈ 17 mM for bovine liver GDH)[VII.33], which implies that the reverse reaction would only occur in the presence of high levels of NH_4^+. Since we used 30 mM L-glutamate and 2.0 mM $NADP^+$ and given the stoichiometry of the reaction, $NADP^+$ would be the limiting substrate, only allowing for a maximum production of 2.0 mM NH_4^+. Therefore, the time dependent decrease in NADPH levels was most likely due to non-enzymatic oxidation. Consequently, the time point used to assess the performance of this enzymatic pathway was chosen based on the highest measured NADPH level in the control condition (GDH alone), i.e., 1 h incubation for the free enzyme assay.

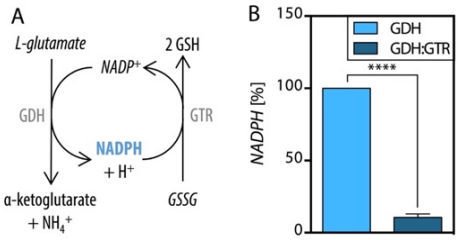


Figure VII.2. Cyclical reactions of GDH and GTR: (**A**) Schematic representation of the employed enzymatic cycle. L-glutamate, GSSG, and $NADP^+$ were the substrates initially added and NADPH was the measured product upon enzymatic conversion. (**B**) Monitored amount of NADPH in solution after 1 h incubation of the substrates with GDH (light blue bar) or with GDH and GTR (dark blue bar). The measurements were normalized to the amount of NADPH generated by GDH alone. N=3. ****$p < 0.0001$ using a two-tailed paired *t*-test. Data represented as mean ± standard deviation (SD).

The second considered pathway consisted of an enzymatic cascade, where each enzyme uses the product from the previous enzyme as

substrate. The enzymes glucose oxidase (GOx) and catalase (Cat) were chosen for this purpose. GOx converts D-glucose into D-glucono-1,5-lactone and H_2O_2.[VII.34] Cat then further converts H_2O_2 into water and oxygen (**Figure VII.3A**).[VII.35]

The amount of H_2O_2 was measured to follow this cascade reaction, using two different conditions. When GOx (10 U mL^{-1}) was incubated with D-glucose in the absence of Cat, a large amount of H_2O_2 was produced over 3 h incubation time. On the other hand, the GOx-produced H_2O_2 was almost completely converted when both enzymes (10 U mL^{-1} each) were incubated with D-glucose for 3 h (**Figure VII.3B**).

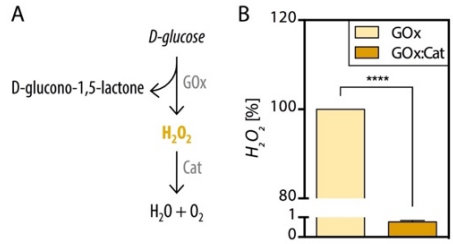


Figure VII.3. Enzymatic cascade of GOx and Cat: (**A**) Schematic representation of the enzymatic pathway, where D-glucose was the initially added substrate and H_2O_2 was the monitored molecule. (**B**) Amount of H_2O_2 after 3 h incubation with GOx (light yellow bar) or with GOx and Cat (dark yellow bar). The measurements were normalized to the amount of H_2O_2 produced by GOx alone. N=3. ****$p < 0.0001$ using a two-tailed paired *t*-test. Data represented as mean ± SD.

Finally, the cascade reaction was taken a step further by adding β-galactosidase (β-Gal), an enzyme that converts D-lactose into D-glucose,[VII.36] which can then serve as the substrate in the above-mentioned cascade reactions (**Figure VII.4A**). D-lactose was incubated for 3 h with either β-Gal and GOx or with β-Gal, GOx, and Cat to characterize this pathway. 10 U mL^{-1} of all enzymes were used for both conditions. In the first case, the combined action of the two enzymes led to an increase in the H_2O_2 levels. In the second case, the monitored amount of H_2O_2 was significantly lower due to the presence of Cat, which consumed part of the produced H_2O_2 (**Figure VII.4B**).

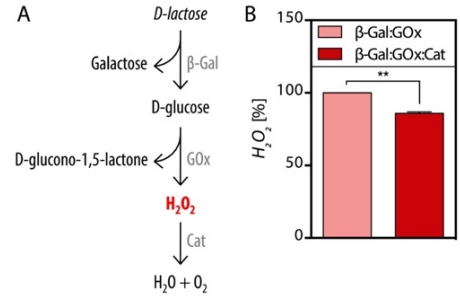


Figure VII.4. Enzymatic cascade of β-Gal, GOx, and Cat: (**A**) Schematic representation of the enzymatic cascade. D-lactose was used as the initial substrate and H_2O_2 was the measured molecule. (**B**) Amount of H_2O_2 generated by the actions of β-Gal and GOx (light red bar) and β-Gal, GOx, and Cat (red bar), after 3 h incubation. The measurements were normalized to the amount of H_2O_2 generated by β-Gal and GOx. N=3. **$p < 0.01$ using a two-tailed paired *t*-test. Data represented as mean ± SD.

The difference observed between the two conditions in the three-step enzymatic cascade is less pronounced than the difference in the two-step enzymatic cascade. Kinetically, these reactions are not in equilibrium due to the concentration of substrate used, which is at least 1000× lower than the respective Km. Thus, a classical biochemical analysis of metabolic flow cannot be performed to elucidate the change in the flow of the pathway.[VII.37] It is however possible to hypothesize that the two reactions necessary for H_2O_2 production (catalyzed by β-Gal and GOx) may not have 100% yield, which could mean that, even though the enzymes were exposed to 10 µM D-lactose, only a fraction of

this substrate was used to produce glucose, leading to an even lower production of H_2O_2. Thus, the 100% in the control condition (β-Gal and GOx, without Cat) would refer to a lower amount of H_2O_2 than in the control condition of the two-step enzymatic cascade and, consequently, the difference in relation to the complete pathway measurement would be smaller.

Additionally, the affinity of GOx toward D-glucose (Km ≈ 22 mM for *Aspergillus niger* GOx)[VII.38] is higher than that of Cat toward H_2O_2 (Km ≈ 33 mM for bovine liver Cat)[VII.39]. Thus, the reaction catalyzed by GOx would occur at a higher rate, not limiting the availability of H_2O_2 for Cat. Since, in conditions where the substrate concentration is significantly lower than the Km, the enzymatic rate is highly dependent on the substrate concentration,[VII.37] Cat would perform at a higher rate when exposed to a higher concentration of H_2O_2. On the other hand, β-Gal shows less affinity toward its substrate (D-lactose, Km ≈ 50–85 mM for *Aspergillus oryzae* β-Gal)[VII.40] than the other two enzymes. In this scenario, the reaction catalyzed by β-Gal would be the limiting step, affecting substrate availability for GOx and Cat. Again, since in these conditions the enzymatic rate is highly dependent on substrate concentration, this could imply that the rate of the reactions catalyzed by GOx and by Cat would be lower, taking more time to convert their respective substrates. This rate reduction would be more accentuated for the reaction catalyzed by Cat, since the slower rate of D-glucose production would amplify the substrate availability issue initiated by β-Gal. Therefore, assuming the rate of the Cat-catalyzed H_2O_2 conversion was low, the measurement performed after 3 h incubation could reflect an incomplete reaction where H_2O_2 in solution had not been consumed by Cat yet.

The interaction between the activity of the different pathways in solution was also considered, using the same enzyme concentrations as described above. For the GDH and GTR cycle, the incomplete and complete pathways were incubated for 1 h with L-glutamate, GSSG, and $NADP^+$ in the presence or absence of either enzymatic cascade and their respective substrate. The presence of the enzymatic cascades did not significantly affect the activity of the GDH and GTR cycle (Chapter VII Supporting Information, **Figure VII.S2**). Regarding the GOx and Cat cascade, both the complete and incomplete pathways were incubated for 3 h with D-glucose, in the presence or absence of the GDH and GTR cycle with or without $NADP^+$. No interaction between the pathways was found (Chapter VII Supporting Information, **Figure VII.S3**). Finally, the β-Gal, GOx, and Cat cascade was incubated for 3 h with D-lactose, in the presence or absence of the GDH and GTR cycle with or without $NADP^+$. No pathway interactions were found but the unexpected potentiation in H_2O_2 production by β-Gal and GOx in the presence of GDH and $NADP^+$ (Chapter VII Supporting Information, **Figure VII.S4**). This apparent potentiation is most likely an artifact of the detection assay due to a slight overlapping of the NADPH and resorufin (used for H_2O_2 detection) spectra.

Enzymatic pathways encapsulated in liposomes

The next step to assemble advanced microreactors required the enzymes to be entrapped in liposomes. These structures are biocompatible and offer optimal protection for fragile

biological cargo, which is illustrated by their successful use in compartmentalized microreactors.[VII.41] To this end, the enzymes were encapsulated in 200 nm monodispersed 1,2-dioleoyl-*sn*-glycero-3-phosphocholine (DOPC) liposomes (Chapter VII Supporting Information, **Figure VII.S5**) and their activity was monitored using the above-mentioned assays. The specific lipid composition and liposome diameter were chosen in order to allow for higher activity of the encapsulated enzymes (Chapter VII Supporting Information, **Figure VII.S6** and **Figure VII.S7**). Enzymes belonging to a specific pathway were mixed in solution (100 U mL^{-1} or 50 U mL^{-1} for the three-step enzymatic cascade at a 1:1 enzymatic activity mixing ratio) prior to being encapsulated in the liposomes. Liposomes not carrying all the enzymes required for a pathway (without either GTR or Cat) were used as control samples. The activity of the encapsulated enzymatic pathways was measured after 24 h or 48 h incubation with the required substrates. 48 h incubation time was chosen for the GDH and GTR cycle based on the highest NADPH measurement for the control condition between different time points (Chapter VII Supporting Information, **Figure VII.S8**), according to the discussion presented above. On the other hand, 24 h incubation time was chosen for both enzymatic cascades to prevent the non-enzymatic degradation of the newly-formed H_2O_2.

The activity of the GDH and GTR cycle was confirmed by the significantly lower level of produced NADPH in the presence of liposomes containing both enzymes, compared to the amount produced by liposomes containing only GDH (**Figure VII.5A**). Although the difference was statistically significant, it was smaller than the difference found for the free enzyme assay. This finding is likely tied to two explanations. First, the enzyme solution encapsulated in the liposomes contained enzymes in the same concentration (U mL^{-1}) as for the free enzyme assay. It is known that the encapsulation efficiency, i.e., how many enzymes are actually encapsulated in liposomes, is never 100%.[VII.42] Indeed, the encapsulation efficiency, expressed as experimental vs. theoretical protein concentration, was calculated for all the produced liposomes and determined to be ~10–20% (Chapter VII Supporting Information, **TableVII.S1**). Thus, it would be expected that fewer enzymes would be inside the liposomes, which would lead to a decrease in NADPH production in the control condition. Indeed, the maximum amount of NADPH measured with GDH-containing liposomes was lower than the one measured with the free enzyme (Chapter VII Supporting Information, **Figure VII.S10**). Furthermore, in the liposomes containing both GDH and GTR, there is no control over the actual ratio of encapsulation, even though the initial enzyme solution contained the enzymes at a 1:1 enzymatic activity ratio. The enzyme ratio could have shifted and the liposomes might have contained more GDH than GTR, which could account for the fact that a higher amount of NADPH was measured in liposomes entrapping both GDH and GTR compared to the free enzymes (Chapter VII Supporting Information, **Figure VII.S10**). Regarding the kinetics of this cycle, the liposome-entrapped enzymes showed a slower activity than the free enzymes in solution, i.e., in the free enzyme assay the highest NADPH amount was measured at 1 h incubation time, while for the enzymes in liposomes the highest

measurement was after 48 h incubation (Chapter VII Supporting Information, **Figure VII.S8**). The change in the kinetics of the pathway could be caused by the liposomes' kinetic barrier. It was previously shown that the entrapment of enzymes in lipidic subunits can affect their activity, namely slowing it down, due to the time that substrates take to diffuse across the lipid layer.[VII.43] All substrates were added outside the liposomes and, consequently, had to cross the lipid bilayer to be in contact with the enzymes. Indeed, when liposomes containing GDH were destroyed using Triton X-100, the production of NADPH after 24 h incubation was ~3× higher compared to intact liposomes (Chapter VII Supporting Information, **Figure VII.S11**). Since it is likely that the different substrates exhibited different abilities to penetrate into the liposomes, the pathway kinetics were probably not only delayed but also altered from the free enzymes in solution situation due to changed substrate concentrations/ratios.

The activity of the encapsulated GOx and Cat cascade was also confirmed, since the amount of H_2O_2 produced by liposomes containing both enzymes was significantly lower compared to liposomes containing only GOx (**Figure VII.5B**). As already observed for the other enzymatic pathway, the difference between the two encapsulated conditions was smaller than the one found for the free enzymes in solution, which is likely due to the reasons discussed above.

Finally, the activity of the encapsulated β-Gal, GOx, and Cat cascade was successfully illustrated. The amount of H_2O_2 generated by liposomes containing β-Gal and GOx was significantly higher than the amount generated by liposomes containing all three enzymes (**Figure VII.5C**).

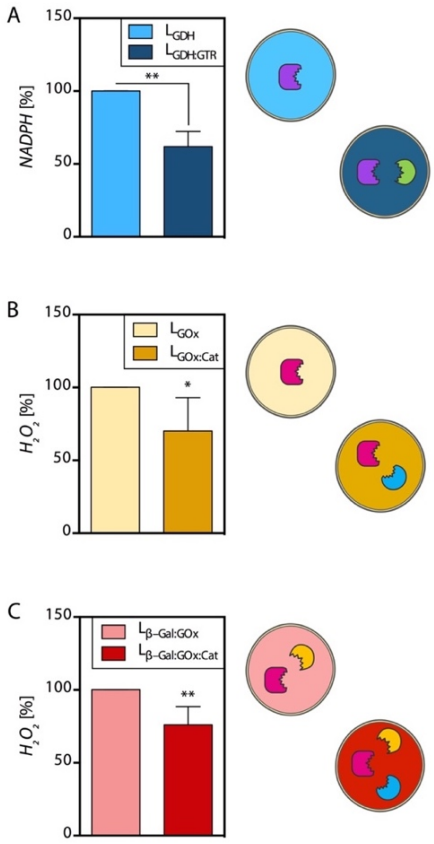


Figure VII.5. Enzymatic pathways encapsulated in liposomes. (**A**) The amount of NADPH produced by either L_{GDH} or $L_{GDH:GTR}$ was measured after 48 h incubation with L-glutamate, GSSG, and $NADP^+$. N=4. **p < 0.01 using a two-tailed paired *t*-test. (**B**) The amount of H_2O_2 generated by L_{GOx} and $L_{GOx:Cat}$ was measured after 24 h incubation with D-glucose. N=5. *p < 0.05 using a two-tailed paired *t*-test. (**C**) The amount of H_2O_2 resulting from the activity of $L_{β\text{-}Gal:GOx}$ and $L_{β\text{-}Gal:GOx:Cat}$ was measured after 24 h incubation with D-lactose. N=5. **p < 0.01 using a two-tailed paired *t*-test. All measurements were normalized to their respective control condition. All data are represented as mean ± SD.

Assembly and activity of microreactors

Capsosomes were chosen to create complex microreactors since they combine the benefits of both liposomal and polymeric components.

While the liposomes provide a protected environment for the encapsulated enzymes, the polymer layers offer protection and would provide structural integrity to the whole structure should the removal of the silica template be required.[VII.44] Furthermore, among different compartmentalized microreactors, capsosomes allow for the formation of the highest number of compartments,[VII.45] with a reported maximum of ~160 000 embedded liposomes,[VII.46] which largely contributes to enhancing the activity of an individual microreactor.

Active microreactors containing different combinations of the described enzyme-loaded liposomes (**Table VII.1**) were assembled by the layer-by-layer (LbL) technique using 2.12 µm SiO_2 template particles, employing a previously described and validated protocol.[VII.47] Briefly, the particles were coated with a layer of poly(L-lysine) (PLL) prior to the first liposome deposition step. Poly(methacrylic acid)-*co*-(cholesteryl methacrylate) (PMAc) and PLL were used as polymer separation layers before the second liposome adsorption step. PMAc and poly(dopamine) (PDA) were used as capping and terminating layers, respectively. PDA was chosen as the terminating layer to improve the biocompatibility and stability of the microreactors, as well as to facilitate subsequent chemical surface modifications[VII.48] of these microreactors in future biomedical/cellular applications, as we for instance recently illustrated.[VII.26] Furthermore, the enzymatic cargo of the liposomal subunits was varied, so that each microreactor contained two different types of enzyme-loaded liposomes (**Table VII.2**). Microreactors M1 were assembled using a mixture of L_{GDH} and L_{GOx}, while a mixture of L_{GDH} and $L_{\beta\text{-Gal:GOx}}$ was used during the liposome deposition steps for microreactors M3. M1 and M3 were employed as control samples since they contained the incomplete enzymatic pathways, i.e., they missed the enzymes GTR and Cat. On the other hand, microreactors M2 contained the complete enzymatic cycle ($L_{GDH:GTR}$) and the two-step enzymatic cascade ($L_{GOx:Cat}$), while microreactors M4 were also equipped with the complete enzymatic cycle ($L_{GDH:GTR}$) but enclosed the three-step enzymatic cascade ($L_{\beta\text{-Gal:GOx:Cat}}$).

Table VII.1. Final concentration of the encapsulated enzymes in liposomes.

Type of liposome	Final enzyme concentration [U mL^{-1}]				
	GDH	GTR	β-Gal	GOx	Cat
L_{GDH}	100	---	---	---	---
$L_{GDH:GTR}$	100	100	---	---	---
L_{GOx}	---	---	---	100	---
$L_{GOx:Cat}$	---	---	---	100	100
$L_{\beta\text{-Gal:GOx}}$	---	---	50	50	---
$L_{\beta\text{-Gal:GOx:Cat}}$	---	---	50	50	50

Table VII.2. Overview of the enzyme-loaded liposomes encapsulated in the different microreactors.

Liposome	M1[a)]	M2	M3[a)]	M4
L_{GDH}	✔	---	✔	---
$L_{GDH:GTR}$	---	✔	---	✔
L_{GOx}	✔	---	---	---
$L_{GOx:Cat}$	---	✔	---	---
$L_{\beta\text{-Gal:GOx}}$	---	---	✔	---
$L_{\beta\text{-Gal:GOx:Cat}}$	---	---	---	✔

[a)]M1 and M3 correspond to the control conditions for M2 and M4, respectively.

Representative bright field images of the assembled microreactors and the population histogram analyzed by flow cytometry confirmed the presence of non-aggregated microreactors (**Figure VII.6A** and Chapter VII Supporting Information, **Figure VII.S12**). Finally, the performance of the microreactors was determined with the aim to confirm the activity of the

encapsulated enzymatic pathways. 10^8 microreactors (M1, M2, M3, and M4) were incubated for 48 h with L-glutamate, GSSG, and $NADP^+$ before the amount of produced NAPDH was measured, to illustrate the successful functionality of the GDH and GTR cycle. As expected, there was a significant higher amount of NADPH measured when M1 and M3 were considered compared to M2 and M4, respectively. Regarding this specific pathway, M1 and M3 only contained GDH which means that the produced NADPH was not enzymatically converted by GTR as it was in M2 and M4 (**Figure VII.6B**).

Alternatively, to assess the activity of the enzymatic cascades, 10^8 microreactors (M1, M2, M3, and M4) were incubated for 24 h with D-glucose (for M1 and M2) or D-lactose (for M3 and M4) before the amount of H_2O_2 was measured. It was observed that M1 and M3 produced a significantly higher amount of H_2O_2 compared to M2 and M4, respectively, since no Cat was present in the former two cases (**Figure VII.6C**). Thus, the two-step as well as the three-step enzymatic cascades were functional when encapsulated in microreactors.

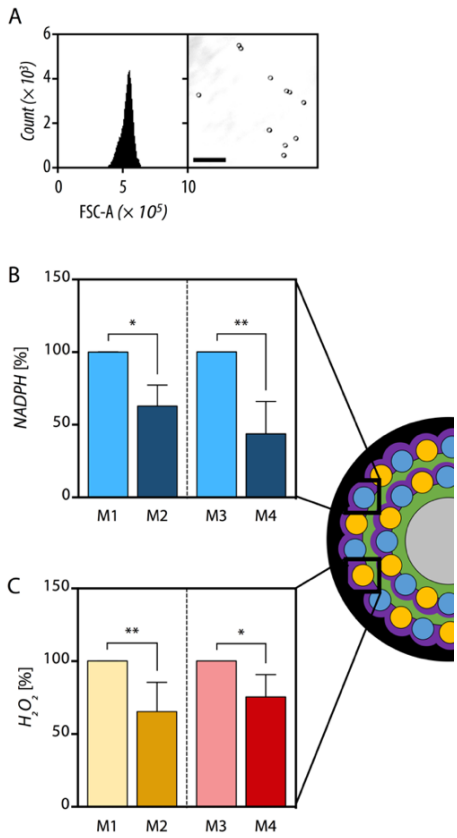


Figure VII.6. Assembly and activity of microreactors with up to five encapsulated enzymes. (**A**) Representative population histogram originated from flow cytometry analysis (left) and bright field microscopy image (right) of the assembled microreactors. Scale bar = 40 µm. (**B**) Amount of produced NADPH measured after 48 h incubation of the different microreactors with L-glutamate, GSSG, and $NADP^+$. M1 and M3 (light blue bars) refer to microreactors with the incomplete pathway (only GDH) and their activity was set to 100%. M2 and M4 (dark blue bars) refer to microreactors with the complete pathway (GDH and GTR) and their activity was normalized to the respective control. N=3. *$p < 0.05$, **$p < 0.01$ for comparison with respective control, using two-tailed paired *t*-tests. (**C**) Amount of generated H_2O_2 measured after 24 h incubation of the different microreactors with D-glucose, for M1 and M2, or D-lactose, for M3 and M4. M1 and M3 (light yellow bar and light red bar, respectively) refer to microreactors with incomplete pathways (without Cat) and their activity was set to 100%. M2 and M4 (dark yellow bar and dark red bar, respectively) refer to microreactors equipped with the complete enzymatic cascade (GOx and Cat or β-Gal, GOx, and Cat, respectively) and their activity was normalized to the respective control. N=4. *$p < 0.05$, **$p < 0.01$ for comparison with respective control, using two-tailed paired *t*-tests. All data are represented as mean ± SD.

Conclusion

Taken together, our results show that we were able to assemble compartmentalized microreactors containing up to five enzymes that formed two different functional enzymatic pathways. This effort represents, to the best of our knowledge, the assembly and characterization of compartmentalized microreactors with the largest number of co-encapsulated enzymes to date. Admittedly, the employed enzymatic pathways have only limited resemblance to biologically relevant designs and substantial further developments, including the performance of the microreactors in complex biological environments and their long-term activity, need to be accomplished. Nonetheless, the reported results signify a relevant advancement toward the fabrication of microreactors with cell-like function in the biocatalytic context.

chapter VII supporting information

The GDH and GTR enzymatic cycle in solution throughout time

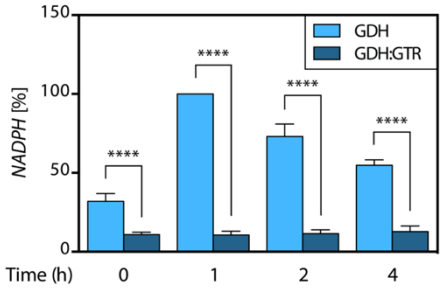


Figure VII.S1. Cyclical reactions of GDH and GTR in solution: The amount of NADPH in solution was measured after 0, 1, 2, and 4 h incubation time of GDH alone (light blue bars) or GDH and GTR (dark blue bars) with L-glutamate, GSSG, and $NADP^+$. Data were normalized to the value for the highest amount of NADPH measured (GDH, 1 h). N=3. ****$p < 0.0001$ for comparison with respective control condition, using two-tailed paired *t*-tests. Data represented as mean ± SD.

Interaction between enzymatic pathways in solution

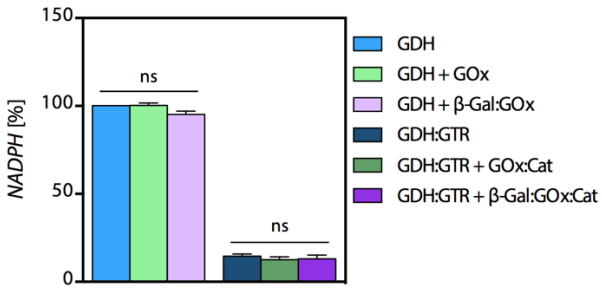


Figure VII.S2. Cyclical reactions of GDH and GTR in solution when incubated with the enzymatic cascades. The incomplete (GDH alone, light blue bar) and complete (GDH and GTR, dark blue bar) pathways were incubated with L-glutamate, GSSG, and $NADP^+$ for 1 h in the presence or absence of the GOx and Cat cascade (light green bar for the incomplete pathway, dark green bar for the complete pathway) or the β-Gal, GOx, and Cat cascade (light purple bar for the incomplete pathway, dark purple bar for the complete pathway) and their respective substrates. Data were normalized to the amount of NADPH generated by GDH alone. N=3. No significant differences ($^{ns}p > 0.05$) were found between the different pathway mixes for both the incomplete and the complete pathways, using one-way ANOVA followed by Sidak's multiple comparison test. Data represented as mean ± SD.

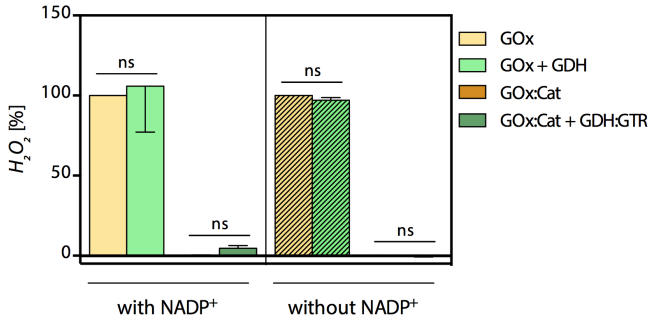


Figure VII.S3. Activity of the GOx and Cat cascade in solution when incubated with the GDH and GTR enzymatic cycle. The incomplete (GOx alone, light yellow bar) and the complete (GOx and Cat, dark yellow bar) pathways were incubated with D-glucose for 3 h in the presence or absence of the GDH and GTR enzymatic cycle (light green bar for the incomplete pathway, dark green bar for the complete pathway) with or without the enzymatic cycle substrate $NADP^+$ (striped and plain bars, respectively). Data were normalized to the amount of H_2O_2 generated by GOx alone, within the conditions with $NADP^+$ and without $NADP^+$. N=3. No significant differences ($^{ns}p > 0.05$) were found in the different conditions between the GOx and Cat cascade alone or incubated with the GDH and GTR enzymatic cycle. Data represented as mean ± SD.

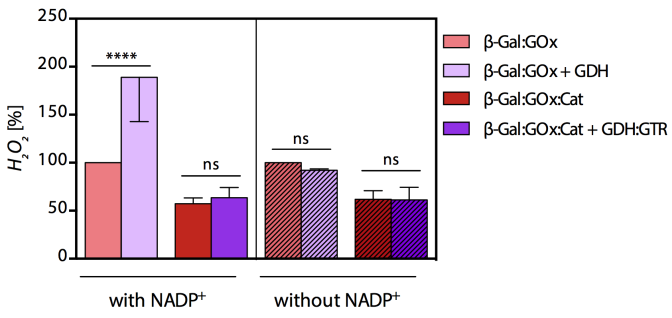


Figure VII.S4. Activity of the β-Gal, GOx, and Cat cascade in solution when incubated with the GDH and GTR enzymatic cycle. The incomplete (β-Gal and GOx, light red bar) and the complete (β-Gal, GOx, and Cat, dark red bar) pathways were incubated with D-lactose for 3 h in the presence or absence of the GDH and GTR enzymatic cycle (light purple bar for the incomplete pathway, dark purple bar for the complete pathway) with or without the enzymatic cycle substrate $NADP^+$ (striped and plain bars, respectively). Values were normalized to the amount of H_2O_2 produced by β-Gal and GOx, within the conditions with $NADP^+$ and without $NADP^+$. N=3. ****$p < 0.0001$. No significant differences ($^{ns}p > 0.05$) were found in the other conditions between the β-Gal, GOx, and Cat cascade alone or incubated with the GDH and GTR enzymatic cycle. Data represented as mean ± SD.

Size characterization of the fabricated enzyme-loaded liposomes

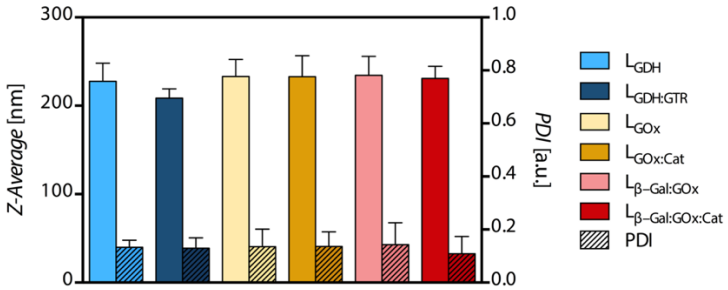


Figure VII.S5. Average size (Z-Average) and polydispersity index (PDI) for all fabricated enzyme-loaded liposomes. Colored bars refer to the average size of each liposome and striped bars refer to their PDI. N=5. No significant differences were found between the average size of different liposomes. Data represented as mean ± SD.

GDH activity when encapsulated in liposomes with different lipid compositions

Materials

β-nicotinamide adenine dinucleotide hydrate (NAD^+) was purchased from Sigma-Aldrich (MO, USA). 1-palmitoyl-2-oleoyl-*sn*-glycero-3-phosphocholine (POPC), 1-palmitoyl-2-oleoyl-*sn*-glycero-3-phospho-L-serine (POPS), 1,2-dimyristoyl-*sn*-glycero-3-phosphocholine (DMPC), 1,2-dipalmitoyl-*sn*-glycero-3-phosphocholine (DPPC), and 1,2-dipalmitoyl-*sn*-glycero-3-phospho-L-serine (DPPS) were purchased from Avanti Polar Lipids (Alabama, USA).

Methods

200 nm monodispersed liposomes with different lipid compositions containing 1.0 mg mL^{-1} GDH were incubated for 24 h with 30 mM L-glutamate and 2.0 mM NAD^+. After this incubation, the absorbance at 340 nm, correspondent to the amount of produced NADH, was measured.

Results

While POPC:POPS (8:2, wt%) liposomes showed a higher GDH activity and, thus, a higher amount of encapsulated GDH, as seen by the amount of NADH measured when the liposomes were disintegrated with Triton X-100, the GDH activity in intact DOPC liposomes was higher than in the other liposomes.

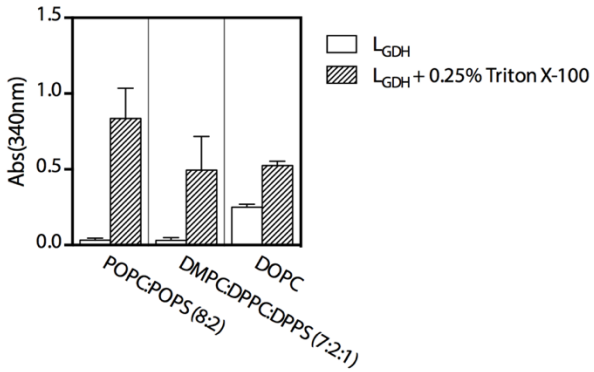


Figure VII.S6. L_{GDH} activity with different lipid compositions. Production of NADH was measured after liposomes with different lipid compositions containing 1.0 mg mL^{-1} GDH were incubated for 24 h with 30 mM L-glutamate and 2.0 mM NAD^+, with or without 0.25% Triton X-100. N=2–5. Data represented as mean ± SD.

GDH activity when encapsulated in liposomes with different diameters

Methods

Monodispersed 100 nm and 200 nm DOPC liposomes containing 1.0 mg mL^{-1} GDH were incubated for 24 h with 30 mM L-glutamate and 2.0 mM NAD^+. Following this incubation, the absorbance at 340 nm, correspondent to the amount of produced NADH, was measured.

Results

The GDH activity was higher in 200 nm liposomes than in 100 nm for both intact and disintegrated liposomes.

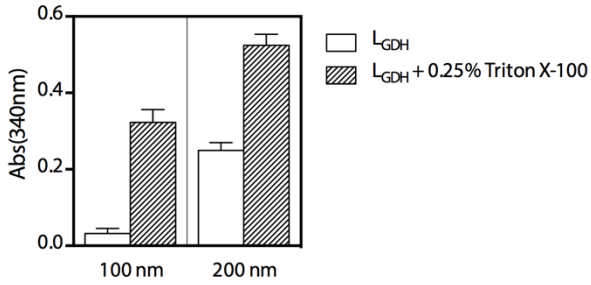


Figure VII.S7. L_{GDH} activity with different liposome sizes. The amount of NADH was measured after 100 nm and 200 nm liposomes were incubated for 24 h with 30 mM L-glutamate and 2.0 mM NAD^+, with or without 0.25% Triton X-100. N=1–2. Data represented as mean ± SD.

Time-dependent performance of the GDH and GTR enzymatic cycle encapsulated in liposomes

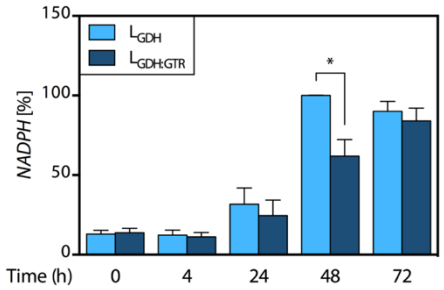


Figure VII.S8. GDH and GTR cyclical reactions encapsulated in liposomes. The amount of NADPH in solution was measured after 0, 4, 24, 48, and 72 h incubation time of L_{GDH} (light blue bars) or $L_{GDH:GTR}$ (dark blue bars) with L-glutamate, GSSG, and $NADP^+$. Data were normalized to the value for the highest amount of NADPH measured (L_{GDH}, 48 h). N=4. *$p < 0.05$ using a two-tailed paired *t*-test. Data represented as mean ± SD.

Enzyme encapsulation efficiency in the different liposomes

Materials

Pierce BCA Protein Assay Kit was purchased from ThermoFisher Scientific (MA, USA).

Methods

Liposomes containing the different enzyme combinations were exposed to 1.0% Triton X-100 for 15 min. 0.1 mL of each sample was then incubated with 1.9 mL of the BCA Protein Assay Kit working reagent for 30 min at 60 °C. Following this incubation, 200 µL of each sample was added to a standard 96-well plate and the absorbance of the solutions was read at 562 nm. The background signal from empty liposomes was subtracted from all results. A calibration curve using BSA was performed to determine the relationship between absorbance and protein concentration (Chapter VII Supporting Information, **Figure VII.S9**).

Results

The amount of encapsulated protein was successfully estimated for all tested enzyme-containing liposomes. The encapsulation efficiencies were determined to be ~10–20%.

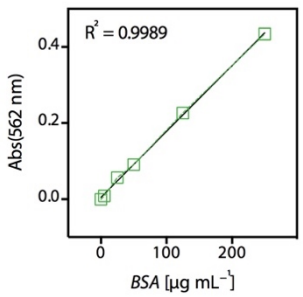


Figure VII.S9. BSA calibration curve for the BCA Protein Assay. A linear regression applied to the values obtained led to R^2 = 0.9989 and the equation Abs(562 nm) = 1.730e(–3) [protein] + 4.904e(–3). N=3. Data represented as mean ± SD.

Table VII.S1. Enzyme encapsulation efficiency.

Type of liposome	Theoretical protein concentration [µg mL^{-1}]	Measured protein concentration [µg mL^{-1}]	Encapsulation efficiency [%]
L_{GDH}	260.4	49.75 ± 10.71	19.10 ± 4.114
$L_{GDH:GTR}$	333.9	59.53 ± 2.217	17.83 ± 0.6638
L_{GOx}	721.9	80.47 ± 8.596	11.15 ± 1.191
$L_{GOx:Cat}$	724.4	81.82 ± 4.143	11.29 ± 0.5719
$L_{β\text{-}Gal:GOx}$	877.5	63.06 ± 2.171	7.186 ± 0.2474
$L_{β\text{-}Gal:GOx:Cat}$	878.8	62.10 ± 1.349	7.067 ± 0.1535

Maximum measured amount of NADPH in solution and liposomes

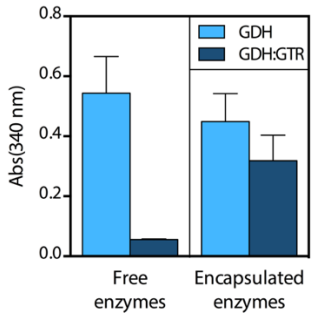


Figure VII.S10. Highest measured amount of NADPH, in raw values. For the free enzyme assay, this measurement corresponds to 1 h incubation, while for the enzymes encapsulated in liposomes it corresponds to 48 h incubation. N=3–4. Data are represented as mean ± SD.

Maximum amount of NADPH in intact and disintegrated GDH-containing liposomes

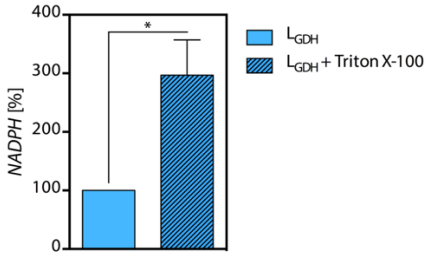


Figure VII.S11. Amount of NADPH measured after liposomes containing GDH (L_{GDH}) were incubated for 24 h with L-Glutamate, GSSG, and $NADP^+$ with or without 0.25% Triton X-100. Data were normalized to the amount of NADPH generated by intact liposomes (without Triton X-100). N=3. *$p < 0.05$ using a two-tailed paired *t*-test. Data represented as mean ± SD.

Microscopy images and size distribution of the different assembled microreactors

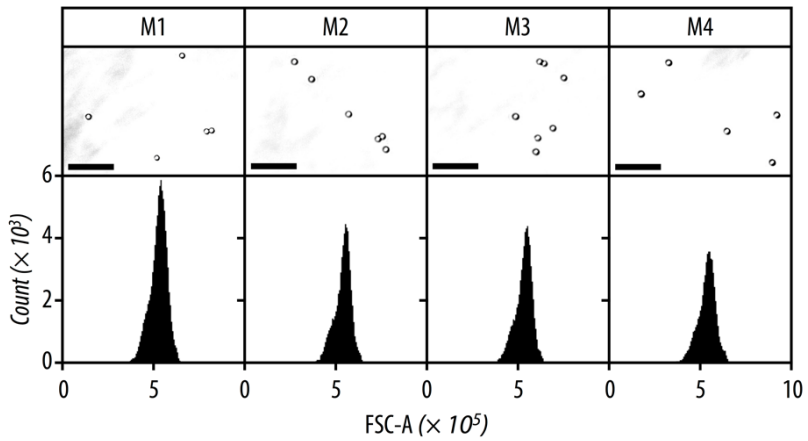


Figure VII.S12. Bright field microscopy images (top row) and population histogram flow cytometry analysis (bottom row) for all the assembled microreactors (M1, M2, M3, and M4). Scale bar = 40 µm.

chapter VII references

VII.1 Buddingh' BC, van Hest JCM. Artificial Cells: Synthetic Compartments with Life-like Functionality and Adaptivity. *Acc Chem Res* **2017**, *50* (4), 769–777.

VII.2 Diekmann Y, Pereira-Leal JB. Evolution of Intracellular Compartmentalization. *Biochem J* **2013**, *449* (2), 319–331.

VII.3 York-Durán MJ, Gallardo MG, Labay CP, Urquhart A, Andresen TL, Hosta-Rigau L. Recent Advances in Compartmentalized Synthetic Architectures as Drug Carriers, Cell Mimics and Artificial Organelles. *Colloids Surf B Biointerfaces* **2017**, *152*, 199–213.

VII.4 Gabaldón T, Pittis AA. Origin and Evolution of Metabolic Sub-Cellular Compartmentalization in Eukaryotes. *Biochimie* **2015**, *119* (Supplement C), 262–268.

VII.5 Zecchin A, Stapor PC, Goveia J, Carmeliet P. Metabolic Pathway Compartmentalization: An Underappreciated Opportunity? *Curr Opin Biotechnol* **2015**, *34* (Supplement C), 73–81.

VII.6 Deamer D. A Giant Step towards Artificial Life? *Trends Biotechnol* **2005**, 23 (7), 336–338.

VII.7 Noireaux V, Maeda YT, Libchaber A. Development of an Artificial Cell, from Self-Organization to Computation and Self-Reproduction. *Proc Natl Acad Sci USA* **2011**, *108* (9), 3473–3480.

VII.8 Walde P. Building Artificial Cells and Protocell Models: Experimental Approaches with Lipid Vesicles. *BioEssays* **2010**, *32* (4), 296–303.

VII.9 Gao C, Wu Z, Lin Z, Lin X, He Q. Polymeric Capsule-Cushioned Leukocyte Cell Membrane Vesicles as a Biomimetic Delivery Platform. *Nanoscale* **2016**, *8* (6), 3548–3554.

VII.10 Hosta-Rigau L, York-Duran MJ, Kang TS, Städler B. Extracellular Microreactor for the Depletion of Phenylalanine Toward Phenylketonuria Treatment. *Adv Funct Mater* **2015**, *25* (25), 3860–3869.

VII.11 Zhang Y, Baekgaard-Laursen M, Städler B. Small Subcompartmentalized Microreactors as Support for Hepatocytes. *Adv Healthc Mater* **2017**, *6* (15), 1601141.

VII.12 Itel F, Schattling PS, Zhang Y, Städler B. Enzymes as Key Features in Therapeutic Cell Mimicry. *Adv Drug Deliv Rev* **2017**, *118*, 94–108.

VII.13 Schoonen L, van Hest JCM. Compartmentalization Approaches in Soft Matter Science: From Nanoreactor Development to Organelle Mimics. *Adv Mater* **2016**, *28* (6), 1109–1128.

VII.14 Chandrawati R, Chong S-F, Zelikin AN, Hosta-Rigau L, Städler B, Caruso F. Degradation of Liposomal Subcompartments in PEGylated Capsosomes. *Soft Matter* **2011**, *7* (20), 9638–9646.

VII.15 Hinzpeter F, Gerland U, Tostevin F. Optimal Compartmentalization Strategies for Metabolic Microcompartments. *Biophys J* **2017**, *112* (4), 767–779.

VII.16 Marguet M, Bonduelle C, Lecommandoux S. Multicompartmentalized Polymeric Systems: Towards Biomimetic Cellular Structure and Function. *Chem Soc Rev* **2012**, *42* (2), 512–529.

VII.17 Peters RJRW, Marguet M, Marais S, Fraaije MW, van Hest JCM, Lecommandoux S. Cascade Reactions in Multicompartmentalized Polymersomes. *Angew Chem Int Ed* **2014**, *53* (1), 146–150.

VII.18 Elani Y, Law RV, Ces O. Vesicle-Based Artificial Cells as Chemical Microreactors with Spatially Segregated Reaction Pathways. *Nat Commun* **2014**, *5*, 5305.

VII.19 Chandrawati R, Odermatt PD, Chong S-F, Price AD, Städler B, Caruso F. Triggered Cargo Release by Encapsulated Enzymatic Catalysis in Capsosomes. *Nano Lett* **2011**, *11* (11), 4958–4963.

VII.20 Hosta-Rigau L, York-Duran MJ, Zhang Y, Goldie KN, Städler B. Confined Multiple Enzymatic (Cascade) Reactions within Poly(Dopamine)-Based Capsosomes. *ACS Appl Mater Interfaces* **2014**, *6* (15), 12771–12779.

VII.21 Schattling P, Dreier C, Städler B. Janus Subcompartmentalized Microreactors. *Soft Matter* **2015**, *11* (26), 5327–5335.

VII.22 Godoy-Gallardo M, Labay C, Jansman MMT, Ek PK, Hosta-Rigau L. Intracellular Microreactors as Artificial Organelles to Conduct Multiple Enzymatic Reactions Simultaneously. *Adv Healthc Mater* **2017**, *6* (4), 1601190.

VII.23 Godoy-Gallardo M, Labay C, Trikalitis VD, Kempen PJ, Larsen JB, Andresen TL, Hosta-Rigau L. Multicompartment Artificial Organelles Conducting Enzymatic Cascade Reactions inside Cells. *ACS Appl Mater Interfaces* **2017**, *9* (19), 15907–15921.

VII.24 Thingholm B, Schattling P, Zhang Y, Städler B. Subcompartmentalized Nanoreactors as Artificial Organelle with Intracellular Activity. *Small* **2016**, *12* (13), 1806–1814.

VII.25 Zhang Y, Schattling PS, Itel F, Städler B. Planar and Cell Aggregate-Like Assemblies Consisting of Microreactors and HepG2 Cells. *ACS Omega* **2017**, *2* (10), 7085–7095.

VII.26 Armada-Moreira A, Taipaleenmäki E, Baekgaard-Laursen M, Schattling PS, Sebastião AM, Vaz SH, Städler B. Platinum Nanoparticle-Based Microreactors as Support for Neuroblastoma Cells. *ACS Appl Mater Interfaces* **2018**, *10* (9), 7581–7592.

VII.27 Liu Y, Du J, Yan M, Lau MY, Hu J, Han H, Yang OO, Liang S, Wei W, Wang H, *et al*. Biomimetic Enzyme Nanocomplexes and Their Use as Antidotes and Preventive Measures for Alcohol Intoxication. *Nat Nanotechnol* **2013**, *8* (3), 187–192.

VII.28 Castellana M, Wilson MZ, Xu Y, Joshi P, Cristea IM, Rabinowitz JD, Gitai Z, Wingreen NS. Enzyme Clustering Accelerates Processing of Intermediates through Metabolic Channeling. *Nat Biotechnol* **2014**, *32* (10), 1011–1018.

VII.29 Lynge ME, Baekgaard Laursen M, Hosta-Rigau L, Jensen BEB, Ogaki R, Smith AAA, Zelikin AN, Städler B. Liposomes as Drug Deposits in Multilayered Polymer Films. *ACS Appl Mater Interfaces* **2013**, *5* (8), 2967–2975.

VII.30 Botman D, Tigchelaar W, Noorden CJFV. Determination of Glutamate Dehydrogenase Activity and Its Kinetics in Mouse Tissues Using Metabolic Mapping (Quantitative Enzyme Histochemistry). *J Histochem Cytochem* **2014**, *62* (11), 802–812.

VII.31 Carlberg I, Mannervik B. Glutathione Reductase. *Methods Enzymol* **1985**, *113*, 484–490.

VII.32 Wu JT, Wu LH, Knight JA. Stability of NADPH: Effect of Various Factors on the Kinetics of Degradation. *Clin Chem* **1986**, *32* (2), 314–319.

VII.33 Thatcher BJ, Storey KB. Glutamate Dehydrogenase from Liver of Euthermic and Hibernating Richardson's Ground Squirrels: Evidence for Two Distinct Enzyme Forms. *Biochem Cell Biol* **2001**, *79* (1), 11–19.

VII.34 Bankar SB, Bule MV, Singhal RS, Ananthanarayan L. Glucose Oxidase - an Overview. *Biotechnol Adv* **2009**, *27* (4), 489–501.

VII.35 Deisseroth A, Dounce AL. Catalase: Physical and Chemical Properties, Mechanism of Catalysis, and Physiological Role. *Physiol Rev* **1970**, *50* (3), 319–375.

VII.36 Juers DH, Matthews BW, Huber RE. LacZ β-Galactosidase: Structure and Function of an Enzyme of Historical and Molecular Biological Importance. *Protein Sci* **2012**, *21* (12), 1792–1807.

VII.37 Johnson KA, Goody RS. The Original Michaelis Constant: Translation of the 1913 Michaelis–Menten Paper. *Biochemistry* **2011**, *50* (39), 8264–8269.

VII.38 Constantinides A, Vieth WR, Fernandes PM. Characterization of Glucose Oxidase Immobilized on Collagen. *Mol Cell Biochem* **1973**, *1* (1), 127–133.

VII.39 Ozyilmaz G, Tukel SS, Alptekin O. Kinetic Properties and Storage Stability of Catalase Immobilized on to Florisil. *Indian J Biochem Biophys* **2007**, *44* (1), 38–43.

VII.40 Crueger A, Crueger W. Carbohydrates. In *Biotransformations*; Biotechnology, A Comprehensive Treatise in 8 Volumes; Kieslich K, Ed.; Verlag Chemie: Weinheim, Germany, **1984**; Vol. 6A, Ch. 12.

VII.41 Brizard AM, van Esch JH. Self-Assembly Approaches for the Construction of Cell Architecture Mimics. *Soft Matter* **2009**, *5* (7), 1320–1327.

VII.42 Nii T, Ishii F. Encapsulation Efficiency of Water-Soluble and Insoluble Drugs in Liposomes Prepared by the Microencapsulation Vesicle Method. *Int J Pharm* **2005**, *298* (1), 198–205.

VII.43 Cioci F, Lavecchia R. Enzyme-Loaded Liposomes as Microreactors. In *Volume III: From Design to Microreactors*; Handbook of Nonmedical Applications of Liposomes; Barenholz Y, Lasic DD, Eds.; CRC Press: Boca Raton, USA, **1996**; Vol. 3, Ch. 16.

VII.44 Städler B, Price AD, Chandrawati R, Hosta-Rigau L, Zelikin AN, Caruso F. Polymer Hydrogel Capsules: En Route toward Synthetic Cellular Systems. *Nanoscale* **2009**, *1* (1), 68–73.

VII.45 Chandrawati R, Caruso F. Biomimetic Liposome- and Polymersome-Based Multicompartmentalized Assemblies. *Langmuir* **2012**, *28* (39), 13798–13807.

VII.46 Chandrawati R, Hosta-Rigau L, Vanderstraaten D, Lokuliyana SA, Städler B, Albericio F, Caruso F. Engineering Advanced Capsosomes: Maximizing the Number of Subcompartments, Cargo Retention, and Temperature-Triggered Reaction. *ACS Nano* **2010**, *4* (3), 1351–1361.

VII.47 Zhu C, Taipaleenmäki E, Zhang Y, Han X, Städler B. Interaction of Cells with Patterned Reactors. *Biomater Sci* **2018**, *6* (4), 793–802.

VII.48 Lynge ME, Schattling P, Städler B. Recent Developments in Poly(Dopamine)-Based Coatings for Biomedical Applications. *Nanomed* **2015**, *10* (17), 2725–2742.

Chapter VIII.

The evolution of the astrosome.

Multicompartment microreactors prevent excitotoxic dysfunctions in rat primary cortical neurons

Armada-Moreira A, Coelho JE, Lopes LV, Sebastião AM, Städler B, Vaz SH

Advanced Biosystems **2020**



Let me summarize what happened in this project so far: (i) I located a biological problem: excitotoxicity; (ii) I went to Denmark, to Städler's lab, where they are specialized in artificial cells and organelles; (iii) while there, I was able to create my first astrosomes, with confirmed biological activity in a cell line; and (iv) I developed a side project that allowed me to gain a lot of knowledge about enzymes in the context of cell mimics.

At this point, I was focused on creating new (more complex) astrosomes using enzymes and platinum nanoparticles, and testing them in a new cell model, that closer resembled the final intended use for the astrosomes.

So, I came back to Portugal, to Sebastião's Lab, and set out to work on these goals. All that work generated the publication presented in this chapter, where we test the first generation of astrosomes with rat primary cortical neurons, create and characterize the new and improved astrosomes, and compare their activity against that of the first generation. We first intended to only perform the same assays as in the cell line publication, performing only a cell viability assay to test biological activity of microreactors. But we used actual neurons in this part of the work, just cell viability would be a waste when we can measure electrical neuronal communication. So, we also did extracellular electrophysiological recordings to functionally test the microreactors. Regarding the new microreactors, we finally incorporated the enzyme glutamate dehydrogenase, working together with the platinum nanoparticles, as was our original plan. However, since we had just published about the enzymatic cycle comprised of glutamate dehydrogenase and glutathione reductase and because excitotoxicity is associated with a redox imbalance, we also tested microreactors containing platinum nanoparticles and these two enzymes.

In this publication, I did all experimental work, data analysis, manuscript writing, and illustrations. Joana E. Coelho and Luísa V. Lopes provided the microelectrode array equipment and taught me the technique.

publication information

Title. Multicompartment microreactors prevent excitotoxic dysfunctions in rat primary cortical neurons.

Authors. Adam Armada-Moreira, Joana E. Coelho, Luísa V. Lopes, Ana M. Sebastião, Brigitte Städler, Sandra H. Vaz.

Status of publication. Published.

Journal. Advanced Biosystems 2020, 2000139.

DOI. 10.1002/adbi.202000139.

JCR impact factor, quartile, and field. N/A.

original research article

Multicompartment microreactors prevent excitotoxic dysfunctions in rat primary cortical neurons

Armada-Moreira A[1,2,3], Coelho JE[2], Lopes LV[2], Sebastião AM[1,2], Städler B[3], Vaz SH[1,2]*

[1]Instituto de Farmacologia e Neurociências, Faculdade de Medicina, Universidade de Lisboa, Lisbon, Portugal.
[2]Instituto de Medicina Molecular, Faculdade de Medicina, Universidade de Lisboa, Lisbon, Portugal.
[3]Interdisciplinary Nanoscience Center (iNANO), Aarhus University, Aarhus, Denmark.
*Corresponding author.

Advanced Biosystems **2020**, 2000139.

Abstract

Excitotoxicity is a cellular phenomenon that comprises the consequences of toxic actions of excitatory neurotransmitters, such as glutamate, and is connected to overproduction of reactive oxygen species (ROS) and ammonia (NH_4^+) toxicity. Platinum nanoparticle (Pt-NP)-based microreactors able to degrade hydrogen peroxide (H_2O_2) and NH_4^+, were previously described as a novel therapeutical approach against excitotoxicity, conferring protection to neuroblasts. Now, it is demonstrated that these microreactors are compatible with rat primary cortical neurons, show high levels of neuronal membrane interaction, and are able to improve cell survival and neuronal activity when neurons are exposed to H_2O_2 or NH_4^+. Furthermore, new microreactors are assembled, including enzyme-loaded liposomes containing glutamate dehydrogenase and glutathione reductase, in addition to Pt-NP. The *in vitro* activity of these microreactors is characterized and they are compared to the Pt-NP-based microreactors in terms of biological activity, concluding that they enhance cell viability similarly or more extensively than the latter ones. Additionally, extracellular electrophysiological recordings are performed, where microreactors rescue neuronal functionality lost upon incubation with H_2O_2 or NH_4^+. This study provides more evidence for the potential application of these microreactors in a biomedical context with more complex cellular environments.

Keywords: rat cortical primary neurons, platinum nanoparticles, excitotoxicity, microreactors, encapsulated catalysis.

Introduction

Excitatory transmission is essential for proper brain function, having an important role not only in neuronal communication *per se*, but also in higher-level functions such as learning and memory. Glutamate is the main excitatory neurotransmitter in the mammalian central nervous system (CNS).[VIII.1] When glutamate is released in a synapse, astrocytes are responsible for the clearance of 80–90% of this synaptically-released neurotransmitter.[VIII.2,3] Due to the major role of astrocytes in glutamate clearance, astrocytic dysfunction can lead to an excessive build-up of glutamate in the synapse that can lead to an extreme activation of neuronal post-synaptic glutamate receptors, inducing excitotoxicity.[VIII.4] This phenomenon can be

described as the toxic actions of excitatory neurotransmitters, namely glutamate in the CNS[VIII.5,6] and, among its many intracellular consequences, it can lead to an overproduction of reactive oxygen species, such as hydrogen peroxide (H_2O_2).[VIII.7,8] Furthermore, since astrocytes are also responsible for ammonia (NH_4^+) detoxification in the brain,[VIII.9] astrocytic dysfunction and associated excitotoxicity often leads to NH_4^+ toxicity.[VIII.10]

Most therapeutic approaches used to counteract excitotoxicity are mainly focused on the blockade of glutamate release or inactivation of glutamate receptors, which is accompanied by undesired and deleterious side effects that impact normal excitatory neuronal communication.[VIII.11]

Therapeutic cell mimicry is a research field focused on creating artificial cells[VIII.12] and organelles[VIII.13] that substitute for lost cellular functions.[VIII.14] Artificial cells showed initial promise to detoxify liver tissue,[VIII.15] to kick-start biomineralization in bone spheroids,[VIII.16] to support *ex vivo* T-cell expansion via antigen-presenting cell mimics,[VIII.17] or in cardiac regeneration using cardiac stem cell mimics.[VIII.18] We recently reported platinum nanoparticle (Pt-NP)-based microreactors as support for neuroblasts, using the human neuroblastoma-derived SH-SY5Y cell line.[VIII.19] Although it was already known that Pt-NP were efficient catalysts for the conversion of H_2O_2 into water and oxygen[VIII.20] and able to convert NH_4^+ into nitric oxide (NO),[VIII.21] this was the first work exploring the potential application of these nanoparticles in the biomedical field, in the context of cell mimicry and artificial cells.

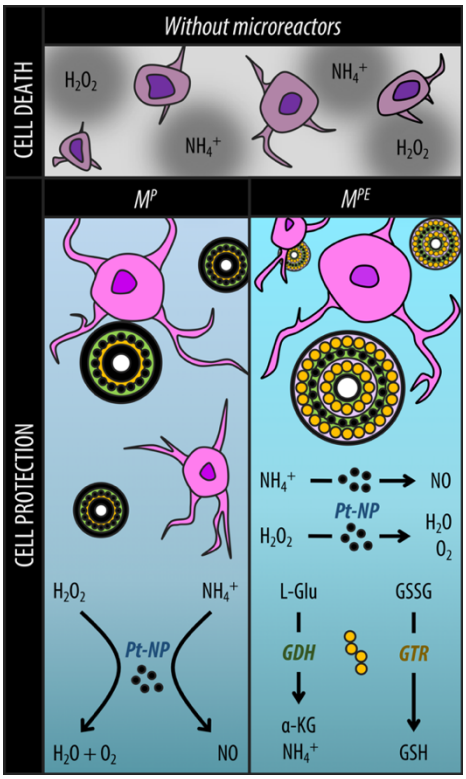


Figure VIII.1. Schematic representation of rat primary cortical neurons exposed to toxic compounds (H_2O_2 or NH_4^+) in the absence (top frame) and in the presence of first (bottom left frame) and second (bottom right frame) generation microreactors. The microreactors are able to protect these cells from cell dysfunction and death caused by either H_2O_2 or NH_4^+. Pt-NP – platinum nanoparticles; NO – nitric oxide; GDH – glutamate dehydrogenase; GTR – glutathione reductase; L-Glu – L-glutamate; α-KG – α-ketoglutarate; GSSG – oxidized glutathione; GSH – reduced glutathione.

We now provide an update that further explores the efficiency of these microreactors as a therapeutical approach against the toxic actions of H_2O_2 and NH_4^+ in a more complex cellular environment. We were able to conclude that Pt-NP-based microreactors are compatible and able to interact with rat primary cortical neurons. These microreactors maintain their biological activity in this cell model against these toxic insults. Additionally, we created new and more

complex microreactors, containing Pt-NP and enzymes, namely glutamate dehydrogenase (GDH) and glutathione reductase (GTR), characterized their activity *in vitro*, and performed biological activity assays with rat primary neuronal cultures exposed to H_2O_2 or NH_4^+. These new microreactors are more efficient in cell protection than the first ones (**Figure VIII.1**). This work is highly meaningful on the road to use these microreactors in a medically relevant application. By showing their biocompatibility and biological activity in rat primary neuronal cultures, we were able to increase the complexity of the biological model and conclude that this therapeutic tool maintains its positive activity in a more relevant cellular setting.

Experimental Section

Materials. 4-(2-hydroxyethyl)piperazine-1-ethanesulfonic acid (HEPES), dopamine hydrochloride (DA), poly(L-lysine) (PLL, MW 40 000–70 000 Da), poly(D-lysine) (PDL, MW 30 000–70 000 Da), hydrogen peroxide (H_2O_2, 30% (w/w)), ammonium acetate, L-glutamic acid dehydrogenase from bovine liver (GDH, EC1.4.1.3, 48 U mg^{-1}), glutathione reductase from baker's yeast (GTR, EC1.8.1.7, 170 U mg^{-1}), glutamic acid, β-nicotinamide adenine dinucleotide phosphate sodium salt hydrate ($NADP^+$), L-glutathione oxidized disodium salt (GSSG), horseradish peroxidase (HRP), ammonia assay kit (AAK, MAK310), paraformaldehyde (PFA), bovine serum albumin (BSA), and Triton X-100 were purchased from Sigma-Aldrich (St. Louis, MO, USA). Tris base and sodium chloride (NaCl) were obtained from VWR (Radnor, PA, USA). Amplex UltraRed, Hank's balanced saline solution (HBSS), fetal bovine serum (FBS), Neurobasal medium, L-glutamine (200 mM), B-27 (50×), gentamycin (50 mg mL^{-1}), trypsin-EDTA (0.5%), and BD Falcon™ Cell Strainer 70 μm were purchased from Thermo Fisher Scientific (Waltham, MA, USA). Hoechst 33342 was purchased from Life Technologies (Carlsbad, CA, USA). Polystyrene (PS) particles (19.30 μm in diameter) were acquired from Microparticles GmbH (Berlin, Germany). Cell counting kit-8 (CCK-8) was obtained from Dojindo EU GmbH (Munich, Germany). 1,2-dioleoyl-*sn*-glycero-3-phosphocholine (DOPC) was purchased from Avanti Polar Lipids (Alabaster, AL, USA). PLL-coated μ-Slides $VI^{0.4}$ were purchased from ibidi GmbH (Martinsried, Germany). Platinum nanoparticles (Pt-NP)[VIII.19] and poly(methacrylic acid)-*co*-cholesteryl methacrylate (PMAc)[VIII.22] were synthesized in house according to previously published procedures.

Buffer solutions. HEPES1 buffer (10 mM HEPES, pH 7.3), HEPES2 buffer (20 mM HEPES, 120 mM NaCl, pH 7.3), Tris buffer (10 mM Tris base, pH 8.5), and phosphate-buffered saline (PBS, pH 7.3).

Liposome preparation. 200 nm in diameter liposomes were prepared by evaporation of 100 μL of a DOPC solution (25 mg mL^{-1} in chloroform) under vacuum for 1 h, followed by rehydration of the lipid film with 200 μL of an enzyme-containing solution (100 U mL^{-1} GDH to generate L_{GDH} or 100 U mL^{-1} GDH and 100 U mL^{-1} GTR to generate $L_{GDH+GTR}$) in HEPES2 buffer. Liposomes were then further hydrated with 800 μL of HEPES2 buffer. The solutions were extruded through 200 nm filters (11×) to obtain monodispersed unilamellar

liposomes. Non-encapsulated enzymes were removed by size exclusion chromatography.

Microreactor assembly. Pt-NP-based microreactors were assembled as previously described.[VIII.19] Briefly, PS particles (19.30 μm in diameter, 10 mg mL^{-1}) were coated with DA (2.5 mg mL^{-1} in Tris buffer, 3 h), generating a coating of polydopamine (PDA). The microreactors were then coated with PLL (1.0 mg mL^{-1} in HEPES1 buffer, 10 min) and Pt-NP were adsorbed to its surface (20 min). The microreactors were coated once more with PLL (1.0 mg mL^{-1} in HEPES1 buffer, 10 min) and received a terminating coat of polydopamine, via a DA solution (2.5 mg mL^{-1} in Tris buffer, 3 h), generating the finished Pt-NP-based microreactors (M^{P}). All coating steps were followed by 3× washing steps with HEPES1 buffer (1 800 rpm, 45 s). To generate microreactors containing Pt-NP and enzyme-loaded liposomes, 19.30 μm PS particles were exposed to DA (2.5 mg mL^{-1} in Tris buffer, 3 h) and incubated with PLL (1.0 mg mL^{-1} in HEPES2 buffer, 10 min). The positively charged particles were incubated with enzyme-loaded liposomes (L_{GDH} for M^{PE1}, or $L_{GDH+GTR}$ for M^{PE2}) for 40 min. All microreactors were then coated with PMAc (2.0 mg mL^{-1} in HEPES2 buffer, 10 min), followed by a coating of PLL (1.0 mg mL^{-1} in HEPES2 buffer, 10 min) and adsorption of Pt-NP (20 min). The three previous coating steps (PLL, liposomes, PMAc) were repeated to increase the amount of adsorbed enzyme-loaded liposomes. Finally, microreactors were incubated with DA (2.5 mg mL^{-1} in Tris buffer, overnight) to generate a capping PDA layer. Different control microreactors without Pt-NP were generated: M^{0}, containing only the first PDA layer; M^{00}, containing empty liposomes; M^{0E1}, containing L_{GDH}; and M^{0E2}, containing $L_{GDH+GTR}$. Additionally, microreactors containing Pt-NP and empty liposomes (M^{P0}) were also fabricated. The summary of all different used microreactors can be found in Chapter VIII Supporting Information, **Table VIII.S1**.

ζ-potential measurements. The ζ-potential of the different assembly steps of microreactors containing Pt-NP and liposomes were determined using a Zetasizer Nano ZS (Malvern Instruments, UK), using a material refractive index of 1.590 and a dispersant refractive index of 1.330.

Fluorescent imaging of microreactors. To label liposomes incorporated into microreactors, microreactors were incubated with di-8-ANEPPS dye (10 μM) for 20 min at room temperature, protected from light. The samples were then imaged using an Axioskop 2 Plus fluorescent microscope (Carl Zeiss Inc., Göttingen, Germany), with a 40× objective.

Transmission electron microscopy (TEM). The grids for TEM were prepared by depositing 5 μL of sample on a formvar coated grid (Agar Scientific Ltd, Stansted, Essex, United Kingdom) followed by washing 2× after 1 min with 5 μL of ultrapure water and staining with 2% (v/v) uranyl acetate. Samples were imaged with a Hitachi H7000 transmission electron microscope (Hitachi High-Technologies Europe GmbH, Krefeld, Germany).

H_2O_2 detection assay. 10^4 microreactors were incubated with 1.0 mM H_2O_2 for 24 h at 37 °C. Following this incubation, each sample was incubated with 0.2 U mL^{-1} HRP and 50 μM Amplex UltraRed at room temperature, protected from light, for 30 min. The fluorescence

of the solutions (λ_{ex} = 545 nm, λ_{em} = 590 nm) was measured by a multiplate reader.

NH_4^+ detection assay. 10^6 microreactors were incubated with 1.0 mM NH_4^+ for 24 h at 37 °C. Following this incubation, NH_4^+ was detected using the commercially available AAK. 10 µL of the samples were incubated with 90 µL of AAK detection mix for 15 min at room temperature, protected from light. The fluorescence of the solutions (λ_{ex} = 360 nm, λ_{em} = 450 nm) was measured by a multiplate reader.

NADPH detection assay. Samples were incubated with 30 mM L-glutamate, 2.0 mM GSSG, and 2.0 mM $NADP^+$ at 37 °C. The amount of NADPH in solution was followed by measuring the absorbance of the solutions (λ = 340 nm) at different time points. For the determination of NADPH produced by the different microreactors, 10^5 microreactors were used and samples were centrifuged (1 800 rpm, 45 s) prior to absorbance measurements.

Cell culture. Primary neuronal cultures were prepared according to a previously established method.[VIII.23] Succinctly, Sprague-Dawley fetuses (pre-natal day 18/19) were euthanized and their brains used to obtain primary neuronal cultures. The fetuses were collected in HBSS, their cerebral cortexes isolated and the meninges removed. Following this, the obtained tissue was mechanically fragmented and digested with 10% (v/v) trypsin-EDTA in HBSS for 15 minutes at 37 °C. Trypsin action was stopped with the addition of 30% (v/v) FBS in HBSS. Cells were then centrifuged 3× at 1 200 rpm, where the supernatant was discarded and replaced with 30% (v/v) FBS in HBSS. Cells were then resuspended in supplemented Neurobasal medium (0.5 mM L-glutamine, 25 µM glutamic acid, 2% (v/v) B-27, and 12 µg mL^{-1} gentamycin). To ensure proper tissue dissociation, cells were strained through a nylon filter (70 µm). Cells were then plated at different densities, depending on the application (150 000 cells mL^{-1} for cell viability assays, 600 000 cells mL^{-1} for Hoechst staining, and 300 000 cells mL^{-1} for extracellular electrophysiological recordings), and were incubated at 37 °C in a humified atmosphere of 95% air–5% CO_2. Importantly, these different plating densities reflect the optimal cell concentration for the different applications,[VIII.24] in order to achieve a linear colorimetric response in the cell viability assay, to be able to examine the interaction between microreactors and cells in the staining assay, and to generate more robust and detectable electrical signals in the electrophysiological recordings. All animals were handled according to Portuguese Law and the European Union Directive (86/609/EEC) on the protection of animals for scientific experimentation.

Cell viability assay. 150 000 cells mL^{-1} were plated on PDL-treated (10 µg mL^{-1}) 96-well plates and allowed to adhere and mature for 7 or 14 DIV. At these times, to study the biocompatibility of the microreactors, M^P were added to the cell medium at different concentrations (5, 10, 20, and 100% of the number of cells). 24 h later, the cell medium was replaced with a solution of 10% (v/v) CCK-8 in supplemented Neurobasal medium. After 2 h of incubation at 37 °C, 100 µL of medium was transferred onto a new 96-well plate and absorbance at 460 nm was measured using a multiplate reader. Regarding the biological activity of the microreactors, the same protocol was performed

except the cells were allowed to adhere and mature for 14 DIV, at which time microreactors (20% of the number of cells; M^P or M^{PE1}) and 10 µM H_2O_2 or 10 mM NH_4^+ were added to the cell medium.

Hoechst staining. 600 000 cells mL^{-1} were plated on PLL-treated ibidi µ-Slides VI$^{0.4}$ for 7 or 14 DIV. Cell medium was renewed every two days, to prevent evaporation. At these time points, M^P were added to each well at different concentrations (10, 20, and 100% of the number of cells). After 24 h of incubation, wells were washed 3× with PBS, fixed for 30 min in 4% (w/v) PFA in PBS, permeabilized and blocked for nonspecific binding sites for 20 min with 0.1% (v/v) Triton X-100 and 1% (w/v) BSA in PBS, and incubated for 10 min at room temperature with Hoechst 33342 (12 µg mL^{-1}) in PBS protected from light. The samples were stored at 4 °C in PBS in the µ-Slides. Bright field and fluorescence images were captured using an Axioskop 2 Plus fluorescent microscope (Carl Zeiss Inc.), with a 10× objective. Images were recorded using the software AxioVision (Carl Zeiss Inc.) and analyzed using the software ImageJ.[VIII.25]

Microelectrode array (MEA) assay. 300 000 cells mL^{-1} were plated on PDL-treated (10 µg mL^{-1}) 6 well round chamber microelectrode array plates with 60 electrodes (60-6wellMEA200/30iR-Ti-rcr, Multi Channel Systems, Reutlingen, Germany) and allowed to adhere for 14 DIV. At this point, extracellular recordings were performed, prior to any cell treatment. Cells were probed with a bi-phasic wave, with ±1000 mV during 200 ms and an inter-stimuli interval of 20 s, during a total recording time of 3 min, resulting in 9 different stimulations. The same electrode was simultaneously used to stimulate and record cells. Cells were then incubated for 24 h with microreactors (M^P or M^{PE1}, at 20% of the number of cells) and 10 µM H_2O_2 or 10 mM NH_4^+. Following this incubation, the same stimulation and recording protocols were performed. The relative position of the electrodes was maintained during all stimulation protocols, in order to stimulate and record the same cells before and after the incubations.

Statistical analysis. All assays include at least three independent repeats (N >= 3). For experiments without cells, concerning the characterization of microreactors, each independent repeat refers to different batches of microreactors, independently assembled. For cell experiments, each independent repeat refers to different independent animal cultures. All cell viability assays were performed with triplicates and at least three independent repeats. For each independent repeat, values were normalized to the cell viability of untreated cells (100%). For Hoechst staining, five random fields were analyzed per condition in each independent repeat. For the quantification of H_2O_2 and NH_4^+ consumption, values were normalized to the initial amount of H_2O_2 or NH_4^+ in solution (100%). Electrophysiological data are normalized as fold-change over 24h (change = value[day 2]/value[day 1]). All data are represented as mean ± standard error of mean (SEM), with $p < 0.05$ representing statistical significance. When considering the whole data set, values outside the range of mean ± 2× standard deviation were considered outliers. Statistical significance was determined using two-tailed paired t-tests when comparing two

conditions and one-way ANOVA when comparing three or more. All data were analyzed in GraphPad Prism (GraphPad Software, Inc., La Jolla, CA, USA).

Results and discussion

Neuronal compatibility and interaction

Neurons generated from rat primary neuronal cultures were allowed to mature for either 7 or 14 DIV, at which points M^P were co-incubated at different concentrations. Cell viability was measured after 24 h (**Figure VIII.2A**). Importantly, the microreactors were tested with 7 DIV and 14 DIV cultures, since these time points are enriched, respectively, with immature and mature neurons.[VIII.26] The assay used in this work to determine cell viability is based on the quantification of a signal that is proportional to the number of live cells in culture. Thus, it only represents cell viability in non-proliferative cell culture, being a proxy for cell proliferation in proliferative cultures. The validity of this assay as a cell viability measure in this work is based on three different premises. Firstly, the cell culture conditions used here (serum-free Neurobasal cell medium) give rise to a mostly neuronal culture.[VIII.27] Secondly, previous findings report very low levels of glial contamination in these time points.[VIII.26,28,29] Finally, it is known that glial proliferation rates are dramatically hindered in the presence of neurons,[VIII.30] which corroborates our argument for the use of this assay to quantify neuronal viability. In this way, it is possible to ascertain the biocompatibility of the microreactors in relation to different phases of neuronal differentiation. There were no significant drops in cell viability at either 7 DIV or 14 DIV when cells were incubated with M^P, regardless of microreactor concentration (**Figure VIII.2B**), which allowed us to conclude that M^P are not neurotoxic.

Interestingly, in a previous study focused on the interaction of these microreactors and the SH-SY5Y cell line, there was a considerable drop in cell viability for the higher microreactor concentrations (c. 50% at a concentration of 100% of the number of cells).[VIII.19] Considering that the SH-SY5Y cell line is a continuously proliferating cell line, the hypothesis used to explain this finding was that the microreactors, when present at a high number in the cell culture, impacted the number of cells in solution through contact inhibition of proliferation, and not due to toxicity. Contact inhibition of proliferation is a phenomenon that leads to a decrease or arrest of proliferation rate, due to a physical constriction of the available space, caused either by high confluence or a mechanical impediment.[VIII.31] Since a microreactor concentration of 100% represents a very large number of microreactors in solution, these microreactors would occupy the space that cells would need to proliferate at their optimal rate. With unavailable free space, cells growing in monolayer decrease their proliferation rate and eventually reach a quiescent state.[VIII.32] This hypothesis was tested with an immunostaining assay targeting dead cells and with a membrane integrity assay, which concluded that, compared to control condition (cells not exposed to microreactors), co-incubation with microreactors had no negative impact in terms of cell death and membrane integrity and, thus, no negative impact on cell viability.[VIII.19] Nevertheless, these experiments only provided an indirect proof of contact

inhibition of proliferation. Our data corroborate the theory that the decrease seen in cell viability when the microreactors were incubated with the SH-SY5Y cell line was due to contact inhibition of proliferation and not microreactor toxicity.

Next, we tested the adherence of M^P to neurons, to ensure that these microreactors are able to interact with the cells. For this, cells were allowed to mature for either 7 or 14 DIV and, at these time points, microreactors were added at different concentrations. 24 h following this incubation, cells were washed and fixed, nuclei were stained, and microscopy images were obtained for each condition (**Figure VIII.2C**). The number of cells and microreactors in each obtained field were counted and the experimental concentration of microreactors was calculated (**Figure VIII.2D**). We were able to conclude that, at either 7 or 14 DIV, the microreactors show high cell adherence, with no significant differences between experimental and theoretical concentrations, using a one sample *t*-test, except for the 100% theoretical concentration (7 DIV: 39.67 ± 16.60, $p < 0.01$; 14 DIV: 57.29 ± 30.81, $p < 0.05$). In this latter case, we hypothesize that the high number of microreactors present in solution caused a physical constraint for the adhesion of more microreactors. With this experiment, we are only able to account for microreactors that are efficiently attached to cells. Due to the size and shape of the microreactors (20 μm in diameter spheres), several sections of cell membrane would be unavailable for attachment, since the already attached microreactors would shadow this neighboring membrane area, impeding the attachment of more microreactors, as illustrated in **Figure VIII.2E**.

Current literature already suggests that polydopamine (PDA)-coated microreactors such as M^P would show high levels of cell adherence. Indeed, PDA has been thoroughly studied to functionalize biomaterials, such as gold, glass, platinum, and different polymers, increasing their biocompatibility towards neurons.[VIII.33] Particularly, a study using PC12 cells had already shown that PDA-coated surfaces promoted cell adhesion and proliferation when compared to uncoated surfaces.[VIII.34] In another study, PDA-coated microreactors were shown to present better cell adhesion towards the SH-SY5Y cell line, compared to uncoated, poly(L-lysine)-coated, and poly(methacrylic acid)-coated microreactors, although with lower absolute cell adherence than the data presented in this study.[VIII.19] Thus, with this study, we were able to further ascertain the potential role of PDA as "biological neuronal glue", where this polymer is able to functionalize biomaterials and increase their biocompatibility towards rat cortical neurons in a highly efficient manner. Furthermore, these data validate primary neuronal cultures as a good model to test the biological activity of the microreactors, since the latter do not induce cell death and show appropriate levels of cell adherence.

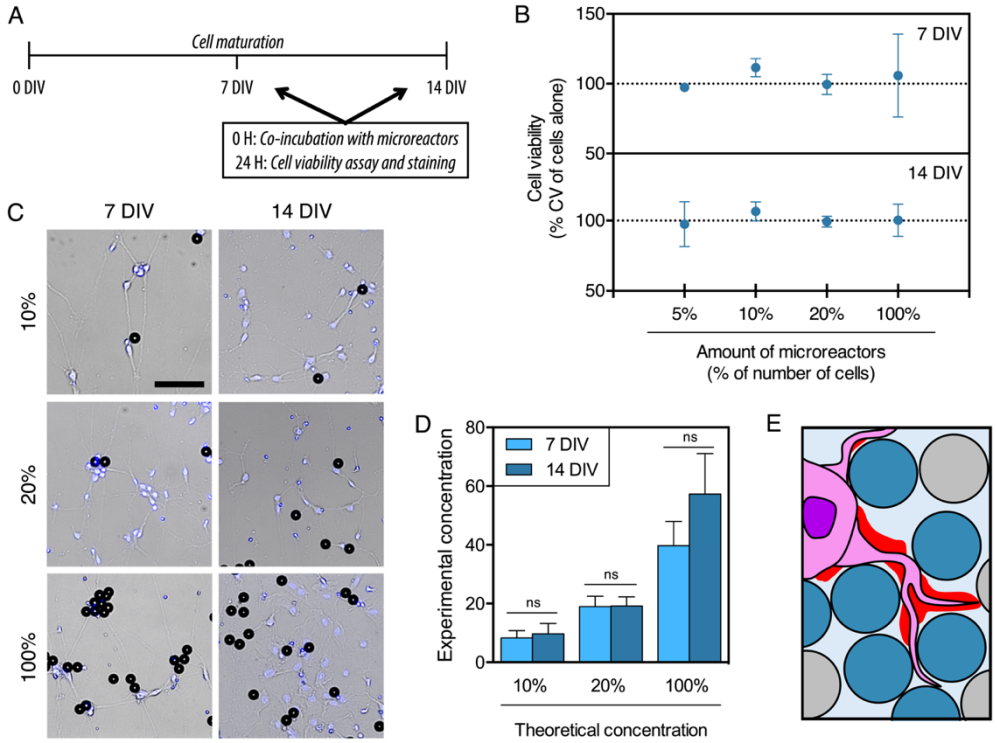


Figure VIII.2. (**A**) Cell viability and adherence of rat primary cortical neurons exposed to different microreactor concentrations: cells matured for either 7 or 14 DIV, at which point M^P were co-incubated for 24 h and the cell viability assay and Hoechst staining were performed. (**B**) Cell viability of rat primary neuronal cultures at 7 DIV and 14 DIV when co-incubated with different concentrations of M^P (5 to 100% of the number of cells). Values were normalized to cell viability of cells not exposed to M^P (100%). N=3–5. No significant differences were found. (**C**) Representative Hoechst staining images, obtained with cells at 7 and 14 DIV with nuclei stained blue, co-incubated with M^P where the theoretical microreactor concentration is either 10%, 20%, or 100% of the number of cells. Scale bar = 100 µm. (**D**) Microreactor concentration, calculated as percentage of the number of cells, after washing, fixing, and staining, at 7 and 14 DIV (N=3–5, $^{ns}p > 0.05$ comparing the same concentrations at 7 and 14 DIV, using one-way ANOVA followed by Sidak's multiple comparison test). (**E**) Schematic representation of the spatial constriction of a high number of microreactors attempting to adhere to a neuron. In blue are the successfully attached microreactors, in gray the ones unable to interact, and in red the cell membrane areas that are unreachable due to the spatial configuration of the already attached microreactors.

Increasing the complexity: comparative *in vitro* characterization of different microreactors

New microreactors, containing Pt-NP and enzyme-filled liposomes, were developed to expand the functions and activity of M^P. The choice of the incorporated enzymes aimed at further mimicking astrocytic functions. Specifically, these new microreactors combine the already described actions of Pt-NP with glutamate consumption and GSH regeneration. Glutamate dehydrogenase (GDH) was chosen to reproduce the astrocytic clearance of synaptically-released glutamate[VIII.2] and glutathione reductase (GTR) was included since astrocytes produce GSH as a strategy to counteract the effects of excitotoxicity and excessive extracellular NH_4^+.[VIII.35,36] With that in mind, two microreactor variations were created: one containing Pt-NP and GDH

(M^{PE1}) and another using Pt-NP and both GDH and GTR (M^{PE2}).

These microreactors were assembled following a combination of previously described protocols.[VIII.19,37] Essentially, 19.30 µm in diameter PS particles were coated with PDA, followed by a coating of PLL and adsorption of L_{GDH} or $L_{GDH+GTR}$ (for M^{PE1} or M^{PE2}, respectively). The liposomes were anchored to the microreactor using a layer of PMAc. A new layer of PLL was used and Pt-NP were allowed to adhere to the structure. In order to obtain higher enzymatic activity, the coating with PLL, liposomes, and PMAc was repeated once more. A finishing layer of PDA ensured the biocompatibility and cell adherence of the microreactors. All assembly steps were followed by the changes in ζ-potential (**Figure VIII.3A**). The relative shifts in ζ-potential are in accordance with previously published assembly protocols,[VIII.37] although the absolute values show clear differences. It is already known that ionic species, specifically NaCl, can quench the signal of ζ-potential, bringing it closer to 0 mV.[VIII.38] Since we used HEPES2 buffer containing NaCl, the absolute values of ζ-potential are not directly comparable to previous studies using different buffer solutions with different ionic strengths. In parallel, the successful deposition of PDA was confirmed by color change (white to brown and brown to black, **Figure VIII.3Ai** and **Figure VIII.3Av** respectively). Liposome presence was evaluated with a fluorescent lipid dye (**Figure VIII.3Aii** for the first liposomal layer and **Figure VIII.3Aiv**, with higher fluorescent intensity for the same exposure time, for microreactors with two liposomal layers). Pt-NP adsorption was monitored using TEM (**Figure VIII.3Aiii**). All these assays indicate a successful assembly of the microreactors.

The successful incorporation of the enzyme-loaded liposomes onto the microreactors was confirmed by determining their enzymatic activity. This activity was measured indirectly via the absorbance at 340 nm, which is proportional to the concentration of NADPH in solution.[VIII.39] NADPH is either a product or a substrate of the incorporated enzymes (**Figure VIII.3B**). It is produced by GDH, with concomitant conversion of L-glutamate and $NADP^+$ into α-ketoglutarate and NH_4^+,[VIII.40] and consumed by GTR during the formation of reduced glutathione (GSH) from oxidized glutathione (GSSG).[VIII.41] Taking this into account, there will be a high production of NADPH, proportional to the consumption of glutamate, when considering GDH alone. On the other hand, with both enzymes, the NADPH produced by GDH will be consumed by GTR, leading to a lower concentration of this compound in solution.

All assembly steps involving enzymes, i.e. free enzymes in solution, enzymes encapsulated in liposomes, and the microreactors M^{PE1} and M^{PE2}, were exposed to L-glutamate, $NADP^+$, and GSSG at 37 °C. The time point corresponding to the highest GDH activity (highest NADPH concentration) is represented (**Figure VIII.3C**). There is a significant difference between GDH and GDH+GTR in all cases, concluding that the enzymes were successfully encapsulated into liposomes and maintain their activity when incorporated into microreactors.

The activity and dynamics of GDH and GTR in solution, liposomes, and incorporated into 2.12 µm sized microreactors were already thoroughly explored in a previous work that also

identified the time point for the highest NADPH production by GDH in each assembly step.[VIII.42] However, contrary to this previous work, we found that the peak NADPH production by M^{PE1} and M^{PE2} was at 72 h and not 48 h. Importantly, we used 19.30 μm PS particles as the microreactor core while the previous study employed 2.12 μm SiO_2 particles. These latter have a higher surface area to volume ratio, which increases microreactor activity and impacts enzyme kinetics. Indeed, the surface area to volume ratio of a 19.30 μm in diameter particle is 0.31 μm^{-1}, while for a 2.12 μm in diameter particle is 2.83 μm^{-1}, almost 10× higher. Regardless, in agreement with previous work, NADPH production in liposomes and microreactors is reduced when compared to free enzymes in solution, which is tied to encapsulation efficiency – only around 10–20% of the enzymes are encapsulated into the liposomes.[VIII.42]

Following on, the microreactors' ability to convert H_2O_2 was compared. For this, microreactors containing Pt-NP (M^P), Pt-NP and empty liposomes (M^{P0}), Pt-NP and L_{GDH} (M^{PE1}), and Pt-NP and $L_{GDH+GTR}$ (M^{PE2}) were incubated with H_2O_2 for 24 h at 37 °C. The equivalent microreactors without Pt-NP were used as control: M^0, M^{00}, M^{0E1}, and M^{0E2}, respectively. A two-way ANOVA considering type of microreactor vs. presence of Pt-NP showed that the differences observed between groups arose from both tested variables (Chapter VIII Supporting Information, **Table VIII.S2**). Considering presence of Pt-NP, all tested Pt-NP-containing microreactors showed significant catalytic activity when compared with the respective control (**Figure VIII.3D**). Considering the type of microreactor, M^{PE1} and M^{PE2} were c. 10× more effective as H_2O_2 scavengers than M^P, but had no significant differences in their activity towards H_2O_2. Interestingly, microreactors containing Pt-NP and empty liposomes (M^{P0}) showed an intermediate activity between that of M^P and that of M^{PE1} and M^{PE2}, although the difference in relation to M^P was not statistically significant (**Figure VIII.3D**).

While the enzymes included in M^{PE1} and M^{PE2} show no direct activity toward H_2O_2, ROS are known to cause lipid peroxidation. In fact, it has been shown that H_2O_2-dependent cell membrane peroxidation is a key player in cell injury induced by oxidative stress, with cells with higher poly unsaturated fatty acid (PUFA) content being more susceptible to this damage.[VIII.43] Additionally, a study in human lymphocytes showed that a 24 h incubation with 10 μM H_2O_2 leads to significant, yet low, lipid peroxidation in cell membranes.[VIII.44] In our work, we used DOPC to form liposomes. DOPC is a phospholipid with two double bonds, making it prone to H_2O_2-induced peroxidation. This peroxidation could be indirectly reducing the amount of H_2O_2 in solution for the M^{PE1} and M^{PE2} conditions.

Next, 10^6 of the different microreactors were incubated with NH_4^+ for 24 h at 37 °C. A higher number of microreactors was used for this assay due to the lower catalytic activity of Pt-NP toward NH_4^+ when compared to H_2O_2.[VIII.19] Following this incubation, the amount of NH_4^+ in solution was determined. A two-way ANOVA considering type of microreactor vs. presence of Pt-NP showed that the differences observed between groups arose from the presence of Pt-NP and not from the type of microreactor (Chapter VIII Supporting Information, **Table VIII.S2**). All Pt-NP-containing

microreactors showed significant catalytic activity toward NH_4^+, with an average consumption of 7–12% of the initial NH_4^+ concentration (**Figure VIII.3E**). Importantly, there were no significant differences between the activity of Pt-NP-containing microreactors.

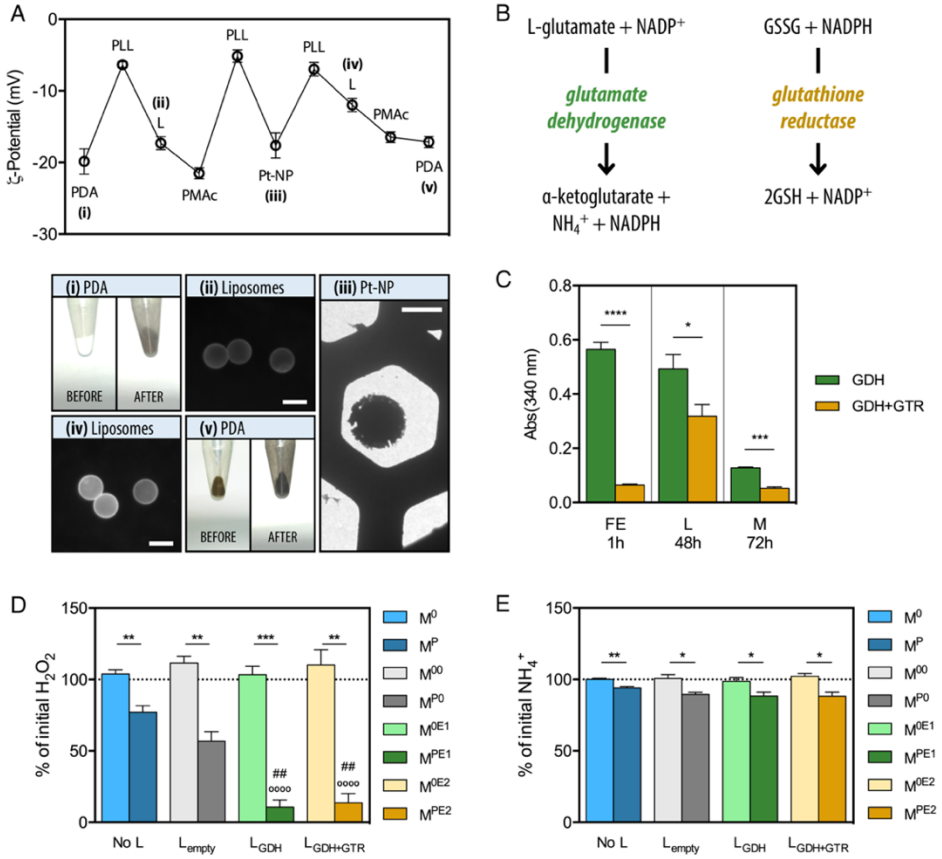


Figure VIII.3. (**A**) ζ-potential measurement of the microreactors at the different assembly steps and representative images. PDA deposition was confirmed by color change (**i** and **v**), liposomal layers were imaged with a fluorescent dye (**ii** and **iv**), and Pt-NP adsorption was observed with TEM (**iii**). Scale bars = 20 µm. (**B**) Chemical reactions catalyzed by the studied enzymes: glutamate dehydrogenase (GDH) converts L-glutamate into α-ketoglutarate and NH_4^+, while glutathione reductase (GTR) reduces oxidized glutathione (GSSG), both using $NADP^+$/NADPH as a co-factor. (**C**) Enzymatic activity of GDH and GTR as free enzymes (FE), enzymes encapsulated in liposomes (L), and microreactors (M, 10^5 microreactors). All samples were incubated with 30 mM L-glutamate, 2.0 mM GSSG, and 2.0 mM $NADP^+$. The amount of NADPH in solution was measured through the absorbance at 340 nm at the time point for which GDH activity was highest (1 h for FE, 48 h for L, and 72 h for M). N=3–8. *p < 0.05, ***p < 0.001, ****p < 0.0001 using a paired *t*-test between the GDH and GDH+GTR conditions. (**D**) Pt-NP activity in different microreactors: H_2O_2 concentration was measured after 10^4 microreactors were incubated with 1.0 mM H_2O_2 for 24 h and is presented as percentage of initial H_2O_2 concentration (100%). N=3–5. **p < 0.01, ***p < 0.001 compared to respective control, using an unpaired *t*-test; $^{\circ\circ\circ\circ}$p < 0.0001 for Pt-NP-containing microreactors compared to M^P, and $^{\#\#}$p < 0.01 for Pt-NP-containing microreactors compared to M^{P0}, using one-way ANOVA followed by Tukey's multiple comparison test. (**E**) Microreactors as NH_4^+ catalysts: 10^6 microreactors were incubated with 1.0 mM NH_4^+ for 24 h at 37 °C. Data is presented as percentage of the initial NH_4^+ concentration (100%). N=3–4. *p < 0.05; **p < 0.01 compared to respective control, using an unpaired *t*-test.

Microreactors and their biological activity

The biological activity of the different microreactors was tested in primary neuronal cultures exposed to H_2O_2 or NH_4^+. Since the focus of this work is reverting excitotoxic dysfunctions on mature neurons, only cells at 14 DIV were used for these assays, to ensure the relevance of the microreactors' biological activity. Furthermore, since no differences were found between the activity of M^{PE1} and M^{PE2}, only M^{PE1} was used for the following assays, where its activity is compared to that of M^P.

In order to ascertain the biological activity of microreactors against H_2O_2 and NH_4^+ toxicity, cell viability was determined and extracellular electrophysiological recordings were performed, following the time points depicted in **Figure VIII.4A**.

For the cell viability assay, 14 DIV cells were incubated with microreactors (M^P or M^{PE1}, 20% of the number of cells) and different concentrations of H_2O_2 or NH_4^+. After 24 h of incubation, cell viability was measured. As a first step, different concentrations of the toxic compounds were explored (Chapter VIII Supporting Information, **Figure VIII.S1**) based on previous studies focused on the effects of these compounds in rat cortical neuronal cultures. Regarding H_2O_2, a study using two different cell densities (high: 2×10^5 cells cm^{-2} and low: 7×10^4 cells cm^{-2}) to explore H_2O_2-induced cell death showed that a 24 h incubation with 10 µM H_2O_2 did not significantly impact cell viability in either studied density, while 30 µM H_2O_2 led to a drop in cell viability of c. 10% for the high cell density and c. 50% for the low cell density. Finally, 100 µM H_2O_2 led to c. 40% cell viability for the high cell density condition and c. 25% for the low cell density condition.[VIII.45] Given that we used an intermediate cell density (9.375×10^4 cells cm^{-2}), the observed cell viability losses in the absence of microreactors are in line with those described above. When considering NH_4^+, our study is in line with previous literature where, in rat primary cortical neurons, a 24 h incubation with 10 mM NH_4^+ led to 50% cell viability.[VIII.46] Taking this into account, we tested 10 mM and higher concentrations of NH_4^+ concentrations to reach a nearly full cell death scenario. Importantly, pathological *in vivo* toxic levels of NH_4^+ are in the range of 0.1–10 mM[VIII.47] and neuronal toxic NH_4^+ levels are around 3 mM.[VIII.48] Microreactors were able to convert NH_4^+ into NO when neurons were incubated with pathologically relevant concentrations of NH_4^+, maintaining sub-toxic levels of both compounds and providing a positive effect in terms of cell survival. Considering the range of action of M^P and physiologically relevant conditions, 10 µM H_2O_2 and 10 mM NH_4^+ were chosen to perform the cell viability assay for all microreactors.

Overall, it is possible to conclude that both M^P and M^{PE1} provide significant neuronal protection against the actions of H_2O_2 and NH_4^+ in terms of cell viability (**Figure VIII.4B**). While no differences were found between M^P and M^{PE1}, both microreactors were able to convert H_2O_2 into water and oxygen, which explains the increase in cell viability from 0.83 to 1.20 when cells were exposed to 10 µM H_2O_2 in the presence of either microreactor. Interestingly, both microreactors elevate cell viability above control level (cells not exposed to microreactors nor H_2O_2). In accordance, a study using rat primary

neuronal and astrocytic cultures showed that astrocytic-generated H_2O_2 has a biphasic effect in terms of neuronal cell viability. In low concentrations, H_2O_2 protects neurons against further oxidative damage, thus buffering the actions of ROS. At high concentrations, H_2O_2 has deleterious effects and leads to cell death, a more common and deeply studied effect of this compound.[VIII.49] Applying these premises to our study, we can hypothesize that, when neurons are exposed to 10 μM H_2O_2 in the presence of the microreactors, the latter are able to convert the majority of H_2O_2, keeping this compound in the range of concentrations where it provides neuronal protection and improves cell viability.

Both M^P and M^{PE1} were able to significantly improve cell viability of cells exposed to NH_4^+ (**Figure VIII.4B**). This effect is likely associated with the catalytic activity of Pt-NP that leads to a decrease of NH_4^+ and concomitant formation of NO in solution, which has a offers neuronal protection at low concentrations.[VIII.50,51] Since these microreactors convert c. 7% of the total amount of NH_4^+ in solution over the course of 24 h[VIII.19] and because NO has an extremely short half-life,[VIII.52] there is never a buildup of NO in cell medium, maintaining this compound at physiological and non-toxic levels. For a review on the different lines of thought concerning what classifies as a physiological concentration of NO, the reader is referred to the work of Hall and Garthwaite.[VIII.53] Surprisingly, M^{PE1} is significantly more effective than M^P in rescuing cell viability.

The second biological activity assay consisted of extracellular electrophysiological recordings, using a microelectrode array (MEA) system. This assay provides more detailed insights into the activity of the microreactors, since it measures how neuronal communication and response to stimuli are altered in the presence of H_2O_2 or NH_4^+, and how microreactors counteract these alterations. In the MEA system, neurons are plated on cell culture inserts with a 60-electrode array, where they adhere and mature, allowing for a direct observation of extracellular neuronal electrical function at a later time point. Since it is not possible to determine how many cells are being recorded by each electrode, internal controls were performed for each experimental condition. Thus, extracellular electrophysiological recordings were performed in two subsequent phases: first a baseline recording was obtained for each individual condition at 14 DIV, without any toxic compounds or microreactors (**Figure VIII.4C**, black traces). These data represent the neural basal activity of those specific neuronal networks, prior to any treatment. Secondly, test phase recordings were performed after cells were incubated for 24 h with microreactors (M^P or M^{PE1}, 20% of the number of cells) and H_2O_2 or NH_4^+ (**Figure VIII.4C**, color traces). Importantly, the relative position of the different electrodes in relation to the cells was maintained over the two recording phases. The same stimulus parameters were used in this phase to ensure normalization to the baseline measurement. This analysis accounts for how much these parameters changed over 24 h and overcomes the possibility of variation in the size of the neuronal networks across cultures, allowing for comparisons between the different conditions. Importantly, cells not exposed to either toxic compounds or microreactors were used as a general control, providing information on how the response parameters change over

24 h without any manipulation, and are represented as a red line in **Figure VIII.4D** and **Figure VIII.4E**. The amplitude and slope of each stimulus response were analyzed (**Figure VIII.4D** and **Figure VIII.4E**, respectively). H_2O_2 led to a decrease in both amplitude and slope, which was completely prevented, in a similar magnitude, by M^P or M^{PE1}. On the other hand, NH_4^+ had the opposite effect, increasing both amplitude and slope. Similarly to the cell viability assay, M^{PE1} appear to have a more extensive capability for preventing these changes when compared to M^P, being able to significantly revert the NH_4^+-induced dysfunctions in both amplitude and slope, while M^P were only able to revert slope dysfunction in a smaller degree. Interestingly, as depicted in the representative traces (**Figure VIII.4B**), exposure to H_2O_2 or NH_4^+ led to a phase shift of the response wave. Given that each depicted wave represents the combined activity of all neurons surrounding the electrode, this shift can be the consequence of structural changes in the neuronal network – either by cell death, as suggested by the cell viability assay, or by axonal and dendritic retraction. Representative signals obtained in different neuron-electrode relative positions can be seen in a review by Obien *et al.*[VIII.54] Importantly, since the phase shifts are only representative of the physical arrangement of neurons, absolute parameter values were used for comparison with other conditions.

Globally, it is possible to conclude that both M^P and M^{PE1} are able to revert the actions of H_2O_2 and NH_4^+ in a rat primary neuronal cultures, with M^{PE1} being significantly more capable to counteract NH_4^+ than M^P. While all biological activity data is in accordance, the *in vitro* data presented above suggested that M^{PE1} would be a better catalyst of H_2O_2 conversion than M^P, a difference which was neither translated into a higher cell viability rescue nor better neuronal function preservation. Since M^P already elevate cell viability to higher than control levels and fully revert electrophysiological neuronal dysfunction, it is possible that cells reached a plateau in both assays, thus masking the actions of M^{PE1}. Focusing on the action of M^{PE1} toward NH_4^+, the *in vitro* characterization also did not foresee such a distinct action between these microreactors and M^P, with M^{PE1} providing significantly more neuronal protection than M^P. This difference might be explained by interaction of GDH with cellular substrates. While this enzyme mainly converts L-glutamate into α-ketoglutarate and NH_4^+,[VIII.55] the reaction can occur to some extent in the opposite direction in the presence of large concentrations of NH_4^+ such as the one used for this assay, leading to the consumption of NH_4^+ and concomitant formation of L-glutamate, explaining the notorious increase in cell viability. In a completely different line of thought, NH_4^+ is known to induce oxidative stress in neuronal cells, leading to an overproduction of ROS,[VIII.56] while M^{PE1} produce NADPH, which can act as an antioxidant, neutralizing toxic free radicals.[VIII.57] Thus, it is possible that M^{PE1} enhanced biological activity arises from the cumulative detoxification of both H_2O_2 and NH_4^+, conjugated with more extensive antioxidant properties. Regardless, these data indicate that the inclusion of enzymes in the microreactors was extremely beneficial, which was anticipated given the important role enzymes have played in encapsulated catalysis over the last years.[VIII.58]

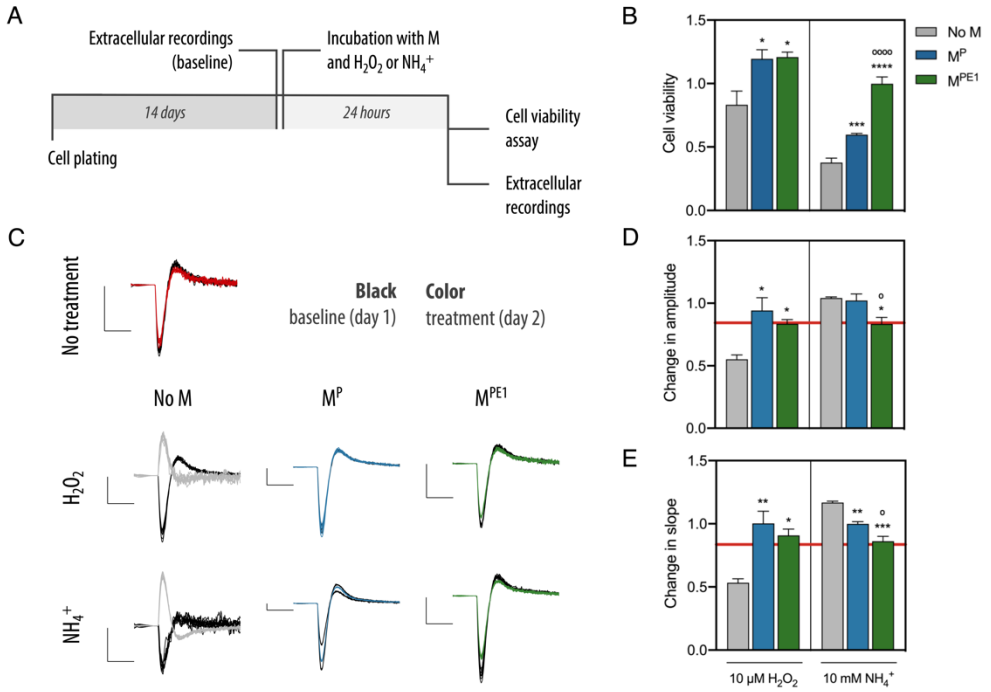


Figure VIII.4. Biological activity of the different microreactors. (**A**) Cells were allowed to mature for 14 days, at which point extracellular electrophysiological recordings were performed to obtain baseline neuronal activity and cells were incubated for 24 h with 10 µM H_2O_2 or 10 mM NH_4^+ in the presence or absence of M^P or M^{PE1}. Following this incubation, cell viability was determined and extracellular electrophysiological recordings were obtained. (**B**) Fold change in cell viability of cells exposed to 10 µM H_2O_2 or 10 mM NH_4^+ in the presence or absence of microreactors (M^P or M^{PE1}, 20% of number of cells), normalized to cells not exposed to toxic compounds. N=3–6. (**C**) Representative traces of neuronal responses obtained in the MEA system. Black traces were obtained prior to any treatment and color traces after cells were treated for 24 h with 10 µM H_2O_2 or 10 mM NH_4^+ in the absence (gray traces) or presence of M^P or M^{PE1} (blue and green traces, respectively). Untreated cells (no microreactors and no toxic compounds) were used as a general control to evaluate the physiological change in parameters over 24 h (red trace). Y-scale bar = 100 µV. X-scale bar = 5.0 ms. Spike amplitude (**D**) and slope (**E**) of the traces were determined and normalized as fold-change over 24 h. Red line represents the fold-change of untreated cells. N=3. *p < 0.05, **p < 0.01, ***p < 0.001, and ****p < 0.0001 compared to cells not exposed to microreactors (No M), °p < 0.05 and °°°°p < 0.0001 compared to M^P, using a one way-ANOVA followed by Tukey's multiple comparison test.

Conclusion

In this study, we further explore the possible therapeutical application of Pt-NP-containing microreactors in the context of excitotoxicity. Regarding microreactors containing only Pt-NP, with this non-proliferating cell model, we were able to exclude the confounding variable of proliferation inhibition in cell viability. With this variable excluded, there was no differences in cell viability in any microreactor concentration tested. Furthermore, these microreactors display good levels of cell adhesion towards neuronal cells, both mature and immature, and maintain the biological activity observed with the SH-SY5Y cell line towards H_2O_2 and NH_4^+. Moreover, we present and thoroughly characterize a new advancement in these microreactors, containing Pt-NP and enzymes. While these findings bring us one step closer to developing a new therapeutic tool to counteract excitotoxicity *in vivo*, with applications in several neurodegenerative

diseases, such as ALS, or in traumatic brain injury, a variety of challenges need to be addressed before such microreactors might have clinical relevance. Among the unsolved issues, the delivery of the microreactor to the brain, the time-limited performance of the microreactors especially when enzymes are used, or the relatively cumbersome and time consuming microreactor assembly still need to be explored. Nonetheless, the promising results shown here are a relevant contribution to the emerging field of artificial biology where bottom-up assembled entities support their natural counterparts.

chapter VIII supporting information

Table VIII.S1. Summary of all the fabricated microreactors.

Microreactor	Pt-NP	L_{empty}	L_{GDH}	$L_{GDH+GTR}$
M^{0}	---	---	---	---
M^{P}	✓	---	---	---
M^{00}	---	✓	---	---
M^{P0}	✓	✓	---	---
M^{0E1}	---	---	✓	---
M^{PE1}	✓	---	✓	---
M^{0E2}	---	---	---	✓
M^{PE2}	✓	---	---	✓

Table VIII.S2. Two-way ANOVA of H_2O_2 and NH_4^+ consumption.

Source of variation	% of variation	F (DFn, DFd)	p-value
	H_2O_2		
Interaction	12.85	F (3,19) = 15.41	**** (< 0.0001)
M type	12.23	F (3,19) = 14.67	**** (< 0.0001)
Pt-NP presence	69.64	F (1,19) = 250.5	**** (< 0.0001)
	NH_4^+		
Interaction	5.201	F (3,17) = 1.196	ns (0.3410)
M type	3.860	F (3,17) = 0.8878	ns (0.4673)
Pt-NP presence	66.30	F (1,17) = 45.75	**** (< 0.0001)

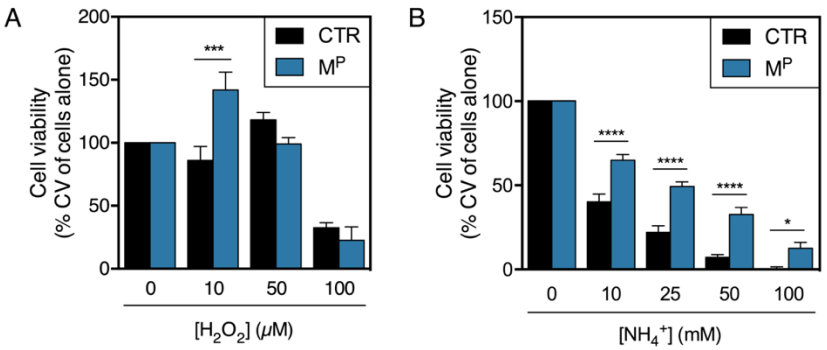


Figure VIII.S1. Cells at 14 DIV were incubated with M^P for 24 h and (**A**) exposed to different concentrations of H_2O_2 (N=3–6, ***p < 0.001 between M^P and CTR) or (**B**) exposed to different concentrations of NH_4^+ (N=4–5, *p < 0.05 and ****p < 0.0001 between M^P and CTR). Cells not incubated with M^P were used as CTR. Following this incubation, cell viability was measured and is represented as percentage of control (absence of H_2O_2 or NH_4^+). Data presented as mean ± SEM.

chapter VIII references

VIII.1 Dong X, Wang Y, Qin Z. Molecular Mechanisms of Excitotoxicity and Their Relevance to Pathogenesis of Neurodegenerative Diseases. *Acta Pharmacol Sin* **2009**, *30* (4), 379–387.

VIII.2 Shigeri Y, Seal RP, Shimamoto K. Molecular Pharmacology of Glutamate Transporters, EAATs and VGLUTs. *Brain Res Rev* **2004**, *45* (3), 250–265.

VIII.3 Gonçalves-Ribeiro J, Pina CC, Sebastião AM, Vaz SH. Glutamate Transporters in Hippocampal LTD/LTP: Not Just Prevention of Excitotoxicity. *Front Cell Neurosci* **2019**, *13*, 357.

VIII.4 Sims NR, Zaidan E. Biochemical Changes Associated with Selective Neuronal Death Following Short-Term Cerebral Ischaemia. *Int J Biochem Cell Biol* **1995**, *27* (6), 531–550.

VIII.5 Connolly NMC, Prehn JHM. The Metabolic Response to Excitotoxicity - Lessons from Single-Cell Imaging. *J Bioenerg Biomembr* **2015**, *47* (1–2), 75–88.

VIII.6 Kritis AA, Stamoula EG, Paniskaki KA, Vavilis TD. Researching Glutamate-Induced Cytotoxicity in Different Cell Lines: A Comparative/Collective Analysis/Study. *Front Cell Neurosci* **2015**, *9*, 91.

VIII.7 Coyle JT, Puttfarcken P. Oxidative Stress, Glutamate, and Neurodegenerative Disorders. *Science* **1993**, *262* (5134), 689–695.

VIII.8 Halliwell B. Antioxidants in Human Health and Disease. *Annu Rev Nutr* **1996**, *16* (1), 33–50.

VIII.9 Bak LK, Schousboe A, Waagepetersen HS. The Glutamate/GABA-Glutamine Cycle: Aspects of Transport, Neurotransmitter Homeostasis and Ammonia Transfer. *J Neurochem* **2006**, *98* (3), 641–653.

VIII.10 Suárez I, Bodega G, Fernández B. Glutamine Synthetase in Brain: Effect of Ammonia. *Neurochem Int* **2002**, *41* (2–3), 123–142.

VIII.11 Jia M, Njapo SAN, Rastogi V, Hedna VS. Taming Glutamate Excitotoxicity: Strategic Pathway Modulation for Neuroprotection. *CNS Drugs* **2015**, *29* (2), 153–162.

VIII.12 Schoonen L, van Hest JCM. Compartmentalization Approaches in Soft Matter Science: From Nanoreactor Development to Organelle Mimics. *Adv Mater* **2016**, *28* (6), 1109–1128.

VIII.13 Godoy-Gallardo M, York-Duran MJ, Hosta-Rigau L. Recent Progress in Micro/Nanoreactors toward the Creation of Artificial Organelles. *Adv Healthc Mater* **2018**, *7* (5), 1700917.

VIII.14 Orive G, Santos E, Poncelet D, Hernández RM, Pedraz JL, Wahlberg LU, De Vos P, Emerich D. Cell Encapsulation: Technical and Clinical Advances. *Trends Pharmacol Sci* **2015**, *36* (8), 537–546.

VIII.15 Zhang Y, Schattling PS, Itel F, Städler B. Planar and Cell Aggregate-Like Assemblies Consisting of Microreactors and HepG2 Cells. *ACS Omega* **2017**, *2* (10), 7085–7095.

VIII.16 Itel F, Skovhus Thomsen J, Städler B. Matrix Vesicles-Containing Microreactors as Support for Bonelike Osteoblasts to Enhance Biomineralization. *ACS Appl Mater Interfaces* **2018**, *10* (36), 30180–30190.

VIII.17 Cheung AS, Zhang DKY, Koshy ST, Mooney DJ. Scaffolds That Mimic Antigen-Presenting Cells Enable Ex Vivo Expansion of Primary T Cells. *Nat Biotechnol* **2018**, *36* (2), 160–169.

VIII.18 Tang J, Shen D, Caranasos TG, Wang Z, Vandergriff AC, Allen TA, Hensley MT, Dinh P-U, Cores J, Li T-S, *et al*. Therapeutic Microparticles Functionalized with Biomimetic Cardiac Stem Cell Membranes and Secretome. *Nat Commun* **2017**, *8*, 13724.

VIII.19 Armada-Moreira A, Taipaleenmäki E, Baekgaard-Laursen M, Schattling PS, Sebastião AM, Vaz SH, Städler B. Platinum Nanoparticle-Based Microreactors as Support for Neuroblastoma Cells. *ACS Appl Mater Interfaces* **2018**, *10* (9), 7581–7592.

VIII.20 Liu Y, Wu H, Li M, Yin J-J, Nie Z. pH Dependent Catalytic Activities of Platinum Nanoparticles with Respect to the Decomposition of Hydrogen Peroxide and Scavenging of Superoxide and Singlet Oxygen. *Nanoscale* **2014**, *6* (20), 11904–11910.

VIII.21 Rafti M, Brunsen A, Fuertes MC, Azzaroni O, Soler-Illia GJAA. Heterogeneous Catalytic Activity of Platinum Nanoparticles Hosted in Mesoporous Silica Thin Films Modified with Polyelectrolyte Brushes. *ACS Appl Mater Interfaces* **2013**, *5* (18), 8833–8840.

VIII.22 Lynge ME, Baekgaard-Laursen M, Hosta-Rigau L, Jensen BEB, Ogaki R, Smith AAA, Zelikin AN, Städler B. Liposomes as Drug Deposits in Multilayered Polymer Films. *ACS Appl Mater Interfaces* **2013**, *5* (8), 2967–2975.

VIII.23 Jerónimo-Santos A, Vaz SH, Parreira S, Rapaz-Lérias S, Caetano AP, Buée-Scherrer V, Castrén E, Valente CA, Blum D, Sebastião AM, *et al*. Dysregulation of TrkB Receptors and BDNF Function by Amyloid-β Peptide Is Mediated by Calpain. *Cereb Cortex* **2015**, *25* (9), 3107–3121.

VIII.24 Biffi E, Regalia G, Menegon A, Ferrigno G, Pedrocchi A. The Influence of Neuronal Density and Maturation on Network Activity of Hippocampal Cell Cultures: A Methodological Study. *PLoS One* **2013**, *8* (12), e83899.

VIII.25 Schneider CA, Rasband WS, Eliceiri KW. NIH Image to ImageJ: 25 Years of Image Analysis. *Nat Methods* **2012**, *9* (7), 671–675.

VIII.26 Sahu MP, Nikkilä O, Lågas S, Kolehmainen S, Castrén E. Culturing Primary Neurons from Rat Hippocampus and Cortex. *Neuronal Signal* **2019**, *3* (2), NS20180207.

VIII.27 Kim MJ, Oh SJ, Park SH, Kang H-J, Won MH, Kang T-C, Park J-B, Kim J-I, Kim J, Lee J-Y. Neuronal Loss in Primary Long-Term Cortical Culture Involves Neurodegeneration-Like Cell Death Via Calpain and P35 Processing, but not Developmental Apoptosis or Aging. *Exp Mol Med* **2007**, *39* (1), 14–26.

VIII.28 Robert F, Cloix JF, Hevor T. Ultrastructural Characterization of Rat Neurons in Primary Culture. *Neuroscience* **2012**, *200*, 248–260.

VIII.29 Valadas JS, Batalha VL, Ferreira DG, Gomes R, Coelho JE, Sebastião AM, Diógenes MJ, Lopes LV. Neuroprotection Afforded by Adenosine A2A Receptor Blockade is Modulated by Corticotrophin-Releasing Factor (CRF) in Glutamate Injured Cortical Neurons. *J Neurochem* **2012**, *123* (6), 1030–1040.

VIII.30 Hatten ME. Neuronal Regulation of Astroglial Morphology and Proliferation In Vitro. *J Cell Biol* **1985**, *100* (2), 384–396.

VIII.31 McClatchey AI, Yap AS. Contact Inhibition (of Proliferation) Redux. *Curr Opin Cell Biol* **2012**, *24* (5), 685–694.

VIII.32 Puliafito A, Hufnagel L, Neveu P, Streichan S, Sigal A, Fygenson DK, Shraiman BI. Collective and Single Cell Behavior in Epithelial Contact Inhibition. *Proc Natl Acad Sci USA* **2012**, *109* (3), 739–744.

VIII.33 Kang K, Choi IS, Nam Y. A Biofunctionalization Scheme for Neural Interfaces Using Polydopamine Polymer. *Biomaterials* **2011**, *32* (27), 6374–6380.

VIII.34 Bhang SH, Kwon S-H, Lee S, Kim GC, Han AM, Kwon YHK, Kim B-S. Enhanced Neuronal Differentiation of Pheochromocytoma 12 Cells on Polydopamine-Modified Surface. *Biochem Biophys Res Commun* **2013**, *430* (4), 1294–1300.

VIII.35 Murthy CR, Bender AS, Dombro RS, Bai G, Norenberg MD. Elevation of Glutathione Levels by Ammonium Ions in Primary Cultures of Rat Astrocytes. *Neurochem Int* **2000**, *37* (2–3), 255–268.

VIII.36 Hilgier W, Węgrzynowicz M, Ruszkiewicz J, Oja SS, Saransaari P, Albrecht J. Direct Exposure to Ammonia and Hyperammonemia Increase the Extracellular Accumulation and Degradation of Astroglia-Derived Glutathione in the Rat Prefrontal Cortex. *Toxicol Sci* **2010**, *117* (1), 163–168.

VIII.37 Zhu C, Itel F, Chandrawati R, Han X, Städler B. Multicompartmentalized Microreactors Containing Nuclei and Catalase-Loaded Liposomes. *Biomacromolecules* **2018**, *19* (11), 4379–4385.

VIII.38 Carneiro-da-Cunha MG, Cerqueira MA, Souza BWS, Teixeira JA, Vicente AA. Influence of Concentration, Ionic Strength and pH on Zeta Potential and Mean Hydrodynamic Diameter of Edible Polysaccharide Solutions Envisaged for Multinanolayered Films Production. *Carbohydr Polym* **2011**, *85* (3), 522–528.

VIII.39 Ziegenhorn J, Senn M, Bücher T. Molar Absorptivities of Beta-NADH and Beta-NADPH. *Clin Chem* **1976**, *22* (2), 151–160.

VIII.40 Botman D, Tigchelaar W, Noorden CJFV. Determination of Glutamate Dehydrogenase Activity and Its Kinetics in Mouse Tissues Using Metabolic Mapping (Quantitative Enzyme Histochemistry). *J Histochem Cytochem* **2014**, *62* (11), 802–812.

VIII.41 Carlberg I, Mannervik B. Glutathione Reductase. *Methods Enzymol* **1985**, *113*, 484–490.

VIII.42 Armada-Moreira A, Thingholm B, Andreassen K, Sebastião AM, Vaz SH, Städler B. On the Assembly of Microreactors with Parallel Enzymatic Pathways. *Adv Biosyst* **2018**, *2* (5), 1700244.

VIII.43 Sheridan AM, Fitzpatrick S, Wang C, Wheeler DC, Lieberthal W. Lipid Peroxidation Contributes to Hydrogen Peroxide Induced Cytotoxicity in Renal Epithelial Cells. *Kidney Int* **1996**, *49* (1), 88–93.

VIII.44 Siddique YH, Ara G, Afzal M. Estimation of Lipid Peroxidation Induced by Hydrogen Peroxide in Cultured Human Lymphocytes. *Dose-Response* **2011**, *10* (1), 1–10.

VIII.45 Whittemore ER, Loo DT, Watt JA, Cotman CW. A Detailed Analysis of Hydrogen Peroxide-Induced Cell Death in Primary Neuronal Culture. *Neuroscience* **1995**, *67* (4), 921–932.

VIII.46 Klejman A, Wegrzynowicz M, Szatmari EM, Mioduszewska B, Hetman M, Albrecht J. Mechanisms of Ammonia-Induced Cell Death in Rat Cortical Neurons: Roles of NMDA Receptors and Glutathione. *Neurochem Int* **2005**, *47* (1–2), 51–57.

VIII.47 Felipo V, Butterworth RF. Neurobiology of Ammonia. *Prog Neurobiol* **2002**, *67* (4), 259–279.

VIII.48 Kosenko E, Kaminsky Y, Grau E, Miñana MD, Marcaida G, Grisolía S, Felipo V. Brain ATP Depletion Induced by Acute Ammonia Intoxication in Rats Is Mediated by Activation of the NMDA Receptor and Na+,K(+)-ATPase. *J Neurochem* **1994**, *63* (6), 2172–2178.

VIII.49 Haskew-Layton RE, Payappilly JB, Smirnova NA, Ma TC, Chan KK, Murphy TH, Guo H, Langley B, Sultana R, Butterfield DA, *et al*. Controlled Enzymatic Production of Astrocytic Hydrogen Peroxide Protects Neurons from Oxidative Stress via an Nrf2-Independent Pathway. *Proc Natl Acad Sci USA* **2010**, *107* (40), 17385–17390.

VIII.50 Yildiz Akar F, Ulak G, Tanyeri P, Erden F, Utkan T, Gacar N. 7-Nitroindazole, a Neuronal Nitric Oxide Synthase Inhibitor, Impairs Passive-Avoidance and Elevated plus-Maze Memory Performance in Rats. *Pharmacol Biochem Behav* **2007**, *87* (4), 434–443.

VIII.51 Paul V, Ekambaram P. Involvement of Nitric Oxide in Learning & Memory Processes. *Indian J Med Res* **2011**, *133* (5), 471–478.

VIII.52 Hakim TS, Sugimori K, Camporesi EM, Anderson G. Half-Life of Nitric Oxide in Aqueous Solutions with and without Haemoglobin. *Physiol Meas* **1996**, *17* (4), 267–277.

VIII.53 Hall CN, Garthwaite J. What Is the Real Physiological NO Concentration in Vivo? *Nitric Oxide* **2009**, *21* (2), 92–103.

VIII.54 Obien MEJ, Deligkaris K, Bullmann T, Bakkum DJ, Frey U. Revealing Neuronal Function through Microelectrode Array Recordings. *Front Neurosci* **2014**, *8*, 423.

VIII.55 Thatcher BJ, Storey KB. Glutamate Dehydrogenase from Liver of Euthermic and Hibernating Richardson's Ground Squirrels: Evidence for Two Distinct Enzyme Forms. *Biochem Cell Biol* **2001**, *79* (1), 11–19.

VIII.56 Bobermin LD, Wartchow KM, Flores MP, Leite MC, Quincozes-Santos A, Gonçalves C-A. Ammonia-Induced Oxidative Damage in Neurons Is Prevented by Resveratrol and Lipoic Acid with Participation of Heme Oxygenase 1. *Neurotoxicology* **2015**, *49*, 28–35.

VIII.57 Kirsch M, De Groot H. NAD(P)H, a Directly Operating Antioxidant? *FASEB J* **2001**, *15* (9), 1569–1574.

VIII.58 Itel F, Schattling PS, Zhang Y, Städler B. Enzymes as Key Features in Therapeutic Cell Mimicry. *Adv Drug Deliv Rev* **2017**, *118*, 94–108.

Chapter IX.

Main discussion

and future directions.

discussion

In this thesis, a novel therapeutic approach against excitotoxicity is designed, created, characterized, and tested in two different biological models. Specifically, astrocyte-inspired artificial microreactors, called astrosomes, were created, containing platinum nanoparticles as an active catalyst. These first astrosomes were able to simultaneously convert hydrogen peroxide and ammonia, preventing their deleterious effects in a human neuroblastoma-derived cell line. With the aim of increasing the functions of the astrosome, the encapsulation of different enzymes in one single microreactor was then explored, to establish, as a proof of concept, that it was possible to incorporate different enzymatic pathways without losing their catalytic activity. For this, an enzymatic cycle comprised of glutamate dehydrogenase and glutathione reductase was considered, together with an enzymatic cascade relying on β-galactosidase, glucose oxidase, and catalase. The expertise gained with this proof of concept was then applied to the original astrosome, with the creation of the second generation of astrosomes, containing platinum nanoparticles and glutamate dehydrogenase, in an attempt to further mimic astrocytes. This second generation was able to prevent excitotoxic dysfunctions in rat primary cortical neurons induced by hydrogen peroxide and ammonia, both in terms of cell viability and neuronal electrical communication.

Each part of this thesis contains its own discussion section, focusing on the specific findings, methodologies, and short-comings of each task. So, for the main discussion of this thesis, I will focus on questions that I consider pivotal for this project, mostly related with the rationale behind the design of the project, that might not have been fully answered in the previous chapters.

Why astrocytes?

I've been admiring astrocytes for a long time now. The elegant control they have over brain homeostasis, the way they regulate and communicate with neurons, all their functions as the interface between blood flow and neuronal metabolism, etc., are rich with new potential therapeutic tools. So, in my opinion, when staring at a blank page thinking how to tackle a disease, astrocytes are a good starting point, as it was highlighted in **Chapter V** of this thesis.

Why excitotoxicity?

I am a firm believer that, when developing pharmaceutical tools to counteract diseases, one should focus on the underlying cellular mechanisms, and not only on the symptoms. Alleviating symptoms will not revert the disease, because all the early processes that occur before symptom onset will still happen. With that premise, excitotoxicity appears as a promising candidate as the first application of the astrosomes, since it is a cellular phenomenon that is behind several neurodegenerative diseases and other disorders, as detailed in **Chapter II** of this thesis. Thus, understanding how to combat or neutralize it can be a useful way to ameliorate many different conditions.

Why synthetic biology?

I come from a biochemistry and neurosciences background. During my MSc degree, I worked with oligodendrogenesis, specifically using pharmacological tools to enhance oligodendrocyte differentiation from stem and progenitor cells. While it was a very interesting line of work, it raised some issues for me. The primordial ones being the lack of control we had over the actions of drugs, and how hard it was to tailor or modify them.

Since I have always had a soft spot for engineering, I started to envy the control of bottom-up techniques, how you could define every parameter and change them at will. Furthermore, my main idea was never to only tackle excitotoxicity. I wanted to create an easy-to-use tool that could be useful for other researchers as well, just by changing the composition, charge, size, or shape.

This is the reason why, instead of creating and testing an unchangeable pharmacological tool, I ventured into synthetic biology, with hopes to create a functional "shell" that could be easily tailored for other and unexpected applications.

Why focus on hydrogen peroxide and ammonia?

This project was started from scratch at the beginning of my PhD. So, as one of the first dilemmas, I had to choose if I wanted to focus on the biological or on the engineering aspects of this project. I chose to focus on the engineering, trying to increasing the complexity of the astrosomes, exploring their catalytic activity, etc. This choice meant that the biological models would have to be simple, in order to eliminate confounding variables and measure astrosome activity.

With that in mind, I, together with my supervisors, made the conscious decision of using directly hydrogen peroxide and ammonia to mimic excitotoxic cellular damage. It is obviously a very rough model that does not capture the subtler aspects of excitotoxicity. But, by using it, we could be sure that our astrosomes were in fact consuming those species and rescuing cells, which is a very important starting point that will allow us to move into more complex cellular models and different excitotoxic stimuli. In fact, we did consider other means of inducing excitotoxicity. Namely, we explored some depolarizing stimuli, such as potassium, cell medium change, or veratridine. It was our initial idea that, if there was enough time, we would move on to inducing excitotoxicity using these means, which, unfortunately, that did not happen.

Why different cell models?

A very important aspect of scientific research, in my opinion, is being conscious. This means that animals should be used to a minimum. There is no way to justify doing the first tests of an unexplored treatment by killing animals, when there are so many options available. Therefore, we started our research using a human neuroblastoma-derived cell line, the SH-SY5Y cell line. This allowed us to perform the first assays, showing that the astrosomes could protect the cells against hydrogen peroxide and ammonia. Only after we confirmed the activity and proper functioning of the astrosomes, did we move to a more complex biological model, using rat primary cortical neurons, where we could explore other actions of the astrosomes, namely in terms of electrical neuronal communication.

Anchoring the astrosome to excitatory synapses

For the astrosomes to be completely functional and for their activity to be directed to the region of interest, these structures must be guided and anchored to excitatory synapses. For that, we researched synaptic cell adhesion proteins that could be possible anchors, concluding that neuroligin-1 was the only cell-adhesion protein that was specific for CNS excitatory synapses.

Neuroligins are type I cell adhesion proteins involved in the formation and maintenance of neuronal synapses. These proteins also modulate neuronal properties by recruiting and stabilizing synaptic components.[IX.1–3] There are, so far, four subtypes of neuroligins described: neuroligin-1, expressed specifically in the CNS at excitatory synapses;[IX.4] neuroligin-2, mainly expressed at both GABAergic and glycinergic CNS inhibitory synapses, but also expressed in tissues such as pancreas, lung, endothelia, uterus, and colon;[IX.5–7] neuroligin-3, expressed in glutamatergic and GABAergic neurons,[IX.8,9] where it forms heterodimers with neuroligin-1 and neuroligin-2 respectively,[IX.9] as well as in a variety of glial cells in mice and rats,[IX.10] and in the heart, skeletal muscle, placenta, and pancreas in humans; and neuroligin-4, which is expressed in both glutamatergic and glycinergic neurons.[IX.8,11]

Neuroligins appear to be important in the maintenance of normal brain activity. Although neuroligins are necessary but not essential for synaptogenesis, since neuroligin deletion does not induce reduction in synapse number,[IX.12,13] alterations in neuroligins have been associated with several neuropsychiatric disorders, such as autism spectrum disorders,[IX.3,14] and neurodegenerative disorders, such as Alzheimer's disease.[IX.15,16] Indeed, neuroligin-1 knock-out in mice is associated with presynaptic immaturity.[IX.17] Furthermore, neuroligin-1 knock-down leads to a decrease in AMPAR and NMDAR-induced EPSCs and in the current ratio of these two receptors.[IX.18–21] Consequently, deletion of neuroligin-1 has been shown to impair hippocampal LTP, having a substantial negative effect in excitatory transmission in this brain area,[IX.22] which is accompanied by learning and memory deficits.[IX.12,23]

Neuroligins are only able to perform their synaptic functions when their extracellular cholinesterase-like domain is transsynaptically bound to neurexins, which are highly variable presynaptic cell adhesion proteins.[IX.24,25] Regarding neurexin variability, these proteins are encoded by three different genes (NRXN1–3), each with two different promoters,[IX.26,27] which lead to the production of α- and β-neurexins.[IX.26] Additionally, more than 2 000 splice variants are possible, which further increases their variability.[IX.28] It should be noted that neuroligin-1 specifically binds to neurexin-1β. One detail that differentiates the neuroligin-1-neurexin-1β complex from other cell adhesion protein complexes is that this complex does not simply offer physical support to the synapse, but it is also a signaling device. Indeed, once neuroligin-1 and neurexin-1β bind, their extracellular domains can lead to intracellular synaptic specializations on either side of the synapse.[IX.8,29]

Neuroligin-1 is composed of a N-linked glycosylated extracellular domain, with a globular structure similar in sequence to acetylcholinesterase and a serine and threonine enriched stalk-like structure connected to N- and O-linked oligosaccharides[IX.24,30,31] that projects the globular domain away from the cell membrane, which allows for neuroligin-1 to span the synaptic cleft and efficiently bind to neurexin-1β.[IX.32] Neuroligin-1 presents a single transmembrane domain that connects to the small C-terminal intracellular domain.[IX.32] It is known that neuroligin-1 forms stable dimers on the neuron membrane.[IX.33,34] Interestingly, neuroligin-1 and neurexin-1β bind in a "cross hand" manner connecting the pre- and postsynaptic regions.[IX.32]

Taking this into account, neuroligin-1 will be chosen as the synaptic anchor for the microreactors, given that it is the only subtype specifically expressed at excitatory synapses. Other typical extracellular synaptic proteins do not show this specificity regarding glutamatergic synapses. Neurexins, the binding partners of neuroligins, are also not a viable option for astrosome anchoring, due to their high variability.

The structure of neuroligin-1/neurexin-1β complex was studied based on the PDB file 3B3Q,[IX.35] where all co-factors and water molecules were removed, leaving only the residues corresponding to the neuroligin-1 dimer and two neurexin-1β structures. With this model, two possible docking pockets were found (**Figure IX.1**), with the following space coordinates:

Pocket 1 (x,y,z) = (-4.572, -49.714, -38.200)

Pocket 2 (x,y,z) = (-1.419, 11.509, 2.164)

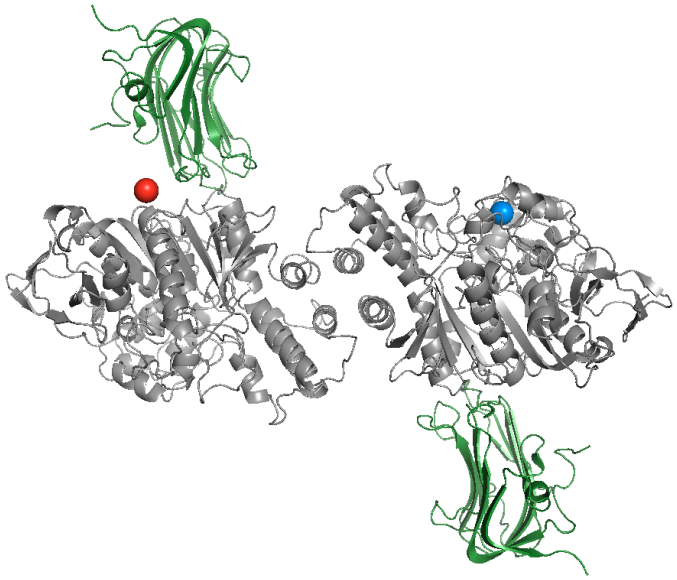


Figure IX.1. 3D structure of the dimeric complex neuroligin-1/neurexin-1β, with the identified pocket locations. Neuroligin-1 sequences are displayed in gray and neurexin-1β in green. Pocket 1 is represented as a red sphere and Pocket 2 as a cyan sphere.

As Pocket 1 was located on the interface between neuroligin-1 and neurexin-1β, we chose it as the anchoring location. This will ensure that the astrosome will be properly directed to excitatory synapses, where neuroligin-1 is interacting with neurexin-1β.

With the location chosen, we used ZINC15 as the starting point to generate a library of candidate ligands for Pocket 1. ZINC15 is a free database of commercially available compounds[IX.36] that allows for the download of 3D structure of thousands of different compounds. We chose in-stock compounds with a molecular weight up to 300 Da and an octanol-water partition coefficient (logP) up to 3, generating a library containing 1 854 123 compounds.

To sort through this ligand library and identify the most promising molecules, 3D protein docking simulations were performed, using the protein-ligand docking software GOLD. This software predicts binding affinity, accuracy, and speed and returns the ligand list ranked by these predictions. For the first run of simulations, very flexible parameters were used (library screening paradigm), in order to quickly sort through

the library and attain the top 10% best ranked ligands. The software returns a .lst file, with all the compounds organized by their ranking. To convert this file into a readable format and export the top 10% ligands, I created the Python script presented in **Annex IX.1**.

Analyzing the top 30 compounds, we were already able to conclude that the ideal ligand will likely have a molecular weight of 250–300 Da, with a logP of 0–2.5, and be of "clean" reactivity (not a nucleophile, electrophile, aggregator, etc.). Importantly, a common chemical characteristic that arises from these top 30 compounds is the existence of rings (**Figure IX.2**), since 27 out of 30 have at least one ring in their structure, together with the concomitant degree of unsaturation. The carbon bond saturation of a molecule can be measured by the fraction sp^3, which is a ratio between the number of sp^3 hybridized carbons (fully saturated) and the total number of carbons.[IX.37] Indeed, among the top 30 ligands, the fraction sp^3 was 0.50 ± 0.24, indicating that the ideal ligand should have unsaturated carbon atoms in its structure. However, more simulations need to be performed, with stricter parameters, to confirm these preliminary conclusions.

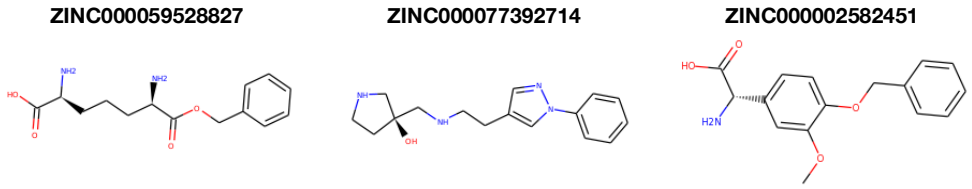


Figure IX.2. Chemical structure of the top 3 more adequate ligands.

Following the identification of 5–10 potential anchors, these compounds will be tested with synaptosomes or rat primary neuronal cultures. Immunocytochemistry will be performed to ensure the co-localization of the ligands with excitatory synapses. Afterwards, the top ligand will be functionalized with a linker, whose size and chemical composition is still to be determined, and connected to the astrosome. The biological activity of anchored astrosomes will be compared to that of non-anchored astrosomes to ascertain the advantages of guiding the location of these microreactors within cell culture.

Annex IX.1. Python script used to convert the best ranking .lst files into .csv files and to select the top 10% of ligands out of the list of PLP scores, where "FILENAME" corresponds to the name of the input file and "NEW-FILENAME" corresponds to the name of the output file.

```
import csv

f = open("FILENAME.lst")
ranking = f.readlines()
f.close()

organized_rank = []

for line in ranking:
    if line:
        if line[0] == "#":
            pass
        else:
            organized_rank.append(line)
    else:
        pass

filtered_rank = []

for line in organized_rank[1:]:
    val1 = line[5:10]
    val2 = line[15:21]
    val3 = line[-18:-2]
    filtered_rank.append([val1, val2, val3])

all_info = []

for line in filtered_rank:
    new_line = line.split(',')
    all_info.append(new_line)

def getKey(item):
    return item[0]

sorted_info = sorted(all_info, key=getKey, reverse=True)
counter = 0

for line in sorted_info:
    counter += 1

cutoff = int(counter * 0.1)
top_ten = []

for i in range(0, cutoff, 1):
    new_line = sorted_info[i]
    top_ten.append(new_line)

filename = 'NEWFILENAME.csv'
fl = open(filename, 'w')
writer = csv.writer(fl, delimiter=',')
for values in top_ten:
    writer.writerow(values)
fl.close()
```

Optimizing astrosome size

In order to advance the astrosomes, an important aspect is to optimize their size. Although we used 20 μm in diameter particles for the first generations of astrosomes, the optimal core size has to be properly explored. Our concept is that the astrosomes should be as small as possible, without being internalized by cells. This ensures that we are creating artificial cells, and not organelles. Furthermore, defining the smallest possible astrosome size will guide us in future research about how to deliver these structures to the brain. The experimental data presented in this section were obtained by Filipa Ribeiro, in the context of our FCT project grant to further study and develop the astrosomes. I was involved in the experimental design and rationale, and participate in data analysis and troubleshooting.

Particle size plays a major role in cell internalization. In fact, different studies using macrophages and epithelial cells show that particles bigger than 1 μm display poor internalization,[IX.38] with particles smaller than 5 μm still being very slowly internalized by pinocytosis,[IX.39] and a limit of internalization for particles with 6.5 μm or more.[IX.40] Regarding neurons, most literature considers these cells as non-phagocytic, which means they cannot internalize structures bigger than 0.5 μm.[IX.41] However, a fairly recent study demonstrated that neurons can uptake 2 μm particles without negative effects in terms of cell viability.[IX.42] Importantly, to our knowledge, neuronal internalization of particles larger than 2 μm is yet to be explored.

In a different approach, it is already known that neuronal hyperexcitability can enhance neurogenesis in neurogenic niches,[IX.43] as a strategy to counteract neuronal death and promote neuroregeneration.[IX.44] The main neurogenic niches in the adult mammalian brain where constitutive neurogenesis takes place are the subventricular zone of the lateral ventricle (SVZ) and in the subgranular zone of the dentate gyrus (DG) in the hippocampus.[IX.45] Indeed, several studies point to enhanced hippocampal neurogenesis following ischemia, which can be considered an excitotoxic scenario.[IX.46,47] Notably, it has also been shown that excitotoxic stimuli promote neurogenesis and long-distance neural circuit integration in zebrafish.[IX.48]

Aim

In this project we aim to evaluate the best microreactor size to generate the astrosomes, so that they can be the small as possible without being incorporated by cells. After choosing the microreactor size we intend to study neurogenesis and gliogenesis promoted by excitotoxicity and by the presence of astrosomes.

Preliminary data

Methods

Materials. 4-(2-hydroxyethyl)piperazine-1-ethanesulfonic acid (HEPES), poly(L-lysine) (PLL, MW 40 000–70 000 Da), poly(D-lysine) (PDL, MW 30 000–70 000 Da), paraformaldehyde (PFA), bovine serum albumin (BSA), Triton X-100 were purchased from Sigma-Aldrich (St. Louis, MO, USA). Polystyrene (PS) particles (1.98 and 7.06 μm in diameter) were acquired from Microparticles GmbH (Berlin, Germany). Hank's balanced saline solution (HBSS), fetal bovine serum (FBS), trypsin-EDTA (0.5%), Dulbecco's modified Eagle's medium / Ham's F-12 medium with glutaMAX (DMEM/F12+GlutaMAX™), 100 U mL^{-1} penicillin and 100 μg mL^{-1} streptomycin (Pen/Strep), B-27 (50×), epidermal growth factor (EGF), basic fibroblast growth factor-2 (FGF-2) were purchased from Thermo Fisher Scientific (Waltham, MA, USA).

Two different buffer solutions were used: HEPES buffer (10 mM HEPES, pH 7.4) and phosphate buffer saline (PBS, 137 mM NaCl, 2.1 mM KCl, 1.8 mM KH_2PO_4, and 10 mM $Na_2HPO_4.2H_2O$, pH 7.4).

Cell culture. Sprague-Dawley fetuses (pre-natal day 18/19) were sacrificed and their brains used to obtain primary neuronal cultures. The fetuses were collected in HBSS, their cerebral cortexes isolated and the meninges removed. Following this, the obtained tissue was mechanically fragmented and digested with 10% (v/v) trypsin-EDTA in HBSS for 15 minutes at 37 °C. Trypsin action was stopped with the addition of 30% (v/v) FBS in HBSS. Cells were then centrifuged 3× at 1 200 rpm, where the supernatant was discarded and replaced with 30% (v/v) FBS in HBSS. Cells were then resuspended in serum-free medium (SFM), composed of DMEM/F12 + GlutaMAX™ supplemented with Pen/Strep, 1% (v/v) B-27, 20 ng mL^{-1} EGF, and 5 ng mL^{-1} FGF-2. 40 000 cells mL^{-1} were then plated in PDL-coated (0.1 mg mL^{-1}) coverslips in 24-well plates and stored at 37 °C in a humified atmosphere of 95% air–5% CO_2. All animals

were handled according to Portuguese Law and the European Union Directive (86/609/EEC) on the protection of animals for scientific experimentation.

Microreactor assembly. PS particles (ø 1.98 or 7.06 µm, 10 wt%) were washed 2× in HEPES buffer (1 800 rpm, 30 s), and then incubated with a PLL-Rhodamine solution (0.1 mg mL^{-1} in HEPES buffer, overnight, at 37 ºC), followed by an incubation with a PLL solution (1.0 mg mL^{-1} in HEPES buffer, 10 min). Finally, the particles were washed 3× in HEPES buffer (1 800 rpm, 30 s).

Immunocytochemistry (ICC). DIV 14 cells were fixed in 4% (w/v) PFA in PBS for 30 min. Cells were permeabilized and non-binding sites blocked with 0.5% (v/v) Triton X-100 and 3% (w/v) BSA in PBS for 1.5 h. Incubation with the primary antibodies was performed overnight at 4 °C according to the information in **Table IX.1**, followed by 1 h with the appropriate donkey Alexa Fluor secondary antibodies (1:200), at room temperature. Nuclei were stained for 10 min with 4',6-diamidino-2-phenylindole (DAPI), and coverslips mounted in Mowiol fluorescent medium. Washes between steps were performed in PBS. To identify particle internalization by neurons and astrocytes, the same protocol was applied, with 4.0×10^5 particles mL^{-1} applied to cell cultures 24 h before fixation.

Table IX.1. Primary antibodies used for ICC, including their origin, type, company, reference, and dilution.

Target	Origin	Type	Company	Reference	Dilution
GFAP	mouse	monoclonal	Millipore	MAB360	1:500
DCX	rabbit	polyclonal	Synaptic Systems	326 003	1:300
MAP2	mouse	monoclonal	Millipore	MAB3418	1:400
O4	mouse	polyclonal	Millipore	MAB345	1:200

Results and discussion

Preliminary data from ICC suggest that neurons, astrocytes, and oligodendrocytes were present in the mixed culture at DIV 14 (**Figure IX.3**). Regarding neurons, ICC was performed against microtubule associated protein-2 (MAP2) and doublecortin (DCX), which have been shown to specifically stain mature[IX.49] and immature neurons.[IX.50] Astrocytes were identified by the expression of the glial fibrillary acidic protein (GFAP), a widely used astrocytic marker.[IX.51] Finally, oligodendrocytic lineage cells were recognized by Olig2, a transcription factor that is expressed throughout oligodendrocyte

differentiation, from early precursor cells to mature oligodendrocytes.[IX.52–54] Oligodendrocytes in later phases of differentiation (pre-oligodendrocytes, immature and mature oligodendrocytes) were differentiated from their progenitor cells by the expression of the oligodendrocyte marker 4 (O4), a membrane protein specific for these cells types.[IX.55]

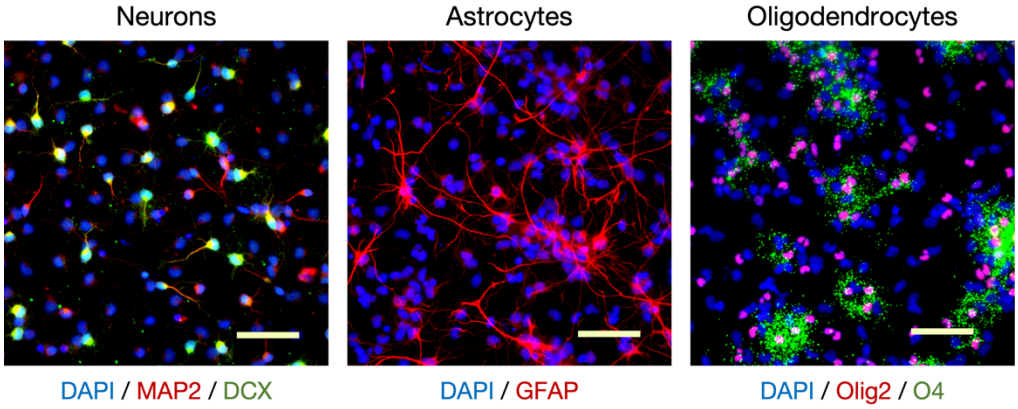


Figure IX.3. Representative fluorescence microscopy images of different cell types in the mixed cell culture. Mature and immature neurons can be identified by MAP2 (red) and DCX (green) staining, respectively. Astrocytes are represented by GFAP staining (red). Oligodendrocytic lineage cells are marked with Olig2 (red) and O4 (green) staining. Cell nuclei are stained in blue. Scale bars = 50 µm.

In order to evaluate whether the different sized particles are incorporated inside cells, namely neurons and astrocytes, rhodamine-labelled particles with different diameters (1.98 or 7.06 µm) were co-incubated with the cells at DIV 14 for 24 h and internalization by different cells was studied by immunocytochemistry against MAP2 and GFAP to identify neurons and astrocytes, respectively. Data suggest that particles with a diameter up to 1.98 µm could be internalized by neurons and astrocytes, while 7.06 µm particles were not (**Figure IX.4**).

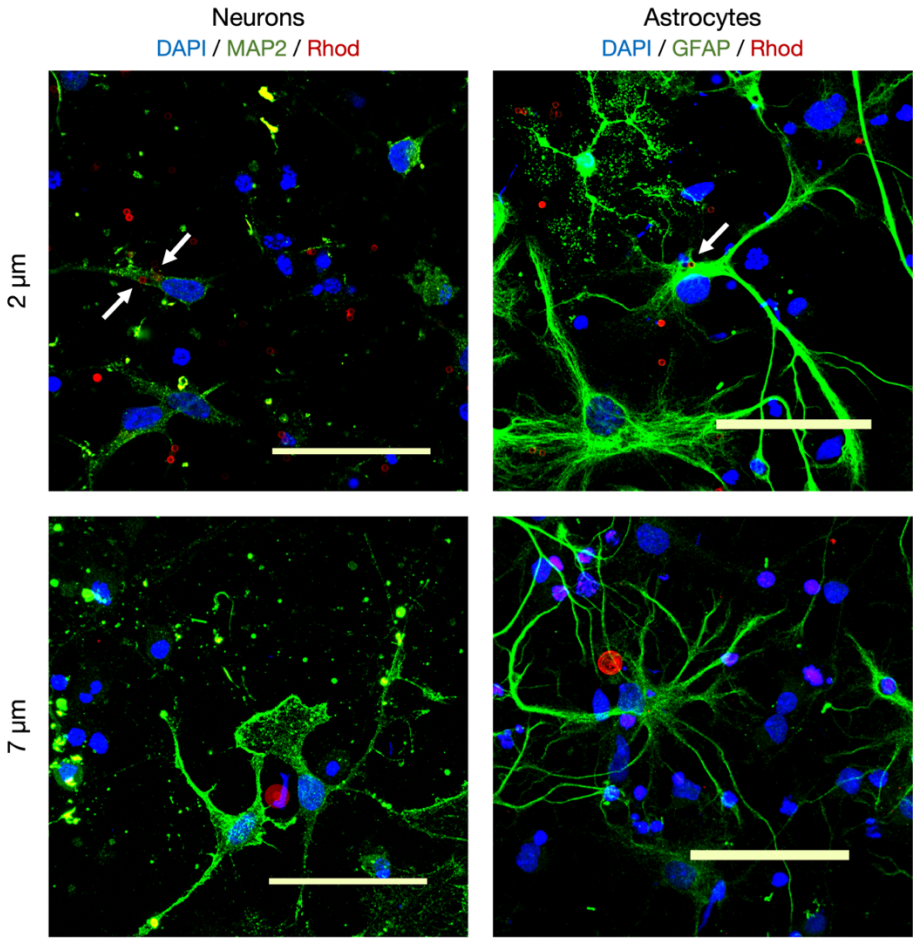


Figure IX.4. Representative fluorescence microscopy images of DIV 14 cells exposed for 24 h to particles with 2 or 7 µm in diameter. Rhodamine-labelled (Rhod) particles are represented in red, cell nuclei in blue, neurons and astrocytes in green. White arrows signal internalized 2 µm particles. Scale bars = 50 µm.

Conclusion

So far, we seem to be able to replicate previous findings that neurons can internalize particles with 2 µm in diameter. Preliminary data also seem to indicate that 7 µm particles cannot be internalized, although further experiments are necessary to reach any conclusion. As a next step, to study neurogenesis and gliogenesis promoted by excitotoxicity and astrosomes, we will apply different concentrations of either glutamate, hydrogen peroxide, or ammonia and/or deliver the astrosomes to both DG- and SVZ-derived cultures. Cell survival and proliferation, neuronal and astrocytic differentiation, and morphology will be evaluated by immunocytochemistry and cell function by calcium signaling.

Change the catalyst, change the application: astrosomes as tools to tackle neuroinflammation

One advantage of the astrosomes is their ability to be tailored to different applications, by changing the catalysts, size, or surface chemistry. So, as a new line of research, the principles behind the astrosome are now being applied to neuroinflammation, using superoxide dismutase or artificial mimics as catalysts. This on-going work will result in the MSc thesis of Oksana K. Savchak, of whom I, together with Sandra H. Vaz, am the supervisor. I have been responsible for the design and organization of the project, personally taught Oksana all the necessary nanoscience techniques, and provided guidance on data analysis and troubleshooting.

Microglia are the prime immune system component of the central nervous system. Their activation is known to lead to neuroinflammation, a process that describes the immune-like response of glial cells, namely microglia and astrocytes. This is an innate immune response and its primary purpose is neuroprotection by eliminating pathogens, repairing damaged brain tissue, and maintaining brain homeostasis. However, in some cases, it can evolve into chronic inflammation, where overactivated cells gain a pathological phenotype, leading to neurotoxicity and neurodegeneration.[IX.56] While several neurodegenerative diseases and other brain disorders have already been linked to inflammatory processes, only recent studies pointed to a more direct and substantial contribution of neuroinflammation for their development.

One of the main pathological mechanisms of neuroinflammation is an overproduction of reactive oxygen species (ROS) by microglia and astrocytes, as a result of oxidative stress. This process leads to cell damage, promoting excessive gliosis, and inducing oxidative stress and mitochondria damage in previously unaffected cells, thus augmenting the pathological impact on the nervous system. Chronical neuroinflammation has been shown to induce neuronal death and to be involved in the pathogenesis of neurodegenerative diseases, such as Alzheimer's disease and amyotrophic lateral sclerosis.[IX.57] Physiological protection mechanisms of the aforementioned cells are based on the action of enzymes, such as superoxide dismutase (SOD), catalase, and glutathione peroxidase.[IX.58] When this mechanism is impaired or

ROS production surpasses the enzymatic capability of the cell, an exogenous source of the of catalysts, either enzymes or enzymes mimics, may be beneficial to prevent further aggravation.

Biology-directed nanotechnology that surfaced in the last years is heavily based on the bottom-up techniques that rely on biological processes for the construction of artificial enzymes, organelles, or even cells. One of the branches of these studies is the development of nanozymes, which are catalytically active nanomaterials that possess enzymatic-like activity without disadvantages of biological enzymes, such as high dependence on the environment and loss of activity over time. As a relevant example of a nanozyme, self-assembled manganese oxide (Mn_3O_4) nanoparticles (Mn-NP) show great antioxidant activity, as these can be used as ROS scavengers, mimicking the activity of SOD, catalase, and glutathione peroxidase.[IX.59]

Aim

Considering these premises, this project aims to develop a novel therapeutic tool to counteract chronic neuroinflammation process, targeting more specifically ROS-inflicted damage, both in short and long term. Two types of microreactors will be generated, one containing Mn-NP and another containing SOD. This will allow us to compare the efficiency of the biological vs. the artificial. The assembly process will follow the same principles explained in this thesis.

Preliminary data

Methods

Materials. Potassium permanganate ($KMnO_4$), oleic acid, stearylamine (SA), 4-(2-hydroxyethyl)piperazine-1-ethanesulfonic acid (HEPES), and superoxide dismutase from bovine erythrocytes (SOD, EC1.15.1.1, 5 441 U mg^{-1}) were obtained from Sigma-Aldrich (St. Louis, MO, USA). Superoxide dismutase activity colorimetric assay kit was attained from Abcam (Cambridge, UK). Tris base and sodium chloride (NaCl) were acquired from VWR (Radnor, PA, USA). Cholesterol and 1,2-dipalmitoyl-*sn*-glycero-3-phosphocholine (DPPC) were purchased from Avanti Polar Lipids (Alabaster, AL, USA). Different buffer solutions were used: phosphate buffer (100 mM sodium phosphate, pH 7.4), phosphate-buffered saline (PBS, 21 mM NaH_2PO_4, 61.2 mM Na_2HPO_4,

pH 7.4), Tris buffer (10 mM Tris base, pH 8.5), citrate buffer (pH 4.0), and HEPES2 buffer (20 mM HEPES, 120 mM NaCl, pH 7.3).

Fabrication of Mn-NP. 6.4 mmol KMn_3O_4 were dissolved in 500 mL of MiliQ water and stirred vigorously for 30 min. Then, 10 mL of oleic acid were added in a continuous flux of 0.25 mL min^{-1} while the solution was stirred for 5 h at 60 ºC, until a dark emulsion was visible. The precipitate was washed 3× with MiliQ water and then 3× with absolute ethanol. The isolated precipitate was then dried at 80 ºC for 10 h and calcinated at 200 ºC for 5 h. The obtained powder was resuspended in the different buffer solutions and sonicated for 10 min.

Liposome preparation. Two types of liposomes with different lipid compositions were fabricated, one using DPPC:Chol:SA (6:3:1, wt%) and another using DPPC:Chol (7:3, wt%). The lipid stock solutions (total of 25 mg mL^{-1} in chloroform) were dried in a rotary evaporator at 300 mbar, followed by further dehydration in vacuum for 2 h. The lipid films were then rehydrated in HEPES2 buffer at 65 ºC for 2 h, followed by four freeze and thaw cycles (10 min at –196 ºC and 10 min at 65 ºC) and extrusion through a 200 nm membrane. The SOD enzyme (500 U mL^{-1}) was then added to the liposome solution and the sample was subjected to two more freeze and thaw cycles and extrusion through a 200 nm membrane. Non-encapsulated enzymes were separated using size exclusion chromatography.

Superoxide dismutase activity assay. Samples were incubated with a tetrazolium salt (WST-1) and xanthine oxidase at 37 ºC for 20 min. The absorbance of the solution at 450 nm was then read with a multiplate reader. This absorbance is proportional to the amount of formazan dye product generated by the reduction of WST-1 catalyzed by O_2^-, which, in turn, is a product of the xanthine oxidase reaction. Since SOD consumes O_2^-, the amount of formazan will decrease with higher SOD activity in the sample.

Results and discussion

Following the described Mn-NP fabrication protocol, we were able to generate manganese nanoflowers, which have already been described as one of the possible physical structures of Mn-NP.[IX.60] The successful fabrication of the nanoflowers was confirmed by TEM (**Figure IX.5A**), where the average size of each structure was 52.12 ± 7.768 nm (N=12). additionally, the surface charge of these Mn-NP was evaluated via

ζ-potential measurement, with an average charge of –24.26 ± 0.4037 mV (N=2) in phosphate buffer and –22.69 ± 2.952 mV (N=3) in PBS. Although the variations in surface charge in different buffer solution was now significant, the catalytic activity of the Mn-NP was also explored in different buffer solutions, with different compositions and pH (**Figure IX.5B**). When compared to the activity of the SOD enzyme, Mn-NP show no activity in phosphate buffer and c. 40% activity in PBS, where activity drops when salt concentration is increased. All these buffer solutions had a pH 7.4. Varying this pH leads to an increase in activity, with c. 50% activity in Tris buffer at pH 8.5 and, remarkably, c. 70% activity in citrate buffer at pH 4.0.

Literature on the characterization of Mn-NP is still very sparse, with contradictory evidence for the variation of activity with pH. Nevertheless, these data point to a pH-dependency of Mn-NP activity.

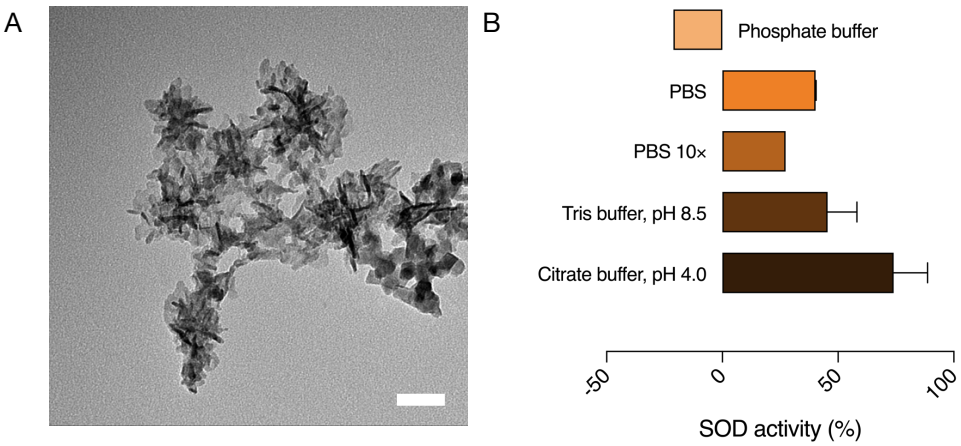


Figure IX.5. Physical and functional analysis of Mn-NP. (**A**) Illustrative TEM image of the fabricated Mn-NP – aggregate of nanoflowers. Scale bar = 50 nm. (**B**) SOD activity of Mn-NP in different buffer composition and pH. Mn-NP solutions were prepared in phosphate buffer pH 7.4, PBS pH 7.4, PBS 10 times concentrated pH 7.4, Tris buffer pH 8.5, and citrate buffer pH 4.0. SOD activity was then measured in these solutions and compared to that of the biological SOD enzyme. N=1–3. Data are normalized to the activity of biological SOD activity (100%) and are represented as mean ± SEM.

Differently, to assemble microreactors containing the biological SOD enzyme, the first step was to determine the ideal lipid composition for the liposomes that will encapsulate the enzyme. Although only anecdotical evidence can be found in literature, one study suggested that the ideal lipid composition for encapsulating SOD was a mixture of 1,2-dipalmitoyl-*sn*-glycero-3-phosphocholine (DPPC), cholesterol (Chol), and stearylamine (SA), in the weight ratio of 6:3:1.[IX.61] With this information, we set out

to fabricate DPPC:Chol:SA liposomes with 200 nm in diameter. We found it impossible to control the size of these liposomes, and isolated SA as the culprit for this issue, since liposomes composed of DPPC:Chol (7:3) presented the desired size. Indeed, DPPC:Chol:SA liposomes were c. 10× larger than DPPC:Chol liposomes, regardless of their cargo, as shown in **Table IX.2**.

Table IX.2. Size distribution of liposomes with different lipid compositions, either empty or containing SOD.

Liposome type	DPPC:Chol:SA [mean ± SD (N)]	DPPC:Chol [mean ± SD (N)]
L_{empty}	2242 ± 629.5 nm (3)	166.9 ± 2.981 nm (1)
L_{SOD}	1945 ± 505.8 nm (2)	134.9 ± 2.591 nm (2)

Next, an enzymatic activity assay was performed with non-encapsulated SOD, and SOD-containing DPPC:Chol liposomes (L_{SOD}). Non-encapsulated SOD exposed to the freeze and thaw protocol necessary for liposome formation was used as a control, to ensure that this protocol did not affect enzymatic activity. L_{SOD} activity was compared before and after size exclusion chromatography (SEC). Since enzyme encapsulation efficiency is never 100%, in the first condition there are still free enzymes in solution together with L_{SOD}, representing the total amount of SOD added to the liposome solution. After SEC, non-encapsulated enzymes have been removed, so it is possible to measure the activity of the encapsulated SOD alone and determine the encapsulation efficiency.

As summarized in **Figure IX.6**, we were able to conclude that SOD does not lose activity when exposed to the freeze and thaw protocol. As for the encapsulated enzymes, L_{SOD} before SEC shows a similar enzymatic activity to that of free SOD. This activity drops after SEC, implying that the encapsulation efficiency is c. 24%.

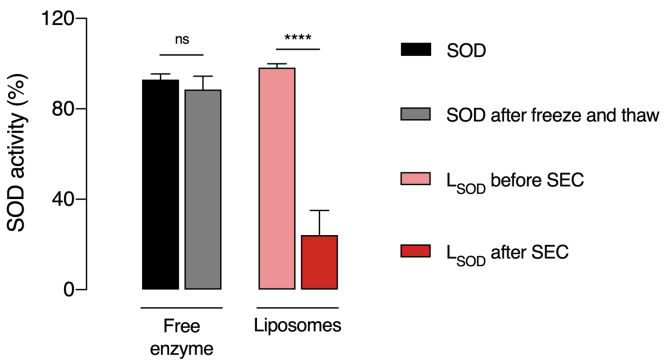


Figure IX.6. SOD enzymatic activity of free SOD and SOD-containing liposomes. SOD exposed to the freeze and thaw protocol and L_{empty} were used as controls. SEC – size exclusion chromatography. N=3–9. $^{ns}p > 0.05$, $^{****}p < 0.0001$ for comparison between the different conditions within free enzyme and liposomes, using a one-way ANOVA followed by Sidak's multiple comparison test. Data represented as mean ± SEM.

Conclusion

Moving forward, we plan to incorporate both the Mn-NP and L_{SOD} into different microreactors, in order to compare artificial and biological enzymes. We then intend to co-incubate these microreactors with a mixed cell culture containing neurons, astrocytes, and microglia and ascertain their biological activity when neuroinflammation is induced.

Moving forward: testing the astrosomes *in vivo*

To further investigate the potential biomedical application of the astrosomes, we are now developing a project that aims to test the activity of the astrosomes in vivo, in a model of chronic stress in which excitotoxicity is involved. This project will rely on the collaboration between Faculdade de Medicina da Universidade de Lisboa, Portugal, and Universidade Federal de São Paulo, Brazil.

The concept of stress is based on the observation that different types of stimuli (external or internal) that can threaten homeostasis, leading to a set of physiological changes called "general adaptation syndrome".[IX.62] The term stimulus or stressor corresponds to events or circumstances that are perceived as aversive by the individual, generating the so-called stress response or stress condition, involving visceral, neuroendocrine and behavioral responses.[IX.63,64] This set of responses aims at maintaining body homeostasis, and are not, per se, pathological changes.[IX.65] However, when aversive stimulation occurs for a prolonged period or exceeds the body's ability to maintain homeostasis, stress can lead to pathological sequelae, such as anxiety and depression, which are understood as stress-related psychiatric disorders.[IX.65] It is well established that the glutamatergic system contributes to the pathophysiology of these disorders. For example, stress exposure, one of the major precipitating factors of anxiety and depression disorders, has been shown to increase glutamate release,[IX.66] alter astrocyte function,[IX.67,68] and cause structural damage to the ventral hippocampus, an important brain structure for depression.[IX.69,70]

In this sense, the general aim of this project is to investigate the activity of the microreactors described in this thesis (astrosomes), administered in the ventral hippocampus of animals submitted or not to the blockade of astrocyte function, and to the model of unpredictable chronic mild stress (UCMS). For that, male Wistar rats will be submitted or not to the UCMS model for 14 consecutive days and on the 15th injected with microreactors or vehicle solution. A group of animals will also be subjected to the blockade of astrocyte function. Five days after the microinjections, the animals will be tested in the open-field and elevated T-maze models (animal models of anxiety and motor activity) and the forced swimming model (animal model of depression). Immediately after the behavioral tests, the animals will be euthanized and their brains processed for immunohistochemical analysis of neurons and glial cells. An additional group of animals will be evaluated for ventral hippocampal electrophysiological activity to better understand how chronic stress and microreactor treatment interfere with the electrophysiology of the investigated structure.

chapter IX references

IX.1 Knight D, Xie W, Boulianne GL. Neurexins and Neuroligins: Recent Insights from Invertebrates. *Mol Neurobiol* **2011**, *44* (3), 426–440.

IX.2 Krueger DD, Tuffy LP, Papadopoulos T, Brose N. The Role of Neurexins and Neuroligins in the Formation, Maturation, and Function of Vertebrate Synapses. *Curr Opin Neurobiol* **2012**, *22* (3), 412–422.

IX.3 Südhof TC. Neuroligins and Neurexins Link Synaptic Function to Cognitive Disease. *Nature* **2008**, *455* (7215), 903–911.

IX.4 Song JY, Ichtchenko K, Südhof TC, Brose N. Neuroligin 1 Is a Postsynaptic Cell-Adhesion Molecule of Excitatory Synapses. *Proc Natl Acad Sci USA* **1999**, *96* (3), 1100–1105.

IX.5 Varoqueaux F, Jamain S, Brose N. Neuroligin 2 Is Exclusively Localized to Inhibitory Synapses. *Eur J Cell Biol* **2004**, *83* (9), 449–456.

IX.6 Hoon M, Bauer G, Fritschy J-M, Moser T, Falkenburger BH, Varoqueaux F. Neuroligin 2 Controls the Maturation of GABAergic Synapses and Information Processing in the Retina. *J Neurosci* **2009**, *29* (25), 8039–8050.

IX.7 Poulopoulos A, Aramuni G, Meyer G, Soykan T, Hoon M, Papadopoulos T, Zhang M, Paarmann I, Fuchs C, Harvey K, *et al*. Neuroligin 2 Drives Postsynaptic Assembly at Perisomatic Inhibitory Synapses through Gephyrin and Collybistin. *Neuron* **2009**, *63* (5), 628–642.

IX.8 Graf ER, Zhang X, Jin S-X, Linhoff MW, Craig AM. Neurexins Induce Differentiation of GABA and Glutamate Postsynaptic Specializations via Neuroligins. *Cell* **2004**, *119* (7), 1013–1026.

IX.9 Budreck EC, Scheiffele P. Neuroligin-3 Is a Neuronal Adhesion Protein at GABAergic and Glutamatergic Synapses. *Eur J Neurosci* **2007**, *26* (7), 1738–1748.

IX.10 Kolozsi E, Mackenzie RN, Roullet FI, deCatanzaro D, Foster JA. Prenatal Exposure to Valproic Acid Leads to Reduced Expression of Synaptic Adhesion Molecule Neuroligin 3 in Mice. *Neuroscience* **2009**, *163* (4), 1201–1210.

IX.11 Hoon M, Soykan T, Falkenburger B, Hammer M, Patrizi A, Schmidt K-F, Sassoè-Pognetto M, Löwel S, Moser T, Taschenberger H, *et al*. Neuroligin-4 Is Localized to Glycinergic Postsynapses and Regulates Inhibition in the Retina. *Proc Natl Acad Sci USA* **2011**, *108* (7), 3053–3058.

IX.12 Blundell J, Blaiss CA, Etherton MR, Espinosa F, Tabuchi K, Walz C, Bolliger MF, Südhof TC, Powell CM. Neuroligin-1 Deletion Results in Impaired Spatial Memory and Increased Repetitive Behavior. *J Neurosci* **2010**, *30* (6), 2115–2129.

IX.13 Varoqueaux F, Aramuni G, Rawson RL, Mohrmann R, Missler M, Gottmann K, Zhang W, Südhof TC, Brose N. Neuroligins Determine Synapse Maturation and Function. *Neuron* **2006**, *51* (6), 741–754.

IX.14 Bourgeron T. A Synaptic Trek to Autism. *Curr Opin Neurobiol* **2009**, *19* (2), 231–234.

IX.15 Saura CA, Servián-Morilla E, Scholl FG. Presenilin/γ-Secretase Regulates Neurexin Processing at Synapses. *PLoS One* **2011**, *6* (4), e19430.

IX.16 Bie B, Wu J, Yang H, Xu JJ, Brown DL, Naguib M. Epigenetic Suppression of Neuroligin 1 Underlies Amyloid-Induced Memory Deficiency. *Nat Neurosci* **2014**, *17* (2), 223.

IX.17 Wittenmayer N, Körber C, Liu H, Kremer T, Varoqueaux F, Chapman ER, Brose N, Kuner T, Dresbach T. Postsynaptic Neuroligin1 Regulates Presynaptic Maturation. *Proc Natl Acad Sci USA* **2009**, *106* (32), 13564–13569.

IX.18 Budreck EC, Kwon O-B, Jung JH, Baudouin S, Thommen A, Kim H-S, Fukazawa Y, Harada H, Tabuchi K, Shigemoto R, *et al*. Neuroligin-1 Controls Synaptic Abundance of NMDA-Type Glutamate Receptors through Extracellular Coupling. *Proc Natl Acad Sci USA* **2013**, *110* (2), 725–730.

IX.19 Chubykin AA, Atasoy D, Etherton MR, Brose N, Kavalali ET, Gibson JR, Südhof TC. Activity-Dependent Validation of Excitatory versus Inhibitory Synapses by Neuroligin-1 versus Neuroligin-2. *Neuron* **2007**, *54* (6), 919–931.

IX.20 Mondin M, Labrousse V, Hosy E, Heine M, Tessier B, Levet F, Poujol C, Blanchet C, Choquet D, Thoumine O. Neurexin-Neuroligin Adhesions Capture Surface-Diffusing AMPA Receptors through PSD-95 Scaffolds. *J Neurosci* **2011**, *31* (38), 13500–13515.

IX.21 Shipman SL, Schnell E, Hirai T, Chen B-S, Roche KW, Nicoll RA. Functional Dependence of Neuroligin on a New Non-PDZ Intracellular Domain. *Nat Neurosci* **2011**, *14* (6), 718–726.

IX.22 Jedlicka P, Vnencak M, Krueger DD, Jungenitz T, Brose N, Schwarzacher SW. Neuroligin-1 Regulates Excitatory Synaptic Transmission, LTP and EPSP-Spike Coupling in the Dentate Gyrus in Vivo. *Brain Struct Funct* **2015**, *220* (1), 47–58.

IX.23 Kim J, Jung S-Y, Lee YK, Park S, Choi J-S, Lee CJ, Kim H-S, Choi Y-B, Scheiffele P, Bailey CH, *et al*. Neuroligin-1 Is Required for Normal Expression of LTP and Associative Fear Memory in the Amygdala of Adult Animals. *Proc Natl Acad Sci USA* **2008**, *105* (26), 9087–9092.

IX.24 Ichtchenko K, Nguyen T, Südhof TC. Structures, Alternative Splicing, and Neurexin Binding of Multiple Neuroligins. *J Biol Chem* **1996**, *271* (5), 2676–2682.

IX.25 Maćkowiak M, Mordalska P, Wędzony K. Neuroligins, Synapse Balance and Neuropsychiatric Disorders. *Pharmacol Rep* **2014**, *66* (5), 830–835.

IX.26 Baudouin S, Scheiffele P. SnapShot: Neuroligin-Neurexin Complexes. *Cell* **2010**, *141* (5), 908, 908.e1.

IX.27 Tanaka H, Miyazaki N, Matoba K, Nogi T, Iwasaki K, Takagi J. Higher-Order Architecture of Cell Adhesion Mediated by Polymorphic Synaptic Adhesion Molecules Neurexin and Neuroligin. *Cell Rep* **2012**, *2* (1), 101–110.

IX.28 Ahmad M, Missler M. Neurexins. In *Encyclopedia of Neuroscience*; Binder M, Hirokawa N, Windhorst U, Eds.; Springer-Verlag: Berlin, Germany, **2009**; pp 261–267.

IX.29 Scheiffele P, Fan J, Choih J, Fetter R, Serafini T. Neuroligin Expressed in Nonneuronal Cells Triggers Presynaptic Development in Contacting Axons. *Cell* **2000**, *101* (6), 657–669.

IX.30 Bolliger MF, Frei K, Winterhalter KH, Gloor SM. Identification of a Novel Neuroligin in Humans Which Binds to PSD-95 and Has a Widespread Expression. *Biochem J* **2001**, *356* (Pt 2), 581–588.

IX.31 Hoffman RC, Jennings LL, Tsigelny I, Comoletti D, Flynn RE, Südhof TC, Taylor P. Structural Characterization of Recombinant Soluble Rat Neuroligin 1: Mapping of Secondary Structure and Glycosylation by Mass Spectrometry. *Biochemistry* **2004**, *43* (6), 1496–1506.

IX.32 Comoletti D, Grishaev A, Whitten AE, Tsigelny I, Taylor P, Trewhella J. Synaptic Arrangement of the Neuroligin/Beta-Neurexin Complex Revealed by X-Ray and Neutron Scattering. *Structure* **2007**, *15* (6), 693–705.

IX.33 Comoletti D, Flynn R, Jennings LL, Chubykin A, Matsumura T, Hasegawa H, Südhof TC, Taylor P. Characterization of the Interaction of a Recombinant Soluble Neuroligin-1 with Neurexin-1beta. *J Biol Chem* **2003**, *278* (50), 50497–50505.

IX.34 Comoletti D, Flynn RE, Boucard AA, Demeler B, Schirf V, Shi J, Jennings LL, Newlin HR, Südhof TC, Taylor P. Gene Selection, Alternative Splicing, and Post-Translational Processing Regulate Neuroligin Selectivity for β-Neurexins. *Biochemistry* **2006**, *45* (42), 12816–12827.

IX.35 Chen X, Liu H, Shim AHR, Focia PJ, He X. Structural Basis for Synaptic Adhesion Mediated by Neuroligin-Neurexin Interactions. *Nat Struct Mol Biol* **2008**, *15* (1), 50–56.

IX.36 Sterling T, Irwin JJ. ZINC 15--Ligand Discovery for Everyone. *J Chem Inf Model* **2015**, *55* (11), 2324–2337.

IX.37 Lovering F, Bikker J, Humblet C. Escape from Flatland: Increasing Saturation as an Approach to Improving Clinical Success. *J Med Chem* **2009**, *52* (21), 6752–6756.

IX.38 Loh JW, Saunders M, Lim L-Y. Cytotoxicity of Monodispersed Chitosan Nanoparticles against the Caco-2 Cells. *Toxicol Appl Pharmacol* **2012**, *262* (3), 273–282.

IX.39 Sahay G, Alakhova DY, Kabanov AV. Endocytosis of Nanomedicines. *J Control Release* **2010**, *145* (3), 182–195.

IX.40 Nicolete R, dos Santos DF, Faccioli LH. The Uptake of PLGA Micro or Nanoparticles by Macrophages Provokes Distinct in Vitro Inflammatory Response. *Int Immunopharmacol* **2011**, *11* (10), 1557–1563.

IX.41 Rabinovitch M. Professional and Non-Professional Phagocytes: An Introduction. *Trends Cell Biol* **1995**, *5* (3), 85–87.

IX.42 Wallace VJ, Cimbro R, Rubio FJ, Fortuno LV, Necarsulmer JC, Koivula PP, Henderson MJ, DeBiase LM, Warren BL, Harvey BK, *et al*. Neurons Internalize Functionalized Micron-Sized Silicon Dioxide Microspheres. *Cell Mol Neurobiol* **2017**, *37* (8), 1487–1499.

IX.43 Pineda JR, Encinas JM. The Contradictory Effects of Neuronal Hyperexcitation on Adult Hippocampal Neurogenesis. *Front Neurosci* **2016**, *10*, 74.

IX.44 Lie DC, Song H, Colamarino SA, Ming G, Gage FH. Neurogenesis in the Adult Brain: New Strategies for Central Nervous System Diseases. *Annu Rev Pharmacol Toxicol* **2004**, *44* (1), 399–421.

IX.45 Alvarez-Buylla A, Lim DA. For the Long Run: Maintaining Germinal Niches in the Adult Brain. *Neuron* **2004**, *41* (5), 683–686.

IX.46 Jin K, Minami M, Lan JQ, Mao XO, Batteur S, Simon RP, Greenberg DA. Neurogenesis in Dentate Subgranular Zone and Rostral Subventricular Zone after Focal Cerebral Ischemia in the Rat. *Proc Natl Acad Sci USA* **2001**, *98* (8), 4710–4715.

IX.47 Nakatomi H, Kuriu T, Okabe S, Yamamoto S, Hatano O, Kawahara N, Tamura A, Kirino T, Nakafuku M. Regeneration of Hippocampal Pyramidal Neurons after Ischemic Brain Injury by Recruitment of Endogenous Neural Progenitors. *Cell* **2002**, *110* (4), 429–441.

IX.48 Skaggs K, Goldman D, Parent JM. Excitotoxic Brain Injury in Adult Zebrafish Stimulates Neurogenesis and Long-Distance Neuronal Integration. *Glia* **2014**, *62* (12), 2061–2079.

IX.49 Dehmelt L, Halpain S. The MAP2/Tau Family of Microtubule-Associated Proteins. *Genome Biol* **2005**, *6* (1), 204.

IX.50 Walker TL, Yasuda T, Adams DJ, Bartlett PF. The Doublecortin-Expressing Population in the Developing and Adult Brain Contains Multipotential Precursors in Addition to Neuronal-Lineage Cells. *J Neurosci* **2007**, *27* (14), 3734–3742.

IX.51 Volterra A, Meldolesi J. Astrocytes, from Brain Glue to Communication Elements: The Revolution Continues. *Nat Rev Neurosci* **2005**, *6* (8), 626–640.

IX.52 Buffo A, Vosko MR, Ertürk D, Hamann GF, Jucker M, Rowitch D, Götz M. Expression Pattern of the Transcription Factor Olig2 in Response to Brain Injuries: Implications for Neuronal Repair. *Proc Natl Acad Sci USA* **2005**, *102* (50), 18183–18188.

IX.53 Rivers LE, Young KM, Rizzi M, Jamen F, Psachoulia K, Wade A, Kessaris N, Richardson WD. PDGFRA/NG2 Glia Generate Myelinating Oligodendrocytes and Piriform Projection Neurons in Adult Mice. *Nat Neurosci* **2008**, *11* (12), 1392–1401.

IX.54 Armada-Moreira A. Exploring the Modulatory Role of A2A Receptors in Oligodendrogenesis Derived from Neural Stem/Progenitor Cells of the Subventricular Zone. MSc Thesis, Faculty of Medicine, University of Lisbon, Lisbon, Portugal, **2015**.

IX.55 Sommer I, Schachner M. Monoclonal Antibodies (O1 to O4) to Oligodendrocyte Cell Surfaces: An Immunocytological Study in the Central Nervous System. *Dev Biol* **1981**, *83* (2), 311–327.

IX.56 Sochocka M, Diniz BS, Leszek J. Inflammatory Response in the CNS: Friend or Foe? *Mol Neurobiol* **2017**, *54* (10), 8071–8089.

IX.57 Streit WJ, Mrak RE, Griffin WST. Microglia and Neuroinflammation: A Pathological Perspective. *J Neuroinflammation* **2004**, *1* (1), 14.

IX.58 Floyd RA. Antioxidants, Oxidative Stress, and Degenerative Neurological Disorders. *Proc Soc Exp Biol Med* **1999**, *222* (3), 236–245.

IX.59 Singh N, Savanur MA, Srivastava S, D'Silva P, Mugesh G. A Manganese Oxide Nanozyme Prevents the Oxidative Damage of Biomolecules without Affecting the Endogenous Antioxidant System. *Nanoscale* **2019**, *11* (9), 3855–3863.

IX.60 Chen H, He J. Self-Assembly of Birnessite Manganese Dioxide into Monodisperse Honeycomb and Hollow Nanospheres. *Chem Lett* **2006**, *36* (1), 174–175.

IX.61 Xu X, Costa A, Burgess DJ. Protein Encapsulation in Unilamellar Liposomes: High Encapsulation Efficiency and a Novel Technique to Assess Lipid-Protein Interaction. *Pharm Res* **2012**, *29* (7), 1919–1931.

IX.62 Sapolsky R. Taming Stress. *Sci Am* **2003**, *289* (3), 86–95.

IX.63 Garnier M, Delamare V. *Dicionário de Termos Técnicos de Medicina*, 20th edition; Organização Andrei Editora Ltda: São Paulo, Brasil, **1984**.

IX.64 Graeff FG. Ansiedade, pânico e o eixo hipotálamo-pituitária-adrenal. *Braz J Psychiatry* **2007**, *29*, s3–s6.

IX.65 Boere V. Behavior and Environment Enrichment. In *Biology, medicine and surgery of South American animals*; Ames IA, Ed.; Iowa University Press: Iowa City, USA, **2001**; pp 263–266.

IX.66 Calabrese F, Guidotti G, Molteni R, Racagni G, Mancini M, Riva MA. Stress-Induced Changes of Hippocampal NMDA Receptors: Modulation by Duloxetine Treatment. *PLoS One* **2012**, *7* (5), e37916.

IX.67 Sanacora G, Banasr M. From Pathophysiology to Novel Antidepressant Drugs: Glial Contributions to the Pathology and Treatment of Mood Disorders. *Biol Psychiatry* **2013**, *73* (12), 1172–1179.

IX.68 Banasr M, Duman RS. Glial Loss in the Prefrontal Cortex Is Sufficient to Induce Depressive-like Behaviors. *Biol Psychiatry* **2008**, *64* (10), 863–870.

IX.69 Christian KM, Miracle AD, Wellman CL, Nakazawa K. Chronic Stress-Induced Hippocampal Dendritic Retraction Requires CA3 NMDA Receptors. *Neuroscience* **2011**, *174*, 26–36.

IX.70 McEwen BS, Magarinos AM, Reagan LP. Structural Plasticity and Tianeptine: Cellular and Molecular Targets. *Eur Psychiatry* **2002**, *17* (Suppl 3), 318–330.

Annex I.

Facs simile of the scientific articles

frontiers in Cellular Neuroscience

REVIEW
published: 24 April 2020
doi: 10.3389/fncel.2020.00090

Going the Extra (Synaptic) Mile: Excitotoxicity as the Road Toward Neurodegenerative Diseases

*Adam Armada-Moreira[1,2,3†], Joana I. Gomes[1,2†], Carolina Campos Pina[1,2], Oksana K. Savchak[1,2], Joana Gonçalves-Ribeiro[1,2], Nádia Rei[1,2], Sara Pinto[1,2], Tatiana P. Morais[4], Robertta Silva Martins[5], Filipa F. Ribeiro[1,2], Ana M. Sebastião[1,2], Vincenzo Crunelli[4,6] and Sandra H. Vaz[1,2]**

[1] Instituto de Farmacologia e Neurociências, Faculdade de Medicina da Universidade de Lisboa, Lisbon, Portugal, [2] Instituto de Medicina Molecular João Lobo Antunes, Faculdade de Medicina da Universidade de Lisboa, Lisbon, Portugal, [3] Interdisciplinary Nanoscience Center (iNANO), Aarhus University, Aarhus, Denmark, [4] Neuroscience Division, School of Bioscience, Cardiff University, Cardiff, United Kingdom, [5] Laboratório de Neurofarmacologia, Instituto Biomédico, Universidade Federal Fluminense, Niterói, Brazil, [6] Department of Physiology and Biochemistry, Faculty of Medicine and Surgery, University of Malta, Msida, Malta

OPEN ACCESS

Edited by:
Balázs Pál,
University of Debrecen, Hungary

Reviewed by:
Christine R. Rose,
Heinrich Heine University of Düsseldorf, Germany
Lucia Wittner,
Research Centre for Natural Sciences (MTA), Hungary

***Correspondence:**
Sandra H. Vaz
svaz@medicina.ulisboa.pt

[†] These authors share first authorship

Specialty section:
This article was submitted to Cellular Neurophysiology, a section of the journal Frontiers in Cellular Neuroscience

Received: 18 December 2019
Accepted: 26 March 2020
Published: 24 April 2020

Citation:
Armada-Moreira A, Gomes JI, Pina CC, Savchak OK, Gonçalves-Ribeiro J, Rei N, Pinto S, Morais TP, Martins RS, Ribeiro FF, Sebastião AM, Crunelli V and Vaz SH (2020) Going the Extra (Synaptic) Mile: Excitotoxicity as the Road Toward Neurodegenerative Diseases. Front. Cell. Neurosci. 14:90. doi: 10.3389/fncel.2020.00090

Excitotoxicity is a phenomenon that describes the toxic actions of excitatory neurotransmitters, primarily glutamate, where the exacerbated or prolonged activation of glutamate receptors starts a cascade of neurotoxicity that ultimately leads to the loss of neuronal function and cell death. In this process, the shift between normal physiological function and excitotoxicity is largely controlled by astrocytes since they can control the levels of glutamate on the synaptic cleft. This control is achieved through glutamate clearance from the synaptic cleft and its underlying recycling through the glutamate-glutamine cycle. The molecular mechanism that triggers excitotoxicity involves alterations in glutamate and calcium metabolism, dysfunction of glutamate transporters, and malfunction of glutamate receptors, particularly N-methyl-D-aspartic acid receptors (NMDAR). On the other hand, excitotoxicity can be regarded as a consequence of other cellular phenomena, such as mitochondrial dysfunction, physical neuronal damage, and oxidative stress. Regardless, it is known that the excessive activation of NMDAR results in the sustained influx of calcium into neurons and leads to several deleterious consequences, including mitochondrial dysfunction, reactive oxygen species (ROS) overproduction, impairment of calcium buffering, the release of pro-apoptotic factors, among others, that inevitably contribute to neuronal loss. A large body of evidence implicates NMDAR-mediated excitotoxicity as a central mechanism in the pathogenesis of many neurodegenerative diseases, including amyotrophic lateral sclerosis (ALS), Alzheimer's disease (AD), and epilepsy. In this review article, we explore different causes and consequences of excitotoxicity, discuss the involvement of NMDAR-mediated

Abbreviations: AD, Alzheimer's Disease; ALS, amyotrophic lateral sclerosis; AMPAR, α-amino-3-hydroxy-5-methylisoxazole-4-propionate receptors; AQP4, aquaporin 4; Aβ, amyloid-β peptide; BDNF, brain-derived neurotrophic factor; CREB, cAMP-regulatory element binding protein; CypD, cyclophilin D; EAAT, excitatory amino acid transporters; eNMDAR, extrasynaptic NMDAR; GABA, γ-aminobutyric acid; GABAR, GABA receptors; iGluR, ionotropic glutamate receptors; KAR, kainate receptors; Kir4.1, input rectifier channels for potassium; mGluR, metabotropic glutamate receptors; NMDAR, N-methyl-D-aspartic acid receptors; NO, nitric oxide; NOS, NO synthase; ROS, reactive oxygen species; sNMDAR, synaptic NMDAR; SOD, superoxide dismutase; TLE, temporal lobe epilepsy; TNF-α, tumor necrosis factor-α.

excitotoxicity and its downstream effects on several neurodegenerative disorders, and identify possible strategies to study new aspects of these diseases that may lead to the discovery of new therapeutic approaches. With the understanding that excitotoxicity is a common denominator in neurodegenerative diseases and other disorders, a new perspective on therapy can be considered, where the targets are not specific symptoms, but the underlying cellular phenomena of the disease.

Keywords: excitotoxicity, astrocytes, NMDA receptors, calcium signaling, neurodegenerative diseases, oxidative stress

EXCITOTOXICITY: WHAT IS IT, WHERE DOES IT COME FROM, HOW DOES IT LIVE?

The Good, the Bad, and the Ugly: General Definition and Summary of Consequences

When looking into the glutamatergic system within the central nervous system, one can see three sides of the same biological phenomenon. First, there is The Good: the glutamatergic system is essential for brain functioning. Indeed, with 40% of glutamatergic synapses in the central nervous system (Fairman and Amara, 1999), glutamate is essential for neuronal communication, as well as for higher-level functions, such as learning and memory. Then, there is The Bad: since glutamate plays such an important role in the brain, dysregulation of the glutamatergic system has long been implicated as a key step in the pathophysiology of neuronal death (Bano et al., 2005). Finally, there is The Ugly: excitotoxicity. This phenomenon, an important aspect of glutamatergic dysregulation, describes the toxic actions of excitatory neurotransmitters, mainly glutamate, that ultimately lead to neuronal death (Connolly and Prehn, 2015). While glutamate does not directly kill neurons, the exacerbated or prolonged activation of glutamate receptors starts a cascade of neurotoxicity (Lipton, 2008; Vincent and Mulle, 2009), which includes cationic influx, mitochondrial dysfunction, energetic and oxidative stress, and overproduction of reactive oxygen species (ROS; Connolly and Prehn, 2015; Prentice et al., 2015). Here, we review the main factors involved in excitotoxicity, as summarized in **Figure 1**, and their role in neurodegenerative diseases and epilepsy.

If These Walls Could Talk... About Excitotoxicity: Historic Review

The term "excitotoxicity" makes its debut in 1969 in a study by Olney where, for the first time, cell death was observed as a consequence of exposure to glutamate or aspartate (Olney, 1969). This type of excitotoxicity can be divided into three steps. It starts with the induction, which begins with the overactivation of ionotropic glutamate receptors (iGluR), such as N-methyl-D-aspartic acid receptors (NMDAR), α-amino-3-hydroxy-5-methylisoxazole-4-propionate receptors (AMPAR) and kainate receptors (KAR). NMDAR display a high permeability to both sodium and calcium (McBain and Mayer, 1994), while AMPAR and KAR activation contributes mainly to sodium influx. This ionic influx is followed by water influx, leading to cell swelling and mitochondrial dysfunction. The final step of induction is the activation of metabotropic glutamate receptors (mGluR), activating pathways regulated by diacylglycerol and inositol 1,4,5-triphosphate (Zivin and Choi, 1991). Amplification and expression are the following stages. These consist of exacerbated metabolic activity, further disruption of ion gradients, elevated electrical neuronal activity, and mitochondria dysfunction (Zivin and Choi, 1991).

Other than this classification system for excitotoxicity, this phenomenon can be further categorized as strong or weak excitotoxicity (Albin and Greenamyre, 1992). Strong excitotoxicity refers to the classical phenomenon described by Olney (1969), where excitotoxicity is elicited by direct exposure to glutamate or another excitotoxic compound. In strong excitotoxicity, the calcium influx is prolonged, there is depolarization of both cell and mitochondria membranes, excessive consumption of NAD(P)H, and an established bioenergetic failure. Furthermore, cell death is generally brought on by necrosis (Castilho et al., 1998; Connolly and Prehn, 2015). On the other hand, weak excitotoxicity results from a prolonged alteration of glutamate receptor function, possibly impacting membrane potential and cellular metabolism and increasing cellular sensitivity to the toxic actions of glutamate (Albin and Greenamyre, 1992). In this scenario, neurons are transiently able to restore calcium homeostasis, membrane potential, and internal ATP and NAD(P)H pools (Ward et al., 2000; Weisová et al., 2009). These neurons can then undergo delayed apoptosis, characterized by delayed calcium dysregulation, nuclear compression, and cellular contraction (Ankarcrona et al., 1995; Bonfoco et al., 1995; Ward et al., 2007; D'Orsi et al., 2012). This is accompanied by a loss of membrane potential, ATP depletion, and overproduction of ROS (Luetjens et al., 2000; Vesce et al., 2004).

A Glutamatergic Mind: Glutamate in Physiological and Excitotoxic Conditions

In central nervous system synapses, glutamate clearance is achieved by diffusion and transporter uptake, mainly into neighboring glial cells (van den Berg and Garfinkel, 1971; Benjamin and Quastel, 1972; Hertz et al., 1999), and is practically independent of enzymatic breakdown (Watkins and Evans, 1981).

It should however be noted that glutamatergic synapses are complex—their morphological characteristics (number of

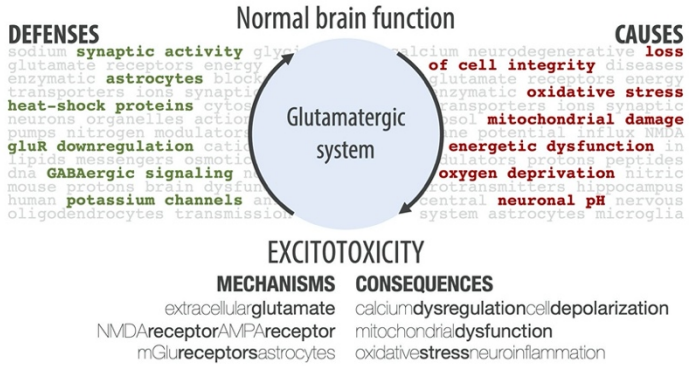


FIGURE 1 | Schematic summary of different aspects of excitotoxicity, including the main cellular defenses against it, the main causes, the players involved in its mechanisms, and general cellular consequences. The shift from normal brain function to an excitotoxic state is brought about by the main causes, and this shift is avoided by the main cellular defenses. If the defenses fail, excitotoxicity is amplified by different mechanisms, causing cellular consequences.

release sites, the existence of dendritic spines, etc.) can differ greatly and synapses in different neural circuitries exhibit different time courses of synaptic communication (Jonas, 2000). Furthermore, the exact time course of glutamate dynamics can be altered by the microanatomical synaptic properties (synaptic contact size, complexity of synaptic morphology, glial wrapping, etc.) and by the density of glutamate transporters (Jonas, 2000).

Even taking all this into account, during a synaptic event, the peak concentration of glutamate in the synapse can be estimated to be 1.1 mM (1.0–1.5 mM), with a decay time constant of 1.2 ms (0.70–2.0 ms; Clements et al., 1992), while in extrasynaptic locations, the peak concentration can reach 190 μM (Dzubay and Jahr, 1999). On the opposite side, the baseline concentration of synaptic glutamate (with no synaptic event occurring) is thought to vary between 25 nM (Herman and Jahr, 2007) and 600 nM (Mark et al., 2001), depending on the study. This basal concentration is unaltered by synaptic activity, being controlled solely by glutamate transporters (Herman and Jahr, 2007). Furthermore, this basal concentration does not activate glutamate receptors (Trussell and Fischbach, 1989; Patneau and Mayer, 1990; Conn and Pin, 1997) nor interferes with neuronal excitability (Herman and Jahr, 2007).

In excitotoxicity, the time course of glutamate dynamics can be affected in several different manners. The synaptic concentration of glutamate can rise above its usual peak concentration (above 1.1 mM), although this value might plateau due to complete depletion of presynaptic glutamate, or this peak concentration can be maintained for an excessive amount of time, which is translated to an increase in the decay time, or even the baseline concentration of glutamate may be increased, regardless of depolarization-induced release. Regarding this last scenario, it is known that neuronal excitotoxic injury occurs with baseline concentrations of glutamate of 2–5 μM (Mark et al., 2001).

Glutamate and the Depolarization Factory: Glutamate Receptors in Excitotoxicity

Glutamatergic neurotransmission is performed through iGluR and mGluR. The iGluR are ligand-gated ion channels permeable to various cations, namely sodium, potassium, and calcium, that produce excitatory glutamate-evoked currents, while mGluR are G protein-coupled receptors that control cellular processes *via* G protein signaling cascades (Reiner and Levitz, 2018). The main characteristics of these receptors are summarized in **Table 1** and reviewed in detail in this section.

iGluR can be divided into three functional classes such as NMDAR, AMPAR, and KAR (Hansen et al., 2017). While all iGluR is in the first line of the excitotoxic response, NMDAR has been pinpointed as the main culprit in glutamate-induced neurotoxicity, due to their permeability to calcium ions. NMDAR exhibits a voltage-dependent magnesium-blockade, high permeability to calcium, and requires simultaneous binding of glutamate and a co-agonist, such as glycine and D-serine, for activation (Guo et al., 2017). NMDAR are tetrameric structures composed of GluN1, GluN2A-D and GluN3A-B subunits that form a central ion channel pore. Diversity in NMDAR subunits and assembly results in different receptor subtypes with distinct functional properties, including different channel kinetics, channel opening probability, and conductance. Therefore, these differences in subunit composition can impact both synaptic plasticity and neuronal function. Previous literature reported that GluN2A-containing receptors present faster kinetics, while GluN2B-containing receptors present slower opening, closing, and glutamate unbinding, indicating that NMDAR containing GluN2A open more reliably and with faster kinetics than

TABLE 1 | Summary of glutamate receptors' characteristics, including their synaptic location, relationship with calcium, and involvement in excitotoxicity.

Receptor type	General description	Receptor subtype	Location	Calcium involvement	Involvement in excitotoxicity
Ionotropic	Ligand-gated ion channels	NMDA	Synaptic and extrasynaptic	Permeable	sNMDA: neuroprotection, cell survival
	Excitatory glutamate-evoked currents				eNMDA: pro-death pathways, excitotoxicity, neuronal dysfunction
		AMPA	Post-synaptic	Permeable if lacking GluA2 subunit	Activation alleviates NMDAR Mg^{2+} block, cell depolarization
		KA	Pre- and post-synaptic	Mostly impermeable	
Metabotropic	GPCR	mGluR1/5	Peri- and extrasynaptic	Ca^{2+} release from internal stores	Activation of the IP_3/Ca^{2+} signaling pathway
	Cellular processes *via* G protein signaling cascades				Delayed cell death

NMDAR containing GluN2B subunits (Erreger et al., 2005). These data suggest that NMDAR containing GluN2A is more likely to sense rapid glutamate transients in the synapse and open with a high probability, while NMDAR containing GluN2B seems to be set to sense basal levels of glutamate and open with much lower probability. Moreover, it is known that NMDAR subunit composition also determines single-channel conductance and blockage by magnesium ions (Kuner and Schoepfer, 1996; Brimecombe et al., 1997; Cull-Candy et al., 2001), where both GluN2A- or GluN2B-containing receptors display a high ionic conductance and stronger magnesium block. In mature neurons, GluN2A subunits are predominantly synaptic (sNMDAR), whereas GluN2B-containing receptors are mostly extrasynaptic (eNMDAR; Rönicke et al., 2011). In rat hippocampal slices, the amount of eNMDAR has been estimated to be 36% of that of sNMDAR (Harris and Pettit, 2007) and it is known that D-serine mainly binds to sNMDAR, while glycine preferentially binds to eNMDAR (Papouin et al., 2012). Furthermore, previous studies reported a neuroprotective role for sNMDAR and a neurotoxic role for eNMDAR by receptor-mediated influx of calcium (Hardingham et al., 2002; Hardingham and Bading, 2010; Samson et al., 2016). Moreover, it has been proposed that the activation of NMDAR containing GluN2A subunits stimulates signaling cascades associated with neuroprotection and regulates survival, while stimulation of NMDAR containing GluN2B subunits leads to the activation of excitotoxic pathways, leading to neuronal death (Zhou et al., 2013). sNMDAR (mainly enriched with GluN2A subunits) activation promotes neuroprotection *via* changes in gene expression that have multiple effects within the cell. Stimulation of sNMDAR is known to result in the enhancement of antioxidant defenses, promoting the transcription of pro-survival factors, including cAMP-regulatory element-binding protein (CREB; Hardingham and Bading, 2010), that results in the transcription of brain-derived neurotrophic factor (BDNF), essential for neuronal survival. sNMDAR activity is also implicated in the generation of anti-apoptotic effects, including the inactivation of pro-death transcription factors, such as forkhead box protein O and p53 (Dick and Bading, 2010). In contrast, stimulation of eNMDAR (mainly enriched with GluN2B subunits) preferentially induces pro-death effects, such as the shut-off of CREB pathway, blocking BDNF expression (Hardingham et al., 2002); the inactivation of extracellular signal-regulated kinases 1 and 2, which are necessary for BDNF function on spines (Hardingham et al., 2002); activation of forkhead box protein O and calpains, with consequent cleavage of the striatal enriched tyrosine phosphatase, which prevents this phosphatase from inhibiting p38 mitogen-activated protein kinase; and oxidative stress with subsequent neurodegeneration (Hardingham et al., 2002; Hardingham and Bading, 2010). Hence, while sNMDAR has a neuroprotective role, eNMDAR preferentially initiates cell death pathways (Hardingham and Bading, 2010). It is known that low levels of eNMDAR activity have no effects on neuronal survival, while high levels of eNMDAR stimulation enhance cell death pathways and exacerbate neurodegenerative processes, consequently reducing neuronal survival (Hardingham and Bading, 2010). eNMDAR

can also be activated by mechanical stimuli and aspartate. Indeed, the GluN2B subunit has been reported to play a role in the mechanosensitive activation of NMDAR (Maneshi et al., 2017). On the other hand, although with lower affinity than glutamate, aspartate can bind and activate NMDAR (Chen et al., 2005). Aspartate levels are severely increased following traumatic brain injury (Palmer et al., 1994; Amorini et al., 2017) and, when present in excessive levels extrasynaptically, are associated with excitotoxicity (Choi et al., 1989). In summary, while sNMDAR signaling is associated with the suppression of pro-apoptotic transcription factors (Dick and Bading, 2010), eNMDAR stimulation increases the activity of pro-apoptotic factors, leading to oxidative stress and cell death (Hardingham et al., 2002; Hardingham and Bading, 2010; Parsons and Raymond, 2014). The activation of these pro-apoptotic factors can affect gene activity regulation of BDNF and vascular endothelial growth factor (Hardingham et al., 2002), essential for the maintenance of synaptic connectivity and architecture (Bading, 2013). Hence, the excessive intracellular calcium levels resulting from the excessive eNMDAR stimulation lead to excitotoxic cell death and contributes to neuronal injury.

Intriguingly, there are conflicting pieces of evidence regarding NMDAR involvement in excitotoxicity. Some studies state that NMDAR has a dichotomic effect in excitotoxicity, where activation of sNMDAR counteracts excitotoxicity and activation of eNMDAR is the main contributor to the excitotoxic cascade (Jia et al., 2015). Other authors propose that NMDAR-induced excitotoxicity requires overactivation of both sNMDAR and eNMDAR (Zhou et al., 2013, 2015). Finally, other studies even suggest neurotoxicity could be solely dependent on sNMDAR activity, since silencing sNMDAR can act as a neuroprotective approach against NMDA-induced excitotoxicity, while inhibiting eNMDAR does not have any protective effect, questioning the role of these receptors in neurotoxicity (Papouin et al., 2012).

AMPAR are tetrameric ionotropic glutamate receptors formed by GluA1–4 subunits. These receptors can be either hetero- or homotetramers and, depending on subunit composition, display different calcium permeability (Pál, 2018), with the GluA2 subunit controlling AMPAR calcium permeability. Assemblies of highly calcium-permeable AMPAR have been implicated in excitotoxicity. Moreover, the GluA2 subunit can also be subjected to RNA editing, with the conversion of a glutamine codon into an arginine one, and AMPAR is calcium-permeable if they contain the unedited GluA2 subunit or if they lack the GluA2 subunit (Wright and Vissel, 2012). Given their high calcium permeability, AMPAR lacking GluA2 is thought to contribute to excitotoxic cell death (Wright and Vissel, 2012).

KAR is composed of GluR5-7 and KA1-2 subunits. KAR properties are similar to AMPAR in that they allow ion flux directly following glutamate exposure, and are mostly impermeable to calcium. Although AMPAR is localized mostly in the postsynaptic membrane, several studies have shown that KAR may be localized in both pre- and post-synaptically (Chittajallu et al., 1996; Castillo et al., 1997). Post-synaptically, KAR, and AMPAR have a similar function in alleviating the magnesium block in NMDAR. This phenomenon leads to an exacerbation of NMDAR activation under glutamate excess.

mGluR are probably the most diverse receptor family of the central nervous system (CNS). The mGluR1 and mGluR5 subtypes are located in the peri- and extrasynaptic neuronal regions (Ferraguti et al., 2008). They are coupled to G_q protein and exert their actions *via* the inositol trisphosphate/calcium signal pathway, being consequently able to stimulate calcium release from neuronal stores, thus triggering delayed cell death (Pál, 2018).

The Gatekeepers of Homeostasis: Astrocytes

In the forebrain, it has been shown that astrocytes are responsible for about 90% of the glutamate clearance from the synaptic cleft. During synaptic transmission, only approximately 20% of synaptically-released glutamate reaches the postsynaptic glutamate receptors, while the remainder can reach the extrasynaptic space (Kojima et al., 1999). Due to the significant role of astrocytes in glutamate re-uptake, impairment of astrocytic glutamate transporters leaves neurons highly susceptible to excitotoxicity (Rothstein et al., 1996). During an acute insult, astrocytes can prevent excitotoxicity by removing extracellular glutamate with high-affinity sodium-dependent glutamate transporters also known as excitatory amino acid transporters (EAAT). These proteins can clear glutamate from the extracellular space into cells, where it can be metabolized or recycled. Several subtypes of EAAT have already been pharmacologically identified. These transporters were divided into four subtypes in rats (GLAST, GLT-1, EAAC1, and EAAT4) and five in humans (EAAT1-5), and can be found in neurons (EAAT3 or EAAC1 and EAAT4) and astrocytes (EAAT1 or GLAST and EAAT2 or GLT-1; Danbolt, 2001; Crino et al., 2002; Beart and O'Shea, 2007; Sarac et al., 2009; Gonçalves-Ribeiro et al., 2019). Additionally, although glutamate transporters activity may come mostly from (if not exclusively) from astrocytes, the role of glutamate transporters in neurons still needs to be further explored. Indeed, neuronal glutamate transporters knockout does not influence in terms of preventing excitotoxicity, since mice with this knockout show no differences in survival, weight gain, and seizure activity compared to wild-type. On the other hand, synaptosomes prepared from these knockout mice showed a reduction of glutamate activity by 40% (Petr et al., 2015), suggesting that the role of neuronal glutamate transporters is yet to be revealed.

Furthermore, astrocytes are responsible for the maintenance of glutamate homeostasis by sustaining its synthesis, uptake and release *via* the glutamate-glutamine cycle (van den Berg and Garfinkel, 1971; Benjamin and Quastel, 1972; Ottersen et al., 1992). Through this cycle, synaptically released glutamate is predominantly taken up into astrocytes, where it is amidated to glutamine by the astrocyte-specific enzyme glutamine synthetase (Norenberg and Martinez-Hernandez, 1979). Glutamine is then released to the synapse and uptake by adjacent neurons, where it is converted to glutamate and γ-aminobutyric acid (GABA), which are then repackaged into vesicles and again released in the

synapse as neurotransmitters (Allen, 2014; Rodríguez-Arellano et al., 2016).

In a different perspective, astrocytes are hypothesized to be the main effectors of glycolysis to produce lactate that is then transferred to neurons through the astrocyte-neuron lactate shuttle. This metabolic link between neurons and astrocytes is because neurons are highly energy-demanding cells but are unable to perform the citric acid cycle without an external supply of lactate, due to the lack of the essential enzyme pyruvate carboxylase (Schousboe et al., 1997; Magistretti and Allaman, 2015). Since astrocytic glutamate re-uptake is electrogenic, for each glutamate molecule entrance, three sodium ions enter the cell, activating the sodium/potassium ATPase. This, in turn, activates the glycolysis pathway in the astrocytes, stimulating the production of the lactate by either increasing glucose uptake or intracellular glycogen breakdown. Produced lactate is later released into the intracellular space by the monocarboxylate transporter 1 expressed in the astrocytes and received by neurons through the monocarboxylate transporter 2 (Stobart and Anderson, 2013). It is later used by the neuron as the carbon source in the Krebs cycle for oxidative phosphorylation. Besides lactate, astrocytes also release citrate, involved in the regulation of neuronal excitability by chelating zinc ions, thus inhibiting NMDAR (Westergaard et al., 1995; Schousboe et al., 1997). Furthermore, although recent literature suggests that neurons are primarily responsible for the synthesis and release of D-serine (Wolosker et al., 2016), several independent studies strongly support that astrocytes are the main source of D-serine, essential for NMDAR function (Henneberger et al., 2010; Bergersen et al., 2012; Martineau et al., 2013; Sultan et al., 2015).

THE BUTTERFLY EFFECT: DETAILED LOOK INTO EXCITOTOXICITY-INDUCED DYSFUNCTIONS

One Ion to Rule Them all: The Central Role of Calcium to Propagate Glutamate Toxicity

One of the first consequences of excessive activation of glutamate receptors, namely NMDAR, is a sustained influx of calcium into the neuron (Mehta et al., 2013). Calcium has long been identified as a key player in glutamate neurotoxicity, as summarized in **Figure 2**. Specifically, early studies proved that scavenging extracellular calcium would decrease excitotoxicity-induced neuronal degeneration, while removal of other cations would not (Berdichevsky et al., 1983; Choi et al., 1988). This influx synergizes with the release of calcium from intracellular stores, such as the mitochondria and the endoplasmic reticulum, due to membrane damage caused by the disruption of ionic gradients (Mehta et al., 2013).

Together, these phenomena lead to a striking increase in the intracellular calcium concentration, which can activate enzymes that degrade proteins, lipids, and nucleic acids (Berliocchi et al., 2005), as well as enzymes involved in arachidonic acid pathways, such as phospholipase A2, cyclooxygenase-2, and lipoxygenases. These latter enzymes, when activated, lead to the production of arachidonic acid and its conversion into prostaglandins, leukotrienes, and thromboxanes with the concomitant production of ROS (Freeman and Crapo, 1982; Pazdernik et al., 1992; Murphy et al., 1994). Among these molecules, prostaglandin E2 has been shown to have a dual role in excitotoxicity: at low concentration (nanomolar range), prostaglandin E2 presents a neuroprotective effect (Akaike et al., 1994); at higher concentrations (micro- to millimolar), as seen in the calcium-induced arachidonic acid cascade, prostaglandin E2 contributes to neurotoxicity and cell death (Hewett et al., 2000). Additionally, calcium-induced activation of phospholipase A2 inhibits GABA receptors (GABAR), thus preventing neuronal hyperpolarization and further contributing to excitotoxicity (Hamano et al., 1996).

Finally, the calcium dysregulation also activates ATP-dependent ion pumps, to counteract the cationic influx, such as the sodium/potassium and calcium ATPases, which will drain all available ATP, creating a low-energy neuronal state (Connolly et al., 2014; Surin et al., 2014).

Eternal Dysfunction for the Mitochondrial Minds: Mitochondrial Damage

Another large contributor to glutamate neurotoxicity are mitochondria (**Figure 2**), which are essential in bioenergetic homeostasis and calcium signaling regulation (Mehta et al., 2013). Indeed, following the excitotoxicity-induced calcium influx, mitochondria capture cytosolic calcium *via* the mitochondrial calcium uniporter, attempting to maintain a low cytosolical calcium concentration (Qiu et al., 2013). While this process temporarily buffers the intracellular calcium concentration, the excessive cationic uptake eventually leads to the depolarization of the mitochondrial membrane, impairing ATP production and anti-oxidant mitochondrial functions (Nicholls and Budd, 2000; Kushnareva et al., 2005) and leaving neurons in a low-energy and oxidative state with high production of ROS (Mehta et al., 2013). Following this cascade, mitochondrial dysfunction contributes to apoptotic cell death, activating both caspases (Lipton, 2008) and calpains (Caldeira et al., 2014).

The Wizard of ROS: Oxidative Stress

The excessive activation of glutamate receptors also leads to an imbalance between ROS and their opposing antioxidant forces (Bondy and LeBel, 1993), a phenomenon named oxidative stress. In an excitotoxic scenario, oxidative stress is brought about by a higher intracellular concentration of ROS, which is directly associated with glutamate neurotoxicity (Nicholls, 2004). ROS are then mediators of enzyme inactivation, lipidic peroxidation and consequent membrane damage, DNA alterations, and apoptosis (Floyd, 1999; Lucca et al., 2009).

The excitotoxic production of ROS is related to the activation of the pro-oxidant enzymes xanthine oxidase and NADPH oxidase (Prentice et al., 2015) and mitochondrial dysfunction. Interestingly, NADPH oxidase, and not mitochondria, has been identified as the major source of ROS following glutamate exposure (Brennan et al., 2009).

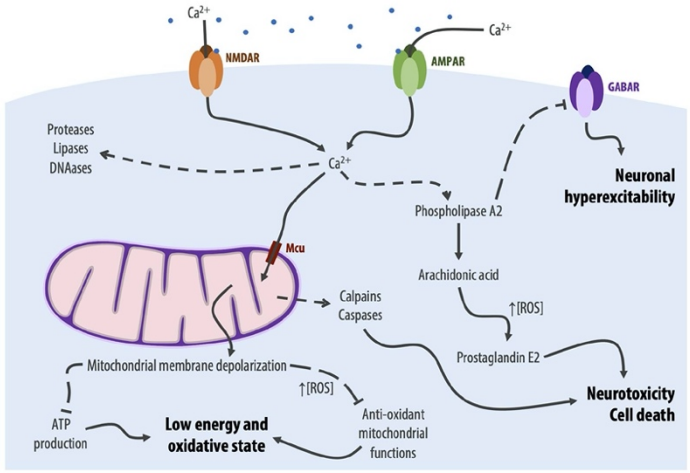


FIGURE 2 | Graphical depiction of the main calcium-dependent processes involved in excitotoxicity, leading to oxidative stress and cell death. Dotted lines with end arrows represent activation, dotted lines with T ends represent inhibition. Mcu, mitochondrial calcium uniporter.

Additionally, studies have demonstrated that glutamate binding to NMDAR results in the production of nitric oxide (NO) as a consequence of nitric oxide synthase (NOS) activation by calcium influx, which is spatially linked to NMDAR *via* the postsynaptic density protein of 95 kDa (Aarts et al., 2002; Zhou et al., 2010; Jones, 2011). It has also been observed that an increase in NO concentration can trigger biochemical pathways that contribute to neuronal death and cognitive impairment (Díaz et al., 2010), since NO can react with the superoxide anion forming peroxynitrite, known to lead to the formation of 3-nitrotyrosine (Butterfield and Kanski, 2001). NO is then responsible for protein degradation by nitration and oxidation, lipid peroxidation, and DNA damage (Jia et al., 2015). Protein nitration results in the dysfunction of several proteins such as superoxide dismutase (SOD), actin, and tyrosine hydroxylase, and can interfere with cell signaling pathways mediated by tyrosine phosphorylation (Butterfield and Stadtman, 1997), contributing to the intracellular signaling dysregulation.

WE NEED TO TALK ABOUT EXCITOTOXICITY: EXCITOTOXICITY AS A CONSEQUENCE OF OTHER PHENOMENA

A possible trigger for excitotoxicity is the physical damage of a neuron. In physiological conditions, the extracellular glutamate concentration is around 0.01% of the intracellular concentration, not reaching the threshold for post-synaptic neuronal activation which maintains the glutamate pools in an inactive state (Mehta et al., 2013). However, this percentage can quickly increase if a damaged neuron releases all its glutamate content into the extracellular space, leading to excitotoxicity in neighboring neurons (Mehta et al., 2013).

Oxidative stress is one of the main consequences of glutamate-induced neurotoxicity. However, it is not possible to define a unidirectional cause/effect relationship between the two phenomena, since oxidative stress and excessive intracellular ROS can also induce excitotoxicity by stimulating extracellular glutamate release (Pellegrini-Giampietro et al., 1990) and releasing calcium from mitochondria into the cytosol (Richter and Kass, 1991). In another perspective, it has already been shown that astrocytic glutamine synthetase is especially susceptible to ROS-induced inactivation, which compromises the whole glutamate-glutamine cycle and contributes to an increase in extracellular glutamate concentration and consequent excitotoxicity (Schor, 1988). Additionally, the presence of ROS has been shown to decrease glutamate transporter activity, impairing synaptic clearance of glutamate further contributing to the increase in extracellular glutamate concentration (Anderson and Swanson, 2000).

Oxygen deprivation can also induce excitotoxicity through different mechanisms. In a straight forward manner, hypoxic-ischemic states directly stimulate glutamate release, increasing the extracellular glutamate concentration to neurotoxic levels (Prentice et al., 2015). Additionally, oxygen deprivation leads to energetic stress by impairing mitochondrial oxidative

phosphorylation and, consequently, blocking ATP production (Doyle et al., 2008). This blockage leads to the depletion of intracellular ATP, which prevents the reuptake of glutamate, creating an excitotoxic concentration of extracellular glutamate (Rossi et al., 2000).

In a different perspective, while mitochondrial damage is one of the main consequences of excitotoxicity, mitochondria can also be originators of excitotoxicity. Mitochondrial toxins, for instance, can cause energetic impairment, preventing ATP production (Dong et al., 2009). Over time, cellular ATP pools are then depleted, with a concomitant decline in the activity of the sodium/potassium ATPase, which will depolarize the neuronal membrane (Mehta et al., 2013). By itself, this depolarization can render neurons more prone to firing action potentials (Dutta and Trapp, 2011). It, however, also affects NMDAR by removing their voltage-dependent magnesium-block, lowering their activation threshold so that non-excitotoxic glutamate concentrations become capable of inducing an excitotoxic response (Stavrovskaya and Kristal, 2005).

Finally, the physiological brain pH is estimated to be pH 7.2–7.3 in rats (Siemkowicz and Hansen, 1981), and pH 7.33 in humans (Mutch and Hansen, 1984). However, some diseases or disorders can drastically alter the CNS pH, inducing either acidosis or alkalosis. For instance, anaerobic conditions of ischemia promote the alteration of the metabolism of the cells from aerobic oxidation of glucose to anaerobic glycolysis. This alteration in metabolism produces lactate and protons, which is responsible for acidosis (Li et al., 2016). Interestingly, a curious phenomenon occurs in acidosis. While severe acidosis ($pH < 6.4$) contributes to excitotoxicity through a loss of ionic gradients (Kraig et al., 1987) and activation of acid-sensing ion channels, which intensifies excitotoxicity by providing another entry for calcium (Waldmann et al., 1997; Cheng et al., 2018; Qiang et al., 2018), mild acidosis (pH 6.5–7.0) appears to partly prevent excitotoxicity (Simon et al., 1993), as well as glutamate-induced neuronal death (Tombaugh and Sapolsky, 1990). This phenomenon occurs due to the inhibitory effects of protons on NMDAR activation (Tang et al., 1990). On the other end of the spectrum, alkalosis ($pH > 8.0$) seems to induce neurotoxicity. When compared to acidosis, alkalosis produces a more severe dysfunction that is more difficult to counteract. Indeed, cortical GABAergic neurons appear to be more susceptible to alkalosis than to acidosis (Zhang et al., 2013). And, considering the inhibitory effect of protons on NMDAR, it is possible to conclude that alkalosis leads to an increase in NMDAR activation. Thus, alkalosis contributes to excitotoxicity by both directly stimulating NMDAR, but also by disrupting inhibitory neurotransmission.

SAVING PRIVATE NEURON: CELLULAR DEFENSES AGAINST EXCITOTOXICITY

During excitotoxicity, neurons mobilize a variety of defenses to decrease the damaging effects of this process, among which are potassium channels, GABA signaling, acid-sensing ion channels, adenosine, and NO (Sapolsky, 2001).

Potassium channels are responsible for limiting and rectifying neuronal excitability during action potentials. The small-conductance calcium-dependent potassium channels (Sah, 1996) are highly calcium-dependent and are quite sensitive to transient increases of cytosolic calcium (Blatz and Magleby, 1987). The small-conductance channels mediate the shift of the excitotoxic calcium mobilization into a protective, hyperpolarizing signal (Madison and Nicoll, 1984; Lancaster and Adams, 1986; Sah, 1996; Honrath et al., 2017). Other key potassium channels are the ATP-dependent potassium channels, whose conductance is enhanced by ATP depletion (Politi and Rogawski, 1991; Riepe et al., 1992), particularly following excitotoxic insults (Trapp and Ballanyi, 1995). At presynaptic sites, ATP-dependent potassium channel activation also inhibits glutamate release (Bancila et al., 2004).

NMDAR-mediated calcium influx also increases sodium/potassium ATPase activity, leading to decreased excitability by stabilizing the resting membrane potential (Marcaida et al., 1996).

Another defense mechanism against excitotoxicity involves the inhibitory neurotransmitter GABA and GABAergic signaling (Bradford, 1995). Also, taurine released from glial cells during insults (Magnusson et al., 1991; Torp et al., 1991), similarly to GABA, also decreases presynaptic neuronal excitability by increasing chloride influx (Huxtable, 1992) through $GABA_AR$ (O'Byrne and Tipton, 2000; Winkler et al., 2019). Moreover, neuronal networks were shown to offer a fast-acting GluN2A-dependent neuroprotective signaling mechanism, which uses the innate capacity of surrounding neuronal networks to quench excitation, through the recruitment of $GABA_BR$ (Samson et al., 2016).

Glutamate receptor number can be also decreased by calcium-mediated activation of calpains. Activation of these proteases can result in the proteolysis of both NMDAR and AMPAR (Bi et al., 1996, 1998a,b). Moreover, calcium-dependent activation of calcineurin and calmodulin can inhibit voltage-gated and NMDAR-gated calcium currents, respectively (Vyklický, 1993; Lieberman and Mody, 1994; Ehlers et al., 1996).

During necrotic insults, energy depletion gives rise to adenosine. Adenosine inhibits presynaptic glutamate release, an action that is accomplished through A_1 adenosine receptors linked by G proteins to both calcium and potassium channels and decreases postsynaptic calcium currents in response to glutamate (Phillis and Wu, 1981; Cunha, 2005). On the other hand, a downstream consequence of glutamatergic excitotoxicity is the generation of NO, which acts intracellularly to inhibit NMDAR activity by nitrosylation (Lipton et al., 1993).

Another response of neurons to cell stress is the expression of heat-shock proteins, which protect against misfolding, conferring resistance to necrotic injury (Yenari et al., 1999). Neurons can also up-regulate and increase the activity of antioxidant agents following necrotic insults, which includes Mn- and Cu/Zn-SOD (Ohtsuki et al., 1993; Fukuhara et al., 1994; Matsuyama et al., 1994), glutathione peroxidase, and catalase (Goss et al., 1997).

Also, recent evidence has shown that synaptic activity can protect primary rat hippocampal neurons against mitochondrial

oxidative stress and mitochondrial dysfunction derived from acute excitotoxicity, since synaptic activity can induce the transcriptional repression of the mitochondrial calcium uniporter, leading to a reduction in excitotoxicity associated with mitochondrial calcium overload (Depp et al., 2018).

A BRIEF HISTORY OF ALS: AMYOTROPHIC LATERAL SCLEROSIS

Amyotrophic Lateral Sclerosis (ALS) is a fatal and progressive neurodegenerative disease, characterized by the degeneration of both upper (motor cortex) and lower (spinal cord) motor neurons that result in motor dysfunction and, ultimately, death. While primary symptoms of ALS are associated with motor dysfunction, other areas of the brain may undergo degeneration, with 40–60% of patients showing evidence of different levels of cognitive impairment (Witgert et al., 2010; Ferrari et al., 2011). Although 90% of ALS cases are sporadic with no known cause, in the 10% of familial cases, more than 30 genes have already been implicated (Chen et al., 2013), with mutations in Cu/Zn-SOD1, transactive response DNA-binding protein, fused in sarcoma, chromosome 9 open reading frame 72, and several others (Ajroud-Driss and Siddique, 2015).

Despite numerous studies demonstrating the involvement of several altered signaling pathways, the pathogenetic mechanisms behind ALS are still unclear. Indeed, it seems that, in ALS, neurodegeneration is the product of a combination of different concomitant mechanisms. Understanding the cause of motor neuron degeneration is critical for unraveling ALS pathogenesis and there are mainly two hypotheses to explain the origin of the disease (Kiernan et al., 2011). The first one is the dying-forward hypothesis, which proposes an anterograde degeneration of motor neurons *via* glutamate excitotoxicity from the cortex. The second one is the dying-back hypothesis, which suggests that ALS may start distally at the nerve terminal or the neuromuscular junction, progressing towards the cell body. Despite the numerous hypotheses proposed, alterations in excitatory neurotransmission appear to have a key role in disease progression, mediated by increased susceptibility to excitotoxicity, as schematically depicted in **Figure 3** (Bae et al., 2013). Physiological studies have demonstrated cortical hyperexcitability in patients with both sporadic and familial ALS before the onset of symptoms (Vucic and Kiernan, 2013). In addition to cortical hyperexcitability, peripheral axons also present changes in their excitability in ALS patients (Vucic and Kiernan, 2006). Changes in neuronal activity can also lead to morphological alterations. In the $SOD1^{G93A}$ mouse model, upper motor neurons display reductions in dendritic length and spine density, suggesting a homeostatic response to heightened pre-synaptic activity or even a stressed state of these neurons (Fogarty et al., 2016; Saba et al., 2016). It is however still unclear whether hyperexcitability is one of the causes of motor neuron degeneration or a compensatory mechanism resulting from motor neuron degeneration.

One of the first proposed mechanisms underpinning neurodegeneration in ALS was glutamate-mediated excitotoxicity (Bendotti and Carrì, 2004). One suggested way in which glutamate excitotoxicity may occur is through a decrease in the levels of the transporters responsible for the removal of glutamate from the synaptic cleft. In ALS, a likely trigger for neuroinflammation is the motor neuronal and astrocytic release of misfolded proteins, like aberrant SOD1, and other toxic molecules. This release stimulates the activation of microglia, unleashing pro-inflammatory and neurotoxic actions (Appel et al., 2011; Zhao et al., 2013; Brites and Vaz, 2014; Pinto et al., 2017), which dysregulate the communication between motor neurons and glial cells, compromising neuronal homeostasis. Microglia are considered the immune cells of the brain and may adopt different polarized activated phenotypes, with the M1 and M2 being the most accepted. The classical M1 phenotype is associated with the release of pro-inflammatory molecules and activation of receptors, and the M2 phenotype is related to the secretion of anti-inflammatory mediators and growth factors. However, recent studies point to the coexistence of different heterogeneous states and mixed phenotypes (Tang et al., 1990; Pinto et al., 2017). In ALS, microglia function changes along with disease progression, displaying the M2 anti-inflammatory phenotype at early stages and switching to the M1 activated subtype as the disease progresses (Zhao et al., 2013; Gravel et al., 2016). Activated microglia contribute and enhance motor neuron death, and can even acquire a distinct and impaired phenotype at the end-stage that accelerates disease progression (Nikodemova et al., 2014; Pinto et al., 2017). In addition to neuroinflammation, glial cells also play a role in glutamate-mediated excitotoxicity. Specifically, astrocyte-mediated downregulation of EAAT2, leading to a decrease in glutamate uptake and subsequent potentiation of excitotoxic effects, has been reported in both ALS patients and $SOD1^{G93A}$ mice (Howland et al., 2002), as well as in the TDP-43 rat model (Tong et al., 2013), correlating with regions of motor neuron loss (Sasaki et al., 2000). Thus, a decrease in the level of these transporters may lead to the accumulation of glutamate in the extracellular space, resulting in postsynaptic glutamate receptor overstimulation and consequent excitotoxic effects (Lin et al., 1998; Zarei et al., 2015). Furthermore, not only have astrocytes in ALS been reported to release lower levels of neurotrophic factors, but they have been shown to release neurotoxic factors that play a role in furthering neurodegeneration (Komine and Yamanaka, 2015; Cunha et al., 2018; Gomes et al., 2019). Moreover, it has been shown that, in ALS patients carrying *SOD1* gene mutations, there is a decrease in motor neuron levels of calcium-binding proteins, which—by decreasing calcium buffering in the cytoplasm—may exacerbate excitotoxicity (Bernard-Marissal et al., 2012; Mattson, 2013). In the $SOD1^{G93A}$ mouse model, overexpression of EAAT2 delays disease onset but not death (Guo et al., 2003) and fails to prevent loss of phrenic nerve motor neurons or rescue respiratory function (Li et al., 2015). Several pathways have been implicated in the modulation of EAAT2 levels, such as tumor necrosis factor-α (TNF-α) and downstream nuclear factor κ-B signaling (Boycott et al., 2008). Recently, membralin, an endoplasmic reticulum membrane protein, was also shown to have a role in EAAT2-mediated glutamate excitotoxicity in ALS. Membralin levels are reduced in human ALS spinal cord and $SOD1^{G93A}$

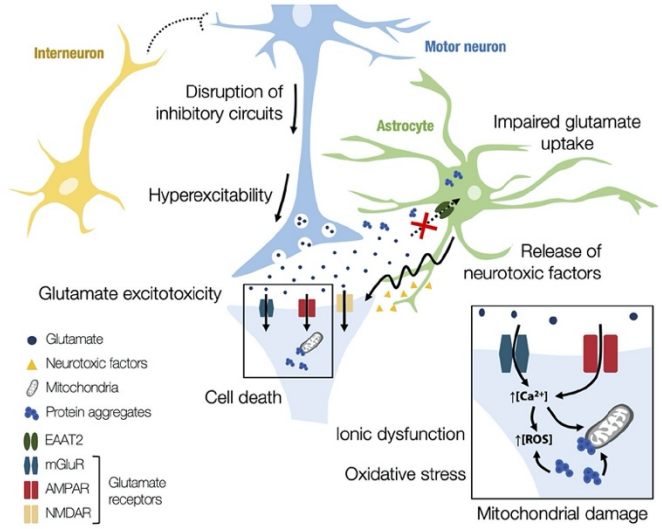


FIGURE 3 | Schematic representation of the alterations in excitatory neurotransmission in amyotrophic lateral sclerosis (ALS). Different pathophysiological mechanisms have been proposed to explain excitotoxicity in ALS. Interneuron alterations are observed in early disease stages, with a loss of cortical and spinal interneurons, leading to the disruption of inhibitory circuits. Consequently, there is an excitation–inhibition imbalance, increasing subsequent excitability and glutamate release to the synaptic cleft. Glutamate-mediated excitotoxicity may happen through an astrocyte-mediated downregulation of excitatory amino acid transporter 2 (EAAT2), which decreases the glutamate uptake from the synaptic cleft and potentiates the excitotoxic effects. Astrocytes in ALS also release neurotoxic factors that trigger changes to motor neuron glutamate receptors and render them susceptible to excitotoxicity, furthering neurodegeneration. Moreover, the excessive firing and the dysregulated calcium influx through atypical glutamate receptors results in an ionic dysfunction in motor neurons. The excessive entry of calcium into motor neurons results in mitochondrial overload and in the generation of reactive oxygen species (ROS), which ultimately causes oxidative stress. The presence of protein aggregates in mitochondria can also lead to alterations in normal cell metabolism, increasing the susceptibility to glutamatergic overstimulation as well as the activation of apoptotic pathways.

mouse models and its deletion suppresses EAAT2 expression through a TNF-α/TNF receptor 1/nuclear factor κ-B pathway. Overexpression of membralin in astrocytes was shown to increase EAAT2 expression and improve motor neuron survival (Jiang et al., 2019).

However, defects in the clearance of glutamate do not seem to be the only origin of excessive extracellular glutamate. In the SOD1^{G93A} mouse model, activation of Group I mGluR or the GABA/glycine heterotransporter abnormally increases the release of glutamate (Raiteri et al., 2003; Giribaldi et al., 2013; Milanese et al., 2015). Recently, Bonifacino and colleagues (Bonifacino et al., 2019) demonstrated that mGluR are overexpressed in the spinal cord of SOD1^{G93A} mice at pre-symptomatic stages and that their function is altered early on in the disease, suggesting that it can represent a cause rather than a consequence of disease progression. Group I mGluR may be potential targets for preventing excitotoxicity in ALS since it has been shown that treatment with an antagonist attenuated cell death, delayed the onset of motor symptoms, and slightly prolonged survival in SOD1^{G93A} mice (Rossi et al., 2008).

Moreover, calcium permeability of AMPAR is largely determined by the presence of the GluA2 subunit and it has been shown that mutant SOD1 astrocytes secrete factors that lower the expression of this subunit in motor neurons, consequently leading to AMPAR-mediated excitotoxicity and cell death (Van Damme et al., 2005, 2007). Moreover, fused in sarcoma-ALS astrocytes trigger changes to motor neuron AMPAR that render them susceptible to excitotoxicity (Kia et al., 2018) and patients with the chromosome 9 open reading frame 72 mutations appear to have increased vulnerability to AMPAR-mediated excitotoxicity (Selvaraj et al., 2018).

Besides glutamate-mediated excitotoxicity, excitotoxicity may arise from an altered regulation by interneurons. Interneurons are one of the main regulators of neuronal signaling and the majority in the cortex is inhibitory, using GABA or glycine as a neurotransmitter. In healthy individuals, a subthreshold stimulus of the motor cortex generally leads to the activation of

inhibitory GABAergic interneurons, thus reducing subsequent excitability, in a process called short intracortical inhibition (Wagle-Shukla et al., 2009). In ALS patients, however, cortical inhibition is impaired, with a reduced or complete absence of short intracortical inhibition. Importantly, the reduction of short intracortical inhibition was shown to be an adverse prognostic factor in ALS (Shibuya et al., 2016). Several post-mortem reports indicate a loss of cortical and spinal interneurons, in addition to motor neuron losses (Stephens et al., 2006). These observations are seen in different mouse models that also exhibit interneuron alterations in early disease stages. The wobbler mouse model displays hippocampal hyperexcitability, together with a reduced number of interneurons (Thielsen et al., 2013). Also, in the $SOD1^{G93A}$ mouse model, decreases in calretinin interneurons and subsequent increases in parvalbumin interneurons in motor and somatosensory cortex may be compensatory changes to improve excitation–inhibition balance (Chung et al., 2005; Minciacchi et al., 2009). In the spinal cord of the $SOD1^{G93A}$ mice, interneurons degenerate before the loss of motor neurons (Martin et al., 2007). Further studies on a mutant SOD1 zebrafish model revealed that interneurons are the first to exhibit neuronal stress and, once more, that the reduction of inhibitory currents or interneurons preceded any defects in motor neurons (McGown et al., 2013).

Another known mechanism involved in ALS neurodegeneration is oxidative stress. The major enzyme involved in the prevention of oxidative damage is the Cu/Zn-SOD1 enzyme. Congruently, mutations in the *SOD1* gene—resulting in either a decrease/loss or a dominant gain of function—have been found to contribute to cytotoxicity. In line with this, a study demonstrated that the cerebrospinal fluid, serum, and urine samples of ALS patients had increased levels of free radicals and concomitant oxidative stress (Zarei et al., 2015). Another source of oxidative damage in mitochondrial dysfunction. The existence of alterations is normal cell metabolism due to misfolded mutant SOD1 deposits in mitochondria has been reported in both ALS patients and mouse models. Furthermore, dysfunctions in energy, alterations in the triggering of apoptotic signals, disruptions in mitochondrial transport along axons, and atypical production of ATP and ROS have been also associated with ALS (Pasinelli et al., 2000; Mattiazzi et al., 2002; Menzies et al., 2002; Damiano et al., 2006). Moreover, the presence of mutant SOD1 in mitochondria can lead to an increase of the motor neurons sensitization to glutamatergic (over)-stimulation and therefore to excitotoxicity. Also, the inflammation and associated microglial activation, both hallmarks of ALS, may contribute to increasing the motor neurons' susceptibility to excitotoxicity.

THE OLD MAN AND THE ALZHEIMER'S DISEASE

Alzheimer's Disease (AD) is an age-dependent neurodegenerative disease, considered the most common form of dementia worldwide (Alzheimer's Association, 2009). AD is firstly manifested by the loss of episodic memory and later loss of executive functions like language, attention, and reasoning (LaFerla et al., 2007). AD is commonly characterized by the presence of senile plaques, large extracellular aggregates of fibrillary amyloid-β peptide (Aβ), originated by the abnormal cleavage of amyloid precursor protein where the sequential cleavage of amyloid precursor protein by β- and γ-secretase produces the neurotoxic Aβ peptide (Scheuner et al., 1996; Ertekin-Taner, 2007). The presence of intracellular neurofibrillary tangles of hyperphosphorylated tau protein is also a characteristic of AD (Grundke-Iqbal et al., 1986; Ferrer, 2012). Many pieces of evidence suggest that $A\beta_{1-42}$ oligomers are the most toxic Aβ species, exerting their pathological actions by disrupting glutamatergic transmission, mainly by acting on NMDAR and mGluR (Walsh et al., 2002). Aβ can also increase glutamate release from both neurons (Brito-Moreira et al., 2011) and astrocytes (Talantova et al., 2013), resulting in abnormally high extracellular glutamate levels capable of activating eNMDAR and, thus, leading to the activation of pro-death pathways and consequent excitotoxicity. Hence, the harmful effects of Aβ in AD may be mediated by the excessive activation of eNMDAR containing predominantly GluN2B subunits (Li et al., 2011). Also, it has been demonstrated that the presence of Aβ can induce a sustained calcium influx *via* NMDAR (Texidó et al., 2011), which can trigger a cascade of events leading to mitochondrial and synaptic dysfunction, excitotoxicity, production of ROS, and neuronal death (Ferreira et al., 2012), as depicted in **Figure 4**.

An imbalance between sNMDAR and eNMDAR activity was observed in brain samples from AD patients, which can contribute to the Aβ-triggered neurotoxicity observed in this disease. In parallel, it is also known that stimulation of eNMDAR plays a critical role in AD. Recent studies performed in rat acute hippocampal slices under Aβ exposure and in Aβ-injected mice support the idea that enhancement of sNMDAR activity, together with the inhibition of eNMDAR, has protective effects against Aβ-induced neurotoxicity (Huang et al., 2017). eNMDAR stimulation is also associated with the inactivation of extracellular signal-regulated kinase/mitogen-activated protein kinase signaling (Mulholland et al., 2008), which is crucial for memory consolidation and synaptic plasticity, suggesting that eNMDAR activation leads to the impairment of the molecular mechanisms underlying memory and learning processes (Schafe et al., 2000). In the presence of Aβ, the exacerbated calcium influx *via* eNMDAR is also associated with excessive activation of calpains, which are calcium-dependent proteases involved in multiple cellular functions, including proliferation, differentiation, and modulation of synaptic function (Wu and Lynch, 2006). The overactivation of calpains in AD is associated with functional changes in several proteins involved in neuronal transmission, such as BDNF. Previous reports have shown that Aβ impairs BDNF function in a calpain-dependent manner (Jerónimo-Santos et al., 2015), whereas inhibition of eNMDAR can prevent Aβ-triggered impairment of BDNF action in long-term synaptic potentiation (Tanqueiro et al., 2018).

Under physiological conditions, mitochondrial calcium signaling stimulates oxidative phosphorylation and ATP synthesis. In AD, as a consequence of the exacerbated calcium

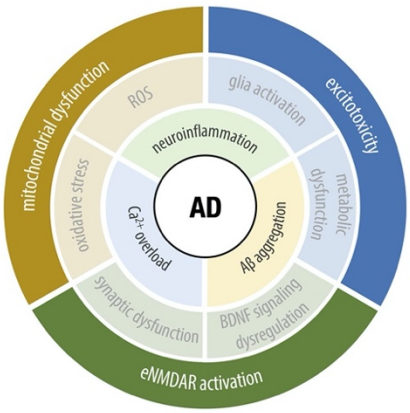


FIGURE 4 | Underlying cellular mechanisms of Alzheimer's disease (AD). The upstream key hallmarks of AD range from ionic dysfunction to the impairment of several cellular processes, including Ca^{2+}-signaling dysregulation, abnormal Aβ production and aggregation and neuroinflammation. The crosstalk between the mentioned factors, leads to the pathological phenotype, involving mitochondrial dysfunction, excitotoxicity, and extrasynaptic NMDA receptor (eNMDAR) activation. As the symptomatic circle closes, the dysfunction of one leads to further activation of the others, altogether contributing to neurodegeneration and cognitive deficits, characteristics of the disease.

levels derived from eNMDAR activation, mitochondria form a non-specific pore in their internal membrane, termed mitochondrial permeability transition pore (Leung et al., 2008). With the pore opening, protons can cross this membrane, leading to the loss of mitochondrial membrane potential and dysregulation of pH gradient. Consequently, this affects ATP synthesis by oxidative phosphorylation, resulting in ionic and metabolic impairment, inevitably leading to cell death. Moreover, this decrease in mitochondrial bioenergetic capacity and consequent impairment of oxidative phosphorylation is associated with free radical production and subsequent oxidative damage. There are evidences of cyclophilin D (CypD), an integral part of the mitochondrial permeability transition pore (Leung et al., 2008), playing a critical role in Aβ-induced mitochondrial and synaptic injury (Du et al., 2008, 2011). Neuronal CypD is linked to Aβ-mediated ROS production, whereas CypD-deficient neurons appear to be resistant to Aβ-mediated inactivation of protein kinase A/CREB signaling, thus revealing that the absence of CypD can prevent Aβ-induced mitochondrial and synaptic dysfunction (Du et al., 2014). Additionally, mitochondrial dysfunction in AD includes respiration deficits, increased generation and accumulation of free radicals, and impaired energy metabolism (Hensley et al., 1994; Manczak et al., 2006; Yao et al., 2009; Calkins et al., 2011). Changes in mitochondrial dynamics, including decreased transport, increased fission, and, eventually, loss of mitochondrial function, are also observed in AD (Hensley et al., 1994; Manczak et al., 2006; Yao et al., 2009; Calkins et al., 2011).

Dysfunctional mitochondria are considered the main generator of ROS and consequent oxidative stress in AD, where oxidative stress can alter protein kinase A/CREB signaling, a signaling pathway necessary for neuronal survival (Wang et al., 2014). Indeed, several reports indicate that alterations in brain glucose metabolism in AD patients contribute to synaptic dysfunction and neuronal loss (Kennedy et al., 1995; Ishii et al., 1997). ROS, as well as reactive nitrogen species, are associated with the formation of protein carbonyls and 3-nitrotyrosine, which correlates with the level of protein oxidation within a cell. The determination of protein carbonyls levels and tyrosine nitration is considered viable measures of oxidative damage, where tyrosine nitration is one specific form of protein oxidation that is associated with AD (Castegna et al., 2003), which culminates in the loss of protein function, cellular dysfunction and, ultimately, cell death (Butterfield and Stadtman, 1997; Butterfield et al., 2006).

In AD, glial cell activation and consequent pro-inflammatory response is associated with an increased expression of NOS, an enzyme responsible for NO production. Indeed, inducible NOS, one of the NOS isoforms, has been found in activated astrocytes and microglia, suggesting a critical role of this enzyme in pathological conditions (Diaz et al., 2011). Also, inducible NOS has been described as the main culprit behind the NO increase to neurotoxic levels, whereas its inhibition was found to be a useful target for neuronal protection against Aβ-mediated toxicity (Diaz et al., 2011). Furthermore, a recent report found that, in adult rats injected with $A\beta_{25-35}$, a neurotoxic Aβ fragment, there is an increase in inducible NOS expression and consequent upsurge of NO levels, which was prevented by the administration of a highly selective cannabinoid receptor 1 agonist, ACEA (Patricio-Martínez et al., 2019). Additionally, animals injected with ACEA and $A\beta_{25-35}$ presented an improvement in learning and memory when compared with animals injected with $A\beta_{25-35}$ alone (Patricio-Martínez et al., 2019), suggesting the involvement of the cannabinoid receptor 1 in neuroprotective mechanisms in AD.

Growing evidence has identified reactive astrocytes as a key player in glutamate-mediated excitotoxicity, since astrogliosis results in the loss of astrocytic physiological function and consequent impairment of neuronal synaptic transmission. This phenomenon is common in AD, where Aβ induces functional, morphological, and metabolic astrocytic dysfunction (Angelova and Abramov, 2014; Brawek and Garaschuk, 2014). Specifically, a downregulation of astrocytic glutamate transporters has been shown in both animal models and AD human brain samples, impairing glutamate uptake and causing excitatory overload in the synaptic cleft. Moreover, in astrocytic cell culture, Aβ reduces the expression of GLT-1 through a mechanism that involves the calcineurin/nuclear factor of activated T cells pathway (Abdul et al., 2009) and oxidative stress (Scimemi et al., 2013). This reduction of GLT-1 expression in astrocytes results in increased glutamate levels at the synapse, which, by acting on eNMDAR, contributes to the progression of AD pathology in

the human brain (Simpson et al., 2010). Additionally, a study performed in postmortem human samples suggests that the preservation of GLT-1 expression in reactive astrocytes could act as a neuroprotective mechanism against AD neuropathological changes (Kobayashi et al., 2018).

Astrocytic glutamate uptake is not only essential for synaptic glutamate clearance, but also the activation of the astrocytic glycolysis cycle. The impaired glutamate uptake will then lead to glycolysis deficiency. In this scenario, neurons not only suffer the consequences of the excessive extracellular glutamate but also of metabolic insufficiency as the astrocytes fail to fulfill the necessary energetic needs. In the hippocampus, glycogen-derived lactate is responsible for memory formation and long-term synaptic potentiation (Newman et al., 2011). Inhibition of lactate production and neuronal delivery weakens synaptic plasticity and memory formation, by impairment of the Krebs cycle and cell signaling dysregulation (Barros, 2013; Schurr, 2014; Dienel, 2017). Indeed, when Long-Evans rats with induced astrocytic metabolic impairment were treated with downstream glycolytic metabolites, such as pyruvate or β-hydroxybutyrate, memory improvement and consolidation were observed (Descalzi et al., 2019). This may suggest that astrocytic metabolic impairment is responsible for memory loss and cognitive impairment, even in the premature stages of AD (Merlini et al., 2011).

Metabolic dysfunction is a very early sign of disease onset. Some studies suggest that glucose hypometabolism is a hallmark of AD that can be detected long before any significant Aβ plaques and neurofibrillary tangles (Mosconi et al., 2009; Chen and Zhong, 2013). As the first aggregates occur with concomitant astrocytic dysfunction, signaling for glycolysis starts to drop and leads to the onset of energetic failure, causing metabolic starvation and consequent excitotoxicity. So far, it has been difficult to determine the causal relationship between astrocytic glutamate uptake dysregulation and metabolic disturbance. Nevertheless, the contribution of the metabolic processes in the pathological excitotoxicity is undeniable.

The role of neuroinflammation in the chemically induced AD animal models has been proven significant for the neurodegenerative profile and assumed to be a crucial factor in disease progression (Liu and Hong, 2003; Reynolds et al., 2007; Taylor et al., 2013). In the early stages of AD, activated microglia express both neurodegenerative (M1) and neuroprotective (M2) phenotypes (Edwards et al., 2006). The M2 phenotype exhibits a great capacity for Aβ and tau protein aggregates clearance through phagocytosis. During disease progression, however, the M2 phenotype appears to undergo polarization into an M1 phenotype, resulting in the overproduction of neurotoxic factors. Indeed, in all stages of AD, significant aggregation of M1 microglia has been observed surrounding neurofibrillary tangles (Sheffield et al., 2000; Yao and Zu, 2020). M1 microglia not only release neurotoxic factors but have also been shown to downregulate or even block neuroprotective mechanisms involved in phagocytosis of Aβ (Yamamoto et al., 2008). This inhibition is mainly due to the impairment of the Aβ receptor complex, complement receptor 3, and insulin-degrading enzyme expression (Koenigsknecht-Talboo and Landreth, 2005). Among neurotoxic factors released by microglia, microglial glutamate release can stimulate excitotoxicity (Barger et al., 2007), while the release of pro-inflammatory cytokines such as interferon γ and TNFα impair the uptake and internal degradation of extracellular glutamate (Hu et al., 2000; Yamamoto et al., 2008). In AD, reactive astrocytes are also able to release pro-inflammatory cytokines, such as, TNFα and interleukin 1-β, which, while not directly cytotoxic, can impair astrocytic glutamate uptake and to enhance NMDAR-induced calcium release, contributing to AD progression. Moreover, it is known that inhibitors of these inflammatory mediators attenuate both synaptic and cognitive deficits in Aβ-treated mice, suggesting that these inflammatory responses mediated by astrocytes have negative effects upon synaptic plasticity mechanisms (Ralay Ranaivo et al., 2006).

Though not often discussed, the cystine-glutamate (Xc-) antiporter system is essential for cysteine homeostasis and considered only a secondary mechanism in the glutamate release and uptake. However, its contribution to pathological states such as glutamate excitotoxicity should not be ignored. The Xc- antiporter system is highly expressed in microglia and astrocytes. It is a sodium-independent anionic amino acid transporter with high specificity for negative species of cysteine and glutamate (Sato et al., 2002). It is also electroneutral, instead of electrogenic as most common EAAT systems (Lo et al., 2008). This antiporter is a heterodimer (Lutgen et al., 2014), composed of heavy 4F2 chain and a specific light chain, named xCT, linked by a disulfide bridge (Lewerenz et al., 2012). It uptakes cystine in exchange for releasing glutamate in the molar ratio 1:1 (Sato et al., 1999). Although less discussed, the Xc- system significantly increases extracellular and, more specifically, synaptic levels of glutamate, releasing up to 60% of all extracellular glutamate in the striatum (Baker et al., 2002). This antiporter can release up to 0.6 μM/s of glutamate into the extracellular space (Warr et al., 1999), which is then uptaken by GLT-1 (Baker et al., 2002; Bridges et al., 2012). Depending on the influx and overall capacity to uptake glutamate, this release can either activate or desensitize the NMDAR (Warr et al., 1999). The cystine-glutamate antiporter was reported to exhibit neuroprotective effects in neurodegenerative diseases, as it is linked to the production of glutathione and the rise of antioxidant cellular capacity (Bridges et al., 2012). This protective effect is observed in AD models, where the Xc- system uptakes cystine, showing great potential at lowering Aβ-induced toxicity, oxidative stress, and later apoptosis. However, when activated either by oxidative stress, TNF-α, or amyloid precursor protein, this antiporter can release cytotoxic amounts of glutamate (Barger and Basile, 2001; Sato et al., 2001). Not only is this antiporter involved in the release of glutamate, contributing to excitotoxicity, but it has also been shown to block microglial neuroprotective functions in AD. Indeed, activated microglia in both AD patients and in AD mouse models show an increased expression of this antiporter and, specifically, the xCT protein (Bridges et al., 2012). In mice, transgenic depletion of the *Slca11* gene ($xCT^{-/-}$ mice) impaired microglial polarization into the neurotoxic phenotype and reduced up to 70% pathological glutamate release in cultured microglial cells (Mesci et al., 2015). Upon blockade of either NMDAR or the Xc- system, microglia act in a neuroprotective way when exposed to Aβ and attenuate neuronal

death. However, when neurons were cultured with microglia depleted of lipid-associated apolipoprotein E expression, the neuroprotective phenotype was lost (Qin et al., 2006), implying that the neuroprotective phenotype of microglia in AD is related to apolipoprotein E. In neuron-microglia co-cultures, the activation of the Xc- system by the Aβ deposits not only exacerbates excitotoxicity, but also lowers the neuronal threshold for glutamate toxicity, allowing non-toxic concentrations of glutamate to exert excitotoxic actions (Qin et al., 2006). Although very sparse in current literature, the neuroprotective role of the Xc- system *in vivo* showed similar effects, where the activation of microglial cells by Aβ can cause both phenotypes, the neurotoxic being mostly related to glutamate release and increased neuronal susceptibility to excitotoxicity, and the neuroprotective related to expression of apolipoprotein E and glutathione (Bannai and Tateishi, 1986; Qin et al., 2006; Shih et al., 2006).

As stated before, another AD hallmark is hypoglycemia. Removal of glucose in mixed astrocyte-neuron cell cultures leads to a glycemic neuronal injury and death (Thorn et al., 2015). However, the neuronal death observed in glucose deprivation conditions is not connected to energy failure but most likely tied to glutamate accumulation in the synaptic cleft (Jackman et al., 2012). Astrocytes express significant levels of the cystine-glutamate antiporter and are also the main metabolic factories and energy suppliers for neurons. As these processes are tightly linked, the dysfunction of one is likely to mediate the function of the other system, for the benefit or damage. Upon glucose deprivation in cultured astrocytes, xCT protein expression rose in a time-dependent matter (Thorn et al., 2015).

In the triple transgenic AD mouse model (3xTg-AD), astrocytic glutamine synthetase expression was found to be decreased in the hippocampus, suggesting a critical role of astrocytes in AD-related disruption of glutamate homeostasis, which may affect the efficiency of glutamatergic transmission, contributing to the cognitive deficits of the disease (Olabarria et al., 2011). Also, it is known that glutamine synthetase activity is sensitive to oxidation and may be impaired by oxidative stress in AD (Smith et al., 1991; Hensley et al., 1994, 1995).

In the 3xTg-AD mouse model, Aβ near to astrocytes leads to the extrasynaptic release of glutamate and consequent eNMDAR activation (Talantova et al., 2013), which contributes to synaptic dysfunction and neuronal death. Furthermore, there are also evidences that eNMDAR activity can trigger the generation of toxic Aβ (Talantova et al., 2013), which suggests a key role of eNMDAR and astrocytic glutamate release in mediating Aβ neurotoxicity.

As mentioned before, astrocytes are responsible for the supply of D-serine to neurons (Henneberger et al., 2010). Indeed, recent evidences reveal that serine racemase, the enzyme responsible for D-serine synthesis is strongly expressed in reactive astrocytes in both human AD samples and AD rat models (Balu et al., 2019). Moreover, changes in intracellular signaling cascades, consistent with excitotoxicity and decreased neuronal survival were found (Balu et al., 2019). Hence, these findings support a model where D-serine released from reactive astrocytes could bind to extrasynaptic GluN2B-containing NMDAR, triggering the activation of excitotoxic signaling pathways and consequent neuronal damage and death. It has however been shown that, in AD-like conditions, the selective blockade of eNMDAR together with the administration of a D-serine-like NMDAR co-agonist significantly improved spatial and related forms of learning and memory (Huang et al., 2017). Moreover, there are evidences that blocking eNMDAR provides neuroprotection against Aβ-triggered deficits, together with the enhancement of sNMDAR activity (Huang et al., 2017). In conclusion, while it is known that D-serine is mainly a co-agonist of sNMDAR, the role of D-serine as a mediator of neuronal excitotoxicity cannot be excluded.

In line with what was described above, many studies support the active involvement of glial cells, in particular astrocytes, in early stages of AD pathogenesis, where Aβ can dysregulate astrocytic calcium signaling both *in vitro* and *in vivo* (Haughey and Mattson, 2003; Kuchibhotla et al., 2009), which can result in the excessive release of glutamate and other gliotransmitters, enhancing extrasynaptic glutamatergic signaling and consequent excitotoxicity in AD, as summarized in **Figure 5**.

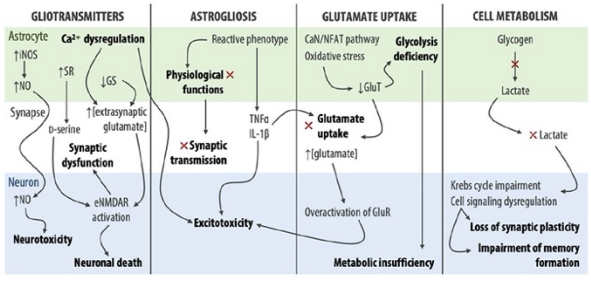


FIGURE 5 | Aβ-induced astrocytic dysfunctions leading to excitotoxicity and AD pathogenesis. iNOS, inducible nitric oxide synthase; NO, nitric oxide; SR, serine racemase; GS, glutamine synthetase; CaN/NFAT—calcineurin/nuclear factor of activated T cells; GluT, glutamate transporters; GluR, glutamate receptors.

THE PHANTOM OF THE BRAIN: EPILEPSY

Epilepsy is one of the most common neurological disorders, estimated to affect more than 70 million people worldwide (Singh and Trevick, 2016). Epilepsy can be regarded as a family of disorders which comprise several diseases and conditions and can be defined by: (i) the unprovoked occurrence of at least two seizures more than 24 h apart; (ii) one unprovoked seizure and further seizure probability of at least 60%; or (iii) diagnosis of an epilepsy syndrome. There are multiple types of seizures, which are characterized in accordance with their onset, physical manifestation, and level of consciousness, differing in the corresponding pathophysiological mechanisms (Fisher et al., 2017). Nevertheless, all epileptic seizures involve persistent changes in synaptic events such as neurotransmitter release, and receptor and transporter activity, and are underpinned by an abnormal excessive or synchronous neuronal firing activity, typically resulting from an imbalance between excitatory and inhibitory processes mediated by the neurotransmitters glutamate and GABA, respectively. Excessive neuronal firing is accompanied by increased extracellular levels of glutamate, leading to excitotoxicity (Soukupová et al., 2014), one of the primary sources of neuronal damage in epilepsy. The processes by which excitotoxicity results in neuronal damage and/or death have previously been described and, in this section, we will focus on the underlying pathophysiological mechanisms of different types of epilepsy and how they correlate with excitotoxicity. The main findings discussed here are summarized in **Figure 6**.

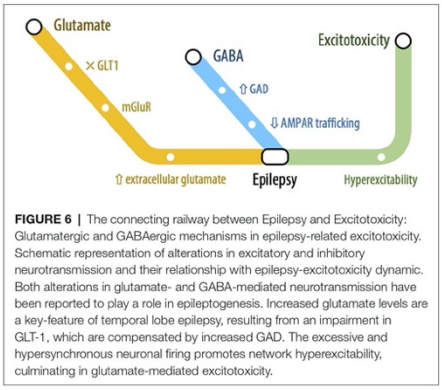


FIGURE 6 | The connecting railway between Epilepsy and Excitotoxicity: Glutamatergic and GABAergic mechanisms in epilepsy-related excitotoxicity. Schematic representation of alterations in excitatory and inhibitory neurotransmission and their relationship with epilepsy-excitotoxicity dynamic. Both alterations in glutamate- and GABA-mediated neurotransmission have been reported to play a role in epileptogenesis. Increased glutamate levels are a key-feature of temporal lobe epilepsy, resulting from an impairment in GLT-1, which are compensated by increased GAD. The excessive and hypersynchronous neuronal firing promotes network hyperexcitability, culminating in glutamate-mediated excitotoxicity.

Temporal Side Story: Temporal Lobe Epilepsy

Temporal lobe epilepsy (TLE) is the most common form of epilepsy, affecting up to 40 million people worldwide (Hubbard et al., 2016; Peterson and Binder, 2019). TLE is characterized by the occurrence of focal seizures that may impair individuals and is often associated with treatment resistance, where approximately 30% of patients taking antiepileptic drugs present drug resistance that prevents them from living seizure-free (Sarac et al., 2009; Hubbard et al., 2016; Peterson and Binder, 2019).

The increase in local excitation and cytotoxicity in the epileptogenic focus of TLE is linked to an increase in extracellular glutamate levels (Proper et al., 2002; Sarac et al., 2009; Albrecht and Zielinska, 2017). Changes in glutamate levels have been reported in the hippocampus of epileptic patients before, during, and after seizures, which may occur due to increased glutamate release or its impaired reuptake (Proper et al., 2002; Hoogland et al., 2004; Hubbard et al., 2016).

As mentioned before, glutamate uptake is a major determinant of extracellular glutamate levels and evidence shows that the alteration of glutamate concentrations in epilepsy may result from aberrant EAAT expression or function (Crino et al., 2002; Proper et al., 2002). Indeed, an increase in EAAT3 expression in the hippocampus of both patients and animal models with TLE has been observed (Crino et al., 2002). This enhanced expression may lead to the increased glutamate release during seizures by increasing intracellular glutamate, which will be stored in vesicles and synaptically released by the classical calcium-dependent pathway (During and Spencer, 1993; Crino et al., 2002). Another mechanism by which increased glutamate release may occur is EAAT3 reversal due to the alteration of cellular excitability promoted during epileptogenesis (Rossi et al., 2000). However, the increase in EAAT3 expression may be a compensatory mechanism, leading to the improvement of GABAergic inhibitory transmission, as shown in the granular cells of the dentate gyrus of TLE animal models, which had increased glutamate decarboxylase expression and GABA release (Sloviter et al., 1996; Crino et al., 2002).

Additionally, reactive astrocytes with morphological and functional alterations may be important in epileptogenesis since they contribute to the increase of neuronal excitability. In TLE, this astrocyte-induced excitotoxicity occurs by dysregulation of glutamate astrocytic transporters (EAAT1 or GLAST and EAAT2 or GLT-1), which are responsible for maintaining extracellular glutamate homeostasis (Hubbard et al., 2016; Peterson and Binder, 2019). Different studies have shown that there is a reduction in EAAT1 and EAAT2 expression in the sclerotic hippocampus of TLE patients at RNA or protein levels (Proper et al., 2002; Rakhade and Loeb, 2008). Furthermore, modifications in GLT-1 function and expression contribute to TLE hyperexcitability and seizure generation (Hubbard et al., 2016; Peterson and Binder, 2019). Different studies have already shown that knockout animal models for GLT-1 exhibit severe spontaneous seizures that can lead to early postnatal death (Tanaka et al., 1997; Hubbard et al., 2016; Peterson and Binder, 2019), and that GLT-1 overexpression may generate pilocarpine-induced epileptogenesis resistant mice (Kong et al., 2012; Sha et al., 2017). In fact, in the intrahippocampal kainic acid mouse model of TLE, a down-regulation of hippocampal astrocytic GLT-1 has been reported, coinciding with the increased excitability (Peterson and Binder, 2019). Also, there seems to be a temporal regulation of GLT-1 expression during epileptic

seizures, with an increase in GLT-1 levels 1–4 days after seizure and a reduction 4–7 days after a seizure (Hubbard et al., 2016; Peterson and Binder, 2019). This difference in GLT-1 expression after epileptic seizures can arise from changes in the membrane anchor and trafficking system, since, upon glutamate release, GLT-1 can be trafficked to synaptic and non-synaptic regions to ensure glutamate clearance (Murphy-Royal et al., 2015). Different drugs can ameliorate epilepsy intensity by targeting GLT-1. Among these drugs, antibiotics such as β-lactam and ceftriaxone show antiepileptic effects and can increase GLT-1 levels (Rothstein et al., 2005; Zeng et al., 2010), and, in a pilocarpine-induced TLE model, a GLT-1 activator was able to promote an increase in GLT-1 expression and reduction of spontaneous seizures frequency by 50% (Kong et al., 2014; Sha et al., 2017). However, GLT-1 internalization and degradation are still observed, suggesting that these are the causes of GLT-1 deficiency and the limiting factors for the use of these drugs in the treatment of TLE (Susarla and Robinson, 2008). Thus, some studies have shown that besides increasing GLT-1 expression, it would be necessary to use inhibitors of proteins responsible for its degradation. Studies have been performed with a Hsp90B inhibitor (17AAG), which is one of the proteins that recruit GLT-1 for degradation (Whitesell and Lindquist, 2005). Not only was this drug able to increase GLT-1 expression, it also maintained GLT-1 protein levels more effectively than ceftriaxone and exhibited a remarkable seizure suppression effect in the TLE model (Sha et al., 2017).

Besides glutamate homeostasis, astrocytes can also modulate water flow and potassium homeostasis in the extracellular space (Devinsky et al., 2013). Potassium concentration is regulated by astrocytes through its uptake by the sodium/potassium ATPase, sodium/potassium/chloride cotransporters, and input rectifier channels for potassium (Kir 4.1; Ransom et al., 2000; D'Ambrosio et al., 2002; Kofuji and Newman, 2004; Nikolic et al., 2019). Increased potassium concentration in the extracellular space can generate sustained neuronal depolarization and neuronal hyperexcitability (Walz, 2000; Devinsky et al., 2013; Nikolic et al., 2019), and evidence in the literature suggests an association between the uncontrolled increase of extracellular potassium levels and epilepsy, both in humans and in animal models (Steinhäuser et al., 2016).

In recent years, studies have shown an association between the glial water channel aquaporin-4 (AQP4) and Kir 4.1, forming an astrocytic protein complex responsible for removing potassium from the extracellular space, being an important mechanism in establishing a hyperpolarized neuronal membrane potential which may play an important role in epilepsy (Aronica et al., 2000; Das et al., 2012; Devinsky et al., 2013). Indeed, reduced expression of Kir 4.1 has been described in the hippocampus of patients with TLE (Das et al., 2012), where astrocytes showed deficits in potassium and glutamate uptake similar to those found in Kir 4.1 knockout animal models (Djukic et al., 2007; Chever et al., 2010; Nikolic et al., 2019). Furthermore, AQP4 knockout animals are also more susceptible to seizures and epilepsy (Dudek and Rogawski, 2005; Devinsky et al., 2013) and, in kainate-induced epileptic animal models, a reduction in AQP4 expression was also reported (Lee et al., 2012; Devinsky et al., 2013). Similarly, patients with TLE who have hippocampal sclerosis show a decrease or loss of AQP4 expression, suggesting the involvement of these channels in early epileptogenesis (Amiry-Moghaddam et al., 2003; Eid et al., 2005; Seifert et al., 2010). Taken together, these findings show that, in addition to the glutamate transporters, the control of potassium homeostasis and water flow is involved in neuronal excitability and TLE, even though further studies are needed to better elucidate their underlying mechanisms for controlling neuronal excitability.

Not only is ion homeostasis, such as sodium and potassium, altered in various forms of epilepsy, but cell metabolism has also been shown to be deeply affected in the epileptic brain. For instance, it is well known that there is a high energy demand during seizures, accompanied by high glucose consumption by neural networks. However, cerebral glucose hypometabolism is a feature of interictal phases in different forms of epilepsy, in regions that encompass but are generally larger than the region of seizure onset (Goffin et al., 2008; Pittau et al., 2014). The exact mechanisms underpinning such alterations are not clear, but mitochondrial dysfunction, linked with deficient glycolysis, remains a plausible hypothesis. Indeed, glutamate is known to promote astrocytic glycolysis (Bittner et al., 2011; Yan et al., 2017), a process in which glucose is converted into lactate. In epilepsy, where extracellular glutamate levels are increased, this process is most likely heightened when in comparison with control conditions. Thus, this results in a rapid depletion of glucose and a quick increase in lactate levels, indicating that, following seizure activity, in which there is a high consumption of glucose, neurons likely rely mostly on astrocyte-derived lactate. The lactate surplus is released into the extracellular space, creating a gradient between astrocytes and neurons (Mächler et al., 2016). Accompanying these alterations, the expression of astroglial monocarboxylate transporters, which lead to an efflux of monocarboxylates in astrocytes, has been reported to be increased in animal models of TLE (Liu et al., 2014), further suggesting that this astroglial-neuronal metabolic coupling pathway is affected in epilepsy. This pathway is vital for several brain functions, including for long-term memory formation (Suzuki et al., 2011), which might indicate a compromise of several neural functions, as a consequence of disrupted energy homeostasis. Due to the accumulating evidence of metabolic disruption in epilepsy, treatment strategies targetting cell metabolism have been gaining more attention, including the revival of the ketogenic diet (Walczyk and Wick, 2017). Pyruvate has been proposed as a possible treatment for epilepsy on account of being an anaplerotic mitochondrial fuel and because of its protective features, including acting as a potent ROS scavenger and normalizing cytosolic redox state. This molecule also facilitates brain-to-blood glutamate flux, preventing neuronal excitability (Popova et al., 2017). Finally, since blood glutamate can be converted into 2-ketoglutarate in the presence of pyruvate, mediated by glutamate-pyruvate transaminase (Gottlieb et al., 2003), treatment with pyruvate can be a protective measure against excitotoxicity (Carvalho et al., 2011).

In addition to alterations in cell metabolism in epilepsy, which include the hypermetabolism and hypometabolism during ictal and interictal phases, respectively, intracellular ATP levels are

also affected. Indeed, depletion of intracellular ATP has been reported in seizures (Wasterlain et al., 2010), and considering that the major source of ATP in the mitochondria, the possibility of mitochondrial dysfunction in epilepsy has gained considerable attention. While it is known that mitochondrial dysfunction is involved in seizure-related neuronal death (Kovac et al., 2013), it has also been associated with increased ROS and NO production during seizures (Frantseva et al., 2000; Jarrett et al., 2008), which is related with the activation of glutamate receptors and depolarization of the mitochondrial membrane. As the major sources of ATP are glycolysis and mitochondrial respiration, alterations in the rate of these processes in epilepsy will also impact ATP production which, reciprocally, influences mitochondrial activity. Mitochondrial dysfunction has been profoundly linked with neuronal damage and death (Rose et al., 2017), and this organelle is particularly relevant for calcium homeostasis. Mitochondria serve as a key regulator of cytosolic calcium, *via* the mitochondrial calcium uniporter and, in its turn, the influx of calcium into the mitochondria can activate the respiratory chain as well as promote the production of ATP. During seizure activity, in which neurons are exposed to high concentrations of glutamate, the subsequent activation of NMDAR induces calcium oscillations and a subsequent depolarization of the mitochondrial membrane (Kovac et al., 2012), which can be a trigger for neuronal death (Vergun et al., 1999). In rats where epileptic status was induced by L-allylglycine and bicuculline, the influx of calcium into neurons led to mitochondrial calcium overload, resulting in cell death (Griffiths et al., 1983; De Stefani et al., 2011). This issue has been overcome in the pilocarpine model of epilepsy by the inhibition of the mitochondrial calcium uniporter system, which decreased neuronal death, suggesting this system plays a role in seizure activity (Wang et al., 2015). Also, increasing ATP production by providing a substrate such as a pyruvate has been demonstrated to prevent neuronal death (Kovac et al., 2012). It should be noted that not only mitochondrial alterations can be observed but also in the endoplasmic reticulum, another intracellular pool of calcium. Indeed, debilitation of endoplasmic reticulum calcium with thapsigargin results in decreased neuronal excitation triggered by bicuculline in cultures (Sokal et al., 2000) as well as in slices, where (RS)-3,5-dihydroxyphenylglycine and pilocarpine-induced ictal discharges were shown to be dependent on the endoplasmic reticulum calcium pool (Rutecki et al., 2002). Although very few studies have focused on the contribution of endoplasmic reticulum calcium stores toward seizure activity, it has been demonstrated that depleting intracellular endoplasmic reticulum calcium stores can counteract neuronal excitability (Sokal et al., 2000).

Another major consequence of intracellular calcium accumulation and mitochondrial dysregulation is the exacerbated production of ROS, which is an essential mechanism in excitotoxicity-induced neuronal injury (Patel et al., 1996). Indeed, oxidative stress has been implicated in both immediate and later excitotoxic neuronal damage and increased ROS production has been reported in the ictal and interictal phases of epilepsy (Liang et al., 2000). Furthermore, this increase is also known to inhibit mitochondrial complex 1 activity and decrease mitochondrial membrane potential (Ryan et al., 2012; Rowley et al., 2015).

Additionally, calcium influx also leads to NOS activation and consequent NO overproduction, which is known to be increased in the cerebral cortex of rodents and epilepsy patients (Mülsch et al., 1994; González-Hernández et al., 2000) and has been suggested to contribute to seizure-induced neuronal death. It has also been demonstrated that NO-mediated activation of the type 1 ryanodine receptor is crucial for seizure-induced neuronal death and that antagonists of this receptor have a neuroprotective effect, emerging as suitable candidates for ameliorating conditions following seizures (Mikami et al., 2016). Supporting this fact, it has been described that non-selectively blocking NOS can potentiate rubidium chloride anti-convulsive effects (Rahimi et al., 2019). Thus, given the onset of metabolic and mitochondrial alterations as a consequence of excitotoxicity in seizure activity and their relevance for neuronal damage, there has been a growing interest in the use of antioxidants and other neuroprotective drugs that prevent neuronal damage following seizures (Petkova et al., 2014; Mishra et al., 2015; Williams et al., 2015; Pauletti et al., 2019).

CURTAIN CALL: CONCLUSIONS

Excitotoxicity relies on multiple pathways that are involved in several regulatory cell mechanisms. Studies reviewed here suggest that, although the glutamatergic system is essential for brain functioning, its dysregulation is implicated as a key step in the pathophysiology of neuronal impairment, which is closely associated with excitotoxicity. This dysregulation may occur at the receptor, transporter, or metabolic levels, leading to different types of cellular responses that ultimately culminate in oxidative stress and neuronal death. Several neurodegenerative diseases display excitotoxic events or characteristics, and possibly this chronic mild excitotoxicity contributes, among other factors, to the neuronal death observed in these pathophysiological conditions. Thus, it is urgent to discover new therapeutic targets that counteract the excitotoxicity mediated by glutamatergic system, with a positive impact on neurological diseases such as ALS, AD, and TLE.

AUTHOR CONTRIBUTIONS

AA-M, JG, CP, OS, JG-R, NR, SP, TM, RM, and FR wrote the manuscript. AA-M designed the illustrations. AS and VC revised the manuscript. SV wrote, designed, and revised the manuscript.

FUNDING

This work was funded by Fundação para a Ciência e Tecnologia (FCT), Portugal (PTDC/BTM-SAL/32147/2017, PD/BD/114278/2016, IMM/BI/2-2020), and by FCT/Ministério da Ciência, Tecnologia e Ensino Superior (MCTES) through Fundos do Orçamento de Estado (UID/BIM/50005/2019). TM was funded by the European Union's Horizon 2020 research and innovation programme under the Marie Skłodowska/Curie grant agreement No. 722053.

REFERENCES

Aarts, M., Liu, Y., Liu, L., Besshoh, S., Arundine, M., Gurd, J. W., et al. (2002). Treatment of ischemic brain damage by perturbing NMDA receptor- PSD-95 protein interactions. *Science* 298, 846–850. doi: 10.1126/science.1072873

Abdul, H. M., Sama, M. A., Furman, J. L., Mathis, D. M., Beckett, T. L., Weidner, A. M., et al. (2009). Cognitive decline in Alzheimer's disease is associated with selective changes in calcineurin/NFAT signaling. *J. Neurosci.* 29, 12957–12969. doi: 10.1523/JNEUROSCI.1064-09.2009

Ajroud-Driss, S., and Siddique, T. (2015). Sporadic and hereditary amyotrophic lateral sclerosis (ALS). *Biochim. Biophys. Acta* 1852, 679–684. doi: 10.1016/j.bbadis.2014.08.010

Akaike, A., Kaneko, S., Tamura, Y., Nakata, N., Shiomi, H., Ushikubi, F., et al. (1994). Prostaglandin E2 protects cultured cortical neurons against N-methyl-D-aspartate receptor-mediated glutamate cytotoxicity. *Brain Res.* 663, 237–243. doi: 10.1016/0006-8993(94)91268-8

Albin, R. L., and Greenamyre, J. T. (1992). Alternative excitotoxic hypotheses. *Neurology* 42, 733–738. doi: 10.1212/wnl.42.4.733

Albrecht, J., and Zielinska, M. (2017). Mechanisms of excessive extracellular glutamate accumulation in temporal lobe epilepsy. *Neurochem. Res.* 42, 1724–1734. doi: 10.1007/s11064-016-2105-8

Allen, N. J. (2014). Astrocyte regulation of synaptic behavior. *Annu. Rev. Cell Dev. Biol.* 30, 439–463. doi: 10.1146/annurev-cellbio-100913-013053

Alzheimer's Association. (2009). 2009 Alzheimer's disease facts and figures. *Alzheimers Dement.* 5, 234–270. doi: 10.1016/j.jalz.2009.03.001

Amiry-Moghaddam, M., Otsuka, T., Hurn, P. D., Traystman, R. J., Haug, F.-M., Froehner, S. C., et al. (2003). An α-syntrophin-dependent pool of AQP4 in astroglial end-feet confers bidirectional water flow between blood and brain. *Proc. Natl. Acad. Sci. U S A* 100, 2106–2111. doi: 10.1073/pnas.0437946100

Amorini, A. M., Lazzarino, G., Di Pietro, V., Signoretti, S., Lazzarino, G., Belli, A., et al. (2017). Severity of experimental traumatic brain injury modulates changes in concentrations of cerebral free amino acids. *J. Cell. Mol. Med.* 21, 530–542. doi: 10.1111/jcmm.12998

Anderson, C. M., and Swanson, R. A. (2000). Astrocyte glutamate transport: review of properties, regulation, and physiological functions. *Glia* 32, 1–14. doi: 10.1002/1098-1136(200010)32:1<1::aid-glia10>3.0.co;2-w

Angelova, P. R., and Abramov, A. Y. (2014). Interaction of neurons and astrocytes underlies the mechanism of Aβ-induced neurotoxicity. *Biochem. Soc. Trans.* 42, 1286–1290. doi: 10.1042/bst20140153

Ankarcrona, M., Dypbukt, J. M., Bonfoco, E., Zhivotovsky, B., Orrenius, S., Lipton, S. A., et al. (1995). Glutamate-induced neuronal death: a succession of necrosis or apoptosis depending on mitochondrial function. *Neuron* 15, 961–973. doi: 10.1016/0896-6273(95)90186-8

Appel, S. H., Zhao, W., Beers, D. R., and Henkel, J. S. (2011). The microglial-motoneuron dialogue in ALS. *Acta Myol.* 30, 4–8.

Aronica, E., van Vliet, E. A., Mayboroda, O. A., Troost, D., da Silva, F. H., and Gorter, J. A. (2000). Upregulation of metabotropic glutamate receptor subtype mGluR3 and mGluR5 in reactive astrocytes in a rat model of mesial temporal lobe epilepsy. *Eur. J. Neurosci.* 12, 2333–2344. doi: 10.1046/j.1460-9568.2000.00131.x

Bading, H. (2013). Nuclear calcium signalling in the regulation of brain function. *Nat. Rev. Neurosci.* 14, 593–608. doi: 10.1038/nrn3531

Bae, J. S., Simon, N. G., Menon, P., Vucic, S., and Kiernan, M. C. (2013). The puzzling case of hyperexcitability in amyotrophic lateral sclerosis. *J. Clin. Neurol.* 9, 65–74. doi: 10.3988/jcn.2013.9.2.65

Baker, D. A., Xi, Z. X., Shen, H., Swanson, C. J., and Kalivas, P. W. (2002). The origin and neuronal function of *in vivo* nonsynaptic glutamate. *J. Neurosci.* 22, 9134–9141. doi: 10.1523/JNEUROSCI.22-20-09134.2002

Balu, D. T., Pantazopoulos, H., Huang, C. C. Y., Muszynski, K., Harvey, T. L., Uno, Y., et al. (2019). Neurotoxic astrocytes express the D-serine synthesizing enzyme, serine racemase, in Alzheimer's disease. *Neurobiol. Dis.* 130:104511. doi: 10.1016/j.nbd.2019.104511

Bancila, V., Nikonenko, I., Dunant, Y., and Bloc, A. (2004). Zinc inhibits glutamate release *via* activation of pre-synaptic KATP channels and reduces ischaemic damage in rat hippocampus. *J. Neurochem.* 90, 1243–1250. doi: 10.1111/j.1471-4159.2004.02587.x

Bannai, S., and Tateishi, N. (1986). Role of membrane transport in metabolism and function of glutathione in mammals. *J. Membr. Biol.* 89, 1–8. doi: 10.1007/bf01870891

Bano, D., Young, K. W., Guerin, C. J., Lefeuvre, R., Rothwell, N. J., Naldini, L., et al. (2005). Cleavage of the plasma membrane Na^+/Ca^{2+} exchanger in excitotoxicity. *Cell* 120, 275–285. doi: 10.1016/j.cell.2004.11.049

Barger, S. W., and Basile, A. S. (2001). Activation of microglia by secreted amyloid precursor protein evokes release of glutamate by cystine exchange and attenuates synaptic function. *J. Neurochem.* 76, 846–854. doi: 10.1046/j.1471-4159.2001.00075.x

Barger, S. W., Goodwin, M. E., Porter, M. M., and Beggs, M. L. (2007). Glutamate release from activated microglia requires the oxidative burst and lipid peroxidation. *J. Neurochem.* 101, 1205–1213. doi: 10.1111/j.1471-4159.2007.04487.x

Barros, L. F. (2013). Metabolic signaling by lactate in the brain. *Trends Neurosci.* 36, 396–404. doi: 10.1016/j.tins.2013.04.002

Beart, P. M., and O'Shea, R. D. (2007). Transporters for L-glutamate: an update on their molecular pharmacology and pathological involvement. *Br. J. Pharmacol.* 150, 5–17. doi: 10.1038/sj.bjp.0706949

Bendotti, C., and Carri, M. T. (2004). Lessons from models of SOD1-linked familial ALS. *Trends Mol. Med.* 10, 393–400. doi: 10.1016/j.molmed.2004.06.009

Benjamin, A. M., and Quastel, J. H. (1972). Locations of amino acids in brain slices from the rat. Tetrodotoxin-sensitive release of amino acids. *Biochem. J.* 128, 631–646. doi: 10.1042/bj1300901c

Berdichevsky, E., Riveros, N., Sánchez-Armáss, S., and Orrego, F. (1983). Kainate, N-methylaspartate and other excitatory amino acids increase calcium influx into rat brain cortex cells *in vitro*. *Neurosci. Lett.* 36, 75–80. doi: 10.1016/0304-3940(83)90489-5

Bergersen, L. H., Morland, C., Ormel, L., Rinholm, J. E., Larsson, M., Wold, J. F. H., et al. (2012). Immunogold detection of L-glutamate and D-serine in small synaptic-like microvesicles in adult hippocampal astrocytes. *Cereb. Cortex* 22, 1690–1697. doi: 10.1093/cercor/bhr254

Berliocchi, L., Bano, D., and Nicotera, P. (2005). Ca^{2+} signals and death programmes in neurons. *Philos. Trans. R. Soc. Lond. B. Biol. Sci.* 360, 2255–2258. doi: 10.1098/rstb.2005.1765

Bernard-Marissal, N., Moumen, A., Sunyach, C., Pellegrino, C., Dudley, K., Henderson, C. E., et al. (2012). Reduced calreticulin levels link endoplasmic reticulum stress and Fas-triggered cell death in motoneurons vulnerable to ALS. *J. Neurosci.* 32, 4901–4912. doi: 10.1523/JNEUROSCI.5431-11.2012

Bi, X., Chang, V., Molnar, E., McIlhinney, R. A. J., and Baudry, M. (1996). The C-terminal domain of glutamate receptor subunit 1 is a target for calpain-mediated proteolysis. *Neuroscience* 73, 903–906. doi: 10.1016/0306-4522(96)00157-1

Bi, X., Chen, J., and Baudry, M. (1998a). Calpain-mediated proteolysis of GluR1 subunits in organotypic hippocampal cultures following kainic acid treatment. *Brain Res.* 781, 355–357. doi: 10.1016/s0006-8993(97)01365-6

Bi, X., Rong, Y., Chen, J., Dang, S., Wang, Z., and Baudry, M. (1998b). Calpain-mediated regulation of NMDA receptor structure and function. *Brain Res.* 790, 245–253. doi: 10.1016/s0006-8993(98)00067-5

Bittner, C. X., Valdebenito, R., Ruminot, I., Loaiza, A., Larenas, V., Sotelo-Hitschfeld, T., et al. (2011). Fast and reversible stimulation of astrocytic glycolysis by K^+ and a delayed and persistent effect of glutamate. *J. Neurosci.* 31, 4709–4713. doi: 10.1523/JNEUROSCI.5311-10.2011

Blatz, A. L., and Magleby, K. L. (1987). Calcium-activated potassium channels. *Trends Neurosci.* 10, 463–467. doi: 10.1016/0166-2236(87)90101-9

Bondy, S. C., and LeBel, C. P. (1993). The relationship between excitotoxicity and oxidative stress in the central nervous system. *Free Radic. Biol. Med.* 14, 633–642. doi: 10.1016/0891-5849(93)90144-j

Bonfoco, E., Krainc, D., Ankarcrona, M., Nicotera, P., and Lipton, S. A. (1995). Apoptosis and necrosis: two distinct events induced, respectively, by mild and intense insults with N-methyl-D-aspartate or nitric oxide/superoxide in cortical cell cultures. *Proc. Natl. Acad. Sci. U S A* 92, 7162–7166. doi: 10.1073/pnas.92.16.7162

Bonifacino, T., Rebosio, C., Provenzano, F., Torazza, C., Balbi, M., Milanese, M., et al. (2019). Enhanced function and overexpression of metabotropic glutamate receptors 1 and 5 in the spinal cord of the SOD1G93A mouse model of

amyotrophic lateral sclerosis during disease progression. *Int. J. Mol. Sci.* 20:E4552. doi: 10.3390/ijms20184552

Boycott, H. E., Wilkinson, J. A., Boyle, J. P., Pearson, H. A., and Peers, C. (2008). Differential involvement of TNFα in hypoxic suppression of astrocyte glutamate transporters. *Glia* 56, 998–1004. doi: 10.1002/glia.20673

Bradford, H. F. (1995). Glutamate, GABA and epilepsy. *Prog. Neurobiol.* 47, 477–511. doi: 10.1016/0301-0082(95)00030-5

Brawek, B., and Garaschuk, O. (2014). Network-wide dysregulation of calcium homeostasis in Alzheimer's disease. *Cell Tissue Res.* 357, 427–438. doi: 10.1007/s00441-014-1798-8

Brennan, A. M., Suh, S. W., Won, S. J., Narasimhan, P., Kauppinen, T. M., Lee, H., et al. (2009). NADPH oxidase is the primary source of superoxide induced by NMDA receptor activation. *Nat. Neurosci.* 12, 857–863. doi: 10.1038/nn.2334

Bridges, R., Lutgen, V., Lobner, D., and Baker, D. A. (2012). Thinking outside the cleft to understand synaptic activity: contribution of the cystine-glutamate antiporter (System X_c^-) to normal and pathological glutamatergic signaling. *Pharmacol. Rev.* 64, 780–802. doi: 10.1124/pr.110.003889

Brimecombe, J. C., Boeckman, F. A., and Aizenman, E. (1997). Functional consequences of NR2 subunit composition in single recombinant N-methyl-D-aspartate receptors. *Proc. Natl. Acad. Sci. U S A* 94, 11019–11024. doi: 10.1073/pnas.94.20.11019

Brites, D., and Vaz, A. R. (2014). Microglia centered pathogenesis in ALS: insights in cell interconnectivity. *Front. Cell. Neurosci.* 8:117. doi: 10.3389/fncel.2014.00117

Brito-Moreira, J., Paula-Lima, A. C., Bomfim, T. R., Oliveira, F. B., Sepúlveda, F. J., De Mello, F. G., et al. (2011). Aβ oligomers induce glutamate release from hippocampal neurons. *Curr. Alzheimer Res.* 8, 552–562. doi: 10.2174/156720511796391917

Butterfield, D. A., and Kanski, J. (2001). Brain protein oxidation in age-related neurodegenerative disorders that are associated with aggregated proteins. *Mech. Ageing Dev.* 122, 945–962. doi: 10.1016/s0047-6374(01)00249-4

Butterfield, D. A., and Stadtman, E. R. (1997). Protein oxidation processes in aging brain. *Adv. Cell Aging Gerontol.* 2, 161–191. doi: 10.1016/S1566-3124(08)60057-7

Butterfield, D. A., Reed, T., Perluigi, M., De Marco, C., Coccia, R., Cini, C., et al. (2006). Elevated protein-bound levels of the lipid peroxidation product, 4-hydroxy-2-nonenal, in brain from persons with mild cognitive impairment. *Neurosci. Lett.* 397, 170–173. doi: 10.1016/j.neulet.2005.12.017

Caldeira, M. V., Salazar, I. L., Curcio, M., Canzoniero, L. M. T., and Duarte, C. B. (2014). Role of the ubiquitin-proteasome system in brain ischemia: friend or foe? *Prog. Neurobiol.* 112, 50–69. doi: 10.1016/j.pneurobio.2013.10.003

Calkins, M. J., Manczak, M., Mao, P., Shirendeb, U., and Reddy, P. H. (2011). Impaired mitochondrial biogenesis, defective axonal transport of mitochondria, abnormal mitochondrial dynamics and synaptic degeneration in a mouse model of Alzheimer's disease. *Hum. Mol. Genet.* 20, 4515–4529. doi: 10.1093/hmg/ddr381

Carvalho, A. S. R., Torres, L. B., Persike, D. S., Fernandes, M. J. S., Amado, D., Naffah-Mazzacoratti, M. D. G., et al. (2011). Neuroprotective effect of pyruvate and oxaloacetate during pilocarpine induced status epilepticus in rats. *Neurochem. Int.* 58, 385–390. doi: 10.1016/j.neuint.2010.12.014

Castegna, A., Thongboonkerd, V., Klein, J. B., Lynn, B., Markesberyl, W. R., and Butterfield, D. A. (2003). Proteomic identification of nitrated proteins in Alzheimer's disease brain. *J. Neurochem.* 85, 1394–1401. doi: 10.1046/j.1471-4159.2003.01786.x

Castilho, R. F., Hansson, O., Ward, M. W., Budd, S. L., and Nicholls, D. G. (1998). Mitochondrial control of acute glutamate excitotoxicity in cultured cerebellar granule cells. *J. Neurosci.* 18, 10277–10286. doi: 10.1523/JNEUROSCI.18-24-10277.1998

Castillo, P. E., Malenka, R. C., and Nicoll, R. A. (1997). Kainate receptors mediate a slow postsynaptic current in hippocampal CA3 neurons. *Nature* 388, 182–186. doi: 10.1038/40645

Chen, P. E., Geballe, M. T., Stansfeld, P. J., Johnston, A. R., Yuan, H., Jacob, A. L., et al. (2005). Structural features of the glutamate binding site in recombinant NR1/NR2A N-methyl-D-aspartate receptors determined by site-directed mutagenesis and molecular modeling. *Mol. Pharmacol.* 67, 1470–1484. doi: 10.1124/mol.104.008185

Chen, S., Sayana, P., Zhang, X., and Le, W. (2013). Genetics of amyotrophic lateral sclerosis: an update. *Mol. Neurodegener.* 8:28. doi: 10.1186/1750-1326-8-28

Chen, Z., and Zhong, C. (2013). Decoding Alzheimer's disease from perturbed cerebral glucose metabolism: implications for diagnostic and therapeutic strategies. *Prog. Neurobiol.* 108, 21–43. doi: 10.1016/j.pneurobio.2013.06.004

Cheng, Y.-R., Jiang, B.-Y., and Chen, C.-C. (2018). Acid-sensing ion channels: dual function proteins for chemo-sensing and mechano-sensing. *J. Biomed. Sci.* 25:46. doi: 10.1186/s12929-018-0448-y

Chever, O., Djukic, B., McCarthy, K. D., and Amzica, F. (2010). Implication of Kir4.1 channel in excess potassium clearance: an *in vivo* study on anesthetized glial-conditional Kir4.1 knock-out mice. *J. Neurosci.* 30, 15769–15777. doi: 10.1523/JNEUROSCI.2078-10.2010

Chittajallu, R., Vignes, M., Dev, K. K., Barnes, J. M., Collingridge, G. L., and Henley, J. M. (1996). Regulation of glutamate release by presynaptic kainate receptors in the hippocampus. *Nature* 379, 78–81. doi: 10.1038/379078a0

Choi, D. W., Koh, J. Y., and Peters, S. (1988). Pharmacology of glutamate neurotoxicity in cortical cell culture: attenuation by NMDA antagonists. *J. Neurosci.* 8, 185–196. doi: 10.1523/JNEUROSCI.08-01-00185.1988

Choi, D. W., Viseskul, V., Amirthanayagam, M., and Monyer, H. (1989). Aspartate neurotoxicity on cultured cortical neurons. *J. Neurosci. Res.* 23, 116–121. doi: 10.1002/jnr.490230115

Chung, Y. H., Joo, K. M., Nam, R. H., Cho, M. H., Kim, D. J., Lee, W. B., et al. (2005). Decreased expression of calretinin in the cerebral cortex and hippocampus of SOD1G93A transgenic mice. *Brain Res.* 1035, 105–109. doi: 10.1016/j.brainres.2004.12.022

Clements, J. D., Lester, R. A., Tong, G., Jahr, C. E., and Westbrook, G. L. (1992). The time course of glutamate in the synaptic cleft. *Science* 258, 1498–1501. doi: 10.1126/science.1359647

Conn, P. J., and Pin, J. P. (1997). Pharmacology and functions of metabotropic glutamate receptors. *Annu. Rev. Pharmacol. Toxicol.* 37, 205–237. doi: 10.1146/annurev.pharmtox.37.1.205

Connolly, N. M. C., Düssmann, H., Anilkumar, U., Huber, H. J., and Prehn, J. H. M. (2014). Single-cell imaging of bioenergetic responses to neuronal excitotoxicity and oxygen and glucose deprivation. *J. Neurosci.* 34, 10192–10205. doi: 10.1523/JNEUROSCI.3127-13.2014

Connolly, N. M. C., and Prehn, J. H. M. (2015). The metabolic response to excitotoxicity—lessons from single-cell imaging. *J. Bioenerg. Biomembr.* 47, 75–88. doi: 10.1007/s10863-014-9578-4

Crino, P. B., Jin, H., Shumate, M. D., Robinson, M. B., Coulter, D. A., and Brooks-Kayal, A. R. (2002). Increased expression of the neuronal glutamate transporter (EAAT3/EAAC1) in hippocampal and neocortical epilepsy. *Epilepsia* 43, 211–218. doi: 10.1046/j.1528-1157.2002.35001.x

Cull-Candy, S., Brickley, S., and Farrant, M. (2001). NMDA receptor subunits: diversity, development and disease. *Curr. Opin. Neurobiol.* 11, 327–335. doi: 10.1016/s0959-4388(00)00215-4

Cunha, R. A. (2005). Neuroprotection by adenosine in the brain: from A1 receptor activation to A2A receptor blockade. *Purinergic Signal.* 1, 111–134. doi: 10.1007/s11302-005-0649-1

Cunha, C., Santos, C., Gomes, C., Fernandes, A., Correia, A. M., Sebastião, A. M., et al. (2018). Downregulated glia interplay and increased miRNA-155 as promising markers to track ALS at an early stage. *Mol. Neurobiol.* 55, 4207–4224. doi: 10.1007/s12035-017-0631-2

D'Ambrosio, R., Gordon, D. S., and Winn, H. R. (2002). Differential role of KIR channel and Na^+/K^+-pump in the regulation of extracellular K^+ in rat hippocampus. *J. Neurophysiol.* 87, 87–102. doi: 10.1152/jn.00240.2001

D'Orsi, B., Bonner, H., Tuffy, L. P., Düssmann, H., Woods, I., Courtney, M. J., et al. (2012). Calpains are downstream effectors of bax-dependent excitotoxic apoptosis. *J. Neurosci.* 32, 1847–1858. doi: 10.1523/JNEUROSCI.2345-11.2012

Damiano, M., Starkov, A. A., Petri, S., Kipiani, K., Kiaei, M., Mattiazzi, M., et al. (2006). Neural mitochondrial Ca^{2+} capacity impairment precedes the onset of motor symptoms in G93A Cu/Zn-superoxide dismutase mutant mice. *J. Neurochem.* 96, 1349–1361. doi: 10.1111/j.1471-4159.2006.03619.x

Danbolt, N. C. (2001). Glutamate uptake. *Prog. Neurobiol.* 65, 1–105. doi: 10.1016/s0301-0082(00)00067-8

Das, A., Wallace, G. C., Holmes, C., McDowell, M. L., Smith, J. A., Marshall, J. D., et al. (2012). Hippocampal tissue of patients with refractory temporal lobe epilepsy is associated with astrocyte activation, inflammation, and altered expression of channels and receptors. *Neuroscience* 220, 237–246. doi: 10.1016/j.neuroscience.2012.06.002

De Stefani, D., Raffaello, A., Teardo, E., Szabò, I., and Rizzuto, R. (2011). A forty-kilodalton protein of the inner membrane is the mitochondrial calcium uniporter. *Nature* 476, 336–340. doi: 10.1038/nature10230

Depp, C., Bas-Orth, C., Schroeder, L., Hellwig, A., and Bading, H. (2018). Synaptic activity protects neurons against calcium-mediated oxidation and contraction of mitochondria during excitotoxicity. *Antioxid. Redox Signal.* 29, 1109–1124. doi: 10.1089/ars.2017.7092

Descalzi, G., Gao, V., Steinman, M. Q., Suzuki, A., and Alberini, C. M. (2019). Lactate from astrocytes fuels learning-induced mRNA translation in excitatory and inhibitory neurons. *Commun. Biol.* 2:247. doi: 10.1038/s42003-019-0495-2

Devinsky, O., Vezzani, A., Najjar, S., De Lanerolle, N. C., and Rogawski, M. A. (2013). Glia and epilepsy: excitability and inflammation. *Trends Neurosci.* 36, 174–184. doi: 10.1016/j.tins.2012.11.008

Díaz, A., De Jesús, L., Mendieta, L., Calvillo, M., Espinosa, B., Zenteno, E., et al. (2010). The amyloid-β25–35 injection into the CA1 region of the neonatal rat hippocampus impairs the long-term memory because of an increase of nitric oxide. *Neurosci. Lett.* 468, 151–155. doi: 10.1016/j.neulet.2009.10.087

Diaz, A., Mendieta, L., Zenteno, E., Guevara, J., and Limon, I. D. (2011). The role of NOS in the impairment of spatial memory and damaged neurons in rats injected with amyloid β 25–35 into the temporal cortex. *Pharmacol. Biochem. Behav.* 98, 67–75. doi: 10.1016/j.pbb.2010.12.005

Dick, O., and Bading, H. (2010). Synaptic activity and nuclear calcium signaling protect hippocampal neurons from death signal-associated nuclear translocation of FoxO3a induced by extrasynaptic N-methyl-D-aspartate receptors. *J. Biol. Chem.* 285, 19354–19361. doi: 10.1074/jbc.m110.127654

Dienel, G. A. (2017). The metabolic trinity, glucose-glycogen-lactate, links astrocytes and neurons in brain energetics, signaling, memory, and gene expression. *Neurosci. Lett.* 637, 18–25. doi: 10.1016/j.neulet.2015.02.052

Djukic, B., Casper, K. B., Philpot, B. D., Chin, L.-S., and McCarthy, K. D. (2007). Conditional knock-out of Kir4.1 leads to glial membrane depolarization, inhibition of potassium and glutamate uptake, and enhanced short-term synaptic potentiation. *J. Neurosci.* 27, 11354–11365. doi: 10.1523/jneurosci.0723-07.2007

Dong, X., Wang, Y., and Qin, Z. (2009). Molecular mechanisms of excitotoxicity and their relevance to pathogenesis of neurodegenerative diseases. *Acta Pharmacol. Sin.* 30, 379–387. doi: 10.1038/aps.2009.24

Doyle, K. P., Simon, R. P., and Stenzel-Poore, M. P. (2008). Mechanisms of ischemic brain damage. *Neuropharmacology* 55, 310–318. doi: 10.1016/j.neuropharm.2008.01.005

Du, H., Guo, L., Fang, F., Chen, D., Sosunov, A. A., McKhann, G. M., et al. (2008). Cyclophilin D deficiency attenuates mitochondrial and neuronal perturbation and ameliorates learning and memory in Alzheimer's disease. *Nat. Med.* 14, 1097–1105. doi: 10.1038/nm.1868

Du, H., Guo, L., Wu, X., Sosunov, A. A., McKhann, G. M., Chen, J. X., et al. (2014). Cyclophilin D deficiency rescues Aβ-impaired PKA/CREB signaling and alleviates synaptic degeneration. *Biochim. Biophys. Acta* 1842, 2517–2527. doi: 10.1016/j.bbadis.2013.03.004

Du, H., Guo, L., Zhang, W., Rydzewska, M., and Yan, S. (2011). Cyclophilin D deficiency improves mitochondrial function and learning/memory in aging Alzheimer disease mouse model. *Neurobiol. Aging* 32, 398–406. doi: 10.1016/j.neurobiolaging.2009.03.003

Dudek, F. E., and Rogawski, M. A. (2005). Regulation of brain water: is there a role for aquaporins in epilepsy? *Epilepsy Curr.* 5, 104–106. doi: 10.1111/j.1535-7511.2005.05310.x

During, M. J., and Spencer, D. D. (1993). Extracellular hippocampal glutamate and spontaneous seizure in the conscious human brain. *Lancet* 341, 1607–1610. doi: 10.1016/0140-6736(93)90754-5

Dutta, R., and Trapp, B. D. (2011). Mechanisms of neuronal dysfunction and degeneration in multiple sclerosis. *Prog. Neurobiol.* 93, 1–12. doi: 10.1016/j.pneurobio.2010.09.005

Dzubay, J. A., and Jahr, C. E. (1999). The concentration of synaptically released glutamate outside of the climbing fiber-Purkinje cell synaptic cleft. *J. Neurosci.* 19, 5265–5274. doi: 10.1523/jneurosci.19-13-05265.1999

Edwards, J. P., Zhang, X., Frauwirth, K. A., and Mosser, D. M. (2006). Biochemical and functional characterization of three activated macrophage populations. *J. Leukoc. Biol.* 80, 1298–1307. doi: 10.1189/jlb.0406249

Ehlers, M. D., Zhang, S., Bernhardt, J. P., and Huganir, R. L. (1996). Inactivation of NMDA receptors by direct interaction of calmodulin with the NR1 subunit. *Cell* 84, 745–755. doi: 10.1016/s0092-8674(00)81052-1

Eid, T., Lee, T.-S. W., Thomas, M. J., Amiry-Moghaddam, M., Bjørnsen, L. P., Spencer, D. D., et al. (2005). Loss of perivascular aquaporin 4 may underlie deficient water and K^+ homeostasis in the human epileptogenic hippocampus. *Proc. Natl. Acad. Sci. U S A* 102, 1193–1198. doi: 10.1073/pnas.0409308102

Erreger, K., Dravid, S. M., Banke, T. G., Wyllie, D. J. A., and Traynelis, S. F. (2005). Subunit-specific gating controls rat NR1/NR2A and NR1/NR2B NMDA channel kinetics and synaptic signalling profiles. *J. Physiol.* 563, 345–358. doi: 10.1113/jphysiol.2004.080028

Ertekin-Taner, N. (2007). Genetics of Alzheimer's disease: a centennial review. *Neurol. Clin.* 25, 611–667. doi: 10.1016/j.ncl.2007.03.009

Fairman, W. A., and Amara, S. G. (1999). Functional diversity of excitatory amino acid transporters: ion channel and transport modes. *Am. J. Physiol.* 277, F481–F486. doi: 10.1152/ajprenal.1999.277.4.f481

Ferraguti, F., Crepaldi, L., and Nicoletti, F. (2008). Metabotropic glutamate 1 receptor: current concepts and perspectives. *Pharmacol. Rev.* 60, 536–581. doi: 10.1124/pr.108.000166

Ferrari, R., Kapogiannis, D., Huey, E. D., and Momeni, P. (2011). FTD and ALS: a tale of two diseases. *Curr. Alzheimer Res.* 8, 273–294. doi: 10.2174/156720511795563700

Ferreira, I. L., Bajouco, L. M., Mota, S. I., Auberson, Y. P., Oliveira, C. R., and Rego, A. C. (2012). Amyloid β peptide 1–42 disturbs intracellular calcium homeostasis through activation of GluN2B-containing N-methyl-d-aspartate receptors in cortical cultures. *Cell Calcium* 51, 95–106. doi: 10.1016/j.ceca.2011.11.008

Ferrer, I. (2012). Defining Alzheimer as a common age-related neurodegenerative process not inevitably leading to dementia. *Prog. Neurobiol.* 97, 38–51. doi: 10.1016/j.pneurobio.2012.03.005

Fisher, R. S., Cross, J. H., French, J. A., Higurashi, N., Hirsch, E., Jansen, F. E., et al. (2017). Operational classification of seizure types by the international league against epilepsy: position paper of the ILAE commission for classification and terminology. *Epilepsia* 58, 522–530. doi: 10.1111/epi.13670

Floyd, R. A. (1999). Antioxidants, oxidative stress, and degenerative neurological disorders. *Proc. Soc. Exp. Biol. Med.* 222, 236–245. doi: 10.1046/j.1525-1373.1999.d01-140.x

Fogarty, M. J., Mu, E. W. H., Noakes, P. G., Lavidis, N. A., and Bellingham, M. C. (2016). Marked changes in dendritic structure and spine density precede significant neuronal death in vulnerable cortical pyramidal neuron populations in the SOD1(G93A) mouse model of amyotrophic lateral sclerosis. *Acta Neuropathol. Commun.* 4:77. doi: 10.1186/s40478-016-0347-y

Frantseva, M. V., Velazquez, J. L., Hwang, P. A., and Carlen, P. L. (2000). Free radical production correlates with cell death in an *in vitro* model of epilepsy. *Eur. J. Neurosci.* 12, 1431–1439. doi: 10.1046/j.1460-9568.2000.00016.x

Freeman, B. A., and Crapo, J. D. (1982). Biology of disease: free radicals and tissue injury. *Lab. Invest.* 47, 412–426.

Fukuhara, T., Nishio, S., Ono, Y., Kawauchi, M., Asari, S., and Ohmoto, T. (1994). Induction of Cu,Zn-superoxide dismutase after cortical contusion injury during hypothermia. *Brain Res.* 657, 333–336. doi: 10.1016/0006-8993(94)90987-3

Giribaldi, F., Milanese, M., Bonifacino, T., Anna Rossi, P. I., Di Prisco, S., Pittaluga, A., et al. (2013). Group I metabotropic glutamate autoreceptors induce abnormal glutamate exocytosis in a mouse model of amyotrophic lateral sclerosis. *Neuropharmacology* 66, 253–263. doi: 10.1016/j.neuropharm.2012.05.018

Goffin, K., Dedeurwaerdere, S., Van Laere, K., and Van Paesschen, W. (2008). Neuronuclear assessment of patients with epilepsy. *Semin. Nucl. Med.* 38, 227–239. doi: 10.1053/j.semnuclmed.2008.02.004

Gomes, C., Cunha, C., Nascimento, F., Ribeiro, J. A., Vaz, A. R., and Brites, D. (2019). Cortical neurotoxic astrocytes with early ALS pathology and miR-146a deficit replicate gliosis markers of symptomatic SOD1G93A mouse model. *Mol. Neurobiol.* 56, 2137–2158. doi: 10.1007/s12035-018-1220-8

Gonçalves-Ribeiro, J., Pina, C. C., Sebastião, A. M., and Vaz, S. H. (2019). Glutamate transporters in hippocampal LTD/LTP: not just prevention of excitotoxicity. *Front. Cell. Neurosci.* 13:357. doi: 10.3389/fncel.2019.00357

González-Hernández, T., García-Marín, V., Pérez-Delgado, M. M., González-González, M. L., Rancel-Torres, N., and González-Feria, L. (2000). Nitric oxide

synthase expression in the cerebral cortex of patients with epilepsy. *Epilepsia* 41, 1259–1268. doi: 10.1111/j.1528-1157.2000.tb04603.x

Goss, J. R., Taffe, K. M., Kochanek, P. M., and DeKosky, S. T. (1997). The antioxidant enzymes glutathione peroxidase and catalase increase following traumatic brain injury in the rat. *Exp. Neurol.* 146, 291–294. doi: 10.1006/exnr.1997.6515

Gottlieb, M., Wang, Y., and Teichberg, V. I. (2003). Blood-mediated scavenging of cerebrospinal fluid glutamate. *J. Neurochem.* 87, 119–126. doi: 10.1046/j.1471-4159.2003.01972.x

Gravel, M., Béland, L.-C., Soucy, G., Abdelhamid, E., Rahimian, R., Gravel, C., et al. (2016). IL-10 controls early microglial phenotypes and disease onset in ALS caused by misfolded superoxide dismutase 1. *J. Neurosci.* 36, 1031–1048. doi: 10.1523/JNEUROSCI.0854-15.2016

Griffiths, T., Evans, M. C., and Meldrum, B. S. (1983). Intracellular calcium accumulation in rat hippocampus during seizures induced by bicuculline or L-allylglycine. *Neuroscience* 10, 385–395. doi: 10.1016/0306-4522(83)90141-0

Grundke-Iqbal, I., Iqbal, K., Tung, Y. C., Quinlan, M., Wisniewski, H. M., and Binder, L. I. (1986). Abnormal phosphorylation of the microtubule-associated protein tau (tau) in Alzheimer cytoskeletal pathology. *Proc. Natl. Acad. Sci. U S A* 83, 4913–4917. doi: 10.1073/pnas.83.13.4913

Guo, H., Camargo, L. M., Yeboah, F., Digan, M. E., Niu, H., Pan, Y., et al. (2017). A NMDA-receptor calcium influx assay sensitive to stimulation by glutamate and glycine/D-serine. *Sci. Rep.* 7:11608. doi: 10.1038/s41598-017-11947-x

Guo, H., Lai, L., Butchbach, M. E. R., Stockinger, M. P., Shan, X., Bishop, G. A., et al. (2003). Increased expression of the glial glutamate transporter EAAT2 modulates excitotoxicity and delays the onset but not the outcome of ALS in mice. *Hum. Mol. Genet.* 12, 2519–2532. doi: 10.1093/hmg/ddg267

Hamano, H., Nabekura, J., Nishikawa, M., and Ogawa, T. (1996). Docosahexaenoic acid reduces GABA response in substantia nigra neuron of rat. *J. Neurophysiol.* 75, 1264–1270. doi: 10.1152/jn.1996.75.3.1264

Hansen, K. B., Yi, F., Perszyk, R. E., Menniti, F. S., and Traynelis, S. F. (2017)."NMDA receptors in the central nervous system," in *NMDA Receptors*, eds N. Burnashev and P. Szepetowski (New York, NY: Springer), 1–80.

Hardingham, G. E., and Bading, H. (2010). Synaptic versus extrasynaptic NMDA receptor signalling: implications for neurodegenerative disorders. *Nat. Rev. Neurosci.* 11, 682–696. doi: 10.1038/nrn2911

Hardingham, G. E., Fukunaga, Y., and Bading, H. (2002). Extrasynaptic NMDARs oppose synaptic NMDARs by triggering CREB shut-off and cell death pathways. *Nat. Neurosci.* 5, 405–414. doi: 10.1038/nn835

Harris, A. Z., and Pettit, D. L. (2007). Extrasynaptic and synaptic NMDA receptors form stable and uniform pools in rat hippocampal slices. *J. Physiol.* 584, 509–519. doi: 10.1113/jphysiol.2007.137679

Haughey, N. J., and Mattson, M. P. (2003). Alzheimer's amyloid β-peptide enhances ATP/gap junction-mediated calcium-wave propagation in astrocytes. *Neuromolecular Med.* 3, 173–180. doi: 10.1385/NMM:3:3:173

Henneberger, C., Papouin, T., Oliet, S. H. R., and Rusakov, D. A. (2010). Long-term potentiation depends on release of d-serine from astrocytes. *Nature* 463, 232–236. doi: 10.1038/nature08673

Hensley, K., Carney, J. M., Mattson, M. P., Aksenova, M., Harris, M., Wu, J. F., et al. (1994). A model forβ-amyloid aggregation and neurotoxicity based on free radical generation by the peptide: relevance to Alzheimer disease. *Proc. Natl. Acad. Sci. U S A* 91, 3270–3274. doi: 10.1073/pnas.91.8.3270

Hensley, K., Hall, N., Subramaniam, R., Cole, P., Harris, M., Aksenov, M., et al. (1995). Brain regional correspondence between Alzheimer's disease histopathology and biomarkers of protein oxidation. *J. Neurochem.* 65, 2146–2156. doi: 10.1073/pnas.91.8.3270

Herman, M. A., and Jahr, C. E. (2007). Extracellular glutamate concentration in hippocampal slice. *J. Neurosci.* 27, 9736–9741. doi: 10.1523/JNEUROSCI.3009-07.2007

Hertz, L., Dringen, R., Schousboe, A., and Robinson, S. R. (1999). Astrocytes: glutamate producers for neurons. *J. Neurosci. Res.* 57, 417–428. doi: 10.1002/(sici)1097-4547(19990815)57:4<417::aid-jnr1 >3.0.co;2-n

Hewett, S. J., Uliasz, T. F., Vidwans, A. S., and Hewett, J. A. (2000). Cyclooxygenase-2 contributes to N-methyl-D-aspartate-mediated neuronal cell death in primary cortical cell culture. *J. Pharmacol. Exp. Ther.* 293, 417–425.

Honrath, B., Krabbendam, I. E., Culmsee, C., and Dolga, A. M. (2017). Small conductance Ca^{2+}-activated K^+ channels in the plasma membrane, mitochondria and the ER: pharmacology and implications in neuronal diseases. *Neurochem. Int.* 109, 13–23. doi: 10.1016/j.neuint.2017.05.005

Hoogland, G., van Oort, R. J., Proper, E. A., Jansen, G. H., van Rijen, P. C., van Veelen, C. W., et al. (2004). Alternative splicing of glutamate transporter EAAT2 RNA in neocortex and hippocampus of temporal lobe epilepsy patients. *Epilepsy Res.* 59, 75–82. doi: 10.1016/j.eplepsyres.2004.03.003

Howland, J. G., Taepavarapruk, P., and Phillips, A. G. (2002). Glutamate receptor-dependent modulation of dopamine efflux in the nucleus accumbens by basolateral, but not central, nucleus of the amygdala in rats. *J. Neurosci.* 22, 1137–1145. doi: 10.1523/JNEUROSCI.22-03-01137.2002

Hu, S., Sheng, W. S., Ehrlich, L. C., Peterson, P. K., and Chao, C. C. (2000). Cytokine effects on glutamate uptake by human astrocytes. *Neuroimmunomodulation* 7, 153–159. doi: 10.1159/000026433

Huang, Y., Shen, W., Su, J., Cheng, B., Li, D., Liu, G., et al. (2017). Modulating the balance of synaptic and extrasynaptic NMDA receptors shows positive effects against amyloid-β-induced neurotoxicity. *J. Alzheimers Dis.* 57, 885–897. doi: 10.3233/jad-161186

Hubbard, J. A., Szu, J. I., Yonan, J. M., and Binder, D. K. (2016). Regulation of astrocyte glutamate transporter-1 (GLT1) and aquaporin-4 (AQP4) expression in a model of epilepsy. *Exp. Neurol.* 283, 85–96. doi: 10.1016/j.expneurol.2016.05.003

Huxtable, R. J. (1992). Physiological actions of taurine. *Physiol. Rev.* 72, 101–163. doi: 10.1152/physrev.1992.72.1.101

Ishii, K., Sasaki, M., Kitagaki, H., Yamaji, S., Sakamoto, S., Matsuda, K., et al. (1997). Reduction of cerebellar glucose metabolism in advanced Alzheimer's disease. *J. Nucl. Med.* 38, 925–928.

Jackman, N. A., Melchior, S. E., Hewett, J. A., and Hewett, S. J. (2012). Non-cell autonomous influence of the astrocyte system xc- on hypoglycaemic neuronal cell death. *ASN Neuro* 4:e00074. doi: 10.1042/an20110030

Jarrett, S. G., Liang, L.-P., Hellier, J. L., Staley, K. J., and Patel, M. (2008). Mitochondrial DNA damage and impaired base excision repair during epileptogenesis. *Neurobiol. Dis.* 30, 130–138. doi: 10.1016/j.nbd.2007.12.009

Jerónimo-Santos, A., Vaz, S. H., Parreira, S., Rapaz-Lérias, S., Caetano, A. P., Buée-Scherrer, V., et al. (2015). Dysregulation of TrkB receptors and BDNF function by amyloid-β peptide is mediated by calpain. *Cereb. Cortex* 25, 3107–3121. doi: 10.1093/cercor/bhu105

Jia, M., Njapo, S. A. N., Rastogi, V., and Hedna, V. S. (2015). Taming glutamate excitotoxicity: strategic pathway modulation for neuroprotection. *CNS Drugs* 29, 153–162. doi: 10.1007/s40263-015-0225-3

Jiang, L. L., Zhu, B., Zhao, Y., Li, X., Liu, T., Pina-Crespo, J., et al. (2019). Membralin deficiency dysregulates astrocytic glutamate homeostasis leading to ALS-like impairment. *J. Clin. Invest.* 129, 3103–3120. doi: 10.1172/jci127695

Jonas, P. (2000). The time course of signaling at central glutamatergic synapses. *Physiology* 15, 83–89. doi: 10.1152/physiologyonline.2000.15.2.83

Jones, N. (2011). Stroke: disruption of the nNOS-PSD-95 complex is neuroprotective in models of cerebral ischemia. *Nat. Rev. Neurol.* 7:61. doi: 10.1038/nrneurol.2010.203

Kennedy, A. M., Frackowiak, R. S. J., Newman, S. K., Bloomfield, P. M., Seaward, J., Roques, P., et al. (1995). Deficits in cerebral glucose metabolism demonstrated by positron emission tomography in individuals at risk of familial Alzheimer's disease. *Neurosci. Lett.* 186, 17–20. doi: 10.1016/0304-3940(95)11270-7

Kia, A., McAvoy, K., Krishnamurthy, K., Trotti, D., and Pasinelli, P. (2018). Astrocytes expressing ALS-linked mutant FUS induce motor neuron death through release of tumor necrosis factor-α. *Glia* 66, 1016–1033. doi: 10.1002/glia.23298

Kiernan, M. C., Vucic, S., Cheah, B. C., Turner, M. R., Eisen, A., Hardiman, O., et al. (2011). Amyotrophic lateral sclerosis. *Lancet* 377, 942–955. doi: 10.1016/S0140-6736(10)61156-7

Kobayashi, E., Nakano, M., Kubota, K., Himuro, N., Mizoguchi, S., Chikenji, T., et al. (2018). Activated forms of astrocytes with higher GLT-1 expression are associated with cognitive normal subjects with Alzheimer pathology in human brain. *Sci. Rep.* 8:1712. doi: 10.1038/s41598-018-19442-7

Koenigsknecht-Talboo, J., and Landreth, G. E. (2005). Microglial phagocytosis induced by fibrillarβ-amyloid and IgGs are differentially regulated by proinflammatory cytokines. *J. Neurosci.* 25, 8240–8249. doi: 10.1523/JNEUROSCI.1808-05.2005

Kofuji, P., and Newman, E. A. (2004). Potassium buffering in the central nervous system. *Neuroscience* 129, 1045–1056. doi: 10.1016/j.neuroscience.2004.06.008

Kojima, S., Nakamura, T., Nidaira, T., Nakamura, K., Ooashi, N., Ito, E., et al. (1999). Optical detection of synaptically induced glutamate transport in hippocampal slices. *J. Neurosci.* 19, 2580–2588. doi: 10.1523/JNEUROSCI.19-07-02580.1999

Komine, O., and Yamanaka, K. (2015). Neuroinflammation in motor neuron disease. *Nagoya J. Med. Sci.* 77, 537–549.

Kong, Q., Chang, L. C., Takahashi, K., Liu, Q., Schulte, D. A., Lai, L., et al. (2014). Small-molecule activator of glutamate transporter EAAT2 translation provides neuroprotection. *J. Clin. Invest.* 124, 1255–1267. doi: 10.1172/jci66163

Kong, Q., Takahashi, K., Schulte, D., Stouffer, N., Lin, Y., and Lin, C. L. (2012). Increased glial glutamate transporter EAAT2 expression reduces epileptogenic processes following pilocarpine-induced status epilepticus. *Neurobiol. Dis.* 47, 145–154. doi: 10.1016/j.nbd.2012.03.032

Kovac, S., Abramov, A. Y., and Walker, M. C. (2013). Energy depletion in seizures: anaplerosis as a strategy for future therapies. *Neuropharmacology* 69, 96–104. doi: 10.1016/j.neuropharm.2012.05.012

Kovac, S., Domijan, A.-M., Walker, M. C., and Abramov, A. Y. (2012). Prolonged seizure activity impairs mitochondrial bioenergetics and induces cell death. *J. Cell Sci.* 125, 1796–1806. doi: 10.1242/jcs.099176

Kraig, R. P., Petito, C. K., Plum, F., and Pulsinelli, W. A. (1987). Hydrogen ions kill brain at concentrations reached in ischemia. *J. Cereb. Blood Flow Metab.* 7, 379–386. doi: 10.1038/jcbfm.1987.80

Kuchibhotla, K. V., Lattarulo, C. R., Hyman, B. T., and Bacskai, B. J. (2009). Synchronous hyperactivity and intercellular calcium waves in astrocytes in Alzheimer mice. *Science* 323, 1211–1215. doi: 10.1126/science.1169096

Kuner, T., and Schoepfer, R. (1996). Multiple structural elements determine subunit specificity of Mg2+ block in NMDA receptor channels. *J. Neurosci.* 16, 3549–3558. doi: 10.1523/JNEUROSCI.16-11-03549.1996

Kushnareva, Y. E., Wiley, S. E., Ward, M. W., Andreyev, A. Y., and Murphy, A. N. (2005). Excitotoxic injury to mitochondria isolated from cultured neurons. *J. Biol. Chem.* 280, 28894–28902. doi: 10.1074/jbc.m503090200

LaFerla, F. M., Green, K. N., and Oddo, S. (2007). Intracellular amyloid-β in Alzheimer's disease. *Nat. Rev. Neurosci.* 8, 499–509. doi: 10.1038/nrn2168

Lancaster, B., and Adams, P. R. (1986). Calcium-dependent current generating the afterhyperpolarization of hippocampal neurons. *J. Neurophysiol.* 55, 1268–1282. doi: 10.1152/jn.1986.55.6.1268

Lee, D. J., Hsu, M. S., Seldin, M. M., Arellano, J. L., and Binder, D. K. (2012). Decreased expression of the glial water channel aquaporin-4 in the intrahippocampal kainic acid model of epileptogenesis. *Exp. Neurol.* 235, 246–255. doi: 10.1016/j.expneurol.2012.02.002

Leung, A. W. C., Varanyuwatana, P., and Halestrap, A. P. (2008). The mitochondrial phosphate carrier interacts with cyclophilin D and may play a key role in the permeability transition. *J. Biol. Chem.* 283, 26312–26323. doi: 10.1074/jbc.m805235200

Lewerenz, J., Maher, P., and Methner, A. (2012). Regulation of xCT expression and system x_c^- function in neuronal cells. *Amino Acids* 42, 171–179. doi: 10.1007/s00726-011-0862-x

Li, K., Hala, T. J., Seetharam, S., Poulsen, D. J., Wright, M. C., and Lepore, A. C. (2015). GLT1 overexpression in SOD1(G93A) mouse cervical spinal cord does not preserve diaphragm function or extend disease. *J. Neurol.* 78, 12–23. doi: 10.1016/j.nbd.2015.03.010

Li, S., Jin, M., Koeglsperger, T., Shepardson, N., Shankar, G., and Selkoe, D. (2011). Soluble Aβ oligomers inhibit long-term potentiation through a mechanism involving excessive activation of extrasynaptic NR2B-containing NMDA receptors. *J. Neurosci.* 31, 6627–6638. doi: 10.1523/JNEUROSCI.0203-11.2011

Li, M.-H., Leng, T.-D., Feng, X.-C., Yang, T., Simon, R. P., and Xiong, Z.-G. (2016). Modulation of acid-sensing ion channel 1a by intracellular pH and its role in ischemic stroke. *J. Biol. Chem.* 291, 18370–18383. doi: 10.1074/jbc.m115.713636

Liang, L. P., Ho, Y. S., and Patel, M. (2000). Mitochondrial superoxide production in kainate-induced hippocampal damage. *Neuroscience* 101, 563–570. doi: 10.1016/s0306-4522(00)00397-3

Lieberman, D. N., and Mody, I. (1994). Regulation of NMDA channel function by endogenous Ca^{2+}-dependent phosphatase. *Nature* 369, 235–239. doi: 10.1038/369235a0

Lin, C. L., Bristol, L. A., Jin, L., Dykes-Hoberg, M., Crawford, T., Clawson, L., et al. (1998). Aberrant RNA processing in a neurodegenerative disease: the cause for absent EAAT2, a glutamate transporter, in amyotrophic lateral sclerosis. *Neuron* 20, 589–602. doi: 10.1016/s0896-6273(00)80997-6

Lipton, S. A. (2008). NMDA receptor activity regulates transcription of antioxidant pathways. *Nat. Neurosci.* 11, 381–382. doi: 10.1038/nn0408-381

Lipton, S. A., Choi, Y. B., Pan, Z. H., Lei, S. Z., Chen, H. S., Sucher, N. J., et al. (1993). A redox-based mechanism for the neuroprotective and neurodestructive effects of nitric oxide and related nitroso-compounds. *Nature* 364, 626–632. doi: 10.1038/364626a0

Liu, B., and Hong, J.-S. (2003). Role of microglia in inflammation-mediated neurodegenerative diseases: mechanisms and strategies for therapeutic intervention. *J. Pharmacol. Exp. Ther.* 304, 1–7. doi: 10.1124/jpet.102.035048

Liu, B., Niu, L., Shen, M.-Z., Gao, L., Wang, C., Li, J., et al. (2014). Decreased astroglial monocarboxylate transporter 4 expression in temporal lobe epilepsy. *Mol. Neurobiol.* 50, 327–338. doi: 10.1007/s12035-013-8619-z

Lo, M., Wang, Y.-Z., and Gout, P. W. (2008). The x_c^- cystine/glutamate antiporter: a potential target for therapy of cancer and other diseases. *J. Cell. Physiol.* 215, 593–602. doi: 10.1002/jcp.21366

Lucca, G., Comim, C. M., Valvassori, S. S., Réus, G. Z., Vuolo, F., Petronilho, F., et al. (2009). Effects of chronic mild stress on the oxidative parameters in the rat brain. *Neurochem. Int.* 54, 358–362. doi: 10.1016/j.neuint.2009.01.001

Luetjens, C. M., Bui, N. T., Sengpiel, B., Münstermann, G., Poppe, M., Krohn, A. J., et al. (2000). Delayed mitochondrial dysfunction in excitotoxic neuron death: cytochrome c release and a secondary increase in superoxide production. *J. Neurosci.* 20, 5715–5723. doi: 10.1523/JNEUROSCI.20-15-05715.2000

Lutgen, V., Resch, J., Qualmann, K., Raddatz, N. J., Panhans, C., Olander, E. M., et al. (2014). Behavioral assessment of acute inhibition of system xc- in rats. *Psychopharmacology* 231, 4637–4647. doi: 10.1007/s00213-014-3612-4

Mächler, P., Wyss, M. T., Elsayed, M., Stobart, J., Gutierrez, R., von Faber-Castell, A., et al. (2016). *in vivo* evidence for a lactate gradient from astrocytes to neurons. *Cell Metab.* 23, 94–102. doi: 10.1016/j.cmet.2015.10.010

Madison, D. V., and Nicoll, R. A. (1984). Control of the repetitive discharge of rat CA 1 pyramidal neurones *in vitro*. *J. Physiol.* 354, 319–331. doi: 10.1113/jphysiol.1984.sp015378

Magistretti, P. J., and Allaman, I. (2015). A cellular perspective on brain energy metabolism and functional imaging. *Neuron* 86, 883–901. doi: 10.1016/j.neuron.2015.03.035

Magnusson, K. R., Koerner, J. F., Larson, A. A., Smullin, D. H., Skilling, S. R., and Beitz, A. J. (1991). NMDA-, kainate- and quisqualate-stimulated release of taurine from electrophysiologically monitored rat hippocampal slices. *Brain Res.* 549, 1–8. doi: 10.1016/0006-8993(91)90592-j

Manczak, M., Anekonda, T. S., Henson, E., Park, B. S., Quinn, J., and Reddy, P. H. (2006). Mitochondria are a direct site of Aβ accumulation in Alzheimer's disease neurons: implications for free radical generation and oxidative damage in disease progression. *Hum. Mol. Genet.* 15, 1437–1449. doi: 10.1093/hmg/ddl066

Maneshi, M. M., Maki, B., Gnanasambandam, R., Belin, S., Popescu, G. K., Sachs, F., et al. (2017). Mechanical stress activates NMDA receptors in the absence of agonists. *Sci. Rep.* 7:39610. doi: 10.1038/srep39610

Marcaida, G., Kosenko, E., Miñana, M. D., Grisolía, S., and Felipo, V. (1996). Glutamate induces a calcineurin-mediated dephosphorylation of Na^+,K^+-ATPase that results in its activation in cerebellar neurons in culture. *J. Neurochem.* 66, 99–104. doi: 10.1046/j.1471-4159.1996.66010099.x

Mark, L. P., Prost, R. W., Ulmer, J. L., Smith, M. M., Daniels, D. L., Strottmann, J. M., et al. (2001). Pictorial review of glutamate excitotoxicity: fundamental concepts for neuroimaging. *Am. J. Neuroradiol.* 22, 1813–1824.

Martin, L. J., Liu, Z., Chen, K., Price, A. C., Pan, Y., Swaby, J. A., et al. (2007). Motor neuron degeneration in amyotrophic lateral sclerosis mutant superoxide dismutase-1 transgenic mice: mechanisms of mitochondriopathy and cell death. *J. Comp. Neurol.* 500, 20–46. doi: 10.1002/cne.21160

Martineau, M., Shi, T., Puyal, J., Knolhoff, A. M., Dulong, J., Gasnier, B., et al. (2013). Storage and uptake of D-serine into astrocytic synaptic-like vesicles specify gliotransmission. *J. Neurosci.* 33, 3413–3423. doi: 10.1523/jneurosci.3497-12.2013

Matsuyama, T., Shimizu, S., Nakamura, H., Michishita, H., Tagaya, M., and Sugita, M. (1994). Effects of recombinant superoxide dismutase on manganese superoxide dismutase gene expression in gerbil hippocampus after ischemia. *Stroke* 25, 1417–1423; discussion 1424. doi: 10.1161/01.str.25.7.1417

Mattiazzi, M., D'Aurelio, M., Gajewski, C. D., Martushova, K., Kiaei, M., Beal, M. F., et al. (2002). Mutated human SOD1 causes dysfunction of oxidative phosphorylation in mitochondria of transgenic mice. *J. Biol. Chem.* 277, 29626–29633. doi: 10.1074/jbc.m203065200

Mattson, M. P. (2013). Excitation BolsTORs motor neurons in ALS mice. *Neuron* 80, 1–3. doi: 10.1016/j.neuron.2013.09.017

McBain, C. J., and Mayer, M. L. (1994). N-methyl-D-aspartic acid receptor structure and function. *Physiol. Rev.* 74, 723–760. doi: 10.1152/physrev.1994.74.3.723

McGown, A., McDearmid, J. R., Panagiotaki, N., Tong, H., Al Mashhadi, S., Redhead, N., et al. (2013). Early interneuron dysfunction in ALS: insights from a mutant sod1 zebrafish model. *Ann. Neurol.* 73, 246–258. doi: 10.1002/ana.23780

Mehta, A., Prabhakar, M., Kumar, P., Deshmukh, R., and Sharma, P. L. (2013). Excitotoxicity: bridge to various triggers in neurodegenerative disorders. *Eur. J. Pharmacol.* 698, 6–18. doi: 10.1016/j.ejphar.2012.10.032

Menzies, F. M., Ince, P. G., and Shaw, P. J. (2002). Mitochondrial involvement in amyotrophic lateral sclerosis. *Neurochem. Int.* 40, 543–551. doi: 10.1016/s0197-0186(01)00125-5

Merlini, M., Meyer, E. P., and Nitsch, A. U. R. M. (2011). Vascular β-amyloid and early astrocyte alterations impair cerebrovascular function and cerebral metabolism in transgenic arcAβ mice. *Acta Neuropathol.* 122, 293–311. doi: 10.1007/s00401-011-0834-y

Mesci, P., Zaidi, S., Lobsiger, C. S., Millecamps, S., Escartin, C., Seilhean, D., et al. (2015). System xC- is a mediator of microglial function and its deletion slows symptoms in amyotrophic lateral sclerosis mice. *Brain* 138, 53–68. doi: 10.1093/brain/awu312

Mikami, Y., Kanemaru, K., Okubo, Y., Nakaune, T., Suzuki, J., Shibata, K., et al. (2016). Nitric oxide-induced activation of the type 1 ryanodine receptor is critical for epileptic seizure-induced neuronal cell death. *EBioMedicine* 11, 253–261. doi: 10.1016/j.ebiom.2016.08.020

Milanese, M., Bonifacino, T., Fedele, E., Rebosio, C., Cattaneo, L., Benfenati, F., et al. (2015). Exocytosis regulates trafficking of GABA and glycine heterotransporters in spinal cord glutamatergic synapses: a mechanism for the excessive heterotransporter-induced release of glutamate in experimental amyotrophic lateral sclerosis. *Neurobiol. Dis.* 74, 314–324. doi: 10.1016/j.nbd.2014.12.004

Minciacchi, D., Kassa, R. M., Del Tongo, C., Mariotti, R., and Bentivoglio, M. (2009). Voronoi-based spatial analysis reveals selective interneuron changes in the cortex of FALS mice. *Exp. Neurol.* 215, 77–86. doi: 10.1016/j.expneurol.2008.09.005

Mishra, V., Shuai, B., Kodali, M., Shetty, G. A., Hattiangady, B., Rao, X., et al. (2015). Resveratrol treatment after status epilepticus restrains neurodegeneration and abnormal neurogenesis with suppression of oxidative stress and inflammation. *Sci. Rep.* 5:17807. doi: 10.1038/srep17807

Mosconi, L., Pupi, A., and De Leon, M. J. (2009). Brain glucose hypometabolism and oxidative stress in preclinical Alzheimer's disease. *Ann. N Y Acad. Sci.* 1147, 180–195. doi: 10.1196/annals.1427.007

Mulholland, P. J., Luong, N. T., Woodward, J. J., and Chandler, L. J. (2008). Brain-derived neurotrophic factor activation of extracellular signal-regulated kinase is autonomous from the dominant extrasynaptic NMDA receptor extracellular signal-regulated kinase shutoff pathway. *Neuroscience* 151, 419–427. doi: 10.1016/j.neuroscience.2007.11.001

Mülsch, A., Busse, R., Mordvintcev, P. I., Vanin, A. F., Nielsen, E. O., Scheel-Krüger, J., et al. (1994). Nitric oxide promotes seizure activity in kainate-treated rats. *Neuroreport* 5, 2325–2328. doi: 10.1097/00001756-199411000-00029

Murphy, E. J., Behrmann, D., Bates, C. M., and Horrocks, L. A. (1994). Lipid alterations following impact spinal cord injury in the rat. *Mol. Chem. Neuropathol.* 23, 13–26. doi: 10.1007/bf02858504

Murphy-Royal, C., Dupuis, J. P., Varela, J. A., Panatier, A., Pinson, B., Baufreton, J., et al. (2015). Surface diffusion of astrocytic glutamate transporters shapes synaptic transmission. *Nat. Neurosci.* 18, 219–226. doi: 10.1038/nn.3901

Mutch, W. A., and Hansen, A. J. (1984). Extracellular pH changes during spreading depression and cerebral ischemia: mechanisms of brain pH regulation. *J. Cereb. Blood Flow Metab.* 4, 17–27. doi: 10.1038/jcbfm.1984.3

Newman, L. A., Korol, D. L., and Gold, P. E. (2011). Lactate produced by glycogenolysis in astrocytes regulates memory processing. *PLoS One* 6:e28427. doi: 10.1371/journal.pone.0028427

Nicholls, D. G. (2004). Mitochondrial dysfunction and glutamate excitotoxicity studied in primary neuronal cultures. *Curr. Mol. Med.* 4, 149–177. doi: 10.2174/1566524043479239

Nicholls, D. G., and Budd, S. L. (2000). Mitochondria and neuronal survival. *Physiol. Rev.* 80, 315–360. doi: 10.1152/physrev.2000.80.1.315

Nikodemova, M., Small, A. L., Smith, S. M. C., Mitchell, G. S., and Watters, J. J. (2014). Spinal but not cortical microglia acquire an atypical phenotype with high VEGF, galectin-3 and osteopontin, and blunted inflammatory responses in ALS rats. *Neurobiol. Dis.* 69, 43–53. doi: 10.1016/j.nbd.2013.11.009

Nikolic, L., Nobili, P., Shen, W., and Audinat, E. (2019). Role of astrocyte purinergic signaling in epilepsy. *Glia* doi: 10.1002/glia.23747 [Epub ahead of print].

Norenberg, M. D., and Martinez-Hernandez, A. (1979). Fine structural localization of glutamine synthetase in astrocytes of rat brain. *Brain Res.* 161, 303–310. doi: 10.1016/0006-8993(79)90071-4

O'Byrne, M. B., and Tipton, K. F. (2000). Taurine-induced attenuation of MPP^+ neurotoxicity *in vitro*. *J. Neurochem.* 74, 2087–2093. doi: 10.1046/j.1471-4159.2000.0742087.x

Ohtsuki, T., Matsumoto, M., Suzuki, K., Taniguchi, N., and Kamada, T. (1993). Effect of transient forebrain ischemia on superoxide dismutases in gerbil hippocampus. *Brain Res.* 620, 305–309. doi: 10.1016/0006-8993(93)90171-i

Olabarria, M., Noristani, H. N., Verkhratsky, A., and Rodríguez, J. J. (2011). Age-dependent decrease in glutamine synthetase expression in the hippocampal astroglia of the triple transgenic Alzheimer's disease mouse model: mechanism for deficient glutamatergic transmission? *Mol. Neurodegener.* 6:55. doi: 10.1186/1750-1326-6-55

Olney, J. W. (1969). Brain lesions, obesity, and other disturbances in mice treated with monosodium glutamate. *Science* 164, 719–721. doi: 10.1126/science.164.3880.719

Ottersen, O. P., Zhang, N., and Walberg, F. (1992). Metabolic compartmentation of glutamate and glutamine: morphological evidence obtained by quantitative immunocytochemistry in rat cerebellum. *Neuroscience* 46, 519–534. doi: 10.1016/0306-4522(92)90141-n

Pál, B. (2018). Involvement of extrasynaptic glutamate in physiological and pathophysiological changes of neuronal excitability. *Cell. Mol. Life Sci.* 75, 2917–2949. doi: 10.1007/s00018-018-2837-5

Palmer, A. M., Marion, D. W., Botscheller, M. L., Bowen, D. M., and DeKosky, S. T. (1994). Increased transmitter amino acid concentration in human ventricular CSF after brain trauma. *Neuroreport* 6, 153–156. doi: 10.1097/00001756-199412300-00039

Papouin, T., Ladépêche, L., Ruel, J., Sacchi, S., Labasque, M., Hanini, M., et al. (2012). Synaptic and extrasynaptic NMDA receptors are gated by different endogenous coagonists. *Cell* 150, 633–646. doi: 10.1016/j.cell.2012.06.029

Parsons, M. P., and Raymond, L. A. (2014). Extrasynaptic NMDA receptor involvement in central nervous system disorders. *Neuron* 82, 279–293. doi: 10.1016/j.neuron.2014.03.030

Pasinelli, P., Houseweart, M. K., Brown, R. H., and Cleveland, D. W. (2000). Caspase-1 and -3 are sequentially activated in motor neuron death in Cu,Zn superoxide dismutase-mediated familial amyotrophic lateral sclerosis. *Proc. Natl. Acad. Sci. U S A* 97, 13901–13906. doi: 10.1073/pnas.240305897

Patel, M., Day, B. J., Crapo, J. D., Fridovich, I., and McNamara, J. O. (1996). Requirement for superoxide in excitotoxic cell death. *Neuron* 16, 345–355. doi: 10.1016/s0896-6273(00)80052-5

Patneau, D. K., and Mayer, M. L. (1990). Structure-activity relationships for amino acid transmitter candidates acting at N-methyl-D-aspartate and quisqualate receptors. *J. Neurosci.* 10, 2385–2399. doi: 10.1523/jneurosci.10-07-02385.1990

Patricio-Martínez, A., Sánchez-Zavaleta, R., Angulo-Cruz, I., Gutierrez-Praxedis, L., Ramírez, E., Martínez-García, I., et al. (2019). The acute activation of the CB1 receptor in the hippocampus decreases neurotoxicity and prevents spatial memory impairment in rats lesioned with β-amyloid 25–35. *Neuroscience* 416, 239–254. doi: 10.1016/j.neuroscience.2019.08.001

Pauletti, A., Terrone, G., Shekh-Ahmad, T., Salamone, A., Ravizza, T., Rizzi, M., et al. (2019). Targeting oxidative stress improves disease outcomes in a rat model of acquired epilepsy. *Brain* 142:e39. doi: 10.1093/brain/awz130

Pazdernik, T. L., Layton, M., Nelson, S. R., and Samson, F. E. (1992). The osmotic/calcium stress theory of brain damage: are free radicals involved? *Neurochem. Res.* 17, 11–21. doi: 10.1007/bf00966860

Pellegrini-Giampietro, D. E., Cherici, G., Alesiani, M., Carla, V., and Moroni, F. (1990). Excitatory amino acid release and free radical formation may cooperate in the genesis of ischemia-induced neuronal damage. *J. Neurosci.* 10, 1035–1041. doi: 10.1523/jneurosci.10-03-01035.1990

Peterson, A. R., and Binder, D. K. (2019). Regulation of synaptosomal GLT-1 and GLAST during epileptogenesis. *Neuroscience* 411, 185–201. doi: 10.1016/j.neuroscience.2019.05.048

Petkova, Z., Tchekalarova, J., Pechlivanova, D., Moyanova, S., Kortenska, L., Mitreva, R., et al. (2014). Treatment with melatonin after status epilepticus attenuates seizure activity and neuronal damage but does not prevent the disturbance in diurnal rhythms and behavioral alterations in spontaneously hypertensive rats in kainate model of temporal lobe epilepsy. *Epilepsy Behav.* 31, 198–208. doi: 10.1016/j.yebeh.2013.12.013

Petr, G. T., Sun, Y., Frederick, N. M., Zhou, Y., Dhamne, S. C., Hameed, M. Q., et al. (2015). Conditional deletion of the glutamate transporter GLT-1 reveals that astrocytic GLT-1 protects against fatal epilepsy while neuronal GLT-1 contributes significantly to glutamate uptake into synaptosomes. *J. Neurosci.* 35, 5187–5201. doi: 10.1523/jneurosci.4255-14.2015

Phillis, J. W., and Wu, P. H. (1981). The role of adenosine and its nucleotides in central synaptic transmission. *Prog. Neurobiol.* 16, 187–239. doi: 10.1016/0301-0082(81)90014-9

Pinto, S., Cunha, C., Barbosa, M., Vaz, A. R., and Brites, D. (2017). Exosomes from NSC-34 cells transfected with hSOD1–G93A are enriched in miR-124 and drive alterations in microglia phenotype. *Front. Neurosci.* 11:273. doi: 10.3389/fnins.2017.00273

Pittau, F., Grouiller, F., Spinelli, L., Seeck, M., Michel, C. M., and Vulliemoz, S. (2014). The role of functional neuroimaging in pre-surgical epilepsy evaluation. *Front. Neurol.* 5:31. doi: 10.3389/fneur.2014.00031

Politi, D. M., and Rogawski, M. A. (1991). Glyburide-sensitive K^+ channels in cultured rat hippocampal neurons: activation by cromakalim and energy-depleting conditions. *Mol. Pharmacol.* 40, 308–315.

Popova, I., Malkov, A., Ivanov, A. I., Samokhina, E., Buldakova, S., Gubkina, O., et al. (2017). Metabolic correction by pyruvate halts acquired epilepsy in multiple rodent models. *Neurobiol. Dis.* 106, 244–254. doi: 10.1016/j.nbd.2017.07.012

Prentice, H., Modi, J. P., and Wu, J.-Y. (2015). Mechanisms of neuronal protection against excitotoxicity, endoplasmic reticulum stress and mitochondrial dysfunction in stroke and neurodegenerative diseases. *Oxid. Med. Cell. Longev.* 2015:964518. doi: 10.1155/2015/964518

Proper, E. A., Hoogland, G., Kappen, S. M., Jansen, G. H., Rensen, M. G., Schrama, L. H., et al. (2002). Distribution of glutamate transporters in the hippocampus of patients with pharmaco-resistant temporal lobe epilepsy. *Brain* 125, 32–43. doi: 10.1093/brain/awf001

Qiang, M., Dong, X., Zha, Z., Zuo, X.-K., Song, X.-L., Zhao, L., et al. (2018). Selection of an ASIC1a-blocking combinatorial antibody that protects cells from ischemic death. *Proc. Natl. Acad. Sci. U S A* 115, E7469–E7477. doi: 10.1073/pnas.1807233115

Qin, S., Colin, C., Hinners, I., Gervais, A., Cheret, C., and Mallat, M. (2006). System X_c^- and apolipoprotein E expressed by microglia have opposite effects on the neurotoxicity of amyloid-β peptide 1–40. *J. Neurosci.* 26, 3345–3356. doi: 10.1523/jneurosci.5186-05.2006

Qiu, J., Tan, Y.-W., Hagenston, A. M., Martel, M.-A., Kneisel, N., Skehel, P. A., et al. (2013). Mitochondrial calcium uniporter Mcu controls excitotoxicity and is transcriptionally repressed by neuroprotective nuclear calcium signals. *Nat. Commun.* 4:2034. doi: 10.1038/ncomms3034

Rahimi, N., Hassanipour, M., Yarmohammadi, F., Faghir-Ghanesefat, H., Pourshadi, N., Bahramnejad, E., et al. (2019). Nitric oxide and glutamate are contributors of anti-seizure activity of rubidium chloride: a comparison with lithium. *Neurosci. Lett.* 708:134349. doi: 10.1016/j.neulet.2019.134349

Raiteri, L., Paolucci, E., Prisco, S., Raiteri, M., and Bonanno, G. (2003). Activation of a glycine transporter on spinal cord neurons causes enhanced glutamate release in a mouse model of amyotrophic lateral sclerosis. *Br. J. Pharmacol.* 138, 1021–1025. doi: 10.1038/sj.bjp.0705142

Rakhade, S. N., and Loeb, J. A. (2008). Focal reduction of neuronal glutamate transporters in human neocortical epilepsy. *Epilepsia* 49, 226–236. doi: 10.1111/j.1528-1167.2007.01310.x

Ralay Ranaivo, H., Craft, J. M., Hu, W., Guo, L., Wing, L. K., Van Eldik, L. J., et al. (2006). Glia as a therapeutic target: selective suppression of human amyloid-β-induced upregulation of brain proinflammatory cytokine production attenuates neurodegeneration. *J. Neurosci.* 26, 662–670. doi: 10.1523/jneurosci.4652-05.2006

Ransom, C. B., Ransom, B. R., and Sontheimer, H. (2000). Activity-dependent extracellular K^+ accumulation in rat optic nerve: the role of glial and axonal Na^+ pumps. *J. Physiol.* 522, 427–442. doi: 10.1111/j.1469-7793.2000.00427.x

Reiner, A., and Levitz, J. (2018). Glutamatergic signaling in the central nervous system: ionotropic and metabotropic receptors in concert. *Neuron* 98, 1080–1098. doi: 10.1016/j.neuron.2018.05.018

Reynolds, A., Laurie, C., Mosley, R. L., and Gendelman, H. E. (2007). Oxidative stress and the pathogenesis of neurodegenerative disorders. *Int. Rev. Neurobiol.* 82, 297–325. doi: 10.1016/S0074-7742(07)82016-2

Richter, C., and Kass, G. E. (1991). Oxidative stress in mitochondria: its relationship to cellular Ca^{2+} homeostasis, cell death, proliferation, and differentiation. *Chem. Biol. Interact.* 77, 1–23. doi: 10.1016/0009-2797(91)90002-o

Riepe, M., Hori, N., Ludolph, A. C., Carpenter, D. O., Spencer, P. S., and Allen, C. N. (1992). Inhibition of energy metabolism by 3-nitropropionic acid activates ATP-sensitive potassium channels. *Brain Res.* 586, 61–66. doi: 10.1016/0006-8993(92)91371-k

Rodríguez-Arellano, J. J., Parpura, V., Zorec, R., and Verkhratsky, A. (2016). Astrocytes in physiological aging and Alzheimer's disease. *Neuroscience* 323, 170–182. doi: 10.1016/j.neuroscience.2015.01.007

Rönicke, R., Mikhaylova, M., Rönicke, S., Meinhardt, J., Schröder, U. H., Fändrich, M., et al. (2011). Early neuronal dysfunction by amyloid β oligomers depends on activation of NR2B-containing NMDA receptors. *Neurobiol. Aging* 32, 2219–2228. doi: 10.1016/j.neurobiolaging.2010.01.011

Rose, J., Brian, C., Woods, J., Pappa, A., Panayiotidis, M. I., Powers, R., et al. (2017). Mitochondrial dysfunction in glial cells: implications for neuronal homeostasis and survival. *Toxicology* 391, 109–115. doi: 10.1016/j.tox.2017.06.011

Rossi, D., Brambilla, L., Valori, C. F., Roncoroni, C., Crugnola, A., Yokota, T., et al. (2008). Focal degeneration of astrocytes in amyotrophic lateral sclerosis. *Cell Death Differ.* 15, 1691–1700. doi: 10.1038/cdd.2008.99

Rossi, D. J., Oshima, T., and Attwell, D. (2000). Glutamate release in severe brain ischaemia is mainly by reversed uptake. *Nature* 403, 316–321. doi: 10.1038/35002090

Rothstein, J. D., Dykes-Hoberg, M., Pardo, C. A., Bristol, L. A., Jin, L., Kuncl, R. W., et al. (1996). Knockout of glutamate transporters reveals a major role for astroglial transport in excitotoxicity and clearance of glutamate. *Neuron* 16, 675–686. doi: 10.1016/s0896-6273(00)80086-0

Rothstein, J. D., Patel, S., Regan, M. R., Haenggeli, C., Huang, Y. H., Bergles, D. E., et al. (2005). β-lactam antibiotics offer neuroprotection by increasing glutamate transporter expression. *Nature* 433, 73–77. doi: 10.1038/nature03180

Rowley, S., Liang, L.-P., Fulton, R., Shimizu, T., Day, B., and Patel, M. (2015). Mitochondrial respiration deficits driven by reactive oxygen species in experimental temporal lobe epilepsy. *Neurobiol. Dis.* 75, 151–158. doi: 10.1016/j.nbd.2014.12.025

Rutecki, P. A., Sayin, U., Yang, Y., and Hadar, E. (2002). Determinants of ictal epileptiform patterns in the hippocampal slice. *Epilepsia* 43, 179–183. doi: 10.1046/j.1528-1157.43.s.5.34.x

Ryan, K., Backos, D. S., Reigan, P., and Patel, M. (2012). Post-translational oxidative modification and inactivation of mitochondrial complex I in epileptogenesis. *J. Neurosci.* 32, 11250–11258. doi: 10.1523/jneurosci.0907-12.2012

Saba, L., Viscomi, M. T., Caioli, S., Pignataro, A., Bisicchia, E., Pieri, M., et al. (2016). Altered functionality, morphology and vesicular glutamate transporter expression of cortical motor neurons from a presymptomatic mouse model of amyotrophic lateral sclerosis. *Cereb. Cortex* 26, 1512–1528. doi: 10.1093/cercor/bhu317

Sah, P. (1996). Ca^{2+}-activated K^+ currents in neurones: types, physiological roles and modulation. *Trends Neurosci.* 19, 150–154. doi: 10.1016/s0166-2236(96)80026-9

Samson, A. J., Robertson, G., Zagnoni, M., and Connolly, C. N. (2016). Neuronal networks provide rapid neuroprotection against spreading toxicity. *Sci. Rep.* 6:33746. doi: 10.1038/srep33746

Sapolsky, R. M. (2001). Cellular defenses against excitotoxic insults. *J. Neurochem.* 76, 1601–1611. doi: 10.1046/j.1471-4159.2001.00203.x

Sarac, S., Afzal, S., Broholm, H., Madsen, F. F., Ploug, T., and Laursen, H. (2009). Excitatory amino acid transporters EAAT-1 and EAAT-2 in temporal lobe and hippocampus in intractable temporal lobe epilepsy. *APMIS* 117, 291–301. doi: 10.1111/j.1600-0463.2009.02443.x

Sasaki, S., Komori, T., and Iwata, M. (2000). Excitatory amino acid transporter 1 and 2 immunoreactivity in the spinal cord in amyotrophic lateral sclerosis. *Acta Neuropathol.* 100, 138–144. doi: 10.1007/s004019900159

Sato, H., Kuriyama-Matsumura, K., Hashimoto, T., Sasaki, H., Wang, H., Ishii, T., et al. (2001). Effect of oxygen on induction of the cystine transporter by bacterial lipopolysaccharide in mouse peritoneal macrophages. *J. Biol. Chem.* 276, 10407–10412. doi: 10.1074/jbc.m007216200

Sato, H., Tamba, M., Ishii, T., and Bannai, S. (1999). Cloning and expression of a plasma membrane cystine/glutamate exchange transporter composed of two distinct proteins. *J. Biol. Chem.* 274, 11455–11458. doi: 10.1074/jbc.274.17.11455

Sato, H., Tamba, M., Okuno, S., Sato, K., Keino-Masu, K., Masu, M., et al. (2002). Distribution of cystine/glutamate exchange transporter, system x_c^-, in the mouse brain. *J. Neurosci.* 22, 8028–8033. doi: 10.1523/jneurosci.22-18-08028.2002

Schafe, G. E., Atkins, C. M., Swank, M. W., Bauer, E. P., Sweatt, J. D., and Ledoux, J. E. (2000). Activation of ERK/MAP kinase in the amygdala is required for memory consolidation of Pavlovian fear conditioning. *J. Neurosci.* 20, 8177–8187. doi: 10.1523/jneurosci.20-21-08177.2000

Scheuner, D., Eckman, C., Jensen, M., Song, X., Citron, M., Suzuki, N., et al. (1996). Secreted amyloid β-protein similar to that in the senile plaques of Alzheimer's disease is increased *in vivo* by the presenilin 1 and 2 and APP mutations linked to familial Alzheimer's disease. *Nat. Med.* 2, 864–870. doi: 10.1038/nm0896-864

Schor, N. F. (1988). Inactivation of mammalian brain glutamine synthetase by oxygen radicals. *Brain Res.* 456, 17–21. doi: 10.1016/0006-8993(88)90341-1

Schousboe, A., Westergaard, N., Waagepetersen, H. S., Larsson, O. M., Bakken, I. J., and Sonnewald, U. (1997). Trafficking between glia and neurons of TCA cycle intermediates and related metabolites. *Glia* 21, 99–105. doi: 10.1002/(sici)1098-1136(199709)21:1<99::aid-glia11 >3.0.co;2-w

Schurr, A. (2014). Cerebral glycolysis: a century of persistent misunderstanding and misconception. *Front. Neurosci.* 8:360. doi: 10.3389/fnins.2014.00360

Scimemi, A., Meabon, J. S., Woltjer, R. L., Sullivan, J. M., Diamond, J. S., and Cook, D. G. (2013). Amyloid-β1–42 slows clearance of synaptically released glutamate by mislocalizing astrocytic GLT-1. *J. Neurosci.* 33, 5312–5318. doi: 10.1523/JNEUROSCI.5274-12.2013

Seifert, G., Carmignoto, G., and Steinhäuser, C. (2010). Astrocyte dysfunction in epilepsy. *Brain Res. Rev.* 63, 212–221. doi: 10.1016/j.brainresrev.2009.10.004

Selvaraj, B. T., Livesey, M. R., Zhao, C., Gregory, J. M., James, O. T., Cleary, E. M., et al. (2018). C9ORF72 repeat expansion causes vulnerability of motor neurons to Ca^{2+}-permeable AMPA receptor-mediated excitotoxicity. *Nat. Commun.* 9:347. doi: 10.1038/s41467-017-02729-0

Sha, L., Wang, X., Li, J., Shi, X., Wu, L., Shen, Y., et al. (2017). Pharmacologic inhibition of Hsp90 to prevent GLT-1 degradation as an effective therapy for epilepsy. *J. Exp. Med.* 214, 547–563. doi: 10.1084/jem.20160667

Sheffield, L. G., Marquis, J. G., and Berman, N. E. J. (2000). Regional distribution of cortical microglia parallels that of neurofibrillary tangles in Alzheimer's disease. *Neurosci. Lett.* 285, 165–168. doi: 10.1016/s0304-3940(00)01037-5

Shibuya, K., Park, S. B., Geevasinga, N., Menon, P., Howells, J., Simon, N. G., et al. (2016). Motor cortical function determines prognosis in sporadic ALS. *Neurology* 87, 513–520. doi: 10.1212/wnl.0000000000002912

Shih, A. Y., Erb, H., Sun, X., Toda, S., Kalivas, P. W., and Murphy, T. H. (2006). Cystine/glutamate exchange modulates glutathione supply for neuroprotection from oxidative stress and cell proliferation. *J. Neurosci.* 26, 10514–10523. doi: 10.1523/jneurosci.3178-06.2006

Siemkowicz, E., and Hansen, A. J. (1981). Brain extracellular ion composition and EEG activity following 10 minutes ischemia in normo- and hyperglycemic rats. *Stroke* 12, 236–240. doi: 10.1161/01.str.12.2.236

Simon, R. P., Niro, M., and Gwinn, R. (1993). Brain acidosis induced by hypercarbic ventilation attenuates focal ischemic injury. *J. Pharmacol. Exp. Ther.* 267, 1428–1431.

Simpson, J. E., Ince, P. G., Lace, G., Forster, G., Shaw, P. J., Matthews, F., et al. (2010). Astrocyte phenotype in relation to Alzheimer-type pathology in the ageing brain. *Neurobiol. Aging* 31, 578–590. doi: 10.1016/j.neurobiolaging.2008.05.015

Singh, A., and Trevick, S. (2016). The epidemiology of global epilepsy. *Neurol. Clin.* 34, 837–847. doi: 10.1016/j.ncl.2016.06.015

Sloviter, R. S., Dichter, M. A., Rachinsky, T. L., Dean, E., Goodman, J. H., Sollas, A. L., et al. (1996). Basal expression and induction of glutamate decarboxylase and GABA in excitatory granule cells of the rat and monkey hippocampal dentate gyrus. *J. Comp. Neurol.* 373, 593–618. doi: 10.1002/(sici)1096-9861(19960930)373:4<593::aid-cne8>3.0.co;2-x

Smith, C. D., Carney, J. M., Starke-Reed, P. E., Oliver, C. N., Stadtman, E. R., Floyd, R. A., et al. (1991). Excess brain protein oxidation and enzyme dysfunction in normal aging and in Alzheimer disease. *Proc. Natl. Acad. Sci. U S A* 88, 10540–10543. doi: 10.1073/pnas.88.23.10540

Sokal, D. M., Mason, R., and Parker, T. L. (2000). Multi-neuronal recordings reveal a differential effect of thapsigargin on bicuculline- or gabazine-induced epileptiform excitability in rat hippocampal neuronal networks. *Neuropharmacology* 39, 2408–2417. doi: 10.1016/s0028-3908(00)00095-2

Soukupová, M., Binaschi, A., Falcicchia, C., Zucchini, S., Roncon, P., Palma, E., et al. (2014). Impairment of GABA release in the hippocampus at the time of the first spontaneous seizure in the pilocarpine model of temporal lobe epilepsy. *Exp. Neurol.* 257, 39–49. doi: 10.1016/j.expneurol.2014.04.014

Stavrovskaya, I. G., and Kristal, B. S. (2005). The powerhouse takes control of the cell: is the mitochondrial permeability transition a viable therapeutic target against neuronal dysfunction and death? *Free Radic. Biol. Med.* 38, 687–697. doi: 10.1016/j.freeradbiomed.2004.11.032

Steinhäuser, C., Grunnet, M., and Carmignoto, G. (2016). Crucial role of astrocytes in temporal lobe epilepsy. *Neuroscience* 323, 157–169. doi: 10.1016/j.neuroscience.2014.12.047

Stephens, B., Guiloff, R. J., Navarrete, R., Newman, P., Nikhar, N., and Lewis, P. (2006). Widespread loss of neuronal populations in the spinal ventral horn in sporadic motor neuron disease. A morphometric study. *J. Neurol. Sci.* 244, 41–58. doi: 10.1016/j.jns.2005.12.003

Stobart, J. L., and Anderson, C. M. (2013). Multifunctional role of astrocytes as gatekeepers of neuronal energy supply. *Front. Cell. Neurosci.* 7:38. doi: 10.3389/fncel.2013.00038

Sultan, S., Li, L., Moss, J., Petrelli, F., Cassé, F., Gebara, E., et al. (2015). Synaptic integration of adult-born hippocampal neurons is locally controlled by astrocytes. *Neuron* 88, 957–972. doi: 10.1016/j.neuron.2015.10.037

Surin, A. M., Gorbacheva, L. R., Savinkova, I. G., Sharipov, R. R., Khodorov, B. I., and Pinelis, V. G. (2014). Study on ATP concentration changes in cytosol of individual cultured neurons during glutamate-induced deregulation of calcium homeostasis. *Biochemistry* 79, 146–157. doi: 10.1134/s0006297914020084

Susarla, B. T., and Robinson, M. B. (2008). Internalization and degradation of the glutamate transporter GLT-1 in response to phorbol ester. *Neurochem. Int.* 52, 709–722. doi: 10.1016/j.neuint.2007.08.020

Suzuki, A., Stern, S. A., Bozdagi, O., Huntley, G. W., Walker, R. H., Magistretti, P. J., et al. (2011). Astrocyte-neuron lactate transport is required for long-term memory formation. *Cell* 144, 810–823. doi: 10.1016/j.cell.2011.02.018

Talantova, M., Sanz-Blasco, S., Zhang, X., Xia, P., Waseem, M., and Okamoto, S. (2013). A β induces astrocytic glutamate release , extrasynaptic NMDA receptor activation, and synaptic loss. *Proc. Natl. Acad. Sci. U S A* 110, E2518–E2527. doi: 10.1073/pnas.1306832110

Tanaka, K., Watase, K., Manabe, T., Yamada, K., Watanabe, M., Takahashi, K., et al. (1997). Epilepsy and exacerbation of brain injury in mice lacking the glutamate transporter GLT-1. *Science* 276, 1699–1702. doi: 10.1126/science.276.5319.1699

Tang, C. M., Dichter, M., and Morad, M. (1990). Modulation of the N-methyl-D-aspartate channel by extracellular H+. *Proc. Natl. Acad. Sci. U S A* 87, 6445–6449. doi: 10.1073/pnas.87.16.6445

Tanqueiro, S. R., Ramalho, R. M., Rodrigues, T. M., Lopes, L. V., Sebastião, A. M., and Diógenes, M. J. (2018). Inhibition of NMDA receptors prevents the loss of BDNF function induced by amyloid β. *Front. Pharmacol.* 9:237. doi: 10.3389/fphar.2018.00237

Taylor, J. M., Main, B. S., and Crack, P. J. (2013). Neuroinflammation and oxidative stress: co-conspirators in the pathology of Parkinson's disease. *Neurochem. Int.* 62, 803–819. doi: 10.1016/j.neuint.2012.12.016

Texidó, L., Martín-Satué, M., Alberdi, E., Solsona, C., and Matute, C. (2011). Amyloid β peptide oligomers directly activate NMDA receptors. *Cell Calcium* 49, 184–190. doi: 10.1016/j.ceca.2011.02.001

Thielsen, K. D., Moser, J. M., Schmitt-John, T., Jensen, M. S., Jensen, K., and Holm, M. M. (2013). The Wobbler mouse model of amyotrophic lateral sclerosis (ALS) displays hippocampal hyperexcitability and reduced number of interneurons, but no presynaptic vesicle release impairments. *PLoS One* 8:e82767. doi: 10.1371/journal.pone.0082767

Thorn, T. L., He, Y., Jackman, N. A., Lobner, D., Hewett, J. A., and Hewett, S. J. (2015). A cytotoxic, co-operative interaction between energy deprivation and glutamate release from system xc- mediates aglycemic neuronal cell death. *ASN Neuro* 7:1759091415614301. doi: 10.1177/1759091415614301

Tombaugh, G. C., and Sapolsky, R. M. (1990). Mild acidosis protects hippocampal neurons from injury induced by oxygen and glucose deprivation. *Brain Res.* 506, 343–345. doi: 10.1016/0006-8993(90)91277-n

Tong, J., Huang, C., Bi, F., Wu, Q., Huang, B., Liu, X., et al. (2013). Expression of ALS-linked TDP-43 mutant in astrocytes causes non-cell-autonomous motor neuron death in rats. *EMBO J.* 32, 1917–1926. doi: 10.1038/emboj.2013.122

Torp, R., Andiné, P., Hagberg, H., Karagülle, T., Blackstad, T. W., and Ottersen, O. P. (1991). Cellular and subcellular redistribution of glutamate-, glutamine- and taurine-like immunoreactivities during forebrain ischemia: a semiquantitative electron microscopic study in rat hippocampus. *Neuroscience* 41, 433–447. doi: 10.1016/0306-4522(91)90339-p

Trapp, S., and Ballanyi, K. (1995). KATP channel mediation of anoxia-induced outward current in rat dorsal vagal neurons *in vitro*. *J. Physiol.* 487, 37–50. doi: 10.1113/jphysiol.1995.sp020859

Trussell, L. O., and Fischbach, G. D. (1989). Glutamate receptor desensitization and its role in synaptic transmission. *Neuron* 3, 209–218. doi: 10.1016/0896-6273(89)90034-2

Van Damme, P., Bogaert, E., Dewil, M., Hersmus, N., Kiraly, D., Scheveneels, W., et al. (2007). Astrocytes regulate GluR2 expression in motor neurons and their vulnerability to excitotoxicity. *Proc. Natl. Acad. Sci. U S A* 104, 14825–14830. doi: 10.1073/pnas.0705046104

Van Damme, P., Braeken, D., Callewaert, G., Robberecht, W., and Van Den Bosch, L. (2005). GluR2 deficiency accelerates motor neuron degeneration in a mouse model of amyotrophic lateral sclerosis. *J. Neuropathol. Exp. Neurol.* 64, 605–612. doi: 10.1097/01.jnen.0000171647.09589.07

van den Berg, C. J., and Garfinkel, D. (1971). A simulation study of brain compartments. Metabolism of glutamate and related substances in mouse brain. *Biochem. J.* 123, 211–218. doi: 10.1042/bj1230211

Vergun, O., Keelan, J., Khodorov, B. I., and Duchen, M. R. (1999). Glutamate-induced mitochondrial depolarisation and perturbation of calcium homeostasis in cultured rat hippocampal neurones. *J. Physiol.* 519, 451–466. doi: 10.1111/j.1469-7793.1999.0451m.x

Vesce, S., Kirk, L., and Nicholls, D. G. (2004). Relationships between superoxide levels and delayed calcium deregulation in cultured cerebellar granule cells exposed continuously to glutamate. *J. Neurochem.* 90, 683–693. doi: 10.1111/j.1471-4159.2004.02516.x

Vincent, P., and Mulle, C. (2009). Kainate receptors in epilepsy and excitotoxicity. *Neuroscience* 158, 309–323. doi: 10.1016/j.neuroscience.2008.02.066

Vucic, S., and Kiernan, M. C. (2006). Axonal excitability properties in amyotrophic lateral sclerosis. *Clin. Neurophysiol.* 117, 1458–1466. doi: 10.1016/j.clinph.2006.04.016

Vucic, S., and Kiernan, M. C. (2013). Utility of transcranial magnetic stimulation in delineating amyotrophic lateral sclerosis pathophysiology. *Handb. Clin. Neurol.* 116, 561–575. doi: 10.1016/b978-0-444-53497-2.00045-0

Vyklický, L. (1993). Calcium-mediated modulation of N-methyl-D-aspartate (NMDA) responses in cultured rat hippocampal neurones. *J. Physiol.* 470, 575–600. doi: 10.1113/jphysiol.1993.sp019876

Wagle-Shukla, A., Ni, Z., Gunraj, C. A., Bahl, N., and Chen, R. (2009). Effects of short interval intracortical inhibition and intracortical facilitation on short interval intracortical facilitation in human primary motor cortex. *J. Physiol.* 587, 5665–5678. doi: 10.1113/jphysiol.2009.181446

Walczyk, T., and Wick, J. Y. (2017). The ketogenic diet: making a comeback. *Consult. Pharm.* 32, 388–396. doi: 10.4140/tcp.n.2017.388

Waldmann, R., Champigny, G., Bassilana, F., Heurteaux, C., and Lazdunski, M. (1997). A proton-gated cation channel involved in acid-sensing. *Nature* 386, 173–177. doi: 10.1038/386173a0

Walsh, D. M., Klyubin, I., Fadeeva, J. V., Cullen, W. K., Anwyl, R., Wolfe, M. S., et al. (2002). Naturally secreted oligomers of amyloid β protein potently inhibit hippocampal long-term potentiation *in vivo*. *Nature* 416, 535–539. doi: 10.1038/416535a

Walz, W. (2000). Role of astrocytes in the clearance of excess extracellular potassium. *Neurochem. Int.* 36, 291–300. doi: 10.1016/s0197-0186(99)00137-0

Wang, C., Xie, N., Wang, Y., Li, Y., Ge, X., and Wang, M. (2015). Role of the mitochondrial calcium uniporter in rat hippocampal neuronal death after pilocarpine-induced status epilepticus. *Neurochem. Res.* 40, 1739–1746. doi: 10.1007/s11064-015-1657-3

Wang, X., Wang, W., Li, L., Perry, G., Lee, H. G., and Zhu, X. (2014). Oxidative stress and mitochondrial dysfunction in Alzheimer's disease. *Biochim. Biophys. Acta* 1842, 1240–1247. doi: 10.1016/j.bbadis.2013.10.015

Ward, M. W., Huber, H. J., Weisová, P., Düssmann, H., Nicholls, D. G., and Prehn, J. H. M. (2007). Mitochondrial and plasma membrane potential of cultured cerebellar neurons during glutamate-induced necrosis, apoptosis, and tolerance. *J. Neurosci.* 27, 8238–8249. doi: 10.1523/JNEUROSCI.1984-07.2007

Ward, M. W., Rego, A. C., Frenguelli, B. G., and Nicholls, D. G. (2000). Mitochondrial membrane potential and glutamate excitotoxicity in cultured cerebellar granule cells. *J. Neurosci.* 20, 7208–7219. doi: 10.1523/jneurosci.20-19-07208.2000

Warr, O., Takahashi, M., and Attwell, D. (1999). Modulation of extracellular glutamate concentration in rat brain slices by cystine-glutamate exchange. *J. Physiol.* 514, 783–793. doi: 10.1111/j.1469-7793.1999.783ad.x

Wasterlain, C. G., Thompson, K. W., Suchomelova, L., and Niquet, J. (2010). Brain energy metabolism during experimental neonatal seizures. *Neurochem. Res.* 35, 2193–2198. doi: 10.1007/s11064-010-0339-4

Watkins, J. C., and Evans, R. H. (1981). Excitatory amino acid transmitters. *Annu. Rev. Pharmacol. Toxicol.* 21, 165–204. doi: 10.1146/annurev.pa.21.040181.001121

Weisová, P., Concannon, C. G., Devocelle, M., Prehn, J. H. M., and Ward, M. W. (2009). Regulation of glucose transporter 3 surface expression by the AMP-activated protein kinase mediates tolerance to glutamate excitation in neurons. *J. Neurosci.* 29, 2997–3008. doi: 10.1523/jneurosci.0354-09.2009

Westergaard, N., Banke, T. U. E., Wahl, P., Sonnewaldt, U., and Schousboe, A. (1995). Citrate modulates the regulation by Zn^{2+} of N-methyl-D-aspartate receptor-mediated channel current and neurotransmitter release. *Proc. Natl. Acad. Sci. U S A* 92, 3367–3370. doi: 10.1073/pnas.92.8.3367

Whitesell, L., and Lindquist, S. L. (2005). HSP90 and the chaperoning of cancer. *Nat. Rev. Cancer* 5, 761–772. doi: 10.1038/nrc1716

Williams, S., Hamil, N., Abramov, A. Y., Walker, M. C., and Kovac, S. (2015). Status epilepticus results in persistent overproduction of reactive oxygen species, inhibition of which is neuroprotective. *Neuroscience* 303, 160–165. doi: 10.1016/j.neuroscience.2015.07.005

Winkler, P., Luhmann, H. J., and Kilb, W. (2019). Taurine potentiates the anticonvulsive effect of the GABAA agonist muscimol and pentobarbital in the immature mouse hippocampus. *Epilepsia* 60, 464–474. doi: 10.1111/epi.14651

Witgert, M., Salamone, A. R., Strutt, A. M., Jawaid, A., Massman, P. J., Bradshaw, M., et al. (2010). Frontal-lobe mediated behavioral dysfunction in amyotrophic lateral sclerosis. *Eur. J. Neurol.* 17, 103–110. doi: 10.1111/j.1468-1331.2009.02801.x

Wolosker, H., Balu, D. T., and Coyle, J. T. (2016). The rise and fall of the d-serine-mediated gliotransmission hypothesis. *Trends Neurosci.* 39, 712–721. doi: 10.1016/j.tins.2016.09.007

Wright, A., and Vissel, B. (2012). The essential role of AMPA receptor GluR2 subunit RNA editing in the normal and diseased brain. *Front. Mol. Neurosci.* 5:34. doi: 10.3389/fnmol.2012.00034

Wu, H. Y., and Lynch, D. R. (2006). Calpain and synaptic function. *Mol. Neurobiol.* 33, 215–236. doi: 10.1385/mn:33:3:215

Yamamoto, M., Kiyota, T., Walsh, S. M., Liu, J., Kipnis, J., and Ikezu, T. (2008). Cytokine-mediated inhibition of fibrillar amyloid-β peptide degradation by human mononuclear phagocytes. *J. Immunol.* 181, 3877–3886. doi: 10.4049/jimmunol.181.6.3877

Yan, X., Shi, Z. F., Xu, L. X., Li, J. X., Wu, M., Wang, X. X., et al. (2017). Glutamate impairs mitochondria aerobic respiration capacity and enhances glycolysis in cultured rat astrocytes. *Biomed. Environ. Sci.* 30, 44–51. doi: 10.3967/bes2017.005

Yao, J., Irwin, R. W., Zhao, L., Nilsen, J., Hamilton, R. T., and Brinton, R. D. (2009). Mitochondrial bioenergetic deficit precedes Alzheimer's pathology in

female mouse model of Alzheimer's disease. *Proc. Natl. Acad. Sci. U S A* 106, 14670–14675. doi: 10.1073/pnas.0903563106

Yao, K., and Zu, H. B. (2020). Microglial polarization: novel therapeutic mechanism against Alzheimer's disease. *Inflammopharmacology* 28, 95–110. doi: 10.1007/s10787-019-00613-5

Yenari, M. A., Giffard, R. G., Sapolsky, R. M., and Steinberg, G. K. (1999). The neuroprotective potential of heat shock protein 70 (HSP70). *Mol. Med. Today* 5, 525–531. doi: 10.1016/s1357-4310(99)01599-3

Zarei, S., Carr, K., Reiley, L., Diaz, K., Guerra, O., Altamirano, P., et al. (2015). A comprehensive review of amyotrophic lateral sclerosis. *Surg. Neurol. Int.* 6:171. doi: 10.4103/2152-7806.169561

Zeng, L. H., Bero, A. W., Zhang, B., Holtzman, D. M., and Wong, M. (2010). Modulation of astrocyte glutamate transporters decreases seizures in a mouse model of tuberous sclerosis complex. *Neurobiol. Dis.* 37, 764–771. doi: 10.1016/j.nbd.2009.12.020

Zhang, S., Sun, P., Sun, Z., Zhang, J., Zhou, J., and Gu, Y. (2013). Cortical GABAergic neurons are more severely impaired by alkalosis than acidosis. *BMC Neurol.* 13:192. doi: 10.1186/1471-2377-13-192

Zhao, W., Beers, D. R., and Appel, S. H. (2013). Immune-mediated mechanisms in the pathoprogression of amyotrophic lateral sclerosis. *J. Neuroimmune Pharmacol.* 8, 888–899. doi: 10.1007/s11481-013-9489-x

Zhou, X., Chen, Z., Yun, W., Ren, J., Li, C., Program, N., et al. (2015). Revisiting the function of extrasynaptic NMDA receptor in excitotoxicity. *Neuroscientist* 21, 337–344. doi: 10.1177/1073858414548724

Zhou, X., Ding, Q., Chen, Z., Yun, H., and Wang, H. (2013). Involvement of the GluN2A and GluN2B subunits in synaptic and extrasynaptic N-methyl-D-aspartate receptor function and neuronal excitotoxicity. *J. Biol. Chem.* 288, 24151–24159. doi: 10.1074/jbc.m113.482000

Zhou, L., Li, F., Xu, H.-B., Luo, C.-X., Wu, H.-Y., Zhu, M.-M., et al. (2010). Treatment of cerebral ischemia by disrupting ischemia-induced interaction of nNOS with PSD-95. *Nat. Med.* 16, 1439–1443. doi: 10.1038/nm.2245

Zivin, J. A., and Choi, D. W. (1991). Stroke therapy. *Sci. Am.* 265, 56–65. doi: 10.1038/scientificamerican0791-56

Conflict of Interest: The authors declare that the research was conducted in the absence of any commercial or financial relationships that could be construed as a potential conflict of interest.

Copyright © 2020 Armada-Moreira, Gomes, Pina, Savchak, Gonçalves-Ribeiro, Rei, Pinto, Morais, Martins, Ribeiro, Sebastião, Crunelli and Vaz. This is an open-access article distributed under the terms of the Creative Commons Attribution License (CC BY). The use, distribution or reproduction in other forums is permitted, provided the original author(s) and the copyright owner(s) are credited and that the original publication in this journal is cited, in accordance with accepted academic practice. No use, distribution or reproduction is permitted which does not comply with these terms.

Nanoscale

MINIREVIEW

View Article Online
View Journal | View Issue

Published on 28 October 2016. Downloaded by Universidade de Lisboa on 12/5/2019 9:27:16 AM.

CrossMark click for updates

Cite this: DOI: 10.1039/c6nr07807a

Droplet-microfluidics towards the assembly of advanced building blocks in cell mimicry

Adam Armada-Moreira,[a,b,c] Essi Taipaleenmäki,[a] Fabian Itel,[a] Yan Zhang[a] and Brigitte Städler*[a]

Received 4th October 2016,
Accepted 27th October 2016
DOI: 10.1039/c6nr07807a
www.rsc.org/nanoscale

Therapeutic cell mimicry is an approach in nanomedicine aiming at substituting for missing or lost cellular functions employing nature-inspired concepts. Pioneered decades ago, only now is this technology empowered with the arsenal of nanotechnological tools and ready to provide radically new solutions such as assembling synthetic organelles and artificial cells. One of these tools is droplet microfluidics (D-μF), which provides the flexibility to generate cargo-loaded particles with tunable size and shape in a fast and reliable manner, an essential requirement in cell mimicry. This minireview aims at outlining the developments in D-μF from the past four years focusing on the assembly of nanoparticles, Janus-shaped and other non-spherical particles as well as their loading with biological payloads.

Introduction

Since its introduction in 2001,[1] droplet microfluidics (D-μF) has been developed into widely applied methods in diverse fields due to its versatility, reliability, low sample consumption, high throughput, *etc.* With the advent of companies selling microfluidic chips and accessories, D-μF has also become even more widespread since access to micro- (or nano-) fabrication facilities became unnecessary.

In the context of nanomedicine and biology,[2] D-μF has been applied for sensing,[3] drug discovery,[4] and assembly of micro/nanoparticles and reaction vessels. Therapeutic cell mimicry is an emerging field of research, which aims at providing nature-inspired approaches to address biomedical challenges by substituting for missing or lost cellular function. The assembly of such mimics, including artificial organelles,[5] artificial cells,[6] and biological nanobots,[7] requires access to flexible yet reliable fabrication methods, which can accommodate for the complexity of natural role models in terms of size, shape, and function, among others. D-μF is such an approach that can fulfil these prerequisites, as recently reviewed for artificial cells by the deMello group.[8] Traditional assembly

[a]*Interdisciplinary Nanoscience Center (iNANO), Aarhus University, Gustav Wieds Vej 14, 8000 Aarhus, Denmark. E-mail: bstadler@inano.au.dk*
[b]*Instituto de Farmacologia e Neurociências, Faculdade de Medicina da Universidade de Lisboa, 1649-028 Lisboa, Portugal*
[c]*Instituto de Medicina Molecular, Faculdade de Medicina da Universidade de Lisboa, 1649-028 Lisboa, Portugal*



Adam Armada-Moreira

Adam Armada-Moreira studied Biochemistry and Neurosciences at the University of Lisbon, where he completed his MSc degree in 2015, and is now pursuing a PhD in Neurosciences at the University of Lisbon, Portugal. Under the supervision of Sandra Henriques and Brigitte Städler, he aims at combining neurosciences and nanoscience. His research is focused on applying nanoscience and artificial particles to yield nature-inspired solutions to counteract excitotoxicity.

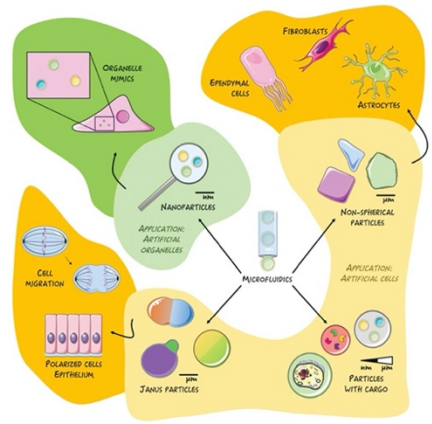


Essi Taipaleenmäki

Essi Taipaleenmäki studied organic chemistry under the nanoscience program of the University of Jyväskylä, Finland, from where she received her diploma in 2016. She joined the Städler lab as a PhD student at the Interdisciplinary Nanoscience Center, Aarhus University, Denmark. Her research interests lie in medical applications of nanoscience, such as nanoparticulate systems for drug delivery focusing on oral delivery.

This journal is © The Royal Society of Chemistry 2016

Published on 28 October 2016. Downloaded by Universidade de Lisboa on 12/5/2019 9:27:16 AM.



Scheme 1 Cartoon illustrating the use of D-μF for the assembly of nanoparticles, Janus particles, and non-spherical particles as well as their loading with biological cargo and potential application in cell mimicry.

methods such as the self-assembly of lipids and block copolymers into liposomes[9,10] and polymersomes,[5] respectively, or layer-by-layer based techniques[11] have been successful in fabricating building blocks for cell mimicry. However, D-μF is uniquely amendable for diverse requirements in terms of sizes (from nanometer particles to large micrometer sized beads), shape or type of loaded cargo.

The aim of this minireview is to highlight the latest developments in D-μF which have the potential to provide innovative tools and methods to be applied in cell mimicry (Scheme 1). Specifically, we will focus on the assembly of nanoparticles, Janus- and other non-spherical particles as well as the use of biological cargo. We will discuss their relevance and envisioned biomedical applications by providing selected examples from the past four years.

Nanoparticles

Artificial organelles are envisioned to be nano-sized entities with intracellular biocatalytic activity. Among the crucial prerequisites for their assembly is the access to sub-300 nm-sized, colloidally stable, monodisperse nanoparticles. D-μF has been applied in the assembly of various kinds of polymeric,[12,13] lipid-based,[14,15] inorganic[16,17] and composite nanoparticles.[18,19] While traditional macroscale methods often lack the precise control over the nucleation and growth processes that are required to produce nanoparticles with well-defined properties, D-μF allows for rapid and uniform heat and mass transfer *via* accurate control of fluids and their interfaces, leading to a more controlled and homogeneous reactive environment.[20] A detailed discussion about what makes D-μF an appealing method for nanoparticle fabrication is available in an excellent review by Capretto *et al.*[20]

In recent years, the most favored fabrication technique for both polymer-[12,13,21–27] and lipid-based[14,15,28–32] nanoparticles has been the hydrodynamic flow focusing (HFF) approach. In HFF, polymers or lipids are dissolved in an organic solvent which is then hydrodynamically focused by two co-axial aqueous streams into a thin sheet (Fig. 1A). This sheet of the organic solvent diffuses into water until a critical concentration is reached, where the nanoparticles start to precipitate.

A variety of biodegradable polymers including poly(lactic-*co*-glycolic acid) (PLGA),[13,23,24,26,33,34] alginate,[21] chitosan,[25,27,35] poly(lactic acid) (PLA),[36,37] and polycaprolactone (PCL)[37,38] have been used to fabricate nanoparticles in microfluidic devices for medical applications. The low flow ratio and fast mixing in HFF allows for one-step synthesis of drug-loaded



Fabian Itel

Fabian Itel obtained his PhD in Nanoscience at the University of Basel, Switzerland, in 2015. Under the supervision of Prof. Wolfgang Meier at the Department of Physical Chemistry in Basel, he worked on artificial membranes made from lipid and block copolymer membranes with functional reconstitution of biological membrane proteins. After obtaining a Swiss National Science Foundation post doc fellowship, he joined the Städler group in 2016. His current research is focused on the generation of artificial cells with potential application in bone tissue engineering.



Yan Zhang

Yan Zhang received her PhD in Materials Science and Engineering from Donghua University, China, in 2013. Currently, she works as a post-doctoral research fellow at iNANO, Aarhus University, Denmark. Her research involves the development of artificial cells and their interaction with hepatocytes.

This journal is © The Royal Society of Chemistry 2016

Published on 28 October 2016. Downloaded by Universidade de Lisboa on 12/5/2019 9:27:16 AM.

polymeric nanoparticles with a higher drug loading, a smaller particle diameter, a smaller size distribution and a slower and more sustained release rate of the drug compared to bulk synthesized nanoparticles. For instance, Majedi *et al.*[27] reported a solvent-free synthesis of paclitaxel-loaded chitosan nanoparticles *via* HFF with loading efficiencies above 95%, with a 1.7-fold higher cellular uptake compared to the particles prepared by a bulk method, and the ability to hold their cargo in physiological pH until they reach the more acidic environment of a tumor. In a similar study, Hasani-Sadrabadi *et al.*[12] utilized HFF to assemble paclitaxel-loaded hydrophobic–hydrophilic core–shell structures of dendritic polyethylene (dPE) and triblock copolymers. It was shown that, within the time period of two weeks, the nanoparticles formed at flow ratios of 0.03, 0.075, and 0.2 released 86%, 76% and 98% of their cargo, respectively, while nanoparticles prepared by the bulk synthesis released almost 100% of the cargo (Fig. 1B).

In addition to polymer-based nanoparticles, liposomes have also been widely applied in pharmaceutical and cosmetic industries.[39] Microfluidic techniques for the preparation of liposomes have recently been critically reviewed by Carugo *et al.*[39] To address the demand for preparation techniques with a high throughput, Hood *et al.*[14] designed a microfluidic vertical flow focusing (VFF) device with an exceptionally high channel aspect ratio (100 : 1). This setting enabled the production of unilamellar, nearly monodisperse 80–200 nm liposomes with a production rate of 1.6 mg min^{-1} which was nearly two orders of magnitude higher than that of a traditional HFF device (Fig. 1C). By applying a proper channel design, it is also possible to have several HFF regions in one chip.[15,29] For instance Conde *et al.*[15] used a 10-inlet channel configuration to produce four parallel HFF regions. The set-up was used to fabricate liposomes loaded with magnetic nanoparticles. These magnetoliposomes had diameters between 90–220 nm and showed responsiveness to external magnetic field gradients. Such particles hold promise in targeted delivery of anticancer drugs[40] and as contrast agents for magnetic resonance imaging.[41]

Examples of lipid–polymer hybrid nanoparticles produced in D-μF have also emerged in the last four years.[42–45] This new class of potential drug carriers enables the loading of a hydrophobic cargo in a polymer core, which also gives rigidity to the assembly, while an outer lipid shell prolongs the circulation half-life. Zhang *et al.*[43] demonstrated the synthesis of PLGA nanoparticles coated with mono- and bi-layered lipid shells by using a two-stage microfluidic chip (Fig. 1D – i). In the first stage of the chip, PLGA-nanoparticles or intermediate liposomes were produced by applying a typical HFF-geometry. These intermediate products were then guided *via* two separated channels to the second stage of the chip where a new inlet channel was introduced in the middle. All three channels combined formed a spiral synthesis channel. The second inlet channel was used to add either lipids to a PLGA-nanoparticle solution or PLGA to a liposome solution to form the final mono- and bi-layered nanoparticles, respectively. These nanoparticles, especially the less flexible monolayered ones, showed good cellular uptake and allowed for dual drug delivery *via* the encapsulation of doxorubicin in the PLGA-core and combretastatin A4 in the lipid shell for tumor growth inhibition *in vivo* (Fig. 1D – ii). A similar kind of multi-stage microfluidic setting was also employed to synthesize nanovesicles consisting of a water core loaded with hydrophilic drugs, a rigid PLGA-core, and an outermost lipid layer to act as a safe and biocompatible nanocarrier for *in vivo* cancer treatment.[44]

For the fabrication of inorganic nanomaterials, such as metallic nanocrystals and quantum dots, microfluidic systems are typically modified to produce a train of discrete droplets which contain the reaction solution.[16,17,46–49] By doing so, the reaction volume is minimized and the reagent concentrations can be easily tuned by varying the droplet size.[47] D-μF has also been presented as a new platform for scaling up the production of inorganic nanocrystals.[50] These nanoparticles are useful not only in biomedicine but also in applications related to photonics, electronics, catalysis, energy conversion, environment protection and information storage, to mention a few.[50] It was demonstrated recently that D-μF enabled not only a high-throughput synthesis, but also allowed for an *in situ* optical detection of the synthesis process when integrated with an online absorbance and fluorescence detection.[46] By using this method, the authors were able to quantitatively measure the growth kinetics of lead-sulfide quantum dots with a millisecond time resolution, which revealed a two-stage mechanism for the nanoparticle formation.

Apart from the direct production of nanoparticles, D-μF has also been used to manufacture innovative composite systems *via* encapsulation of nanoparticles. Recently, Araújo *et al.*[51] developed a PLGA- and mesoporous silica (PSi)-based composite system for oral delivery of two peptide drugs for the treatment of type 2 diabetes mellitus. The system was composed of an antidiabetic peptide, glucagon-like peptide-1 (GLP-1), loaded on PLGA or PSi nanoparticles which were further functionalized with mucoadhesive chitosan and cell penetrating



Brigitte Städler

Brigitte Städler received her PhD from ETH Zürich, Switzerland (2007). She then worked as a post doc at the University of Melbourne, Australia. She was Assistant Professor at iNANO, Aarhus University, Denmark between 2010 and 2014 before she became Associate Professor in 2015. She has published over 60 papers (h-factor 25). Her interdisciplinary group works at the interface of (liposomal) drug delivery, polymer science, surface science, cell biology, and microfluidics to provide nature inspired solutions to address medical challenges.

Published on 28 October 2016. Downloaded by Universidade de Lisboa on 12/5/2019 9:27:16 AM.

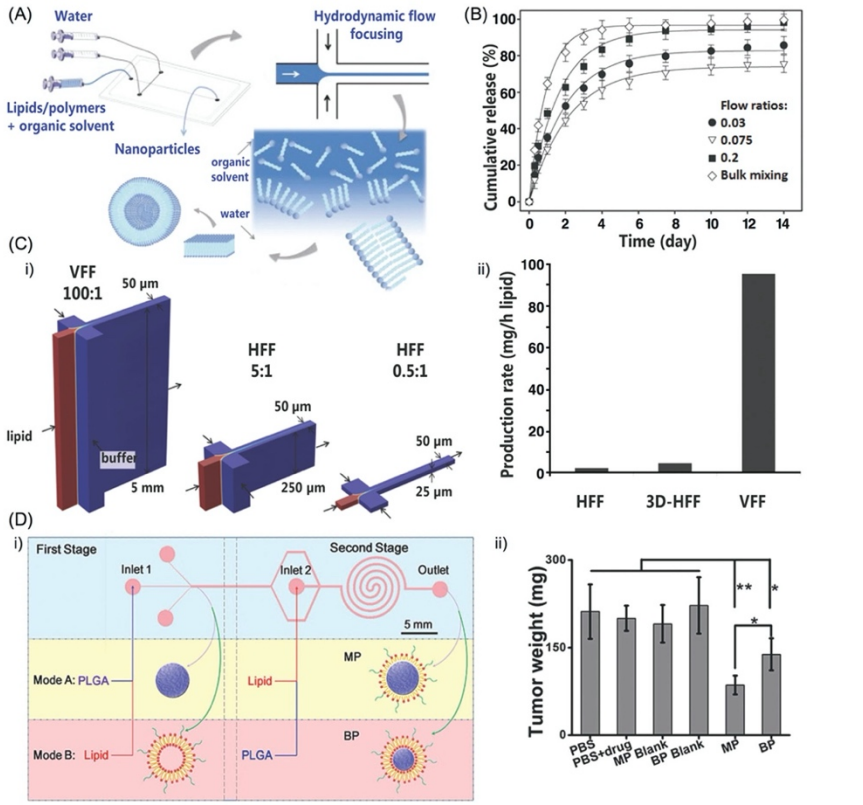


Fig. 1 Nanoparticle assembly: (A) Schematic representation of a HFF set-up where an organic stream is focused into a narrow sheet by two aqueous streams. When the organic sheet mixes with aqueous solvent, nanoparticle precursors, originally dissolved in the organic phase, self-assemble into nanoparticles. Adapted from ref. 29 with permission from Elsevier. (B) Cumulative *in vitro* release of paclitaxel from dPE-based nanoparticles formed at different flow ratios by using HFF illustrating the sustained drug release of microfluidically fabricated nanoparticles. Adapted with permission from ref. 12. (C) (i) Schematic representation of a microfluidic VFF device with an exceptionally high channel aspect ratio of 100 : 1 compared with common HFF devices with channel aspect ratios of 5 : 1 and 0.5 : 1. Adapted with permission from ref. 14 (ii) Comparison of liposome production rates across various microfluidic methods illustrating that VFF enables the generation of liposomes at a significantly higher rate than a planar HFF device. Reprinted with permission from ref. 14. (D) (i) Schematic representation of a two-stage microfluidic chip for the production of PLGA nanoparticles coated with mono- and bi-layered lipid shells. Stage one: PLGA nanoparticles or liposomes are formed *via* HFF; stage two: lipids or PLGA are introduced to produce mono- and bi-layered core–shell nanoparticles, respectively. Reprinted with permission from ref. 43. Copyright 2015 American Chemical Society. (ii) The effect of doxorubicin and combretastatin A4 loaded polymer-lipid nanoparticles with mono- (MP) and bi-layered (BP) lipid shells on tumor growth *in vivo* is shown. Reprinted with permission from ref. 43. Copyright 2015 American Chemical Society.

peptides to enhance the delivery across intestinal endothelial cells protected by a mucus layer. These functionalized nanoparticles were further encapsulated within an enteric polymer, hydroxypropylmethylcellulose acetylsuccinate (HPMC-AS), to protect the peptides from degradation. This was carried out in a microfluidic setting with flow-focusing geometry where functionalized nanoparticles along with the dipeptidyl peptidase 4 (DPP4) enzyme inhibitor were dissolved in ethyl acetate. Then, an aqueous solution of F127 was used to force the organic stream through a narrow orifice where high shear and capillary

Published on 28 October 2016. Downloaded by Universidade de Lisboa on 12/5/2019 9:27:16 AM.

instability broke bubbles off the tip resulting in the formation of monodisperse particles. The drug delivery system was tested *in vivo* in a non-obese type 2 diabetes mellitus rat model and an increase in hypoglycemic effects was observed.[52]

Janus particles

Cell polarity, *i.e.*, the asymmetric, non-random arrangement of cellular components and structures, is a central feature of cells that allows them to perform specialized tasks such as neurotransmitter release and uptake in specialized sites in neurons,[53] or asymmetric front–back polarity in migrating cells as they move towards attractive cues.[54] Although the biological relevance of cell polarity is tremendous,[55] our group was the first one to consider this aspect in cell mimicry employing Janus-shaped particles.[56] Janus particles possess asymmetrical spatial regions with physical and/or chemical differences, as recently discussed in two reviews,[57,58] which is the fundamental prerequisite for polarity. Compared to other assembly methods of Janus particles (*e.g.*, pickering emulsions,[59] self-assembly,[60] surface modification,[61] particle lithography,[62] photo-polymerization,[63] biphasic electro-jetting/spraying,[64] *etc.*), D-μF-based assembly benefits from the highly adjustable nature of microfluidic devices, providing a flexible platform to construct Janus particles from monomers,[65] polymers,[66] hydrogels,[67] or nanoparticles,[68] equipped with multiple functions or multiple components.[69,70] It is straightforward to assemble Janus particles by D-μF using either two miscible[71–75] or immiscible regions,[76] followed by parallel crosslinking or polymerization of the building blocks. Furthermore, Janus particles can be assembled by phase separation of mixed droplets employing different driving forces including temperature,[77] copolymerization,[78] solvent diffusion,[79] or gravity.[79,80]

When assembling Janus droplets using two miscible phases, the main obstacle is the risk of their mixing, thus breaking the Janus configuration, due to the interface convection effect. The major preventive strategies are controlling the size of the droplet by adjusting the viscosities of the two dispersed phases, matching the flow rates of both the continuous phase and the dispersed phase, and increasing the solidifying rate of the Janus droplets.[67,72,75] Alternatively, when the Janus particles are assembled based on two immiscible phases, undesired mixing can be inherently avoided. An interesting example in this context was reported by Khan *et al.*[65] They constructed amphiphilic poly(acrylamide)(PAAm)/poly(methyl acrylate)(PAM) Janus particles from hydrophilic acrylamide and hydrophobic methyl acrylate monomers through UV-initiated polymerization (Fig. 2A). In those Janus particles, hydrophobic ketoprofen and hydrophilic fluorescein model cargos were encapsulated separately in two parts. In this system, the flow rates of the two dispersed phases and the presence of surfactants in the dispersed phase were the key factors for yielding asymmetric droplet/particle structures. In the absence of surfactants and together with high flow rates of the hydrophobic monomer phase, "acorn-like" Janus particles were obtained. On the other hand, when there was a low amount of surfactant (0.75%) in the hydrophilic dispersed phase, Janus particles were obtained. In addition, they managed to form "helmet-like" and "UFO-like" Janus particles by changing the acrylamide monomer composition. Phase separation of a single droplet is a common strategy for Janus particle formation. The following section highlights a selection of new strategies which are particularly interesting in the context of this minireview. Lone *et al.* applied a light- and thermo-responsive random copolymer of poly(isopropyl acrylamide) (pNIPAAm) modified with a fluorescent dye and photochromic spironaphthoxazine (named poly(NIPAAm-*co*-SPO-*co*-fluorophore)) to assemble Janus particles with a poly(NIPAAm-*co*-SPO-*co*-fluorophore) copolymer part and a hollow poly(*N*,*N*-methylenebisacrylamide) (PMBA) part.[78] First, the light-responsive polymer poly(NIPAAm-*co*-SPO-*co*-fluorophore) and MBA-monomer mixed droplets were formed, followed by UV-exposure which led to the phase separation of the copolymer poly(NIPAAm-*co*-SPO-*co*-fluorophore) to one side of the droplet while the MBA monomers in the droplets polymerized at the water/oil interface to form a hollow structure with a PMBA shell (Fig. 2B). In another example, Cao and co-workers fabricated PLGA and PCL (patchy) Janus particles by phase separation.[81] The authors controlled the particle architectures by adjusting the polymer ratios and the solvent compositions (Fig. 2C). When dimethyl carbonate (DMC) was used as the sole solvent, due to the complete phase separation of PLGA and PCL during the particle solidification, Janus particles with clear demarcation between two regions were obtained. However, when a dichloromethane and DMC mixture was used, patchy Janus particles with a smooth PLGA hemisphere and a rough PCL hemisphere were formed. In another report, Janus particles with a polystyrene (PS) part and a poly(vinylpyrrolidone) (PVP) containing Fe_3O_4 part (named PS/Fe_3O_4@PVP Janus particle) were assembled by solvent diffusion-induced phase separation (Fig. 2D).[82] The mixture droplets, containing polystyrene (PS), PVP, and PVP-coated Fe_3O_4 nanoparticles (NPs) in dichloromethane, were first formed. Following on, water diffused into the droplets and formed reversed PVP and NP tiny droplets, followed by coalescence of those tiny droplets. During this process, Fe_3O_4@PVP were located on one side of the droplet under magnetic field, while the hydrophilic PVP with located NPs totally phase separated from hydrophobic PS regions with the assist of solvent evaporation, and thus PS/Fe_3O_4@PVP Janus particles were obtained. Replacing PVP with PAA or polyethylene glycol (PEG) allowed for the assembly of other amphiphilic Janus particles. These Janus particles were used to assemble hydrophilic or hydrophobic monolayers for cell adhesion studies.

Non-spherical particles

In nature, particles exist in several different shapes and sizes. In fact, this shape diversity is crucial for the optimization of

Published on 28 October 2016. Downloaded by Universidade de Lisboa on 12/5/2019 9:27:16 AM.

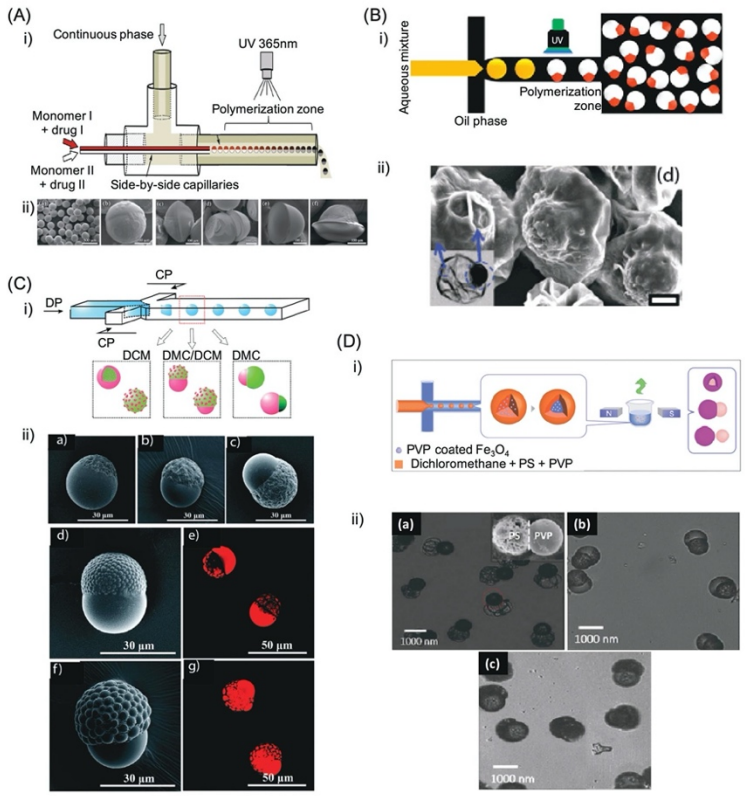


Fig. 2 Janus-shaped particles: (A) (i) schematic of cargo loaded Janus poly(acrylamide)/poly(methyl acrylate) particles fabricated from a side-by-side capillary-based microfluidic setup; (ii) SEM images of Janus PAAm/PMA particles in different morphologies. Reprinted with permission from ref. 65. (B) (i) Schematic representation of the poly(NIPAAm-*co*-SPO-*co*-fluorophore)/PMBA Janus particle forming process. (ii) SEM of dried Janus particles with two distinct regions (inset: optical image of the Janus particle). Reprinted with permission from ref. 78. (C) (i) Schematic illustration of Janus PLGA/PCL particle formation through solvent diffusion-induced phase separation. (ii) SEM and CLSM images of Janus PLGA/PCL particles made from different solvent, PLGA, and PCL ratios. Reprinted with permission from ref. 81. (D) (i) Schematic illustration of the Janus PS/Fe_3O_4@PVP particle formation. (ii) TEM images of PS/Fe_3O_4@PVP (a), PS/Fe_3O_4@PAA (b) and PS/Fe_3O_4@PEG (c) Janus particles. Reprinted with permission from ref. 82.

different functions. When considering artificial particles, however, most are spherical, due to fabrication techniques generally involving emulsion and suspension polymerization,[83] where the surface tension between the polymer and surrounding solutions comes into play, leading to contact area minimization and, thus, the creation of spherical particles.[84] Despite this fact, particle morphology plays a very important role in particle function, and is the main factor in several applications such as intracellular particle delivery,[85] particle stability in emulsions,[86] Brownian motion,[87] three-dimensional tissue formation,[88] as well as drug delivery, bioimaging, and biomimetics.[89] For a recent comprehensive review on non-spherical particles, their fabrication techniques, and their applications, the reader is referred to Mathaes *et al.*[90] Indeed, non-spherical particles offer larger surface areas, display anisotropic behaviour in response to external stimuli[91] and can, for example, be packed more densely than spherical particles.[92] Numerous techniques can be used to produce non-spherical

This journal is © The Royal Society of Chemistry 2016

Published on 28 October 2016. Downloaded by Universidade de Lisboa on 12/5/2019 9:27:16 AM.

particles. Batch methods include dispersion and precipitation polymerization, copolymer self-assembly, and phase-separated polymer precipitation, as recently reviewed by Chu and co-workers.[34] These methods, however, lack control over the precise shape and size of the produced particles. Microfluidic systems solve this problem by allowing a stronger control over particle characteristics. With microfluidics, non-spherical particles can be generated from spherical ones *via* simple processing steps such as arrested coalescence, asymmetric polymer solidification, polymerization in microfluidic flow, and evaporation-driven clustering, as discussed in two recent reviews.[84,93]

In the last few years, several innovations based on differently shaped particles fabricated by microfluidics have emerged. Interesting examples include the production of bullet-shaped magnetic microparticles useful for drug delivery and cell-based therapies,[94] the assembly of biconcave microlenses for microoptics,[95] the use of a magnetic-field-assisted method of fabrication to obtain differently shaped particles ranging from spheres to rods,[83] or the assembly of hollow microcapsules capable of maintaining complex rod-like shapes.[96] A more detailed discussion on this subject can be found in specific reviews.[70,93]

Specifically regarding biotechnological applications, numerous advances have been accomplished over the last couple of years and a selection will be highlighted here.

Cheng and collaborators developed a microfluidic technique to create anisotropic colloidal crystal particles (CCPs), using silica nanoparticles and hexadecane, and achieving different colours by using different concentrations of PEG diacrylate (PEG-DA) (Fig. 3A). With this technique, it was possible to generate anisotropic non-close-packed CCPs by photo-polymerizing droplet templates in a capillary. Applying a thermal process to these non-close-packed CCPs, the group created anisotropic close-packed CCPs. The authors showed that this technique could be used to generate CCPs with several sizes, colours, and shapes (rods, cuboids, and disks) with dimensions in the range of 200 μm to 1 mm. These crystals were employed as a marker for DNA multiplex detection as an example for a high-throughput assay.[97] Notably, this is one of the rare examples where the authors went beyond the assembly and characterization of non-spherical particles, but illustrated their relevance in a nanomedicine-related application. In a different effort, Hu and collaborators created mushroom-shaped alginate/pNIPAAm microgels with tuneable size and shape, originated from 300 μm spherical droplets (Fig. 3B). For the fabrication of these particles, Hu and collaborators used a glass capillary microfluidic device, with which they created single water-in-oil emulsions. These alginate/pNIPAAm emulsions were then collected in a solution containing barium acetate and different concentrations of glycerol. By adjusting the glycerol concentration and the initial droplet size, the authors were able to fully control the final particle size and morphology. These non-spherical, mushroom-like particles could be valuable for applications in stimulus-responsive drug delivery, cell attachment, and constructing complex and porous 3D tissues and scaffolds.[77]

Apart from the particle shape, it is also important to address the surface morphology and texture. Indeed, texturized and wrinkled particles are widely found in nature, for example in plant biology[98] and in the mammalian immune system.[99] Therefore, artificial wrinkled particles have been produced, and their different surface morphologies and textures might make them quite unique in controlled drug delivery,[100] fabrication of absorbent materials,[101] inkjet recording,[102] and self-assembly (due to wrinkle alignment).[103] Within this field, Li and collaborators were able to generate wrinkled PEG-DA particles, with a diameter of around 50 μm with controllable morphology, size, and wrinkle pattern (Fig. 3C). The authors resorted to stop-flow lithography combined with a rapid wrinkling post-process that consisted of UV exposure and different concentrations of washing agents. The originated particles were able to promote cell attachment in cell cultures without any extra chemical treatment, showing great promise in the field of cell attachment and scaffold fabrication.[104]

Microfluidics also allows for the creation of multicompartmental particles, where it is possible to individually control the function of each compartment, meaning that these particles are capable of controllably releasing several different payloads, in response to diverse external cues,[105,106] aiming towards controlled and sustained drug delivery.[107] Guo and collaborators were able to produce different shapes of anisotropic polyacrylamide (PAM)/PEG core/shell droplets and hydrogels with diameters of 250 μm using polymerization-induced phase separation and droplet coalescence.[108] More importantly, this group was able to create multicore emulsion droplets using single-core droplets as building blocks, producing several complex two- and three-dimensional structures that can display different release rates depending on their hierarchical organization (Fig. 3D). As a proof of concept, the authors compared the release rate of bovine serum albumin (BSA) in single and quadruple core PAM/PEG hydrogels and concluded that the kinetics of release changes significantly within those particles. While both particles are able to release most of the entrapped BSA, the quadruple core particles show a much faster release rate when compared to single core particles (70% of release in one hour *vs.* four hours, respectively).[108]

Biological cargo

The use of nano/microparticles in the context of nanobiomedicine requires their loading with bioactive cargo, *i.e.*, biomolecules, such as proteins or enzymes, but also entire living cells. In this way, their encapsulation offers the possibility to create new materials in the fields of drug delivery, cell mimicry, tissue engineering, and diagnosis. In addition to the prior outlined advantages, D-μF allows for 100% cargo loading at efficient rates (10^3–10^9 particles per second).[8,109] Small cargo, *e.g.* enzymes, proteins, and DNA, can be easily loaded homogeneously within the particles. For larger cargo, on the other hand, such as living cells, it has to be considered that the particles can contain zero to multiple

Published on 28 October 2016. Downloaded by Universidade de Lisboa on 12/5/2019 9:27:16 AM.

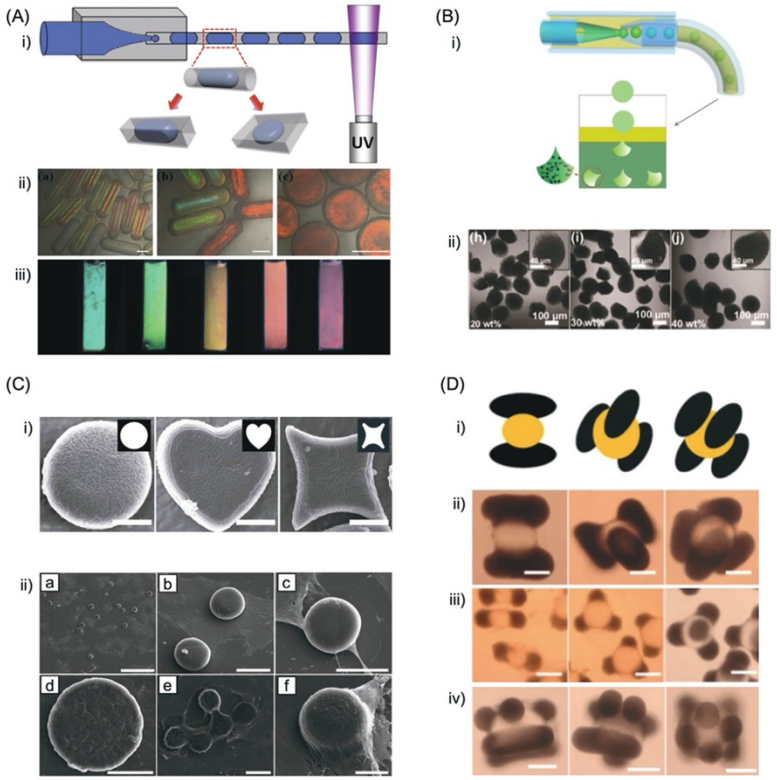


Fig. 3 Non-spherical particles: (A) (i) schematic representation of the microfluidic production of anisotropic particles with different geometries. (ii) Optical microscopy images of CCPs with different geometries: (a) rods, (b) cuboids, (c) disks. Scale bars: 200 μm. (iii) Digital photographs of different types of colloidal crystal PEG-DA solutions. Reprinted with permission from ref. 97. (B) (i) Schematic representation of the microfluidic device used for the creation of mushroom-like shaped particles. (ii) Optical microscopy images of the resulting particles. Reprinted with permission from ref. 77. (C) (i) Wrinkled particles with different shapes. Scale bars: 20 μm. (ii) Smooth (top) *vs.* wrinkled particles (bottom) in cell cultures: the cells ignore the smooth particles but attach to the wrinkled ones. Scale bars: (a) 300 μm, (b, c, e) 40 μm, (d, f) 20 μm. Reprinted with permission from ref. 104. (D) (i) Model for multiple rod-like cores. (ii) Optical microscopy images of multiple rod-like cores. (iii) and (iv) Optical microscopy images of other multicore particle shapes. Scale bars: 200 μm. Reprinted with permission from ref. 108.

cells per particle. An approach to avoid empty particles has recently been reported by either improving the cell-to-particle ratio before forming the particles or by sorting the particles after their formation.[110] Sorting of particles is also important in cell-free protein expression and flow-PCR techniques, where proteins are expressed and DNA is amplified, respectively, within water–oil droplets. After analysis and particle sorting, the cargo could then be recovered and the particles were discarded.[111,112] However, in the context of cell mimicry, the particles have to be structurally stable, *i.e.*, they need to be manipulated in order to be handled over an extended period of time or to modify their surfaces. As such, stable particles have been generated as soft particles from biocompatible/biodegradable polymers (PEG,[113,114] PLGA,[115] PCL,[116] PLA[117]), as hydrogel particles from alginate,[118,119] agarose,[120] chitosan,[121] polyacrylamide,[122] DNA,[123] (Kahn, 2016[137]) *etc.*, as fibrous particles from natural collagen fibrils[124] or peptides,[125] and as hollow structures like liposomes,[126,127] polymersomes,[105,128]

This journal is © The Royal Society of Chemistry 2016

Published on 28 October 2016. Downloaded by Universidade de Lisboa on 12/5/2019 9:27:16 AM.

or capsules.[129,130] Stable particles are useful for delivering and producing drugs, as microreactors/nanoreactors or to encapsulate cells for tissue engineering.[131] On the other hand, the field of microfluidics is still relatively new and other techniques to encapsulate protein moieties have been used, *e.g.*, droplet emulsification. Therefore, the number of publications regarding enzyme/protein/DNA-loaded particles prepared by D-μF remains scarce.

The loading of sensitive biomolecules, such as enzymes or proteins, into polymer matrices can result in the loss of the protein 3D structure and, therefore, the biomolecules can lose their activity due to the small mesh sizes of certain polymers. In addition, denatured proteins can aggregate within the particles, which can lead to strong immunological responses when administered *in vivo*.[132] Thus, hydrogels are more suited to encapsulate proteins due to their large water content and increased mesh sizes. On the other hand, the larger mesh size might involve the need for a covalent immobilization of the proteins to avoid uncontrolled cargo leakage. As an alternative, the particle surface can be made less permeable by depositing interacting polymer layers in order to keep the enzymes entrapped as illustrated, for instance, by Fischlechner and coworkers (Fig. 4A).[130] They recently generated gel–shell beads, where an agarose hydrogel core served as the interior compartment while a polyelectrolyte shell functioned as the membrane. In order to functionalize one single droplet with the specific plasmid and expressed enzyme of one specific *E. coli* cell, one of the aqueous channels contained the *E. coli* cells while the second aqueous channel contained the supplements for *E. coli* cell lysis and the third channel contained the non-fluorescent substrate for the enzyme. Within the still-liquid core of the droplets, the enzyme converted the substrate to the fluorescent product. After gelation by cooling below 30 °C and consequent gel–shell bead formation, the beads were sorted by FACS. By doing so, a directed evolution of the enzyme was established and the positive mutants could be analyzed at a rate of ~10^7 particles per hour. The plasmid was selectively isolated from the positive beads. These gel–shell beads offer a promising tool for the encapsulation of enzymes or multiple enzymes and proteins to fulfil cascade reactions for the generation of artificial cells. Besides protein encapsulation, proteins can also be immobilized on the surface of particles for applications in affinity tests, disease diagnosis, *etc*. In a one-step synthesis, Chen *et al.* prepared antibody-presenting alginate microparticles to be used in binding affinity assays.[138] *E. coli* bacteria bound onto the anti-*E. coli* IgG-functionalized alginate microparticles at a comparable specificity than that of an ELISA. Although the non-specific binding has to be further

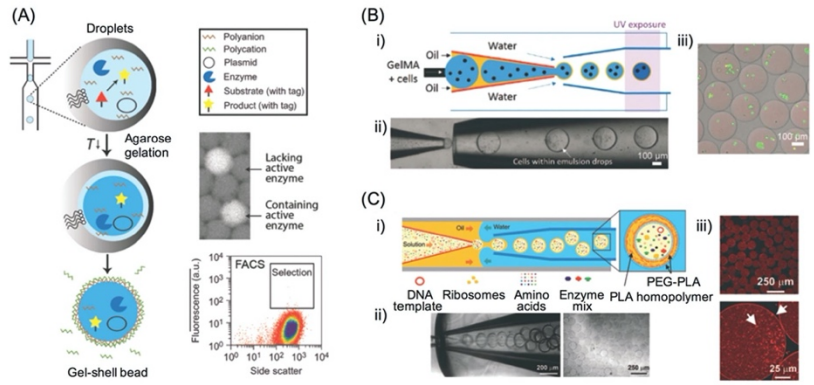


Fig. 4 Cargo loading: (A) assembly and directed evolution in gel–shell beads (GSBs). Single *E. coli* cells harboring the expressed enzyme and its encoding plasmid are mixed with the non-fluorescent substrate and a lysis agent to form the droplets. The aqueous solution, containing agarose and alginate, gelates on cooling to form solid beads. After FACS sorting the positive beads, the coding plasmid is recovered and selected variants are sequenced or further characterized. Adapted with the permission of Macmillan Publishers Ltd: Nature Chemistry,[130] copyright 2014. (B) Production of cell-laden microparticles. (i) Schematic illustration showing the encapsulation of living cells using the thin shell double emulsion drops formed with a photo-crosslinkable polymer. (ii) Optical image showing cell encapsulation within the drops. (iii) Fluorescence microscopy image showing calcein-AM stained (living) and ethidium homodimer-stained (dead) cells embedded within microgels. Adapted from ref. 134 with permission of the Royal Society of Chemistry. (C) PEG-*b*-PLA polymersomes made by D-μF and encapsulation of cell-free protein expression machinery. (i) Schematic illustration of the double emulsion technique. (ii) Optical micrographs of the droplets and the generated polymersomes. (iii) Fluorescence microscopy images of expressed MreB-RFP proteins within the giant polymersomes. Arrows indicate the formation of polymerized MreB-RFP patches dispersed in the inner phase and the adhesion of the protein on the membrane. Reproduced with permission of John Wiley & Sons from ref. 135.

Published on 28 October 2016. Downloaded by Universidade de Lisboa on 12/5/2019 9:27:16 AM.

improved, the large surface to volume ratio of microparticles offers a promising approach to a simpler operation procedure and lower costs than ELISA.

In the field of tissue engineering, cell-laden microgels are an approach to engineer a physiologically relevant microenvironment for cells.[133,134] In general, the single-emulsion technique in D-μF has the disadvantage that the cell viability is drastically reduced, as recently reported even down to 20%.[134] The reason for this is the long time the cells are exposed to the different chemical components for the droplet formation, while they endure reduced nutrient- and oxygen-availability due to the oil phase, cell membrane-active surfactants, toxic photo-initiators, UV-light exposure, *etc*. A possibility to overcome this problem was recently shown, where the gelation of the particles happens without the addition of a polymerization initiator.[133] In this case, three different aqueous microchannels were used, and all of them were mixed just before the droplet formation. The cell-containing solution was mixed with a solution of dithiolated PEG macro-cross-linker, which reacted with the third solution containing acrylated hyperbranched PEG (hPEG) *via* nucleophilic Michael addition. Thus, the cross-linking happens almost immediately after mixing. Yeast and mammalian (lymphoblasts and fibroblasts) cell viability within these particles was increased up to 90%. Another approach was recently reported by the Weitz group.[134] A double emulsion microfluidic technique reduced the time of contact between the cell-loaded particles and the oil phase, which led to an improved cell viability (Fig. 4B).[134] Specifically, monodisperse PEG-diacrylate or gelatin-methacrylate droplets were polymerized in the presence of a photoinitiator for only 2 s after droplet formation. Upon polymerization, the thin oil-shell around the particles spontaneously de-wetted and the oil separated immediately from the particles. In this way, the authors were able to reduce the preparation time of the particles and minimize oil-related toxicity effects that are harmful to living cells. This double-emulsion technique showed 100% cell viability for three different cell types (myelogenous leukemia cells (K562), Madin-Darby canine kidney epithelial (MDCK) cells, and NIH/3T3 fibroblast cells). In addition, the cells were cultured in 3D tissues and it was shown that the cells were viable, growing within the microgels, and even forming cell–cell connections between the microparticles after four days (NIH/3T3 fibroblasts).

D-μF also allowed the generation of giant polymersomes loaded with the complete protein expression machinery (Fig. 4C).[135] To mimic the bacterial cytoskeleton, actin-like proteins (MreB) were selectively expressed within PEG-PLA block copolymer vesicles. The advantage of the D-μF technique is that the giant polymersomes can be generated in homogeneous sizes without any loss of material (block copolymer and cell-free machinery). Within a few hours, a fluorescent version of MreB was expressed inside the giant polymersomes and a network of actin filaments was achieved. Another work showed the feasibility of having an induced polymersome membrane rupture on demand.[136] Catalase-loaded giant polymersomes, with diameters between 50–100 μm, were prepared by double-emulsion D-μF, with the membrane consisting of a PEG-*b*-polybutadiene (PEG-PB) block copolymer. The polymersomes were then incubated within a glucose and glucose oxidase (GOx) solution, which produces hydrogen peroxide (H_2O_2). H_2O_2 enters the polymersomes and is enzymatically converted to oxygen and water. However, due to solvent evaporation, large clusters of the polymer stuck on the polymersome membrane and, in addition, catalase partially associated with the membrane. Thus, the polymersome membrane ruptured upon H_2O_2 generation. Nevertheless, the exact mechanism of membrane rupture is not clear and might be not applicable for other enzymes/proteins. These two examples of polymersome preparation by D-μF showed the feasibility of creating artificial cells by improving the homogeneity and loading of giant polymersomes with biomolecules.

Conclusions and future perspective

This minireview emphasizes selected aspects that illustrate the impact D-μF could have in different areas of cell mimicry and nanomedicine.

Examples from recent years demonstrated the applicability of D-μF for the production of several different types of nanoparticles. Advantages compared to the traditional bulk synthesis methods include better control over the synthesis process leading to an increased uniformity of the produced nanoparticles. Multiple inlet channel set-ups allow for the fabrication of complex core–shell structures and combination of different materials into hybrid nanoparticles. Moreover, D-μF provides a possibility for *in situ* monitoring of the nanomaterial production process. It also offers great opportunities to assemble Janus particles. Diverse types of non-spherical particles were assembled by D-μF including wrinkled particles, multi-core particles, and other particles with controlled shape and size. In the context of loading biological cargo, the generation of artificial cells became technically feasible by D-μF and examples were shown, such as enzyme encapsulation into hydrogel particles, cell-laden hydrogel particles for tissue engineering and giant polymersomes/liposomes. The advantages of D-μF lie mainly in the extremely high efficiency of cargo loading and the generation of uniform particles at high rates.

Despite all the outlined advantages, the use of D-μF-assembled particles in cell mimicry and biomedicine in general remains largely unexplored, given that most examples found in the literature refer only to proof of concept and simple applications. Future directions will involve the combination of the above outlined aspects, such as cargo loading of non-spherical particles or obtaining Janus-shaped nanoparticles, as well as the performance assessment in biologically relevant environment. Non-spherical particles are ideal models which could be used to explore in detail how different shapes might interact with biological cells and tissues, with the aim to understand how biological entities interact with different neighbouring stimuli and objects. Furthermore, producing Janus particles while avoiding organic solvents or long

This journal is © The Royal Society of Chemistry 2016

Published on 28 October 2016. Downloaded by Universidade de Lisboa on 12/5/2019 9:27:16 AM.

phase separation processes is imperative when loading with biological cargo is envisioned. The more challenging issue will be related to the assembly of functionalized Janus microreactors (*e.g.*, different cargo separated within Janus particles), and comparing the structural to non-structural compartmentalization. The D-μF based nanoparticle fabrication needs to overcome small production rates. Additionally, for all nanoparticles that will be used inside the human body several important aspects, such as renal clearance, immunogenicity and biodistribution, have to be assessed. Yet, in many cases, studies are either limited to *in vitro* testing or lack this aspect completely. More work is therefore necessary to prove the suitability of D-μF-fabricated nanoparticles for biomedical applications. Finally, cell encapsulation became feasible using D-μF, but improving cell retention and cell survival (*e.g.*, shortening the time cell loaded particles stay in contact with the oil-phase), and thus prolonging the life-time of the artificial cells, are challenges to be addressed. Key requirements for effective artificial cells include long-term stability and long-term function of the particles together with the prevention of possible immune responses. This requires the use of non-toxic and biocompatible and, if needed, biodegradable building blocks.

Note added after first publication

This article replaces the version published on 18th November 2016. The name and gender of the first author have since changed. No scientific changes have been made.

Acknowledgements

This work was supported by grants from the Innovation Fund Denmark, the Swiss National Science Foundation (Postdoctoral Fellowship F. I.) and Fundação para a Ciência e Tecnologia (FCT), Portugal (A. A.-M.).

Notes and references

1 T. Thorsen, R. W. Roberts, F. H. Arnold and S. R. Quake, *Phys. Rev. Lett.*, 2001, **86**, 4163.
2 S. Mashaghi, A. Abbaspourrad, D. A. Weitz and A. M. van Oijen, *Trends Anal. Chem.*, 2016, **82**, 118.
3 M. T. Guo, A. Rotem, J. A. Heyman and D. A. Weitz, *Lab Chip*, 2012, **12**, 2146.
4 N. Shembekar, C. Chaipan, R. Utharala and C. A. Merten, *Lab Chip*, 2016, **16**, 1314.
5 R. J. R. W. Peters, I. Louzao and J. C. M. van Hest, *Chem. Sci.*, 2012, **3**, 335.
6 L. Schoonen and J. C. M. van Hest, *Adv. Mater.*, 2016, **28**, 1109.
7 S. Sánchez, L. Soler and J. Katuri, *Angew. Chem., Int. Ed.*, 2015, **54**, 1414.
8 C. Martino and A. J. deMello, *Interface Focus*, 2016, DOI: 10.1098/rsfs.2016.0011.
9 L. Hosta-Rigau, P. Schattling, B. M. Teo, M. E. Lynge and B. Stadler, *J. Mater. Chem. B*, 2014, **2**, 6686.
10 G. Bozzuto and A. Molinari, *Int. J. Nanomed.*, 2015, **10**, 975.
11 J. Cui, J. J. Richardson, M. Björnmalm, M. Faria and F. Caruso, *Acc. Chem. Res.*, 2016, **49**, 1139.
12 M. M. Hasani-Sadrabadi, V. Karimkhani, F. S. Majedi, J. J. Van Dersarl and E. Dashtimoghadam, *Adv. Mater.*, 2014, **26**, 3118.
13 J.-M. Lim, N. Bertrand, P. M. Valencia, M. Rhee and R. Langer, *Nanomedicine*, 2014, **10**, 401.
14 R. R. Hood and D. L. DeVoe, *Small*, 2015, **11**, 5790.
15 A. J. Conde, M. Batalla, B. Cerda, O. Mykhaylyk and C. Plank, *Lab Chip*, 2014, **14**, 4506.
16 L. Zhang, Y. Wang, L. Tong and Y. Xia, *Nano Lett.*, 2014, **14**, 4189.
17 Y. H. Kim, L. Zhang, T. Yu, M. Jin and D. Qin, *Small*, 2013, **9**, 3462.
18 M. Lu, Y.-P. Ho, C. L. Grigsby, A. A. Nawaz and K. W. Leong, *ACS Nano*, 2014, **8**, 332.
19 M. Lu, S. Yang, Y.-P. Ho, C. L. Grigsby and K. W. Leong, *ACS Nano*, 2014, **8**, 10026.
20 L. Capretto, D. Carugo, S. Mazzitelli, C. Nastruzzi and X. Zhang, *Adv. Drug Delivery Rev.*, 2013, **65**, 1496.
21 S. Bazban-Shotorbani, E. Dashtimoghadam, A. Karkhaneh, M. M. Hasani-Sadrabadi and K. I. Jacob, *Langmuir*, 2016, **32**, 4996.
22 G. Tresset, C. Marculescu, A. Salonen, M. Ni and C. Iliescu, *Anal. Chem.*, 2013, **85**, 5850.
23 L. Martín-Banderas, E. Saez-Fernandez, M. Angeles Holgado, M. Matilde Duran-Lobato and J. C. Prados, *Int. J. Pharm.*, 2013, **443**, 103.
24 P. M. Valencia, E. M. Pridgen, M. Rhee, R. Langer and O. C. Farokhzad, *ACS Nano*, 2013, **7**, 10671.
25 E. Dashtimoghadam, H. Mirzadeh, F. A. Taromi and B. Nystrom, *Polym.*, 2013, **54**, 4972.
26 J. Sun, Y. Xianyu, M. Li, W. Liu and L. Zhang, *Nanoscale*, 2013, **5**, 5262.
27 F. S. Majedi, M. M. Hasani-Sadrabadi, J. J. VanDersarl, N. Mokarram and S. Hojjati-Emami, *Adv. Funct. Mater.*, 2014, **24**, 432.
28 R. R. Hood, D. L. DeVoe, J. Atencia, W. N. Vreeland and D. M. Omiatek, *Lab Chip*, 2014, **14**, 2403.
29 T. A. Balbino, N. T. Aoki, A. A. M. Gasperini, C. L. P. Oliveira and A. R. Azzoni, *Chem. Eng.*, 2013, **226**, 423.
30 A. U. Andar, R. R. Hood, W. N. Vreeland, D. L. DeVoe and P. W. Swaan, *Pharm. Res.*, 2014, **31**, 401.
31 R. R. Hood, C. Shao, D. M. Omiatek, W. N. Vreeland and D. L. DeVoe, *Pharm. Res.*, 2013, **30**, 1597.
32 M. Mijajlovic, D. Wright, V. Zivkovic, J. X. Bi and M. J. Biggs, *Colloids Surf., B*, 2013, **104**, 276.
33 J. Wang, W. Chen, J. Sun, C. Liu and Q. Yin, *Lab Chip*, 2014, **14**, 1673.
34 W. Wang, M.-J. Zhang and L.-Y. Chu, *Acc. Chem. Res.*, 2014, **47**, 373.

Published on 28 October 2016. Downloaded by Universidade de Lisboa on 12/5/2019 9:27:16 AM.

35 F. S. Majedi, M. M. Hasani-Sadrabadi, S. H. Emami, M. A. Shokrgozar and J. J. VanDersarl, *Lab Chip*, 2013, **13**, 204.
36 R. Othman, G. T. Vladisavljevic, N. L. Thomas and Z. K. Nagy, *Colloids Surf., B*, 2016, **141**, 187.
37 R. Othman, G. T. Vladisavljevic and Z. K. Nagy, *Chem. Eng. Sci.*, 2015, **137**, 119.
38 A. Bains, J. E. Wulff and M. G. Moffitt, *J. Colloid Interface Sci.*, 2016, **475**, 136.
39 D. Carugo, E. Bottaro, J. Owen, E. Stride and C. Nastruzzi, *Sci. Rep.*, 2016, **6**, 25876.
40 S. Dandamudi and R. B. Campbell, *Biomaterials*, 2007, **28**, 4673.
41 G. Mikhaylov, U. Mikac, A. A. Magaeva, V. I. Itin and E. P. Naiden, *Nat. Nanotechnol.*, 2011, **6**, 594.
42 Q. Feng, L. Zhang, C. Liu, X. Li and G. Hu, *Biomicrofluidics*, 2015, **9**, 052604.
43 L. Zhang, Q. Feng, J. Wang, S. Zhang and B. Ding, *ACS Nano*, 2015, **9**, 9912.
44 L. Zhang, Q. Feng, J. Wang, J. Sun and X. Shi, *Angew. Chem., Int. Ed.*, 2015, **54**, 3952.
45 J. Sun, L. Zhang, J. Wang, Q. Feng and D. Liu, *Adv. Mater.*, 2015, **27**, 1402.
46 I. Lignos, S. Stavrakis, A. Kilaj and A. J. deMello, *Small*, 2015, **11**, 4009.
47 J. Dai, X. Yang, M. Hamon and L. Kong, *Chem. Eng.*, 2015, **280**, 385.
48 Y. Shu, P. Jiang, D.-W. Pang and Z.-L. Zhang, *Nanotechnology*, 2015, **26**, 275701.
49 H. Gu, F. Rong, B. Tang, Y. Zhao and D. Fu, *Langmuir*, 2013, **29**, 7576.
50 G. Niu, A. Ruditskiy, M. Vara and Y. Xia, *Chem. Soc. Rev.*, 2015, **44**, 5806.
51 F. Araújo, N. Shrestha, M.-A. Shahbazi, D. Liu and B. Herranz-Blanco, *ACS Nano*, 2015, **9**, 8291.
52 F. Araújo, N. Shrestha, M. J. Gomes, B. Herranz-Blanco and D. Liu, *Nanoscale*, 2016, **8**, 10706.
53 S. Yamada and W. J. Nelson, *Annu. Rev. Biochem.*, 2007, **76**, 267.
54 P. A. Iglesias and P. N. Devreotes, *Curr. Opin. Cell Biol.*, 2008, **20**, 35.
55 D. M. Bryant and K. E. Mostov, *Nat. Rev. Mol. Cell Biol.*, 2008, **9**, 887.
56 P. Schattling, C. Dreier and B. Stadler, *Soft Matter*, 2015, **11**, 5327.
57 A. Walther and A. H. E. Müller, *Chem. Rev.*, 2013, **113**, 5194.
58 C. Kaewsaneha, P. Tangboriboonrat, D. Polpanich, M. Eissa and A. Elaissari, *ACS Appl. Mater. Interfaces*, 2013, **5**, 1857.
59 T. M. Ruhland, H. S. McKenzie, T. S. Skelhon, S. A. F. Bon, A. Walther and A. H. E. Müller, *Polym.*, 2015, **79**, 299.
60 C. Maggi, J. Simmchen, F. Saglimbeni, J. Katuri, M. Dipalo, F. De Angelis, S. Sanchez and R. Di Leonardo, *Small*, 2016, **12**, 446.
61 L. C. Bradley, K. J. Stebe and D. Lee, *J. Am. Chem. Soc.*, 2016, **138**, 11437.
62 P. Seidel and B. J. Ravoo, *Macromol. Chem. Phys.*, 2016, **217**, 1467.
63 J. W. Kim, J. Cho, J. Cho, B. J. Park, Y.-J. Kim, K.-H. Choi and J. W. Kim, *Angew. Chem., Int. Ed.*, 2016, **55**, 4509.
64 Y. Nakagawa, H. Kageyama, Y. Oaki and H. Imai, *J. Am. Chem. Soc.*, 2014, **136**, 3716.
65 I. U. Khan, C. A. Serra, N. Anton, X. Li, R. Akasov, N. Messaddeq, I. Kraus and T. F. Vandamme, *Int. J. Pharm.*, 2014, **473**, 239.
66 X.-T. Sun, C.-G. Yang and Z.-R. Xu, *RSC Adv.*, 2016, **6**, 12042.
67 M. Marquis, D. Renard and B. Cathala, *Biomacromolecules*, 2012, **13**, 1197.
68 Y. Hu, J. Wang, C. Li, Q. Wang, H. Wang, J. Zhu and Y. Yang, *Langmuir*, 2013, **29**, 15529.
69 S. Lone and I. W. Cheong, *RSC Adv.*, 2014, **4**, 13322.
70 J. H. Kim, T. Y. Jeon, T. M. Choi, T. S. Shim, S.-H. Kim and S.-M. Yang, *Langmuir*, 2014, **30**, 1473.
71 S.-N. Yin, C.-F. Wang, Z.-Y. Yu, J. Wang, S.-S. Liu and S. Chen, *Adv. Mater.*, 2011, **23**, 2915.
72 L. B. Zhao, L. Pan, K. Zhang, S. S. Guo, W. Liu, Y. Wang, Y. Chen, X. Z. Zhao and H. L. W. Chan, *Lab Chip*, 2009, **9**, 2981.
73 K. Maeda, H. Onoe, M. Takinoue and S. Takeuchi, *Adv. Mater.*, 2012, **24**, 1340.
74 M. Liu, X.-T. Sun, C.-G. Yang and Z.-R. Xu, *J. Colloid Interface Sci.*, 2016, **466**, 20.
75 J. Lan, J. Chen, N. Li, X. Ji, M. Yu and Z. He, *Talanta*, 2016, **151**, 126.
76 Y.-T. Yang, J. Wei, X. Li, L.-J. Wu, Z.-Q. Chang and C. A. Serra, *Adv. Powder Technol.*, 2015, **26**, 156.
77 Y. Hu, S. Wang, A. Abbaspourrad and A. M. Ardekani, *Langmuir*, 2015, **31**, 1885.
78 S. Lone, S. H. Kim, S. W. Nam, S. Park, J. Joo and I. W. Cheong, *Chem. Commun.*, 2011, **47**, 2634.
79 J. Jeong, E. Um, J.-K. Park and M. W. Kim, *RSC Adv.*, 2013, **3**, 11801.
80 Y. Chen, G. Nurumbetov, R. Chen, N. Ballard and S. A. F. Bon, *Langmuir*, 2013, **29**, 12657.
81 X. Cao, W. Li, T. Ma and H. Dong, *RSC Adv.*, 2015, **5**, 79969.
82 X. Wang, X. Feng, G. Ma, L. Yao and M. Ge, *Adv. Mater.*, 2016, **28**, 3131.
83 T. Zhu, R. Cheng, G. R. Sheppard, J. Locklin and L. Mao, *Langmuir*, 2015, **31**, 8531.
84 H. C. Shum, A. R. Abate, D. Lee, A. R. Studart, B. Wang, C.-H. Chen, J. Thiele, R. K. Shah, A. Krummel and D. A. Weitz, *Macromol. Rapid Commun.*, 2010, **31**, 108.
85 S. Muro, C. Garnacho, J. A. Champion, J. Leferovich, C. Gajewski, E. H. Schuchman, S. Mitragotri and V. R. Muzykantov, *Mol. Ther.*, 2008, **16**, 1450.
86 B. Madivala, S. Vandebril, J. Fransaer and J. Vermant, *Soft Matter*, 2009, **5**, 1717.
87 Y. Han, A. M. Alsayed, M. Nobili, J. Zhang, T. C. Lubensky and A. G. Yodh, *Science*, 2006, **314**, 626.

This journal is © The Royal Society of Chemistry 2016

Published on 28 October 2016. Downloaded by Universidade de Lisboa on 12/5/2019 9:27:16 AM.

88 Y. Du, E. Lo, S. Ali and A. Khademhosseini, *Proc. Natl. Acad. Sci. U. S. A.*, 2008, **105**, 9522.
89 K. A. Whitehead, J. Colligon and J. Verran, *Colloids Surf., B*, 2005, **41**, 129.
90 R. Mathaes, G. Winter, A. Besheer and J. Engert, *Expert Opin. Drug Delivery*, 2015, **12**, 481.
91 J. A. Champion, Y. K. Katare and S. Mitragotri, *Proc. Natl. Acad. Sci. U. S. A.*, 2007, **104**, 11901.
92 A. Donev, I. Cisse, D. Sachs, E. A. Variano, F. H. Stillinger, R. Connelly, S. Torquato and P. M. Chaikin, *Science*, 2004, **303**, 990.
93 S. Seiffert, *ChemPhysChem*, 2013, **14**, 295.
94 B.-U. Moon, N. Hakimi, D. K. Hwang and S. S. H. Tsai, *Biomicrofluidics*, 2014, **8**, 052103.
95 T. Nisisako, T. Ando and T. Hatsuzawa, *Small*, 2014, **10**, 5116.
96 L. Chen, H. Z. An and P. S. Doyle, *Langmuir*, 2015, **31**, 9228.
97 Y. Cheng, C. Zhu, Z. Xie, H. Gu, T. Tian, Y. Zhao and Z. Gu, *J. Colloid Interface Sci.*, 2014, **421**, 64.
98 A. F. Edlund, R. Swanson and D. Preuss, *Plant Cell*, 2004, **16**, S84.
99 M. B. Hallett and S. Dewitt, *Trends Cell Biol.*, 2007, **17**, 209.
100 H. K. Chan and N. Y. K. Chew, *Adv. Drug Delivery Rev.*, 2003, **55**, 793.
101 F. W. Stanley, J. C. Lamphere and L. R. Wilson, *US Pat.*, 5744564, 1998.
102 C. L. Landry-Coltrain and J. W. Leon, *US Pat.*, 6753051B1, 2004.
103 J. Yin, E. Bar-Kochba and X. Chen, *Soft Matter*, 2009, **5**, 3469.
104 M. Li, D. Joung, B. Hughes, S. D. Waldman, J. A. Kozinski and D. K. Hwang, *Sci. Rep.*, 2016, **6**, 30463.
105 S.-H. Kim, H. C. Shum, J. W. Kim, J.-C. Cho and D. A. Weitz, *J. Am. Chem. Soc.*, 2011, **133**, 15165.
106 R. Luo, Y. Cao, P. Shi and C.-H. Chen, *Small*, 2014, **10**, 4886.
107 S. Mitragotri and J. Lahann, *Nat. Mater.*, 2009, **8**, 15.
108 S. Guo, T. Yao, X. Ji, C. Zeng, C. Wang and L. Zhang, *Angew. Chem., Int. Ed.*, 2014, **53**, 7504.
109 S.-Y. Teh, R. Lin, L.-H. Hung and A. P. Lee, *Lab Chip*, 2008, **8**, 198.
110 L. Mazutis, J. Gilbert, W. L. Ung, D. A. Weitz, A. D. Griffiths and J. A. Heyman, *Nat. Protocols*, 2013, **8**, 870.
111 A. Fallah-Araghi, J.-C. Baret, M. Ryckelynck and A. D. Griffiths, *Lab Chip*, 2012, **12**, 882.
112 M. Leman, F. Abouakil, A. D. Griffiths and P. Tabeling, *Lab Chip*, 2015, **15**, 753.
113 I. Ziemecka, V. van Steijn, G. J. M. Koper, M. Rosso, A. M. Brizard, J. H. van Esch and M. T. Kreutzer, *Lab Chip*, 2011, **11**, 620.
114 K. W. Wang, K. G. Lee, T. J. Park, Y.-C. Lee, J.-W. Yang, D. H. Kim, S. J. Lee and J. Y. Park, *Biotechnol. Bioeng.*, 2012, **109**, 289.
115 C. M. Kim, S. J. Park and G. M. Kim, *Int. J. Precision Eng. Manufacturing*, 2015, **16**, 2545.
116 C. H. Yang, K. S. Huang, Y. S. Lin, K. Lu, C. C. Tzeng, E. C. Wang, C. H. Lin, W. Y. Hsu and J. Y. Chang, *Lab Chip*, 2009, **9**, 961.
117 T. Watanabe, T. Ono and Y. Kimura, *Soft Matter*, 2011, **7**, 9894.
118 K.-S. Huang, T.-H. Lai and Y.-C. Lin, *Lab Chip*, 2006, **6**, 954.
119 C. J. Martinez, J. W. Kim, C. Ye, I. Ortiz, A. C. Rowat, M. Marquez and D. Weitz, *Macromol. Biosci.*, 2012, **12**, 946.
120 Y.-J. Eun, A. S. Utada, M. F. Copeland, S. Takeuchi and D. B. Weibel, *ACS Chem. Biol.*, 2011, **6**, 260.
121 C.-H. Yang, K.-S. Huang and J.-Y. Chang, *Biomed. Microdevices*, 2007, **9**, 253.
122 H. Shibata, Y. J. Heo, T. Okitsu, Y. Matsunaga, T. Kawanishi and S. Takeuchi, *Proc. Natl. Acad. Sci. U. S. A.*, 2010, **107**, 17894.
123 R. C. H. Ruiz, P. Kiatwuthinon, J. S. Kahn, Y. H. Roh and D. Luo, *Ind. Biotechnol.*, 2012, **8**, 372.
124 S.-B. Huang, Y.-H. Chang, H.-C. Lee, S.-W. Tsai and M.-H. Wu, *Biomed. Microdevices*, 2014, **16**, 345.
125 Y. Tsuda, Y. Morimoto and S. Takeuchi, *Langmuir*, 2010, **26**, 2645.
126 Y.-C. Tan, K. Hettiarachchi, M. Siu, Y.-R. Pan and A. P. Lee, *J. Am. Chem. Soc.*, 2006, **128**, 5656.
127 S. Deshpande, Y. Caspi, A. E. C. Meijering and C. Dekker, *Nat. Commun.*, 2016, **7**, 10447.
128 C. Martino, T. Y. Lee, S.-H. Kim and A. J. deMello, *Biomicrofluidics*, 2015, **9**, 024101.
129 L. Liu, F. Wu, X.-J. Ju, R. Xie, W. Wang, C. H. Niu and L.-Y. Chu, *J. Colloid Interface Sci.*, 2013, **404**, 85.
130 M. Fischlechner, Y. Schaerli, M. F. Mohamed, S. Patil, C. Abell and F. Hollfelder, *Nat. Chem.*, 2014, **6**, 791.
131 B. G. Chung, K.-H. Lee, A. Khademhosseini and S.-H. Lee, *Lab Chip*, 2012, **12**, 45.
132 M. M. C. van Beers, W. Jiskoot and H. Schellekens, *J. Interferon Cytokine Res.*, 2010, **30**, 767.
133 T. Rossow, J. A. Heyman, A. J. Ehrlicher, A. Langhoff, D. A. Weitz, R. Haag and S. Seiffert, *J. Am. Chem. Soc.*, 2012, **134**, 4983.
134 C.-H. Choi, H. Wang, H. Lee, J. H. Kim, L. Zhang, A. Mao, D. J. Mooney and D. A. Weitz, *Lab Chip*, 2016, **16**, 1549.
135 C. Martino, S.-H. Kim, L. Horsfall, A. Abbaspourrad, S. J. Rosser, J. Cooper and D. A. Weitz, *Angew. Chem., Int. Ed.*, 2012, **51**, 6416.
136 W.-S. Jang, S. C. Park, E. H. Reed, K. P. Dooley, S. F. Wheeler, D. Lee and D. A. Hammer, *Soft Matter*, 2016, **12**, 1014.
137 J. S. Kahn, R. C. H. Ruiz, S. Sureka, S. Peng, T. L. Derrien, D. An and D. Luo, *Biomacromolecules*, 2016, **17**, 2019.
138 W. Chen, J.-H. Kim, D. Zhang, K.-H. Lee, G. A. Cangelosi, S. D. Soelberg, C. E. Furlong, J.-H. Chung and A. Q. Shen, *J. R. Soc., Interface*, 2013, **10**, 88.

ACS APPLIED MATERIALS & INTERFACES

Forum Article

Cite This: ACS Appl. Mater. Interfaces XXXX, XXX, XXX-XXX

www.acsami.org

Platinum Nanoparticle-Based Microreactors as Support for Neuroblastoma Cells

A[redacted] Armada-Moreira,[†,‡,§] Essi Taipaleenmäki,[†] Marie Baekgaard-Laursen,[†] Philipp Sebastian Schattling,[†] Ana M. Sebastião,[‡,§] Sandra H. Vaz,[‡,§] and Brigitte Städler*[,†]

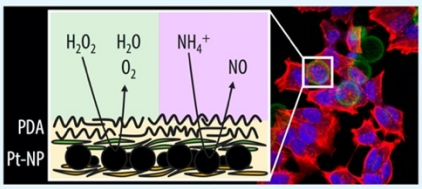
[†]Interdisciplinary Nanoscience Center (iNANO), Aarhus University, Gustav Wieds Vej 14, 8000 Aarhus, Denmark

[‡]Instituto de Farmacologia e Neurociências, Faculdade de Medicina da Universidade de Lisboa, 1649-028 Lisboa, Portugal

[§]Instituto de Medicina Molecular, Faculdade de Medicina da Universidade de Lisboa, 1649-028 Lisboa, Portugal

Supporting Information

ABSTRACT: Excitotoxicity is a common phenomenon in several neurological diseases, associated with an impaired clearance of synaptically released glutamate, which leads to an overactivation of postsynaptic glutamate receptors. This will, in turn, start an intracellular cascade of neurotoxic events, which include exacerbated production of reactive oxygen species and ammonia toxicity. We report the assembly of microreactors equipped with platinum nanoparticles as artificial enzymes and polymer terminating layers including poly(dopamine). The biological response to these microreactors is assessed in human neuroblastoma cell culture. The microreactors' function to deplete hydrogen peroxide (H_2O_2) and ammonia is confirmed. While the proliferation of the cells depends on the number of microreactors present, no inherent toxicity is found. Furthermore, the microreactors are able to ameliorate the effects of excitotoxicity in cell culture by scavenging H_2O_2 and ammonia, thus having the potential to provide a therapeutic approach for several neurological diseases in which excitotoxicity is observed.



KEYWORDS: *Polydopamine, neuroblastoma cells, excitotoxicity, oxidative stress, ammonia toxicity, platinum nanoparticles*

INTRODUCTION

Excitotoxicity can be described as neuronal injury and death triggered by toxic actions of excitatory neurotransmitters, mainly glutamate in the central nervous system (CNS).[1] Excitotoxicity is present in several neurodegenerative diseases,[2] as well as in cerebral ischemia and traumatic brain injury.[3,4] In the mammalian CNS, this phenomenon involves a rise in intracellular calcium levels, as well as mitochondria dysfunction, free radical accumulation, and production of reactive oxygen species (ROS), among other toxic intracellular events.[5,6] Furthermore, if associated with an impairment of the glutamate/glutamine cycle, which is the main mechanism of ammonia (NH_4^+) detoxification in the brain,[7] excitotoxicity can lead to NH_4^+ toxicity,[8] exacerbating the overactivation of NMDA glutamate receptors.[9]

Although excitotoxicity is a very complex and not yet fully understood phenomenon (the reader is referred to a review on excitotoxicity by Mehta et al.),[2] it is widely accepted that excitotoxicity-induced production of ROS is an important contributor to the onset of pathology.[10,11] It is known that high intracellular ROS levels induce oxidative stress by causing irreversible oxidative damage to lipids, membranes, proteins, and nucleic acids.[12] Importantly, some intracellularly produced ROS, for example hydrogen peroxide (H_2O_2), are capable of crossing cell membranes and affecting neighboring cells.[13]

Several treatments to counteract excitotoxicity focus on limiting glutamate release or blocking glutamate receptors, as reviewed by Jia et al.[14] However, this type of permanent blockage interferes with physiological glutamate functions, generating considerable side effects.[4] Therefore, there is a need for the development of alternative therapeutic strategies.

Therapeutic cell mimicry aims at replacing missing or lost cellular functions. A core focus of this field comprises the bottom-up fabrication of micro- and nanostructures with tunable size, shape, chemistry, and biological activity,[15] including the assembly of artificial cells, organelles, and enzymes.[16]

The field of artificial enzymes, which includes organic or inorganic materials with enzyme-like activity, has attracted considerable interest in the past few years.[17] Nanozymes are a particular subset of artificial enzymes that are based on nanomaterials and nanoparticles that possess catalytic activity, including metal oxides, noble metals, and carbon,[18] with potential applications in biomedicine[19] or prodrug therapy.[20]

Special Issue: 10 Years of Polydopamine: Current Status and Future Directions

Received: July 21, 2017
Accepted: October 17, 2017

ACS Publications © XXXX American Chemical Society

DOI: 10.1021/acsami.7b10724
ACS Appl. Mater. Interfaces XXXX, XXX, XXX−XXX

Inorganic nanoparticles show great promise as enzyme mimics since they circumvent problems that natural enzymes face (such as low stability, progressive loss of activity, and high purification costs),[21] although they predominantly exhibit peroxidase, oxidase, catalase, and/or superoxide dismutase (SOD) activity.[18] Noble metals-based nanozymes have inherent beneficial properties, including low susceptibility to corrosion, higher resistance toward oxidation, inertness, and absence of complex formation with other elements, giving them higher stability and lower levels of toxicity.[18] Platinum nanoparticles (Pt-NP) are interesting artificial enzyme candidates.[22] For instance, citrate-capped Pt-NP have been shown to be more efficient peroxidases than horseradish peroxidase (HRP) at the same concentration.[23] Moreover, while soluble platinum ($PtCl_4$) is cytotoxic and leads to oxidative stress, Pt-NP do not dissolve in cell medium and do not lead to a rise in the intracellular ROS levels and consequent cytotoxicity or apoptosis.[23,24] Thus, Pt-NP have been widely used in biomedical applications.[25,26] For a detailed discussion on the applications of noble metal-based nanozymes and Pt-NP, the reader is referred to the review by Cheng and Liu.[27]

From a different perspective, the field of artificial cells considers two different approaches. The top-down approach includes the encapsulation of whole cells or components of cells, as reviewed by Orive et al.[28] On the other hand, the bottom-up approach aims to construct microreactors often with biocatalytic activity, using polymers, lipids, and enzymes as building blocks.[29,30] Although impressive progress in the assembly of artificial cells has been accomplished, yielding multicompartmentalized systems[31,32] hosting up to three enzymes simultaneously,[33] only few reports have succeeded in confirming their biocatalytic activity in the presence of their natural counterparts. Unlike artificial organelles,[34] artificial cells are expected to show extracellular biocatalytic function and no cell internalization is required.

Poly(dopamine) (PDA), first introduced by Lee et al.,[35] is assembled via the self-oxidative polymerization of dopamine at slightly basic pH, and has been proven useful for several biomedical applications as recently extensively outlined in reviews providing an excellent historical overview over the developments of PDA.[36,37] The early findings illustrating the biocompatibility of PDA in cell culture[38] and in vivo[39] contributed to the wide use of this material, which is known to possess strong adhesive properties, being able to adhere to virtually any type of substrate.[40] In addition to rendering surfaces adhesive to proteins and cells, PDA has been used as a building block for the assembly of colloidal carriers, such as polymer capsules introduced by the Caruso group,[41] and microreactors.[33,42]

The aim of this report was to create a microreactor that can act as an artificial astrocyte toward counteracting ROS production and NH_4^+ toxicity triggered by excitotoxicity (Figure 1). Specifically, we (i) assessed the conversion of H_2O_2 and NH_4^+ by Pt-NP in solution, (ii) assembled Pt-NP-based microreactors with different surface charges and assessed their catalytic activity toward H_2O_2 and NH_4^+, (iii) determined the effects of different microreactor to cell ratios in terms of cell viability and proliferation, (iv) compared the microreactors' cell adhesive properties, and (v) demonstrated the protective effects of the microreactors toward H_2O_2 and NH_4^+ cell toxicity.

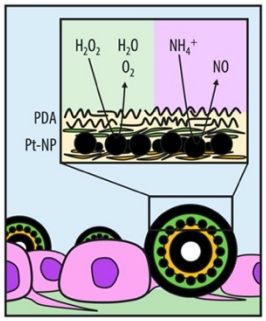


Figure 1. Schematic overview of the interaction between neuroblastoma cells and microreactors. The inset shows the protective activity of the Pt-NP, which can convert hydrogen peroxide (H_2O_2) into water and oxygen as well as ammonia (NH_4^+) into nitric oxide (NO). The microreactors consist of a polystyrene carrier particle (white) coated with poly(L-lysine) (PLL, yellow and green), Pt-NP (black circles), and poly(dopamine) (PDA, black layers), PLL, or poly(methacrylic acid) as terminating layers.

EXPERIMENTAL SECTION

Materials. 4-(2-Hydroxyethyl)piperazine-1-ethanesulfonic acid (HEPES), hexachloroplatinic acid, sodium borohydride, trisodium citrate, poly(L-lysine) (PLL, M_W 40 000−70 000 Da), poly(methacrylic acid) (PMA, M_W 18 600 Da), fluorescein 5(6)-isothiocyanate (FITC), tris(hydroxymethyl)aminomethane (TRIS), fluorescein *O*-methacrylate, *N*-hydroxysuccinimide 2-(dodecylthiocarbonothioylthio)isobutyrate (CTA-NHS), dopamine hydrochloride (DA), phosphate buffered saline (PBS), Hoechst 33342, fluorescein diacetate (FDA), propidium iodide (PI), horseradish peroxidase (HRP, 250−330 units per mg solid), cell counting kit CCK-8, hydrogen peroxide (H_2O_2, 30% (w/w)), ammonium acetate (NH_4^+), SH-SY5Y cells, ammonia assay kit (AAK, MAK310), paraformaldehyde (PFA), bovine serum albumin (BSA), Triton X-100, and o-dianisidine were purchased from Sigma-Aldrich (St. Louis, MO). Amplex UltraRed and Pierce LDH Cytotoxicity Assay Kit were obtained from ThermoFisher Scientific (Waltham, MA). Dulbecco's modified Eagle's medium (DMEM, high glucose), Ham's F12 Nutrient Mix (Ham's F12), fetal bovine serum (FBS), and 100 U mL^{-1} penicillin and 100 μg mL^{-1} streptomycin (Pen/Strep) were purchased from Life Technologies (Camarillo, CA). Diethyl ether and dimethylformamide (DMF) were purchased from VWR (Radnor, PA). Methacrylic acid and azobis(isobutyronitrile) (AIBN) were purchased for Merck (Kenilworth, NJ). Polystyrene (PS) particles (19.30 μm in diameter) were purchased from Microparticles GmbH (Berlin, Germany). Uncoated, IbiTreat- and PLL-coated μ-Slides VI$^{0.4}$ were purchased from ibidi GmbH (Martinsried, Germany). Ultrapure water (18.2 MΩ cm^{-1} resistance) was provided by an ELGA Purelab Ultra system (ELGA LabWater, Lane End, UK). FITC-labeled PLL (PLL_{FI}) was synthesized according to the procedure previously published.[43]

Two types of buffer solutions were used throughout all experiments: HEPES buffer consisting of 10 mM HEPES, pH 7.3, and TRIS buffer consisting of 10 mM TRIS, pH 8.5. All buffer solutions were prepared using ultrapure water.

Pt-NP Fabrication. 1 mL of an aqueous solution of hexachloroplatinic acid (16 mM) and 1 mL of an aqueous solution of trisodium citrate (40 mM) were added to 32 mL of ultrapure water and stirred for 30 min at room temperature. After the addition of 200 μL of an aqueous solution of sodium borohydride (50 mM), the solution

DOI: 10.1021/acsami.7b10724
ACS Appl. Mater. Interfaces XXXX, XXX, XXX−XXX

turned brownish. The reaction was allowed to proceed for 1 h at room temperature.

Synthesis of Fluorescein *O*-Methacrylate Labeled PMA (PMA_F). 1 g (11.6 mmol) of methacrylic acid, 116 mg (0.3 mmol) of fluorescein O-methacrylate, 30.8 mg (0.07 mmol) of CTA-NHS, and 1.10 mg (6.7 μmol) of AIBN were dissolved in 3 mL of DMF. The solution was purged with Argon for 2 min. Oxygen was removed by three consecutive freeze thaw cycles. Between each cycle the tubes were backfilled with Argon. The solution was placed in an oil bath preheated at 75 °C and stirred overnight. After the solution was cooled down to room temperature, the polymer was purified by precipitation with diethyl ether. The purification was repeated three times, by dissolving the polymer again in DMF. The polymer was dried under reduced pressure.

Microreactor Assembly. PS particles (ø 19.30 μm, 0.1 g mL^{-1}) were washed 2× in TRIS buffer (1800 rpm, 30 s). The particles were suspended in a DA solution (2.5 mg mL^{-1} in TRIS buffer, 3 h) to generate inactive PDA-coated particles (M^0). To assemble active microreactors, the particles were then incubated with either a PLL or a PLL_F solution (1 mg mL^{-1} in HEPES buffer, 10 min), followed by incubation with a Pt-NP solution (20 min) to obtain Pt-NP-coated particles (M^{Pt}). The assemblies were always washed 3× in HEPES buffer between the different coating steps. To generate microreactors with a positively charged terminating layer (M^+), M^{Pt} were incubated with a solution of either PLL or PLL_F (1 mg mL^{-1} in HEPES buffer, 10 min). To obtain microreactors with a PDA terminating layer (M^{PDA}) and with a negatively charged terminating layer (M^-), M^+ were exposed to a DA solution (2.5 mg mL^{-1} in TRIS buffer, 3 h) and to a solution of either PMA or PMA_F (4 mg mL^{-1} in HEPES buffer, 15 min), respectively.

ζ-Potential Measurements. The ζ-potential of the different layers in the microreactors assembly were analyzed using a Zetasizer Nano ZS (Malvern Instruments, Malvern, UK), employing a material refractive index of 1.590 and a dispersant (water at 25 °C) refractive index of 1.330.

H_2O_2 Detection Assay. H_2O_2 detection was achieved using the Amplex UltraRed assay for H_2O_2 detection. 50 μL of the samples were incubated with 0.2 U mL^{-1} HRP and 50 μM Amplex UltraRed in ultrapure water, in a total volume of 100 μL. The mix was incubated at room temperature protected from light for 30 min. The fluorescence of the solutions (λ_{ex} = 545 nm, λ_{em} = 590 nm) was measured by a multiplate reader.

NH_4^+ Detection Assay. NH_4^+ was detected using the commercially available AAK. 10 μL of the samples were incubated with 90 μL of the AAK detection mix and left to incubate for 15 min at room temperature, protected from light. The fluorescence of the solutions (λ_{ex} = 360 nm, λ_{em} = 450 nm) was measured by a multiplate reader.

Confocal Laser Scanning Microscopy (CLSM). Microreactors were deposited in uncoated Ibidi μ-Slides VI$^{0.4}$ and imaged with a confocal laser scanning microscope (CLSM, LSM700, Carl Zeiss, Germany), with a 40× objective. Images were recorded with the software ZEN (Carl Zeiss).

Transmission Electron Microscopy (TEM). Microreactors with and without Pt-NP were imaged by TEM (Tecnai G^2 Spirit TWIN/BioTWIN, FEI Company, Hillsboro, OR). The grids for TEM were prepared by depositing 5 μL of sample on a glow discharge-treated (20 s, PELCO easiGlow, Ted Pella Inc., Redding, CA) grid followed by washing after 1 min with 2 × 5 μL ultrapure water and staining with 2 × 5 μL 2% (v/v) uranyl acetate.

Cell Culture. The human neuroblastoma cell line (SH-SY5Y) was obtained from European Collection of Cell Cultures. The cells were cultured at a density of 3000 cells cm^{-2} in 75 cm^2 culture flasks in DMEM/Ham's F12 medium (1:1) supplemented with 10% (v/v) FBS and 1% (v/v) Pen/Strep, at 37 °C in a humidified atmosphere of 95% air−5% CO_2.

Immunocytochemistry (ICC). For the cell attachment assay, 50 000 cells cm^{-2} were adhered for 48 h onto IbiTreat-coated μ-Slides VI$^{0.4}$. Microreactors were then added, at a 1:1 or 1:10 microreactor to cell ratio. After 24 h of incubation, cells were washed 3× with PBS, fixed for 30 min in 4% (w/v) PFA in PBS, and permeabilized and blocked for nonspecific binding sites for 20 min with 0.1% (v/v) Triton X-100 and 1% (w/v) BSA in PBS. Cells were subsequently incubated for 30 min at room temperature with Hoechst 33342 (12 μg mL^{-1}) and 1% (w/v) BSA in PBS protected from light. The samples were stored at 4 °C in PBS in the μ-Slides. For the Live/Dead assay, 50 000 cells cm^{-2} were adhered for 48 h onto PLL-coated μ-Slides VI$^{0.4}$. Microreactors were then added, at a 1:1 microreactor to cell ratio. After 24 h of incubation, cells were washed 3× with PBS and incubated for 5 min at room temperature, protected from light, with FDA (8 μg mL^{-1}) and PI (20 μg mL^{-1}) in PBS. The samples were stored at 4 °C in PBS in the μ-Slides.

Fluorescence images were captured using an Olympus XM10 monochrome digital camera (Olympus Corp., Tokyo, Japan) mounted on an Olympus IX81 inverted wide field fluorescence microscope (Olympus Corp.), with either a 10× or a 40× objective. Images were recorded using the software CellSens (Olympus Corp.).

Lactate Dehydrogenase (LDH) Cytotoxicity Assay. 100 000 cells cm^{-2} were plated in 96-well plates and allowed to adhere for 24 h. At this point, microreactors were added to the cell medium, at a ratio of one microreactor per one cell, and left to incubate for 24 h. Then, the activity of released LDH was measured for the different conditions by using Pierce LDH Cytotoxicity Assay Kit. Cells grown in the absence of microreactors were used as a negative control, in order to establish the baseline spontaneous LDH activity, and cells exposed to lysis buffer for 45 min were used as a positive control, to determine the maximum LDH activity. 50 μL of each sample was mixed with 50 μL of the LDH cytotoxicity assay reaction mix and incubated for 30 min at room temperature, after which 10 μL of stop solution was added to each well. Absorbance of samples was measured at 490 and 680 nm. The absorbance at 680 nm corresponds to background absorbance and was subtracted from that at 490 nm in order to determine LDH release.

Cell Viability Assay. 100 000 cells cm^{-2} were plated in 96-well plates and allowed to adhere for 24 h. Then, to study the effects of the microreactors in cell proliferation, microreactors were added to the cell medium at different microreactor to cell ratios (1:20, 1:10, 1:2, and 1:1) and incubated for 24 h. Alternatively, for the determination of the biological activity of the microreactors, microreactors (1:10 ratio) and different concentrations of H_2O_2 or NH_4^+ were incubated with the cells during 24 h instead. Then, the cell medium was renewed and 10% (v/v) of CCK-8 was added to each well. After 2 h of incubation at 37 °C in a humidified atmosphere of 95% air−5% CO_2, 100 μL of the cell medium was transferred into a new 96-well plate and the solution absorbance (λ = 460 nm), which is proportional to the number of cells, was measured using a multiplate reader.

Statistical Analysis. All assays in solution were performed with duplicates, with at least three independent repeats. For cell viability assays, every condition was measured in triplicates within every independent repeat. For ICC, five random fields were imaged per condition in each independent repeat. Data are expressed as mean ± standard deviation (SD). Statistical significance was determined using one-way analysis of variance followed by Sidak's multiple comparison test, with $p < 0.05$ considered to represent statistical significance. All data were analyzed in GraphPad Prism (GraphPad Software, Inc., La Jolla, CA).

■ RESULTS AND DISCUSSION

Pt-NP Activity in Solution. Pt-NP can act as ROS scavengers due to their SOD- and catalase-like activity and ability to quench superoxide anion (O_2^-), H_2O_2, and free radicals.[22] This property of Pt-NP has been extensively studied, proving that Pt-NP decompose H_2O_2, converting it into hydroxyl radicals in acidic pH, and into water and oxygen in neutral and basic pH.[22] Likewise, it was shown that Pt-NP scavenge O_2^- at neutral pH but not at acidic pH, and that the Pt-NP scavenging activity for $^1O_2$ increases with pH.[22] In addition, smaller Pt-NP show higher catalytic activity due to the

DOI: 10.1021/acsami.7b10724
ACS Appl. Mater. Interfaces XXXX, XXX, XXX−XXX

increased surface-to-volume ratio.[23] Multiple studies showed that Pt-NP, acting as ROS and free radical scavengers, reduced oxidative damage both in vitro[44,45] and in vivo for several applications, including bone diseases and pulmonary inflammation.[46,47] In the context of neuronal applications, Pt-NP were able to restore ROS homeostasis in an in vitro model of an oxidative stress-related disorder, proving that these particles can act as active ROS scavengers in the brain.[23] Furthermore, Pt-NP have been used as scavengers of O_2^- and H_2O_2 in an mouse model of ischemic stroke,[48] where an i.v. injection of Pt-NP improved neurological function and motor performance and decreased neuronal damage.[48,49]

We aimed to employ Pt-NP as the active entities in microreactors. Therefore, citrate-capped Pt-NP were synthesized by a procedure published earlier,[25] yielding ~2 nm in diameter Pt-NP with narrow dispersity, as confirmed using TEM (Figure 2).

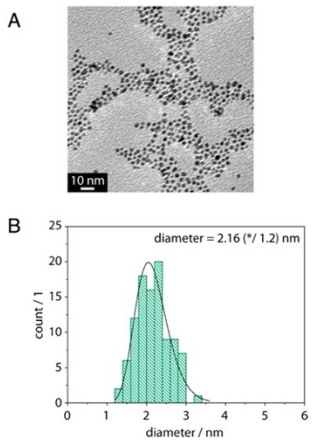


Figure 2. Pt-NP synthesis. Representative TEM image (A) and the size distribution (B) of the Pt-NP is shown. Scale bar = 10 nm.

With the goal to characterize the activity of these Pt-NP in solution, 0.25 mM, 0.50 mM, or 1.0 mM H_2O_2 were incubated with Pt-NP and its consumption was measured after 2, 4, and 24 h. As expected, the Pt-NP were capable of drastically reducing the concentration of H_2O_2 in solution, that is, after 2 h of incubation less than 5% of the original H_2O_2 concentration was left for all tested conditions, with no further significant reduction observed for the later time points (Figure 3A). It should be noted that the amount of H_2O_2 left in every condition refers to a baseline amount, equal for every condition (SI Figure S1).

From a different perspective, in bulk, platinum can catalyze the conversion of NH_4^+ into nitric oxide (NO) with high efficiency.[50,51] Interestingly, Pt-NP enclosed in mesoporous silica films were shown to maintain platinum catalytic activity in NH_4^+ degradation in a near ultrahigh-vacuum regime.[51] However, to the best of our knowledge, biomedical applications of this specific Pt-NP activity remain so far unexplored.

With the goal to assess the ability of the Pt-NP to convert NH_4^+ in solution, Pt-NP were exposed to different concentrations of NH_4^+ and the remaining amount of NH_4^+ in solution was monitored after 2, 4, and 24 h. After 2 and 4 h of incubation, it was possible to detect a significant decrease in NH_4^+ for 0.25 mM and 0.50 mM NH_4^+ starting concentrations. Importantly, after 24 h of incubation, it was possible to observe that the Pt-NP converted a significant amount of NH_4^+ for all tested conditions (Figure 3B).

In order to investigate if the Pt-NP activity was affected by the presence of both H_2O_2 and NH_4^+, Pt-NP were incubated with different concentrations of both compounds simultaneously for 24 h. The results showed that adding increasing amounts of NH_4^+ had no effect on the ability of Pt-NP to convert H_2O_2 (Figure 3C). On the other hand, adding increasing amounts of H_2O_2 to a Pt-NP solution containing 0.25 mM NH_4^+ significantly improved the Pt-NP-catalyzed conversion of NH_4^+ by ~20% in the presence of 1.0 mM H_2O_2 in comparison to the H_2O_2-free condition. This effect could only be detected for the lowest concentration of NH_4^+ tested, with no H_2O_2-dependent significant changes in NH_4^+ conversion by the Pt-NP observed for higher NH_4^+ starting concentrations (Figure 3D). This observation might be explainable, considering that H_2O_2 can be used as a source of hydroxyl radicals and these oxidizing molecules can lead to the oxidation of NH_4^+.[52] Indeed, mixtures of NH_4^+ and H_2O_2 have been used in wet chemical cleaning processes, in the form of ammonium hydroxide-hydrogen peroxide mixtures.[53] It was shown that, in these mixtures, the concentration of both NH_4^+ and H_2O_2 decreased over time, probably due to the decomposition of H_2O_2 and the hydroxyl-induced conversion of NH_4^+.[53] In our work, since the Pt-NP decompose H_2O_2 and NH_4^+ simultaneously, it is possible to hypothesize that the products of H_2O_2 degradation might, by themselves, exacerbate the oxidation of NH_4^+, thus contributing to an enhanced decrease in NH_4^+ in solution.

Microreactor Assembly. Microreactors were assembled by the layer-by-layer (LbL) technique using 19.30 μm PS particles coated with PDA (M^i) and PLL prior to the deposition of the catalytically active Pt-NP (M^{Pt}) and different terminating polymer layers. The deposition of the initial PDA layer makes the assembly of the microreactors independent of the template particles, that is, instead of PS, other materials such as silica, melamine resin, or poly(methyl methacrylate) could be used without the need to re-evaluate the assembly protocol. First, the LbL film deposition was confirmed on planar surfaces using quartz crystal microbalance with dissipation monitoring (SI Figure S2). Following on, the multilayers were assembled onto PS particles and the ζ-potential was monitored after each adsorption step. The assembly of M^i was confirmed by the color change of the initially white PS particles into dark gray particles (Figure 4A). The subsequent deposition of PLL was illustrated by the ζ-potential change from ~ −34 mV to ~26 mV and visualized using CLSM employing PLL_F (Figure 4B). The successful Pt-NP adsorption onto the PDA/PLL precoated carrier particles yielding M^{Pt} was confirmed by the ζ-potential change from ~26 mV to ~2 mV and TEM images (Figure 4C). In the latter case, the particle surfaces were smooth and rough in the absence and presence of the Pt-NP, respectively. Different terminating layers were employed with the aim to optimize the interaction of the microreactors with the neuroblastoma cells. To this end, positively and negatively charged microreactors were assembled. Additionally, PDA was

DOI: 10.1021/acsami.7b10724
ACS Appl. Mater. Interfaces XXXX, XXX, XXX−XXX

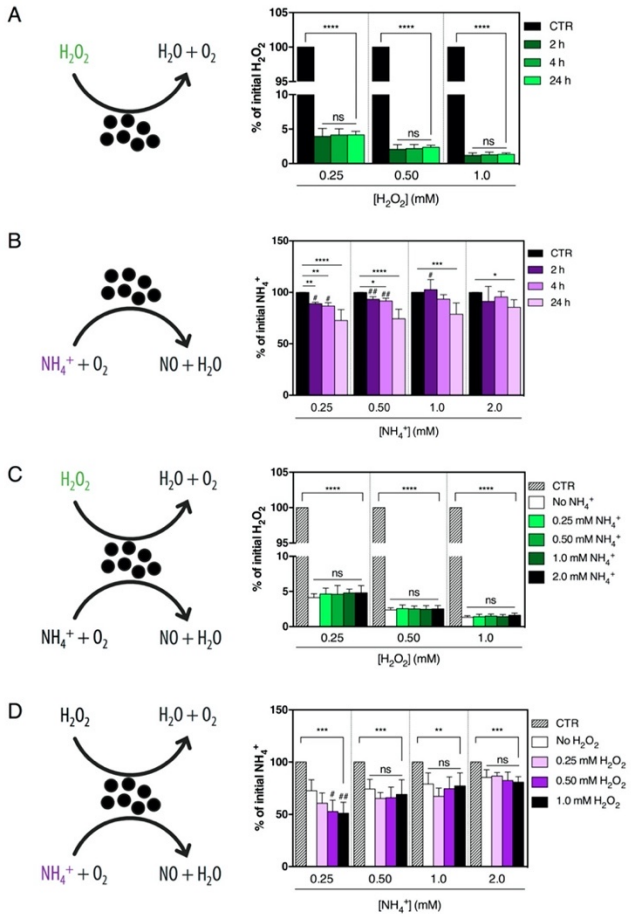


Figure 3. Pt-NP as enzyme mimics in solution. (A) H_2O_2 degradation. The remaining amount of H_2O_2 was measured at different time points (2, 4, and 24 h) when incubated with Pt-NP using different initial concentrations of H_2O_2 (0.25 mM, 0.50 mM, and 1.0 mM). $N = 3$. $^{****}p < 0.0001$ compared to control, $^{ns}p > 0.05$ between time points. (B) NH_4^+ conversion. The remaining concentration of NH_4^+ in solution was measured after 2, 4, and 24 h when incubated with Pt-NP using different initial NH_4^+ concentrations (0.25 mM, 0.50 mM, 1.0 mM, and 2.0 mM). $N = 4$. $^{*}p < 0.05$, $^{**}p < 0.01$, $^{***}p < 0.001$, $^{****}p < 0.0001$ compared to respective control. $^{\#}p < 0.05$, $^{\#\#}p < 0.01$ for comparison with the 24 h time point. (C) H_2O_2 degradation in the presence of NH_4^+. Pt-NP were incubated with different combinations of initial concentrations of H_2O_2 (0.25 mM, 0.50 mM, and 1.0 mM) and NH_4^+ (0.25 mM, 0.50 mM, 1.0 mM, and 2.0 mM) for 24 h. $N = 3$. $^{****}p < 0.0001$ for all conditions compared to control, $^{ns}p > 0.05$ between conditions. (D) Degradation of NH_4^+ in the presence of H_2O_2. Pt-NP were incubated with different combinations of initial concentrations of NH_4^+ (0.25 mM, 0.50 mM, 1.0 mM, and 2.0 mM) and H_2O_2 (0.25 mM, 0.50 mM, and 1.0 mM) for 24 h. $N = 4$–9. $^{**}p < 0.01$, $^{***}p < 0.001$ compared to control. $^{ns}p > 0.05$, $^{\#}p < 0.05$, $^{\#\#}p < 0.01$ for comparison of conditions with the H_2O_2-free condition. All values were normalized to the control condition (no Pt-NP) and are represented as mean ± SD. All controls were set to 100%. All graphs are accompanied by a schematic representation of the measured reaction.

chosen as a terminating layer due to its known beneficial effects on cell adhesion as, for instance, shown by Yang et al.[54] and Xu et al.[55] Positively charged microreactors (M^+) were obtained by coating M^{Pt} with PLL. The obtained positive ζ-potential (~19 mV) and the visualization by CLSM using PLL_F confirmed the deposition of this PLL layer (Figure 4D). PDA-coated (M^{PDA})

DOI: 10.1021/acsami.7b10724
ACS Appl. Mater. Interfaces XXXX, XXX, XXX−XXX

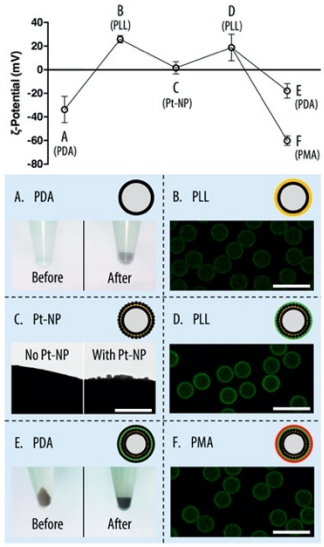


Figure 4. ζ-potential measurements of the microreactors at the different steps in the LbL assembly (N = 2) including representative images. The PDA deposition is confirmed by color change (A: M^i: color change from white to dark gray, E: M^{PDA}: color change from dark gray to black). The deposition of the PLL_F and PMA_F layers are imaged using CLSM (B, D: M^+, F: M^-). Pt-NP deposition is confirmed by TEM (C: M^{Pt}). CLSM scale bar = 40 μm. TEM scale bar = 1 μm.

and negatively charged (M^-) microreactors were yielded by an additional deposition of PDA and PMA, respectively, on M^+. The deposition of the PDA terminating layer was illustrated by the negative ζ-potential (∼ −18 mV) and the color change of the microreactors from dark gray to black (Figure 4E). The negative ζ-potential (∼ −60 mV) and the green fluorescence in the CLSM images originating from the deposited PMA_F confirmed the assembly of M^- (Figure 4F). Microreactors without a terminating layer (M^{Pt}) were used as control, to ensure that the terminating layers did not block the catalytic activity of Pt-NP.

Following on, the catalytic activity of the microreactors was assessed. 10^4 or 10^5 microreactors were incubated with 1.0 mM H_2O_2 for 24 h before the remaining H_2O_2 was detected. In the first case (10^4 microreactors) ∼ 30% of H_2O_2 was consumed, while almost all H_2O_2 was used up in the latter case (10^5 microreactors) (Figure 5A). The average conversion of a single microreactor was estimated to be $(2.59 \pm 0.249) \times 10^{-4}$ nmol H_2O_2 h^{-1}. The terminating layer did not significantly affect the Pt-NP activity (SI Figure S3), indicating that neither the deposition of the terminating layer(s) displaced Pt-NP from the carrier particle surface, nor did their presence hinder the access of H_2O_2 to the Pt-NP surface. As expected, M^i did not show catalytic activity toward H_2O_2. In addition, it was confirmed that the catalytic activity toward H_2O_2 of M^{PDA} was maintained in cell medium (SI Figure S4). Furthermore, although PDA

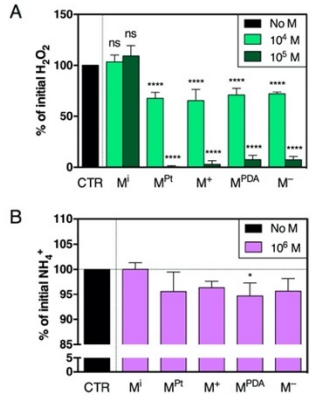


Figure 5. Pt-NP-based microreactors in solution. (A) Pt-NP-based microreactors as H_2O_2 scavengers. The amount of remaining H_2O_2 in solution after incubation of 1.0 mM H_2O_2 with 10^4 or 10^5 microreactors (M) for 24 h is shown. N = 3. $^{ns}p > 0.05$, $^{****}p < 0.0001$ compared to control (no microreactors). (B) Pt-NP-based microreactors for NH_4^+ degradation. The remaining amount of NH_4^+ was measured after 10^6 microreactors (M) were incubated with 1.0 mM NH_4^+ for 24 h. N = 3–4. $^*p < 0.05$ compared to control (no microreactors). Controls were set to 100%. All values were normalized to the respective control and are represented as mean ± SD.

degradation due to H_2O_2 was shown before,[56] the H_2O_2 concentrations used here were ∼2000× lower and the pH was neutral and not basic.

Similarly, 10^6 microreactors were exposed to 1.0 mM NH_4^+ for 24 h and the amount of remaining NH_4^+ in solution was measured (Figure 5B). It was observed that all microreactors were catalytically active, consuming similar amounts of NH_4^+. It was estimated that, in average, a single microreactor converted $(1.84 \pm 0.291) \times 10^{-6}$ nmol NH_4^+ h^{-1}. M^i did not show catalytic activity toward NH_4^+.

Taken together, functional Pt-NP-based microreactors, with controllable surface chemistry and capability to convert H_2O_2 and NH_4^+, were assembled.

Microreactors and Neuroblastoma Cells: Proliferation. With the aim to assess the effects of the microreactors on the cell viability and proliferation of neuroblastoma cells, 100 000 cells cm^{-2} were seeded in 96 well-plates and incubated for 24 h at 37 °C in a humidified atmosphere of 95% air−5% CO_2. Subsequently, different numbers of microreactors were added to the cell medium and incubated for 24 h before the cell viability was measured. The cell viability was normalized to cells grown in the absence of microreactors. In general, increasing the number of microreactors led to a decrease in the number of cells, compared to the control condition.

Incubating the cells with microreactors, regardless of the terminating layer, at a ratio of one microreactor per one or two cells led to a decrease of ∼50% or more in the number of cells present in culture, compared to the control condition (no microreactors). In these conditions, the differences between the terminating layers of the microreactors might be caused by how these different coatings interact with the cells. Since the neuronal cell membrane has a negative charge, both M^+ (Figure

DOI: 10.1021/acsami.7b10724
ACS Appl. Mater. Interfaces XXXX, XXX, XXX−XXX

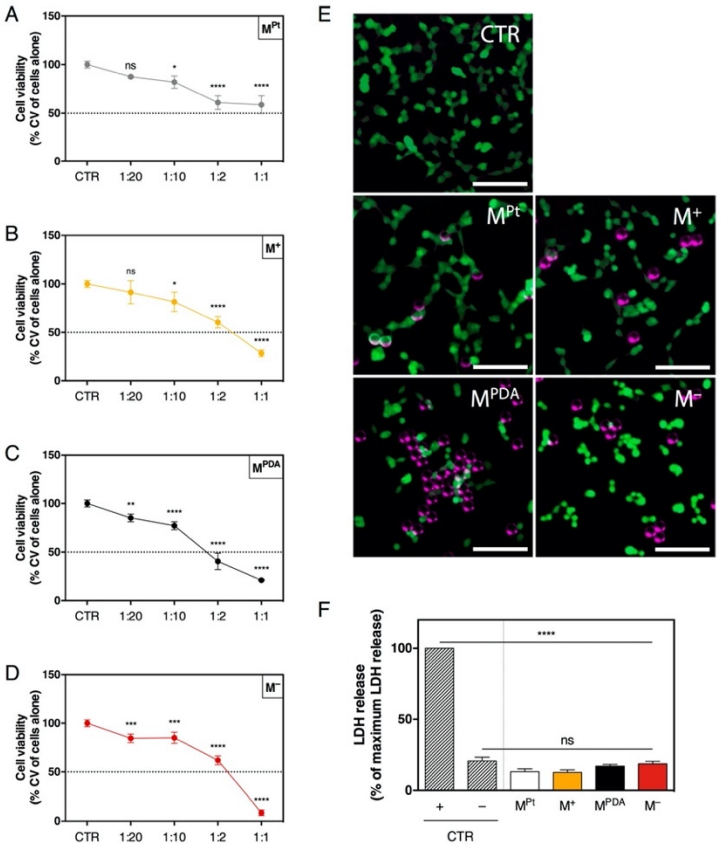


Figure 6. Cell viability/proliferation of neuroblastoma cells incubated with (A) Pt-NP-coated microreactors (M^{Pt}; $N = 3$; $^{*}p < 0.05$, $^{**}p < 0.01$, $^{****}p < 0.0001$ compared to control), (B) positively charged microreactors (M^{+}; $N = 3$; $^{ns}p > 0.05$, $^{*}p < 0.01$, $^{****}p < 0.0001$ compared to control), (C) PDA-coated microreactors (M^{PDA}; $N = 4–5$; $^{**}p < 0.01$, $^{****}p < 0.0001$ compared to control), and (D) negatively charged microreactors (M^{-}; $N = 3$; $^{****}p < 0.0001$ compared to control). All values were normalized to the control (no microreactors) and are represented as mean ± SD. Controls were set to 100% of cell viability. (E) Representative fluorescent images of the Live/Dead assay, showing live cells (green) and microreactors (magenta). No dead cells (magenta cells) were found in any condition. Scale bars = 100 μm. (F) LDH cytotoxicity assay. The levels of LDH release were measured in cells treated with lysis buffer (positive control), cells grown in the absence of microreactors (negative control), and cells exposed to the differently coated microreactors, at a 1:1 ratio, for 24 h. The maximum LDH release, shown in the negative control, was set to 100% and other values were normalized to it. $N = 3$. $^{ns}p > 0.05$ for comparison with negative control, $^{****}p < 0.0001$ for comparison with positive control. Data are represented as mean ± SD.

6B) and M^{PDA} (Figure 6C) will adhere more to the cells compared to M^{Pt} (Figure 6A), causing a bigger impact in the reduction of number of cells. For the same reason, M^{-} might not interact as much with the cells, possibly impeding their proliferation due to its surface charge (Figure 6D). Interestingly, at lower ratios, no significant differences in the number of cells were found between different microreactors co-cultured at the same ratio (SI Figure S5). The decreasing cell numbers with increasing number of microreactors could be explained by either the microreactors inducing more cell death, or their presence having a negative effect in cell proliferation. In order to clarify the reason for the decreased cell count, a Live/Dead staining assay was employed. 50 000 cells cm^{-2} were grown for 48 h and then exposed to 10^{5} microreactors for 24 h. Then, the cells were stained with FDA and PI to visualize the live and dead cells, respectively. The number of dead cells (magenta

DOI: 10.1021/acsami.7b10724
ACS Appl. Mater. Interfaces XXXX, XXX, XXX−XXX

cells) was negligible in every condition (Figure 6E). Additionally, a LDH cytotoxicity assay was performed, to ensure the cell membrane integrity when the cells were exposed to the microreactors. LDH release occurs when cell membranes are compromised and the cells begin processes of cell death.[57] This assay was performed on cell cultures prepared in the same manner as for the cell viability assay described above. After the 24 h incubation, the activity of released LDH was measured for all conditions, using cells not exposed to microreactors as a negative control (to establish baseline spontaneous LDH release) and using cells exposed to lysis buffer as a positive control (to determine the maximum LDH release). It was observed that the levels of LDH release in cells exposed to microreactors were undistinguishable from the baseline spontaneous LDH release (Figure 6F). On the other hand, cells exposed to the lysis buffer, that is, cells with compromised membranes, showed significantly higher levels of LDH release. Thus, it can be concluded that the microreactors did not interfere with the membrane integrity. Therefore, taking all these assays into account, it can be hypothesized that the microreactors are not cytotoxic, but interfere with cell proliferation, likely due to contact inhibition of proliferation (CIP). CIP refers to the process by which cells stop or slow their proliferation due to high confluence and mechanical constraints, and is one of the factors that lead to monolayer cell growth. For a review on the subject, the reader is referred to the publication of McClatchey and Yap.[58] Indeed, it has been shown that, when the free space available per cell was reduced, the affected cells slowed their proliferation and eventually reached a quiescent state.[59] In our experimental setup, increasing the number of microreactors in culture led to less available space for the cells and, thus, might have caused a higher mechanical stress with concomitant arrest of proliferation.

In light of these results, a ratio of one microreactor per ten cells was chosen for most of the following experiments, to ensure high catalytic activity while minimizing the negative effects on the cell proliferation.

Microreactors and Neuroblastoma Cells: Attachment. In a next step, the cell attachment to the microreactors was analyzed in more detail. To this end, the microreactors were incubated with the neuroblastoma cells in a theoretical microreactor to cell ratio of 1:1 and 1:10 and allowed to adhere for 24 h, followed by medium change, cell fixing and staining for microscopy analysis. In this experimental set up, only microreactors which were attached to the cells were detected – the free or loosely bound microreactors were washed away. The experimental microreactor to cell ratios were then calculated. When incubated at a theoretical ratio of 1:1, that is, when the number of microreactors and cells should be the same, all microreactors were present at a much lower ratio (Figure 7A, left bars). For instance, there were 10× more cells than M^{Pt} present in the culture. While M^{Pt}, M^{+}, and M^{-} attached in the same amounts, significantly more M^{PDA} could be found, indicating that PDA had a beneficial effect on the cell adhesion to the microreactors. Similarly, at the theoretical ratio 1:10, that is, the number of microreactors should be 10× lower than the number of cells, the experimental microreactor to cell ratio was significantly lower for all the tested microreactors (Figure 7A, right bars). Representative microscopy images reflect these observations (Figure 7B), where the number of microreactors (green) in comparison to the number of cells

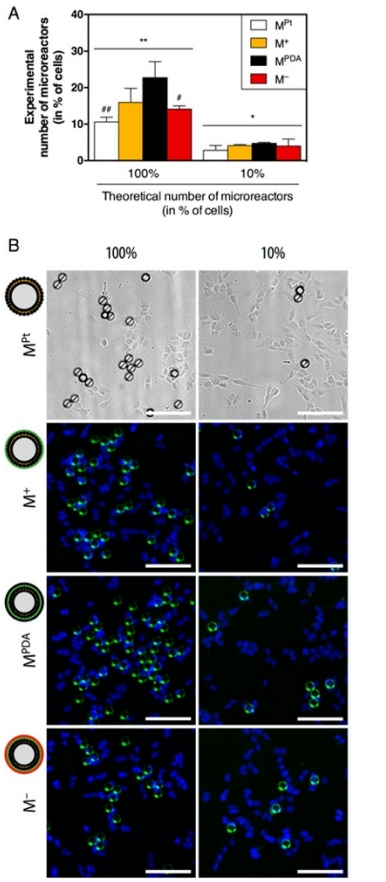


Figure 7. Surface coating dependent cell adhesion. (A) Number of microreactors, expressed as % of cells, present after medium change and ICC. The number of microreactors and cells per field was counted. The total number of cells was set to 100% and the number of microreactors was normalized to it. $N = 3–4$. $^{*}p < 0.05$, $^{**}p < 0.01$ compared to the theoretical ratio. $^{\#}p < 0.05$, $^{\#\#}p < 0.01$ compared to M^{PDA}. (B) Representative fluorescence images of microreactors (green: PLL_{fc}) incubated with neuroblastoma cells (blue nuclei). For M^{Pt}, representative bright field images are shown. Scale bars = 100 μm.

(blue nuclei) varies with the microreactor surface coating. For M^{Pt}, representative bright field images are shown.

Taking these results into account, M^{PDA} were chosen for further studies, due to their higher cell adhesive properties. PDA was previously shown to be noncytotoxic[60,61] and beneficial for neuronal cells.[62,63] Specifically, PDA-coated substrates exhibited increased neuronal adhesion, causing no

DOI: 10.1021/acsami.7b10724
ACS Appl. Mater. Interfaces XXXX, XXX, XXX–XXX

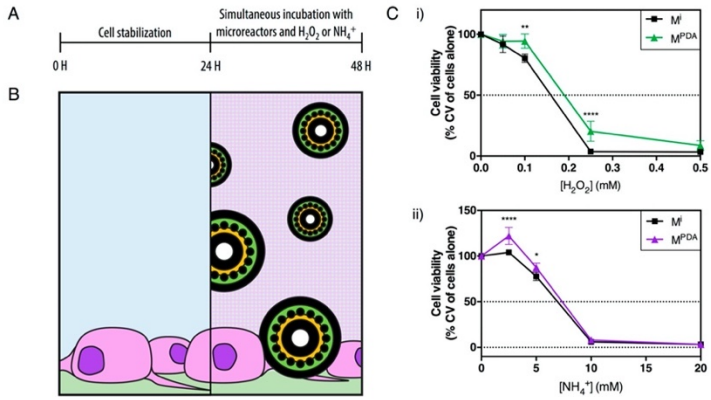


Figure 8. M^{PDA} offer protection against H_2O_2 and NH_4^+ toxicity. (A) Schematic representation of the experimental setup. (B) Illustration of microreactor-cell interaction. In the first frame, cells grow and stabilize for 24 h. In the second frame, microreactors (M^{PDA} or M^i) and toxic compounds (either H_2O_2 or NH_4^+) are incubated with the cells for more 24 h. (C) Cell viability assays performed in the presence of different concentrations of H_2O_2 or NH_4^+, with active (M^{PDA}) or inactive (M^i) microreactors. (i) Neuroblastoma cells were exposed to different concentrations of H_2O_2 and M^{PDA} or M^i (1:10 ratio) for 24 h. $N = 3$. $^{**}p < 0.01$, $^{****}p < 0.0001$ compared to M^i. (ii) Neuroblastoma cells were incubated for 24 h with M^{PDA} or M^i (1:10 ratio) and different concentrations of NH_4^+. $N = 3–5$. $^{*}p < 0.05$, $^{****}p < 0.0001$ compared to M^i. For each condition, cell viability in the absence of toxic compounds was set to 100%. All values were normalized to the respective cell viability in the absence of toxic compounds and are represented and mean ± SD.

alterations in neuronal communication and excitability, and possessing no neurotoxic effects.[63] Furthermore, while detailed studies on PDA degradation in biological environments are rare, it was shown that PDA neither led to the formation of monomeric dopamine[39] nor did it present dopaminergic activity.[64]

Microreactors and Neuroblastoma Cells: Activity. Prior efforts have been attempted to enzymatically alleviate the toxic effects of H_2O_2 in neuronal cell cultures. For instance, it has been shown, in rat striatal neuronal culture, that pharmacological-induced production of H_2O_2 could be blocked by co-administration of the inducing drug and catalase.[65] Additionally, catalase-containing nanoparticles have also been recently used to prevent the toxic effects of H_2O_2, in a study where primary human neuronal cultures were exposed to exogenous H_2O_2.[66]

In contrast to these prior reports, we employed a simple microreactor to support neuroblastoma cells. To evaluate the protective effects of M^{PDA} toward cell toxicity, neuroblastoma cells were incubated with M^{PDA} (one microreactor per ten cells ratio) and different concentrations of H_2O_2 or NH_4^+. Control experiments were performed using inactive microreactors (M^i) at the same ratio. It should be noted that, in the absence of toxic compounds, there were no significant differences in cell viability of cells incubated with M^i and with M^{PDA} at a 1:10 ratio (SI Figure S6). 100 000 cells cm^{-2} were plated and allowed to stabilize for 24 h and, then, microreactors (M^i or M^{PDA}) and different concentrations of H_2O_2 or NH_4^+ were simultaneously added to the cell medium and incubated for another 24 h (Figure 8A). The range of concentrations for both toxic compounds was determined by performing the same assay in neuroblastoma cells not exposed to microreactors (SI Figure S7). In the described experimental setup, not all microreactors are attached to the cells, as discussed in the attachment section above, being present both loose in solution and adhered to cells (Figure 8B). Thus, their catalytic activity will affect the cell medium in general, and not only in the immediate surrounding of cells. Cell viability data showed that M^{PDA} have a significant protective effect against the cytotoxic effects of H_2O_2, compared to cells exposed to M^i (Figure 8Ci). Although these findings are not surprising, since Pt-NP were expected to have a protective effect toward H_2O_2 due to their catalase-like activity, converting H_2O_2 into H_2O and O_2, nontoxic products,[22] this is the first time that Pt-NP were integrated into microreactors to be used as artificial cells.

Additionally, M^{PDA} also showed a beneficial effect toward NH_4^+ toxicity as illustrated by the cell viability data (Figure 8Cii). Interestingly, while no cell toxicity in the presence of low NH_4^+ concentrations and M^i was detected, M^{PDA} increased the cell viability at these NH_4^+ concentrations. This observation could be explained by the fact that NH_4^+ is converted into NO by M^{PDA}.[51] Although NH_4^+ and NO can be neurotoxic at high concentrations,[8,67,68] it is possible to hypothesize that the cells were only exposed to low concentrations of NO due to the NH_4^+ conversion by M^{PDA}. More specifically, according to our in vitro data (Figure 5B), only ~7% of the initial low concentration NH_4^+ (max. 5 mM) would be converted into NO. NO, in lower concentrations, is known to promote neuronal activity,[69,70] illustrating that M^{PDA} could not only prevent the cytotoxic actions of H_2O_2, but these artificial entities seemed to also convert the toxic compound NH_4^+, yielding a positive cell response.

■ CONCLUSION

Taken together, we demonstrated the assembly of a microreactor using Pt-NP as ROS and NH_4^+ scavengers and showed

DOI: 10.1021/acsami.7b10724
ACS Appl. Mater. Interfaces XXXX, XXX, XXX−XXX

their protective and stimulating effects on neuroblastoma cells. Furthermore, this work represents the first attempt to create a simple artificial astrocyte to counteract excitotoxicity and it is, to our knowledge, the first study that focuses on PDA/Pt-NP-based cell mimics as a therapeutic approach in a neuronal setting. Admittedly, the supportive effect of the microreactors needs to be improved, for instance by adding multiple layers of Pt-NP. Moreover, more in-depth biological evaluations, including the effect of the microreactors on endogenous H_2O_2 or assessing the intracellular responses to the presence of the microreactors, are required. Nonetheless, these findings are considerably advancing the field of cell mimicry, opening up vast possibilities to address the tremendous need for novel therapeutic concepts to counteract neurological medical challenges. Considering the diverse assembly possibilities of microreactors (e.g., subcompartmentalization, targeting, multiple biocatalytic cargo, etc.), tailor-made artificial cells might be feasible depending on the targeted neurological condition.

■ ASSOCIATED CONTENT

Supporting Information

The Supporting Information is available free of charge on the ACS Publications website at DOI: 10.1021/acsami.7b10724.

Non-essential figures and descriptions that complement the findings and discussion of the manuscript: raw fluorescence intensity data for Pt-NP-catalyzed H_2O_2 degradation, QCM-D measurements of the microreactor assembly method on planar surface, effect of different terminating layers on microreactor H_2O_2 scavenging properties, H_2O_2 consumption by M^{PDA} in cell medium, comparison between different microreactor terminating layers and different microreactor to cell ratios in terms of cell viability, cell viability in the presence of active and inactive microreactors at a one microreactor to ten cells ratio, dose–response curves for neuroblastoma cells in the presence of H_2O_2 or NH_4^+, and description of the necessary steps to determine the average activity per microreactor toward H_2O_2 and NH_4^+ (PDF)

■ AUTHOR INFORMATION

Corresponding Author

*E-mail: bstadler@inano.au.dk.

ORCID

Brigitte Städler: 0000-0002-7335-3945

Notes

The authors declare no competing financial interest.

■ ACKNOWLEDGMENTS

This work was supported by Fundação para a Ciência e Tecnologia (FCT), Portugal (A. A.-M., PD/BD/114278/2016 and S.H.V., SFRH/BPD/81627/2011), the Mind-brain college of ULisboa and SynaNet H2020 Twinning action, and the Aarhus University Research Foundation, Denmark.

■ REFERENCES

(1) Dong, X.; Wang, Y.; Qin, Z. Molecular Mechanisms of Excitotoxicity and Their Relevance to Pathogenesis of Neurodegenerative Diseases. *Acta Pharmacol. Sin.* **2009**, *30* (4), 379–387.

(2) Mehta, A.; Prabhakar, M.; Kumar, P.; Deshmukh, R.; Sharma, P. L. Excitotoxicity: Bridge to Various Triggers in Neurodegenerative Disorders. *Eur. J. Pharmacol.* **2013**, *698* (1–3), 6–18.

(3) Yi, J.-H.; Hazell, A. S. Excitotoxic Mechanisms and the Role of Astrocytic Glutamate Transporters in Traumatic Brain Injury. *Neurochem. Int.* **2006**, *48* (5), 394–403.

(4) Sattler, R.; Tymianski, M. Molecular Mechanisms of Glutamate Receptor-Mediated Excitotoxic Neuronal Cell Death. *Mol. Neurobiol.* **2001**, *24* (1–3), 107–129.

(5) Connolly, N. M. C.; Prehn, J. H. M. The Metabolic Response to Excitotoxicity - Lessons from Single-Cell Imaging. *J. Bioenerg. Biomembr.* **2015**, *47* (1–2), 75–88.

(6) Kritis, A. A.; Stamoula, E. G.; Paniskaki, K. A.; Vavilis, T. D. Researching Glutamate - Induced Cytotoxicity in Different Cell Lines: A Comparative/Collective Analysis/Study. *Front. Cell. Neurosci.* **2015**, *9*, 91.

(7) Bak, L. K.; Schousboe, A.; Waagepetersen, H. S. The Glutamate/GABA-Glutamine Cycle: Aspects of Transport, Neurotransmitter Homeostasis and Ammonia Transfer. *J. Neurochem.* **2006**, *98* (3), 641–653.

(8) Suárez, I.; Bodega, G.; Fernández, B. Glutamine Synthetase in Brain: Effect of Ammonia. *Neurochem. Int.* **2002**, *41* (2–3), 123–142.

(9) Marcaida, G.; Felipo, V.; Hermenegildo, C.; Miñana, M. D.; Grisolía, S. Acute Ammonia Toxicity Is Mediated by the NMDA Type of Glutamate Receptors. *FEBS Lett.* **1992**, *296* (1), 67–68.

(10) Coyle, J. T.; Puttfarcken, P. Oxidative Stress, Glutamate, and Neurodegenerative Disorders. *Science* **1993**, *262* (5134), 689–695.

(11) Kontos, H. A. Oxygen Radicals in Cerebral Ischemia: The 2001 Willis Lecture. *Stroke* **2001**, *32* (11), 2712–2716.

(12) Poli, G.; Leonarduzzi, G.; Biasi, F.; Chiarpotto, E. Oxidative Stress and Cell Signalling. *Curr. Med. Chem.* **2004**, *11* (9), 1163–1182.

(13) Halliwell, B. Antioxidants in Human Health and Disease. *Annu. Rev. Nutr.* **1996**, *16* (1), 33–50.

(14) Jia, M.; Njapo, S. A. N.; Rastogi, V.; Hedna, V. S. Taming Glutamate Excitotoxicity: Strategic Pathway Modulation for Neuroprotection. *CNS Drugs* **2015**, *29* (2), 153–162.

(15) Armada-Moreira, A.; Taipaleenmäki, E.; Itel, F.; Zhang, Y.; Städler, B. Droplet-Microfluidics towards the Assembly of Advanced Building Blocks in Cell Mimicry. *Nanoscale* **2016**, *8* (47), 19510–19522.

(16) Itel, F.; Schattling, P. S.; Zhang, Y.; Städler, B. Enzymes as Key Features in Therapeutic Cell Mimicry. *Adv. Drug Delivery Rev.* **2017**, DOI: 10.1016/j.addr.2017.09.006.

(17) Mancin, F.; Prins, L. J.; Pengo, P.; Pasquato, L.; Tecilla, P.; Scrimin, P. Hydrolytic Metallo-Nanozymes: From Micelles and Vesicles to Gold Nanoparticles. *Molecules* **2016**, *21* (8), E1014.

(18) Wei, H.; Wang, E. Nanomaterials with Enzyme-like Characteristics (Nanozymes): Next-Generation Artificial Enzymes. *Chem. Soc. Rev.* **2013**, *42* (14), 6060–6093.

(19) Rai, M.; Ingle, A. P.; Birla, S.; Yadav, A.; Santos, C. A. D. Strategic Role of Selected Noble Metal Nanoparticles in Medicine. *Crit. Rev. Microbiol.* **2016**, *42* (5), 696–719.

(20) Du, B.; Li, D.; Wang, J.; Wang, E. Designing Metal-Contained Enzyme Mimics for Prodrug Activation. *Adv. Drug Delivery Rev.* DOI: **2017**10.1016/j.addr.2017.04.002.

(21) Lin, Y.; Ren, J.; Qu, X. Catalytically Active Nanomaterials: A Promising Candidate for Artificial Enzymes. *Acc. Chem. Res.* **2014**, *47* (4), 1097–1105.

(22) Liu, Y.; Wu, H.; Li, M.; Yin, J.-J.; Nie, Z. pH Dependent Catalytic Activities of Platinum Nanoparticles with Respect to the Decomposition of Hydrogen Peroxide and Scavenging of Superoxide and Singlet Oxygen. *Nanoscale* **2014**, *6* (20), 11904–11910.

(23) Moglianetti, M.; De Luca, E.; Pedone, D.; Marotta, R.; Catelani, T.; Sartori, B.; Amenitsch, H.; Retta, S. F.; Pompa, P. P. Platinum Nanozymes Recover Cellular ROS Homeostasis in an Oxidative Stress-Mediated Disease Model. *Nanoscale* **2016**, *8* (6), 3739–3752.

(24) Horie, M.; Kato, H.; Endoh, S.; Fujita, K.; Nishio, K.; Komaba, L. K.; Fukui, H.; Nakamura, A.; Miyauchi, A.; Nakazato, T.; Kinugasa, S.; Yoshida, Y.; Hagihara, Y.; Morimoto, Y.; Iwahashi, H. Evaluation of Cellular Influences of Platinum Nanoparticles by Stable Medium Dispersion. *Met. Integr. Biometal Sci.* **2011**, *3* (11), 1244–1252.

(25) Wu, G.-W.; He, S.-B.; Peng, H.-P.; Deng, H.-H.; Liu, A.-L.; Lin, X.-H.; Xia, X.-H.; Chen, W. Citrate-Capped Platinum Nanoparticle as a Smart Probe for Ultrasensitive Mercury Sensing. *Anal. Chem.* **2014**, *86* (21), 10955−10960.
(26) Yan, L.; Bo, X.; Zhu, D.; Guo, L. Well-Dispersed Pt Nanoparticles on Polydopamine-Coated Ordered Mesoporous Carbons and Their Electrocatalytic Application. *Talanta* **2014**, *120*, 304−311.
(27) Cheng, Q.; Liu, Y. Multifunctional Platinum-Based Nanoparticles for Biomedical Applications. *Wiley Interdiscip. Rev. Nanomed. Nanobiotechnol.* **2017**, *9* (2), E1410.
(28) Orive, G.; Santos, E.; Poncelet, D.; Hernández, R. M.; Pedraz, J. L.; Wahlberg, L. U.; De Vos, P.; Emerich, D. Cell Encapsulation: Technical and Clinical Advances. *Trends Pharmacol. Sci.* **2015**, *36* (8), 537−546.
(29) Zhang, Y.; Baekgaard-Laursen, M.; Städler, B. Small Subcompartmentalized Microreactors as Support for Hepatocytes. *Adv. Healthcare Mater.* **2017**, DOI: 10.1002/adhm.201601141.
(30) Gao, C.; Wu, Z.; Lin, Z.; Lin, X.; He, Q. Polymeric Capsule-Cushioned Leukocyte Cell Membrane Vesicles as a Biomimetic Delivery Platform. *Nanoscale* **2016**, *8* (6), 3548−3554.
(31) Marguet, M.; Bonduelle, C.; Lecommandoux, S. Multicompartmentalized Polymeric Systems: Towards Biomimetic Cellular Structure and Function. *Chem. Soc. Rev.* **2012**, *42* (2), 512−529.
(32) Trantidou, T.; Friddin, M.; Elani, Y.; Brooks, N. J.; Law, R. V.; Seddon, J. M.; Ces, O. Engineering Compartmentalized Biomimetic Micro- and Nanocontainers. *ACS Nano* **2017**, *11* (7), 6549−6565.
(33) Hosta-Rigau, L.; York-Duran, M. J.; Zhang, Y.; Goldie, K. N.; Städler, B. Confined Multiple Enzymatic (Cascade) Reactions within Poly(dopamine)-Based Capsosomes. *ACS Appl. Mater. Interfaces* **2014**, *6* (15), 12771−12779.
(34) Schoonen, L.; van Hest, J. C. M. Compartmentalization Approaches in Soft Matter Science: From Nanoreactor Development to Organelle Mimics. *Adv. Mater.* **2016**, *28* (6), 1109−1128.
(35) Lee, H.; Dellatore, S. M.; Miller, W. M.; Messersmith, P. B. Mussel-Inspired Surface Chemistry for Multifunctional Coatings. *Science* **2007**, *318* (5849), 426−430.
(36) Lynge, M. E.; Schattling, P.; Städler, B. Recent Developments in Poly(dopamine)-Based Coatings for Biomedical Applications. *Nanomedicine* **2015**, *10* (17), 2725−2742.
(37) Liu, Y.; Ai, K.; Lu, L. Polydopamine and Its Derivative Materials: Synthesis and Promising Applications in Energy, Environmental, and Biomedical Fields. *Chem. Rev.* **2014**, *114* (9), 5057−5115.
(38) Ku, S. H.; Ryu, J.; Hong, S. K.; Lee, H.; Park, C. B. General Functionalization Route for Cell Adhesion on Non-Wetting Surfaces. *Biomaterials* **2010**, *31* (9), 2535−2541.
(39) Hong, S.; Kim, K. Y.; Wook, H. J.; Park, S. Y.; Lee, K. D.; Lee, D. Y.; Lee, H. Attenuation of the in Vivo Toxicity of Biomaterials by Polydopamine Surface Modification. *Nanomedicine* **2011**, *6* (5), 793−801.
(40) Sedó, J.; Saiz-Poseu, J.; Busqué, F.; Ruiz-Molina, D. Catechol-Based Biomimetic Functional Materials. *Adv. Mater.* **2013**, *25* (5), 653−701.
(41) Postma, A.; Yan, Y.; Wang, Y.; Zelikin, A. N.; Tjipto, E.; Caruso, F. Self-Polymerization of Dopamine as a Versatile and Robust Technique to Prepare Polymer Capsules. *Chem. Mater.* **2009**, *21* (14), 3042−3044.
(42) Zhang, L.; Shi, J.; Jiang, Z.; Jiang, Y.; Qiao, S.; Li, J.; Wang, R.; Meng, R.; Zhu, Y.; Zheng, Y. Bioinspired Preparation of Polydopamine Microcapsule for Multienzyme System Construction. *Green Chem.* **2011**, *13* (2), 300−306.
(43) Schattling, P.; Dreier, C.; Städler, B. Janus Subcompartmentalized Microreactors. *Soft Matter* **2015**, *11* (26), 5327−5335.
(44) Hamasaki, T.; Kashiwagi, T.; Imada, T.; Nakamichi, N.; Aramaki, S.; Toh, K.; Morisawa, S.; Shimakoshi, H.; Hisaeda, Y.; Shirahata, S. Kinetic Analysis of Superoxide Anion Radical-Scavenging and Hydroxyl Radical-Scavenging Activities of Platinum Nanoparticles. *Langmuir* **2008**, *24* (14), 7354−7364.
(45) Watanabe, A.; Kajita, M.; Kim, J.; Kanayama, A.; Takahashi, K.; Mashino, T.; Miyamoto, Y. In Vitro Free Radical Scavenging Activity of Platinum Nanoparticles. *Nanotechnology* **2009**, *20* (45), 455105.
(46) Nomura, M.; Yoshimura, Y.; Kikuiri, T.; Hasegawa, T.; Taniguchi, Y.; Deyama, Y.; Koshiro, K.; Sano, H.; Suzuki, K.; Inoue, N. Platinum Nanoparticles Suppress Osteoclastogenesis through Scavenging of Reactive Oxygen Species Produced in RAW264.7 Cells. *J. Pharmacol. Sci.* **2011**, *117* (4), 243−252.
(47) Onizawa, S.; Aoshiba, K.; Kajita, M.; Miyamoto, Y.; Nagai, A. Platinum Nanoparticle Antioxidants Inhibit Pulmonary Inflammation in Mice Exposed to Cigarette Smoke. *Pulm. Pharmacol. Ther.* **2009**, *22* (4), 340−349.
(48) Takamiya, M.; Miyamoto, Y.; Yamashita, T.; Deguchi, K.; Ohta, Y.; Abe, K. Strong Neuroprotection with a Novel Platinum Nanoparticle against Ischemic Stroke- and Tissue Plasminogen Activator-Related Brain Damages in Mice. *Neuroscience* **2012**, *221*, 47−55.
(49) Takamiya, M.; Miyamoto, Y.; Yamashita, T.; Deguchi, K.; Ohta, Y.; Ikeda, Y.; Matsuura, T.; Abe, K. Neurological and Pathological Improvements of Cerebral Infarction in Mice with Platinum Nanoparticles. *J. Neurosci. Res.* **2011**, *89* (7), 1125−1133.
(50) Nowak, E. J. Catalytic Oxidation of Ammonia on Platinum. *Chem. Eng. Sci.* **1966**, *21* (1), 19−27.
(51) Rafti, M.; Brunsen, A.; Fuertes, M. C.; Azzaroni, O.; Soler-Illia, G. J. A. A. Heterogeneous Catalytic Activity of Platinum Nanoparticles Hosted in Mesoporous Silica Thin Films Modified with Polyelectrolyte Brushes. *ACS Appl. Mater. Interfaces* **2013**, *5* (18), 8833−8840.
(52) Huang, L.; Li, L.; Dong, W.; Liu, Y.; Hou, H. Removal of Ammonia by OH Radical in Aqueous Phase. *Environ. Sci. Technol.* **2008**, *42* (21), 8070−8075.
(53) Siddiqui, S.; Keswani, M.; Brooks, B.; Fuerst, A.; Raghavan, S. A Study of Hydrogen Peroxide Decomposition in Ammonia-Peroxide Mixtures (APM). *Microelectron. Eng.* **2013**, *102*, 68−73.
(54) Yang, Z.; Tu, Q.; Zhu, Y.; Luo, R.; Li, X.; Xie, Y.; Maitz, M. F.; Wang, J.; Huang, N. Mussel-Inspired Coating of Polydopamine Directs Endothelial and Smooth Muscle Cell Fate for Re-Endothelialization of Vascular Devices. *Adv. Healthcare Mater.* **2012**, *1* (5), 548−559.
(55) Xu, M.; Zhang, Y.; Zhai, D.; Chang, J.; Wu, C. Mussel-Inspired Bioactive Ceramics with Improved Bioactivity, Cell Proliferation, Differentiation and Bone-Related Gene Expression of MC3T3 Cells. *Biomater. Sci.* **2013**, *1* (9), 933−941.
(56) Lin, J.-H.; Yu, C.-J.; Yang, Y.-C.; Tseng, W.-L. Formation of Fluorescent Polydopamine Dots from Hydroxyl Radical-Induced Degradation of Polydopamine Nanoparticles. *Phys. Chem. Chem. Phys.* **2015**, *17* (23), 15124−15130.
(57) Decker, T.; Lohmann-Matthes, M. L. A Quick and Simple Method for the Quantitation of Lactate Dehydrogenase Release in Measurements of Cellular Cytotoxicity and Tumor Necrosis Factor (TNF) Activity. *J. Immunol. Methods* **1988**, *115* (1), 61−69.
(58) McClatchey, A. I.; Yap, A. S. Contact Inhibition (of Proliferation) Redux. *Curr. Opin. Cell Biol.* **2012**, *24* (5), 685−694.
(59) Puliafito, A.; Hufnagel, L.; Neveu, P.; Streichan, S.; Sigal, A.; Fygenson, D. K.; Shraiman, B. I. Collective and Single Cell Behavior in Epithelial Contact Inhibition. *Proc. Natl. Acad. Sci. U. S. A.* **2012**, *109* (3), 739−744.
(60) Liu, X.; Cao, J.; Li, H.; Li, J.; Jin, Q.; Ren, K.; Ji, J. Mussel-Inspired Polydopamine: A Biocompatible and Ultrastable Coating for Nanoparticles in Vivo. *ACS Nano* **2013**, *7* (10), 9384−9395.
(61) van der Westen, R.; Hosta-Rigau, L.; Sutherland, D. S.; Goldie, K. N.; Albericio, F.; Postma, A.; Städler, B. Myoblast Cell Interaction with Polydopamine Coated Liposomes. *Biointerphases* **2012**, *7* (1−4), 8.
(62) Bhang, S. H.; Kwon, S.-H.; Lee, S.; Kim, G. C.; Han, A. M.; Kwon, Y. H. K.; Kim, B.-S. Enhanced Neuronal Differentiation of Pheochromocytoma 12 Cells on Polydopamine-Modified Surface. *Biochem. Biophys. Res. Commun.* **2013**, *430* (4), 1294−1300.

DOI: 10.1021/acsami.7b10724
ACS Appl. Mater. Interfaces XXXX, XXX, XXX−XXX

(63) Kang, K.; Choi, I. S.; Nam, Y. A Biofunctionalization Scheme for Neural Interfaces Using Polydopamine Polymer. *Biomaterials* **2011**, *32* (27), 6374−6380.
(64) Park, J.; Brust, T. F.; Lee, H. J.; Lee, S. C.; Watts, V. J.; Yeo, Y. Polydopamine-Based Simple and Versatile Surface Modification of Polymeric Nano Drug Carriers. *ACS Nano* **2014**, *8* (4), 3347−3356.
(65) Okuda, S.; Nishiyama, N.; Saito, H.; Katsuki, H. Hydrogen Peroxide-Mediated Neuronal Cell Death Induced by an Endogenous Neurotoxin, 3-Hydroxykynurenine. *Proc. Natl. Acad. Sci. U. S. A.* **1996**, *93* (22), 12553−12558.
(66) Singhal, A.; Morris, V. B.; Labhasetwar, V.; Ghorpade, A. Nanoparticle-Mediated Catalase Delivery Protects Human Neurons from Oxidative Stress. *Cell Death Dis.* **2013**, *4* (11), e903.
(67) Dawson, V. L.; Dawson, T. M.; Bartley, D. A.; Uhl, G. R.; Snyder, S. H. Mechanisms of Nitric Oxide-Mediated Neurotoxicity in Primary Brain Cultures. *J. Neurosci. Off. J. Soc. Neurosci.* **1993**, *13* (6), 2651−2661.
(68) Dawson, V. L.; Dawson, T. M. Nitric Oxide Neurotoxicity. *J. Chem. Neuroanat.* **1996**, *10* (3−4), 179−190.
(69) Paul, V.; Ekambaram, P. Involvement of Nitric Oxide in Learning & Memory Processes. *Indian J. Med. Res.* **2011**, *133* (5), 471−478.
(70) Yildiz Akar, F.; Ulak, G.; Tanyeri, P.; Erden, F.; Utkan, T.; Gacar, N. 7-Nitroindazole, a Neuronal Nitric Oxide Synthase Inhibitor, Impairs Passive-Avoidance and Elevated plus-Maze Memory Performance in Rats. *Pharmacol., Biochem. Behav.* **2007**, *87* (4), 434−443.

DOI: 10.1021/acsami.7b10724
ACS Appl. Mater. Interfaces XXXX, XXX, XXX−XXX

ADVANCED BIOSYSTEMS
www.adv-biosys.com

On the Assembly of Microreactors with Parallel Enzymatic Pathways

A[redacted] Armada-Moreira, Bo Thingholm, Kristine Andreassen, Ana M. Sebastião, Sandra H. Vaz, and Brigitte Städler*

Cell mimicry aims to create artificial structures capable of mimicking certain functions of living cells. However, cell mimics are tremendously simpler than their natural role models. Thus, increasing their complexity is of great importance for the advancement of cell mimicry concepts and for further understanding of biological intracellular processes. Here, the successful co-encapsulation of two enzymatic pathways with up to five enzymes into compartmentalized microreactors is reported. The microreactors are assembled by combining polymer layers and enzyme-loaded liposomal subunits, which physically separate the two encapsulated enzymatic pathways. Specifically, this report confirms the activity of an encapsulated enzymatic cycle that conjugates the actions of glutamate dehydrogenase and glutathione reductase, using $NADP^+$/NADPH as a common co-factor, as well as an encapsulated enzymatic cascade combining β-galactosidase, glucose oxidase, and catalase. This work represents a relevant advancement in encapsulated catalysis toward the assembly of therapeutic cell mimics.

1. Introduction

Living cells are complex structures and yet represent the simplest form of life. In terms of function, it is possible to look at cells as advanced catalytic reactors.[1] A notable feature of living cells that enables the performance of catalytic activity is compartmentalization, i.e., the presence of several different organelles enclosed by a lipid bilayer.[2,3] This hierarchical structure allows for the performance of multiple and simultaneous complex biochemical processes with high specificity and selectivity[3] in confined microenvironments, often with different physical and biochemical characteristics, without interference of unwanted external stimuli.[4] In fact, there is a large consensus that compartmentalization and catalyst separation are important mechanisms in the spatial and temporal control of intracellular processes and flux regulation of metabolic pathways.[2] For a detailed review on the control of specific cellular functions by compartmentalization, the reader is referred to a report by Zecchin et al.[5]

Researchers have been fascinated with the complexity and efficiency of living cells and, consequently, dedicated a considerable effort toward creating artificial cells and organelles that mimic specific cellular features. With that aim, bottom-up synthetic biology focuses on creating artificial structures with functions and architectures similar to those of living cells[6–8] by combining both biological and synthetic building blocks (such as polymers, enzymes, enzyme mimics, lipids, among others)[9–11] to construct functional artificial structures, namely artificial cells and organelles,[12] capable of interacting with cells.[13]

Taking all this into account, a simple model of an artificial cell can be achieved by creating compartmentalized assemblies where the encapsulated cargo is protected from unwanted degradation or interference and where exchange of molecules between the interior and exterior of the reactor is possible. The latter aspect gives the cargo the opportunity to react to external cues.[14] Moreover, being able to mimic biological compartmentalization is essential in the field of cell mimicry, since it creates an isolated micro/nano-environment for the entrapped catalyst, avoiding biocompatibility problems and enhancing the selectivity and efficiency of the catalyst.[13,15] Furthermore, compartmentalization in cell mimics allows for the entrapment of different cargo in each compartment, making it possible to combine different therapeutic compounds in a single carrier.[16] For an overview on recent advances in compartmentalization approaches in cell mimicry, as well as their applications, the reader is referred to reviews by York-Durán et al.[3] and Buddingh' and van Hest.[1]

A recent highlight from polymersomes-in-polymersome assemblies was reported by Peters et al., where three incompatible enzymes were encapsulated in different compartments to form an enzymatic cascade, and communication between the different compartments was achieved by substrate and product diffusion.[17] Alternatively, Elani et al. designed a complex artificial structure based on liposomes-in-liposomes comprised of

A. Armada-Moreira, B. Thingholm, K. Andreassen, Prof. B. Städler
Interdisciplinary Nanoscience Center (iNANO)
Aarhus University
Gustav Wieds Vej 14, 8000 Aarhus, Denmark
E-mail: bstadler@inano.au.dk
A. Armada-Moreira, Prof. A. M. Sebastião, Dr. S. H. Vaz
Instituto de Farmacologia e Neurociências
Faculdade de Medicina da Universidade de Lisboa
1649-028 Lisboa, Portugal
A. Armada-Moreira, Prof. A. M. Sebastião, Dr. S. H. Vaz
Instituto de Medicina Molecular
Faculdade de Medicina da Universidade de Lisboa
1649-028 Lisboa, Portugal
The ORCID identification number(s) for the author(s) of this article can be found under https://doi.org/10.1002/adbi.201700244.

DOI: 10.1002/adbi.201700244

 © 2018 WILEY-VCH Verlag GmbH & Co. KGaA, Weinheim

a network of tightly bound aqueous liposomal compartments, used to encapsulate a three-step enzymatic cascade, where transmembrane protein pores were used to navigate substrates and products toward adjacent compartments.[18]

Capsosomes (structures combining polymer capsules and liposomes), on the other hand, were employed to trigger release of encapsulated cargo using the actions of an entrapped enzyme on its substrate,[19] to catalyze a two-enzyme coupled reaction in parallel with a single-enzyme conversion by incorporating three types of liposomal subunits, each encapsulating a different type of enzyme,[20] and to perform localized encapsulated catalysis in Janus capsosomes.[21] Also, capsosomes are the only compartmentalized system that has been proven functional in biologically relevant settings, as both nanoreactors with organelle-like function[22–24] and microreactors with cell-like function.[9,10] Furthermore, capsosome-like microreactors composed of catalase (Cat) containing liposomes entrapped in alginate hydrogel particles were used to detoxify hydrogen peroxide when co-cultured with HepG2 cells, both in planar cell cultures and in the form of microreactor-cell aggregates.[25] Another recent variation of capsosomes with demonstrated biological activity entailed the replacement of enzyme-loaded liposomes with platinum nanoparticles acting as catalysts. These microreactors were able to detoxify both hydrogen peroxide and ammonia when co-cultured with human neuroblastoma cells.[26] Although still scarce in the literature, these successful examples describing the biological activity of microreactors demonstrate the potential of these systems as therapeutic strategies in a biological and biomedical context.

It should be noted that, although tremendous advances were made in assembling functional compartmentalized microreactors, metabolic clustering, i.e., the encapsulation of enzymatic pathways within not only the same microreactor but also the same compartment, is largely unexplored. Together with compartmentalization, metabolic clustering is relevant for the field of cell mimicry. Indeed, biological compartments often contain several enzymes that work together, forming enzymatic pathways.[27] Furthermore, computational simulations of enzyme kinetics have already shown that enzymatic clustering, i.e., the physical proximity of the elements of enzymatic pathways, increases the efficiency of the pathway flux by sixfold for a simple two-step enzymatic pathway, compared to the distribution of these elements in a bigger structure, such as the cytosol.[28] Within the field of cell mimicry, some notable examples highlight the advantages of metabolic clustering. For instance, Liu et al. describe the assembly and activity in vivo of noncompartmentalized polymer capsules containing two enzymes working in tandem. In their work, the authors compared the activity of two polymer capsules containing one enzyme each with that of a capsule containing both, concluding that metabolic clustering led to a significant enhancement of the enzymatic pathway activity.[27]

Taking into account that the highest number of co-encapsulated enzymes in a single microreactor is 3 and that metabolic clustering is often overlooked, the aim of this work was to create a compartmentalized microreactor containing up to five liposome-entrapped enzymes forming two enzymatic pathways—an enzymatic cycle containing the enzymes glutamate dehydrogenase (GDH) and glutathione reductase (GTR), using

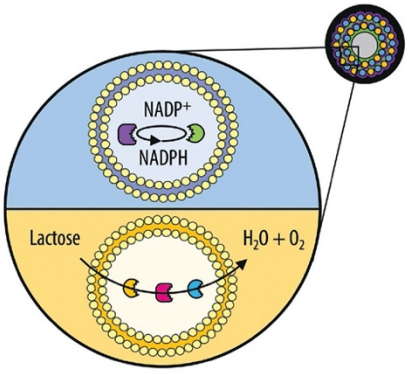


Figure 1. Overview schematic of the microreactors containing two different encapsulated enzymatic pathways.

$NADP^+$/NADPH as a self-renewable co-factor, and an enzymatic cascade combining the enzymes β-galactosidase (β-Gal), glucose oxidase (GOx), and Cat, using lactose as substrate and generating water and oxygen (**Figure 1**). Specifically, we assessed the performance of the two different enzymatic pathways using either free enzymes in solution (i) or enzymes entrapped in liposomes (ii) and confirmed the biocatalytic activity of microreactors containing these enzyme-loaded liposomes (iii). The microreactors were successfully assembled, maintaining the activity of both encapsulated enzymatic pathways.

2. Results and Discussion

2.1. Enzymatic Pathways Using Free Enzymes in Solution

As a first step, we aimed to illustrate that the activity of the envisioned enzymatic pathways could be monitored. To this end, we employed enzymes in solution considering two different enzymatic pathways. The first investigated pathway consisted of two cyclical reactions catalyzed by GDH and GTR. GDH reversibly converts L-glutamate into α-ketoglutarate and ammonia (NH_4^+), while simultaneously converting nicotinamide adenine dinucleotide phosphate ($NADP^+$) into its reduced form, NADPH.[29] GTR, on the other hand, catalyzes the reduction of glutathione disulphide (GSSG) into glutathione, concomitantly converting NADPH into $NADP^+$ (**Figure 2**A).[30] Thus, it was expected that the activity of GDH alone would lead to a high production of NADPH, while the presence of both enzymes would only lead to the generation of a basal amount of NADPH, which would be constant over time. The successful performance of this enzymatic pathway was confirmed. The amount of NADPH in solution was followed by changes in the absorbance (λ = 340 nm), using two different conditions. On the one hand, when only GDH (10 U mL^{-1}) was incubated for 1 h with L-glutamate, GSSG, and $NADP^+$, the enzymatic pathway was incomplete

© 2018 WILEY-VCH Verlag GmbH & Co. KGaA, Weinheim

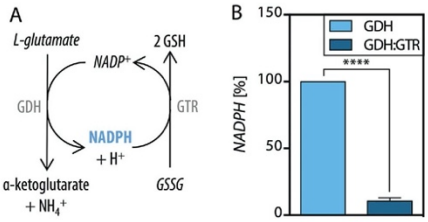


Figure 2. Cyclical reactions of GDH and GTR: A) Schematic representation of the employed enzymatic cycle. L-glutamate, GSSG, and $NADP^+$ were the substrates initially added and NADPH was the measured product upon enzymatic conversion. B) Monitored amount of NADPH in solution after 1 h incubation of the substrates with GDH (light blue bar) or with GDH and GTR (dark blue bar). The measurements were normalized to the amount of NADPH generated by GDH alone. $N = 3$. $^{****}p < 0.0001$ using a two-tailed paired *t*-test. Data represented as mean ± standard deviation (SD).

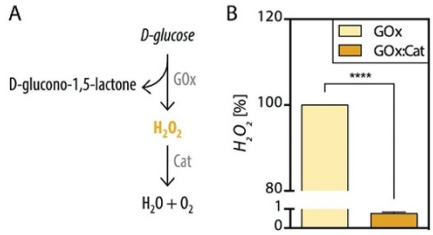


Figure 3. Enzymatic cascade of GOx and Cat: A) Schematic representation of the enzymatic pathway, where D-glucose was the initially added substrate and H_2O_2 was the monitored molecule. B) Amount of H_2O_2 in solution after 3 h incubation of D-glucose with GOx (light yellow bar) or with GOx and Cat (dark yellow bar). The measurements were normalized to the amount of H_2O_2 produced by GOx alone. $N = 3$. $^{****}p < 0.0001$ using a two-tailed paired *t*-test. Data represented as mean ± SD.

and NADPH was enzymatically generated, serving as the control condition. On the other hand, when GDH and GTR (1:1 enzymatic activity ratio, 10 U mL^{-1}) were employed with the same substrates for 1 h, the enzymatic pathway was complete and the NADPH generated by GDH was consumed by GTR. Indeed, the normalized amount of NADPH produced by GDH was significantly higher than the monitored amount of NADPH when both enzymes were present (Figure 2B). Furthermore, in the latter case, equilibrium was reached, where the amount of NADPH in solution was constant over time (Figure S1, Supporting Information). Additionally, although there was a significant difference between the two conditions in all measured time points, the levels of NADPH produced by GDH alone decreased with increasing incubation time (Figure S1, Supporting Information). This finding might be due to the nonenzymatic oxidation of NADPH into $NADP^+$, given the instability of the former molecule,[31] or due to the reversal of the GDH-catalyzed reaction. However, the reaction catalyzed by GDH is known to mainly occur in the direction of α-ketoglutarate formation, since GDH shows very low affinity for NH_4^+ ($K_m \approx 17 \times 10^{-3}$ M for bovine liver GDH),[32] which implies that the reverse reaction would only occur in the presence of high levels of NH_4^+. Since we used 30×10^{-3} M L-glutamate and 2.0×10^{-3} M $NADP^+$ and given the stoichiometry of the reaction, $NADP^+$ would be the limiting substrate, only allowing for a maximum production of 2.0×10^{-3} M NH_4^+. Therefore, the time-dependent decrease in NADPH levels was most likely due to nonenzymatic oxidation. Consequently, the time point used to assess the performance of this enzymatic pathway was chosen based on the highest measured NADPH level in the control condition (GDH alone), i.e., 1 h incubation for the free enzyme assay.

The second considered pathway consisted of an enzymatic cascade, where each enzyme uses the product from the previous enzyme as substrate. The enzymes GOx and Cat were chosen for this purpose. GOx converts D-glucose into D-glucono-1,5-lactone and H_2O_2.[33] Cat then further converts H_2O_2 into water and oxygen (**Figure 3**A).[34]

The amount of H_2O_2 was measured to follow this cascade reaction, using two different conditions. When GOx (10 U mL^{-1}) was incubated with D-glucose in the absence of Cat, a large amount of H_2O_2 was produced over 3 h incubation time. On the other hand, the GOx-produced H_2O_2 was almost completely converted when both enzymes (10 U mL^{-1} each) were incubated with D-glucose for 3 h (Figure 3B).

Finally, the cascade reaction was taken a step further by adding β-Gal, an enzyme that converts D-lactose into D-glucose,[35] which can then serve as the substrate in the above-mentioned cascade reactions (**Figure 4**A). D-lactose was incubated for 3 h with either β-Gal and GOx or with β-Gal, GOx, and Cat to characterize this pathway. 10 U mL^{-1} of all enzymes were used for both conditions. In the first case, the combined action of the two enzymes led to an increase in the H_2O_2 levels. In the second case, the monitored amount of H_2O_2

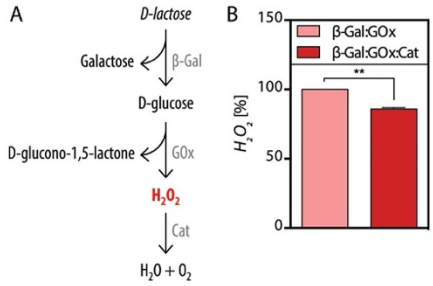


Figure 4. Enzymatic cascade of β-Gal, GOx, and Cat: A) Schematic representation of the enzymatic cascade. D-lactose was used as the initial substrate and H_2O_2 was the measured molecule. B) Amount of H_2O_2 generated by the actions of β-Gal and GOx (light red bar) and β-Gal, GOx, and Cat (red bar), after 3 h incubation with D-lactose. The measurements were normalized to the amount of H_2O_2 generated by β-Gal and GOx. $N = 3$. $^{**}p < 0.01$ using a two-tailed paired *t*-test. Data represented as mean ± SD.

© 2018 WILEY-VCH Verlag GmbH & Co. KGaA, Weinheim

was significantly lower due to the presence of Cat, which consumed part of the produced H_2O_2 (Figure 4B).

The difference observed between the two conditions in the three-step enzymatic cascade is less pronounced than the difference in the two-step enzymatic cascade. Kinetically, these reactions are not in equilibrium due to the concentration of substrate used, which is at least 1000× lower than the respective K_m. Thus, a classical biochemical analysis of metabolic flow cannot be performed to elucidate the change in the flow of the pathway.[36] It is however possible to hypothesize that the two reactions necessary for H_2O_2 production (catalyzed by β-Gal and GOx) may not have 100% yield, which could mean that even though the enzymes were exposed to 10×10^{-6} M D-lactose, only a fraction of this substrate was used to produce glucose, leading to an even lower production of H_2O_2. Thus, the 100% in the control condition (β-Gal and GOx, without Cat) would refer to a lower amount of H_2O_2 than in the control condition of the two-step enzymatic cascade and, consequently, the difference in relation to the complete pathway measurement would be smaller.

Additionally, the affinity of GOx toward D-glucose ($K_m \approx 22 \times 10^{-3}$ M for *Aspergillus niger* GOx)[37] is higher than that of Cat toward H_2O_2 ($K_m \approx 33 \times 10^{-3}$ M for bovine liver Cat).[38] Thus, the reaction catalyzed by GOx would occur at a higher rate, not limiting the availability of H_2O_2 for Cat. Since, in conditions where the substrate concentration is significantly lower than the K_m, the enzymatic rate is highly dependent on the substrate concentration,[36] Cat would perform at a higher rate when exposed to a higher concentration of H_2O_2. On the other hand, β-Gal shows less affinity toward its substrate (D-lactose, $K_m \approx 50–85 \times 10^{-3}$ M for *Aspergillus oryzae* β-Gal)[39] than the other two enzymes. In this scenario, the reaction catalyzed by β-Gal would be the limiting step, affecting substrate availability for GOx and Cat. Again, since in these conditions the enzymatic rate is highly dependent on substrate concentration, this could imply that the rate of the reactions catalyzed by GOx and by Cat would be lower, taking more time to convert their respective substrates. This rate reduction would be more accentuated for the reaction catalyzed by Cat, since the slower rate of D-glucose production would amplify the substrate availability issue initiated by β-Gal. Therefore, assuming the rate of the Cat-catalyzed H_2O_2 conversion was low, the measurement performed after 3 h incubation could reflect an incomplete reaction where H_2O_2 in solution had not been consumed by Cat yet.

The interaction between the activity of the different pathways in solution was also considered, using the same enzyme concentrations as described above. For the GDH and GTR cycle, the incomplete and complete pathways were incubated for 1 h with L-glutamate, GSSG, and $NADP^+$ in the presence or absence of the enzymes and substrates from the enzymatic cascade reaction. The presence of the enzymatic cascades did not significantly affect the activity of the GDH and GTR cycle (Figure S2, Supporting Information). Regarding the GOx and Cat cascade, both the complete and incomplete pathways were incubated for 3 h with D-glucose, in the presence or absence of the GDH and GTR cycle with or without $NADP^+$. No interaction between the pathways was found (Figure S3, Supporting Information). Finally, the β-Gal, GOx, and Cat cascade was incubated for 3 h with D-lactose, in the presence or absence of the GDH and GTR cycle with or without $NADP^+$. No pathway interactions were found but the unexpected potentiation in H_2O_2 production by β-Gal and GOx in the presence of GDH and $NADP^+$ (Figure S4, Supporting Information). This apparent potentiation is most likely an artifact of the detection assay due to a slight overlapping of the NADPH and resorufin (used for H_2O_2 detection) spectra.

2.2. Enzymatic Pathways Encapsulated in Liposomes

The next step to assemble advanced microreactors required the enzymes to be entrapped in liposomes. These structures are biocompatible and offer optimal protection for fragile biological cargo, which is illustrated by their successful use in compartmentalized microreactors.[40] To this end, the enzymes were encapsulated in 200 nm monodispersed 1,2-dioleoyl-*sn*-glycero-3-phosphocholine (DOPC) liposomes (Figure S5, Supporting Information) and their activity was monitored using the above-mentioned assays. The specific lipid composition and liposome diameter were chosen in order to allow for higher activity of the encapsulated enzymes (Figures S6 and S7, Supporting Information). Enzymes belonging to a specific pathway were mixed in solution (100 U mL^{-1} or 50 U mL^{-1} for the three-step enzymatic cascade at a 1:1 enzymatic activity mixing ratio) prior to being encapsulated in the liposomes. Liposomes not carrying all the enzymes required for a pathway (without either GTR or Cat) were used as control samples. The activity of the encapsulated enzymatic pathways was measured after 24 or 48 h incubation with the required substrates. The 48 h incubation time was chosen for the GDH and GTR cycle based on the highest NADPH measurement for the control condition between different time points (Figure S8, Supporting Information), according to the discussion presented above. On the other hand, 24 h incubation time was chosen for both enzymatic cascades to prevent the nonenzymatic degradation of the newly formed H_2O_2.

The activity of the GDH and GTR cycle was confirmed by the significantly lower level of produced NADPH by liposomes containing both enzymes, compared to the amount produced by liposomes containing only GDH (**Figure 5**A). Although the difference was statistically significant, it was smaller than the difference found for the free enzyme assay. This finding is likely tied to two explanations. First, the enzyme solution encapsulated in the liposomes contained enzymes in the same concentration (U mL^{-1}) as for the free enzyme assay. It is known that the encapsulation efficiency, i.e., how many enzymes are actually encapsulated in liposomes, is never 100%.[41] Indeed, the encapsulation efficiency, expressed as experimental versus theoretical protein concentration, was calculated for all the produced liposomes and determined to be ≈10–20% (Table S1, Supporting Information). Thus, it would be expected that fewer enzymes would be inside the liposomes, which would lead to a decrease in NADPH production in the control condition. Indeed, the maximum amount of NADPH measured with GDH-containing liposomes was lower than that measured with the free enzyme (Figure S10, Supporting Information). Furthermore, in the liposomes containing both GDH and GTR, there is no control over the actual ratio of encapsulation, even though the initial enzyme solution contained the enzymes at a 1:1

© 2018 WILEY-VCH Verlag GmbH & Co. KGaA, Weinheim

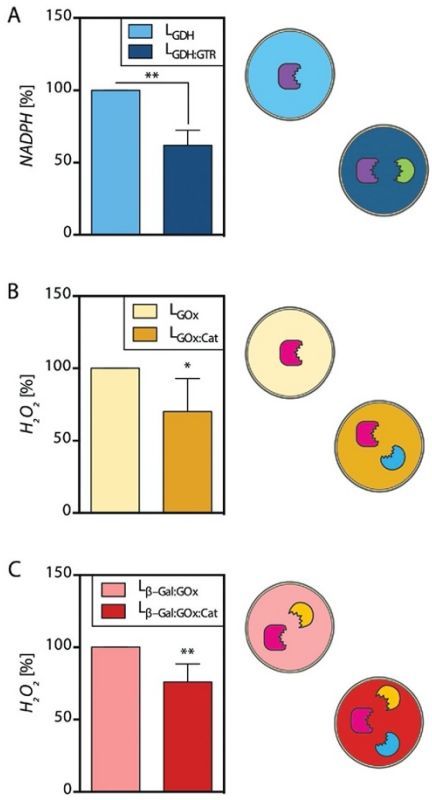


Figure 5. Enzymatic pathways encapsulated in liposomes. A) The amount of NADPH produced by either L_{GDH} or $L_{GDH:GTR}$ was measured after 48 h incubation with L-glutamate, GSSG, and $NADP^+$. $N = 4$. $^{**}p < 0.01$ using a two-tailed paired *t*-test. B) The amount of H_2O_2 generated by L_{GOx} and $L_{GOx:Cat}$ was measured after 24 h incubation with D-glucose. $N = 5$. $^{*}p < 0.05$ using a two-tailed paired *t*-test. C) The amount of H_2O_2 resulting from the activity of $L_{\beta\text{-}Gal:GOx}$ and $L_{\beta\text{-}Gal:GOx:Cat}$ was measured after 24 h incubation with D-lactose. $N = 5$. $^{**}p < 0.01$ using a two-tailed paired *t*-test. All measurements were normalized to their respective control condition. All data are represented as mean ± SD.

enzymatic activity ratio. The enzyme ratio could have shifted and the liposomes might have contained more GDH than GTR, which could account for the fact that a higher amount of NADPH was measured in liposomes entrapping both GDH and GTR compared to the free enzymes (Figure S10, Supporting Information). Second, regarding the kinetics of this cycle, the liposome-entrapped enzymes showed a slower activity than the free enzymes in solution, i.e., in the free enzyme assay the highest NADPH amount was measured at 1 h incubation time, while for the enzymes in liposomes the highest measurement was after 48 h incubation (Figure S8, Supporting Information). The change in the kinetics of the pathway could be caused by the liposomes' kinetic barrier. It was previously shown that the entrapment of enzymes in lipidic subunits can affect their activity, namely slowing it down, due to the time that substrates take to diffuse across the lipid layer.[42] All substrates were added outside of the liposomes and, consequently, had to cross the lipid bilayer to be in contact with the enzymes. Indeed, when liposomes containing GDH were destroyed using Triton X-100, the production of NADPH after 24 h incubation was approximately three times higher compared to intact liposomes (Figure S11, Supporting Information). Since it is likely that the different substrates exhibited different abilities to penetrate into the liposomes, the pathway kinetics were probably not only delayed but also altered from the free enzymes in solution situation due to changed substrate concentrations/ratios.

The activity of the encapsulated GOx and Cat cascade was also confirmed, since the amount of H_2O_2 produced by liposomes containing both enzymes was significantly lower compared to liposomes containing only GOx (Figure 5B). As already observed for the other enzymatic pathway, the difference between the two encapsulated conditions was smaller than the one found for the free enzymes in solution, which is likely due to the reasons discussed above.

Finally, the activity of the encapsulated *β*-Gal, GOx, and Cat cascade was successfully illustrated. The amount of H_2O_2 generated by liposomes containing *β*-Gal and GOx was significantly higher than the amount generated by liposomes containing all three enzymes (Figure 5C).

2.3. Assembly and Activity of Microreactors

Capsosomes were chosen to create complex microreactors since they combine the benefits of both liposomal and polymeric components. While the liposomes provide a protected environment for the encapsulated enzymes, the polymer layers offer protection and would provide structural integrity to the whole structure should the removal of the silica template be required.[43] Furthermore, among different compartmentalized microreactors, capsosomes allow for the formation of the highest number of compartments,[44] with a reported maximum of ≈160 000 embedded liposomes,[45] which largely contributes to enhancing the activity of an individual microreactor.

Active microreactors containing different combinations of the described enzyme-loaded liposomes (**Table 1**) were assembled by the layer-by-layer technique using 2.12 µm SiO_2 template particles, employing a previously described and validated protocol.[46] Briefly, the particles were coated with a layer of poly(L-lysine) (PLL) prior to the first liposome deposition step. Poly(methacrylic acid)-*co*-(cholesteryl methacrylate) (PMAc) and PLL were used as polymer separation layers before the second liposome adsorption step. PMAc and poly(dopamine) (PDA) were used as capping and terminating layers, respectively. PDA was chosen as the terminating layer to improve the biocompatibility and stability of the microreactors, as well as to facilitate subsequent chemical surface modifications[47]

© 2018 WILEY-VCH Verlag GmbH & Co. KGaA, Weinheim

Table 1. Final concentration of the encapsulated enzymes in liposomes.

Type of liposome	Final enzyme concentration [U mL^{-1}]				
	GDH[a]	GTR[b]	β-Gal[c]	GOx[d]	Cat[e]
L_{GDH}	100	–	–	–	–
$L_{GDH:GTR}$	100	100	–	–	–
L_{GOx}	–	–	–	100	–
$L_{GOx:Cat}$	–	–	–	100	100
$L_{\beta Gal:GOx}$	–	–	50	50	–
$L_{\beta Gal:Gox:Cat}$	–	–	50	50	50

[a]Glutamate dehydrogenase; [b]Glutathione reductase; [c]β-galactosidase; [d]Glucose oxidase; [e]Catalase.

of these microreactors in future biomedical/cellular applications, as we, for instance, recently illustrated.[26] Furthermore, the enzymatic cargo of the liposomal subunits was varied, so that each microreactor contained two different types of enzyme-loaded liposomes (**Table 2**). Microreactors M1 were assembled using a mixture of L_{GDH} and L_{GOx}, while a mixture of L_{GDH} and $L_{\beta Gal:GOx}$ was used during the liposome deposition steps for microreactors M3. M1 and M3 were employed as control samples since they contained the incomplete enzymatic pathways, i.e., they missed the enzymes GTR and Cat. On the other hand, microreactors M2 contained the complete enzymatic cycle ($L_{GDH:GTR}$) and the two-step enzymatic cascade ($L_{GOx:Cat}$), while microreactors M4 were also equipped with the complete enzymatic cycle ($L_{GDH:GTR}$) but enclosed the three-step enzymatic cascade ($L_{\beta Gal:GOx:Cat}$).

Representative bright field images of the assembled microreactors and the population histogram analyzed by flow cytometry confirmed the presence of nonaggregated microreactors (**Figure 6**A and Figure S12, Supporting Information). Finally, the performance of the microreactors was determined with the aim to confirm the activity of the encapsulated enzymatic pathways. 10^8 microreactors (M1, M2, M3, and M4) were incubated for 48 h with L-glutamate, GSSG, and $NADP^+$ before the amount of produced NAPDH was measured, to illustrate the successful functionality of the GDH and GTR cycle. As expected, there was a significantly higher amount of NADPH measured when M1 and M3 were considered compared to M2 and M4, respectively. Regarding this specific pathway, M1 and M3 only contained GDH, which means that the produced NADPH was not enzymatically converted by GTR as it was in M2 and M4 (Figure 6B).

Table 2. Overview of the enzyme-loaded liposomes incorporated in the different microreactors.

Type of liposome	M1[a]	M2	M3[a]	M4
L_{GDH}	✓	–	✓	–
$L_{GDH:GTR}$	–	✓	–	✓
L_{GOx}	✓	–	–	–
$L_{GOx:Cat}$	–	✓	–	–
$L_{\beta Gal:GOx}$	–	–	✓	–
$L_{\beta Gal:Gox:Cat}$	–	–	–	✓

[a]M1 and M3 correspond to the control conditions for M2 and M4, respectively.

Alternatively, to assess the activity of the enzymatic cascades, 10^8 microreactors (M1, M2, M3, and M4) were incubated for 24 h with D-glucose (for M1 and M2) or D-lactose (for M3 and M4) before the amount of H_2O_2 was measured. It was observed that M1 and M3 produced a significantly higher amount of H_2O_2 compared to M2 and M4, respectively, since no Cat was present in the former two cases (Figure 6C). Thus, the two-step as well as the three-step enzymatic cascades were functional when encapsulated in microreactors.

3. Conclusion

Taken together, our results show that we were able to assemble compartmentalized microreactors containing up to five enzymes that formed two different functional enzymatic pathways. This effort represents, to the best of our knowledge, the assembly and characterization of compartmentalized microreactors with the largest number of co-encapsulated enzymes to date. Admittedly, the employed enzymatic pathways have only limited resemblance to biologically relevant designs and substantial further developments, including the performance of the microreactors in complex biological environments and their long-term activity, need to be accomplished. Nonetheless, the reported results signify a relevant advancement toward the fabrication of microreactors with cell-like function in a biocatalytic context.

4. Experimental Section

Materials: 4-(2-Hydroxyethyl)piperazine-1-ethanesulfonic acid (HEPES), tris(hydroxymethyl)aminomethane (TRIS), sodium chloride (NaCl), L-glutamic acid dehydrogenase from bovine liver (GDH, EC1.4.1.3, 48 U mg^{-1}), glutathione reductase from baker's yeast (GTR, EC1.8.1.7, 170 U mg^{-1}), β-galactosidase from *A. oryzae* (β-Gal, EC3.2.1.23, 12 U mg^{-1}), glucose oxidase from *A. niger* (GOx, EC1.1.3.4, 173 U mg^{-1}), catalase from bovine liver (Cat, EC1.11.1.6, 5000 U mg^{-1}), L-glutamic acid monosodium salt hydrate (L-glutamate), L-glutathione oxidized disodium salt (GSSG), β-nicotinamide adenine dinucleotide phosphate sodium salt hydrate ($NADP^+$), D-glucose, D-lactose, PLL (M_W 30 000–70 000 Da), dopamine hydrochloride (DA), horseradish peroxidase (HRP, 250–330 units per milligram solid), hydrogen peroxide (H_2O_2, 30% (w/w)), and Triton X-100 were purchased from Sigma-Aldrich (MO, USA). Amplex UltraRed was obtained from Thermo Fisher Scientific (MA, USA). DOPC was purchased from Avanti Polar Lipids (Alabama, USA). SiO_2 particles (2.12 ± 0.06 μm in diameter) were

© 2018 WILEY-VCH Verlag GmbH & Co. KGaA, Weinheim

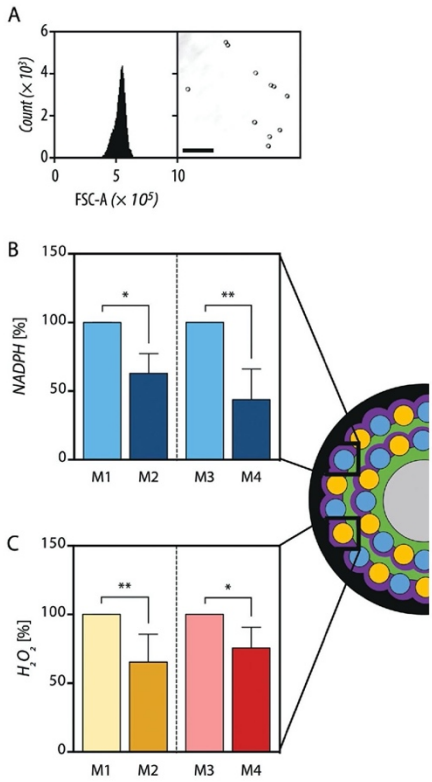


Figure 6. Assembly and activity of microreactors with up to five encapsulated enzymes. A) Representative population histogram originated from flow cytometry analysis (left) and bright field microscopy image (right) of the assembled microreactors. Scale bar = 40 µm. B) Amount of produced NADPH measured after 48 h incubation of the different microreactors with L-glutamate, GSSG, and $NADP^+$. M1 and M3 (light blue bars) refer to microreactors with the incomplete pathway (only GDH) and their activity was set to 100%. M2 and M4 (dark blue bars) refer to microreactors with the complete pathway (GDH and GTR) and their activity was normalized to the respective control. $N = 3$. $^*p < 0.05$ and $^{**}p < 0.01$ for comparison with respective control, using two-tailed paired *t*-tests. C) Amount of generated H_2O_2 measured after 24 h incubation of the different microreactors with D-glucose, for M1 and M2, or D-lactose, for M3 and M4. M1 and M3 (light yellow bar and light red bar, respectively) refer to microreactors with incomplete pathways (without Cat) and their activity was set to 100%. M2 and M4 (dark yellow bar and dark red bar, respectively) refer to microreactors equipped with the complete enzymatic cascade (GOx and Cat or β-Gal, GOx, and Cat, respectively) and their activity was normalized to the respective control. $N = 4$. $^*p < 0.05$ and $^{**}p < 0.01$ for comparison with respective control, using two-tailed paired *t*-tests. All data are represented as mean ± SD.

purchased from Microparticles GmbH (Berlin, Germany). Ultrapure water (18.2 MΩ cm^{-1} resistance) was provided by an ELGA Purelab Ultra system (ELGA LabWater, Lane End, UK).

PMAc was synthesized according to a previously published protocol.[48]

Two types of buffer solutions were used: HEPES2 buffer consisting of 20×10^{-3} M HEPES and 130×10^{-3} M NaCl, pH 7.4, and TRIS buffer consisting of 10×10^{-3} M TRIS, pH 8.5. All buffer solutions were prepared using ultrapure water.

Liposome Preparation: Unilamellar liposomes were prepared by evaporation of 100 µL of a DOPC solution (25 mg mL^{-1} in chloroform) under vacuum for 1 h, followed by rehydration of the lipids with 200 µL of an enzyme-containing solution (see Table 1 for specific enzymes and concentrations used) in HEPES2 buffer. The liposomes were then further hydrated with 800 µL of HEPES2 buffer. The solutions were extruded through 200 nm filters (13×) to obtain monodispersed liposomes. Nonencapsulated enzymes were removed by size exclusion chromatography, which diluted each sample by a factor of two. Liposome formation was confirmed through dynamic light scattering (Zetasizer Nano S90, Malvern Instruments, UK) using a material refractive index of 1.590 and a dispersant (water at 25 °C) refractive index of 1.330.

Microreactor Assembly: Silica particles (2.12 µm in diameter, 50 mg mL^{-1}) were washed three times in HEPES2 buffer (1 800 rpm, 45 s). The particles were then incubated with a PLL solution (1.0 mg mL^{-1} in HEPES2 buffer, 10 min). The assemblies were washed three times in HEPES2 buffer between coating steps, unless otherwise stated. The positively charged particles were incubated with enzyme-loaded liposomes (1:1 mix of L_{GDH} and L_{GOx} for M1; $L_{GDH:GTR}$ and $L_{GOx:Cat}$ for M2; L_{GDH} and $L_{\beta Gal:GOx}$ for M3; and $L_{GDH:GTR}$ and $L_{\beta Gal:GOx:Cat}$ for M4) for 40 min. In order to anchor and fix the liposomes, the microreactors were incubated with PMAc (2.0 mg mL^{-1} in HEPES2 buffer, 10 min). These three coating steps were repeated to increase the amount of adsorbed enzyme-loaded liposomes. Finally, the microreactors were washed two times in HEPES2 buffer and one time in TRIS buffer and incubated with a DA solution (2.5 mg mL^{-1} in TRIS buffer, overnight) to generate a PDA layer. The final concentration of microreactors was determined by flow cytometry (C6 Flow Cytometer, Accuri Cytometers, Inc., MI, USA).

NADPH Detection Assay: Samples were incubated with 30×10^{-3} M L-glutamate, 2.0×10^{-3} M GSSG, and 2.0×10^{-3} M $NADP^+$ in HEPES2 buffer at 37 °C. The production of NADPH was followed by measuring the absorbance of the solutions (λ = 340 nm) at different time points. For the determination of NADPH produced by the different microreactors, samples were centrifuged (1800 rpm, 45 s) prior to absorbance measurements.

H_2O_2 Detection Assay: Samples were incubated with 10×10^{-6} M D-glucose (for the two-step enzymatic cascade) or 10×10^{-6} M D-lactose (for the three-step enzymatic cascade) during 3 h (for the free enzyme assay) or 24 h (for the liposome and microreactor assays) at 37 °C. After these incubations, H_2O_2 was detected using the Amplex UltraRed assay for H_2O_2 detection. 50 µL of the samples were incubated with 0.2 U mL^{-1} HRP and 50×10^{-6} M Amplex UltraRed in ultrapure water (reaction mix), in a total volume of 100 µL. The mix was incubated at room temperature protected from light for 30 min. The fluorescence of the solutions (λ_{ex} = 545 nm, λ_{em} = 590 nm) was measured by a multiplate reader. For the microreactor assay, samples were centrifuged (1800 rpm, 45 s) prior to incubation with the reaction mix.

Statistical Analysis: All assays were performed with duplicates, with at least three independent repeats ($n >= 3$). All data are presented as percentage of enzymatically generated NADPH, for the GDH and GTR cycle, or H_2O_2, for the two-step and the three-step enzymatic cascades. For each independent repeat, the amount of the monitored molecules generated by the incomplete pathways (GDH alone, GOx alone, or β-Gal and GOx) was set to 100% and the amount of the monitored molecules generated by the respective complete pathways was normalized to it. Considering the data from all the repeats, values outside of the range mean ± 2 × standard deviation (SD) were considered outliers. Data are represented as mean ± SD. Statistical significance was determined using

© 2018 WILEY-VCH Verlag GmbH & Co. KGaA, Weinheim

two-tailed paired *t*-tests comparing incomplete and complete pathway values, with $p < 0.05$ considered to represent statistical significance. All data were analyzed in GraphPad Prism (GraphPad Software, Inc., CS, USA).

Supporting Information

Supporting Information is available from the Wiley Online Library or from the author.

Acknowledgements

This work was supported by Fundação para a Ciência e Tecnologia (FCT), Portugal (PD/BD/114278/2016 to A.A.-M. and SFRH/BPD/81627/2011 to S.H.V.) and the Aarhus University Research Foundation, Denmark.

Conflict of Interest

The authors declare no conflict of interest.

Keywords

encapsulated catalysis, enzymatic cascades, enzymatic cycles, microreactors

Received: December 12, 2017
Revised: January 29, 2018
Published online:

[1] B. C. Buddingh', J. C. M. van Hest, *Acc. Chem. Res.* **2017**, *50*, 4.
[2] Y. Diekmann, J. B. Pereira-Leal, *Biochem. J.* **2013**, *449*, 2.
[3] M. J. York-Durán, M. G. Gallardo, C. P. Labay, A. Urquhart, T. L. Andresen, L. Hosta-Rigau, *Colloids Surf., B* **2017**, *152*, 199.
[4] T. Gabaldón, A. A. Pittis, *Biochimie* **2015**, *119*, 262.
[5] A. Zecchin, P. C. Stapor, J. Goveia, P. Carmeliet, *Curr. Opin. Biotechnol.* **2015**, *34*, 73.
[6] D. Deamer, *Trends Biotechnol.* **2005**, *23*, 7.
[7] P. Walde, *BioEssays News Rev. Mol. Cell. Dev. Biol.* **2010**, *32*, 4.
[8] V. Noireaux, Y. T. Maeda, A. Libchaber, *Proc. Natl. Acad. Sci. USA* **2011**, *108*, 9.
[9] L. Hosta-Rigau, M. J. York-Duran, T. S. Kang, B. Städler, *Adv. Funct. Mater.* **2015**, *25*, 25.
[10] Y. Zhang, M. Baekgaard-Laursen, B. Städler, *Adv. Healthcare Mater.* **2017**, *6*, 15.
[11] C. Gao, Z. Wu, Z. Lin, X. Lin, Q. He, *Nanoscale* **2016**, *8*, 6.
[12] F. Itel, P. S. Schattling, Y. Zhang, B. Städler, *Adv. Drug Delivery Rev.* **2017**, *118*, 94.
[13] L. Schoonen, J. C. M. van Hest, *Adv. Mater.* **2016**, *28*, 6.
[14] R. Chandrawati, S.-F. Chong, A. N. Zelikin, L. Hosta-Rigau, B. Städler, F. Caruso, *Soft Matter* **2011**, *7*, 20.
[15] F. Hinzpeter, U. Gerland, F. Tostevin, *Biophys. J.* **2017**, *112*, 4.
[16] M. Marguet, C. Bonduelle, S. Lecommandoux, *Chem. Soc. Rev.* **2012**, *42*, 2.
[17] R. J. R. W. Peters, M. Marguet, S. Marais, M. W. Fraaije, J. C. M. van Hest, S. Lecommandoux, *Angew. Chem., Int. Ed.* **2014**, *53*, 1.
[18] Y. Elani, R. V. Law, O. Ces, *Nat. Commun.* **2014**, *5*, 5305.
[19] R. Chandrawati, P. D. Odermatt, S.-F. Chong, A. D. Price, B. Städler, F. Caruso, *Nano Lett.* **2011**, *11*, 11.
[20] L. Hosta-Rigau, M. J. York-Duran, Y. Zhang, K. N. Goldie, B. Städler, *ACS Appl. Mater. Interfaces* **2014**, *6*, 15.
[21] P. Schattling, C. Dreier, B. Städler, *Soft Matter* **2015**, *11*, 26.
[22] B. Thingholm, P. Schattling, Y. Zhang, B. Städler, *Small* **2016**, *12*, 13.
[23] M. Godoy-Gallardo, C. Labay, M. M. T. Jansman, P. K. Ek, L. Hosta-Rigau, *Adv. Healthcare Mater.* **2017**, *6*, 4.
[24] M. Godoy-Gallardo, C. Labay, V. D. Trikalitis, P. J. Kempen, J. B. Larsen, T. L. Andresen, L. Hosta-Rigau, *ACS Appl. Mater. Interfaces* **2017**, *9*, 19.
[25] Y. Zhang, P. S. Schattling, F. Itel, B. Städler, *ACS Omega* **2017**, *2*, 10.
[26] A. Armada-Moreira, E. Taipaleenmäki, M. Baekgaard-Laursen, P. S. Schattling, A. M. Sebastião, S. H. Vaz, B. Städler, *ACS Appl. Mater. Interfaces* **2018**, *10*, 7581.
[27] Y. Liu, J. Du, M. Yan, M. Y. Lau, J. Hu, H. Han, O. O. Yang, S. Liang, W. Wei, H. Wang, J. Li, X. Zhu, L. Shi, W. Chen, C. Ji, Y. Lu, *Nat. Nanotechnol.* **2013**, *8*, 3.
[28] M. Castellana, M. Z. Wilson, Y. Xu, P. Joshi, I. M. Cristea, J. D. Rabinowitz, Z. Gitai, N. S. Wingreen, *Nat. Biotechnol.* **2014**, *32*, 10.
[29] D. Botman, W. Tigchelaar, C. J. F. Van Noorden, *J. Histochem. Cytochem.: Off. J. Histochem. Soc.* **2014**, *62*, 11.
[30] I. Carlberg, B. Mannervik, *Methods Enzymol.* **1985**, *113*.
[31] J. T. Wu, L. H. Wu, J. A. Knight, *Clin. Chem.* **1986**, *32*, 2.
[32] B. J. Thatcher, K. B. Storey, *Biochem. Cell Biol.* **2001**, *79*, 1.
[33] S. B. Bankar, M. V. Bule, R. S. Singhal, L. Ananthanarayan, *Biotechnol. Adv.* **2009**, *27*, 4.
[34] A. Deisseroth, A. L. Dounce, *Physiol. Rev.* **1970**, *50*, 3.
[35] D. H. Juers, B. W. Matthews, R. E. Huber, *Protein Sci. Publ. Protein Soc.* **2012**, *21*, 12.
[36] K. A. Johnson, R. S. Goody, *Biochemistry* **2011**, *50*, 39.
[37] A. Constantinides, W. R. Vieth, P. M. Fernandes, *Mol. Cell. Biochem.* **1973**, *1*, 1.
[38] G. Ozyilmaz, S. S. Tukel, O. Alptekin, *Indian J. Biochem. Biophys.* **2007**, *44*, 1.
[39] A. Crueger, W. Crueger, in *Biotechnology, Vol. 6A: Biotransformations* (Ed: K. Kieslich), Verlag-Chemie, Weinheim **1984**, Ch. 12.
[40] A. M. Brizard, J. H. van Esch, *Soft Matter* **2009**, *5*, 7.
[41] T. Nii, F. Ishii, *Int. J. Pharm.* **2005**, *298*, 1.
[42] F. Cioci, R. Lavecchia, in *Handbook of Nonmedical Applications of Liposomes*, Vol. *3* (Eds: Y. Barenholz, D. D. Lasic), CRC Press, Boca Raton, FL **1996**, Ch. 16.
[43] B. Städler, A. D. Price, R. Chandrawati, L. Hosta-Rigau, A. N. Zelikin, F. Caruso, *Nanoscale* **2009**, *1*, 1.
[44] R. Chandrawati, F. Caruso, *Langmuir* **2012**, *28*, 39.
[45] R. Chandrawati, L. Hosta-Rigau, D. Vanderstraaten, S. A. Lokuliyana, B. Städler, F. Albericio, F. Caruso, *ACS Nano* **2010**, *4*, 3.
[46] C. Zhu, E. Taipaleenmaki, Y. Zhang, X. Han, B. Städler, *Biomater. Sci.* **2018**, https://doi.org/10.1039/C7BM00838D.
[47] M. E. Lynge, P. Schattling, B. Städler, *Nanomedicine* **2015**, *10*, 17.
[48] M. E. Lynge, M. Baekgaard Laursen, L. Hosta-Rigau, B. E. B. Jensen, R. Ogaki, A. A. A. Smith, A. N. Zelikin, B. Städler, *ACS Appl. Mater. Interfaces* **2013**, *5*, 8.

 © 2018 WILEY-VCH Verlag GmbH & Co. KGaA, Weinheim

ADVANCED BIOSYSTEMS
www.adv-biosys.com

Check for updates

Multicompartment Microreactors Prevent Excitotoxic Dysfunctions In Rat Primary Cortical Neurons

*Adam Armada-Moreira, Joana E. Coelho, Luísa V. Lopes, Ana M. Sebastião, Brigitte Städler, and Sandra H. Vaz**

Excitotoxicity is a cellular phenomenon that comprises the consequences of toxic actions of excitatory neurotransmitters, such as glutamate. This process is usually related to overproduction of reactive oxygen species (ROS) and ammonia (NH_4^+) toxicity. Platinum nanoparticle (Pt-NP)-based microreactors able to degrade hydrogen peroxide (H_2O_2) and NH_4^+, are previously described as a novel therapeutical approach against excitotoxicity, conferring protection to neuroblasts. Now, it is demonstrated that these microreactors are compatible with rat primary cortical neurons, show high levels of neuronal membrane interaction, and are able to improve cell survival and neuronal activity when neurons are exposed to H_2O_2 or NH_4^+. Additionally, more complex microreactors are assembled, including enzyme-loaded liposomes containing glutamate dehydrogenase and glutathione reductase, in addition to Pt-NP. The in vitro activity of these microreactors is characterized and they are compared to the Pt-NP-based microreactors in terms of biological activity, concluding that they enhance cell viability similarly or more extensively than the latter. Extracellular electrophysiological recordings demonstrate that these microreactors rescue neuronal functionality lost upon incubation with H_2O_2 or NH_4^+. This study provides more evidence for the potential application of these microreactors in a biomedical context with more complex cellular environments.

1. Introduction

Excitatory transmission is essential for proper brain function, having an important role not only in neuronal communication per se, but also in higher-level functions such as learning and memory. Glutamate is the main excitatory neurotransmitter in the mammalian central nervous system (CNS).[1] When glutamate is released in a synapse, astrocytes are responsible for the clearance of 80–90% of this synaptically released neurotransmitter.[2,3] Due to the major role of astrocytes in glutamate clearance, astrocytic dysfunction can lead to an excessive build-up of glutamate in the synapse that can lead to an extreme activation of neuronal post-synaptic glutamate receptors, inducing excitotoxicity.[4] This phenomenon can be described as the toxic actions of excitatory neurotransmitters, namely glutamate in the CNS,[5,6] and, among its many intracellular consequences, it can lead to an overproduction of reactive oxygen species, such as hydrogen peroxide (H_2O_2).[7,8] Furthermore, since astrocytes are also responsible for ammonia (NH_4^+) detoxification in the brain,[9] astrocytic dysfunction and associated excitotoxicity often leads to NH_4^+ toxicity.[10]

Most therapeutic approaches used to counteract excitotoxicity are mainly focused on the blockade of glutamate release or inactivation of glutamate receptors, which is accompanied by undesired and deleterious side effects that impact normal excitatory neuronal communication.[11]

Therapeutic cell mimicry is a research field focused on creating artificial cells[12] and organelles[13] that substitute for lost cellular functions.[14] Artificial cells showed initial promise to detoxify liver tissue,[15] to kick-start biomineralization in bone spheroids,[16] to support ex vivo T-cell expansion via antigen-presenting cell mimics,[17] or in cardiac regeneration using cardiac stem cell mimics.[18] We recently reported platinum nanoparticle (Pt-NP)-based microreactors as support for neuroblasts, using the human neuroblastoma-derived SH-SY5Y cell line.[19] Although it was already known that Pt-NP were efficient catalysts for the conversion of H_2O_2 into water and oxygen[20] and able to convert NH_4^+ into nitric oxide (NO),[21] this was the first work exploring the potential application of these nanoparticles in the biomedical field, in the context of cell mimicry and artificial cells.

We now further explored the efficiency of these microreactors as a therapeutical approach against the toxic actions of H_2O_2 and NH_4^+ in a more complex cellular environment.

A. Armada-Moreira, Prof. A. M. Sebastião, Dr. S. H. Vaz
Instituto de Farmacologia e Neurociências
Faculdade de Medicina
Universidade de Lisboa
Avenida Professor Egas Moniz
Edifício Egas Moniz, Lisboa 1649-028, Portugal
E-mail: svaz@medicina.ulisboa.pt
A. Armada-Moreira, Dr. J. E. Coelho, Dr. L. V. Lopes, Prof. A. M. Sebastião, Dr. S. H. Vaz
Instituto de Medicina Molecular João Lobo Antunes
Faculdade de Medicina
Universidade de Lisboa
Lisboa 1649-028, Portugal
A. Armada-Moreira, Prof. B. Städler
Interdisciplinary Nanoscience Center (iNANO)
Aarhus University
Aarhus 8000, Denmark
The ORCID identification number(s) for the author(s) of this article can be found under https://doi.org/10.1002/adbi.202000139.

DOI: 10.1002/adbi.202000139

© 2020 Wiley-VCH GmbH

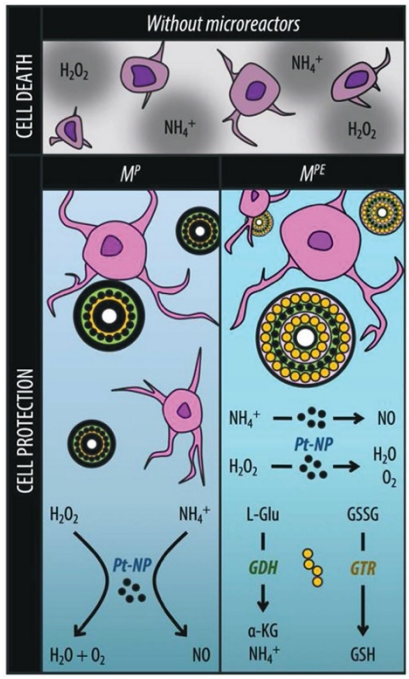


Figure 1. Schematic representation of rat primary cortical neurons exposed to toxic compounds (H_2O_2 or NH_4^+) in the absence (top frame) and in the presence of first (bottom left frame) and second (bottom right frame) generation microreactors. The microreactors are able to protect these cells from cell dysfunction and death caused by either H_2O_2 or NH_4^+. Pt-NP-platinum nanoparticles; NO-nitric oxide; GDH-glutamate dehydrogenase; GTR-glutathione reductase; L-Glu-L-glutamate; α-KG-α-ketoglutarate; GSSG-oxidized glutathione; GSH-reduced glutathione.

We were able to conclude that Pt-NP-based microreactors are compatible and able to interact with rat primary cortical neurons. These microreactors maintain their biological activity in this cell model against these toxic insults. Additionally, we created new and more complex microreactors, containing Pt-NP and enzymes, namely glutamate dehydrogenase (GDH) and glutathione reductase (GTR), characterized their activity in vitro, and performed biological activity assays with rat primary neuronal cultures exposed to H_2O_2 or NH_4^+. These new microreactors are more efficient in cell protection than the first ones (**Figure 1**). This work is highly meaningful on the road to use these microreactors in a medically relevant application. By showing their biocompatibility and biological activity in rat primary neuronal cultures, we were able to increase the complexity of the biological model and conclude that this therapeutic tool maintains its positive activity in a more relevant cellular setting.

2. Results and Discussion

2.1. Neuronal Compatibility and Interaction

Neurons generated from rat primary neuronal cultures were allowed to mature for either 7 or 14 DIV, at which points microreactors containing Pt-NP (M^P) were co-incubated at different concentrations. Cell viability was measured after 24 h (**Figure 2**A). Importantly, the microreactors were tested with 7 DIV and 14 DIV cultures, since these time points are enriched, respectively, with immature and mature neurons.[22] The assay used in this work to determine cell viability is based on the quantification of a signal that is proportional to the number of live cells in culture. Thus, it only represents cell viability in non-proliferative cell culture, being a proxy for cell proliferation in proliferative cultures. The validity of this assay as a cell viability measure in this work is based on three different premises. First, the cell culture conditions used here (serum-free Neurobasal cell medium) give rise to a mostly neuronal culture.[23] Second, previous findings report very low levels of glial contamination in these time points.[22,24,25] Finally, it is known that glial proliferation rates are dramatically hindered in the presence of neurons,[26] which corroborates our argument for the use of this assay to quantify neuronal viability. In this way, it is possible to ascertain the biocompatibility of the microreactors in relation to different phases of neuronal differentiation. There were no significant drops in cell viability at either 7 DIV or 14 DIV when cells were incubated with M^P, regardless of microreactor concentration (Figure 2B), which allowed us to conclude that M^P are not neurotoxic.

Interestingly, in a previous study focused on the interaction of these microreactors and the SH-SY5Y cell line, there was a considerable drop in cell viability for the higher microreactor concentrations (≈50% at a concentration of 100% of the number of cells).[19] Considering that the SH-SY5Y cell line is a continuously proliferating cell line, the hypothesis used to explain this finding was that the microreactors, when present at a high number in the cell culture, impacted the number of cells in solution through contact inhibition of proliferation, and not due to toxicity. Contact inhibition of proliferation is a phenomenon that leads to a decrease or arrest of proliferation rate, due to a physical constriction of the available space, caused either by high confluence or a mechanical impediment.[27] Since a microreactor concentration of 100% represents a very large number of microreactors in solution, these microreactors would occupy the space that cells would need to proliferate at their optimal rate. With unavailable free space, cells growing in monolayer decrease their proliferation rate and eventually reach a quiescent state.[28] This hypothesis was tested with an immunostaining assay targeting dead cells and with a membrane integrity assay, which concluded that, compared to control condition (cells not exposed to microreactors), co-incubation with microreactors had no negative impact in terms of cell death and membrane integrity and, thus, no negative impact on cell viability.[19] Nevertheless, these experiments only

© 2020 Wiley-VCH GmbH

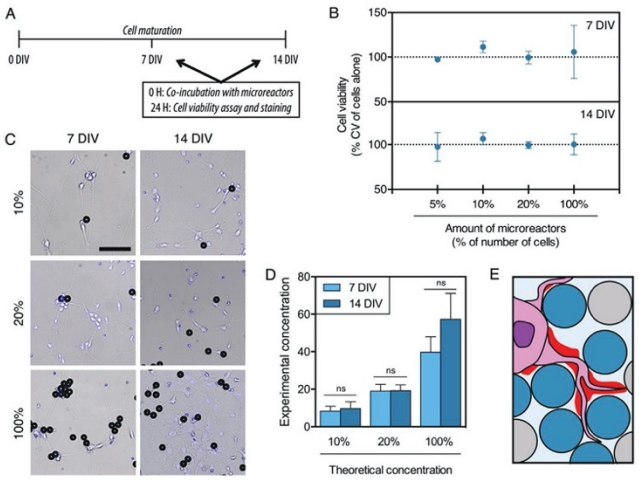


Figure 2. A) Cell viability and adherence of rat primary cortical neurons exposed to different microreactor concentrations: cells matured for either 7 or 14 DIV, at which point M^P were co-incubated for 24 h and the cell viability assay and Hoechst staining were performed. B) Cell viability of rat primary neuronal cultures at 7 DIV and 14 DIV when co-incubated with different concentrations of M^P (5 to 100% of the number of cells). Values were normalized to cell viability of cells not exposed to M^P (100%). $N = 3–5$. No significant differences were found. C) Representative Hoechst staining images, obtained with cells at 7 or 14 DIV with nuclei stained blue, co-incubated with M^P where the theoretical microreactor concentration is either 10%, 20%, or 100% of the number of cells. Scale bar = 100 µm. D) Microreactor concentration, calculated as percentage of the number of cells, after washing, fixing, and staining, at 7 and 14 DIV ($N = 3–5$, $^{ns}p > 0.05$ comparing the same concentrations at 7 and 14 DIV, using one-way ANOVA followed by Sidak's multiple comparison test). E) Schematic representation of the spatial constriction of a high number of microreactors attempting to adhere to a neuron. In blue are the successfully attached microreactors, in gray the ones unable to interact, and in red the cell membrane areas that are unreachable due to the spatial configuration of the already attached microreactors.

provided an indirect proof of contact inhibition of proliferation. Our data corroborate the theory that the decrease seen in cell viability when the microreactors were incubated with the SH-SY5Y cell line was due to contact inhibition of proliferation and not microreactor toxicity.

Next, we tested the adherence of M^P to neurons, to ensure that these microreactors are able to interact with the cells. For this, cells were allowed to mature for either 7 or 14 DIV and, at these time points, microreactors were added at different concentrations. 24 h following this incubation, cells were washed and fixed, nuclei were stained, and microscopy images were obtained for each condition (Figure 2C). The number of cells and microreactors in each obtained field were counted and the experimental concentration of microreactors was calculated (Figure 2D). We were able to conclude that, at either 7 or 14 DIV, the microreactors show high cell adherence, with no significant differences between experimental and theoretical concentrations, using a one sample *t*-test, except for the 100% theoretical concentration (7 DIV: 39.67 ± 16.60, $p < 0.01$; 14 DIV: 57.29 ± 30.81, $p < 0.05$). In this latter case, we hypothesize that the high number of microreactors present in solution caused a physical constraint for the adhesion of more microreactors. With this experiment, we are only able to account for microreactors that are efficiently attached to cells. Due to the size and shape of the microreactors (20 µm in diameter spheres), several sections of cell membrane would be unavailable for attachment, since the already attached microreactors would shadow this neighboring membrane area, impeding the attachment of more microreactors, as illustrated in Figure 2E.

Current literature already suggests that polydopamine (PDA)-coated microreactors such as M^P would show high levels of cell adherence. Indeed, PDA has been thoroughly studied to functionalize biomaterials, such as gold, glass, platinum, and different polymers, increasing their biocompatibility toward neurons.[29] Particularly, a study using PC12 cells had already shown that PDA-coated surfaces promoted cell adhesion and proliferation when compared to uncoated surfaces.[30] In another study, PDA-coated microreactors were shown to present better cell adhesion toward the SH-SY5Y cell line, compared to uncoated, poly(L-lysine)-coated, and poly(methacrylic acid)-coated microreactors, although with lower absolute cell adherence than the data presented in this study.[19] Thus, with this study, we were able to further ascertain the potential role of PDA as "biological neuronal glue", where this polymer is able to functionalize biomaterials and increase their biocompatibility toward rat cortical neurons in a highly efficient manner. Furthermore, these data validate primary neuronal cultures as a good model to test the biological activity of the microreactors,

© 2020 Wiley-VCH GmbH

since the latter do not induce cell death and show appropriate levels of cell adherence.

2.2. Increasing the Complexity: Comparative In Vitro Characterization of Different Microreactors

New microreactors, containing Pt-NP and enzyme-filled liposomes, were developed to expand the functions and activity of M^P. The choice of the incorporated enzymes aimed at further mimicking astrocytic functions. Specifically, these new microreactors combine the already described actions of Pt-NP with glutamate consumption and GSH regeneration. Glutamate dehydrogenase (GDH) was chosen to reproduce the astrocytic clearance of synaptically released glutamate[2] and glutathione reductase (GTR) was included since astrocytes produce GSH as a strategy to counteract the effects of excitotoxicity and excessive extracellular NH_4^+.[31,32] With that in mind, two microreactor variations were created: one containing Pt-NP and GDH (M^{PE1}) and another using Pt-NP and both GDH and GTR (M^{PE2}).

These microreactors were assembled following a combination of previously described protocols.[19,33] Essentially, 19.30 µm in diameter PS particles were coated with PDA, followed by a coating of PLL and adsorption of L_{GDH} or $L_{GDH+GTR}$ (for M^{PE1} or M^{PE2}, respectively). The liposomes were anchored to the microreactor using a layer of PMAc. A new layer of PLL was used and Pt-NP were allowed to adhere to the structure. In order to obtain higher enzymatic activity, the coating with PLL, liposomes, and PMAc was repeated once more. A finishing layer of PDA ensured the biocompatibility and cell adherence of the microreactors. All assembly steps were followed by the changes in ζ-potential (**Figure 3**A). The relative

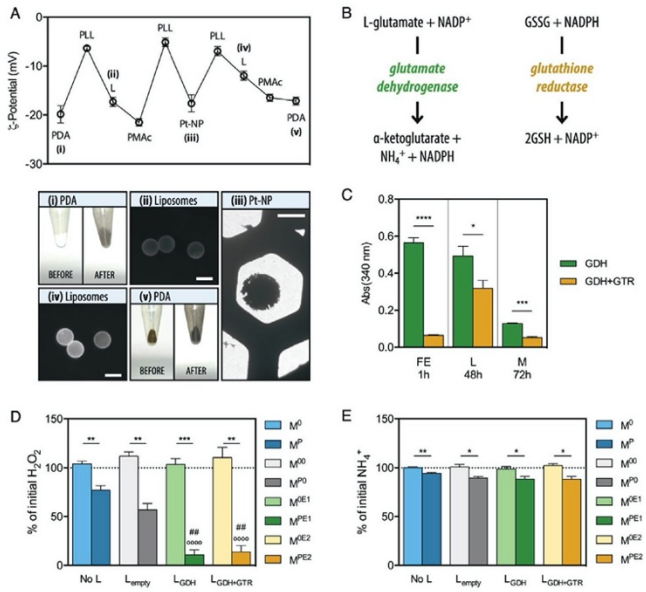


Figure 3. A) ζ-potential measurement of the microreactors at the different assembly steps and representative images. i,v) PDA deposition was confirmed by color change, ii,iv) liposomal layers were imaged with a fluorescent dye, and iii) Pt-NP adsorption was observed with TEM. Scale bars = 20 µm. B) Chemical reactions catalyzed by the studied enzymes: glutamate dehydrogenase (GDH) converts L-glutamate into α-ketoglutarate and NH_4^+, while glutathione reductase (GTR) reduces oxidized glutathione (GSSG), both using $NADP^+$/NADPH as a co-factor. C) Enzymatic activity of GDH and GTR as free enzymes (FE), enzymes encapsulated in liposomes (L), and microreactors (M, 10^5 microreactors). All samples were incubated with 30×10^{-3} M L-glutamate, 2.0×10^{-3} M GSSG, and 2.0×10^{-3} M $NADP^+$. The amount of NADPH in solution was measured through the absorbance at 340 nm at the time point for which GDH activity was highest (1 h for FE, 48 h for L, and 72 h for M). $N = 3$–8. $^*p < 0.05$, $^{***}p < 0.001$, $^{****}p < 0.0001$ using a paired t-test between the GDH and GDH+GTR conditions. D) Pt-NP activity in different microreactors: H_2O_2 concentration was measured after 10^4 microreactors were incubated with 1.0×10^{-3} M H_2O_2 for 24 h and is presented as percentage of initial H_2O_2 concentration (100%). $N = 3$–5. $^{**}p < 0.01$, $^{***}p < 0.001$ compared to respective control, using an unpaired t-test; $^{\circ\circ\circ\circ}p < 0.0001$ for Pt-NP-containing microreactors compared to M^P, and $^{\#\#}p < 0.01$ for Pt-NP-containing microreactors compared to M^{P0}, using one-way ANOVA followed by Tukey's multiple comparison test. E) Microreactors as NH_4^+ catalysts: 10^6 microreactors were incubated with 1.0×10^{-3} M NH_4^+ for 24 h at 37 °C. Data is presented as percentage of the initial NH_4^+ concentration (100%). $N = 3$–4. $^*p < 0.05$; $^{**}p < 0.01$ compared to respective control, using an unpaired t-test.

© 2020 Wiley-VCH GmbH

shifts in ζ-potential are in accordance with previously published assembly protocols,[33] although the absolute values show clear differences. It is already known that ionic species, specifically NaCl, can quench the signal of ζ-potential, bringing it closer to 0 mV.[34] Since we used HEPES2 buffer containing NaCl, the absolute values of ζ-potential are not directly comparable to previous studies using different buffer solutions with different ionic strengths. In parallel, the successful deposition of PDA was confirmed by color change (white to brown and brown to black, Figure 3A-i,v respectively). Liposome presence was evaluated with a fluorescent lipid dye (Figure 3A-ii for the first liposomal layer and Figure 3A-iv, with higher fluorescent intensity for the same exposure time, for microreactors with two liposomal layers). Pt-NP adsorption was monitored using TEM (Figure 3A-iii). All these assays indicate a successful assembly of the microreactors.

The successful incorporation of the enzyme-loaded liposomes onto the microreactors was confirmed by determining their enzymatic activity. This activity was measured indirectly via the absorbance at 340 nm, which is proportional to the concentration of NADPH in solution.[35] NADPH is either a product or a substrate of the incorporated enzymes (Figure 3B). It is produced by GDH, with concomitant conversion of L-glutamate and $NADP^+$ into α-ketoglutarate and NH_4^+,[36] and consumed by GTR during the formation of reduced glutathione (GSH) from oxidized glutathione (GSSG).[37] Taking this into account, there will be a high production of NADPH, proportional to the consumption of glutamate, when considering GDH alone. On the other hand, with both enzymes, the NADPH produced by GDH will be consumed by GTR, leading to a lower concentration of this compound in solution.

All assembly steps involving enzymes, i.e., free enzymes in solution, enzymes encapsulated in liposomes, and the microreactors M^{PE1} and M^{PE2}, were exposed to L-glutamate, $NADP^+$, and GSSG at 37 °C. The time point corresponding to the highest GDH activity (highest NADPH concentration) is represented (Figure 3C). There is a significant difference between GDH and GDH+GTR in all cases, concluding that the enzymes were successfully encapsulated into liposomes and maintain their activity when incorporated into microreactors.

The activity and dynamics of GDH and GTR in solution, liposomes, and incorporated into 2.12 µm sized microreactors were already thoroughly explored in a previous work that also identified the time point for the highest NADPH production by GDH in each assembly step.[38] However, contrary to this previous work, we found that the peak NADPH production by M^{PE1} and M^{PE2} was at 72 h and not 48 h. Importantly, we used 19.30 µm PS particles as the microreactor core while the previous study employed 2.12 µm SiO_2 particles. These latter have a higher surface area to volume ratio, which increases microreactor activity and impacts enzyme kinetics. Indeed, the surface area to volume ratio of a 19.30 µm in diameter particle is 0.31 μm^{-1}, while for a 2.12 µm in diameter particle is 2.83 μm^{-1}, almost 10x higher. Regardless, in agreement with previous work, NADPH production in liposomes and microreactors is reduced when compared to free enzymes in solution, which is tied to encapsulation efficiency – only around 10–20% of the enzymes are encapsulated into the liposomes.[38]

Following on, the microreactors' ability to convert H_2O_2 was compared. For this, microreactors containing Pt-NP (M^P), Pt-NP and empty liposomes (M^{P0}), Pt-NP and L_{GDH} (M^{PE1}), and Pt-NP and $L_{GDH+GTR}$ (M^{PE2}) were incubated with H_2O_2 for 24 h at 37 °C. The equivalent microreactors without Pt-NP were used as control: M^0, M^{00}, M^{0E1}, and M^{0E2}, respectively. A two-way ANOVA considering type of microreactor versus presence of Pt-NP showed that the differences observed between groups arose from both tested variables (Table S1, Supporting Information). Considering presence of Pt-NP, all tested Pt-NP-containing microreactors showed significant catalytic activity when compared with the respective control (Figure 3D). Considering the type of microreactor, M^{PE1} and M^{PE2} were ≈10x more effective as H_2O_2 scavengers than M^P, but had no significant differences in their activity toward H_2O_2. Interestingly, microreactors containing Pt-NP and empty liposomes (M^{P0}) showed an intermediate activity between that of M^P and that of M^{PE1} and M^{PE2}, although the difference in relation to M^P was not statistically significant (Figure 3D).

While the enzymes included in M^{PE1} and M^{PE2} show no direct activity toward H_2O_2, ROS are known to cause lipid peroxidation. In fact, it has been shown that H_2O_2-dependent cell membrane peroxidation is a key player in cell injury induced by oxidative stress, with cells with higher poly unsaturated fatty acid (PUFA) content being more susceptible to this damage.[39] Additionally, a study in human lymphocytes showed that a 24 h incubation with 10 µm H_2O_2 leads to significant, yet low, lipid peroxidation in cell membranes.[40] In our work, we used DOPC to form liposomes. DOPC is a phospholipid with two double bonds, making it prone to H_2O_2-induced peroxidation. This peroxidation could be indirectly reducing the amount of H_2O_2 in solution for the M^{PE1} and M^{PE2} conditions.

Next, 10^6 of the different microreactors were incubated with NH_4^+ for 24 h at 37 °C. A higher number of microreactors was used for this assay due to the lower catalytic activity of Pt-NP toward NH_4^+ when compared to H_2O_2.[19] Following this incubation, the amount of NH_4^+ in solution was determined. A two-way ANOVA considering type of microreactor versus presence of Pt-NP showed that the differences observed between groups arose from the presence of Pt-NP and not from the type of microreactor (Table S1, Supporting Information). All Pt-NP-containing microreactors showed significant catalytic activity toward NH_4^+, with an average consumption of 7–12% of the initial NH_4^+ concentration (Figure 3E). Importantly, there were no significant differences between the activity of Pt-NP-containing microreactors.

2.3. Microreactors and their Biological Activity

The biological activity of the different microreactors was tested in primary neuronal cultures exposed to H_2O_2 or NH_4^+. Since the focus of this work is reverting excitotoxic dysfunctions on mature neurons, only cells at 14 DIV were used for these assays, to ensure the relevance of the microreactors' biological activity. Furthermore, since no differences were found between the activity of M^{PE1} and M^{PE2}, only M^{PE1} was used for the following assays, where its activity is compared to that of M^P.

© 2020 Wiley-VCH GmbH

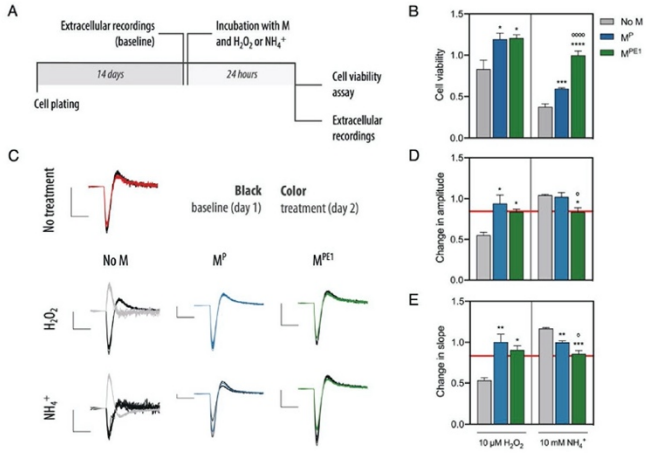


Figure 4. Biological activity of the different microreactors. A) Cells were allowed to mature for 14 days, at which point extracellular electrophysiological recordings were performed to obtain baseline neuronal activity and cells were incubated for 24 h with 10×10^{-6} M H_2O_2 or 10×10^{-3} M NH_4^+ in the presence or absence of M^P or M^{PE1}. Following this incubation, cell viability was determined and extracellular electrophysiological recordings were obtained. B) Fold change in cell viability of cells exposed to 10×10^{-6} M H_2O_2 or 10×10^{-3} M NH_4^+ in the presence or absence of microreactors (M^P or M^{PE1}, 20% of number of cells), normalized to cells not exposed to toxic compounds. $N = 3$–6. C) Representative traces of neuronal responses obtained in the MEA system. Black traces were obtained prior to any treatment and color traces after cells were treated for 24 h with 10×10^{-6} M H_2O_2 or 10×10^{-3} M NH_4^+ in the absence (gray traces) or presence of M^P or M^{PE1} (blue and green traces, respectively). Untreated cells (no microreactors and no toxic compounds) were used as a general control to evaluate the physiological change in parameters over 24 h (red trace). *Y*-scale bar = 100 µV. *X*-scale bar = 5.0 ms. D) Spike amplitude and E) slope of the traces were determined and normalized as fold-change over 24 h. Red line represents the fold-change of untreated cells. $N = 3$. $^*p < 0.05$, $^{**}p < 0.01$, $^{***}p < 0.001$, and $^{****}p < 0.0001$ compared to cells not exposed to microreactors (No M), $^\circ p < 0.05$ and $^{\circ\circ\circ\circ}p < 0.0001$ compared to M^P, using a one way-ANOVA followed by Tukey's multiple comparison test.

In order to ascertain the biological activity of microreactors against H_2O_2 and NH_4^+ toxicity, cell viability was determined and extracellular electrophysiological recordings were performed, following the time points depicted in **Figure 4**A.

For the cell viability assay, 14 DIV cells were incubated with microreactors (M^P or M^{PE1}, 20% of the number of cells) and different concentrations of H_2O_2 or NH_4^+. After 24 h of incubation, cell viability was measured. As a first step, different concentrations of the toxic compounds were explored (Figure S1, Supporting Information) based on previous studies focused on the effects of these compounds in rat cortical neuronal cultures. Regarding H_2O_2, a study using two different cell densities (high: 2×10^5 cells cm^{-2} and low: 7×10^4 cells cm^{-2}) to explore H_2O_2-induced cell death showed that a 24 h incubation with 10×10^{-6} M H_2O_2 did not significantly impact cell viability in either studied density, while 30 µm H_2O_2 led to a drop in cell viability of ≈10% for the high cell density and ≈50% for the low cell density. Finally, 100×10^{-6} M H_2O_2 led to ≈40% cell viability for the high cell density condition and ≈25% for the low cell density condition.[41] Given that we used an intermediate cell density (9.375×10^4 cells cm^{-2}), the observed cell viability losses in the absence of microreactors are in line with those described above. When considering NH_4^+, our study is in line with previous literature where, in rat primary cortical neurons, a 24 h incubation with 10×10^{-3} M NH_4^+ led to 50% cell viability.[42] Taking this into account, we tested 10×10^{-3} M and higher concentrations of NH_4^+ concentrations to reach a nearly full cell death scenario. Importantly, pathological in vivo toxic levels of NH_4^+ are in the range of $0.1–10 \times 10^{-3}$ M[43] and neuronal toxic NH_4^+ levels are around 3×10^{-3} M.[44] Microreactors were able to convert NH_4^+ into NO when neurons were incubated with pathologically relevant concentrations of NH_4^+, maintaining sub-toxic levels of both compounds and providing a positive effect in terms of cell survival. Considering the range of action of M^P and physiologically relevant conditions, 10×10^{-6} M H_2O_2 and 10×10^{-3} M NH_4^+ were chosen to perform the cell viability assay for all microreactors.

Overall, it is possible to conclude that both M^P and M^{PE1} provide significant neuronal protection against the actions of H_2O_2 and NH_4^+ in terms of cell viability (Figure 4B). While no differences were found between M^P and M^{PE1}, both microreactors were able to convert H_2O_2 into water and oxygen, which explains the increase in cell viability from 0.83 to 1.20 when cells were exposed to 10×10^{-6} M H_2O_2 in the presence of either microreactor. Interestingly, both microreactors elevate cell viability above control level (cells not exposed to microreactors nor H_2O_2). In accordance, a study using rat primary neuronal and astrocytic cultures showed that astrocytic-generated H_2O_2 has a biphasic effect in terms of neuronal cell viability. In low

© 2020 Wiley-VCH GmbH

concentrations, H_2O_2 protects neurons against further oxidative damage, thus buffering the actions of ROS. At high concentrations, H_2O_2 has deleterious effects and leads to cell death, a more common and deeply studied effect of this compound.[45] Applying these premises to our study, we can hypothesize that, when neurons are exposed to 10×10^{-6} M H_2O_2 in the presence of the microreactors, the latter are able to convert the majority of H_2O_2, keeping this compound in the range of concentrations where it provides neuronal protection and improves cell viability.

Both M^P and M^{PE1} were able to significantly improve cell viability of cells exposed to NH_4^+ (Figure 4B). This effect is likely associated with the catalytic activity of Pt-NP that leads to a decrease of NH_4^+ and concomitant formation of NO in solution, which has a offers neuronal protection at low concentrations.[46,47] Since these microreactors convert ≈7% of the total amount of NH_4^+ in solution over the course of 24 h[19] and because NO has an extremely short half-life,[48] there is never a buildup of NO in cell medium, maintaining this compound at physiological and non-toxic levels. For a review on the different lines of thought concerning what classifies as a physiological concentration of NO, the reader is referred to the work of Hall and Garthwaite.[49] Surprisingly, M^{PE1} is significantly more effective than M^P in rescuing cell viability.

The second biological activity assay consisted of extracellular electrophysiological recordings, using a microelectrode array (MEA) system. This assay provides more detailed insights into the activity of the microreactors, since it measures how neuronal communication and response to stimuli are altered in the presence of H_2O_2 or NH_4^+, and how microreactors counteract these alterations. In the MEA system, neurons are plated on cell culture inserts with a 60-electrode array, where they adhere and mature, allowing for a direct observation of extracellular neuronal electrical function at a later time point. Since it is not possible to determine how many cells are being recorded by each electrode, internal controls were performed for each experimental condition. Thus, extracellular electrophysiological recordings were performed in two subsequent phases: first a baseline recording was obtained for each individual condition at 14 DIV, without any toxic compounds or microreactors (Figure 4C, black traces). These data represent the neural basal activity of those specific neuronal networks, prior to any treatment. Secondly, test phase recordings were performed after cells were incubated for 24 h with microreactors (M^P or M^{PE1}, 20% of the number of cells) and H_2O_2 or NH_4^+ (Figure 4C, color traces). Importantly, the relative position of the different electrodes in relation to the cells was maintained over the two recording phases. The same stimulus parameters were used in this phase to ensure normalization to the baseline measurement. This analysis accounts for how much these parameters changed over 24 h and overcomes the possibility of variation in the size of the neuronal networks across cultures, allowing for comparisons between the different conditions. Importantly, cells not exposed to either toxic compounds or microreactors were used as a general control, providing information on how the response parameters change over 24 h without any manipulation, and are represented as a red line in Figure 4D,E.

The amplitude and slope of each stimulus response were analyzed (Figure 4D,E, respectively). H_2O_2 led to a decrease in both amplitude and slope, which was completely prevented, in a similar magnitude, by M^P or M^{PE1}. On the other hand, NH_4^+ had the opposite effect, increasing both amplitude and slope. Similarly to the cell viability assay, M^{PE1} appear to have a more extensive capability for preventing these changes when compared to M^P, being able to significantly revert the NH_4^+-induced dysfunctions in both amplitude and slope, while M^P were only able to revert slope dysfunction in a smaller degree. Interestingly, as depicted in the representative traces (Figure 4B), exposure to H_2O_2 or NH_4^+ led to a phase shift of the response wave. Given that each depicted wave represents the combined activity of all neurons surrounding the electrode, this shift can be the consequence of structural changes in the neuronal network–either by cell death, as suggested by the cell viability assay, or by axonal and dendritic retraction. Representative signals obtained in different neuron-electrode relative positions can be seen in a review by Obien et al.[50] Importantly, since the phase shifts are only representative of the physical arrangement of neurons, absolute parameter values were used for comparison with other conditions.

Globally, it is possible to conclude that both M^P and M^{PE1} are able to revert the actions of H_2O_2 and NH_4^+ in a rat primary neuronal cultures, with M^{PE1} being significantly more capable to counteract NH_4^+ than M^P. While all biological activity data is in accordance, the in vitro data presented above suggested that M^{PE1} would be a better catalyst of H_2O_2 conversion than M^P, a difference that was not translated into higher cell viability rescue nor into better neuronal function preservation. Since M^P already elevate cell viability to higher than control levels and fully revert electrophysiological neuronal dysfunction, it is possible that cells reached a plateau in both assays, thus masking the actions of M^{PE1}. Focusing on the action of M^{PE1} toward NH_4^+, the in vitro characterization also did not foresee such a distinct action between these microreactors and M^P, with M^{PE1} providing significantly more neuronal protection than M^P. This difference might be explained by interaction of GDH with cellular substrates. While this enzyme mainly converts L-glutamate into α-ketoglutarate and NH_4^+,[51] the reaction can occur to some extent in the opposite direction in the presence of large concentrations of NH_4^+ such as the one used for this assay, leading to the consumption of NH_4^+ and concomitant formation of L-glutamate, explaining the notorious increase in cell viability. In a completely different line of thought, NH_4^+ is known to induce oxidative stress in neuronal cells, leading to an overproduction of ROS,[52] while M^{PE1} produce NADPH, which can act as an antioxidant, neutralizing toxic free radicals.[53] Thus, it is possible that M^{PE1} enhanced biological activity arises from the cumulative detoxification of both H_2O_2 and NH_4^+, conjugated with more extensive antioxidant properties. Regardless, these data indicate that the inclusion of enzymes in the microreactors was extremely beneficial, which was anticipated given the important role enzymes have played in encapsulated catalysis over the last years.[54]

3. Conclusion

In this study, we further explore the possible therapeutical application of Pt-NP-containing microreactors in the context of

© 2020 Wiley-VCH GmbH

excitotoxicity. Regarding microreactors containing only Pt-NP, with this non-proliferating cell model, we were able to exclude the confounding variable of proliferation inhibition in cell viability. With this variable excluded, there were no differences in cell viability in any microreactor concentration tested. Furthermore, these microreactors display good levels of cell adhesion toward neuronal cells, both mature and immature, and maintain the biological activity observed with the SH-SY5Y cell line toward H_2O_2 and NH_4^+. Moreover, we present and thoroughly characterize a new advancement in these microreactors, containing Pt-NP and enzymes. These novel microreactors are able to prevent cellular death caused by H_2O_2 or NH_4^+ as well as restore disrupted neuronal activity in a more complex cellular model that closer mimics a true neuronal environment. While these findings bring us one step closer to developing a new therapeutic tool to counteract excitotoxicity in vivo, with applications in several neurodegenerative diseases, such as ALS, or in traumatic brain injury, a variety of challenges need to be addressed before such microreactors might have clinical relevance. Among the unsolved issues, the delivery of the microreactor to the brain, the time-limited performance of the microreactors especially when enzymes are used, or the relatively cumbersome and time consuming microreactor assembly still need to be explored. Nonetheless, the promising results shown here are a relevant contribution to the emerging field of artificial biology where bottom-up assembled entities support their natural counterparts.

4. Experimental Section

Materials: 4-(2-hydroxyethyl)piperazine-1-ethanesulfonic acid (HEPES), dopamine hydrochloride (DA), poly(L-lysine) (PLL, MW 40 000–70 000 Da), poly(D-lysine) (PDL, MW 30 000–70 000 Da), hydrogen peroxide (H_2O_2, 30% w/w), ammonium acetate, L-glutamic acid dehydrogenase from bovine liver (GDH, EC1.4.1.3, 48 U mg^{-1}), glutathione reductase from baker's yeast (GTR, EC1.8.1.7, 170 U mg^{-1}), glutamic acid, β-nicotinamide adenine dinucleotide phosphate sodium salt hydrate ($NADP^+$), L-glutathione oxidized disodium salt (GSSG), horseradish peroxidase (HRP), ammonia assay kit (AAK, MAK310), paraformaldehyde (PFA), bovine serum albumin (BSA), and Triton X-100 were purchased from Sigma-Aldrich (St. Louis, MO, USA). Tris base and sodium chloride (NaCl) were obtained from VWR (Radnor, PA, USA). Amplex UltraRed, Hank's balanced saline solution (HBSS), fetal bovine serum (FBS), Neurobasal medium, L-glutamine (200×10^{-3} M), B-27 (50x), gentamycin (50 mg mL^{-1}), trypsin-EDTA (0.5%, no phenol red), and BD Falcon Cell Strainer 70 µm were purchased from Thermo Fisher Scientific (Waltham, MA, USA). Hoechst 33 342 was purchased from Life Technologies (Carlsbad, CA, USA). Polystyrene (PS) particles (19.30 µm in diameter) were acquired from Microparticles GmbH (Berlin, Germany). Cell counting kit 8 (CCK-8) was obtained from Dojindo EU GmbH (Munich, Germany). 1,2-dioleoyl-*sn*-glycero-3-phosphocholine (DOPC) was purchased from Avanti Polar Lipids (Alabaster, AL, USA). PLL-coated μ-Slides VI$^{0.4}$ were purchased from ibidi GmbH (Martinsried, Germany). Platinum nanoparticles (Pt-NP)[19] and poly(methacrylic acid)-*co*-cholesteryl methacrylate (PMAc)[55] were synthesized in house according to previously published procedures.

Buffer solutions: HEPES1 buffer (10×10^{-3} M HEPES, pH 7.3), HEPES2 buffer (20×10^{-3} M HEPES, 120×10^{-3} M NaCl, pH 7.3), Tris buffer (10×10^{-3} M Tris base, pH 8.5), and phosphate-buffered saline (PBS, pH 7.3).

Liposome Preparation: 200 nm in diameter liposomes were prepared by evaporation of 100 µL of a DOPC solution (25 mg mL^{-1} in chloroform) under vacuum for 1 h, followed by rehydration of the lipid film with 200 µL of an enzyme-containing solution (100 U mL^{-1} GDH to generate L_{GDH} or 100 U mL^{-1} GDH and 100 U mL^{-1} GTR to generate $L_{GDH+GTR}$) in HEPES2 buffer. Liposomes were then further hydrated with 800 µL of HEPES2 buffer. The solutions were extruded through 200 nm filters (11x) to obtain monodispersed unilamellar liposomes. Non-encapsulated enzymes were removed by size exclusion chromatography.

Microreactor Assembly: Pt-NP-based microreactors were assembled as previously described.[19] Briefly, PS particles (19.30 µm in diameter, 10 mg mL^{-1}) were coated with DA (2.5 mg mL^{-1} in Tris buffer, 3 h), generating a coating of polydopamine (PDA). The microreactors were then coated with PLL (1.0 mg mL^{-1} in HEPES1 buffer, 10 min) and Pt-NP were adsorbed to its surface (20 min). The microreactors were coated once more with PLL (1.0 mg mL^{-1} in HEPES1 buffer, 10 min) and received a terminating coat of polydopamine, via a DA solution (2.5 mg mL^{-1} in Tris buffer, 3 h), generating the finished Pt-NP-based microreactors (M^P). All coating steps were followed by 3x washing steps with HEPES1 buffer (1800 rpm, 45 s). To generate microreactors containing Pt-NP and enzyme-loaded liposomes, 19.30 µm PS particles were exposed to DA (2.5 mg mL^{-1} in Tris buffer, 3 h) and incubated with PLL (1.0 mg mL^{-1} in HEPES2 buffer, 10 min). The positively charged particles were incubated with enzyme-loaded liposomes (L_{GDH} for M^{PE1}, or $L_{GDH+GTR}$ for M^{PE2}) for 40 min. All microreactors were then coated with PMAc (2.0 mg mL^{-1} in HEPES2 buffer, 10 min), followed by a coating of PLL (1.0 mg mL^{-1} in HEPES2 buffer, 10 min) and adsorption of Pt-NP (20 min). The three previous coating steps (PLL, liposomes, PMAc) were repeated to increase the amount of adsorbed enzyme-loaded liposomes. Finally, microreactors were incubated with DA (2.5 mg mL^{-1} in Tris buffer, overnight) to generate a capping PDA layer. Different control microreactors without Pt-NP were generated M^0, containing only the first PDA layer; M^{00}, containing empty liposomes; M^{0E1}, containing L_{GDH}; and M^{0E2}, containing $L_{GDH+GTR}$. Additionally, microreactors containing Pt-NP and empty liposomes (M^{P0}) were also fabricated. The summary of all different used microreactors can be found in Table S2 (Supporting Information).

ζ-potential Measurements: The ζ-potential of the different assembly steps of microreactors containing Pt-NP and liposomes were determined using a Zetasizer Nano ZS (Malvern Instruments, UK), using a material refractive index of 1.590 and a dispersant refractive index of 1.330.

Fluorescent Imaging of Microreactors: To label liposomes incorporated into microreactors, microreactors were incubated with di-8-ANEPPS dye (10×10^{-6} M) for 20 min at room temperature, protected from light. The samples were then imaged using an Axioskop 2 Plus fluorescent microscope (Carl Zeiss Inc., Göttingen, Germany), with a 40x objective.

Transmission Electron Microscopy (TEM): The grids for TEM were prepared by depositing 5 µL of sample on a formvar coated grid (Agar Scientific Ltd, Stansted, Essex, United Kingdom) followed by washing 2x after 1 min with 5 µL of ultrapure water and staining with 2% v/v uranyl acetate. Samples were imaged with a Hitachi H7000 transmission electron microscope (Hitachi High-Technologies Europe GmbH, Krefeld, Germany).

H_2O_2 Detection Assay: 10^4 microreactors were incubated with 1.0×10^{-3} M H_2O_2 for 24 h at 37 °C. Following this incubation, each sample was incubated with 0.2 U mL^{-1} HRP and 50 µm Amplex UltraRed at room temperature, protected from light, for 30 min. The fluorescence of the solutions (λ_{ex} = 545 nm, λ_{em} = 590 nm) was measured by a multiplate reader.

NH_4^+ Detection Assay: 10^6 microreactors were incubated with 1.0×10^{-3} M NH_4^+ for 24 h at 37 °C. Following this incubation, NH_4^+ was detected using the commercially available AAK. 10 µL of the samples were incubated with 90 µL of AAK detection mix for 15 min at room temperature, protected from light. The fluorescence of the solutions (λ_{ex} = 360 nm, λ_{em} = 450 nm) was measured by a multiplate reader.

NADPH Detection Assay: Samples were incubated with 30×10^{-3} M L-glutamate, 2.0×10^{-3} M GSSG, and 2.0×10^{-3} M $NADP^+$ at 37 °C. The amount of NADPH in solution was followed by measuring the absorbance of the solutions (λ = 340 nm) at different time points. For the determination of NADPH produced by the different microreactors,

© 2020 Wiley-VCH GmbH

10^5 microreactors were used and samples were centrifuged (1800 rpm, 45 s) prior to absorbance measurements.

Cell Culture: Primary neuronal cultures were prepared according to a previously established method.[56] Succinctly, Sprague-Dawley fetuses (pre-natal day 18/19) were euthanized and their brains used to obtain primary neuronal cultures. The fetuses were collected in HBSS, their cerebral cortexes isolated and the meninges removed. Following this, the obtained tissue was mechanically fragmented and digested with 10% v/v trypsin-EDTA in HBSS for 15 min at 37 °C. Trypsin action was stopped with the addition of 30% v/v FBS in HBSS. Cells were then centrifuged 3x at 1 200 rpm, where the supernatant was discarded and replaced with 30% v/v FBS in HBSS. Cells were then resuspended in supplemented Neurobasal medium (0.5×10^{-3} M L-glutamine, 25×10^{-6} M glutamic acid, 2% v/v B-27, and 12 µg mL^{-1} gentamycin). To ensure proper tissue dissociation, cells were strained through a nylon filter (70 µm). Cells were then plated at different densities, depending on the application (150 000 cells mL^{-1} for cell viability assays, 600 000 cells mL^{-1} for Hoechst staining, and 300 000 cells mL^{-1} for extracellular electrophysiological recordings), and were incubated at 37 °C in a humified atmosphere of 95% air–5% CO_2. Importantly, these different plating densities reflect the optimal cell concentration for the different applications,[57] in order to achieve a linear colorimetric response in the cell viability assay, to be able to examine the interaction between microreactors and cells in the staining assay, and to generate more robust and detectable electrical signals in the electrophysiological recordings. All animals were handled according to Portuguese Law and the European Union Directive (86/609/EEC) on the protection of animals for scientific experimentation.

Cell Viability Assay: 150 000 cells mL^{-1} were plated on PDL-treated (10 µg mL^{-1}) 96-well plates and allowed to adhere and mature for 7 or 14 DIV. At these times, to study the biocompatibility of the microreactors, M^P were added to the cell medium at different concentrations (5, 10%, 20%, and 100% of the number of cells). 24 h later, the cell medium was replaced with a solution of 10% v/v CCK-8 in supplemented Neurobasal medium. After 2 h of incubation at 37 °C, 100 µL of medium was transferred onto a new 96-well plate and absorbance at 460 nm was measured using a multiplate reader. Regarding the biological activity of the microreactors, the same protocol was performed except the cells were allowed to adhere and mature for 14 DIV, at which time microreactors (20% of the number of cells; M^P or M^{PE1}) and 10×10^{-6} M H_2O_2 or 10×10^{-3} M NH_4^+ were added to the cell medium.

Hoechst Staining: 600 000 cells mL^{-1} were plated on PLL-treated ibidi µ-Slides VI$^{0.4}$ for 7 or 14 DIV. Cell medium was renewed every two days, to prevent evaporation. At these time points, M^P were added to each well at different concentrations (10%, 20%, and 100% of the number of cells). After 24 h of incubation, wells were washed 3x with PBS, fixed for 30 min in 4% w/v PFA in PBS, permeabilized and blocked for nonspecific binding sites for 20 min with 0.1% v/v Triton X-100 and 1% w/v BSA in PBS, and incubated for 10 min at room temperature with Hoechst 33 342 (12 µg mL^{-1}) in PBS protected from light. The samples were stored at 4 °C in PBS in the µ-Slides. Bright field and fluorescence images were captured using an Axioskop 2 Plus fluorescent microscope (Carl Zeiss Inc.), with a 10x objective. Images were recorded using the software AxioVision (Carl Zeiss Inc.) and analyzed using the software ImageJ.[58]

Microelectrode Array (MEA) Assay: 300 000 cells mL^{-1} were plated on PDL-treated (10 µg mL^{-1}) 6 well round chamber microelectrode array plates with 60 electrodes (60-6wellMEA200/30iR-Ti-rcr, Multi Channel Systems, Reutlingen, Germany) and allowed to adhere for 14 DIV. At this point, extracellular recordings were performed, prior to any cell treatment. Cells were probed with a bi-phasic wave, with ±1000 mV during 200 ms and an inter-stimuli interval of 20 s, during a total recording time of 3 min, resulting in 9 different stimulations. The same electrode was simultaneously used to stimulate and record cells. Cells were then incubated for 24 h with microreactors (M^P or M^{PE1}, at 20% of the number of cells) and 10 µm H_2O_2 or 10×10^{-3} M NH_4^+. Following this incubation, the same stimulation and recording protocols were performed. The relative position of the electrodes was maintained during all stimulation protocols, in order to stimulate and record the same cells before and after the incubations.

Statistical Analysis: All assays include at least three independent repeats ($N >= 3$). For experiments without cells, concerning the characterization of microreactors, each independent repeat refers to different batches of microreactors, independently assembled. For cell experiments, each independent repeat refers to different independent animal cultures. All cell viability assays were performed with triplicates and at least three independent repeats. For each independent repeat, values were normalized to the cell viability of untreated cells (100%). For Hoechst staining, five random fields were analyzed per condition in each independent repeat. For the quantification of H_2O_2 and NH_4^+ consumption, values were normalized to the initial amount of H_2O_2 or NH_4^+ in solution (100%). Electrophysiological data are normalized as fold-change over 24 h (change = value[day 2]/value[day 1]). All data are represented as mean ± standard error of mean (SEM), with $p < 0.05$ representing statistical significance. When considering the whole data set, values outside the range of mean ± 2 x standard deviation were considered outliers. Statistical significance was determined using two-tailed paired t-tests when comparing two conditions and one-way ANOVA when comparing three or more. All data were analyzed in GraphPad Prism (GraphPad Software, Inc., La Jolla, CA, USA).

Supporting Information

Supporting Information is available from the Wiley Online Library or from the author.

Acknowledgements

This work was supported by Fundação para a Ciência e Tecnologia (FCT), Portugal (PTDC/BTM-SAL/32147/2017, PD/BD/114278/2016, IMM/BI/2-2020) and the Aarhus University Research Foundation, Denmark.

Conflict of Interest

The authors declare no conflict of interest.

Keywords

encapsulated catalysis, excitotoxicity, microreactors, platinum nanoparticles, rat cortical primary neurons

Received: May 28, 2020
Revised: July 29, 2020
Published online:

[1] X. Dong, Y. Wang, Z. Qin, *Acta Pharmacol. Sin.* **2009**, *30*, 379.
[2] Y. Shigeri, R. P. Seal, K. Shimamoto, *Brain Res. Rev.* **2004**, *45*, 250.
[3] J. Gonçalves-Ribeiro, C. C. Pina, A. M. Sebastião, S. H. Vaz, *Front. Cell. Neurosci.* **2019**, *13*, 357.
[4] N. R. Sims, E. Zaidan, *Int. J. Biochem. Cell Biol.* **1995**, *27*, 531.
[5] N. M. C. Connolly, J. H. M. Prehn, *J. Bioenerg. Biomembr.* **2015**, *47*, 75.
[6] A. A. Kritis, E. G. Stamoula, K. A. Paniskaki, T. D. Vavilis, *Front. Cell. Neurosci.* **2015**, *9*, 91.
[7] J. T. Coyle, P. Puttfarcken, *Science* **1993**, *262*, 689.
[8] B. Halliwell, *Annu. Rev. Nutr.* **1996**, *16*, 33.
[9] L. K. Bak, A. Schousboe, H. S. Waagepetersen, *J. Neurochem.* **2006**, *98*, 641.
[10] I. Suárez, G. Bodega, B. Fernández, *Neurochem. Int.* **2002**, *41*, 123.

 © 2020 Wiley-VCH GmbH

[11] M. Jia, S. A. N. Njapo, V. Rastogi, V. S. Hedna, *CNS Drugs* **2015**, *29*, 153.
[12] L. Schoonen, J. C. M. van Hest, *Adv. Mater.* **2016**, *28*, 1109.
[13] M. Godoy-Gallardo, M. J. York-Duran, L. Hosta-Rigau, *Adv. Healthcare Mater.* **2018**, *7*, 1700917.
[14] G. Orive, E. Santos, D. Poncelet, R. M. Hernández, J. L. Pedraz, L. U. Wahlberg, P. De Vos, D. Emerich, *Trends Pharmacol. Sci.* **2015**, *36*, 537.
[15] Y. Zhang, P. S. Schattling, F. Itel, B. Städler, *ACS Omega* **2017**, *2*, 7085.
[16] F. Itel, J. Skovhus Thomsen, B. Städler, *ACS Appl. Mater. Interfaces* **2018**, *10*, 30180.
[17] A. S. Cheung, D. K. Y. Zhang, S. T. Koshy, D. J. Mooney, *Nat. Biotechnol.* **2018**, *36*, 160.
[18] J. Tang, D. Shen, T. G. Caranasos, Z. Wang, A. C. Vandergriff, T. A. Allen, M. T. Hensley, P.-U. Dinh, J. Cores, T.-S. Li, J. Zhang, Q. Kan, K. Cheng, *Nat. Commun.* **2017**, *8*, 13724.
[19] A. Armada-Moreira, E. Taipaleenmäki, M. Baekgaard-Laursen, P. S. Schattling, A. M. Sebastião, S. H. Vaz, B. Städler, *ACS Appl. Mater. Interfaces* **2018**, *10*, 7581.
[20] Y. Liu, H. Wu, M. Li, J.-J. Yin, Z. Nie, *Nanoscale* **2014**, *6*, 11904.
[21] M. Rafti, A. Brunsen, M. C. Fuertes, O. Azzaroni, G. J. A. A. Soler-Illia, *ACS Appl. Mater. Interfaces* **2013**, *5*, 8833.
[22] M. P. Sahu, O. Nikkilä, S. Lågas, S. Kolehmainen, E. Castrén, *Neuronal Signaling* **2019**, *3*, NS20180207.
[23] M. J. Kim, S. J. Oh, S. H. Park, H.-J. Kang, M. H. Won, T.-C. Kang, J.-B. Park, J.-I. Kim, J. Kim, J.-Y. Lee, *Exp. Mol. Med.* **2007**, *39*, 14.
[24] F. Robert, J. F. Cloix, T. Hevor, *Neuroscience* **2012**, *200*, 248.
[25] J. S. Valadas, V. L. Batalha, D. G. Ferreira, R. Gomes, J. E. Coelho, A. M. Sebastião, M. J. Diógenes, L. V. Lopes, *J. Neurochem.* **2012**, *123*, 1030.
[26] M. E. Hatten, *J. Cell Biol.* **1985**, *100*, 384.
[27] A. I. McClatchey, A. S. Yap, *Curr. Opin. Cell Biol.* **2012**, *24*, 685.
[28] A. Puliafito, L. Hufnagel, P. Neveu, S. Streichan, A. Sigal, D. K. Fygenson, B. I. Shraiman, *Proc. Natl. Acad. Sci. USA* **2012**, *109*, 739.
[29] K. Kang, I. S. Choi, Y. Nam, *Biomaterials* **2011**, *32*, 6374.
[30] S. H. Bhang, S.-H. Kwon, S. Lee, G. C. Kim, A. M. Han, Y. H. K. Kwon, B.-S. Kim, *Biochem. Biophys. Res. Commun.* **2013**, *430*, 1294.
[31] C. R. Murthy, A. S. Bender, R. S. Dombro, G. Bai, M. D. Norenberg, *Neurochem. Int.* **2000**, *37*, 255.
[32] W. Hilgier, M. Węgrzynowicz, J. Ruszkiewicz, S. S. Oja, P. Saransaari, J. Albrecht, *Toxicol. Sci.* **2010**, *117*, 163.
[33] C. Zhu, F. Itel, R. Chandrawati, X. Han, B. Städler, *Biomacromolecules* **2018**, *19*, 4379.
[34] M. G. Carneiro-da-Cunha, M. A. Cerqueira, B. W. S. Souza, J. A. Teixeira, A. A. Vicente, *Carbohydr. Polym.* **2011**, *85*, 522.
[35] J. Ziegenhorn, M. Senn, T. Bücher, *Clin. Chem.* **1976**, *22*, 151.
[36] D. Botman, W. Tigchelaar, C. J. F. V. Noorden, *J. Histochem. Cytochem.* **2014**, *62*, 802.
[37] I. Carlberg, B. Mannervik, *Methods Enzymol.* **1985**, *113*, 484.
[38] A. Armada-Moreira, B. Thingholm, K. Andreassen, A. M. Sebastião, S. H. Vaz, B. Städler, *Adv. Biosyst.* **2018**, *2*, 1700244.
[39] A. M. Sheridan, S. Fitzpatrick, C. Wang, D. C. Wheeler, W. Lieberthal, *Kidney Int.* **1996**, *49*, 88.
[40] Y. H. Siddique, G. Ara, M. Afzal, *Dose-Response* **2012**, *10*, 1.
[41] E. R. Whittemore, D. T. Loo, J. A. Watt, C. W. Cotman, *Neuroscience* **1995**, *67*, 921.
[42] A. Klejman, M. Wegrzynowicz, E. M. Szatmari, B. Mioduszewska, M. Hetman, J. Albrecht, *Neurochem. Int.* **2005**, *47*, 51.
[43] V. Felipo, R. F. Butterworth, *Prog. Neurobiol.* **2002**, *67*, 259.
[44] E. Kosenko, Y. Kaminsky, E. Grau, M. D. Miñana, G. Marcaida, S. Grisolía, V. Felipo, *J. Neurochem.* **1994**, *63*, 2172.
[45] R. E. Haskew-Layton, J. B. Payappilly, N. A. Smirnova, T. C. Ma, K. K. Chan, T. H. Murphy, H. Guo, B. Langley, R. Sultana, D. A. Butterfield, S. Santagata, M. J. Alldred, I. G. Gazaryan, G. W. Bell, S. D. Ginsberg, R. R. Ratan, *Proc. Natl. Acad. Sci. USA* **2010**, *107*, 17385.
[46] F. Yildiz Akar, G. Ulak, P. Tanyeri, F. Erden, T. Utkan, N. Gacar, *Pharmacol., Biochem. Behav.* **2007**, *87*, 434.
[47] V. Paul, P. Ekambaram, *Indian J. Med. Res.* **2011**, *133*, 471.
[48] T. S. Hakim, K. Sugimori, E. M. Camporesi, G. Anderson, *Physiol. Meas.* **1996**, *17*, 267.
[49] C. N. Hall, J. Garthwaite, *Nitric Oxide* **2009**, *21*, 92.
[50] M. E. J. Obien, K. Deligkaris, T. Bullmann, D. J. Bakkum, U. Frey, *Front. Neurosci.* **2014**, *8*, 423.
[51] B. J. Thatcher, K. B. Storey, *Biochem. Cell Biol.* **2001**, *79*, 11.
[52] L. D. Bobermin, K. M. Wartchow, M. P. Flores, M. C. Leite, A. Quincozes-Santos, C.-A. Gonçalves, *Neurotoxicology* **2015**, *49*, 28.
[53] M. Kirsch, H. De Groot, *FASEB J.* **2001**, *15*, 1569.
[54] F. Itel, P. S. Schattling, Y. Zhang, B. Städler, *Adv. Drug Delivery Rev.* **2017**, *118*, 94.
[55] M. E. Lynge, M. Baekgaard Laursen, L. Hosta-Rigau, B. E. B. Jensen, R. Ogaki, A. A. A. Smith, A. N. Zelikin, B. Städler, *ACS Appl. Mater. Interfaces* **2013**, *5*, 2967.
[56] A. Jerónimo-Santos, S. H. Vaz, S. Parreira, S. Rapaz-Lérias, A. P. Caetano, V. Buée-Scherrer, E. Castrén, C. A. Valente, D. Blum, A. M. Sebastião, M. J. Diógenes, *Cereb. Cortex* **2015**, *25*, 3107.
[57] E. Biffi, G. Regalia, A. Menegon, G. Ferrigno, A. Pedrocchi, *PLoS One* **2013**, *8*, 83899.
[58] C. A. Schneider, W. S. Rasband, K. W. Eliceiri, *Nat. Methods* **2012**, *9*, 671.

 © 2020 Wiley-VCH GmbH